ISTANBUL TECHNICAL UNIVERSITY ★ GRADUATE SCHOOL

INVESTIGATION OF THE EFFECTS OF ALTERNATIVE FUEL USE ON PERFORMANCE AND EMISSIONS IN A COMPRESSION IGNITION (CI) DIESEL ENGINE

Ph.D. THESIS

Ferhat EKİN

Department of Naval Architecture and Marine Engineering

Naval Architecture and Marine Engineering Programme

JANUARY 2024

ISTANBUL TECHNICAL UNIVERSITY ★ GRADUATE SCHOOL

INVESTIGATION OF THE EFFECTS OF ALTERNATIVE FUEL USE ON PERFORMANCE AND EMISSIONS IN A COMPRESSION IGNITION (CI) DIESEL ENGINE

Ph.D. THESIS

Ferhat EKİN
(508162013)

Department of Naval Architecture and Marine Engineering

Naval Architecture and Marine Engineering Programme

Thesis Advisor: Prof. Dr. Osman Azmi ÖZSOYSAL
Thesis Co-Advisor: Assist. Prof. Dr. Hikmet ARSLAN

JANUARY 2024

İSTANBUL TEKNİK ÜNİVERSİTESİ ★ LİSANSÜSTÜ EĞİTİM ENSTİTÜSÜ

SIKIŞTIRMALI ATEŞLEMELİ BİR DİZEL MOTORDA ALTERNATİF YAKIT KULLANIMININ PERFORMANS VE EMİSYON DEĞERLERİ ÜZERİNDEKİ ETKİLERİNİN ARAŞTIRILMASI

DOKTORA TEZİ

Ferhat EKİN
(508162013)

Gemi İnşaatı ve Gemi Makineleri Mühendisliği Programı

Gemi İnşaatı ve Gemi Makineleri Mühendisliği Anabilim Dalı

Tez Danışmanı: Prof. Dr. Osman Azmi ÖZSOYSAL
Eş Danışman: Dr. Öğr. Üyesi Hikmet ARSLAN

OCAK 2024

Ferhat EKİN, a Ph.D. student of İTU Graduate School student ID 508162013, successfully defended the thesis/dissertation entitled "INVESTIGATION OF THE EFFECTS OF ALTERNATIVE FUEL USE ON PERFORMANCE AND EMISSIONS IN A COMPRESSION IGNITION (CI) DIESEL ENGINE", which he prepared after fulfilling the requirements specified in the associated legislations, before the jury whose signatures are below.

Thesis Advisor :	**Prof. Dr. Osman Azmi ÖZSOYSAL** İstanbul Technical University	.....
Co-advisor :	**Assist. Prof. Dr. Hikmet ARSLAN** İstanbul Technical University	.....
Jury Members :	**Assoc. Prof. Dr. Osman Akın KUTLAR** İstanbul Technical University	.....
	Prof. Dr. Yasin ÜST Yıldız Technical University	.....
	Prof. Dr. Güven GONCA Yıldız Technical University	.....
	Prof. Dr. Oğuz Salim SÖĞÜT İstanbul Technical University	.....
	Prof. Dr. Nurten VARDAR Yıldız Technical University	.....

Date of Submission : 1 December 2023
Date of Defense : 11 January 2024

To my wife and my sons,

FOREWORD

Compression Ignition (CI) engines are of great significance, especially in commercial terms, due to their ability to provide high torque and low fuel consumption. However, there has been a prejudice against CI engines due to their high emissions of harmful exhaust gases and their inadequacy in meeting continuously tightened emission standards. In the scope of the thesis, the use of alternative fuels in these engines has been facilitated as a motivational source to overcome these negatives, aiming to achieve high performance and low emissions comprehensively.

In the challenging process I have gone through, I owe a debt of gratitude to my invaluable advisor Prof. Dr. Osman Azmi ÖZSOYSAL, who has consistently guided me with his knowledge and experience, and to my co-advisor Assist. Prof. Dr. Hikmet ARSLAN, as well as to the thesis monitoring committee members Prof. Dr. Yasin ÜST and Prof. Dr. Güven GONCA. I extend my thanks to Assoc. Prof. Dr. Osman Akın KUTLAR and Assist. Prof. Dr. Hikmet ARSLAN, who not only provided valuable contributions through the courses they offered before the thesis period but also served as members of the thesis monitoring committee. I also express my gratitude to my esteemed colleagues Assist. Prof. Dr. Gökhan BUDAK, Assist. Prof. Dr. Mustafa KAFALI, Dr. Muhammet AYDIN, Dr. Halil İbrahim SÖNMEZ, Research Assistant Öncel ÖNCÜOĞLU and Research Assistant Mikail Rıza ONAT, who dedicated their time and shared their experiences during my thesis process. Special thanks go to Mr. Dr. Erdal TUNÇER, Technical Affairs Manager at Erin Motor Inc., for his assistance and willingness to share knowledge, which significantly contributed to my studies.

Throughout my professional life, I express my gratitude to my dear wife, Latife Ümran EKİN, who has always been spiritually by my side, providing unwavering support, patience, and understanding in the face of all challenges, and who has never hesitated to make sacrifices when needed. Her constant encouragement has kept my motivation alive. I extend my thanks to my beloved parents, who have played an immeasurable role in bringing me to this point. My gratitude to them can never be fully repaid. I also feel honored to express my thanks to all my loved ones, especially my wife's family, who have been a constant source of support and presence in my life.

December 2023

Ferhat EKİN
(Naval Architecture and Marine Engineer)

TABLE OF CONTENTS

Page

ABBREVIATIONS

AFR : Air-Fuel Ratio
ATDC : After Top Dead Center
BDC : Bottom Dead Center
BMEP : Break Mean Effective Pressure
BSFC : Break Specific Fuel Consumption
BTDC : Before Top Dead Center
CA : Crank Angle
CD : Combustion Duration
CFD : Computational Fluid Dynamics
CI : Compression Ignition
CN : Cetane Number
CNG : Compressed Natural Gas
DI : Direct Injection
EGR : Exhaust Gas Recirculation
EGT : Exhaust Gas Temperature
EVC : Exhaust Valve Closure
EVO : Exhaust Valve Open
HCCI : Homogeneous Charge Compression Ignition
HRR : Rate of Heat Release
ICE : Internal Combustion Engine
ID : Ignition Delay
IMEP : Indicated Mean Effective Pressure
IMO : International Maritime Organization
IVC : Inlet Valve Closure
IVO : Inlet Valve Open
LHV : Lower Heating Value
LPG : Liquefied Petroleum Gas
LTC : Low Temperature Combustion
MON : Motor Octane Number
MPRR : Rate of Maximum Pressure Rise

NG **:** Natural Gas

PCCI **:** Premixed Charge Compression Ignition

PI **:** Pilot Injection

PM **:** Particulate Matter

RCCI **:** Reactivity Controlled Compression Ignition

RON **:** Research Octane Number

RPM **:** Revolutions Per Minute

SCR **:** Selective Catalytic Reduction

SI **:** Spark Ignition

SOI **:** Start of Injection

SOWI **:** Start of Water Injection

SOWVI **:** Start of Water Vapor Injection

TDC **:** Top Dead Center

TE **:** Thermal Efficiency

TKE **:** Turbulence Kinetic Energy

WI **:** Water Injection

WVI **:** Water Vapor Injection

SYMBOLS

C_c	: Cavitation Coefficient
C_d	: Discharge Coefficient
CH_4	: Methane
CH_3OH	: Methanol
C_2H_5OH	: Ethanol
CO	: Carbon Monoxide
CO_2	: Carbon Dioxide
c_p, c_v	: Specific Heat Coefficients
E_A	: Energy of Activation
g	: Gravitational Acceleration
H_2	: Hydrogen
k	: Specific Heat Ratio
N	: Engine Rotation Speed
N_2	: Nitrogen
$n\text{-}C_7H_{16}$	: N-Heptane
$n\text{-}C_{14}H_{30}$	: N-Tetradecane
NH_3	: Ammonia
NO_x	: Nitrogen Oxides
O_2	: Oxygen
P_e	: Effective Power
P_f	: Friction Power
P_i	: Indicated Power
p_{me}	: Mean Effective Pressure
p_{mf}	: Mean Friction Pressure
p_{mi}	: Mean Indicated Pressure
R	: Ideal Gas Constant
R_e	: Reynolds Number
SO_x	: Sulphur Oxides
St	: Stokes Number
T	: Taylor Number

UHC : Unburned Hydrocarbon

$\mathbf{V_C}$: Clearance Volume

$\mathbf{V_H}$: Total Stroke Volume

$\mathbf{W_e}$: Weber Number

Z : Ohnesorge Number

$\boldsymbol{\varepsilon}$: Compression Ratio

$\boldsymbol{\beta}$: Pressure Increase Rate

$\boldsymbol{\rho}$: Pre-compression Ratio

$\boldsymbol{\lambda}$: Excess Air Ratio

$\boldsymbol{\phi}$: Equivalence Ratio

$\boldsymbol{\upsilon}$: Kinematic Viscosity

$\boldsymbol{\mu}$: Dynamic Viscosity

$\boldsymbol{\eta_c}$: Combustion Efficiency

$\boldsymbol{\eta_e}$: Effective Efficiency

$\boldsymbol{\eta_m}$: Mechanical Efficiency

$\boldsymbol{\eta_{th}}$: Thermal Efficiency

$\boldsymbol{\eta_v}$: Volumetric Efficiency

LIST OF TABLES

Page

LIST OF FIGURES

Page

INVESTIGATION OF THE EFFECTS OF ALTERNATIVE FUEL USE ON PERFORMANCE AND EMISSIONS IN A COMPRESSION IGNITION (CI) DIESEL ENGINE

SUMMARY

Undoubtedly, one of the most crucial options under investigation for enhancing performance and emission characteristics in internal combustion engines (ICEs) is the adoption of alternative fuels. It is of utmost importance that these alternative fuels are compatible with engine operation and do not lead to substantial structural alterations in the engine. These fuels need to be thermodynamically compatible with the engine and environmentally friendly. Key characteristics to look for in alternative fuels include having high reserves, high energy density, and causing minimal emissions. Due to possessing all these features, natural gas and hydrogen fuels hold significant importance among alternative fuels. Natural gas and hydrogen fuels are thermodynamically compatible with engines that operate on both Otto and Diesel cycles. Their ability to be used in internal combustion engines as alternative fuels without causing significant structural changes paves the way for their application. Furthermore, their lower emissions contribute to their appeal. In a compression-ignition (CI) engine, natural gas and hydrogen fuels, along with diesel fuel, can be used by mixing the gaseous fuel with intake air through a low-pressure injector in the manifold. Subsequently, ignition is achieved by injecting pilot diesel fuel onto the compressed charge during the compression process. The combustion technology that occurs in CI engines through this method is called "Dual-Fuel" combustion.

The combination of the high energy density of natural gas and its environmentally friendly nature, coupled with the high thermal efficiency of the diesel engine, results in both efficient and environmentally friendly operating conditions. In high compression ratio CI (Compression Ignition) engines, natural gas with a high octane number can be used directly in a premixed form without causing knock up to a certain compression ratio. When it comes to hydrogen fuel, it is known that its use in compression-ignition engines is highly suitable, just like natural gas, and it does not require any structural changes in the engine. The advantages of natural gas, such as its low carbon-to-hydrogen ratio, and the absence of this ratio in hydrogen, combined with their high energy densities, have increased the interest in these gaseous fuels. This situation has motivated the current thesis work. The impact of CI engines on air pollution worldwide, along with the economic and high-energy capacity characteristics of natural gas and hydrogen, strengthens the case for the alternative use of these gas fuels. The environmentally friendly and high-performance attributes of natural gas, combined with hydrogen's rapid and extensive ignition range, along with its high mass-specific energy density, have shed light on the application of these two gas fuels together in CI engines. Utilizing these advantages, the current thesis work has not only improved performance values but has also met the increasingly stringent emission limit values.

The thesis work involved the numerical modeling of an experimental study based on the literature, utilizing the ANSYS Forte CFD program. In the experimental part, the energy in a partially loaded (25% - 4.05 BMEP) compression-ignition diesel engine was supplied by 25% diesel fuel and 75% natural gas fuel. Different diesel fuel injection advances (10°, 14°, 18°, 22°, 26°, 30°, 34°, 38°, 42°, 46°, and 50° CA BTDC) were investigated at a constant engine speed (910 rpm) to explore their effects on performance and emission values. The test results were compared with the obtained numerical results to validate the established model. Subsequently, using the validated numerical model, parametric studies involving hydrogen in combustion were conducted.

Parametric studies were conducted in two stages. In the first stage, the effects of energy fractions of natural gas and hydrogen, as well as diesel fuel injection advances, were examined. Two fundamental principles guided the energy fractionation. In the first principle, the total fuel input energy under test conditions remained constant, while a portion of the natural gas energy was gradually transferred to hydrogen fuel. The diesel-derived energy fraction was kept constant at 25%, while the remaining 75% was allocated between natural gas and hydrogen fuels. These operating points were named Mode 1, also known as the energy-sharing mode for gas fuels. For Mode 1, the energy sharing ratios were established as D25NG75H00 (test case), D25NG65H10, D25NG50H25, D25NG25H50, and D25NG00H75. The second principle involved maintaining the diesel and natural gas energy ratios (25% diesel and 75% natural gas) constant, while providing extra energy input to the system through the inclusion of hydrogen. These operating points were labeled as Mode 2, also referred to as the hydrogen enrichment mode. For Mode 2, the operating points resulting from hydrogen enrichment were designated as D25NG75H00 (test case), D25NG75H05, D25NG75H10, D25NG75H15, D25NG75H20, and D25NG75H25. Various fuel energy fractions for both Mode 1 and Mode 2, combined with different diesel fuel injection timings (10°, 14°, 18°, 22°, 26°, 30°, 34°, and 38° CA BTDC), were examined to analyze their effects on performance and emission values. Among the examined values, it was observed that the operating points D25NG50H25 (14° CA BTDC for SOI) for Mode 1 and D25NG75H15 (10° CA BTDC for SOI) for Mode 2 produced more reasonable results in terms of both engine performance and exhaust gas emissions compared to other operating points. The optimal condition obtained for Mode 1 resulted in improvements of 21%, 29%, 88%, 86%, and 77% for power, BSFC, HC, CO, and SOOT (PM), respectively. For Mode 2, the optimal condition yielded improvements of 36%, 22%, 76%, 80%, and 83% for the same parameters. However, when comparing both Mode 1 and Mode 2 test conditions, the higher cylinder combustion temperatures due to hydrogen led to higher NO_x and MPRR values. While there was a 12% increase in NOx for Mode 1, Mode 2 showed an increase of 11%. Although significant results were achieved in terms of performance and emission values in the first stage, especially for NO_x and MPRR, the same situation did not occur. Therefore, the second stage of the study was carried out to implement some processes to maintain the improvements obtained in other emission types, especially NO_x and MPRR.

In the second stage, Exhaust Gas Recirculation (EGR), pilot diesel fuel injection (PI), water injection into the combustion chamber (WI), and water vapor direct injection (WVI) processes were applied to reduce NO_x and MPRR values. The PI strategy aimed to reduce the MPRR value, and the other processes were intended to improve NO_x. The PI strategy, along with other processes (EGR-PI, WI-PI, and WVI-PI), was

applied to achieve simultaneous reasonable results for MPRR and NO_x. In the PI application, the injection advance and duration were kept constant at 40° CA BTDC and 2.5° CA, respectively, for all conditions. The study investigated the effects of different Exhaust Gas Recirculation (EGR) ratios (0%, 10%, 15%, and 20%) and EGR temperatures (100 °C, 200 °C, and 300 °C) along with various pilot diesel fuel injection ratios (0%, 20%, 30%, and 50% - as the mass fraction of fuel sent with the main injection) on the points where the EGR effect was analyzed. When the D25NG50H25-20PI-10EGR100°C working point obtained for Mode 1 was compared with the test conditions (D25NG75H00 14° CA BTDC for SOI), improvements of 17%, 28.4%, 87.4%, 84.4%, and 32% were observed for power, BSFC, HC, CO, and NO_x, respectively. Similarly, for Mode 2, the D25NG75H15-20PI-10EGR100°C working point showed improvements of 31.15%, 21%, 74%, 77.15%, and 30%, respectively, compared to the test conditions (D25NG75H00 10° CA BTDC for SOI).

In the analysis conducted for water injection, the effects of different water injection ratios (0%, 5%, 10%, 15%, 20%, and 25% - as the mass fraction of diesel fuel sent with the main injection) and temperatures (25 °C, 60 °C, 75 °C, and 90 °C) along with various water injection timings (20° CA BTDC, 10° CA BTDC, 0° CA BTDC - TDC, and 10° CA ATDC) were investigated. The PI value for WI was chosen as 20%, which was obtained from EGR studies and yielded significant results. For Mode 1, the working point D25NG50H25-20PI-25WI75°C, in terms of WI-PI strategies, showed improvements of 14.26%, 20.7%, 88.33%, 85.7%, and 23.42% for power, BSFC, HC, CO, and NO_x, respectively, compared to the test conditions (D25NG75H00 14° CA BTDC for SOI). Similarly, for Mode 2, the operating point D25NG75H15-20PI-25WI75°C showed improvements of 30.33%, 15%, 77.29%, 79.5%, and 17%, respectively, for the same magnitudes compared to the test conditions (D25NG75H00 10° CA BTDC for SOI) at the 20° CA BTDC water injection timing (SOWI - Start of Water Injection).

In the study conducted for water vapor injection (WVI) into the combustion chamber, similar to the water jet analysis, the effects of different water vapor ratios (0%, 5%, 10%, 15%, 20%, and 25% - as the mass fraction of diesel fuel sent with the main injection) and temperatures (100 °C, 125 °C, 150 °C, and 200 °C) were investigated at various water vapor injection timings (20° CA BTDC, 10° CA BTDC, 0° CA BTDC - TDC, and 10° CA ATDC). Similar to WI, PI was chosen as 20% for WVI. For Mode 1, the operating point D25NG50H25-20PI-15WVI100°C, obtained with WVI-PI processes, showed significant improvements of 17.39%, 25%, 89.12%, 88%, and 14.56% for power, BSFC, HC, CO, and NO_x, respectively, compared to the test conditions (D25NG75H00 14° CA BTDC for SOI) at the 20° CA BTDC water vapor injection timing (SOWVI - Start of Water Vapor Injection). Similarly, for Mode 2, the operating point D25NG75H15-20PI-15WVI100°C showed improvements of 33.2%, 18.89%, 78.68%, 82%, and 9.8%, respectively, for the same engine parameters compared to the test conditions (D25NG75H00 10° CA BTDC for SOI) at the 20° CA BTDC water vapor injection timing (SOWVI - Start of Water Vapor Injection).

Within the scope of the thesis, the goal for Mode 1 operating points is to achieve higher performance and lower overall emissions with the same fuel energy input. For Mode 2 operating points, the goal is to achieve higher efficiency, higher performance, and lower overall emissions by including additional hydrogen in the combustion chamber. When examining the obtained numerical results, it is observed that both Mode 1 and Mode 2 have successfully achieved these goals.

SIKIŞTIRMALI ATEŞLEMELİ BİR DİZEL MOTORDA ALTERNATİF YAKIT KULLANIMININ PERFORMANS VE EMİSYON DEĞERLERİ ÜZERİNDEKİ ETKİLERİNİN ARAŞTIRILMASI

ÖZET

Enerji insanoğlunun ihtiyaç duyduğu en temel unsurların başında gelmektedir. Enerjinin üretilmesi çeşitli yollarla sağlanabilmektedir. Ancak hangi yöntemle karşılanırsa karşılansın enerji üretirken çevreyi de kirletiyoruz. Hava kirliliğinin en temel sebebi enerji üretimine bağlı oluşan zararlı gazların havaya salınımıdır. İçten yanmalı motorlar enerji üretiminde en çok kullanılan araçlardır. Hava kirliliğine sebep olan unsurların en başında gelmektedir. Günümüzün en önemli sorunlarından biri olan hava kirliliğinin önlenmesine yönelik bilim insanları tarafından çeşitli çalışmalar yapılmaktadır. Enerji üretimini gerçekleştirirken önemli iki unsur sağlanmalıdır. Bunlar sırasıyla ihtiyaç duyulan enerjiyi daha ekonomik elde etmek ve havaya daha az emisyon salınımına neden olmaktır.

İçten yanmalı motorların enerji ihtiyacı sıvı hidrokarbon yakıtlardan sağlanmaktadır. Bu yakıtların mevcut rezervlerinin kısıtlı olması ve sürekli daraltılan uluslararası emisyon standartlarını karşılamada sahip oldukları bazı problemler söz konusudur. Bu problemleri aşmak için çalışmalar üç ana koldan ilerlemektedir. Üzerinde yoğun bir şekilde çalışılan birinci yol mevcut motorlarda bazı müdahaleler yapılarak zararlı emisyon gazlarının azaltılmasına yöneliktir. Bu yöntemlerin başında After-Treatment Systemler gelmektedir. Bu yöntemler içerisinde farklı metotlar vardır. SCR (Selective Catalytic Reduction) ve Scrubber bu metotlardan bazılarıdır. Bu yöntemler ekonomik olarak uygun değillerdir. Ayrıca sıvı hidrokarbon yakıtlarının rezervlerinin çok az olmasından dolayı uzun ömürlü bir çözüm olarak görülmemektedir. Diğer bir yöntem ise içten yanmalı motorların işletme ve dizayn parametreleri üzerinde parametrik çalışılarak optimum performans ve emisyon değerlerinin araştırılmasına yöneliktir. Parametre çalışmaları ile mevcut motorun performans ve emisyon değerlerinin iyileştirilmeleri son derece önemli olmasına rağmen sıvı hidro karbon yakıt rezervlerinin kısıtlı olması sebebiyle geçici bir önlem olarak görülmektedir. Üzerinde çalışılan diğer bir seçenek şüphesiz alternatif yakıtlar seçeneğidir. Söz konusu bu seçenek motorları ciddi bir yapısal değişikliğe maruz bırakmadan onların çalışmalarına uygun olan yakıtların araştırılmasıdır. Bu yakıtların motor termodinamiğine uygun olması ve çevreci yakıt olmaları gerekmektedir.

Alternatif yakıtlarda aranması gereken özellikler rezervi ve enerji yoğunluğu fazla ve çevreye az emisyon salınımına neden olmalarıdır. Sayılan tüm bu özelliklere sahip olmasından dolayı doğalgaz ve hidrojen yakıtları alternatif yakıtlar arasında büyük bir öneme sahiptir. Doğalgaz ve hidrojen yakıtları hem otto hem de dizel çevrimi ile çalışan motorlara termodinamik olarak uyumlu olması ve motorda yapısal büyük bir değişikliğe sebep olmaması bu yakıtların içten yanmalı motorlarda alternatif yakıt olarak kullanılmalarının önünü açmaktadır. Ayrıca çevreye verdikleri zararlı gazların daha az olması da bir başka özellikleridir. Doğalgaz ve hidrojen yakıtlarının dizel yakıtıyla birlikte sıkıştırmalı ateşlemeli (CI) bir motorda kullanılmasında manifoldda

bulunan düşük basınç enjektörü vasıtasıyla emme havası ile gaz yakıtının ön karışımı sağlanır. Daha sonra sıkıştırma prosesi sırasında dolgunun üzerine pilot dizel yakıtının püskürtülmesiyle ateşlemenin gerçekleştirilmesine dayanmaktadır. Sıkıştırılan dolgunun ısınması sonucu üzerine püskürtülen yakıt buharlaşır ve kendi kendine tutuşur. CI motorlarda bu şekilde oluşan yanma teknolojisine ‘‘Dual-Fuel’’ yanması denilmektedir.

Doğalgazın yüksek enerji yoğunluğu ve çevreci yakıt oluşu, dizel motorunun yüksek termal verimliliği ile birleştirilince hem verimli hem de çevreci çalışma koşulları ortaya konabilmektedir. Yüksek sıkıştırma oranına sahip CI motorlarda belli bir sıkıştırma oranına kadar yüksek oktan sayısına sahip doğalgazın vuruntuya neden olmadan direkt ön karışım olarak kullanılabilmektedir. Hidrojen yakıtı açısından incelendiğinde sıkıştırmalı ateşlemeli motorlarda kullanımının son derece uygun olduğu tıpkı doğalgaz yakıtında olduğu gibi motorda herhangi bir yapısal değişikliğe gerek olmadığı bilinmektedir. Doğalgaz yakıtında C/H oranının düşük olması ve hidrojende hiç olmaması avantajlarının yanı sıra yüksek enerji yoğunlukları da bu gaz yakıtlarına olan ilgiyi arttırmıştır. Bu durum yapılan mevcut tez çalışması için bir motivasyon kaynağı oluşturmuştur. Dünya üzerinde CI motorların hava kirliliği üzerindeki etkisi başta olmak üzere doğalgaz ve hidrojenin ekonomik ve yüksek enerji kapasitesi özelliklerine sahip olmaları bu gaz yakıtlarının alternatif olarak kullanılmalarını güçlendirmektedir. Doğalgazın çevreci ve performans değerleri yüksek bir yakıt olması ile hidrojenin hızlı ve geniş bir tutuşma menziline sahip olması özelliklerinin yanı sıra ayrıca hidrojenin yüksek kütlesel enerji yoğunluğunun mevcut oluşu bu iki gaz yakıtının birlikte CI motorlara uygulanmasına ışık tutmuştur. Bu avantajlar kullanılarak mevcut tez çalışması kapsamında hem performans değerleri iyileştirilmiş hem de giderek kısıtlanan emisyon sınırları değerleri karşılanabilmiştir. Elde edilen sonuçlar literatürde ki çalışmalar ile karşılaştırıldığında benzer eğilimde bilgiler sunmuştur.

Tez çalışması literatür üzerinden elde edilen bir deneysel çalışma referans alınarak ANSYS Forte CFD programında sayısal olarak modellenmiştir. Deneysel çalışma kısmi yükte (25% - 4.05 BMEP) sıkıştırmalı ateşlemeli bir dizel motorda enerjinin 25%’i dizel yakıtından 75%’i doğalgaz yakıtından karşılanacak şekilde farklı dizel yakıt enjeksiyon avanslarının (10°, 14°, 18°, 22°, 26°, 30°, 34°, 38°, 42°, 46° and 50° CA BTDC) sabit motor hızında (910 rpm) performans ve emisyon değerlerine olan etkilerini araştırmıştır. Test sonuçları ile elde edilen sayısal sonuçlar karşılaştırılarak kurulan modelin validasyonu sağlanmıştır. Daha sonra validasyonu sağlanan sayısal model kullanılarak yanmaya hidrojeninde dahil edildiği parametrik çalışmalara geçilmiştir.

Parametrik çalışmalar iki aşamada gerçekleştirilmiştir. İlk aşama olarak doğalgaz ve hidrojenin enerji fraksiyonları ile dizel yakıtının püskürtme avanslarının etkileri irdelenmiştir. Enerji fraksiyonu olarak iki temel kaide üzerinden hareket edilmiştir. Birinci kaide test koşullarındaki toplam yakıt girdi enerjisi sabit kalacak şekilde doğalgaz enerjisinin bir kısmı kademeli olarak hidrojen yakıtına aktarılmıştır. Dizel kaynaklı enerji oranı 25% olarak sabit tutularak kalan 75% oranı doğalgaz ve hidrojen yakıtları arasında paylaştırılmıştır. Bu çalışma noktaları Mode 1 olarak isimlendirilmiştir. Mode 1 gaz yakıtları enerji paylaşım modu olarakta anılabilir. Mode 1 için enerji paylaşım oranları D25NG75H00 (test case), D25NG65H10, D25NG50H25, D25NG25H50 ve D25NG00H75 şeklinde oluşturulmuştur. İkinci kaide ise test koşullarındaki dizel ve doğalgaz enerji oranları (25% diesel and 75% Natural Gas) sabit kalacak şekilde sisteme ekstra enerji girdisi olarak hidrojenin dahil

edilmesi sağlanmıştır. Bu çalışma noktaları ise Mode 2 olarak kodlanmıştır. Mode 2 hidrojence zenginleştirme modu olarakta isimlendirilebilir. Mode 2 için hidrojen zenginleştirme sonucu oluşturulan çalışma noktaları D25NG75H00 (test case), D25NG75H05, D25NG75H10, D25NG75H15, D25NG75H20 ve D25NG75H25 olarak belirlenmiştir. Mode 1 ve Mode 2 için oluşturulan bu çeşitli yakıt enerji fraksiyonları farklı dizel yakıt püskürtme avansları (10°, 14°, 18°, 22°, 26°, 30°, 34° and 38° CA BTDC) ile birlikte kombine edilerek performans ve emisyon değerleri incelenmiştir. İncelenen değerlerden Mode 1 için D25NG50H25 (14° CA BTDC for SOI) ve Mode 2 için D25NG75H15 (10° CA BTDC for SOI) çalışma noktalarının hem motor performansı hem de egzoz gazı emisyonları açısından diğer çalışma noktalarına göre daha makul sonuçlar ürettikleri görülmüştür. Mode 1 için elde edilen optimum durum ile güç, BSFC, HC, CO ve SOOT (PM) açısından sırasıyla 21%, 29%, 88%, 86% ve 77% oranlarında iyileşme sağlanırken Mode 2 için elde edilen optimum durum ile bu değerler sırasıyla 36%, 22%, 76%, 80% ve 83% oranlarında gerçekleşmiştir. Ancak hem Mode 1 hem de Mode 2 test koşulları ile karşılaştırıldığında hidrojenin silindir içi yanma sıcaklıklarını yükseltmesinden dolayı daha yüksek NO_x ve MPRR değerlerinin oluşmasına yol açmıştır. Mode 1 ile NO_x için 12% bir artış söz konusu iken Mode 2 için 11% oranında bir artışın oluştuğu görülmüştür. İlk aşama ile sonuçların performans ve emisyon değerleri açısından kayda değer olarak elde edilmesi sağlanmasına rağmen özellikle NO_x ve MPRR için aynı durum oluşmamıştır. Bu yüzden NO_x ve MPRR başta olmak üzere diğer emisyon türlerinde elde edilen iyileştirmeleri de koruyacak şekilde bazı proseslerin uygulanması için çalışmanın ikinci aşaması gerçekleştirilmiştir.

İkinci aşamada NO_x ve MPRR değerlerininde düşürülmesi için EGR, pilot dizel yakıt enjeksiyonu (PI), yanma odasına su jeti (WI) ve su buharı (WVI) direkt enjeksiyonu prosesleri uygulanmıştır. PI stratejisi ile MPRR değerinin düşürülmesi amaçlanmış diğer proseslerle de NO_x iyileştirilmesi hedeflenmiştir. PI stratejisi diğer prosesler ile birlikte uygulanarak (EGR-PI, WI-PI and WVI-PI) MPRR ve NO_x için eş zamanlı olarak makul sonuçların elde edilmesi sağlanmıştır. PI uygulamasında püskürtme avansı ve süresi sırasıyla 40° CA BTDC ve 2.5° CA olacak şekilde tüm koşullarda sabit tutulmuştur. EGR etkisinin araştırıldığı çalışma noktalarında farklı EGR oranları (0%, 10%, 15% and 20%) ve EGR sıcaklıklarının (100 °C, 200 °C and 300 °C) çeşitli pilot dizel yakıt enjeksiyon oranları (0%, 20%, 30% and 50% - ana püskürtme ile gönderilen yakıtın kütlesel fraksiyonu olarak) ile birlikte etkileri incelenmiştir. EGR analizlerinden Mode 1 için elde edilen D25NG50H25-20PI-10EGR100°C çalışma noktası test koşulları (D25NG75H00 14° CA BTDC for SOI) ile karşılaştırıldığında güç, BSFC, HC, CO ve NO_x için sırasıyla 17%, 28.4%, 87.4%, 84.4% ve 32% oranlarında iyileşmeler göstermiştir. Benzer şekilde Mode 2 için elde edilen D25NG75H15-20PI-10EGR100°C çalışma noktasınında test koşullarına (D25NG75H00 10° CA BTDC for SOI) göre aynı büyüklükler için sırasıyla 31.15%, 21%, 74%, 77.15% ve 30% oranlarında iyileşmeler gösterdiği gözlemlenmiştir.

Su jeti enjeksiyonu için gerçekleştirilen analizlerde farklı su jeti oranlarının (0%, 5%, 10%, 15%, 20% and 25% - ana püskürtme ile gönderilen dizel yakıtının kütlesel fraksiyonu olarak) ve sıcaklıklarının (25 °C, 60 °C, 75 °C and 90 °C) etkisi ile çeşitli su jeti enjeksiyon avanslarının (20° CA BTDC, 10° CA BTDC, 0° CA BTDC - TDC and 10° CA ATDC) etkileri araştırılmıştır. WI için PI değeri EGR çalışmalarından elde edilen ve kayda değer sonuçlar üreten 20% oranı olarak tercih edilmiştir. Mode 1 için WI-PI stratejileri açısından elde edilen D25NG50H25-20PI-25WI75°C çalışma noktası su jeti enjeksiyonu avansının 20° CA BTDC değerinde test koşulları

(D25NG75H00 14° CA BTDC for SOI) ile karşılaştırıldığında güç, BSFC, HC, CO ve NO_x açısından sırasıyla 14.26%, 20.7%, 88.33%, 85.7% ve 23.42% oranlarında düzelmeler göstermiştir. Benzer şekilde Mode 2 için D25NG75H15-20PI-25WI75°C operasyon noktası 20° CA BTDC su jeti enjeksiyon avansında (SOWI – Start of Water Injection) test koşullarına göre (D25NG75H00 10° CA BTDC for SOI) aynı büyüklükler için sırasıyla 30.33%, 15%, 77.29%, 79.5% ve 17% değerlerinde iyileşmeler sağlamıştır.

Yanma odasına suyun buhar fazında enjeksiyonu (WVI) için yapılan çalışmada da su jeti analizlerinde ki gibi farklı su buharı oranlarının (0%, 5%, 10%, 15%, 20% and 25% - ana püskürtme ile gönderilen dizel yakıtının kütlesel fraksiyonu olarak) ve sıcaklıklarının (100 °C, 125 °C, 150 °C and 200 °C) etkisi çeşitli su buharı enjeksiyon avanslarında (20° CA BTDC, 10° CA BTDC, 0° CA BTDC - TDC and 10° CA ATDC) gerçekleştirilmiştir. Tıpkı WI için olduğu gibi WVI içinde PI 20% oranında seçilmiştir. Mode 1 için WVI-PI prosesleri ile elde edilen D25NG50H25-20PI-15WVI100°C operasyon noktası su buharı avansının 20° CA BTDC değerinde test koşulları (D25NG75H00 14° CA BTDC for SOI) ile karşılaştırıldığında güç, BSFC, HC, CO ve NO_x bakımından sırasıyla 17.39%, 25%, 89.12%, 88% ve 14.56% oranlarında kayda değer iyileşme sağlamıştır. Mode 2 için D25NG75H15-20PI-15WVI100°C çalışma noktası yine 20° CA BTDC su buharı enjeksiyon avansında (SOWVI – Start of Water Vapour Injection) test koşullarına göre (D25NG75H00 10° CA BTDC for SOI) aynı motor terimleri için sırasıyla 33.2%, 18.89%, 78.68%, 82% ve 9.8% oranlarında gelişme göstermiştir.

Tez çalışması kapsamında Mode 1 çalışma noktaları ile elde edilmek istenen aynı yakıt enerji girdisi ile daha yüksek performans ve daha düşük tüm emisyonlar hedefidir. Mode 2 operasyon noktaları için hedef ise yanma odasına ekstra hidrojen dahil edilerek daha yüksek verimde daha yüksek performans ve daha düşük tüm emisyonların elde edilmesidir. Elde edilen sayısal sonuçlar incelendiğinde hem Mode 1 hem de Mode 2 için belirlenen bu hedeflerin başarılı bir şekilde gerçekleştiği görülmüştür.

1. INTRODUCTION

Scientists are conducting various studies to address one of today's most critical issues, air pollution. Due to the cost implications of applying certain systems (After-Treatment System) to meet increasingly stringent emission standards in existing internal combustion engines, alternative solutions have always been considered. In addition to their economic disadvantages, the limited lifespan granted to current liquid hydrocarbon fuels (gasoline and diesel) has led to the temporary use of these systems. Given the constrained reserves of these liquid hydrocarbon fuels, a series of studies is being conducted globally to ensure the continued operation of internal combustion engines. At the forefront of these efforts is the use of alternative fuels in internal combustion engines without undergoing significant structural changes. These fuels must be both abundant in supply and have a more environmentally friendly characteristic. Due to their compliance with these desired features, natural gas and hydrogen are of great importance.

The susceptibility of natural gas and hydrogen fuels to both Otto and diesel cycles paves the way for their future use. Compared to hydrogen, the use of natural gas in internal combustion engines dates back much earlier. In the literature, there are numerous studies on the use of natural gas in diesel engines. The utilization of natural gas and diesel fuel in a compression ignition engine is as follows: A premixture of natural gas is provided with intake air, and subsequently, pilot diesel fuel is injected onto it. The combustion relies on reaching the autoignition temperature of the injected diesel fuel, leading to the initiation of combustion. Engines operating with this system are referred to as "Dual-Fuel" engines. In gasoline engines operating on the Otto cycle, natural gas is commonly preferred as a standalone fuel. Air and natural gas are homogeneously mixed to create a charge, which is then sent to the combustion chamber. The combustion process is initiated by igniting the mixture using a spark plug. These types of engines are often referred to as "Gas Engines" in the literature.

There are numerous studies in the literature regarding the use of hydrogen as an alternative fuel in both diesel and gasoline (Otto cycle) engines. In diesel engines, a

pre-mixture of air and hydrogen is generally created, and this mixture is sent to the combustion chamber. Diesel fuel is then injected into the chamber when the piston is near the Top Dead Center (TDC), initiating combustion. Hydrogen usage is more commonly observed in Otto cycle engines. A homogenous mixture of hydrogen and air is introduced into the cylinder. The compressed mixture, as the piston moves towards the Top Dead Center, is ignited by a spark plug, leading to combustion. There are also studies exploring the co-utilization of hydrogen with natural gas as a combined fuel in Otto engines.

The mixture of hydrogen and natural gas is referred to as hydrogen-enriched natural gas or, briefly, Hythane fuel. Although not very common in diesel engines, there are studies on the use of Hythane fuel. There are several reasons for the preference for the co-utilization of hydrogen and natural gas. Hydrogen combustion results in water vapor as the only environmentally harmless byproduct. Furthermore, considering the efficient cycle of separating water vapor back into hydrogen and oxygen, an environmentally friendly cycle can be achieved. Additionally, natural gas is known for its slow combustion, while hydrogen is a fast-burning fuel. Combining the two can overcome the individual disadvantages when used as a standalone fuel, providing a significant advantage. When considering emissions, literature indicates positive improvements. In the combustion process with hydrogen fuel, it has been observed that regional temperatures inside the cylinder are high. However, when used in conjunction with natural gas, regional temperatures decrease. The reduction in regional temperatures is associated with a decrease in NO_x emissions, and the proportion of harmful gases resulting from dissociation decreases. Hydrogen, as a fuel, is not a hydrocarbon fuel. Therefore, combustion end products do not include unburned hydrocarbons (HC) or carbon monoxide gas (CO). Additionally, compared to liquid hydrocarbon fuels, methane (CH_4), considered as natural gas fuel, has a lower proportion of carbon atoms. Taking all these factors into account, there is no doubt that hydrogen and natural gas fuels will play a crucial role as alternative fuels in the future.

1.1 Purpose of Thesis

Fuels used in internal combustion engines are desired to vaporize easily and mix homogeneously with the air taken into the cylinder. Furthermore, it is desirable for the

mixture to provide a high amount of energy per unit volume and to ignite easily. Liquid hydrocarbon fuels, particularly gasoline and diesel fuels, have been the types of fuel that could meet all these requirements until our recent past. One of the most significant characteristics of these fuels is their ease of acquisition and the presence of a well-established global trade network. However, these fuels, which have been the unrivaled energy source for internal combustion engines until recently, will be depleted in a relatively short period due to their limited reserves. Additionally, considering their adverse environmental effects, finding alternatives has become extremely important. Scientists have conducted numerous studies on this issue for approximately the last 40 years.

Despite the existence of many alternative fuel types, obtaining a renewable high-energy fuel is not an easy task. Scientists have conducted numerous experimental and numerical studies on alternative fuels, including natural gas, alcohols, biogas, biodiesel, and liquefied petroleum gas (LPG). The most important feature of these studies has been the reduction of air pollution and the achievement of energy efficiency. Certain negative changes occurring in the ecosystem and natural balance have necessitated the implementation of some national and international measures. These measures aim to reduce the environmental impact of emissions from internal combustion engines. Over the years, these rules, gradually tightening, aim to at least minimize the damage to the disrupted natural balance.

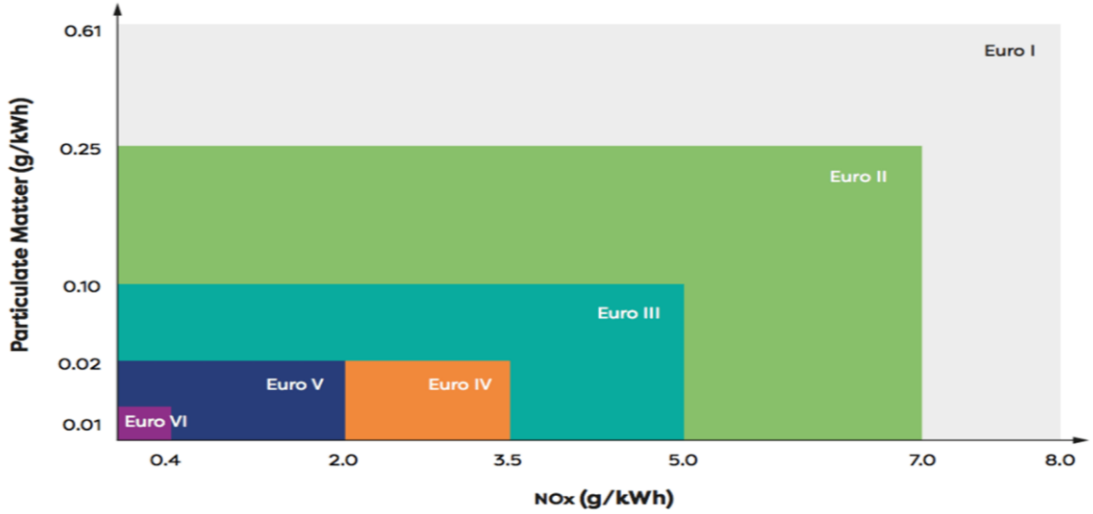

Figure 1.1 : Euro emission standards for NO_x and PM emissions [1].

One of these standards is the "European Emission Standards," which has gradually set certain limit values for NO_x and PM emissions on a yearly basis. The applicable years

for limitations are set as follows: Euro I for 1992–1998, Euro II for 1998–2000, Euro III for 2000–2005, Euro IV for 2005–2008, Euro V for 2008–2014, and Euro VI for 2014 and beyond. The NO_x and PM emission limit values specified in the European emission standards are provided in Figure 1.1. For emissions from ships, limits set by the International Maritime Organization (IMO) have been gradually implemented over the years. IMO has categorized these limitations for NO_x as Tier I, Tier II, and Tier III. Tier I applies to ships built between 2000 and 2011, Tier II applies to ships built between 2011 and 2016, and Tier III applies to ships built after 2016.

Tier	Ship construction date on or after	Total weighted cycle emission limit (g/kWh) n = engine's rated speed (rpm)		
		n < 130	n = 130 - 1999	n ≥ 2000
I	1 January 2000	17.0	$45 \cdot n^{(-0.2)}$ e.g., 720 rpm – 12.1	9.8
II	1 January 2011	14.4	$44 \cdot n^{(-0.23)}$ e.g., 720 rpm – 9.7	7.7
III	1 January 2016	3.4	$9 \cdot n^{(-0.2)}$ e.g., 720 rpm – 2.4	2.0

Figure 1.2 : Calculation of IMO emission standard based on RPM for NO_x emisssions [2].

The NOx upper limit values determined by IMO, considering the years and engine speeds, are illustrated in Figure 1.2. Figure 1.3 displays the graphical representation of these values.

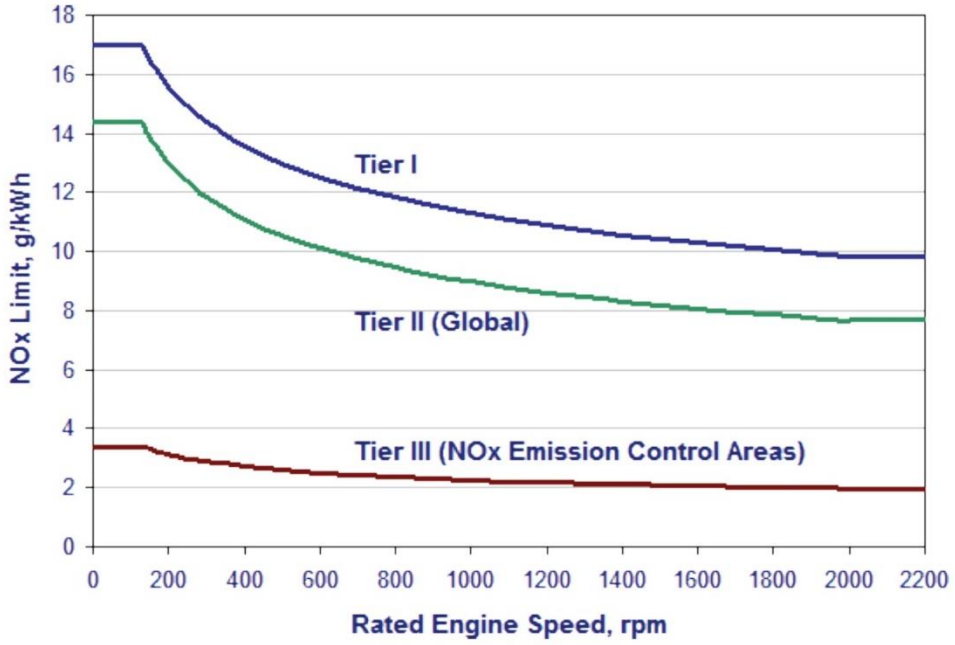

Figure 1.3 : IMO emission standards for NO_x [3].

IMO has also mandated the limitation of sulfur content in fuel. Sulfur is an unwanted substance found in liquid hydrocarbons obtained from underground reserves. Complete removal of sulfur from fuel content is not entirely feasible. Therefore, the presence of sulfur in fuel content leads to the formation of gases and derivatives called SO_x after combustion. IMO aims to reduce SO_x emissions from ships. Over the years, the volumetric limits of sulfur (S) content in fuel are shown in Figure 1.4.

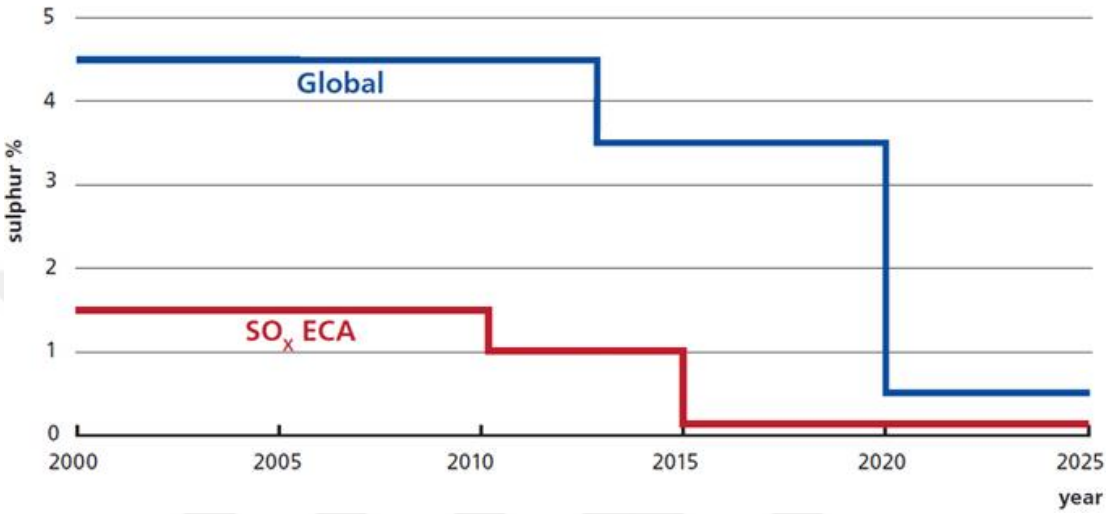

Figure 1.4 : IMO emission standards for SO_x [4].

It is known that conventional diesel and gasoline engines face some challenges in meeting these limits. Scientists have aimed to overcome these challenges through two main approaches. One of these approaches relies on making certain chemical and physical interventions in the exhaust gas. In the literature, this method is referred to as "After-Treatment Systems".

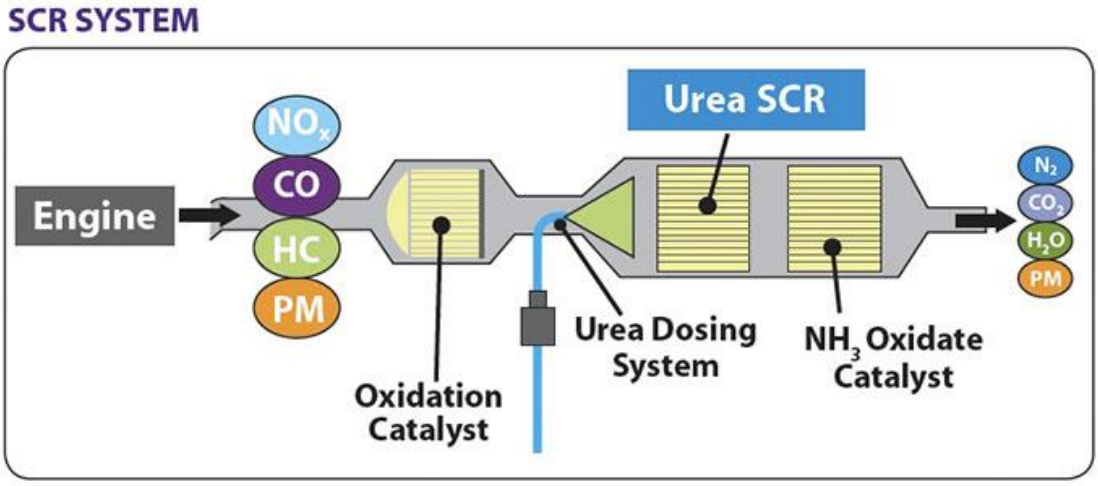

Figure 1.5 : SCR system scheme [5].

Within this method, there are various techniques, with SCR (Selective Catalytic Reduction) and scrubber being among the most prominent ones. The working principle of the Selective Catalytic Reduction (SCR) system is adapted to the gradual passage of exhaust gases through certain processes and sections to mitigate their harmful effects. The exhaust gases, containing NO_x, CO, UHC, and PM emissions, initially enter the catalytic converter. Inside the catalytic converter, CO and UHC gases are transformed into CO_2 and H_2O gases. No processing is done in this section for NO_x and PM. Subsequently, in the SCR section, AdBlue (a urea-ammonia solution) is sprayed onto the NO_x, converting it into N_2 and H_2O gases. The gases, mainly N_2, H_2O, and CO_2, along with PM components, finally enter the particulate filter, reducing PM emissions. This process results in approximately a 90% reduction in NO_x. The basic working diagram of the SCR system is presented in Figure 1.5.

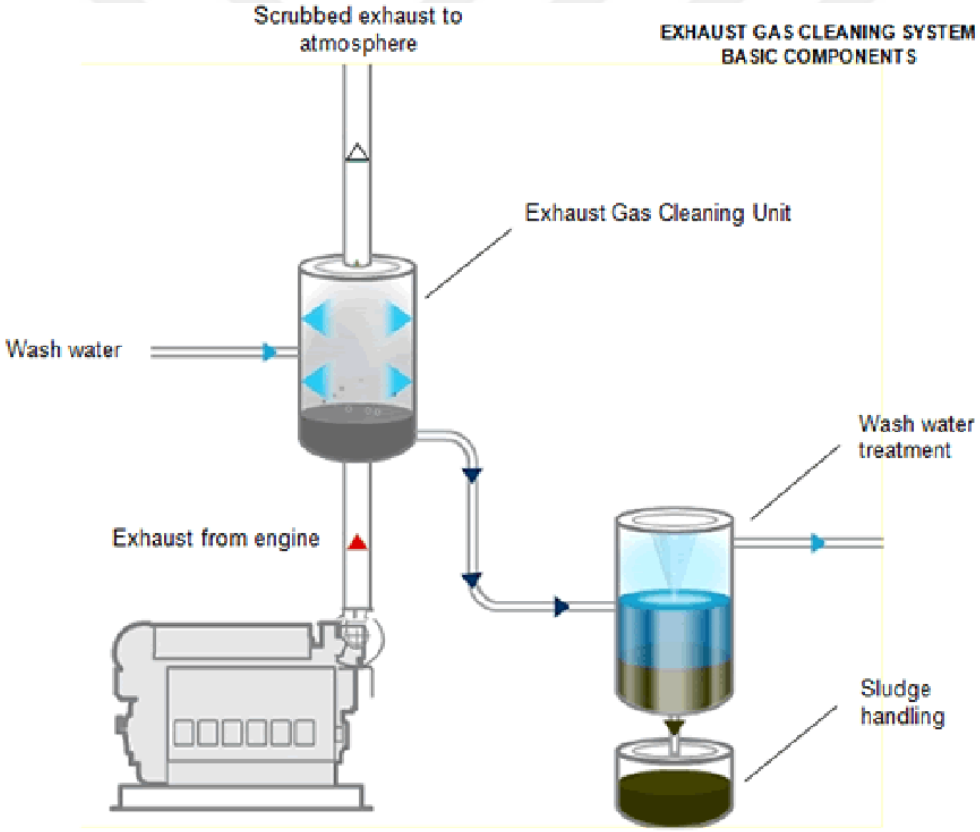

Figure 1.6 : Scrubber system basic operating scheme [6].

The Scrubber system is based on the principle of washing exhaust gases with water to reduce SO_x emissions. It involves the collision of SO_x gases from the engine exhaust with water. The harmful byproducts resulting from the wash (H_2SO_4 or SO_x gases) are transferred to another tank, where, through some chemical processes, they are transformed into harmless waste.

The basic operational diagram of the Scrubber system is shown in Figure 1.6. Although SCR and Scrubber systems are effective methods, they are expensive and not economically viable for their applicability. Moreover, these methods are temporary solutions to meet emission standards for liquid hydrocarbon fuels.

Therefore, another more effective method to be considered is the discovery of alternative and renewable fuels. Natural gas stands out as a primary alternative fuel due to its abundant reserves and high energy potential per unit volume. The preference for hydrogen has increased, as its environmental impact is significantly lower when compared to liquid hydrocarbon fuels. Recently, hydrogen has become one of the most popular fuels as a renewable energy source. One of the most significant advantages of using hydrogen fuels is their minimal impact on air pollution. Unlike hydrocarbon fuels, the combustion of hydrogen with air does not produce gases like CO, CO_2, SO_x, and unburned hydrocarbons. Consequently, phenomena such as acid rain, photochemical smog, and the greenhouse effect, which are associated with combustion by-products, are not relevant when hydrogen is used as fuel. One of the most important features of hydrogen is its ability to exist in both liquid and gas states. Hydrogen gas is approximately 14 times lighter than air of the same volume. When compared to fuels used in ICEs, liquid hydrogen is about 10 times lighter than liquid hydrocarbon fuels, and gaseous hydrogen is 10 times lighter than gases like methane and natural gas. Another crucial advantage of using hydrogen as a fuel in engines is its wide flammability limits, spanning across a broad range of fuel-air mixtures. Hydrogen can ignite in air within the range of 4% to 75%. While gasoline-air mixtures can ignite within an air excess ratio range of 0.3 to 1.7, hydrogen-air mixtures have a broader range of 0.14 to 4.35 for ignition. Hydrogen-air mixtures also have wider ignition limits compared to gas fuels. For example, for methane-air mixtures to ignite, the air excess ratio must be between 0.6 and 1.9. The lower heating value of hydrogen is higher than other conventional motor fuels (119.93 kJ/g for hydrogen, 43.4 kJ/g for gasoline). However, when considered volumetrically, the lower heating value of hydrogen is lower than other fuels (8.41 MJ/liter for hydrogen, 31.8 MJ/liter for gasoline, 15.9 MJ/liter for methanol, 20.8 MJ/liter for methane). Hydrogen's adiabatic flame temperature is comparable to gasoline. (Hydrogen 2318 K, Gasoline 2470 K, Methane 2148 K). The level of NO_x components resulting from hydrogen combustion is higher compared to other fuels due to the increase in temperature levels. The

production and storage costs of hydrogen are still high today, which is one of the reasons why hydrogen is not widely used. However, as the widespread use of hydrogen and the increase in production capacity occur, the cost will naturally decrease. Some characteristics of diesel, hydrogen, and natural gas fuels are shown in Table 1.1.

Table 1.1 : Fuel properties for diesel, hydrogen and natural gas.

Properties	Diesel	Hydrogen	Natural Gas
Main compenent	C and H	H	Methane (CH_4)
Auto-ignition temperature (K)	553	858	923
LHV (MJ/kg)	42.5	120	50
Density (kg/m^3)	833 – 881	0.08	0.692
Molecular weight (g/mol)	170	2.016	16.043
Flammability limits in air (vol %)	0.7 – 5	4 – 75	5 – 15
Flame velocity (m/s)	0.3	2.65 – 3.25	0.45
Specific gravity	0.83	0.091	0.55
Boiling point (K)	453 – 653	20.2	111.5
Cetane number	40 – 60	-	-
Octane number	30	130	120
CO_2 emissions (%)	13.4	0	9.5
Mass diffusivity in air (cm^2/s)	-	0.61	0.16
Minimum ignition energy (MJ)	-	0.02	0.28

Natural gas can be used in both diesel and gasoline engines without any structural conversion to the engines. In diesel engines with a high compression ratio, natural gas can be directly used as a premix since it does not cause knock up to a certain compression ratio with a high octane number. However, in some applications where the tendency for knock is reduced by lowering the compression ratios, the top dead center has been brought closer to the bottom dead center, and the compression ratio has been reduced. In gasoline engines, the low compression ratio has been increased to improve thermal efficiency. This action has become an advantage because the octane number of natural gas fuel is higher than that of gasoline.

When the hydrogen is in turn as a fuel, it is well-known that its use in both compression-ignition and spark-ignition engines is highly suitable, just like natural gas fuel, without the need for any structural changes to the engine. In diesel engine applications, a low-pressure injector in the manifold injects hydrogen and/or natural gas in gas form onto the air, creating a premixture with the air, and the cylinder is filled with an air-natural gas/hydrogen mixture. The compressed mixture is ignited by injecting pilot diesel fuel near the TDC. In SI engines, instead of gasoline, a mixture of natural gas and/or hydrogen with air is created, and ignition is achieved by spark

near the top dead center. The use of natural gas and hydrogen fuels in conventional gasoline and diesel engines is becoming increasingly common due to their fuel properties, such as low carbon-to-hydrogen ratio in natural gas and the absence of carbon in hydrogen, as well as their high energy density and abundant reserves in nature.

This dissertation has sparked a detailed interest in the combustion of diesel/natural gas/hydrogen. The impact of internal combustion engines on air pollution worldwide, along with economic reasons and high energy capacity, encourages the use of these gas fuels as alternatives. The environmentally friendly and high-performance values of natural gas, along with hydrogen's rapid and broad ignition range, as well as its high mass energy density, shed light on the application of these two gas fuels in internal combustion engines. Along with these advantages, improvements in emission values have been observed, especially considering the increasingly restricted emission limits. Literature studies also provide information in line with this trend. The increase in NO_x emissions due to the high temperatures in hydrogen combustion can be mitigated by using hydrogen in conjunction with natural gas fuel. For all these reasons, within the scope of this thesis, the effects of both natural gas and hydrogen fuels on the performance and emission values of a compression ignition diesel engine have been examined. The main goal in in-cylinder combustion studies is to achieve high performance and low overall emissions. It is possible to achieve this goal by utilizing the physical, chemical, and thermodynamic properties of hydrogen.

In pursuit of the goal of high energy and low environmental pollution, scientists have conducted numerous studies, and they continue to do so. The main objective of the current dissertation has also been to achieve this principle. When looking at studies in the literature, various liquid and gas fuels have been investigated as alternative fuels. The application of these alternatives to compression ignition engines has contributed various pieces of information to the literature. Natural gas and hydrogen, due to their properties, have become among the most researched fuels in recent times. In general, a review of the literature reveals the examination of the effects of these gas fuels when used individually in internal combustion engines. Although limited in number, there are also studies focusing on the simultaneous use of both gas fuels. This thesis investigates comprehensively the effects of using natural gas, hydrogen, and hydrogen-enriched natural gas as alternative fuels in a compression ignition engine,

comparing their performance and emission characteristics. The study is based on the previous experimental study in the literature. The experimental work involved a dual-fuel diesel-natural gas engine, operating at a constant engine speed (910 RPM) and a constant indicated mean effective pressure (4.05 BMEP) under 25% load (partial load). Different diesel fuel injection timings (10°, 14°, 18°, 22°, 26°, 30°, 34°, 38°, 42°, 46°, and 50° CA BTDC) were examined to understand their impact on the engine performance at partial load conditions [7–9].

This experimental study intends to be a pioneer work for creating a numerical model using the ANSYS Forte CFD program. The numerical model was validated by comparing the numerical results with the experimental findings. The numerical investigations were evaluated in two stages. The first stage involves the effects of alternative fuels and diesel fuel injection timings on the performance characteristics and exhaust emission levels. The second stage consists of different processes and strategies affecting engine performance and emissions. The second stage contains the application of EGR (Exhaust Gas Recirculation) and water jet/vapor injection processes in conjunction with a pilot diesel injection strategy.

The first stage of the numerical study covers some essential parametric variations based on two different modes, including also hydrogen. These modes were identified as Mode 1 and Mode 2. In Mode 1, the shared energy fractions of gas fuel mixtures (natural gas/hydrogen) were gradually changed. The total fuel energy was distributed between hydrogen and natural gas at different energy fractions while keeping the test conditions the same. The effects of these energy-shared operating points on engine performance and emission values were investigated at different diesel fuel injection timings (10°, 14°, 18°, 22°, 26°, 30°, 34°, and 38° CA BTDC). For Mode 2, the amounts of diesel and natural gas fuel were kept constant (25% diesel and 75% natural gas), and extra energy in the form of hydrogen was introduced into the combustion chamber. The effects of different diesel fuel injection timings (10°, 14°, 18°, 22°, 26°, 30°, 34°, and 38° CA BTDC) were taken into account. The description "energy sharing mode" can be attributed to Mode 1, and "hydrogen enrichment mode" can be attributed to Mode 2. In the second stage, the effects of Exhaust Gas Recirculation (EGR), water injection/vapor (WI – Water Injection and WVI – Water Vapor Injection), and pilot diesel fuel injection (PI – Pilot Injection) were investigated. Despite achieving high-performance and low-emission results in the first stage, some engine outputs did not

reach desirable values. These outputs include the crank angle-resolved pressure rise rate (MPRR) and NO_x emission values. The goal was to achieve higher performance and lower overall emissions by improving both parameters. Thus, information about which gas mixture fractions and which diesel fuel injection timings result in more optimal operating points in terms of performance and emissions has been added to the literature. The knowledge of how the results would change and improve with the implemented processes was obtained. The processes were further expanded by delving into more specific details. In studies where the EGR with pilot diesel fuel injection process was examined, different EGR ratios and temperatures, as well as different pilot diesel fuel injection rates and timings, were considered. In the analyses examining seperately water injection and steam injection with pilot diesel fuel injection strategies, different water/steam ratios, temperatures, and injection timings were investigated, and numerical results were evaluated. The aim was to improve the negative outcomes observed in cases involving hydrogen in the numerical studies conducted in the first and second stages and to open the way for increased presence of hydrogen in the gas mixture. Recently, there has been a considerable number of computational fluid dynamics-based software packages that are highly economical and reliable. Through numerical studies, diversifying various parameters and conditions allows for the emergence of more information and knowledge, enabling the acquisition of reliable results in a shorter time frame. In this thesis, the ANSYS Forte CFD program was utilized to establish a numerical model and conduct parametric studies.

1.2 Literature Survey

In order to improve engine performance and emission values, scientists have conducted numerous numerical and experimental studies on alternative fuels. In the literature, various liquid and gaseous fuels have been used as alternative fuels in diesel engines, including natural gas, hydrogen, and hydrogen-enriched natural gas fuel. While these studies have led to increased efficiency of diesel fuel in compression ignition (CI) engines, complete replacement of diesel fuel has not been a common practice. In cases where this substitution has occurred, it is observed that there is often a limited operational range. Generally, these studies have used alternative fuels to create a homogenous mixture with air, which serves as the main power source, while diesel fuel is used to ignite the mixture. In some cases, gaseous and liquid alternative

fuels have been directly injected into the combustion chamber. Studies on the effects of hydrogen in CI engines have provided valuable insights into the literature. Below are findings from various experimental and numerical studies on hydrogen-diesel combustion.

While hydrogen is directly injected into the combustion chamber in CI (compression ignition) engines, diesel fuel injection can be carried out in two stages, involving pilot injection and main injection, to control the combustion process more effectively.

The study demonstrates the feasibility of achieving operational points with hydrogen energy fractions of up to 90% in a single-cylinder compression-ignition light-duty engine utilizing hydrogen-diesel dual-fuel mode [10]. Hydrogen injection is facilitated through a dedicated gas injector positioned at the cylinder center. Operating across a range of 20%-90% hydrogen energy fraction, tests were conducted at an engine speed of 2000 rpm. Variations in the injection advance of hydrogen, spanning from 0° CA (TDC) to 180° CA BTDC, were explored. Notably, at a 90% hydrogen energy fraction, the IMEP (Indicated Mean Effective Pressure) reached 9.43 bar, accompanied by a 57.2% improvement in Brake Specific Fuel Consumption (BSFC) compared to pure diesel conditions. However, the study highlights a significant increase in NO_x emissions with high hydrogen content. The timing of hydrogen injection is identified as a critical factor influencing combustion characteristics and control. Different injection advances demonstrated distinct combustion behaviors high injection advance showcased premix combustion characteristics, while later advances (40° CA BTDC and beyond) exhibited effects akin to mixture-controlled combustion. For the case of a 90% hydrogen energy fraction with a high injection advance, while maximum efficiency and IMEP were achieved, undesirable increases in NO_x were observed due to elevated combustion temperatures. The study underscores the importance of carefully selecting the hydrogen injection advance to balance performance and emissions. It is recommended that a hydrogen injection advance of 40° CA BTDC can prevent NO_x escalation and yield performance values comparable to diesel combustion conditions. Additionally, direct injection of hydrogen into the combustion chamber at this advance could lead to an 85.9% reduction in CO_2 emissions and a 13.3% increase in IMEP.

The performance and emission effects of hydrogen direct injection into the combustion chamber of a diesel engine have been numerically investigated [11]. Numerical results

were obtained for different hydrogen injection rates and injection timings. The study was conducted under 25% load conditions in a single-cylinder, four-stroke diesel engine. According to the numerical results, the injection of H15 (15% hydrogen fraction) at 20° CA BTDC resulted in the maximum pressure, temperature, and Heat Release Rate (HRR). It was stated that increasing hydrogen fraction and advance led to higher power, thermal efficiency, and IMEP values. The increase in hydrogen fraction led to higher combustion temperatures, causing an increase in NO_x emissions. It was also noted that earlier hydrogen injection into the combustion chamber had negative effects on NO_x. The study emphasized that selecting the appropriate hydrogen fraction and advance could result in both higher performance and lower emissions.

The experimental investigation explored the impact of hydrogen on the performance and emission characteristics of a compression-ignition diesel engine [12]. Hydrogen was introduced into the combustion chamber by mixing it with air in the intake manifold, with the energy of diesel fuel being gradually replaced by hydrogen in various fractions (ranging from 0% to 30%). At full load with a 30% hydrogen energy fraction, there were significant increases of 13%, 46%, and 35% in the maximum combustion pressure, heat release rate, and maximum pressure increase rate, respectively. The results indicated that there should be a limit on hydrogen addition due to its effect on shortening the burning time, influenced by the accelerated combustion rate. At 14% and 25% hydrogen energy fractions (DH14 and DH25), the BSFC value improved by approximately 17%. However, at 30% hydrogen (DH30), substantial deteriorations in engine stability were observed. For DH25, there was a notable reduction of 85%, 57%, and 27% in particulate matter (PM), carbon monoxide (CO), and carbon dioxide (CO_2) emissions, respectively. High hydrogen addition (DH30) to the combustion chamber resulted in an increase in hydrocarbon (HC) and nitrogen oxides (NO_x) emissions by 80%. These results highlight the delicate balance required in adjusting hydrogen ratios to optimize combustion efficiency, reduce emissions, and maintain engine stability. While moderate hydrogen addition showed positive effects, exceeding certain levels (such as DH30) led to challenges in terms of engine stability and increased emissions.

In a four-cylinder diesel engine equipped with a common-rail injection system, the introduction of hydrogen fuel into the combustion chamber at different volumetric rates (0 L/min, 20 L/min, and 40 L/min) was facilitated, and the experimental values

for engine performance and emissions were obtained [13]. The engine was operated at a constant speed (1750 rpm) under different loads (50 Nm, 75 Nm, and 100 Nm). While diesel fuel was injected into the cylinder at high pressure, hydrogen fuel was mixed with intake air through a low-pressure injector in the intake port and sent to the combustion chamber. It was shown that at 50 Nm load, hydrogen with a volumetric rate of 20 L/min constituted 12.63% of all energy, at 75 Nm load it was 8.93%, and at 100 Nm load it was 7.12%. It was reported that as the load increased, there was a decrease in the corresponding ratios of energy for hydrogen fuel with the same volumetric rate. According to the results, it was stated that the cylinder pressure increased when the volumetric ratio of hydrogen was increased under all load conditions. Additionally, it was mentioned that the crank angle value where the peak pressure occurred approached TDC (Top Dead Center). Compared to diesel engine conditions at 50 Nm and 75 Nm loads, HC and CO_2 emissions decreased, NO_x emissions decreased for H_2O conditions (20 L/min hydrogen), while increased for H40 conditions (40 L/min hydrogen). In terms of thermal efficiency, the addition of hydrogen improved thermal efficiency except for the volumetric hydrogen ratio of H40 under 100 Nm load. Exhaust gas temperatures increased as the amount of hydrogen increased under all loads. Under 100 Nm load, NO_x emissions remained at lower values compared to diesel engine conditions. In this study, it was emphasized that hydrogen-enriched intake filling in a diesel engine should be preferred as hydrogen increased thermal efficiency and reduced carbon emissions.

The research conducted involved experimental exploration into the impact of diesel-hydrogen dual fuel combustion on both the emissions and performance of a turbocharged four-cylinder direct injection diesel engine [14]. The study also delved into the influence of various ratios between hydrogen and diesel fuels on knock tendency and ignition capability. The experiments were conducted at a consistent engine speed of 2400 rpm but at different loads (30%, 60%, and 100%). Each load condition had a distinct maximum hydrogen ratio: 80% for 30% load, 60% for 60% load, and 40% for 100% load. Comparative analysis revealed a reduction of about 54.2% in diesel-specific fuel consumption when 80% hydrogen was substituted at 30% load, as opposed to pure diesel combustion at 100% load. While augmenting hydrogen at all engine loads enhanced specific fuel consumption and lowered CO_2 emissions, the NO_x emissions varied depending on the engine load conditions.

The impact of hydrogen addition on the combustion process, particularly NO_x emissions, in a compression ignition diesel engine was investigated through numerical simulation [15]. The numerical model was developed using the AVL Fire CFD program, focusing on a heavy-duty diesel engine with Exhaust Gas Recirculation (EGR) applied. The validation of the model included cases where hydrogen was added up to 6% by volume to the combustion chamber, and these results were compared with experimental data. Subsequently, the validated numerical model was extended to explore the effects of different hydrogen ratios (ranging from 6% to 18%) on combustion and NO_x formation. The numerical model was validated by comparing results, particularly for cases where hydrogen was added up to 6% by volume, with experimental data. At 1200 rpm and 70% load, hydrogen addition resulted in increased ignition delay and positive effects on premix fuel development and diesel diffusion combustion. It was found that 12% volumetric hydrogen addition led to the maximum cylinder pressure, while the addition of 16% volumetric hydrogen resulted in the maximum heat release rate. Hydrogen addition was identified as having a dominant effect on NO_x emissions. Although hydrogen had a positive impact on Particulate Matter (PM) emissions, it unfortunately had an adverse effect on NO_x emissions. It was emphasized that appropriate combinations of EGR and hydrogen could yield preferable results in terms of both engine performance and the balance between PM and NO_x emissions. In summary, the numerical study highlighted the complex interplay between hydrogen addition, combustion characteristics, and emissions in a compression ignition diesel engine. While hydrogen showed promise for PM emissions, the challenge lies in finding the right combinations with EGR to achieve a balanced and favorable outcome for both PM and NO_x emissions alongside overall engine performance.

In a numerical investigation, the impact of hydrogen addition on the performance and emission characteristics of a diesel engine was examined [16]. The simulations involved a comparison between pure diesel combustion and scenarios with varying levels of hydrogen inclusion, exploring constant compression ratios (set at 17.5:1), different diesel-hydrogen ratios (0%, 5%, 10%, 20%, 30%, and 40% by volume), diverse engine speeds (ranging from 1000 to 4000 rpm), and a spectrum of air-fuel ratios (from 10 to 80 air/fuel). The results indicated that the introduction of hydrogen into the combustion chamber led to enhanced engine performance and reduced

emissions. Notably, even at low volumetric levels of hydrogen supplementation, there was a smoother start of combustion attributed to the shortened ignition delay compared to pure diesel combustion. This resulted in a reduction in the rate of pressure increase per crank angle, indicating a more controlled combustion process. These findings underscore the potential benefits of hydrogen addition in terms of optimizing combustion characteristics and improving overall engine performance while mitigating emissions.

The primary objective of directly injecting hydrogen into the combustion chamber of a diesel engine is to enhance both knock resistance and ignition limits in comparison to combustion through port injection. This involves placing a high-pressure gas injector adjacent to the diesel injector within the combustion chamber. Operating the engine at a medium load ensures a consistent energy input to the combustion chamber [17]. To maintain stability in the combustion phase, there is a deliberate reduction in the diesel fuel fraction despite an increase in the hydrogen ratio. Analyzing heat release rates and emission values, it was observed that conditions with high advance hydrogen injection were indistinguishable from port injection conditions. However, it has been emphasized that the critical factor in low-advance hydrogen injection lies in the fraction of hydrogen introduced into the combustion chamber. By employing a 50% hydrogen fraction and optimizing the injection advance to 40° CA BTDC, notable improvements were achieved, including a 6 dB reduction in noise emissions and an 11% enhancement in NO_x emissions. The reported thermal efficiency at these optimized conditions was 47%.

The experimental investigation aimed to explore the effects of introducing hydrogen at different volumetric ratios (10 l/min, 20 l/min, and 30 l/min) into the combustion chamber of an Audi/VW 1.9 TDI turbocharged Compression Ignition (CI) engine [18]. The study considered various engine speeds (1900 rpm and 2500 rpm) and loads (4 bar, 6 bar, and 8 bar BMEP), comparing the results with those obtained from pure diesel combustion. At all loads, the low hydrogen fraction (maximum 15.74%) exhibited noticeable impacts on both engine performance and emissions. Under low and partial load conditions, a modest rate of hydrogen supplementation (10 l/min and 20 l/min) at both engine speeds led to a reduction in ignition delay, resulting in decreased cylinder pressure, pressure increase rate, and thermal efficiency. This was accompanied by an increase in Brake Specific Fuel Consumption (BSFC) compared

to pure diesel combustion. However, with an increased hydrogen ratio (30 l/min), a decrease in BSFC and an increase in thermal efficiency were observed compared to the pure diesel results. The results were further validated numerically using AVL Boost, reinforcing the experimental findings. This suggests that the addition of hydrogen, particularly at higher ratios, can positively influence engine performance and emissions under certain operating conditions.

In an experimental investigation, the impact of hydrogen on the performance, emissions, and combustion characteristics of a compression ignition engine was systematically examined [19]. The tests were conducted at various engine speeds (1500 rpm, 2000 rpm, and 2500 rpm) and different volumetric hydrogen ratios (21.4 lpm, 28.5 lpm, 36.2 lpm, 42.8 lpm, and 49.6 lpm). Hydrogen ratios of 21.4 lpm and 42.8 lpm were found to have a substantial impact on the engine coefficient of variation (COV) and overall engine performance. Carbon monoxide (CO), carbon dioxide (CO_2), and particulate matter (PM) emissions showed improvement, suggesting a positive effect of hydrogen addition. Positive outcomes for both engine performance and emission values were attributed to the formation of an ideal combustion time at a hydrogen ratio of 21.4 lpm. The study emphasized that hydrogen, as an alternative fuel, is expected to receive increased attention in the future, considering its positive impacts on engine performance and emissions.

In an experimental investigation, the impact of different hydrogen ratios on performance, emissions, and combustion characteristics was examined across various energy fractions (ranging from 50% to 90%), loads (3 bar, 7 bar, and 9 bar BMEP), and engine speeds (600 rpm, 1000 rpm, and 1500 rpm) in a single-cylinder compression-ignition engine [20]. The findings revealed that the addition of hydrogen at high loads contributed to an increase in thermal efficiency when compared to the diesel engine baseline. However, it was noted that elevated values of hydrogen energy fraction led to the initiation of combustion before diesel ignition. As a consequence, it was emphasized that there should be limitations on the amount of hydrogen in the combustion chamber to manage and control the combustion process effectively. These results underscore the complexity of optimizing hydrogen addition in compression-ignition engines, necessitating a careful balance to achieve improved performance without compromising combustion stability and control. With the ideal hydrogen ratio, higher performance values are achieved more stable and efficient.

The use of hydrogen in diesel engines has been reported to result in higher temperatures and an increased tendency for knocking. As a consequence of the elevated temperatures, the levels of NO_x have also significantly risen. To overcome these issues, particularly in the case of hydrogen, different alternative fuels (such as alcohol-derived fuels, biodiesel, biogas, and ammonia) and combustion technologies (RCCI and PCCI) have been utilized in conjunction with hydrogen to control NO_x and MPRR values. The introduction of various fuels into the combustion chamber along with hydrogen has led to improvements in undesirable outcomes associated with hydrogen combustion.

The experimental investigation aimed to assess the effects of three different fuel combinations-diesel-hydrogen, diesel-biogas, and hydrogen-biogas-diesel on the performance and emission characteristics of a compression ignition engine [21]. In comparison to pure diesel fuel combustion, the results revealed that hydrogen-biogas-diesel combustion yielded increased performance values and reduced emissions. Specifically, in the presence of hydrogen-biogas-diesel fuel, a noteworthy improvement of 3.09% in thermal efficiency was observed, accompanied by a significant 71.05% reduction in Brake Specific Fuel Consumption (BSFC). Emission reductions were also prominent, with an 88.09% improvement in carbon monoxide (CO), a 5.68% reduction in hydrocarbons (HC), and an 83.01% decrease in nitrogen oxides (NO_x). The injection advance timing of 21° CA BTDC during hydrogen-biogas-diesel combustion was highlighted as crucial for achieving optimal values in the tests. This suggests that the specific fuel combination, along with a carefully tuned injection strategy, can lead to improved engine performance and reduced emissions compared to conventional diesel fuel combustion.

The experimental investigation delved into the impact of hydrogen on the combustion of diesel and biodiesel in a compression ignition engine [22]. The biodiesel was produced by blending diesel fuel with 20% by volume of honge oil. In the intake manifold, a mixture of hydrogen (at rates of 10 lt/min and 13 lt/min) with air, at various volumetric ratios, was introduced, filling the combustion chamber during the intake stroke. The study examined the effects of hydrogen enrichment on performance, emissions, and combustion characteristics. Comparatively, it was observed that biodiesel combustion exhibited higher thermal efficiency when contrasted with pure diesel combustion. For instance, the combination of 20% biodiesel and 13% hydrogen

showed improvements of 2.2% in thermal efficiency and 6% in Brake Specific Fuel Consumption (BSFC). Carbon monoxide (CO) and hydrocarbon (HC) emissions also demonstrated notable improvements, with reductions of 21% and 24%, respectively. However, there was an increase in nitrogen oxide (NO_x) emissions due to higher in-cylinder temperatures resulting from increased hydrogen content. This elevation in NO_x was associated with higher cylinder pressure, an increased heat release rate, a heightened maximum pressure increase rate, and a shortened combustion time. These results emphasize the complex relationship between the addition of hydrogen, combustion properties, and emissions in compression ignition engines operating on biodiesel blends.

In an experimental investigation, the impact of hydrogen enrichment in a compression ignition engine fueled by diesel and diesel-biodiesel blends (specifically, P20 - 20% Palm Oil + 80% Diesel by volume) was explored [23]. Different volumetric ratios of hydrogen (7 lpm and 10 lpm) were introduced into the intake manifold, and the mixture was sent to the combustion chamber under various engine loads (30%, 60%, 80%, 90%, and 100%). Thermal efficiency, cylinder pressure, and rate of heat release increased due to the high lower heating value of hydrogen. Hydrocarbon (HC), carbon monoxide (CO), and carbon dioxide (CO_2) emissions decreased due to the carbon-free nature of hydrogen. NO_x emissions increased as a result of elevated in-cylinder temperature values associated with hydrogen enrichment. Hydrogen addition led to a reduction in ignition delay, attributed to an increase in the combustion rate. Under 90% load conditions with 10% hydrogen added to P20, there was a 28% increase in thermal efficiency compared to P20 without hydrogen, along with a 20% improvement in specific energy consumption (BSEC). Emissions such as HC, CO, and CO_2 were reduced, but there was a 13% increase in NO_x emissions. At full load, the P20+10% H_2 operating point reduced combustion time by 12.5% compared to the P20 case. However, it increased cylinder pressure and heat release rate in the range of 1-5%. These results emphasize the trade-offs and complexities associated with hydrogen enrichment in compression ignition engines, showcasing the potential for performance gains and emission reductions but also highlighting challenges related to NO_x emissions and combustion characteristics, particularly at higher loads.

In a numerical investigation, the objective was to augment the hydrogen ratio under medium load conditions (9.4 bar BMEP) within the RCCI engine [24]. Gaseous fuels,

namely natural gas enriched with hydrogen or syngas (80% H_2 + 20% CO), were employed. The approach involved maintaining a constant injection of diesel fuel while adjusting the proportions of hydrogen or syngas mixed with natural gas, along with appropriate Exhaust Gas Recirculation (EGR) ratios, to achieve the concept of low-temperature combustion and provide requisite energy. Gas mixture ratios were tailored for each cycle. The numerical results revealed that the hydrogen energy fraction could be increased to 40.43% in the gas mixture without inducing diesel knocking, with only a 1% power loss. When considering the total fuel energy, the hydrogen energy fraction reached 27.05%, resulting in a power increase of over 4%. Enriching natural gas with hydrogen led to a substantial 46.6% reduction in HC emissions, while a 33.86% improvement was observed in the syngas and natural gas mixture. The study emphasized a remarkable 50% increase in engine efficiency compared to the RCCI engine utilizing diesel and natural gas.

An experimental investigation was conducted to examine the impact of hydrogen on combustion, performance, and emission characteristics in a compression ignition engine operating with rapeseed methyl ester (RME) and a 7% RME blended diesel fuel (RME7) [25]. The primary objective of the study was to enhance the hydrogen ratio in the combustion chamber, achieved by increasing the hydrogen fraction up to 44%. The elevated hydrogen ratio led to a reduction in ignition delay, as well as decreased emissions of hydrocarbons (HC), particulate matter (PM), and carbon monoxide (CO). It's noteworthy that the hydrogen fraction was capped at 35% due to the propensity for knock at higher ratios. This limitation suggests a careful balance between maximizing hydrogen content for improved combustion and mitigating potential issues related to knock tendencies in the engine.

Several formations of various fuels enrichened with hydrogen at different ratios, as well as the application of various processes (such as EGR, split injection, water injection, and different injection strategies), have allowed for the emergence of highly effective studies in the literature. The implementation of EGR and water injection for reducing combustion temperatures has successfully improved NO_x emissions, while injection-related studies have aimed to enhance power output and mitigate knocking tendencies.

The experimental investigation focused on assessing the impact of a hydrogen-diesel dual fuel mode on the emissions and performance of a compression-ignition single-

cylinder engine [26]. Recognizing the tendency of hydrogen combustion to increase NO_x emissions, the Exhaust Gas Recirculation (EGR) method was applied at varying rates (0%, 5%, and 10%) in the tests. Experiments were conducted across different loads (25%, 50%, 75%, and 100%) and hydrogen energy share rates (HES - 0%, 10%, and 30%). The findings underscored that combining EGR with hydrogen yielded highly favorable outcomes in emission values, albeit with a marginal loss in thermal efficiency. Notably, at a 30% hydrogen energy fraction and 10% EGR, there was a substantial reduction of 38.4%, 27.4%, 33.4%, 32.3%, and 20% in NO_x, CO_2, CO, HC, and PM emissions, respectively. This underscores the significant impact of the EGR method on all emissions when utilizing hydrogen in the combustion chamber. The results emphasize the effectiveness of employing a combined approach for emissions reduction while acknowledging a minor compromise in thermal efficiency.

In an experimental investigation, the impact of utilizing hydrogen in a heavy-duty diesel engine was studied, focusing on engine performance and emissions under low and medium load operating conditions at a constant engine speed of 1500 rpm [27]. The study considered the effects of Exhaust Gas Recirculation (EGR), diesel fuel injection pressure, and injection strategies on combustion at various hydrogen energy sharing rates (42%, 60%, 81%, 93%, and 98%). Diesel-hydrogen combustion was achievable up to 98% hydrogen energy fraction without any modifications to the engine under low load conditions. Emissions exhibited significant improvements, with hydrocarbon (HC) and nitrogen oxides (NO_x) decreasing by approximately 90%, and particulate matter (PM) emissions improving by 85% compared to pure diesel fuel combustion. It was emphasized that hydrogen had a negative impact on NO_x emissions in the medium load region, suggesting challenges in maintaining emission reductions observed at low loads. These results highlight the potential for significant emission reductions, especially under low load conditions, when incorporating hydrogen into heavy-duty diesel engines. However, the study underscores the importance of carefully managing hydrogen utilization, especially as load conditions vary, to achieve optimal emission performance across different operating regimes.

In an experimental study conducted on a 6-cylinder turbocharged compression-ignition heavy-duty engine, the impact of Exhaust Gas Recirculation (EGR) on stoichiometric air-fuel ratios was investigated in the context of diesel-natural gas dual-fuel combustion mode [28]. The study maintained a constant total fuel input to the

combustion chamber, with the diesel fuel injection strategy held consistent. Different inert gases, namely N_2, Ar, and CO_2, were utilized as components of the EGR content. Reducing the N_2 and Ar ratios in the EGR content resulted in an increase in engine power. Reducing the CO_2 ratio in the EGR content led to a decrease in engine power. It was noted that the order of dilution effect factors for increasing engine power is Ar, N_2, and CO_2. Each inert gas (N_2, Ar, CO_2) exhibited different effects on engine performance and emission values. The study emphasizes the need for caution when adjusting ratios, as different gases in the EGR content have distinct effects when applied in the engine.

In a diesel engine, an investigation was conducted to examine the effects of different Exhaust Gas Recirculation (EGR) ratios and injection advances on performance and emission values across various engine loads [29]. This analysis utilized a two-zone numerical model. The study aimed to validate the established numerical model by comparing its results with experimental data, literature findings, and reinforcing the validation study. The established numerical model was validated by demonstrating agreement with experimental results and comparing them with literature data. Results obtained from the numerical model were compared with literature findings, reinforcing the validation of the established model. The study explored the combined effects of various pilot diesel fuel advances with different EGR rates and temperatures at different engine loads. Results from the numerical model provided significant insights into local combustion mechanisms and the formation of regional emissions. The study emphasized that using a numerical model enables faster and cost-effective exploration of results compared to experimental approaches. This eliminates the need to face challenges in terms of economy and time associated with experiments. The numerical model facilitates obtaining information for a wider range of working points, providing comprehensive insights into engine performance and emissions. In summary, the two-zone numerical model proved effective in analyzing the effects of EGR ratios and injection advances on diesel engine performance and emissions. Its advantages include efficiency, cost-effectiveness, and the ability to explore a broader range of working points, providing valuable information for understanding combustion mechanisms and optimizing engine operation.

In a comprehensive three-stage study, waste fuel oil (WFO) derived from waste frying oil was introduced in the initial phase [30]. The second stage delved into investigating

the effects of the engine's fuel composition, pilot fuel injection pressure (PFIP), and pilot fuel injection time (PFIT). The final stage of experiments explored the impact of hydrogen in dual fuel mode, considering both hydrogen manifold injection (HMI) and hydrogen port injection (HPI). Additionally, the study examined the effects of different Exhaust Gas Recirculation (EGR) ratios. The engine utilized in the experiments was a compression-ignition (CI) single-cylinder diesel engine with a compression ratio of 17.5:1 and featured a Common Rail Direct Injection (CRDI) system. PFIT variations between 0° and 15° CA BTDC and PFIP changes from 600 to 1000 bar were investigated. Adjustments to PFIT and PFIP had notable impacts on combustion parameters and emissions. Hydrogen injection was explored in both manifold (HMI) and port (HPI) modes. Injection advance and duration of induced hydrogen were significant parameters in achieving optimal combustion and emission results. Different EGR ratios in the range of 0-15% by volume were combined with other parameters. Results showed improvements in NO_x emissions and trade-offs in thermal efficiency and emissions with varying EGR levels. Specific operating points with adjusted PFIT, PFIP, hydrogen injection parameters, and EGR showed a 5.8% lower thermal efficiency but increases in PM, HC, and CO emissions. NO_x emissions demonstrated improvement compared to the case without EGR under 80% load. Proper adjustments of injection time and pressure contributed to reduced combustion pressure (CP) and heat release rates (HRR), along with improvements in combustion time (CD) and ignition delay (ID) values. In summary, the study provided insights into optimizing combustion and emissions in a CI engine through careful adjustments of various parameters, including PFIT, PFIP, hydrogen injection, and EGR.

In a single-cylinder diesel engine, experimental studies were conducted where the energy of diesel fuel was transferred to hydrogen fuel at different rates (ranging from 0% to 20%) under a constant speed (1800 rpm) and various Exhaust Gas Recirculation (EGR) rates (ranging from 0% to 40%) [31]. It was reported that specific fuel consumption decreased with the addition of hydrogen under various EGR rates, while there was no difference in terms of thermal efficiency. Increasing the EGR ratio in the diesel-hydrogen mixture was reported to cause ignition delay. The increased hydrogen ratio increased cylinder pressure and heat release rate values, but the increase in EGR ratio showed a decrease in both quantities. It was stated that the additions of hydrogen and EGR did not lead to any instability in the in-cylinder combustion process. Under

conditions of 60% load and 40% EGR, the addition of 20% hydrogen resulted in an 84% reduction in CO emissions. The maximum decrease in CO_2 emissions, approximately 17.46%, was observed when no EGR was applied at 60% load. The diesel-hydrogen energy distribution system, connected to EGR, increased HC emissions. The increase in hydrogen or EGR ratio was observed to reduce NO_x emissions. On the other hand, while the addition of hydrogen reduced soot emissions, an increase in the EGR ratio was reported to adversely affect this emission value. Under 60% load, the addition of 40% EGR and 20% hydrogen to the intake air resulted in approximately 37.6% reduction in soot emissions and 59.5% improvement in NO_x emissions. It was reported that among all the conditions tested in the study, the ratios of 20% hydrogen and 40% EGR showed more favorable results in terms of performance and emissions when compared to diesel engine conditions.

The absence of CO, CO_2, and unburned HC components in hydrogen and the high thermal efficiency of diesel engines have led scientists to explore the potential advantages of these two characteristics. In another study, the effects of using hydrogen as a dual fuel in a diesel engine were experimentally and numerically investigated in terms of performance and emission characteristics [32]. Additionally, the effects of different Exhaust Gas Recirculation (EGR) rates and pilot diesel fuel injection timing advances were examined under dual-fuel conditions with hydrogen. Energy was distributed between hydrogen and diesel fuel at various ratios, and an optimization study was conducted by altering EGR rates and injection timing advances under these conditions. It was highlighted that increasing EGR rates reduced NO_x emissions, but there was a slight loss in thermal efficiency, which was compensated by improvements in injection timing advances. These studies were conducted both experimentally and numerically. In the numerical study, the authors established their own chemical kinetic models for reaction mechanisms and species, emphasizing that the obtained results aligned with experimental findings.

To address NO_x emissions in a diesel engine, a strategy involving the application of cooled heavy Exhaust Gas Recirculation (EGR) was employed [33]. However, the implementation of EGR was constrained to a specific value due to the observed increase in Hydrocarbon (HC) emissions and the decrease in thermal efficiency. Concurrently, varying amounts of hydrogen were introduced into the intake manifold, maintaining the hydrogen fraction within the range of 2% to 10% of the total energy

fraction. While keeping other diesel engine test conditions constant, such as injection timing, engine speed, and diesel fuel injection ratio, the experimental investigation aimed to examine the effects of different hydrogen ratios on engine performance and emission characteristics. The test results revealed that thermal efficiency increased, and NO_x emissions decreased at suitable combinations of EGR (2%, 16%, and 31%) and hydrogen ratios. It was emphasized that lower NO_x emissions were achieved at higher EGR rates when compared to pure diesel conditions with the addition of hydrogen. For instance, under conditions involving 31% EGR and 10% hydrogen energy fraction, there was an observed improvement of approximately 25% in NO_x emissions, with only a slight increase in thermal efficiency. This suggests that the introduction of hydrogen, combined with controlled EGR, can be an effective strategy for enhancing engine performance while mitigating NO_x emissions.

The pilot injection timing and injection pressure also play a crucial role in mitigating the adverse effects of hydrogen. Properly-timed pilot injection results in a reduction in MPRR, and the injection pressure significantly contributes to fuel vaporization and the creation of homogeneous fuel mixtures, which are important for both homogeneous and diffusion combustion processes. Additionally, achieving a gradual and smoother start of combustion helps avoid high temperatures and pressures associated with abrupt combustion. This leads to significant improvements in both NO_x emissions and performance values.

The experimental study investigates the effects of pilot fuel injection pressure (FIP) and timing (FIT) on combustion and emissions in a dual-fuel compression ignition engine using biodiesel derived from Jatropha oil and hydrogen [34]. Hydrogen volumetric fractions of 5 lt/min, 7 lt/min, and 9 lt/min were used in the tests. Three different fuel injection pressures (FIP) were considered: 500 bar, 1000 bar, and 1500 bar. Biodiesel fuel injection advances (FIT) of 5° CA, 11° CA, and 17° CA BTDC were examined. Under pure diesel operating conditions, thermal efficiency was 25.02%. In biodiesel-hydrogen dual fuel mode with 1500 bar FIP, 17° CA BTDC FIT, and 9 lt/min hydrogen fraction, thermal efficiency increased to 32.15%. However, there was a notable increase of 20.61% in NO_x emissions. Higher FIP values resulted in increased cylinder pressure and heat release rates. Increasing the injection advance (FIT) had a similar effect on cylinder pressure and heat release rates. Biodiesel-hydrogen dual fuel mode with 1500 bar FIP, 11° CA BTDC FIT, and 9 lt/min hydrogen

fraction improved HC and PM emissions by 59.52% and 46.15%, respectively, compared to 100% diesel conditions. The study emphasizes that higher FIP and FIT values are appropriate for improving engine combustion, performance, and emissions in biodiesel-hydrogen dual fuel operating conditions. Optimizing injection pressure and timing is crucial for achieving a balance between combustion efficiency, thermal efficiency, and emissions in dual-fuel compression ignition engines using biodiesel derived from Jatropha oil and hydrogen. The interplay of these parameters influences various aspects of engine performance and environmental impact. The study emphasizes the need for a careful selection of injection parameters to attain the desired trade-off between efficiency and emissions, highlighting the importance of precise control strategies for achieving optimal results in dual-fuel operations.

The study aimed to investigate the effects of various fuel injection strategies on diesel-hydrogen combustion using a numerical approach [35]. Two injection strategies were considered: single injection and split injection. The engine had a compression ratio of 19.5:1, and the analyses were conducted at a constant speed of 1500 rpm. The strategies investigated were single injection (Fuel injected for 2° CA – 23° CA between BTDC with 100% mass fraction) and split injection (Pilot injection for 12° CA - 24° CA BTDC with 4° CA incremental increases and Fixed main injection at 8° CA BTDC with 90%, 80%, 70% mass fractions). The numerical model was created using the CONVERGE CFD program, and validation was performed by comparing the results with experimental data conducted at a hydrogen energy fraction of 18.5%. The results suggested that the optimum pilot injection rate was 10%. The optimum injection advance was found to be 16° CA BTDC. This injection strategy (10% pilot injection rate, 16° CA BTDC) led to higher indicated mean effective pressure (IMEP). The proposed strategy resulted in lower NO_x, PM, HC, and CO emissions. Indeed, the numerical study suggests that a split injection strategy with a 10% pilot injection rate at 16° CA BTDC is a promising approach for achieving improved performance and reduced emissions in diesel-hydrogen combustion. This discovery emphasizes the significance of injection timing and strategy when it comes to optimizing the combustion process in dual-fuel engines, ultimately leading to more efficient and environmentally friendly combustion. EGR (Exhaust Gas Recirculation) process enriched with hydrogen is another method that has been applied. EGR helps reduce NO_x emissions, and with the addition of hydrogen to the combustion, performance

values can be maintained. Thus, it is achieved that both performance and emission values is controlled.

In a compression ignition diesel engine, an investigation was conducted to observe the effects on performance and emissions at various loads (0%, 20%, 40%, 60%, 80%, and 100%) in conditions with and without Exhaust Gas Recirculation (EGR) (basic diesel) [36]. Additionally, the study explored the impact of hydrogen-enriched EGR (H_2EGR), involving hydrogen addition ranging from 9.3% to 14.4% by volume. Comparing the results with EGR and base diesel scenarios, H_2EGR demonstrated substantial improvements in Particulate Matter (PM), Hydrocarbons (HC), and all carbon-containing emissions. Notably, H_2EGR achieved an approximate 46% reduction in NO_x emissions compared to baseline diesel conditions. In summary, the study emphasized that H_2EGR led to decreases in both NO_x and PM emissions, with positive outcomes on thermal efficiency.

The study investigated the impact of Exhaust Gas Recirculation (EGR) with different ratios of intake air supply on a supercharged diesel-hydrogen dual-fuel compression-ignition engine [37]. The experiments were conducted at various engine loads, and the addition of hydrogen with energy fractions of 15% and 28% was explored. The supercharged system contributed to a rich oxygen concentration in the combustion chamber, resulting in positive effects on performance values. EGR had a positive impact on reducing NO_x emissions. The addition of EGR, combined with the supercharged system, contributed to improvements in NO_x emissions. The presence of rich oxygen in the combustion chamber, facilitated by the supercharged system, led to positive results in reducing Particulate Matter (PM) emissions. Increasing the hydrogen ratio was associated with an increase in NO_x emissions and a decrease in PM and CO_2 emissions. Hydrogen addition had a more significant effect on PM emissions, particularly in low and medium-sized intake air boost conditions. High EGR rates resulted in a reduction of about 2% in oxygen concentration in the combustion chamber. The addition of hydrogen with a 15% energy fraction led to a significant reduction (75%) in particles formed at the end of combustion. The overarching goal of the study was to determine appropriate intake air, EGR, and hydrogen ratios to enhance both performance and emission values. In summary, the study aimed to optimize the combination of intake air, EGR, and hydrogen ratios to achieve improved performance and emission characteristics. The findings highlight the synergistic effects of

supercharging, EGR, and hydrogen addition on combustion and emissions in a dual-fuel compression-ignition engine.

In an experimental investigation conducted on a compression ignition diesel engine, the impact of enriched hydrogen ratios (13.4%, 20.9%, and 29.3% for 30% load; 10.8%, 17.2%, and 24.1% for 45% load; 8.4%, 13.8%, and 19.5% for 60% load, hydrogen energy fractions) on engine performance and emission characteristics was studied [38]. The experiments were carried out under varying load conditions (30%, 45%, and 60%), incorporating cooled Exhaust Gas Recirculation (EGR) at different ratios (20%, 30%, and 40%) and employing different intake air scenarios (temperatures of 30 °C, 45 °C, and 60 °C). The experimental setup involved combining intake air with a methanol mixture at different flow rates (6.5 g/min, 10 g/min, and 13.5 g/min) with the addition of cooled EGR. The temperature of the intake air was controlled using a heater, and a mixture of aqueous methanol was introduced into the intake air with a rich hydrogen fraction. Cooled EGR was applied to the combustion chamber from the intake port to regulate NO_x emissions. The objective was to achieve optimum Brake Specific Fuel Consumption (BSFC), thermal efficiency, and emission values (CO, HC, and NO_x). All obtained results were compared with those of the engine operating under pure diesel conditions. The optimal outcomes demonstrated notable improvements, with a 31.58% reduction in CO emissions, a 15% reduction in HC emissions, a 41.35% reduction in NO_x emissions, a 29.27% reduction in PM emissions, and 5.13% improvements in both BSFC and thermal efficiency values. These findings underscore the positive impact of enriched hydrogen ratios, cooled EGR, and varying intake air conditions on the overall performance and emission profile of the diesel engine.

Exhaust Gas Recirculation (EGR) is implemented to mitigate NO_x emissions, but it tends to increase Particulate Matter (PM) emissions. A numerical study was conducted to address both concerns, recommending the application of EGR under high pressure for a comprehensive solution [39]. The approach involves a turbocharger system to introduce high-pressure intake air into the engine. Exhaust gases are then cooled and mixed with the high-pressure intake air. This process, when applied to the combustion chamber, reduces combustion temperatures without significantly decreasing oxygen concentration, resulting in decreased NO_x emissions. The presence of high oxygen facilitates the combustion of particles, enhancing the reduction of soot formation. In

this numerical study, a two-zone combustion model was established, and various EGR rates (ranging from 0% to 30%) and temperatures (varying between 90 °C and 240 °C in 50 °C increments) were introduced into the combustion chamber under high pressure. The effects of these parameters on performance, emissions, and combustion were examined under full load conditions. The need for a turbocharger system to introduce high-pressure intake air for EGR application was emphasized. The application of EGR under high pressure effectively reduces combustion temperatures, leading to a decrease in NO_x emissions. The high oxygen concentration in the combustion chamber facilitates the combustion of particles, contributing to the reduction of soot formation. The study found that decreasing EGR temperature had more positive effects on Brake Specific Fuel Consumption (BSFC) and PM emissions. However, its impact on NO_x emissions was relatively weaker. The effects of EGR temperatures were noted to be more pronounced at high EGR rates. In summary, the proposed approach of applying EGR under high pressure, facilitated by a turbocharger system, demonstrates promise in simultaneously reducing NO_x emissions and mitigating PM emissions. The study highlights the importance of carefully managing EGR rates and temperatures, especially at high EGR rates, to optimize engine performance and emissions.

In an experimental study, the energy and exergy analyses of diesel-biogas dual-fuel combustion mode in a compression ignition engine were conducted [40]. The investigation included the effects of different Exhaust Gas Recirculation (EGR) rates (5%, 10%, and 15%) and EGR temperatures (35 °C and 65 °C) on engine performance and emission values at various compression ratios (16.5, 17.5, 18.5, and 19.5). Initial tests focused on varying compression ratios, revealing that an increase in compression ratio led to improvements in thermal efficiency and reductions in emissions. At low loads, EGR slightly increased engine efficiency and significantly reduced nitrogen oxides (NO_x) emissions. However, applying EGR at high loads caused a slight decrease in engine efficiency. In the third stage of experiments, hot EGR was applied, and results were compared with cold EGR. Hot EGR yielded more positive results in terms of engine efficiency and exhaust emissions at both low and high loads. These findings underscore the intricate relationship between compression ratio, EGR (Exhaust Gas Recirculation) rates, and temperatures in a diesel-biogas dual-fuel combustion mode. While increasing compression ratio and applying EGR showed

benefits in certain aspects, the introduction of hot EGR emerged as a favorable strategy, particularly for enhancing engine efficiency and mitigating emissions under varied load conditions.

The study explored engine performance and emissions in the context of hydrogen-diesel dual fuel combustion by introducing oxygen into the combustion chamber (ranging from 21% to 27% by volume) during partial and low loads [41]. Notable enhancements were observed, particularly in carbon-based emissions. Elevating the oxygen concentration resulted in a 1.6% increase in thermal efficiency, accompanied by a 4% reduction in specific fuel consumption. The rise in oxygen levels led to elevated in-cylinder temperatures, prompting the application of Exhaust Gas Recirculation (EGR) as a mitigation strategy. The introduction of oxygen without EGR resulted in a substantial 63% increase in NO_x emissions. However, a significant 72% reduction in particulate matter (PM) emissions was noted. In specific scenarios, such as combining 27% oxygen enrichment with a 24% EGR ratio, a 79% improvement in NO_x emissions and a 2.6% enhancement in thermal efficiency were achieved at a 45% hydrogen by volume operating point.

In an experiment with a compression ignition engine, a mixture of air and biogas was introduced into the intake port and sent to the combustion chamber, where it was ignited with diesel fuel [42]. The study aimed to analyze engine performance and exhaust emissions at a constant compression ratio (18:1). The experimental results were compared across tests with different biogas ratios (Biogas 1# H_2:CO:CH_4:N_2 = 5:40:5:50 and Biogas 2# H_2:CO:CH_4:N_2 = 15:30:5:50) and various Exhaust Gas Recirculation (EGR) ratios. Increasing EGR ratios were found to prolong combustion time and ignition delay. NO_x emissions exhibited a monotonic decrease at EGR ratios of 50% and above. PM emissions were notably high in the Biogas 1# (H_2:CO:CH_4:N_2 = 5:40:5:50) gas mixture. It was emphasized that as the EGR ratio increased, the thermal efficiency value gradually decreased. Biogas 2# with a higher hydrogen (H_2) concentration at similar EGR rates showed more positive results in terms of combustion reactivity. Biogas 2# (H_2:CO:CH_4:N_2 = 15:30:5:50) caused higher in-cylinder temperatures, resulting in higher thermal efficiency and NO_x emissions. The study concluded that positive results in performance and emission values could be achieved in biogas-diesel dual-fuel combustion mode by applying EGR, split diesel fuel injection, and hydrogen addition together. These findings highlight the

significance of considering a combination of strategies, such as EGR, fuel injection techniques, and hydrogen addition, to optimize performance and emissions in a biogas-diesel dual-fuel combustion mode.

Since hydrogen usage in the engine tends to increase NO_x and MPRR values, various strategies have been combined in studies to improve these values. In most studies, EGR and injection strategies have been applied together to expedite obtaining more reasonable results.

The experimental study investigates the effects of PCCI (Premixed Charge Compression Ignition) technology on a compression-ignition engine [43]. High premix-combustion rates in PCCI technology lead to lower temperatures compared to traditional compression-ignition combustion, resulting in lower NO_x emissions. However, at high loads, the sudden formation of knock tendency and high temperatures limit the positive effects on NO_x emissions. PCCI technology is considered applicable up to medium loads. Adjusting injection timing and providing in-cylinder pressure-temperature control can improve the applicability of PCCI technology. Splitting the injection time and applying suitable EGR ratios help reduce knocking tendency and temperature spikes, leading to improved NOx emissions. Tests considered various pilot injection advances (30°, 35°, and 40° CA BTDC) and main injection advances (12°, 16°, 20°, and 24° CA BTDC) with different EGR rates (0%, 15%, and 30%). The combination of a 35° CA BTDC pilot injection advance and a 15% EGR ratio was recommended for optimum results. Delaying the pilot injection (30° CA BTDC) resulted in higher NO_x and PM emissions, while too much advance (40° CA BTDC) led to lower engine power. Appropriate EGR rates (15% and below) had a positive effect on combustion and emission values. High EGR rates (above 15%) caused a decrease in cylinder temperatures, leading to a deterioration in performance. The study emphasizes the importance of split fuel strategies (Pilot and Main injection) with an appropriate EGR ratio to increase the PCCI combustion limit. These findings highlight the complexity of optimizing PCCI technology, considering factors such as injection timing, EGR rates, and their impact on combustion efficiency and emissions at different engine loads.

The tests aimed to investigate the effects of different injection strategies in hydrogen-diesel dual-fuel mode at low load (2 bar BMEP) [44]. Four injection strategies were compared (Single pulse injection = 100% of the fuel injected in a single pulse, double

pulse phase 1 injection = 50% of the fuel in the first pulse - 50% of the fuel in the second pulse, double pulse phase 2 injection = 30% of the fuel in the first pulse - 70% of the fuel in the second pulse and multi pulse injection = 45% of the fuel in the first pulse - 45% of the fuel in the second pulse - 10% of the fuel in the third pulse). The maximum hydrogen energy shares (HES) that could be substituted into the combustion chamber with the applied injection strategies were found to be 73.99%, 48.98%, 34.46%, and 24.39%, respectively. Double Pulse Phase 2 injection exhibited the highest thermal efficiency at 21.61%, while single pulse injection had a slightly lower efficiency at 19.5%. With the increase in temperatures, NO_x emissions also increased slightly. Multi-pulse injection led to a decrease in NO_x emissions. Multi-pulse injection resulted in increased PM emissions, while other strategies showed varying effects. Multi-pulse injection had a moderate positive effect on BTE. At the maximum HES, there was a significant improvement in NO_x emissions, and engine stability was maintained despite a small increase in PM emissions. In summary, the choice of injection strategy had notable impacts on thermal efficiency, emissions, and overall engine performance in hydrogen-diesel dual-fuel mode, with different strategies showing varying trade-offs between efficiency and emissions.

The combination of n-butanol and diesel fuels, brought together through a post-injection strategy, has resulted in extremely low soot emissions [45]. However, it has been observed that the inclusion of n-butanol in the combustion chamber leads to an increase in NO_x emissions. The EGR process has proven effective in mitigating NO_x formation to some extent. In study, the impact of n-butanol and EGR ratios on emissions and combustion performance was experimentally investigated on a turbocharged diesel engine. The effects of different fuels and EGR ratios in compression ignition engines were also explored. Tests utilized different fuels: pure diesel (D100), diesel with 10% n-butanol (NB10), diesel with 20% n-butanol (NB20), and diesel with 30% n-butanol (NB30). The results indicate that while post-injection timing has little effect on brake thermal efficiency (BTE), it reduces CO, HC, NO_x, and soot emissions by 33.3%, 10%, 25%, and 50%, respectively. Under specific post-injection strategies, the addition of n-butanol (at 10%, 20%, and 30%) leads to a significant reduction in CO and soot emissions. In the 10% and 20% EGR range, it is suggested that NB20 fuel can strike a balance between combustion performance and emissions under certain post-injection strategies. Furthermore, it was emphasized that

NB30 fuel results in the lowest soot and CO emissions and has the highest heat release rate. The reason which the lowest soot composed with NB30 was explained that it has lower C content than diesel fuel.

A numerical investigation was conducted to assess the impact of hydrogen on a diesel engine, aiming to reduce hydrocarbon emissions and enhance performance values [46]. Various hydrogen fractions were introduced with air into the combustion chamber, and ignition was facilitated through the injection of pilot diesel fuel. As the hydrogen ratio increased, particulate matter (PM) emissions exhibited a decrease, and there was an improvement in thermal efficiency. However, nitrogen oxide (NO_x) emissions increased due to elevated cylinder temperatures resulting from the higher hydrogen ratio. The augmentation in the hydrogen ratio led to a decrease in the formation rate of OH radicals, causing an increase in ignition delay. To address the elevated NO_x emissions, the Exhaust Gas Recirculation (EGR) method and various injection advance strategies were employed. These additional measures were implemented to mitigate the adverse effects on NO_x emissions, thereby striking a balance between reducing hydrocarbon emissions, improving performance, and managing the trade-offs associated with increased hydrogen content in the combustion process.

In the literature, numerous studies have explored the combined effects of certain processes (such as EGR and injection strategies) and various engine parameters (including compression ratio and combustion chamber geometry) on performance and emission values.

In a numerical investigation, the influence of the interplay between different compression ratios and hydrogen ratios on engine performance and emission characteristics in a compression ignition engine was examined [47]. Hydrogen was introduced into the intake air using a low-pressure injector on the intake port, considering compression ratio values of 14.5:1, 16.5:1, and 19.5:1. Analyses were conducted for varying ratios of hydrogen energy fraction, ranging from 0% to 55%. The numerical results indicated that to counteract the increasing tendency for knock with rising compression ratios, it is advisable to reduce the hydrogen fraction. Specifically, as the compression ratio increased from 14.5 to 19.5, the hydrogen fraction decreased from 45% to 20%. In terms of emissions, all pollutants except nitrogen oxides (NO_x) demonstrated improvements with an increasing hydrogen

energy fraction. These findings highlight the delicate balance required in adjusting hydrogen ratios to mitigate knock tendencies associated with higher compression ratios while simultaneously improving emissions in compression ignition engines.

The study emphasizes the intricate relationship between compression ratios and fuel injection timing when utilizing ammonia-hydrogen mixtures in a compression ignition engine [48]. Delaying the injection timing was observed to reduce engine performance and increase ignition delay. This delay was associated with a gradual increase in particulate matter (PM) and carbon monoxide (CO) emissions. Interestingly, delaying the injection timing had a positive effect on NO_x emissions. Increasing the compression ratio was found to enhance combustion performance but also increased NO_x and nitrous oxide (N_2O) emissions. The study identified an operating point with a 12° CA BTDC injection advance and a compression ratio of 13.5 as meeting the Tier III standards set by the International Maritime Organization (IMO) for NO_x emissions. It's noteworthy that the NO_x emissions caused by each compression ratio and injection timing were found to be suitable for Tier II standards. This suggests that careful tuning of injection timing and compression ratio is essential for achieving a balance between combustion performance and emissions, especially when dealing with alternative fuel mixtures like ammonia-hydrogen. The study's findings contribute valuable insights for meeting stringent emissions standards in compression ignition engines using such alternative fuels.

The numerical study explores the impacts of different piston bowl geometries (P1, P2 and P3), injection advances (1.5°, 2°, 3° and 4° CA BTDC), and EGR ratios (0%, 10% and 20%) on the performance and emissions of a compression ignition engine [49]. P2 piston geometry resulted in 12% better results in terms of thermal efficiency and power compared to P1. P2 geometry showed a 10.5% reduction in PM (Particulate Matter) emissions compared to P1, while maintaining similar NO_x emissions. The study suggests that an injection advance of 2° CA BTDC is optimal in terms of performance and emissions. The introduction of 10% EGR (Exhaust Gas Recirculation) reduced NO_x emissions by 37%, indicating the effectiveness of EGR in NO_x reduction. However, 10% EGR also led to a 6.4% increase in CO_2 emissions. P2 geometry provided better results in terms of combustion efficiency compared to other geometries. Approximately a 20% improvement was observed in CO emissions with the P2 geometry. It's interesting to note that the optimal injection advance and piston

bowl geometry play crucial roles in achieving improved efficiency and reduced emissions. Additionally, the trade-offs between NO_x reduction and CO_2 emissions, especially with the introduction of EGR, highlight the complexity of optimizing combustion in internal combustion engines.

Direct or indirect water jet/vapor injection into the combustion chamber leads to significant and reasonable improvements in NO_x emissions. In CI engines, the application of water injection methods during the combustion of various fuels makes it possible to achieve a decrease in all emissions, including NO_x, with very little loss in performance values.

The numerical analysis of the effects of direct water injection (DWI) into the combustion chamber of a ship diesel engine on performance and emission characteristics has been conducted [50]. The study investigated parameters such as the amount of water injected, water injection temperature, and injection timing. In the numerical study, comparisons between DWI and Exhaust Gas Recirculation (EGR) were performed, expanding the scope of the research. With an increasing ratio of DWI, power, in-cylinder pressure, temperature, and NO_x values decreased. When DWI advance was chosen as the compression stroke, a 55.6% improvement in NO_x was reported. It was stated that the temperature of DWI had a minimal impact on engine performance and emission values. As the DWI advance increased, engine power decreased, while an increase in advance led to an increase in power. Among the examined parameters, DWI advance was observed to be the most influential parameter on NO_x emissions. When comparing DWI with EGR in terms of power and NO_x, the results indicated that the DWI process resulted in higher power output and lower NO_x emissions.

In a Compression Ignition engine fueled by hydrogen (HFCI - Hydrogen-Fueled Compression Ignition), various advances and ratios of water injection into the combustion chamber were provided to mitigate the increased NO_x emissions associated with hydrogen use [51]. Hydrogen was introduced into the cylinder through an injector at a constant flow rate of 5 LPM (Liters Per Minute) over a period of 40° CA. Water injection was provided between 20° CA Before Top Dead Center (BTDC) and 20° CA After Top Dead Center (ATDC) with injection durations of 20° CA and 40° CA. It was observed that thermal efficiency and power values increased in the case of water injection with an advance of 20° CA ATDC and an injection duration of 20°

CA. The lowest NO_x and lower Exhaust Gas Temperature (EGT) values were obtained at 2500 rpm across all speed ranges. The highest Heat Release Rate (HRR) and the longest ignition delay time were observed in the case of water injection with an advance of 20° CA BTDC and an injection duration of 40° CA. The study suggests that water injection is a promising technique to effectively enhance the performance and emission quality of HFCI engines.

The effects of water injection into the combustion chamber as a measure to mitigate the increase in NO_x and MPRR values caused by hydrogen in a Compression Ignition diesel engine have been investigated [52]. Water injection was provided into the combustion chamber at various volumetric ratios (0%, 5%, 10%, and 15%) with different advances (9° CA BTDC, 3° CA BTDC, and 3° CA ATDC). The effects of water injection were also examined considering different water jet temperatures (27 °C – room temperature and 60 °C). Results for water injection in diesel fuel and diesel+hydrogen fuel conditions were obtained and interpreted. It was mentioned that the condition of 15% Water Injection (WI) and 60 °C water jet temperature provided the highest pressure value, more torque, higher thermal efficiency, and greater engine power. The lowest emission values were achieved under the conditions of 5% WI and 27 °C water jet temperature.

The effects of different gaseous fuels (hydrogen, methane, and hythane) and nozzle hole sizes in a Compression Ignition (CI) engine were investigated both numerically and experimentally [53]. Tests were conducted based on energy fractionation with 50% diesel-50% methane (D50M50), 50% diesel-50% hydrogen (D50H50), and 50% diesel-50% hythane (D50Hy50) ratios. The results were compared with pure diesel outcomes. Additionally, due to the high temperatures encountered in points involving hydrogen and hythane, volumetric water injection at a rate of 10% was included in the combustion chamber. The results showed that under D50H50 fuel fractionation and a 1 mm nozzle hole size condition, Brake Specific Fuel Consumption (BSFC) was 28% higher compared to pure diesel conditions, indicating that diesel fuel consumption was more dominant at smaller nozzle sizes. The injection of water vapor into the combustion chamber contributed to the maximum pressure, and as a result, the D50Hy40W10 (50% diesel, 40% hythane, and 10% Water Injection) condition produced a high torque value at smaller nozzle hole sizes. An increase in nozzle hole size led to a decrease in combustion temperature and an increase in CO content in

exhaust gases. The increasing of nozzle diameter led to lower surface area/volume rate for fuel droplets. Thus, the combustion temperature declined and NOx emission decreased.

The experimental study aimed at improving NO_x emissions due to biodiesel fuel, which leads to higher combustion temperatures compared to diesel fuel, through water injection into the combustion chamber in a Compression Ignition (CI) engine [54]. The study was conducted on a four-cylinder, four-stroke, direct-injection (DI), and turbocharged diesel engine. The 3 kg/h water injection rate was found to be not very effective for Brake Specific Fuel Consumption (BSFC), but it resulted in approximately a 50% improvement in NO_x emissions. The study indicated that water injection into the intake manifold had very little effect on the cylinder pressure and heat release rate of the CI engine under different operating conditions.

There is a significant amount of research in the literature regarding the use of natural gas in compression ignition (CI) engines in conjunction with hydrogen. It has been observed that natural gas fuel leads to very reasonable results in controlling the fast combustion characteristic of hydrogen to some extent. Compared to other fuels, the collaboration of hydrogen and natural gas has shown to be more environmentally friendly and provide more favorable results in terms of engine performance.

The experimental investigation explored the impact of high hydrogen ratios (20%, 30%, 40%, and 50% by volume) on the performance, emissions, and knock tendency in a dual-fuel engine using diesel and natural gas [55]. Increased hydrogen ratios at high loads resulted in heightened maximum pressure and rate of heat release (HRR). Notably, the addition of hydrogen positively influenced the combustion of gas mixtures, with the most significant HRR and pressure values observed at a 50% hydrogen mixture. The introduction of hydrogen led to a reduction in combustion time and an enhancement in thermal efficiency across all volumetric fractions. Particularly, at 50% hydrogen enrichment, there was a noteworthy improvement of approximately 16% in thermal efficiency compared to pure natural gas dual-fuel combustion. Hydrogen supplementation proved effective in reducing carbon monoxide (CO) and hydrocarbon (HC) emissions, especially in medium and high load operating conditions. Positive outcomes were observed in terms of nitrogen oxides (NO_x) emissions with hydrogen addition at low and medium loads; however, caution was advised against its use at high loads. It was emphasized that the enrichment of natural

gas with 80% or more hydrogen significantly increased the tendency for knocking. These results underscore the potential benefits of hydrogen addition in terms of improving combustion dynamics, enhancing thermal efficiency, and reducing specific emissions in dual-fuel engines. However, careful consideration is crucial, particularly at high loads, to manage challenges associated with increased knock tendency.

In a comprehensive numerical study using AVL Fire CFD program, the effects of hydrogen addition to natural gas (HCNG - Hydrogen Compressed Natural Gas) and the application of Exhaust Gas Recirculation (EGR) to the combustion chamber were investigated [56]. The diesel fuel's energy was gradually replaced by natural gas and hydrogen, ranging from 0% Hydrogen for 0% HCNG to 15.59% Hydrogen for 40% HCNG. The energy fraction for the gas mixture was varied from 0% to 40%. To mitigate the knock tendency resulting from hydrogen addition, the compression ratio of the diesel engine was reduced from 17:1 to 15:1. The analyses were conducted on a three-cylinder compression-ignition engine at different loads (40% and 80%) and engine speeds ranging from 1000 rpm to 1800 rpm. EGR rates of 5%, 10%, and 15% were considered in the study. The increase in EGR led to a longer combustion time and a decrease in thermal efficiency, engine power, and Brake Specific Fuel Consumption (BSFC). While EGR increased the cumulative heat release in the cylinder, it did not significantly affect the in-cylinder pressure. Enriching natural gas with hydrogen resulted in increased combustion temperatures and, consequently, higher NO_x emissions. Optimum values for performance and emission parameters were recommended at 6.35% EGR and 31% HCNG. The reduction in compression ratio (from 17:1 to 15:1) aimed to address the knock tendency associated with hydrogen addition. In summary, the study emphasized the trade-offs involved in adjusting EGR rates and HCNG composition in terms of combustion characteristics, performance, and emissions. The recommended optimum values provide insights for achieving a balance between these factors in the context of a compression-ignition engine.

In a numerical study, a D19 diesel engine was modeled both in one-dimensional and three-dimensional forms, and the engine was converted into dual fuel mode with natural gas at different rates (0%, 20%, 40%, and 60% natural gas content) under specific operating conditions (2200 rpm and 50% load). The integration of natural gas into the model involved using the GRI-Mech 3.0 skeletal mechanism and the 95/55vv

diesel fuel mechanism [57]. A reduced mechanism with 79 species and 224 chemical kinetic reactions was employed. The study aimed to investigate the combustion performance and exhaust emissions (NO_x and PM) of the engine in both diesel and diesel-natural gas dual fuel modes. The numerical model was validated by comparing the simulation results with experimental data obtained at different operating conditions (1500 rpm, 60% load, and 42% natural gas content & 2200 rpm, 80% load, and 27% natural gas content). The results indicated that the thermal effects of Exhaust Gas Recirculation (EGR) on the engine were greater than the chemical effects. EGR content, consisting of CO_2 and H_2O gases, played a dominant role in thermal effects, with CO_2 being more influential. At 50% EGR, the efficiency rates were observed to be 65.3% for thermal effects and 36.7% for chemical effects in 100% diesel (pure diesel mode) conditions. In diesel-natural gas dual fuel mode at the same 50% EGR ratio, the thermal and chemical effects were 62.2% and 39.2%, respectively. The application of EGR in dual fuel mode was found to be less effective for thermal values but had a more decisive impact on chemical reactions. In summary, the study highlighted the complex interplay between EGR, combustion performance, and emissions in both diesel and dual fuel modes. The findings contribute to understanding the relative importance of thermal and chemical effects in different operating conditions.

The experimental setup aimed at reducing NO_x and PM emissions involved converting a compression ignition diesel engine to dual-fuel combustion mode with natural gas [58]. The study observed that natural gas-diesel combustion led to high HC and CO emissions with low thermal efficiency at low loads. To address these issues, the effects of single and split injection strategies (pilot injection, main injection, and post injection) on diesel-natural gas combustion were investigated in terms of performance and emission values. The tests were conducted in a single-cylinder engine at a constant speed of 1500 rpm and under different load conditions (20%, 40%, 60%, 80%, and 100%). Two types of split injection strategies were employed. First strategy is pilot – main injection (Pilot injection at 11° CA, 16° CA and 20° CA BTDC, contributing 20% of the fuel - Main injection at 4.5° CA BTDC, constituting 80% of the fuel). Second strategy is pilot – main – post injections (Pilot injection at 11° CA BTDC, contributing 20% of the fuel – Main injection at 4.5° CA BTDC, constituting 60% of the fuel – Post injection at various injection advance by timings of 4° CA, 8° CA, 12°

CA, 20° CA, and 28° CA BTDC, contributing 20% of the fuel). The results indicated that the split fuel application had a significant impact on engine combustion and emissions. Notably, the split injection strategy led to a 25.6% improvement in thermal efficiency compared to single injection at low load conditions. At 20% load, employing 11° CA BTDC pilot injection resulted in a 20.4% improvement in BSFC, along with reduced HC, NO_x, and noise emissions. Furthermore, the study emphasized the positive effects of early post-injection advances on thermal efficiency. Delaying the post-injection advance at low and medium loads was found to decrease NO_x emissions. Overall, the findings highlight the effectiveness of split injection strategies in enhancing engine performance and emission characteristics in dual-fuel combustion mode with natural gas.

In an experimental study aimed at improving NO_x and PM emissions, a diesel engine was operated in dual fuel mode with compressed natural gas (CNG) at a constant engine speed of 1500 rpm [59]. The investigation involved varying diesel-natural gas ratios at different energy fractions (D + 10% CNG, D + 15% CNG, D + 20% CNG) across various loads (low, medium, and high) and Exhaust Gas Recirculation (EGR) ratios (5%, 10%, and 15%). Compared to pure diesel conditions, dual fuel combustion mode resulted in a decrease in thermal efficiency by 1-2% across all loads. The Brake Specific Fuel Consumption (BSFC) value at high loads showed an improvement of approximately 2-3% under dual fuel combustion conditions. HC and CO emissions were found to be higher under low and high load conditions in dual fuel combustion compared to diesel combustion conditions. There was an improvement of 21% and 18% for NO_x and PM emissions, respectively, under dual fuel combustion conditions. The findings suggest that while there is a trade-off with a slight reduction in thermal efficiency, the dual fuel mode led to improvements in NO_x and PM emissions. The study provides insights into the potential benefits and challenges associated with using compressed natural gas in dual fuel combustion for diesel engines.

In an experimental investigation conducted on a compression-ignition CRDI engine, the effects of pilot diesel fuel and gaseous fuels with different energy compositions on combustion and emission values at high loads were explored [60]. Three dual-fuel approaches were examined (DFA1: 100% hydrogen, DFA2: 95% hydrogen + 5% CNG and DFA3: 90% hydrogen + 10% CNG). Three different pilot diesel injection pressures were considered: 500 bar, 750 bar, and 1000 bar. Improved combustion was

observed at dual-fuel operating points. In-cylinder pressure values increased, indicating enhanced combustion efficiency. Ignition delay and combustion time were significantly affected at dual-fuel operating points. Brake Specific Fuel Consumption (BSFC) and emissions showed improvements. Hydrogen substitution led to a reduction in HC and CO_2 emissions by 30-35% and 3-4%, respectively. A 5-10% decrease in soot emissions was observed compared to pure diesel. Performance values were 37.2% higher with dual-fuel approaches compared to pure diesel. DFA2 type fuel composition (95% hydrogen + 5% CNG) yielded more positive results in terms of performance and emissions compared to DFA1 and DFA3. In summary, the study highlights the advantages of using gaseous fuels in a dual-fuel approach, particularly emphasizing the positive impact on combustion efficiency, emissions, and overall engine performance. The specific composition of DFA2 (95% hydrogen + 5% CNG) showed superior results among the examined fuel approaches.

In a study aimed at reducing engine exhaust emissions by utilizing natural gas as a dual fuel in a compression ignition diesel engine, various diesel fuel injection strategies were investigated in diesel-natural gas dual combustion mode [61]. The primary goal is to reduce CO and HC emissions in a diesel-natural gas dual-fuel combustion engine. Different diesel main injection advances were analyzed (4° CA, 8° CA, 12° CA, and 16° CA BTDC). Split injection strategies were implemented. The effects of pilot fuel injection at different fractions (15%, 30%, and 45%) were investigated under a constant main injection advance (8° CA BTDC). Numerical results were obtained by varying the pilot injection timing between 12° CA BTDC and 30° CA BTDC. An 8° CA BTDC injection advance for the main injection was identified as causing optimum values for both performance and emission parameters. For the split injection strategy, HC and CO emissions improved with a 24° CA BTDC value for pilot injection advance. Advances greater than 24° CA BTDC increased HC and CO emissions significantly (by 30% and 45%, respectively) for all pilot fuel fractions (15%, 30%, and 45%). Increasing the pilot fuel injection fraction did not yield positive results for HC and CO emissions in the 24°–30° CA BTDC injection advance range. The optimum conditions identified for diesel-natural gas dual fuel combustion were a 24° CA BTDC pilot fuel injection advance, 8° CA BTDC main injection advance, and a 15% fuel fraction for the split injection strategy. In summary, the study highlights the significance of injection strategies in the context of dual-fuel

combustion, pinpointing specific injection advances and fractions that result in enhanced performance and decreased emissions in diesel-natural gas engines. These findings offer valuable insights for optimizing engine operation in dual-fuel mode, contributing to the ongoing efforts to develop more efficient and environmentally friendly combustion systems.

The study investigates the effects of different injection pressures and various EGR rates in a diesel-natural gas dual fuel compression ignition engine [62]. Increasing injection pressure (from 800 bar to 1600 bar) resulted in increased natural gas flame propagation speed and thermal efficiency. However, higher injection pressure led to an increase in the unburned natural gas ratio near the cylinder walls, contributing to higher UHC (Unburned Hydrocarbon) emissions. EGR (Exhaust Gas Recirculation) increased thermal efficiency up to a certain value (up to 20%) but then started decreasing it. The increase in thermal efficiency was accompanied by increased unburned CH_4 emissions due to the chemical reactions involving diesel fuel. Low EGR rates (10% and below) were not effective in reducing CO (Carbon Monoxide) and HC (Hydrocarbon) emissions. CO and HC emissions decreased at high EGR rates (30% and above) due to the increase in thermal efficiency. The study suggests that the conditions of 1600 bar injection pressure and 20% EGR rate are suitable for achieving optimum thermal efficiency and low emissions. These findings highlight the intricate balance between injection parameters, EGR rates, and their impact on combustion efficiency, emissions, and thermal efficiency in dual fuel compression ignition engines. Optimal conditions may vary depending on the specific requirements and trade-offs of the application.

The experimental investigation of the impact of adding hydrogen, a pre-mixture fuel, to natural gas in a single-cylinder diesel-natural gas dual-fuel engine (HCNG) on performance and emission values was conducted [63]. In the study, the combustion chamber was recorded with an imaging system, and the obtained images were interpreted. Dual-fuel engines, taking advantage of the high compression ratio characteristic of diesel engines and the environmentally friendly nature of natural gas used as an alternative fuel, are known for their high thermal efficiency and low emissions. However, during the initial study, the drawback of knocking in cold weather and high unburned HC emissions at low loads was identified. To overcome this issue, hydrogen, with its wide ignition limit, was introduced to natural gas used as

a premixed fuel in varying volumetric ratios (from 0% to 30%). The energy ratio of the natural gas-hydrogen mixture (HCNG) was intended to be kept at the 70% limit. According to the results, an increase in the volumetric ratio of hydrogen in the mixture led to an increase in cylinder maximum pressure and heat release rates, while reducing the ignition delay. The combustion inside the cylinder was explained by dividing it into five phases: ignition delay phase, diesel premixed combustion phase, diesel mixture-controlled combustion phase, ignition (HCNG) premixed combustion phase, and the remaining diesel mixture combustion phase. The impact of hydrogen was felt more in the initial combustion phase than in the final combustion phase. The study also highlighted that the premixed combustion with blue flames was observed, while diffusion combustion was seen with yellow flames. Increasing the volume of hydrogen in the premixed mixture was stated to increase the number of yellow flame zones, representing diffusion combustion.

A single-cylinder air-cooled diesel engine was operated in conventional diesel mode, diesel-natural gas dual-fuel mode, and with the addition of hydrogen to natural gas in premixed combustion (HCNG - hydrogen + natural gas) mode, and both performance and emission values were experimentally obtained and compared [64]. Various volumetric ratios of hydrogen were added to natural gas (10%, 20%, 30%, and 70%), and their effects were examined. According to the results, adding hydrogen to natural gas fuel generally improved the gas mixture combustion phase, leading to increases in cylinder peak pressure and heat release rates, especially at high loads (4.1 bar and 70% load). The highest cumulative heat release and heat release rates were reported to occur with a 10% volumetric ratio of added hydrogen. This improvement was attributed to an increase in combustion rate and enhanced ignitability of the mixture. It was stated that increasing the hydrogen ratio shortened the combustion phase duration of gaseous fuels and increased combustion stability. The coefficient of variation of indicated mean effective pressure (COV_{IMEP}) did not exceed 10% for all hydrogen mixture ratios, indicating that combustion noise did not increase significantly. Ignition delay did not vary significantly for all mixture ratios. When examined from a thermal efficiency perspective, adding hydrogen improved the gas fuel combustion phase, resulting in approximately 32.5% maximum thermal efficiency. The specific fuel consumption reached a minimum value of approximately 236 g/kW.h at 70% load with 10% hydrogen added to the mixture. It was noted that compared to the conventional diesel

engine, the dual-fuel diesel-natural gas mode had higher combustion noise but became similar in combustion noise characteristics with the addition of hydrogen. Regarding combustion duration, the diesel engine was reported to have a shorter combustion duration, especially at low and medium loads, compared to the dual-fuel diesel-natural gas mode. When hydrogen was added to the dual-fuel mixture with higher combustion duration than the conventional diesel engine, the combustion duration slightly decreased due to the combustible properties, rapid combustion characteristics, and wide combustion range of hydrogen. It was mentioned that there was not much difference in ignition delay between the traditional diesel engine and the dual-fuel diesel-natural gas mode at low loads, but this difference increased towards high loads. This was explained by the fact that at low loads, the premixed gas fuel ratio was very low, and therefore, no significant difference was observed with the diesel engine. At approximately 70% load, where a portion of the premixed mixture consisted of gas fuel, it was stated that the oxygen concentration decreased and the ignition delay time increased, but the addition of hydrogen did not significantly affect this time. The changes in the dual-fuel mode were reported to be lower compared to the conventional diesel engine. The COV_{IMEP} coefficient is the most important parameter used to determine combustion stability. After the improvement in combustion due to the enrichment of natural gas with hydrogen, the decrease in cycle-to-cycle variations and the fact that the COV_{IMEP} value did not exceed 10% were emphasized. In low-load regions, compared to the diesel engine, the dual-fuel mode with lower thermal efficiency was stated to lead to higher specific energy consumption, but with the addition of hydrogen to the premix, it was mentioned that this situation improved due to the improvement in gas mixture combustion.

The results in the literature have generally shown that using hydrogen as the sole fuel in a compression ignition (CI) engine is quite challenging. The results also emphasize that the combination of hydrogen with another alternative fuel in CI engines, ignited by pilot diesel fuel, would yield more significant results. It has been observed from the studies that natural gas can provide more consistent and preferable results when combined with hydrogen. The importance of hydrogen and natural gas becomes more significant for achieving lower fuel consumption, higher performance, and lower overall emissions. Various processes such as EGR, injection strategies, and water injection play an indispensable role in achieving these goals.

1.3 Hypothesis

Diesel engines have become indispensable on a global scale due to their high torque and efficient operation. In today's world, especially with the rapidly increasing global population, transportation has gained significant importance, and diesel engines play a crucial role. However, as pollutant emissions have reached levels that threaten our planet, national and international regulations have been introduced to restrict diesel engines. As a result, some engine manufacturers have discontinued diesel engine production, while others have taken various measures to address these restrictions. Despite the prejudice against diesel engines due to their high emissions, no one can deny their significant contribution to meeting global energy needs. The key here is to mitigate the harmful effects of diesel engines as much as possible, allowing them to continue their operations while addressing environmental concerns. Using clean alternative fuels suitable for the diesel engine cycle leads to a significant reduction in diesel engine emissions. Clean alternative fuels, such as natural gas and hydrogen, should be given top priority. For compression ignition (CI) engines, a fuel with automatic ignition capability is required to provide ignition. Within the broad operating range of an engine, there is no fuel other than diesel fuels with the automatic ignition feature. Therefore, in CI engines, diesel fuel is used for ignition. The most direct approach here is to minimize the contribution of diesel fuel to the combustion process and allow alternative fuels to be the primary source of power. Diesel fuel should become a mere ignition source, and the main power should be generated by alternative fuels. Globally, vehicles and machinery that require high power (commercial ships, trucks, lorries, and agricultural equipment) also require high torque. To meet this need, engines with high fuel efficiency and torque values, like CI engines, should be used.

The primary scientific contribution of this thesis work is to provide clear answers to the questions of the permissible limits for the use of natural gas and hydrogen as alternative fuels in partial loads for compression ignition (CI) engines and how they affect performance and emission values. It aims to provide insights into the effects of EGR, water injection, and pilot diesel fuel injection strategies on diesel/natural gas/hydrogen combustion. The current study has demonstrated that by incorporating hydrogen into the combustion with constant fuel input energy, higher performance and lower overall emissions can be achieved. Furthermore, by introducing hydrogen as an

additional energy input into the combustion process, the goal of achieving higher performance and lower unit power per emissions has been realized. The dissertation will be a valuable and original resource for those interested in research on hydrogen, natural gas, or hydrogen-enriched natural gas fuels in CI engines.

2. FUELS AND COMBUSTION IN THE DIESEL ENGINES

In diesel engines, pressure and temperature of the air in cylinders increase due to the piston's movement through TDC from BDC. Combustion is initiated by injecting diesel liquid hydrocarbon fuel into the heated air through injectors. The self-ignition property of the fuel leads to the ignition of the mixture. To mathematically express this combustion process in thermodynamic terms, it is necessary to formulate the event known as the diesel cycle. To quantify the energy released as a result of this cycle, specific engine parameters are required. Furthermore, combustion is a chemical process, and each fuel has different thermodynamic properties. Not all fuels are suitable for diesel engines due to differences in their thermodynamic characteristics. Therefore, it is essential to thoroughly analyze both the fuel and the cycle to derive meaningful engine parameters. In this section, diesel cycle types, engine performance parameters, phases and chemistry of combustion events, combustion technologies used in diesel engines, alternative fuels compatible with the diesel engine cycle, the formation of polluting emissions resulting from diesel engine combustion, and some methods used to reduce these emissions will be discussed.

2.1 Diesel Engine Cycles

Diesel engines are known as compression-ignition internal combustion engines. In these engines, the air drawn into the cylinder is compressed, reaching high temperatures. Diesel fuel self-ignites due to the high temperature and pressure in the cylinder. Therefore, there is no need for an external ignition source, such as a spark plug, as is the case in gasoline engines. The downward motion of the piston is transformed into rotary motion that drives the engine's crankshaft through the piston pin and crank pin bearings.

In four-stroke diesel engines, fuel is efficiently injected into the cylinder using fuel pumps and injectors to ensure optimal combustion. This process involves increasing the fuel pressure during injection, which helps in better fuel atomization. Diesel engines operate through a series of synchronized steps in which the crankshaft moves

in a specific timing to generate power. This operating cycle consists of the following stages sequentially:

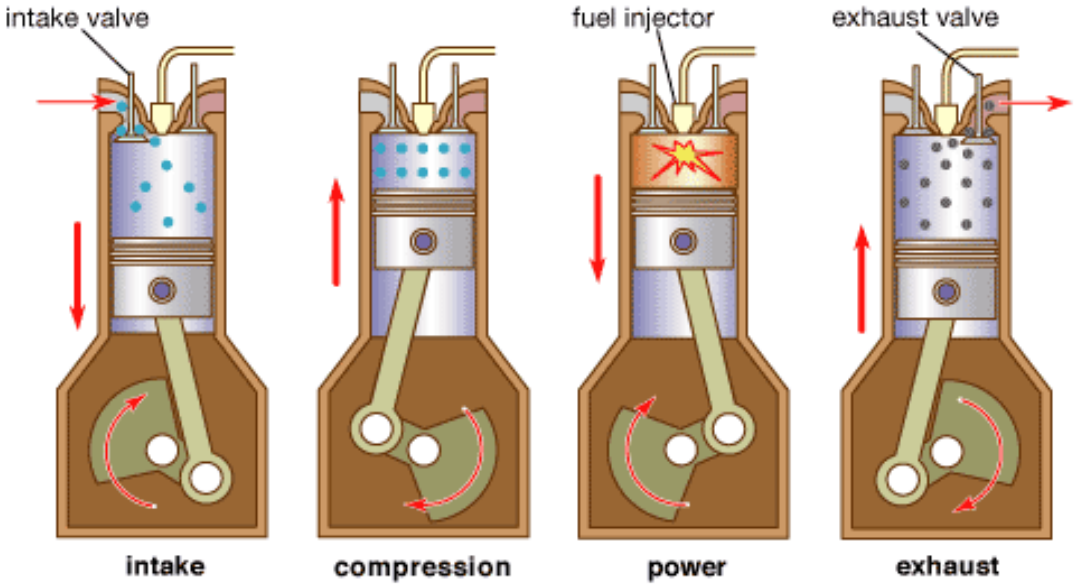

Figure 2.1 : Diesel engine operating diagram [65].

Intake Stroke: During this stage, the intake valve on the cylinder head is open, and the piston moves downward. As the piston moves downward, air from the intake manifold is drawn into the cylinder.

Compression Stroke: In this phase, the piston begins to move upward. The piston compresses the air that has been drawn into the cylinder. The compressed air can reach temperatures of up to 900 °C, depending on the type of engine. Both the intake and exhaust valves are closed at this point. As the cycle approaches its end, the diesel fuel, typically having an auto-ignition temperature ranging from 320 to 360 °C, is injected into the cylinder with the help of injectors.

Ignition and Combustion Stroke: This stage is where the actual work is done. Fuel particles spontaneously ignite when mixed with the very hot compressed air, causing an explosion in the cylinder. This explosion rapidly forces the piston downward. During the explosion, the internal pressure can rise up to 180 bar, depending on the engine type, and the temperature can vary from 2000 to 2500 °C.

Exhaust Stroke: This stage begins with the opening of the exhaust valve, and the gases produced by the combustion inside the cylinder start escaping into the exhaust manifold. As the piston moves upward, it pushes the gases in the cylinder toward the manifold. The schematic of all these processes is shown in Figure 2.1.

The working principle (cycle) of a diesel engine has been mathematically modeled based on thermodynamic principles. However, in order to make practical calculations easier, an ideal (theoretical) cycle model is created by making certain assumptions. In the ideal cycle, intake and exhaust losses, pumping losses, and heat losses are neglected.

2.1.1 Real (actual) cycle

Real cycles can present challenges in thermodynamic calculations. Idealized models, such as the Otto and Diesel cycles, provide a simplified framework for analysis. However, real-world systems often involve complexities such as heat losses, friction, and non-ideal behaviors of gases. In theoretical systems, it is assumed that heat is given at constant volume and/or constant pressure. However, in reality, the combustion process takes place over a very short period. During this short time frame, the piston continues to move, and it moves away from the point where maximum pressure should occur. This affects power generation and efficiency negatively.

Ideal air cycles do not cover any combustion models. Performing the real cycle models to examine the events occurring in diesel engines is very difficult and laborious and takes a rather time to produce the realistic results. However, studying the ideal air cycle with simple assumptions gives fast but acceptable approximate values. Adding some suitable assumptions into the mathematical model of an ideal air cycle, produces also more satisfactory results. The differences between ideal and real cycles are indicated in the table below (Table 2.1).

Table 2.1 : Comparison of ideal and real diesel cycle.

	Ideal Cycle	Real Cycle
Working Fluid	* Only air through the whole cycle	Air flows in the compressor only; fuel is added to the flow in the combustor
Specific Heats	Assumed constant	Vary with the temperature variation
Heat Addition	* Assumed at constant pressure	* Pressure drop occurs across the combustor due the friction
	* Assumed from an external source	* Fuel is physically added to the flow, combustion efficiency is not 100%
Inlet Pressure	Equals to the ambient pressure	Losses in the inlet ducts reduce the value of the pressure at the compressor inlet
Compression and Expansion	Assumed reversible processes	Real processes are irreversible with isentropic efficiency less than 100%

The assumptions of the ideal cycle provide convenience for thermodynamic calculations, and the results obtained are often very close to real results. Regarding the losses compared to the ideal cycle, approximately 12% are due to heat losses, 2% are due to exhaust losses, and 6% result from valve opening and closing timings.

2.1.2 Ideal cycles

Two types of ideal cycles have been defined: the Diesel cycle, in which heat addition occurs at constant pressure, and the Seilinger (dual) cycle, in which heat addition first occurs at constant volume and then at constant pressure.

2.1.2.1 Diesel cycle

The Diesel cycle assumes that the working fluid in the cycle is air. It assumes that the air taken into the cylinders is compressed reversibly and adiabatically (isentropically) and that when the piston reaches the top dead center (TDC), there is heat addition at constant pressure. Similarly, it assumes that the expansion stroke is reversible and adiabatic and that there is heat rejection at constant volume during the exhaust process. In reversible and adiabatic processes, the entropy (s) remains constant. Figure 2.2 shows the P-V (Pressure-Volume) and T-S (Temperature-Entropy) diagrams for the Diesel cycle.

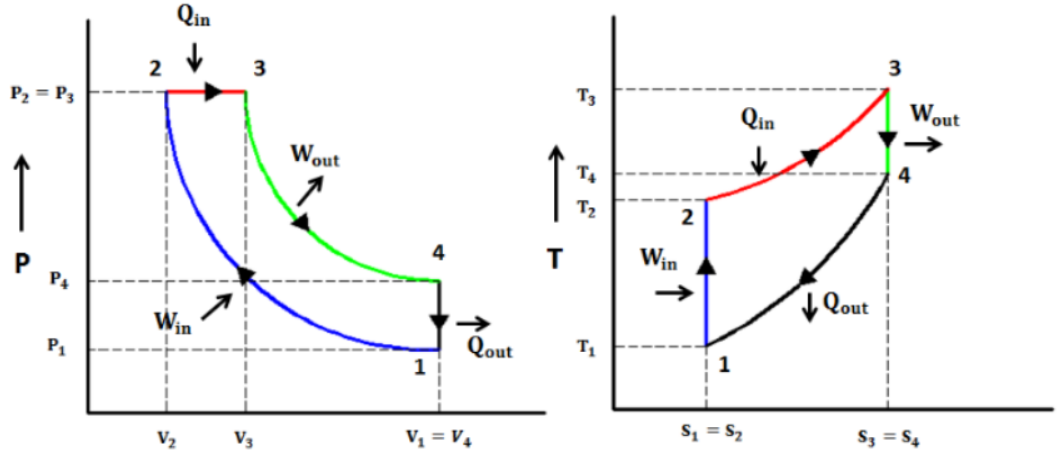

Figure 2.2 : P-V and T-S diagram for ideal diesel cycle.

The thermodynamic relationships for these processes are provided below. For isentropic process in the range 1-2 (Equation 2.1):

$$P_1.V_1^k = P_2.V_2^k = c \qquad (2.1)$$

equality is ensured. Here, k is known as the isentropic index. The equation for the exponent k is as follows (Equation 2.2):

$$k = \frac{c_p}{c_v} \tag{2.2}$$

The specific heat at constant pressure, denoted as c_p, and the specific heat at constant volume, denoted as c_v, are here. In reality, as temperature changes, the value of k also changes. As the temperature increases, k decreases. Point 1 represents the position of the piston in BDC, while point 2 represents its position in TDC. The ratio of the volume that the cylinder possesses between these two positions is equal to the compression ratio (ε) value (Equation 2.3).

$$\varepsilon = \frac{V_1}{V_2} \tag{2.3}$$

Therefore;

$$\left(\frac{V_1}{V_2}\right)^k = \varepsilon^k = \frac{P_2}{P_1} \tag{2.4}$$

obtained. For points 1 and 2 from the ideal gas equation:

$$\frac{P_1 . V_1}{m_1 . R . T_1} = \frac{P_2 . V_2}{m_2 . R . T_2} \tag{2.5}$$

The relation is obtained. Where $m_1 = m_2$ (since the derivation of mass by time is zero), the final version of the expression is as follows (Equation 2.6):

$$\frac{P_1 . V_1}{T_1} = \frac{P_2 . V_2}{T_2} => \frac{V_1}{V_2} = \frac{P_2 . T_1}{P_1 . T_2} => \varepsilon = \varepsilon^k . \frac{T_1}{T_2} => \frac{T_1}{T_2} = \varepsilon^{1-k} \tag{2.6}$$

The ideal gas equation for the heat input process range at constant pressure 2 – 3 (Equation 2.7):

$$\frac{P_2 . V_2}{m_2 . R . T_2} = \frac{P_3 . V_3}{m_3 . R . T_3} \tag{2.7}$$

Since $P_2 = P_3$ and $m_2 = m_3$ (no mass loss), the final version of the expression is as follows (Equation 2.8):

$$\frac{V_2}{T_2} = \frac{V_3}{T_3} => \frac{T_3}{T_2} = \frac{V_3}{V_2} = \rho \quad (2.8)$$

Here, ρ is referred to as the pre-compression ratio. In addition, the heat entering the system is determined as follows (Equation 2.9):

$$Q_{2,3} = m.c_p.\Delta T = m.c_p.(T_3 - T_2) \quad (2.9)$$

For the isentropic process in the range 3 – 4 (Equation 2.10):

$$P_3.V_3^k = P_4.V_4^k = c = \left(\frac{V_3}{V_4}\right)^k = \frac{P_4}{P_3} \quad (2.10)$$

Similarly, if the ideal gas equation is written for points 3 and 4:

$$\frac{P_3.V_3}{T_3} = \frac{P_4.V_4}{T_4} => \frac{V_3}{V_4} = \frac{P_4.T_3}{P_3.T_4} => \frac{V_3}{V_4} = \left(\frac{V_3}{V_4}\right)^k.\frac{T_3}{T_4} => \left(\frac{V_3}{V_4}\right)^{1-k} = \frac{T_3}{T_4} \quad (2.11)$$

The value of ρ was obtained previously with equation (2.8).

$$\frac{V_3}{V_2} = \rho => V_3 = \rho.V_2 \quad (2.12)$$

When the equation is rearranged for ρ and the equation $V_4 = V_1$ is used;

$$\left(\frac{\rho.V_2}{V_4}\right)^{1-k} = \frac{T_3}{T_4} = \left(\frac{\rho.V_2}{V_1}\right)^{1-k} = \left(\frac{\rho}{\varepsilon}\right)^{1-k} = \frac{T_3}{T_4} \quad (2.13)$$

If the ideal gas equation is rewritten for the 4 – 1 constant volume heat release process range:

$$\frac{P_4.V_4}{m_4.R.T_4} = \frac{P_1.V_1}{m_1.R.T_1} \quad (2.14)$$

Where $V_4 = V_1$ and $m_4 = m_1$ (since the derivation of mass by time is zero), the final version of the expression is as follows:

$$\frac{P_4}{P_1} = \frac{T_4}{T_1} \quad (2.15)$$

The magnitude of the heat released from the system is found by the equation below.

$$Q_{4,1} = m.c_v.\Delta T = m.c_v.(T_4 - T_1) \tag{2.16}$$

Thermal efficiency is the ratio of the net heat in the system to the heat entering the system. If the following equations are followed step by step by substituting the previously obtained data (Equation 2.17-2.20):

$$\eta_{th} = \frac{Q_{net}}{Q_{inlet}} = \frac{Q_{2,3} - Q_{4,1}}{Q_{2,3}} = \frac{m.c_p.(T_3 - T_2) - m.c_v.(T_4 - T_1)}{m.c_p.(T_3 - T_2)} \tag{2.17}$$

$$\eta_{th} = 1 - \frac{(T_4 - T_1)}{k.(T_3 - T_2)} = 1 - \frac{T_2.\left(\frac{T_4}{T_2} - \frac{T_1}{T_2}\right)}{k.T_2.\left(\frac{T_3}{T_2} - 1\right)} \tag{2.18}$$

$$\eta_{th} = 1 - \frac{\left(\frac{T_4}{T_2} - \varepsilon^{1-k}\right)}{k.(\rho - 1)} = 1 - \frac{\left(\frac{T_4}{T_3} x \frac{T_3}{T_2} - \varepsilon^{1-k}\right)}{k.(\rho - 1)} = 1 - \frac{\left(\left(\frac{\rho}{\varepsilon}\right)^{k-1}.\rho - \varepsilon^{1-k}\right)}{k.(\rho - 1)} \tag{2.19}$$

Thermal efficiency expression in the diesel cycle will be obtained:

$$\eta_{th} = 1 - \frac{1}{\varepsilon^{k-1}}.\frac{(\rho^k - 1)}{k.(\rho - 1)} \tag{2.20}$$

2.1.2.2 Seilinger (dual) cycle

In the Seilinger cycle, the working fluid is assumed to be air. It is assumed that the air taken into the cylinders is compressed reversibly and adiabatically (isentropically), and there is heat input at a constant volume and pressure to the system when the piston reaches TDC. Similarly, it is stated that the expansion stroke is reversible and adiabatic, with heat output at a constant volume during the exhaust process. The difference from the Diesel cycle is the presence of heat input at constant volume in the 2-3 process. P-V and T-S diagrams for the Seilinger cycle are given in Figure 2.3. Similar thermodynamic expressions are also valid for this cycle. Below, some of the expressions are shown (Equations 2.21-2.36).

The equations obtained earlier are valid for the isentropic process in the 1-2 range in the Diesel cycle.

$$\frac{T_1}{T_2} = \varepsilon^{1-k} \tag{2.21}$$

The ideal gas equation between points 2 and 3 for the process range of 2 – 3 constant volume heat input:

$$\frac{P_2.V_2}{m_2.R.T_2} = \frac{P_3.V_3}{m_3.R.T_3} \tag{2.22}$$

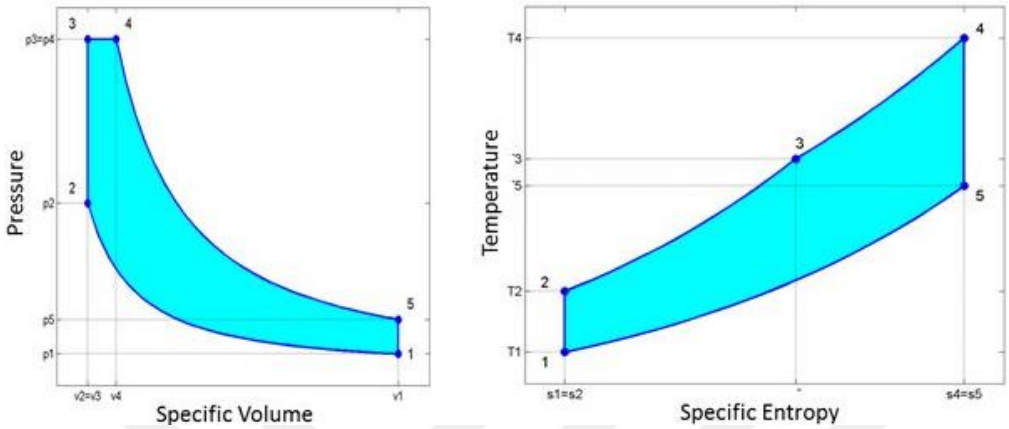

Figure 2.3 : P-V and T-S diagram for ideal seilinger cycle.

Where $V_2 = V_3$ and $m_2 = m_3$ (since the derivation of mass by time is zero), the final version of the expression is as follows:

$$\frac{P_2}{P_3} = \frac{T_2}{T_3} => \frac{P_3}{P_2} = \frac{T_3}{T_2} = \beta \tag{2.23}$$

Here β is called the pressure increase rate. Additionally, the heat entering the system is found as follows:

$$Q_{2,3} = m.c_v.\Delta T = m.c_v.(T_3 - T_2) \tag{2.24}$$

For the process range of 3 – 4 constant pressure heat input: Since $P_3 = P_4$ and $m_3 = m_4$ (no mass loss), when the conversions in the diesel cycle are applied, the final version of the expression is as follows:

$$\frac{T_4}{T_3} = \frac{V_4}{V_3} = \rho \tag{2.25}$$

Additionally, the heat entering the system is found as follows:

$$Q_{3,4} = m.c_p.\Delta T = m.c_p.(T_4 - T_3) \tag{2.26}$$

When the transformations made in the diesel cycle are applied in the isentropic process in the range 4 - 5, the following equations are obtained (Equations 2.27-2.30):

$$P_4.V_4^k = P_5.V_5^k = \left(\frac{V_4}{V_5}\right)^k = \frac{P_5}{P_4} \tag{2.27}$$

$$\frac{P_4.V_4}{T_4} = \frac{P_5.V_5}{T_5} => \frac{V_4}{V_5} = \frac{P_5.T_4}{P_4.T_5} => \frac{V_4}{V_5} = \left(\frac{V_4}{V_5}\right)^k . \frac{T_4}{T_5} => \left(\frac{V_4}{V_5}\right)^{1-k} = \frac{T_4}{T_5} \tag{2.28}$$

$$\frac{V_4}{V_3} = \rho => V_4 = \rho.V_3 \tag{2.29}$$

$$\left(\frac{\rho.V_3}{V_5}\right)^{1-k} = \frac{T_4}{T_5} = \left(\frac{\rho.V_2}{V_1}\right)^{1-k} = \left(\frac{\rho}{\varepsilon}\right)^{1-k} \tag{2.30}$$

Ideal gas equation for the process range 5 – 1 constant volume heat release:

$$\frac{P_5.V_5}{m_5.R.T_5} = \frac{P_1.V_1}{m_1.R.T_1} \tag{2.31}$$

Since $V_5 = V_1$ and $m_5 = m_1$ (no mass loss), the final version of the expression is as follows:

$$\frac{P_5}{P_1} = \frac{T_5}{T_1} \tag{2.32}$$

The magnitude of the heat released from the system is found by the equation below (Equation 2.33).

$$Q_{5,1} = m.c_v.\Delta T = m.c_v.(T_5 - T_1) \tag{2.33}$$

Thermal efficiency is the ratio of the net heat in the system to the heat entering the system. By using the previously obtained equations, the thermal efficiency expression for the Seilinger cycle is obtained (Equation 2.34-2.36). As seen from equation (2.36), thermal efficiency has higher value with increasing compression ratio. Thus, CI engines operates than SI engines by higher thermal efficiency.

$$\eta_{th} = \frac{Q_{2,3} + Q_{3,4} - Q_{5,1}}{Q_{2,3} + Q_{3,4}} = \frac{m.c_v.(T_3 - T_2) + m.c_p.(T_4 - T_3) - m.c_v.(T_5 - T_1)}{m.c_v.(T_3 - T_2) + m.c_p.(T_4 - T_3)} \tag{2.34}$$

$$\eta_{th} = 1 - \frac{c_v.(T_5 - T_1)}{c_v.(T_3 - T_2) + c_p.(T_4 - T_3)}$$

$$= 1 - \frac{c_v.T_2.\left(\frac{T_5}{T_2} - \frac{T_1}{T_2}\right)}{c_v.T_2.\left(\frac{T_3}{T_2} - 1 + k.\frac{T_4}{T_2} - k.\frac{T_3}{T_2}\right)} \quad (2.35)$$

$$\eta_{th} = 1 - \frac{1}{\varepsilon^{k-1}}.\frac{\left(\rho^k.\beta - 1\right)}{(\rho - 1) + k.\rho.(\beta - 1)} \quad (2.36)$$

2.2 Engine Performance Parameters

Each of the engine parameters is of great importance, as they provide crucial information about engines. Understanding the meaning of each parameter and how to calculate them is essential. In the previous section, we derived some thermodynamic expressions for ideal Diesel cycles. However, the values obtained after the cycle in the engine are smaller than the values obtained during the cycle. This decrease occurs due to reasons such as friction between engine components, heat, and combustion losses. The values obtained during the cycle are called indicated values, while the values obtained at the engine output are referred to as effective values.

2.2.1 Power

Power is defined as work done per unit time. In a diesel engine, work is the area under the p-V diagram (Equation 2.37).

$$W = \oint p.dV \quad (2.37)$$

Specific work and volume per unit mass:

$$w = \frac{W}{m} \quad \& \quad v = \frac{V}{m} \quad (2.38)$$

If the specific values are written in their place in the equation:

$$w = \oint p.dv \quad (2.39)$$

The w value here is the indicated value. There are differences between indicated and effective quantities due to friction.

$$w_i = w_e + w_f \tag{2.40}$$

Here w_i is considered as indicated work, w_e as effective work and w_f as losses due to friction. From the above integral, the dv differential emerges as V_H stroke volume and the equation is:

$$w = p.V_H \tag{2.41}$$

While +W in the graph indicates positive work, –W indicates negative work due to pumping losses.

The sum of these two works is the indicated work, which means the net work in the cylinder (Figure 2.4).

$$p_{mi} = \frac{w_i}{V_H} \tag{2.42}$$

Therefore, the ratio of the indicated work to the stroke volume provides the average indicated pressure.

To convert to power, the engine speed and the fact that a four-stroke engine's crankshaft completes one cycle every two revolutions should also be taken into account. Expression of power:

$$P_i = \frac{p_{mi}.V_H.N}{60.i} \tag{2.43}$$

Here, the value of "i" is taken as 2 for four-stroke engines. "N" represents the engine speed in RPM (revolutions per minute), and "P_i" indicates the indicated power.

By subtracting friction losses, effective values are obtained. The equation mentioned above can include friction losses as well.

$$P_f = \frac{p_{mf}.V_H.N}{60.i} \tag{2.44}$$

"P_f" represents friction power, and "p_{mf}" denotes the average friction pressure. With these two values obtained, the transition to effective power is made.

$$P_e = P_i - P_f \tag{2.45}$$

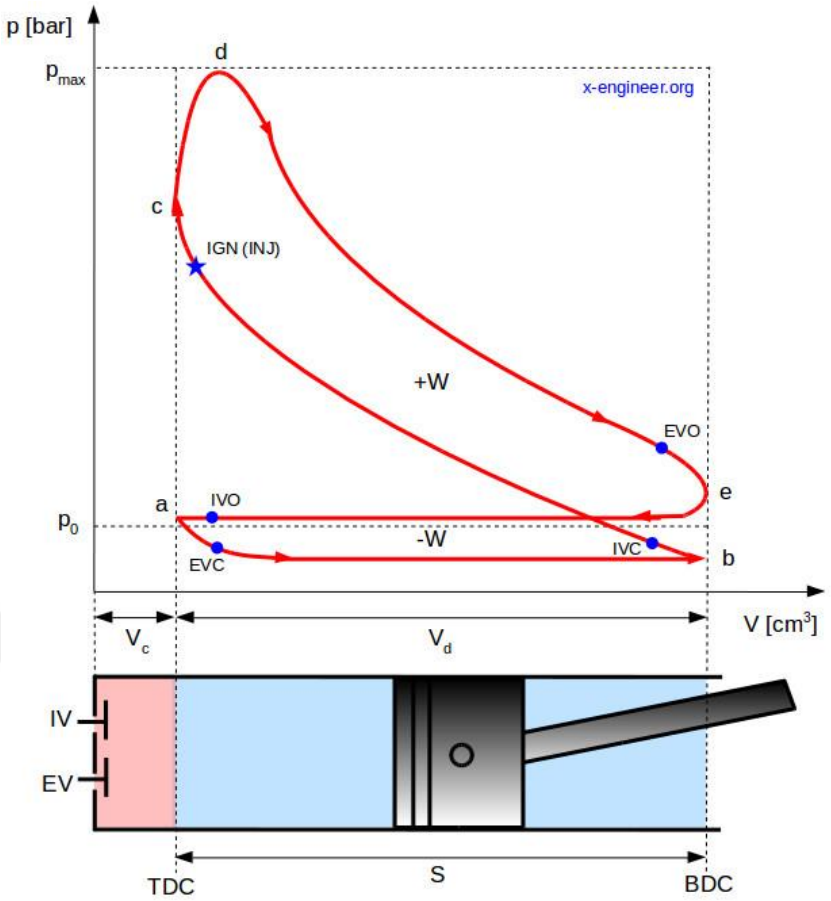

Figure 2.4 : Indicator (p-V) diagram for diesel engines.

2.2.2 Efficiencies

Combustion efficiency is the ratio of the energy released during combustion to the energy possessed by the fuel entering the cylinders (Equation 2.46).

$$\eta_c = \frac{w_i}{m_f . H_u} \tag{2.46}$$

H_u is the lower heating value of the fuel (in kJ/kg), and m_f represents the amount of fuel entering the cylinder. The symbol η_c represents the combustion efficiency.

The thermal efficiency is the ratio of the difference between the energy input to the system and the energy output from the system to the energy input into the system (Equation 2.47). It measures how effectively the system converts input energy into useful work or output.

$$\eta_{th} = \frac{Q_{in} - Q_{out}}{Q_{in}} = 1 - \frac{Q_{out}}{Q_{in}} \tag{2.47}$$

Mechanical efficiency is the ratio of the power extracted from the crankshaft to the power generated as a result of combustion (Equation 2.48). It measures how efficiently the engine converts the energy released during combustion into useful mechanical work.

$$\eta_m = \frac{P_e}{P_i} = \frac{P_i - P_f}{P_i} = 1 - \frac{P_f}{P_i} \tag{2.48}$$

The mechanical efficiency value typically ranges between 75% and 95%. As the engine speed increases, friction-related losses tend to increase, which can lead to a decrease in mechanical efficiency. This relationship between engine speed and mechanical efficiency is an important consideration in engine design and performance analysis.

Effective efficiency is the ratio of the energy measured from the engine with the help of a dynamo (generator) to the energy possessed by the fuel entering the engine (Equation 2.49).

$$\eta_e = \frac{w_e}{m_f . H_u} = \frac{P_e}{\dot{m}_f . H_u} = \frac{3600}{H_u . b_e} \tag{2.49}$$

Here b_e is the specific fuel consumption in g/kW.h. H_u is the lower calorific value of the fuel. And its unit is taken as kJ/kg.

Volumetric efficiency is the ratio of the actual amount of air taken into the cylinders to the theoretically required amount of air (Equation 2.50). It measures how effectively the engine's induction system fills the cylinders with air. A higher volumetric efficiency indicates that the engine is better at drawing in air, which can lead to improved performance.

$$\eta_v = \frac{V_a}{V_H + V_C} \tag{2.50}$$

V_a represents the amount of air drawn into the cylinders, V_H denotes the total stroke volume, and V_C represents the total clearance volume. In naturally aspirated engines, the volumetric efficiency value is typically less than one, indicating that the engine cannot completely fill the cylinders with air during the intake stroke. However, in

supercharged or turbocharged engines, the overall volumetric efficiency can be greater than one, indicating that the engine is capable of filling the cylinders with more air than their actual volume, thanks to forced induction. This leads to increased power output in such engines.

2.2.3 Air excess ratio

The amount of air needed for the complete combustion of fuel is called the stoichiometric air quantity. The ratio of the actual amount of air taken into the combustion chamber to the air quantity at stoichiometric conditions is referred to as the air-fuel ratio, denoted by the symbol λ (lambda) (Equation 2.51). Conversely, the reciprocal of the air-fuel ratio is known as the equivalence ratio, symbolized by ϕ (phi).

$$\lambda = \frac{\left(\frac{m_a}{m_f}\right)_r}{\left(\frac{m_a}{m_f}\right)_{st}} = \frac{1}{\phi} \tag{2.51}$$

- Fuel rich mixture for $\lambda<1$ or $\phi>1$
- Stoichiometric mixture for $\lambda= \phi =1$
- Fuel-lean mixture for $\lambda>1$ or $\phi<1$

Diesel engines generally operate in the lean mixture combustion region, especially at partial and medium loads. However, at full load conditions, the λ value can be less than one. When the λ value in diesel engines drops below 1.2, significant increases in soot emissions are observed. As the air-fuel ratio increases, combustion worsens due to reduced fuel density in the air, leading to decreased engine performance. Therefore, for diesel engine operating conditions, a λ value in the range of 1.2 to 2 is more suitable in terms of performance and emission values. For instance, in the Figure 2.5, values for a gasoline engine are shown.

It can be seen that the stoichiometric value is at a ratio of 14.7:1, and the maximum power is reached at a rich mixture of 12.6:1. The most efficient value, in terms of efficiency, is 15.4:1 in the lean mixture region. As observed, the air-fuel ratio plays a critical role in both performance and fuel consumption. The combustion speed is at its maximum around stoichiometric mixture, while it decreases in lean and rich mixture regions.

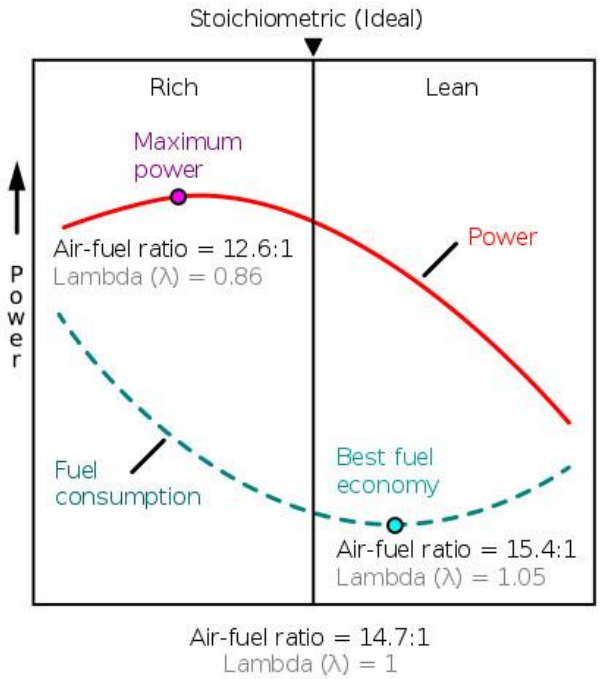

Figure 2.5 : Air excess ratio – power & BSFC graphic for a SI engine [66].

2.2.4 Compression ratio

The ratio of the volume the cylinder possesses when the piston is at the BDC (Bottom Dead Center) to the volume it possesses when the piston is at the TDC (Top Dead Center) is called the compression ratio. It is of utmost importance for engine performance values.

$$V_{BDC} = V_H + V_C \;\&\; V_{TDC} = V_{Total} \tag{2.52}$$

$$\varepsilon = \frac{V_{BDC}}{V_{TDC}} = \frac{V_H + V_C}{V_C} = 1 + \frac{V_H}{V_C} \tag{2.53}$$

In diesel engines, the compression ratio typically falls within the range of 14:1 to 22:1, while in gasoline engines, this value is in the range of 8:1 to 10:1. The compression ratio is particularly important, especially concerning thermal efficiency. When we examine the expression for thermal efficiency in diesel engines, it becomes evident that as the compression ratio (ε) increases, the thermal efficiency also increases.

$$\eta_t = 1 - \frac{1}{\varepsilon^{k-1}} \cdot \frac{\left(\rho^k . \beta - 1\right)}{(\rho - 1) + k.\rho.(\beta - 1)} \tag{2.54}$$

The most significant factor limiting the compression ratio in an engine is knocking, also known as engine knock. At very high compression ratios, the fuel begins to auto-

ignite in the hot air before the desired ignition time, leading to decreased engine performance. High compression ratios have allowed diesel engines to achieve high torque values. Diesel fuel needs a longer stroke length to form a homogeneous mixture with air and reach its self-ignition temperature. Time is required for mixture formation and the beginning of the combustion process. A longer stroke length results in a higher moment arm, which gives diesel engines their high torque characteristic [67].

2.3 Phases of Combustion

In diesel engines, combustion occurs in four stages. These are the ignition delay phase, premixed combustion phase, mixture-controlled combustion phase, and the post-combustion phase. The positions of these phases relative to the crank angle can be observed in the Figure 2.6.

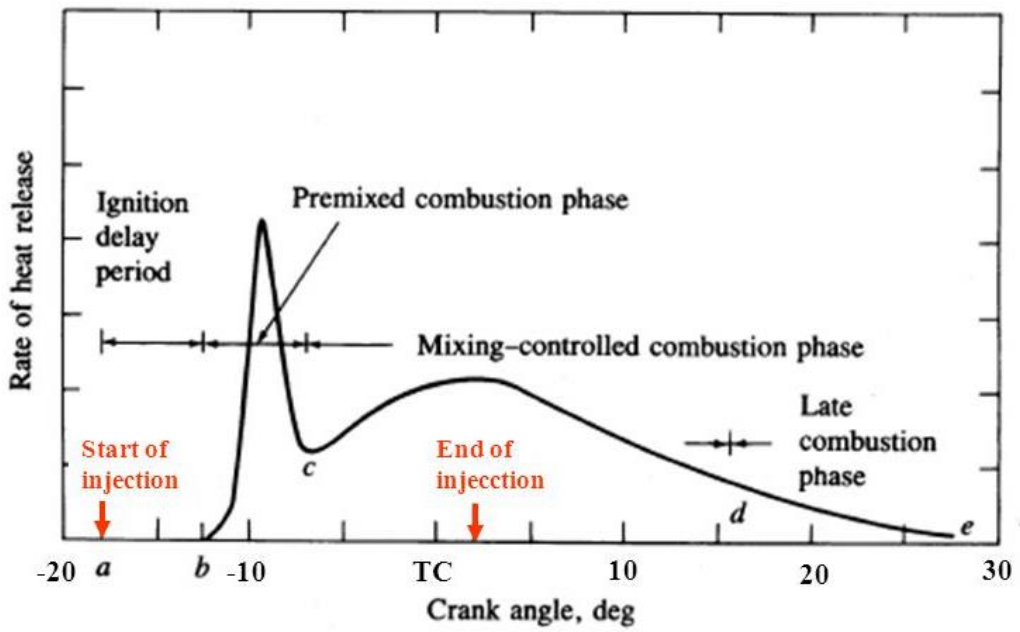

Figure 2.6 : The state of combustion phases depending on CA.

2.3.1 Ignition delay phase

The time interval between the injection of fuel into the combustion chamber and the start of combustion is called ignition delay. During the ignition delay period, the injected fuel mixes with air in the combustion chamber, creating an almost homogeneous mixture and becoming ready for combustion.

Ignition delay consists of both physical and chemical stages. The physical delay represents the time between fuel injection and the establishment of chemical reaction

conditions. During this stage, the fuel atomizes, vaporizes, and the mixture temperature increases. The chemical delay, on the other hand, refers to the time from the establishment of reaction conditions to the beginning of ignition. In this stage, the reaction starts slowly and accelerates until ignition takes place [67,68]. The ignition delay time is extremely important. As the delay increases, more fuel will accumulate in the cylinders as a result of injection. Excess fuel can lead to sudden explosions, resulting in high pressure and temperatures. High pressure can cause an increase in noise emissions and mechanical stresses on the engine structure. High temperatures can lead to increased NO_x emissions and thermal wear on engine materials. The ignition delay and the rate of pressure rise should be at appropriate values. Otherwise, it can lead to an increase in knocking tendencies [69]. After fuel injection begins, it will absorb heat from the surroundings to vaporize. For the vaporized fuel to have a tendency to ignite, certain chemical mechanisms need to occur. Fuel particles with the activation energy required for combustion will start to ignite. All of these factors indicate that there is a need for some time for fuel combustion. Naturally, it is desired that this process doesn't take too long or happen too quickly. Early ignition results in the maximum pressure occurring earlier than TDC (Top Dead Center), leading to deteriorated combustion and decreased engine performance.

Ignition delay is influenced by factors such as the air-fuel ratio, intake air temperature and pressure, and the physical and chemical properties of the fuel (vaporization heat, cetane number, surface tension, etc.). These factors can vary the ignition delay, and engine performance and emissions are sensitive to these variations [70]. Some empirical expressions have been developed to estimate the ignition delay time in diesel engines. Hardenberg proposed the equation 2.55 for ignition delay [71].

$$t_{ID} = (k_1 + k_2 . u_p) . \exp\left[E_A \left(\frac{1}{R.T} - \frac{1}{k_3}\right)\left(\frac{k_4}{P_{TDC} - k_5}\right)^{k_6}\right] \qquad (2.55)$$

For diesel engines, based on experimental data, the values k_1=0.36, k_2=0.22, k_3=17190, k_4=21.2, k_5=12.4, and k_6=0.63 are appropriate. In the equation, E_A represents the activation energy of the fuel, up represents the piston mean speed, and P_{TDC} represents the cylinder internal pressure at TDC (Top Dead Center). It's important to note that the activation energy of each fuel can be different, and even fuels with the same name can have different activation energies depending on their specific composition. For

instance, when we refer to diesel fuel, its ignition characteristics vary depending on the ratio of hydrocarbons in the composition. Cetane number is a parameter that best expresses the ignition characteristics of diesel fuels. Diesel fuels with a higher cetane number ignite more easily. Therefore, the activation energy is related to the cetane number. Hardenberg and others have proposed the equation 2.56 for the activation energy of the fuel [71]:

$$E_A = \frac{618840}{CN + 25} \tag{2.56}$$

Another empirical expression for estimating ignition delay was suggested by Wolfer.

$$t_{ID} = \frac{0.44e^{\left(\frac{4650}{T}\right)}}{P^{1.19}} \tag{2.57}$$

In the formula, T stands for temperature and P stands for pressure [68].

Another recommended equation for ignition delay time for atmospheric direct injection diesel engines is as follows (Equation 2.58).

$$t_{ID} = \frac{2.4}{\left(\frac{1}{\lambda}\right)^{0.2} . P^{1.02}} \exp\left(\frac{Ea}{R.T}\right) \tag{2.58}$$

In the equation where λ represents the air-fuel ratio, P represents the maximum cylinder pressure (kPa), T represents the average cylinder temperature (K), R represents the universal gas constant (8.31434 kJ/kmol.K), and Ea represents the activation energy for the fuel (kJ/kmol·K), the ignition delay time can be obtained from the expression in milliseconds (ms) [72].

2.3.2 Premixed combustion phase

During the ignition delay phase, some of the fuel that continues to be injected into the combustion chamber while the mixture is ready to ignite will also ignite as the ready-to-burn mixture ignites. The injection of fuel into the cylinder can continue during the second stage or be terminated before this stage is completed. After the controlled ignition delay period, the mixture burns very rapidly. This premixed combustion has a similar characteristic to spark-ignited (SI) engine combustion, where ignition is initiated by a spark plug.

The duration of the premixed combustion phase depends on the following factors:

- Ignition delay phase,
- Distribution of fuel in the combustion chamber,
- The amount of fuel injected during the ignition delay phase,
- The amount of fuel injected during the premixed combustion phase,

These factors are important factors affecting the duration of the premixed combustion phase [67,68].

2.3.3 Controlled combustion phase

This phase is also known as the diffusion-controlled combustion phase. After the premixed phase, as injection continues, the fuel continues to vaporize and mix with air due to the heat generated by the combustion during the premixed phase. Chemical reactions in this stage are extremely rapid, and the combustion process is controlled by the mixture ratio. As the piston moves from top dead center (TDC) to bottom dead center (BDC), swirls are created at the edges of the combustion chamber due to the gas pressure of the burned mixture. Under specific conditions, these swirls create turbulence and help in achieving a homogeneous mixture between fuel and air. The end of the main combustion phase marks the moment when the maximum temperature is reached in the combustion chamber.

The controlled combustion period depends on several factors, including [67,68]:

- Fuel droplet characteristics (average droplet diameter)
- Air motion
- Air-fuel ratio
- Degree of turbulence

2.3.4 Post-combustion phase

As combustion progresses, the pressure and temperature ahead of the flame decrease, and simultaneously, chemical reactions slow down. The conversion of unburned fuel toward the end of the process decreases significantly because the intermediate products formed due to oxygen deficiency during the main combustion phase oxidize during the post-combustion phase. Therefore, the post-combustion phase is particularly crucial for the oxidation of pre-existing carbon compounds.

2.4 Wiebe Function

Wiebe factor, also known as the Wiebe function, is an important parameter in the field of internal combustion engines, especially in explaining the combustion rate within a cylinder. The Wiebe factor is used to model the progression of the combustion process in an engine cylinder. It represents the relationship between the burned fuel volume and the crankshaft angle and helps us understand the pressure changes inside the cylinder and the work generated by the engine more effectively. In 1967, Wiebe proposed the following equation as a percentage of the burned fuel:

$$x_b = 1 - \exp\left[-a \cdot \left(\frac{\theta - \theta_0}{\Delta\theta}\right)^{m+1}\right] \quad (2.59)$$

In this equation:

- x_b represents the percentage of burned fuel mass.
- θ represents the instantaneous crank angle.
- θ_0 represents the crank angle at the start of combustion.
- $\Delta\theta$ represents the total crank angle over which combustion occurs.
- a and m are empirical coefficients.

For the constants *a* and *m,* Heywood suggests values of 6.908 and 2, respectively. These values are used to fit the Wiebe function to experimental data and may vary depending on the specific engine and operating conditions [67].

The double Wiebe function is another variation of the Wiebe function used in the field of internal combustion engines. It is applied as a method to approximate the measured heat characteristics of a diesel engine. In this context, two separate motion functions are defined: the first is used to model the peak of premixed combustion, while the second is used to model diffusion-controlled combustion. When the fuel distribution is known for both of these motion functions, the heat release from these two motion functions can be combined. The use of a double Wiebe function allows for a more accurate modeling of the combustion process in a diesel engine, taking into account both premixed and diffusion-controlled combustion. This can help in better understanding and optimizing the combustion characteristics and performance of the engine.

$$x_{bb} = \lambda.\left\{1 - \exp\left[-a_1.\left(\frac{\theta - \theta_0}{\Delta\theta_1}\right)^{m_1+1}\right]\right\} + (1-\lambda).\left\{1 - \exp\left[-a_2.\left(\frac{\theta - \theta_0}{\Delta\theta_2}\right)^{m_2+1}\right]\right\} \quad (2.60)$$

In the double Wiebe function equation, the terms with a subscript of 1 are related to the premixed combustion phase, while the terms with a subscript of 2 are related to the diffusion-controlled combustion phase. The weight factor λ helps combine these two phases to provide a more comprehensive model for the combustion process in a diesel engine, considering both premixed and diffusion-controlled combustion. For example, a study was conducted comparing the standard Wiebe and double Wiebe functions, and the effect of different m values was also investigated. The results of the study are shown in the Figure 2.7 below.

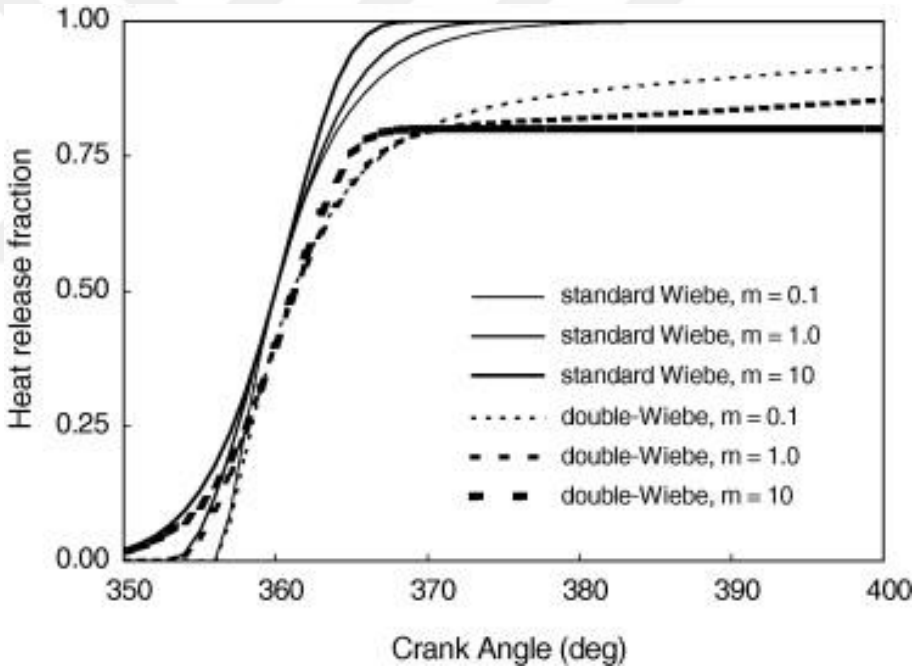

Figure 2.7 : Comparison of standard and double Wiebe functions for different m factors [73].

2.5 Diesel Engine Technologies

To reduce emissions from diesel engines, strategies have been developed to operate the engine at lower combustion temperatures. The aim of these strategies is to achieve efficient combustion in lean mixture regions while also obtaining low NO_x emissions as a result of lower temperatures. These combustion strategies differ from traditional diesel combustion in that they involve sending the fuel to the combustion chamber

well before ignition. This provides a longer time for the air-fuel mixture to form, allowing for combustion in leaner mixture limits. Additionally, the elimination of diffusion combustion leads to significant improvements in soot emissions. One disadvantage of these combustion technologies is that they have limited operating ranges and may not be suitable for engines that require high maneuverability. Some prominent types of these combustion technologies include Homogeneous Charge Compression Ignition (HCCI), Premixed Charged Compression Ignition (PCCI), and Reactivity Controlled Compression Ignition (RCCI), which is used in dual-fuel engines. These technologies aim to provide a balance between efficiency and emissions reduction in diesel engines.

2.5.1 HCCI engine

HCCI engines are a combined version of combustion technology used in gasoline and diesel engines. Like other internal combustion engine types, HCCI engines are built on a four-stroke working principle, which includes intake, compression, combustion-expansion, and exhaust strokes. In HCCI engines, during the intake stroke, the piston moves from top dead center to bottom dead center. During this movement, the intake valve is opened, allowing a homogeneous air-fuel mixture to fill the cylinder due to low cylinder pressure. When transitioning from the HCCI mode, a homogeneous air-fuel mixture can be prepared using port injection or early direct injection. When transitioning from CI mode to HCCI mode, early direct injection is used to create a homogeneous air-fuel mixture for achieving HCCI combustion.

The piston, at the end of the intake stroke, moves from bottom dead center to top dead center, compressing the homogeneous air-fuel mixture inside the cylinder. Toward the end of the compression stroke, the air-fuel mixture reaches suitable pressure and temperature values and spontaneously ignites, initiating the combustion process. Since the combustion process starts simultaneously at various points inside the cylinder, the combustion duration is shortened, leading to an increase in thermal efficiency. During the expansion stroke, the heat energy released as a result of combustion drives the piston from top dead center to bottom dead center. This means the conversion of chemical energy into mechanical energy. At the end of the expansion stroke, the piston moves from top dead center to bottom dead center to initiate the exhaust stroke, where it expels the combustion residues through the exhaust manifold.

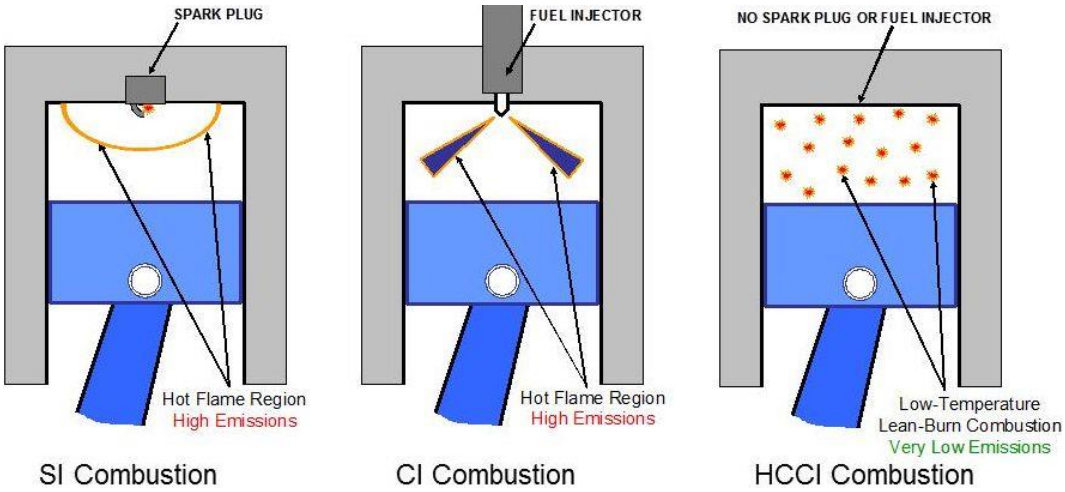

Figure 2.8 : Comparison of SI, CI and HCCI engines in terms of combustion characteristics [74].

HCCI engines offer advantages over conventional internal combustion engines, including simultaneous combustion and better thermal efficiency and emission performance. HCCI engines combine the advantages of spark-ignited (SI) and compression-ignited (CI) engines.

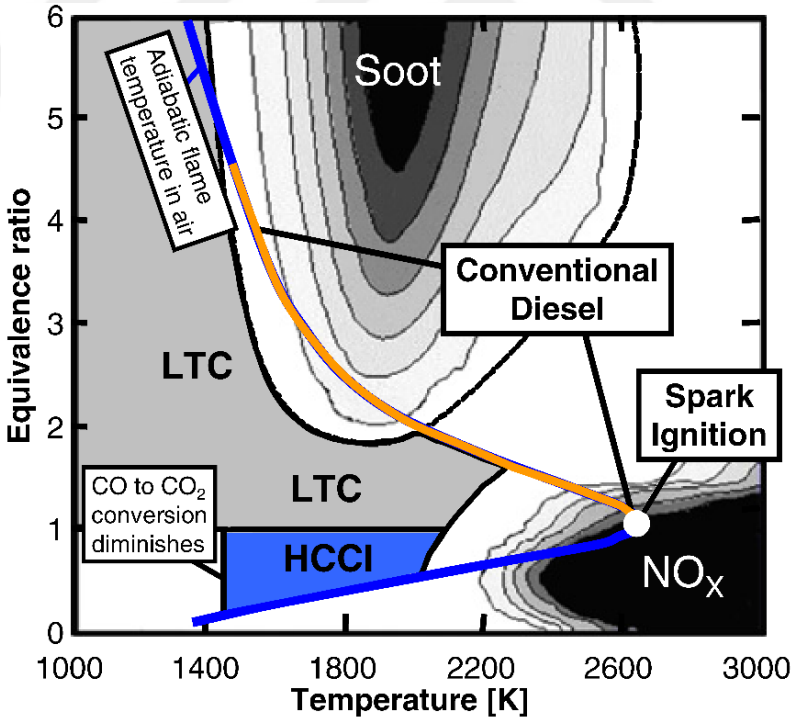

Figure 2.9 : The temperature and equivalence ratio range at which HCCI engines operate [75].

They have higher thermal efficiency compared to traditional gasoline (SI) and diesel (CI) engines, and they produce lower NO_x and soot emissions. Additionally, they offer the ability to simultaneously reduce NO_x and soot emissions, which is typically

challenging in conventional diesel engines. HCCI engines are well-suited for running on alternative fuels. Since the fuel and air mixture is premixed during the intake phase, it results in a homogenous charge inside the cylinder [76–78]. However, HCCI engines do have some disadvantages. For example, it is not possible to directly control the initiation of combustion, and their operating range is limited. Additionally, they face issues such as knocking at low loads and detonation at high loads, which can hinder their use in industrial applications [79,80]. Therefore, researchers are conducting studies to expand the operating range of HCCI engines and address issues like knocking at low loads and detonation at high loads. They are focusing on factors such as compression ratio, intake air temperature, exhaust gas recirculation (EGR), variable valve timing, alternative fuels, fuel injection strategies, and supercharging to achieve these goals [81–85].

2.5.2 PCCI engine

It is a combustion technology that stands for **P**remixed **C**harged **C**ompression **I**gnition. The goal here is to send the fuel into the cylinder earlier than in a conventional diesel engine to achieve homogeneous air-fuel mixture [86]. In HCCI engines, controlling ignition has been a challenge. In PCCI engines, to overcome this difficulty, a small amount of fuel is taken into the cylinders at a high advance, while a larger amount of fuel is injected into the cylinders later. This way, the ignition timing is controlled by the secondary injection [87–89].

Transition to the PCCI combustion mode can be achieved in a conventional diesel engine by introducing a high level of EGR (Exhaust Gas Recirculation) and increasing the injection advance. It is recommended to apply EGR to PCCI engines because in regions with homogeneous air-fuel mixtures, the high concentration of oxygen leads to increased NO_x emissions. This is especially prevalent in high-temperature regions (above 1800 K) that encompass burned gas regions, where the air-fuel mixture's air excess ratio is relatively high compared to other regions [43,90,91]. Compared to HCCI engines, PCCI engines produce higher levels of NO_x and soot emissions. The formation of soot is based on the oxidation of unburned and non-vaporized fuels when they come into contact with the burned gases. This oxidation primarily occurs in regions with rich fuel mixtures, especially in the fuel spray core. In PCCI engines, this phenomenon is more pronounced than in HCCI engines [92,93].

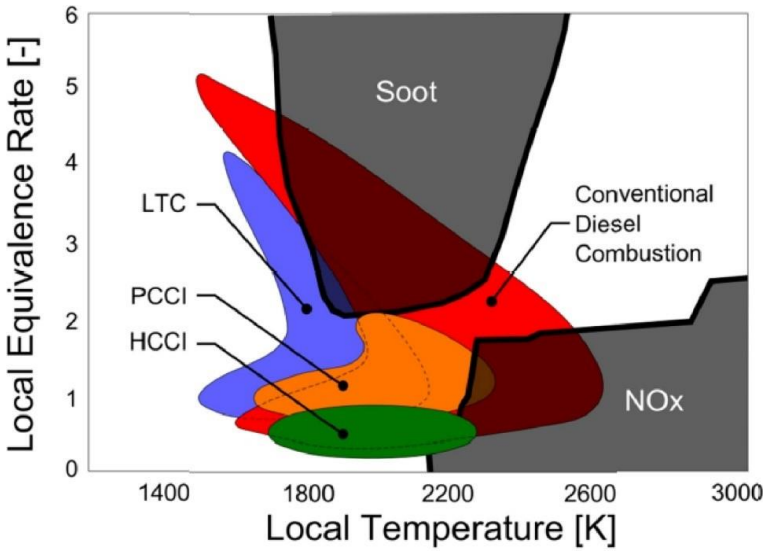

Figure 2.10 : Operating regions of PCCI and HCCI combustion in terms of NO_x and SOOT emissions [94].

As seen in the Figure 2.10, HCCI combustion is closer to NO_x and soot emission limits compared to PCCI combustion.

Table 2.2 : Basic combustion characteristics for diesel, HCCI and PCCI engines [95].

	Diesel Engine	HCCI Engine	PCCI Engine
Injection	Near the TDC	High advance	Near the TDC and High advance
Combustion Mode	Diffused	Premixed	Diffused + Premixed
Ignition	Auto ignition (Controlled by injection time)	Auto ignition (Controlled by Chemical Kinetics)	Auto ignition (Controlled by injection time)
Temperature	Relatively High	Relatively Low	Relatively Low
NO_x	High NO_x due to high temperature	Low NO_x due to low temperature	Low NO_x due to low temperature and EGR rate
SOOT	High SOOT due to diffusion combustion	Low SOOT due to homogeneous lean mixture	Low SOOT due to homogeneous lean mixture

In a diesel engine, combustion occurs in a stratified manner during the injection process, resulting in a combustion pattern known as diffusion combustion. In PCCI engines, combustion is more homogeneous within the combustion chamber due to the simultaneous occurrence of multiple points of ignition. It can be thought of as if there were a spark plug at each ignition point, similar to how combustion is initiated around a spark plug in gasoline engines. However, controlling these simultaneous ignitions, especially in high-load regions, is very challenging in PCCI engines. Therefore, just

like HCCI engines, the operating range of PCCI engines is very narrow. PCCI engines combine elements of both the HCCI combustion mode and the conventional diesel combustion mode.

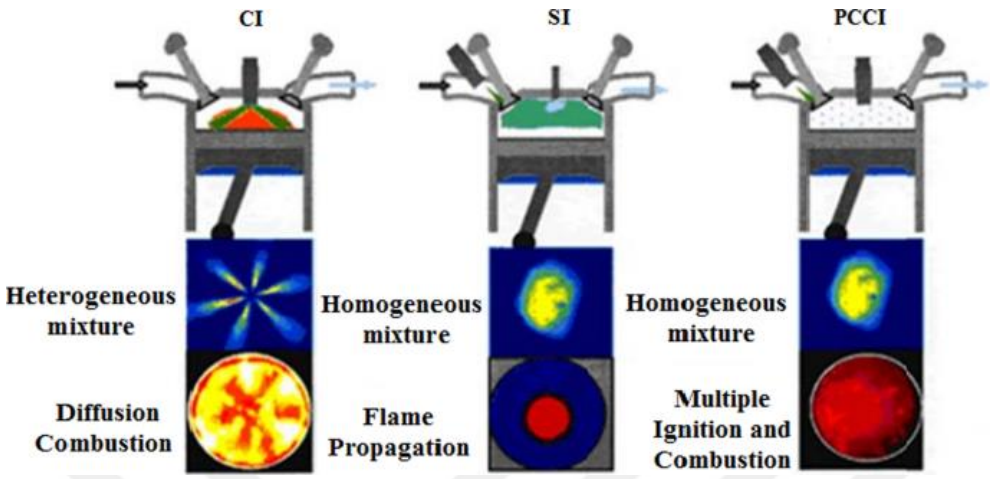

Figure 2.11 : Flame propagation for CI, SI and PCCI engines [94].

The partial premixing achieved by injecting a portion of the fuel with high advance is similar to HCCI engines. Sending a significant portion of the fuel to the cylinders with low advance is similar to diesel engine combustion. Having these two modes allows it to have low NO_x and soot emissions while also increasing the operating range compared to HCCI engines. This is because the flexibility of the second injection timing allows control of the combustion phase.

2.5.3 RCCI (dual fuel) engine

RCCI stands for **R**eactivity **C**ontrolled **C**ompression **I**gnition. Its operating principle is based on using different fuels with low and high reactivity. The high reactivity fuel is referred to as the primary fuel, while the low reactivity fuel is called the secondary fuel. The secondary fuel (low reactivity) is premixed with air in advance and this air-fuel mixture is introduced into the cylinder. Then, to initiate combustion, the primary fuel (high reactivity) is directly injected into the combustion chamber to enable the engine to operate. Typically, diesel or dimethyl ether is used as the high reactivity primary fuel, while gasoline, natural gas, ethanol, or methanol is used as the low reactivity secondary fuel. The secondary fuel is injected into the intake port with a low-pressure injector [96,97]. The secondary fuel should have the characteristics of easy vaporization but challenging ignition. If a high-reactivity fuel is chosen, early ignition tendencies occur inside the cylinder, and maximum pressure force is generated before the piston reaches TDC (Top Dead Center). On the other hand, the primary fuel

is desired to be highly reactive. When the fuel is injected (typically around 10°-20° CA BTDC), the ambient temperatures are around 500 K on average. In such an environment, the high-reactivity fuel that is sprayed first vaporizes and then ignites within the temperature range of its ignition limits. RCCI combustion exhibits lower NO_x and soot emissions compared to other LTC (**L**ow-**T**emperature **C**ombustion) strategies. It also provides higher thermal efficiency. However, one issue with RCCI is that, like other LTC methods, its operating range is limited, and during high load conditions, NO_x and soot emissions can significantly increase [98].

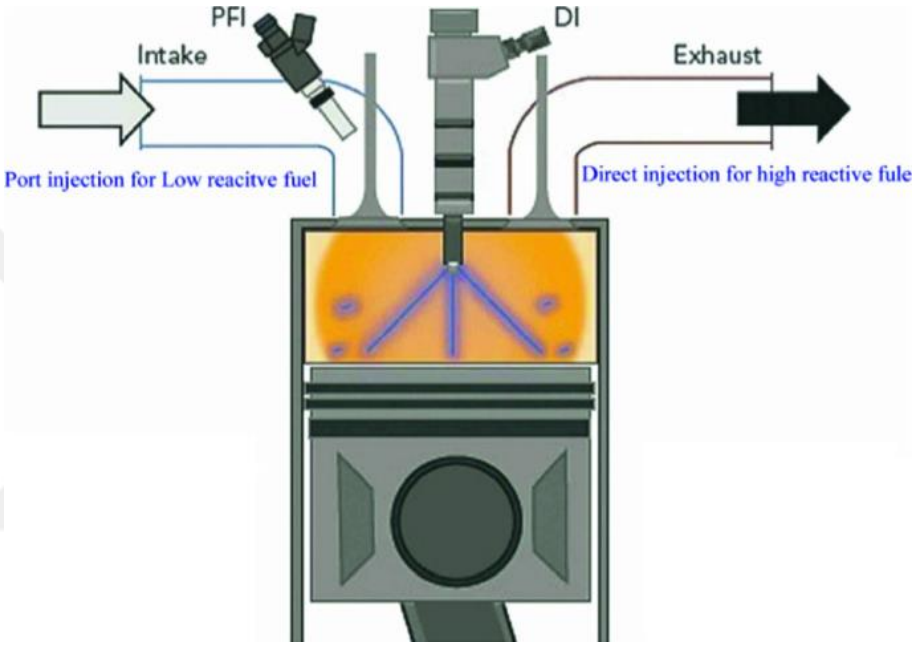

Figure 2.12 : Representation of RCCI combustion on the engine [99].

2.6 Alternative Fuels

In recent times, intensive research is ongoing regarding alternative fuels that can be used instead of diesel fuel in compression ignition (CI) engines. The primary focus of these studies is on alternative fuels with good combustion characteristics and low pollutant properties. Among the alternative fuels used in diesel engines, alcohol derivatives (such as methanol and ethanol) in liquid phase, biodiesel, and more recently, ammonia, have emerged as prominent choices. In the gaseous phase, natural gas, hydrogen, and biogas are among the options.

2.6.1 Liquid fuels

The most significant advantage of taking the fuel into the engine in liquid form is that it generally contains a higher amount of energy per unit volume compared to the gas

phase. Additionally, since it occupies less volume within the cylinder, it provides more positive results in terms of volumetric efficiency. The fuel introduced into the combustion chamber in the liquid phase will absorb heat from the environment to vaporize. The heat taken from the environment will partially reduce the increase in post-combustion temperatures. This situation leads to positive outcomes in terms of NO_x emissions.

2.6.1.1 Methanol

Methanol is a compound containing methyl alcohol and can be obtained through the distillation of fossil fuels such as wood or coal at high temperatures, the distillation of natural gas, or the synthesis of CO and H_2 in a catalytic environment. However, obtaining methanol from renewable sources may not be possible, making its use as an alternative fuel a temporary solution. Additionally, the current production of methanol is energy-intensive, meaning that the energy used for methanol production may exceed the energy obtained in the end. Methanol has a boiling point of 65.1°C and a freezing point of -97.6°C, and it can mix with water in any proportion. Therefore, methanol can be easily used in vehicles with minimal modifications. Despite having a high octane number, methanol has a very low cetane number. As a result, there may be some issues related to its use in diesel engines. Due to its low cetane number, high ignition temperature, and resistance to autoignition, methanol can pose some challenges in the combustion process when injected into the compressed air at the end of the compression stroke in a diesel engine. It can delay ignition and lead to knocking in a diesel engine [100,101]. However, methanol's resistance to autoignition allows for an increase in the compression ratio in Otto engines, making methanol more suitable for use in Otto engines. Therefore, the use of methanol in diesel engines often requires the use of spark plugs or blending with diesel fuel. Various studies have been conducted to address the combustion issues associated with low-cetane-number fuels in diesel engines. The Table 2.3 illustrates these studies. Methanol has a lower energy density per unit volume compared to gasoline, which means that you might need to use more methanol to travel the same distance. For example, you may need 1.7 liters of methanol to provide the same energy as 1 liter of gasoline. This could lead to larger and heavier fuel tanks in vehicles, resulting in a loss of storage space. Additionally, if standard fuel pumps are used, you might need to inject a larger quantity of methanol to achieve the

same energy output. Therefore, the amount of fuel passing through the pump and injectors is crucial. Methanol has a lower heating value than petroleum, which means it has a higher vaporization temperature. This can make it more challenging to start engines in cold weather conditions.

Table 2.3 : Methods developed for the use of methanol in diesel engines.

Method	Advantage	Disadvantage
Chemical Additives	No need for changes in the engine.	The high cost and the large quantity required of additives.
Emülsion	It requires very few changes in the engine.	Requiring two separate fuel tanks due to 50% of the fuel being diesel.
The Separate Use of Methanol and Diesel Injector	Minimal diesel fuel requirement for pilot injection.	The requirement for two separate injection systems.
The Use of Methanol with Diesel Fuel	Economic than using two separate injectors.	Requiring two separate fuels due to 50% of the fuel being diesel.
Surface Ignition	Requires only a single fuel.	The high energy requirement for obtaining hot surfaces.
Spark Ignition	Requires only a single fuel.	The cost of the ignition system.

2.6.1.2 Ethanol

Ethanol is a type of alcohol obtained through the fermentation of substances like sugar, cellulose, or starch. It can be produced from agricultural products such as potatoes, grains, sugarcane, and sugar beets. The energy required for the production of ethanol is generally higher than the energy it would provide when used in diesel engines, making it an inefficient choice for diesel engines. Ethanol is a clean, colorless, and non-toxic liquid. Its heating value is lower than that of gasoline. Additionally, ethanol can mix with water in any proportion. While ethanol has a high octane rating, it can pose some challenges when used in diesel engines due to its low cetane rating and self-ignition resistance. Therefore, the use of spark plugs or blending with diesel fuel is often required for ethanol to be used in diesel engines. Ethanol has a lower heating value than petroleum and a higher vaporization temperature. It also has a lower vapor pressure. This higher vaporization temperature can make it difficult to start engines in cold weather conditions. The physical and chemical properties of liquid fuels are shown in the Table 2.4.

Table 2.4 : Physical and chemical characteristics of liquid fuels.

	Gasoline	Diesel	Methanol	Ethanol
Chemical Equation	C_7H_{17}	$C_{11}H_{19}$	CH_3OH	C_2H_5OH
Rate of C/H	0.41	0.58	0.25	0.333
Molecular Mass (g/mole)	101.17	151.2	32.04	46.07
Specific Density as Liquid (kg/dm^3)	0.74	0.84	0.79	0.79
Calorific Value (Mj/kg)	42.5	42.5	20.1	26.9
Stoichiometric Air/Fuel as mass	14.7	14.3	6.44	8.96
Heat of Vaporization (Mj/kg)	0.31	0.28	1.10	0.856
Ignition Limits (%Volume)	1.4-7.6	0.7-5	6-37	3.5-19
Laminar Flame Speed (m/s)	0.58	0.3	0.52	0.47
Adiabatic Flame Temperature (°C)	2200	2390	1878	1924
Auto-Ignition Temperature (°C)	370	235	470	392
Octane Number - ROS	95	-	110	106
Octane Number - MOS	85	-	87	89

The methods applied to enable the use of ethanol in diesel engines are similar to those used for methanol, as mentioned in the Table 2.3.

2.6.1.3 Biodiesel

Biodiesel, a fuel alternative for diesel engines, is defined as the monoalkyl esters of long-chain fatty acids obtained from raw materials containing vegetable or animal oil. Biodiesel is produced through chemical reactions involving vegetable or animal oils and alcohols like methanol or ethanol, with the aid of homogeneous or heterogeneous catalysts. This alternative fuel is non-toxic, biologically degradable, and referred to as methyl/ethyl ester or biodiesel. The biodiesel production process is illustrated in Figure 2.13.

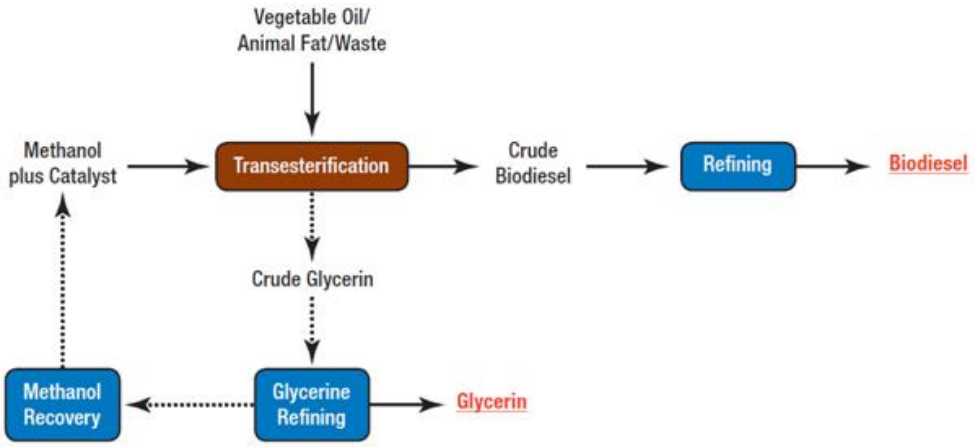

Figure 2.13 : Scheme of production of biodiesel.

Animal or vegetable oils, along with various alcohol and base mixtures (Methanol/Ethanol-NaOH/KOH), are introduced into a reactor. The reactor is heated to approximately 55°C – 60°C. The animal or vegetable oils are allowed to dissolve in the alcohol-base mixture for about 1-2 hours. At the end of this period, two types of products, biodiesel and glycerin, are formed in the environment. This process is called transesterification. The resulting mixture of biodiesel and glycerin is separated using a separation funnel. Glycerin passes through the separation funnel since it is denser than biodiesel, leaving crude biodiesel, which is called fatty acid alkyl ester, in the reactor. However, there are alcohol residues in both biodiesel and glycerin to a certain extent. The separation of alcohol in glycerin and biodiesel is required. Distillation is used for this separation process. The alcohol that has been separated is recycled back into the system for later use. Pure biodiesel is obtained by removing alcohol from crude biodiesel.

2.6.1.4 Ammonia

Under stoichiometric ($\lambda=1$) conditions, the required air-to-fuel ratio for the combustion of ammonia is approximately 6.1. This value is lower compared to diesel or other fuels, making ammonia less efficient in terms of combustion. Considering the ignition temperature of ammonia, which is 651°C, it becomes evident that it is resistant to high compression ratios. The laminar flame speed of ammonia is minimal among all fuels, indicating that high engine speeds cannot be achieved with ammonia. In terms of adiabatic flame temperature, ammonia exhibits characteristics similar to diesel and gasoline fuels. The high adiabatic temperature suggests the creation of a high-pressure zone during combustion. Ammonia falls into the category of low-reactivity fuels, having lower activity compared to diesel fuel. In a study, the effects of different concentrations of ammonia as a secondary fuel on engine performance and emissions were investigated in a diesel engine. The study showed that increasing the amount of ammonia delayed ignition and reduced the tendency for autoignition in the engine [102]. Ammonia has a higher heat of vaporization compared to other fuels and also has a lower lower heating value. For pure ammonia (100%) to be burned in a compression ignition diesel engine, the engine compression ratio needs to be at least 35:1. However, this is impractical and costly in reality, so using 100% ammonia in diesel engines is not suitable. Instead, a mixture of diesel and ammonia should be used in specific proportions. Studies have shown that the required amount of ammonia to

be used should be in the range of 20% to 40% of the mass of the diesel used [102,103]. In compression-ignition engines, the high-temperature formation due to ammonia content has an effect on NO_x formation. At low ammonia usage rates, the rate of NO_x formation is low, while at high ammonia rates, it increases the NO_x formation rate. Because of the high ignition temperature of ammonia, it results in more effective outcomes when used with a certain amount of diesel fuel. This is because the compression-ignition engines have high compression end temperatures, and including a certain amount of liquid ammonia in the combustion chamber will lower the ambient temperature. As ammonia evaporates, the heat it takes from the environment reduces the post-combustion temperatures, and consequently, NO_x formation improves as temperatures decrease [104]. A high input of ammonia would increase ignition delay, resulting in an accumulation of excess fuel in the chamber. As a consequence, combustion begins abruptly, and the rate of pressure rise per unit crank angle increases. This, in turn, shortens the combustion duration. The primary goal of using ammonia in diesel engines at the moment is to reduce NO_x emissions by lowering the combustion chamber temperatures in a certain fraction and, by utilizing its energy, to decrease the contribution of diesel to combustion. This leads to an improvement in HC, CO, and CO_2 emissions [105].

Ammonia theoretically shows a combustion reaction under stoichiometric conditions (complete combustion) according to the equation (2.61).

$$4NH_3 + \lambda.3(O_2 + 3.76N_2) \rightarrow 6H_2O + 13.28N_2 \tag{2.61}$$

The equation used in case of incomplete combustion (incomplete combustion) is shown in equation (2.62).

$$\begin{aligned} aNH_3 + \lambda.3b(O_2 + 3.76N_2) \\ \rightarrow xH_2O + yN_2O + zNO + mNO_2 + nNH_3 + kN_2 + sO_2 \end{aligned} \tag{2.62}$$

When examining the products part of the equation, it can be observed that the amount of unburned ammonia and NO_x components, which are incomplete combustion products, affect the quality of combustion. Using a higher fraction of ammonia in diesel engines increases both NO_x emissions and the amount of unburned ammonia. By balancing the equation above, it is possible to express each unknown in terms of one another. The combustion characteristics of ammonia are shown in Table 2.5.

Table 2.5 : Combustion characteristics for ammonia.

	Ammonia
Chemical Equation	NH_3
Molecular Mass (g/mole)	17.03
Specific Density as Liquid (kg/dm^3)	0.68
Calorific Value (MJ/kg)	18.8
Stoichiometric Air/Fuel as mass	6.05
Stoichiometric Air/Fuel as volumetric	3.57
Heat of Vaporization (MJ/kg)	1.37
Ignition Limits (%Volume)	15-28
Laminar Flame Speed (m/s)	0.015
Adiabatic Flame Temperature (°C)	1717
Boiling Point (°C)	-33.5
Auto-Ignition Temperature (°C)	651
Octane Number - ROS	>130

2.6.2 Gaseous fuels

The gaseous state of matter has more freedom of movement and interparticle space compared to the liquid state, which means that it occupies more volume. Therefore, gaseous fuels exhibit more dispersion inside the cylinder compared to liquid fuels. This situation has both advantages and disadvantages. The advantage is that it leads to higher air-fuel homogenization due to the turbulence generated inside the cylinder. When the ignition temperature is reached, gaseous fuel will ignite directly. The disadvantage is that it occupies more volume inside the cylinder, which leads to a reduction in oxygen concentration to some extent. In gaseous fuels, it is desirable for the fuel to carry a large amount of energy per unit volume. This allows for the extraction of more energy. Among alternative fuels, the most important ones in the gaseous phase are natural gas, hydrogen, and biogas.

2.6.2.1 Natural gas (CNG)

Natural gas is one of the gaseous fuels that can be used in diesel engines. Especially preferred as a dual fuel, natural gas has drawn the attention of researchers due to its abundant reserves, ease of implementation, and cost-effectiveness.

The majority of natural gas consists of methane (CH_4) gas, typically around 90-96%. The remaining composition includes approximately 2.411% ethane (C_2H_6), 0.736% propane (C_3H_8), 0.371% butane (C_4H_{10}), 0.776% nitrogen (N_2), 0.164% pentane (C_5H_{12}), and 0.085% carbon dioxide (CO_2). Natural gas has low density and is a lighter gas than air. However, it has a relatively high diffusion coefficient. The diffusion

coefficient of natural gas is about twice that of gasoline (0.08). This characteristic allows natural gas to mix and spread easily and quickly with air. Natural gas has a high air excess ratio. While the stoichiometric air/fuel ratio is 14.7 for gasoline and 14.5 for diesel, the stoichiometric air/fuel ratio for natural gas is 17.2. This means that natural gas can combust under lean conditions with a lower fuel density, providing a significant advantage in terms of fuel efficiency. Additionally, the laminar flame speed of natural gas is lower compared to a gasoline-air mixture, resulting in a slightly longer combustion duration [106]. Natural gas has a wide flammability range. While the flammability range for gasoline is approximately 1.4-7.6, and for diesel, it's 0.7-5.0, natural gas has a range of about 5-15. In other words, natural gas cannot burn with air mixtures that have less than 5% or more than 15% gas content.

Natural gas has a relatively low boiling point, making it storable under high pressure. Additionally, the auto-ignition temperature of natural gas is higher than that of gasoline and diesel. While the auto-ignition temperature for gasoline is 27-216 °C, for diesel, it's 160-382 °C, but natural gas has an auto-ignition temperature of approximately 632 °C. This indicates that the use of natural gas is advantageous from a safety perspective [107]. Furthermore, natural gas has a lower carbon-to-hydrogen (C/H) ratio compared to gasoline and diesel. Gasoline and diesel have a C/H ratio of approximately 0.5, whereas natural gas has a C/H ratio of 0.25. This means that the use of natural gas contributes to the reduction of carbon-containing pollutants, especially CO_2 emissions.

Finally, natural gas has a higher heating value compared to gasoline and diesel. The lower heating value of gasoline and diesel is approximately 43 MJ/kg, while the lower heating value of liquid natural gas is approximately 50 MJ/kg. This lowers the cost of providing a unit of energy content. The use of natural gas in diesel engines is typically implemented in dual-fuel mode. In this mode, the engine can run on both natural gas and diesel fuel without the need for major modifications. The combustion of natural gas in this method is achieved by using a small amount of pilot diesel fuel injected into the cylinder. The pilot diesel fuel injected at the end of the compression stroke rapidly ignites due to the compression temperature, subsequently igniting the natural gas-air mixture in the cylinder. The primary advantage of these dual-fuel systems is their cost-effectiveness and the ability to switch between single and dual fuels as needed. Therefore, dual-fuel systems are often a preferred option [108–110].

2.6.2.2 Hydrogen

One of the important characteristics of hydrogen is that it can be used in both liquid and gaseous states. In its gaseous form, hydrogen is approximately 14 times lighter than the same volume of air. When compared to other internal combustion engine fuels, liquid hydrogen is approximately 10 times lighter than liquid hydrocarbon fuels, while gaseous hydrogen is about 10 times lighter than other gaseous fuels like methane or natural gas. One of the advantages of using hydrogen in internal combustion engines is the wide flammability limits it offers. Hydrogen can burn in a mixture with air in a range of approximately 4% to 75%. This provides a more flexible combustion capability compared to other fuels [111,112]. For example, the appropriate mixture ratio for gasoline-air mixtures is typically between 0.3 to 1.7, while for hydrogen-air mixtures, this range is wider, spanning from 0.14 to 4.35. Hydrogen-air mixtures have broader flammability limits compared to other gas fuels. For instance, methane-air mixtures typically require an air-fuel ratio within the range of 0.6 to 1.9. Hydrogen has a higher lower heating value compared to many conventional motor fuels. However, when considered volumetrically, hydrogen has a lower energy content compared to other fuels. Additionally, hydrogen has a similar adiabatic flame temperature to gasoline. The use of hydrogen can potentially increase NO_x emissions, but this can be mitigated by co-firing hydrogen with natural gas [113]. While the current production and storage costs of hydrogen are high, it is expected that these costs will decrease in the future.

Table 2.6 : Comparison of physical and chemical characteristics of natural gas and hydrogen with diesel and gasoline.

	Gasoline	Diesel	Natural Gas	Hydrogen
Chemical Equation	C_7H_{17}	$C_{11}H_{19}$	CH_4	H_2
Rate of C/H	0.41	0.58	0.25	-
Molecular Mass (g/mole)	101.17	151.2	16.04	2.02
Specific Density as Liquid (kg/dm^3)	0.74	0.84	0.424	0.7
Calorific Value (MJ/kg)	42.5	42.5	50.8	120
Stoichiometric Air/Fuel as mass	14.7	14.3	17.2	34.32
Heat of Vaporization (MJ/kg)	0.31	0.28	0.509	0.446
Ignition Limits (%Volume)	1.4-7.6	0.7-5	5-15.4	4-75
Laminar Flame Speed (m/s)	0.58	0.3	0.37	2.93
Adiabatic Flame Temperature (°C)	2200	2390	1954	2110
Auto-Ignition Temperature (°C)	370	235	537	500
Octane Number - ROS	95	-	130	>130
Octane Number - MOS	85	-	105	60

Therefore, as hydrogen becomes more widely used and production capacity increases, costs are likely to decrease. The comparison of gas fuels with diesel and gasoline in terms of physical and chemical properties has been made in the Table 2.6.

2.6.2.3 Biogas

Biogas is a gas mixture formed as a result of the anaerobic fermentation of organic waste. This gas is colorless, odorless, lighter than air, and burns with a bright blue flame. The composition of biogas varies depending on the organic materials it contains, but it typically consists of different proportions of methane, carbon dioxide, nitrogen, and hydrogen, with trace amounts of hydrogen sulfide. 1 m^3 of biogas generates approximately 19-24 MJ/m^3 of heat energy. Additionally, 1 m^3 of biogas is equivalent to approximately 0.66 liters of diesel, 0.75 liters of gasoline, and 0.25 m^3 of propane in terms of fuel quantities. Due to the carbon dioxide it contains, biogas has a higher density than methane. Also, the amount of carbon dioxide affects the calorific value of biogas. As the carbon dioxide content increases, the density of biogas increases, but its calorific value decreases [114]. The ignition temperature is the temperature at which a fuel can spontaneously ignite. Biogas has a high ignition temperature, which means that to use it in diesel engines, either external energy must be supplied to the combustion chamber or the engine needs to be converted into a dual-fuel system. This is because in compression-ignition engines, the compression end temperature does not typically exceed 700°C [115]. The heat value of biogas is primarily derived from the methane gas it contains, along with small amounts of hydrogen gas. For biogas to burn effectively, the methane content should be at least 50%. Following methane, the gas found in the highest proportion in biogas is carbon dioxide. The table below provides the basic characteristics of biogas with a composition of 60% CH_4 and 40% CO_2, along with other gas fuels. The environmental impact of biogas suggests that it has the potential to be a more environmentally friendly fuel when compared to fossil fuels. The most critical factors determining these environmental impacts are the gases present in the composition of biogas and their ratios. In other words, as the methane content in biogas increases, its environmental impacts are positively affected, making it a more sustainable fuel [114]. Gas-fueled diesel engines generally exhibit performance quite close to that of regular diesel engines. However, a decrease in the calorific value of the gas and an increase in the gas fuel volume required for power can lead to a decrease in performance. In these

types of engines, diesel fuel is replaced by a gas-air mixture in the cylinders, which means that gas fuel takes the place of air entering the cylinders, resulting in a reduced air-fuel ratio. Consequently, the decrease in both diesel fuel and air can lead to a lower generated power compared to single-fuel operation. However, noticeable performance degradation is generally not observed under low and medium load conditions since more air is taken into the cylinders in dual-fuel operation. Additionally, in dual-fuel operation, the exhaust gas temperature is typically higher compared to single-fuel operation. Due to the slower combustion rate, the combustion process shifts towards the exhaust timing during dual-fuel operation. This situation can lead to overheating and damage to the exhaust valves. The thermodynamic properties of gas fuels are given in Table 2.7 [116].

Table 2.7 : Basic physical and chemical characteristics of gaseous fuels [116].

	Natural Gas	Hydrogen	Biogas
Chemical Equation	CH_4	H_2	60% CH_4 + 40% CO_2
Calorific Value (MJ/kg)	50.8	120	18
Stoichiometric Air/Fuel as mass	17.2	34.32	10.2
Ignition Limits (%Volume)	5-15.4	4-75	5-15
Auto-Ignition Temperature (°C)	537	500	650
Octane Number - ROS	130	>130	130

2.7 Emissions

Combustion in internal combustion engines is one of the most significant contributors to air pollution. Various substances and gases produced from the combustion of fossil fuels are the major factors in the formation of air pollution. These substances and gases include NO_x (nitrogen oxides), particulate matter (soot), HC (hydrocarbons), CO (carbon monoxide), and CO_2 (carbon dioxide). Among these, especially CO, NO_x, and particulate matter are of great importance in terms of air pollution. When these gases and particles are released into the environment, they lead to health issues, acid rain, the greenhouse effect, and, in general, the degradation of air quality. Therefore, controlling and reducing emissions resulting from the combustion of fossil fuels is critically important in reducing air pollution and its environmental impacts.

2.7.1 NO_x emissions

The attainment of high temperatures during combustion leads to the formation of nitrogen oxides as atmospheric nitrogen combines with oxygen. When looking at this

formation process, some important parameters come into play. These parameters include the combustion chamber temperature and the air-fuel ratio.

The quantity calculated from chemical equilibrium reactions differs from the quantity formed as a result of the combustion occurring in the engine. This difference arises because under engine conditions, there is not enough time for the combustion products to reach chemical equilibrium. Since reaction rates are temperature-dependent, once the highest temperature is reached, the temperatures of the burned gases start to decrease before they can reach chemical equilibrium. During the cooling of the burned gases, differences from the chemical equilibrium state are also observed. As the temperature decreases, it is expected that NO_x components will dissociate into N_2 and O_2 gases. However, due to the very slow reaction rates at low temperatures, these dissociation reactions slow down. Therefore, the NO_x quantities obtained at higher temperatures become fixed at lower temperatures, as if they were frozen. Initially, the amount of NO_x components is low because the reaction rates are insufficient to reach the equilibrium conditions (due to limited reaction rates). However, after a certain time, as the temperatures drop, the reactions stop, and the NO_x amount in the exhaust gases becomes fixed, proportional to the maximum temperature level reached earlier. This situation indicates that the formation of nitrogen oxides depends on reaction rates and the time required for the reactions to complete [67].

The formation of NO_x is also dependent on the oxygen content. Therefore, in very rich mixtures, the NO levels decrease due to incomplete combustion. When the air-fuel mixture's air content is significantly increased, the combustion temperatures will decrease, and the NO levels will decrease as well. Hence, another parameter that affects NO_x emissions is the air-fuel ratio. There is a range of values within which the air-fuel ratio affects temperature and pressure, depending on the amount of injected fuel. Controlling the air-fuel ratio within this range is an important factor in managing NO_x emissions [67,117].

2.7.2 SOOT (PM) emissions

In diffusion flames that occur in diesel engines, soot is typically formed under conditions of time and, especially, oxygen deficiency because hydrogen is generally more reactive towards oxygen compared to carbon. Soot consists of solid carbon particles that form under these conditions. The amount of soot formed varies as a

function of the air-fuel ratio (AFR), which changes depending on the engine's load condition. This, in turn, has an effect on the engine's power output. Typically, soot formation is a part of the diesel combustion process. Therefore, initially, a significant portion of the formed carbon will re-burn. However, when a large amount of fuel is injected into the combustion chamber to increase power, insufficient oxygen will be available, resulting in some soot in the exhaust gases.

Soot emission formation can be defined as the oxidation of unburned fuel vapors in high-temperature regions with high oxygen concentration inside the cylinder. Soot emissions are particularly observed in the rich fuel content of the inner core region of the fuel spray [67,118]. Soot formation can lead to cylinder wear and the clogging of piston ring grooves, potentially causing damage to the engine.

2.7.3 HC emission

The use of all saturated and unsaturated hydrocarbons as well as aromatic compounds as fuels causes the formation of HC (hydrocarbon) emissions. The presence of HC substances in exhaust gases is not due to high temperatures, unlike CO (carbon monoxide) and NO_x (nitrogen oxides) emissions.

The primary factor contributing to the formation of HC emissions is the incomplete combustion that occurs when temperatures are low or when there is insufficient oxygen. This occurs due to the following reasons:

- Having a very lean or very rich local mixture ratio can slow down oxidation reactions and lead to flame extinction due to heat loss.
- A high surface-to-volume ratio of the mixture in different regions of the combustion chamber can cause significant heat losses that prevent the mixture in these areas from igniting.
- Heat losses towards the cold walls of the combustion chamber can result in the immediate extinction of the flame reaching this region.

The richness or leanness of the mixture also affects HC (hydrocarbon) emissions. When the air-fuel equivalence ratio is high, the combustion chamber temperature decreases, preventing complete combustion, which leads to increased HC emissions. In the case of a rich mixture, not enough oxygen is present for complete combustion, causing an increase in HC emissions [67].

2.7.4 CO emission

The primary reason for the formation of CO is the lack of oxygen during combustion. CO emissions occur when there is generally an oxygen deficiency in the combustion chamber, or when fuel and air do not mix homogeneously, or when there is local oxygen deficiency in specific areas of the combustion chamber.

CO formation primarily depends on the air-fuel equivalence ratio. Therefore, correcting combustion conditions and ensuring sufficient oxygen are important for reducing CO emissions. Diesel engines often operate with lean mixture ratios, which means that the overall mixture in the combustion chamber is lean. This condition contributes to lower CO emissions because there is sufficient oxygen under these conditions, allowing for the complete combustion of CO. Therefore, CO emissions from diesel engines are generally low [67,117].

2.7.5 CO_2 emission

The combustion of hydrocarbon fuels results in the formation of water and CO_2 gas. Accumulated CO_2 gases in the atmosphere prevent sunlight from being reflected back into space. Intense ultraviolet radiation absorbed by atmospheric CO_2 causes warming of the Earth's surface. This excessive warming phenomenon is called the greenhouse effect.

The greenhouse effect leads to global warming, which, in turn, disrupts the world's climatic and ecological balance. Melting polar ice caps, sudden meteorological events, or climate shifts are all recent events exacerbated by global warming. Reducing CO_2 emissions is most effectively achieved by shifting to alternative fuels that do not contain carbon. Especially in contrast to the high carbon content in diesel and gasoline fuels, green fuels that are carbon-free should be used in these engines. Otherwise, the effects of global warming will intensify, leading to an irreversible scenario.

From a performance perspective, a high CO_2 content in exhaust gases indicates efficient combustion. However, considering the environmental impact, the transition to alternative fuels without carbon is of utmost importance.

2.7.6 Noise emission

Emission sources related to noise and vibration are a result of engine knock. While the impact of knocking in diesel and gasoline engines may appear to be the same, the

formation of knocking differs between them. Knock in gasoline engines is due to auto-ignition of the fuel inside the cylinder before spark plug ignition occurs. Early ignition results in engine knocking, misfiring, and a loss of performance, as maximum pressure occurs before top dead center (TDC).

Knocking in diesel engines is related to the value of the pressure increase per unit crank angle. Three types of combustion performance are possible: mild combustion with values of 1-5 bar/CA (crank angle), severe combustion with values of 5-10 bar/CA, and knocking combustion with values of 10 bar/CA or higher.

Reducing noise and vibration in engines depends on achieving knock-free operation. To mitigate knocking tendencies, adjustments to ignition/injection timing, fuel quantities, and the suitability of the chosen fuel for the engine cycle should be carefully considered. In the literature, extensive studies have been conducted on various engine parameters to reduce knocking and noisy operation in diesel engines [119–123].

2.8 Methods for Emission Reduction

Reducing emissions without sacrificing engine performance has been a major goal in the literature's research efforts. Achieving lower emissions can involve adjustments to engine operating parameters and is highly influenced by the composition of the fuel used. Interventions in operating parameters typically revolve around optimizing parameters like injection timing and angle, intake air temperature and pressure, turbulence levels, the implementation of Exhaust Gas Recirculation (EGR), injection strategies (such as split injection), and the injection of additives into the combustion chamber to reduce emissions. These measures are aimed at minimizing emissions while maintaining engine performance [124–127].

Within the scope of the thesis, the methods used to improve emissions include the use of alternative fuels, adjusting injection timing, implementing Exhaust Gas Recirculation (EGR), applying injection strategies (pilot injection), and introducing water jet/vapour into the combustion chamber.

2.8.1 Fuel injection strategies

The advancement of fuel injection timing in diesel engines has a significant impact on performance and emission values. Studies in the literature have shown improvements

in emissions through the optimization of fuel injection timing or the application of various strategies, such as split injection. Injection strategies consist of three main types: pilot injection, main injection, and post-injection. Each type of injection serves a specific purpose. Pre-injection introduces fuel to the combustion chamber in advance, facilitating the formation of a homogeneous mixture by allowing the fuel to mix with air for a longer time. This results in a smoother combustion environment with reduced tendencies for knocking and noise emissions, as well as improved NO_x emissions. Main injection is the type of injection used to initiate combustion, following the pre-injection, and it ignites the vaporized fuel along with the fuel introduced into the combustion chamber. Post-injection is applied especially towards the end of the combustion process, aiming to burn oxidized fuel particles, thus extending the combustion duration and improving soot emissions. While there are three main injection strategies, these strategies can also be applied in a split manner, involving multiple injections of pre-injection or other types as part of the application [128].

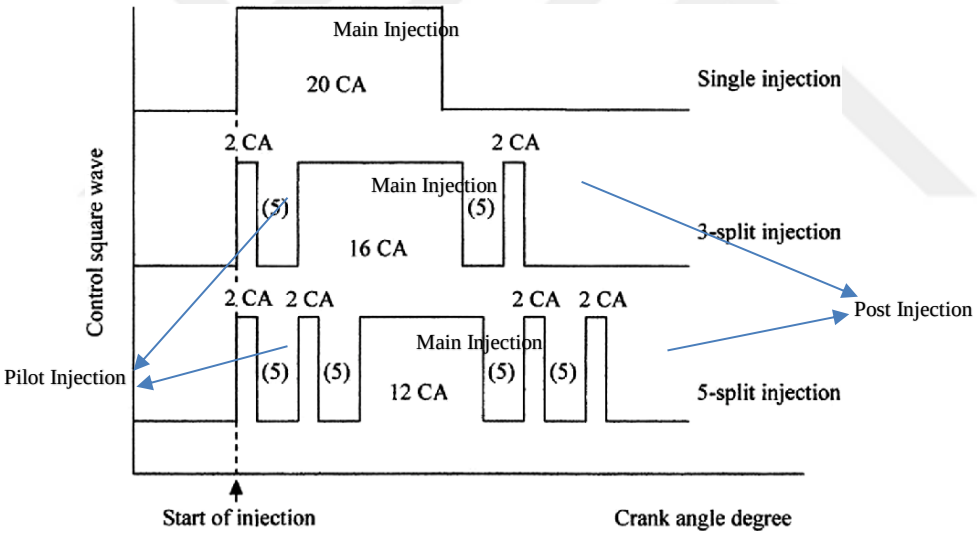

Figure 2.14 : Scheme of multi split injection for a diesel engine [128].

2.8.2 EGR

EGR is the process of passing a certain portion of the exhaust gases, sometimes after passing through an intercooler, through a valve and back into the cylinder along with the intake air. The primary purpose of this practice is to reduce the oxygen concentration inside the cylinder, leading to a decrease in post-combustion temperatures. Lower temperatures result in reduced NO_x emissions. EGR is essentially an application designed to improve NO_x emissions, even if it involves a certain degree of compromise in performance. With increasingly stringent emission standards, the

practical use of this application has become quite common in the field. The EGR operation diagram is given in Figure 2.15.

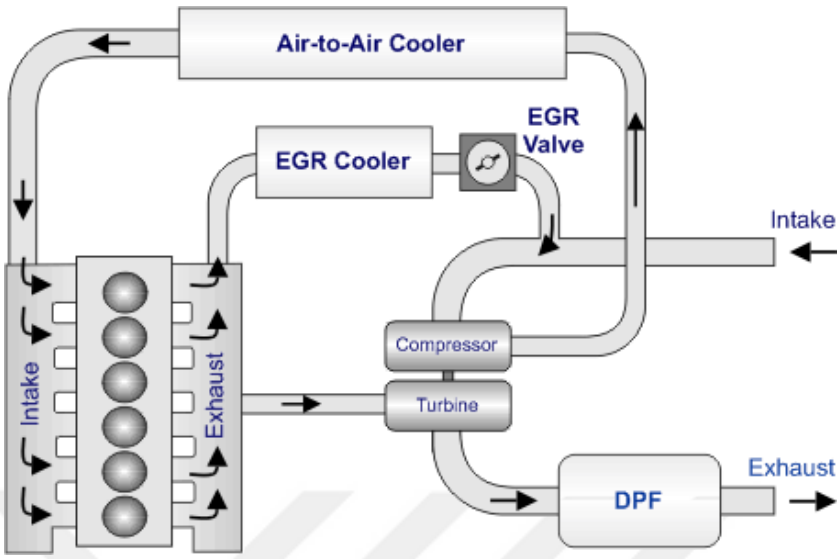

Figure 2.15 : Schematic representation of engine EGR application [129].

EGR application in engines results in the following observations:

- It prolongs the ignition delay period.
- It causes an improvement in NO_x emissions due to the deteriorating combustion leading to a decrease in regional temperatures.
- It causes a certain increase in specific fuel consumption.
- It leads to a decrease in performance values.
- It increases HC, CO, and soot emissions.

All studies have primarily focused on achieving the maximum reduction in NOx emissions with minimal performance loss [124,125,130].

2.8.3 Water jet/vapor injection into the combustion chamber

There are two main methods for injecting water or steam into the combustion chamber. The first method involves mixing water with the intake air. Here, an injector in the intake manifold blends water and air, and the cylinder receives humid air. The other type is direct injection into the combustion chamber. When comparing liquid and steam phase injections, it has been observed that the liquid phase reduces NO_x emissions more effectively. The main reason for this is that the liquid phase absorbs heat from the surroundings during vaporization, leading to a greater decrease in combustion chamber temperatures compared to the steam phase. As a result, it leads to a more significant reduction in NO_x emissions. The injection of water or steam into

the combustion chamber can potentially lead to decreases in performance values due to the temperature drop within the combustion chamber. However, by creating an appropriate turbulence environment inside the cylinder and ensuring reasonable water injection into the combustion chamber, it has been observed that there is a likelihood of increasing performance values [131,132]. The increase in performance in the study is attributed to the fact that water droplets with low surface tension cause fuel droplets to break into smaller pieces. Smaller fuel droplets have a larger surface area, which leads to improved combustion efficiency and, consequently, better performance parameters [131].

3. MATERIAL AND METHOD

Mathematical models are created for systems by making certain assumptions in control volumes where many physical and chemical events take place. Assumptions are made to simplify the mathematical modeling of the process. In the in-cylinder combustion process, the motion and properties of the fluid, as well as chemical reactions, are the physical and chemical events that occur. Physical and chemical events are interrelated. Fluid dynamics are fundamentally controlled by the Navier-Stokes equations, and transport equations describe the turbulent properties of a flow. When a liquid is injected into a flow or sprayed, exchange functions are used to describe the interaction between the gas phase and liquid droplets. Fick's Law is used for mass diffusion, and Fourier's Law is used for heat diffusion. The goal of the turbulent combustion model approach is to maintain the fundamental effects of turbulence on flow and combustion properties while eliminating the need to resolve all small-scale structures and fluctuations. To achieve this goal, the Favre average is used to represent the instantaneous quantities. Under the mathematical model, information about conservation equations, turbulence models, chemical kinetics, combustion model, collision model and evaporation models will be given.

3.1 Conservation Equations

When creating a numerical model, the fundamental assumptions are the continuity equation, conservation of momentum, conservation of energy, and the ideal gas state equations for the gases in the system.

3.1.1 Continuity equation

This is the most fundamental equation from which the conservation equations are derived. Its form for compressible and incompressible flows is shown in equation (3.1).

$$\frac{\partial \overline{\rho}}{\partial t} + \nabla . (\overline{\rho} \tilde{u}) = \overline{\rho}_k^s \tag{3.1}$$

3.1.2 Conservation of the momentum (Navier-stokes equation)

The closed form of the momentum conservation equation is shown in equation (3.2) below.

$$\frac{\partial \overline{\rho}\tilde{u}}{\partial t} + \nabla.(\overline{\rho}\tilde{u}\tilde{u}) = -\nabla\overline{p} + -\nabla\overline{\sigma} - \frac{2}{3}\overline{\rho}\tilde{k}I + \overline{F}^{s} + \overline{\rho g} \tag{3.2}$$

The term $\overline{\sigma}$ represents the Viscous Stress Tensor, and it is shown in equation (3.3). Here, I is the unit tensor, $\overline{F}^{s}$ is the rate of gain of momentum per unit volume, and g is the specific body force.

$$\overline{\sigma} = (\mu + \mu_T)\left[\nabla\tilde{u} + \nabla\tilde{u}^{T} - \frac{2}{3}(\nabla.\tilde{u})I\right] \tag{3.3}$$

The term μ represents the laminar dynamic viscosity, while μ_T represents the turbulent dynamic viscosity. In equation (3.2), $\tilde{k}$ represents turbulent kinetic energy. The expression for $\tilde{k}$ is calculated as shown in equation (3.4).

$$\tilde{k} = \frac{1}{2}\widetilde{u''u''} \tag{3.4}$$

The turbulent dynamic viscosity μ_T is calculated based on turbulent kinetic energy and turbulent kinetic energy dissipation rate ($\tilde{\varepsilon}$), as shown in equation (3.5).

$$\mu_T = c_\mu \overline{\rho}\frac{\tilde{k}^2}{\tilde{\varepsilon}} \tag{3.5}$$

The parameter c_μ is a model-specific constant for the turbulence model. After determining the value of μ_T, thermal diffusivity (α_T) and mass diffusivity (D_T) can be calculated using equation (3.6) and equation (3.7), respectively.

$$\alpha_T = \frac{V_T}{Pr_T} = \frac{\mu_T}{\overline{\rho}Pr_T} \tag{3.6}$$

$$D_T = \frac{V_T}{Sc_T} = \frac{\mu_T}{\overline{\rho}Sc_T} \tag{3.7}$$

The V_T term represents the turbulence kinetic viscosity, Pr_T is the turbulence Prandtl number, and Sc_T is the turbulence Schmidt number. Pr_T is a dimensionless number

used to represent the ratio of momentum diffusion to thermal diffusion. Sc_T, on the other hand, is a dimensionless number defined as the ratio of momentum diffusivity (kinematic viscosity) to mass diffusivity.

When considering the general expression for the viscous stress tensor in Equation (3.3), the expression for the Reynolds stress tensor arising due to turbulence is represented in equation (3.8) [133].

$$\overline{\tau} = (\mu_T)\left[\nabla\tilde{u} + \nabla\tilde{u}^T - \frac{2}{3}(\nabla.\tilde{u})I\right] - \frac{2}{3}\overline{\rho}\tilde{k}I \tag{3.8}$$

3.1.3 Conservation of the energy

The conservation equation for internal energy is represented by equation (3.9).

$$\frac{\partial\overline{\rho}\tilde{I}}{\partial t} = \nabla.(\overline{\rho}\tilde{u}\tilde{I}) = -\nabla\overline{\rho}\tilde{u} - \nabla\tilde{J} + \overline{\rho}\tilde{\varepsilon} + \widetilde{\dot{Q}^c} + \widetilde{\dot{Q}^s} \tag{3.9}$$

$\tilde{I}$ represents specific internal energy, and $\tilde{J}$ is the heat flux term. Heat flux is created within the control volume through heat conduction and enthalpy diffusion. The $\tilde{J}$ term is represented by equation (3.10).

$$\tilde{J} = -\lambda\nabla\widetilde{T} - \tilde{\rho}D_T\sum_k \tilde{h}_k\nabla\left(\frac{\overline{\rho}_k}{\overline{\rho}}\right) \tag{3.10}$$

λ represents the thermal conductivity, $\widetilde{T}$ is the flow temperature, and $\tilde{h}_k$ corresponds to the specific enthalpy values of the species. $\widetilde{\dot{Q}^c}$ and $\widetilde{\dot{Q}^s}$ terms represent the chemical heat release and spray interaction coefficients, respectively. The thermal conductivity λ is determined using equation (3.11) [133].

$$\lambda = \tilde{\rho}c_p\alpha_T \tag{3.11}$$

3.1.4 Ideal gas equation of state

The equation of state for all species and mixtures in the control volume, both before and after combustion, is derived from the ideal gas law as given in equation (3.12).

$$\overline{p} = R_u\widetilde{T}\sum_k\left(\frac{\overline{\rho}_k}{W_k}\right) \tag{3.12}$$

Where R_u is the universal gas constant, and W_k represents the molecular weight of each species in the control volume [133].

3.2 Turbulence Models

Turbulence is the term used to describe the irregular distribution of flow within a system. It is caused by pressure and velocity fluctuations, as well as the diffusion of low momentum and the transport of high momentum within the control volume.

Fully defining turbulence, which represents chaotic flow, is challenging. The system is shaped by viscosity and the kinetic energy of moving particles. Numerous regional vortices form within the control volume, and these vortices interact with each other. Turbulence has a significant impact, especially before and after combustion. Therefore, an appropriate turbulence modeling approach is necessary for an accurate representation.

In many physical phenomena, turbulence is commonly encountered, and turbulence models have been developed to help explain turbulent environments. Therefore, choosing the appropriate turbulence model is crucial for solving fluid dynamics problems. Ansys Forte includes standard k-epsilon and RNG k-ε turbulence models.

3.2.1 Standard k-ε turbulence model

The Standard k- ε turbulence model, which is used at high Reynolds numbers, includes two transport equations for turbulence kinetic energy (k) and the rate of turbulence kinetic energy dissipation (ε). The equation for k is shown in equation (3.13) below.

k is the turbulence kinetic energy:

$$\frac{\partial}{\partial t}(\rho k) + \frac{\partial}{\partial x_j}\left[\rho u_j k - \left(\mu + \frac{\mu_t}{\sigma_k}\right)\frac{\partial k}{\partial x_j}\right] = \mu_t\left(S_{ij}\frac{\partial u_i}{\partial x_j} - \frac{g_i}{\sigma_{h,t}}\frac{1}{\rho}\frac{\partial \rho}{\partial x_i}\right) - \rho\varepsilon - \frac{2}{3}\left(\mu_t\frac{\partial u_i}{\partial x_i} + \rho k\right)\frac{\partial u_i}{\partial x_i} \quad (3.13)$$

The first term on the right-hand side of equation (3.13) represents turbulence due to normal and shear stresses, the second term accounts for viscous dissipation, and the third term represents the effects caused by compression.

The turbulence dissipation rate ε is represented by equation (3.14).

The turbulence dissipation rate ε:

$$\frac{\partial}{\partial t}(\rho\varepsilon)+\frac{\partial}{\partial x_j}\left[\rho u_j\varepsilon-\left(\mu+\frac{\mu_t}{\sigma_\varepsilon}\right)\frac{\partial\varepsilon}{\partial x_j}\right] = C_{e_1}\frac{\varepsilon}{k}\left[\mu_t S_{ij}\frac{\partial u_i}{\partial x_j}-\frac{2}{3}\left(\mu_t\frac{\partial u_i}{\partial x_i}+\rho k\right)\frac{\partial u_i}{\partial x_i}\right]-C_{e_2}\rho\frac{\varepsilon^2}{k} - C_{e_3}\frac{\varepsilon}{k}\mu_t\frac{g_i}{\sigma_{h,t}}\frac{1}{\rho}\frac{\partial\rho}{\partial x_i}+C_{e_4}\rho\varepsilon\frac{\partial u_i}{\partial x_j} \quad (3.14)$$

The equations contain the following variables: u_i represents the absolute velocity, σ stands for the turbulence Prandtl number, ε is the turbulence dissipation rate, k represents the turbulence kinetic energy, S_{ij} is the mean strain rate, and ρ is the density.

C_{e1}, C_{e2}, C_{e3} and C_{e4} are coefficients representing constants. The first term on the right-hand side of equation (3.14) represents the linear strain, the second term accounts for the dissipation of turbulence spreading, and the third and fourth terms denote the distribution due to buoyancy and transient mean density changes, respectively [133].

3.2.2 RNG k-ε turbulence model

The most fundamental difference between the RNG k-ε turbulence model and the standard k-epsilon turbulence model is that the RNG model takes into account the effects of smaller-scale motions.

Another difference is that it includes calculations for various scales of motion, providing more precise results. RNG stands for **R**e-**N**ormalization **G**roup, and this theory was initially developed and used by Yakhot and Orszag [134].

The RNG k-ε turbulence model also includes two transport equations for turbulence kinetic energy k and its dissipation rate ε. For k, equation (3.15) is shown below, and this equation is the same as the one used in the standard k-epsilon turbulence model.

Turbulence kinetic energy k:

$$\frac{\partial}{\partial t}(\rho k)+\frac{\partial}{\partial x_j}\left[\rho u_j k-\left(\mu+\frac{\mu_t}{\sigma_k}\right)\frac{\partial k}{\partial x_j}\right] = \mu_t\left(S_{ij}\frac{\partial u_i}{\partial x_j}-\frac{g_i}{\sigma_{h,t}}\frac{1}{\rho}\frac{\partial\rho}{\partial x_i}\right)-\rho\varepsilon-\frac{2}{3}\left(\mu_t\frac{\partial u_i}{\partial x_i}+\rho k\right)\frac{\partial u_i}{\partial x_i} \quad (3.15)$$

The equation for the turbulence dissipation rate ε is represented by equation (3.16).

Compared to the standard k-epsilon turbulence model, it can be observed that an additional term has been added to the end of the equation on the right-hand side.

Turbulence dissipation rate ε:

$$\frac{\partial}{\partial t}(\rho\varepsilon) + \frac{\partial}{\partial x_j}\left[\rho u_j \varepsilon - \left(\mu + \frac{\mu_t}{\sigma_\varepsilon}\right)\frac{\partial \varepsilon}{\partial x_j}\right] = C_{e_1}\frac{\varepsilon}{k}\left[\mu_t S_{ij}\frac{\partial u_i}{\partial x_j} - \frac{2}{3}\left(\mu_t \frac{\partial u_i}{\partial x_i} + \rho k\right)\frac{\partial u_i}{\partial x_i}\right] - C_{e_2}\rho\frac{\varepsilon^2}{k} - C_{e_3}\frac{\varepsilon}{k}\mu_t \frac{g_i}{\sigma_{h,t}}\frac{1}{\rho}\frac{\partial \rho}{\partial x_i} + C_{e_4}\rho\varepsilon\frac{\partial u_i}{\partial x_j} - \frac{C_\mu \eta^3\left(1 - \frac{\eta}{\eta_0}\right)}{1 + \beta\eta^3}\frac{\rho\varepsilon^2}{k} \quad (3.16)$$

The term η in the equation for turbulence dissipation rate ε, given by equation (3.16), is calculated using equation (3.17).

The values of η_0 and β are experimentally determined, with values of 4.38 and 0.012, respectively.

The constants C_{e1}, C_{e2}, C_{e3} and C_{e4} are the same as those in the standard k-ε turbulence model.

$$\eta = S\frac{k}{\varepsilon} \quad (3.17)$$

The expression for S is calculated using the equation given by equation (3.18).

$$S = (2\overline{S}:\overline{S})^{\frac{1}{2}} \quad (3.18)$$

The $\overline{S}$ term is calculated using the equation given by equation (3.19).

$$\overline{S} = \frac{1}{2}(\nabla\tilde{u} + \nabla\tilde{u}^T) \quad (3.19)$$

All the constants used for the RNG k-ε turbulence model are shown in Table 3.1 below [133].

Table 3.1 : Coefficients for standard k-ε and RNG k-ε turbulence models [133].

	C_μ	C_{e_1}	C_{e_2}	C_{e_3}	$1/Pr_k$	$1/Pr_\varepsilon$	η_0	β
Standart k-ε	0.09	1.44	1.92	-1.0	1.0	0.769		
RNG k- ε	0.0845	1.42	1.68	1.44	1.39	1.39	4.38	0.012

3.3 Chemical Kinetic Formulation

ANSYS Forte carries out the chemical reactions in the combustion process using chemical kinetic mechanisms. Chemical kinetic mechanisms describe the reaction rates that change species concentrations based on the chemical, thermophysical, and thermodynamic properties of the fuel. Chemical kinetic mechanisms calculate the concentrations of K species, whether reversible or irreversible, using the equation (3.20).

$$\sum_{k=1}^{K} V'_{ki}\, X_k \Leftrightarrow \sum V''_{ki} X_k \;\; (i = 1,2, \dots \dots \dots, I) \tag{3.20}$$

The production rate of species i in the k-th reaction is expressed by equation (3.21).

$$\dot{\omega}_{ki} = (V''_{ki} - V'_{ki}) q_i \; (k = 1,2, \dots \dots \dots, K) \tag{3.21}$$

The term q_i in the equation represents the reaction progress rate. The chemical source term in the species continuity equation, considering the production rate of all reactions, is determined by equation (3.22).

$$\dot{\rho}^c_k = W_k \sum_{i=1}^{I} \dot{\omega}_{ki} \tag{3.22}$$

Equation (3.23) is used for the chemical heat release term in the energy conservation equation.

$$\dot{Q}^c = -\sum_{i=1}^{I} \sum_{k=1}^{K} (V''_{ki} - V'_{ki})(\Delta h^0_f)_k q_i \tag{3.23}$$

The term Δh^0_f represents the standard heat of formation for species i [133].

3.3.1 SOOT (PM) model

When calculating SOOT emissions in ANSYS Forte, a two-step approach is followed. In the first step, it focuses on the formation of soot, and in the second step, it investigates the oxidation reactions. During these steps, Hiroyasu soot formation is used in the first step, and Nagle and Strickland-Constable oxidation models are used in the second step [135,136].

The expressions used for the SOOT model are shown below with equations (3.24), (3.25), (3.26), and (3.27).

$$\frac{dM_s}{dt} = \frac{dM_{sf}}{dt} - \frac{dM_{so}}{dt} \tag{3.24}$$

$$\frac{dM_{sf}}{dt} = K_f M_{pre} \tag{3.25}$$

$$K_f = A_{sf} p^n \exp\left(-\frac{E_f}{RT}\right) \tag{3.26}$$

$$\frac{dM_{so}}{dt} = \frac{6MW_c}{\rho_s D_s} M_s R_{total} \tag{3.27}$$

In the equations, P represents pressure, n is a constant, Ms denotes soot mass, M_{sf} is the formed soot mass, M_{so} is the soot mass undergoing oxidation, M_{pre} is the initial formed soot mass, K_f is the soot formation rate, A_{sf} is the pre-exponential factor, E_f is the activation energy required for soot formation, MW_c is the molecular weight of carbon, ρ_s is the soot density, D_s is the soot particle diameter, and R_{total} represents the Nagle and Strickland-Constable oxidation rate. In ANSYS Forte, by default, the SOOT model uses the values n = 0.5, A_{sf} = 40 cm^3/mol, E_f = 12500 cal/mol, ρ_s = 2 g/cm^3, and D_s = 25 nm [133].

3.3.2 Turbulence-kinetics interaction model

ANSYS Forte uses the turbulence-kinetic interaction model proposed by Kong in combustion simulations for diesel engines [137,138].

The turbulence-kinetic interaction model examines the effects of turbulence on combustion. The mixture time-scale model is based on the idea that turbulence can be partially controlled by the termination of turbulent effects due to the incomplete mixing of combustion chemistry, fuel, and oxidizer in a real engine process. This model is especially based on the assumption that the effective time scales (τ_{eff}) of each species approach equilibrium values within a certain time frame, and therefore, the formation rate of species (k) is expressed by the following equation (3.28).

$$\tilde{\omega}_{k,eff} = \frac{Y_{k,EQ} - Y_k}{\tau_{eff}} \tag{3.28}$$

The effective time scale occurs based on the chemical time scale and depends on the turbulent scalar mixing time scale. Equation (3.29) represents the effective time scale.

$$\tau_{eff} = \tau_{chem} + \tau_{mix} \tag{3.29}$$

The chemical time scale (τ_{chem}) defines the time it takes for the mixture to reach equilibrium under the conditions inside the computational cell.

The turbulent mixing time scale (τ_{mix}) is obtained from the rate of turbulent kinetic energy and dissipation, as shown in equation (3.30) below.

$$\tau_{mix} = C_{tki}\tau_{turb} = C_{tki}\frac{K}{\varepsilon} \tag{3.30}$$

The model constant (C_{tki}) is one of the turbulence model coefficients and is a user-provided input parameter in ANSYS Forte. It is typically chosen as a value of 0.5, especially in shear flow turbulence analyses.

The relationship between the effective species production rate and the species production rate due to kinetic effects is shown by equation (3.31).

$$\tilde{\dot{\omega}}_{k,eff} = \frac{\tau_{chem}\dot{\omega}_k}{\tau_{eff}} \tag{3.31}$$

The progression of the effective species production rate is shown by equation (3.32).

$$\tilde{\omega}_{k,eff}\Delta t = Y_k^{n+1} - Y_k^n = \frac{\tau_{chem}\dot{\omega}_k}{\tau_{eff}}\Delta t = \frac{\tau_{chem}\left(Y_k^{kin} - Y_k^n\right)}{\tau_{chem} + f\tau_{mix}} \tag{3.32}$$

The progress variable f is obtained using equation (3.33).

$$f = \frac{1 - \exp\left(-Y_{product}\right)}{1 - \exp(-1)} \tag{3.33}$$

Here, $Y_{product}$ represents the mass fraction of all combustion products. When f = 0, the Turbulence-Kinetic Interaction Model approximates ignition in a CFD cell entirely controlled by chemical kinetics.

As the combustion process progresses, combustion products are formed, indicating an increase in turbulence effects [133].

3.4 Combustion Model and Submodels

The G-Equation model is used as the combustion model in ANSYS Forte. This model provides significant results for premixed, partially premixed, and diffusion combustion. It also enables accurate prediction of the types of emissions generated.

3.4.1 G-equation model

The foundation of the G-Equation combustion model is based on Peters' flame theory [139].

According to this theorem:

- In the wrinkled flamelet regime, it is assumed that the size of the eddies within the reactive-diffusive flame structure is embedded in the Kolmogorov length scale.
- Kolmogorov eddies (turbulence) can penetrate into the preheat region of the chemically reactive and diffusive flame structure in the thin reaction zone regime but chemical reactions cannot reach the inner layer.

The G-Equation model was further developed by Tan et al, as well as by Liang et al [140–142].

The G-Equation model consists of Favre-averaged level-set equations, including the Favre-mean ($\widetilde{G}$) and Favre variance ($\widetilde{G}^{n^2}$) terms. Within the model, turbulent/laminar flame surface area ratio is used to calculate turbulent flame speed (S_T^0).

The Reynolds-averaged Navier-Stokes equations and turbulence modeling equations together form a complete set of equations to describe the propagation of a premixed turbulent flame in front, and for the G-Equation Combustion Model used in ANSYS Forte, the equation set is given as equation (3.34) and equation (3.35) [133].

$$\frac{\partial \widetilde{G}}{\partial t} + (\vec{u} + \vec{u}_{vertex}).\nabla\widetilde{G} = \frac{\overline{\rho}_u}{\overline{\rho}_b} S_T^0 \left|\nabla\widetilde{G}\right| - D_T \widetilde{K} \left|\nabla\widetilde{G}\right| \tag{3.34}$$

$$\frac{\partial \widetilde{G}^{n^2}}{\partial t} + \vec{u}\nabla\widetilde{G}^{n^2} = \nabla_{II}\left(\frac{\overline{\rho}_u}{\overline{\rho}_b} D_T \nabla_{II}\widetilde{G}^{n^2}\right) + 2D_T\left(\nabla\widetilde{G}\right)^2 - C_s\frac{\widetilde{\varepsilon}}{\widetilde{k}}\widetilde{G}^{n^2} \tag{3.35}$$

∇_{II} tangential gradient operator; $\vec{u}$ fluid velocity vector; $\vec{u}_{vertex}$ velocity of a moving vertex; $\overline{\rho}_b$ and $\overline{\rho}_u$ are the burnt and unburned mixture densities, respectively; D_T

turbulent diffusivity; $\widetilde{K}$ Favre mean flame front curvature; C_s model constant; $\tilde{k}$ Favre mean turbulent kinetic energy and $\tilde{\varepsilon}$ Favre mean dissipation rate terms.

Predicting turbulent combustion speed accurately is crucial. To obtain an accurate prediction of a turbulent flame, calculating the laminar flame speed is necessary. In the ANSYS Forte G-Equation combustion model, two parameters are used to calculate the laminar flame speed. These parameters are determined by the Power-Law correlation and values in the flame speed table [133].

The Power-Law equation is shown below with equation (3.36):

$$S_L^0 = S_{L,ref}^0 \left(\frac{T_u}{T_{u,ref}}\right)^{\alpha} \left(\frac{p}{p_{ref}}\right)^{\beta} F_{dil} \tag{3.36}$$

For the ref index terms in the equation, values at 298 K temperature and 1 atm pressure are generally used. F_{dil} is the diluent's effect term. Two different formulas are used for the reference laminar flame spread rate $S_{L,ref}^0$. These are Metghalchi formulation and Gülder formulation. Metghalchi formula is shown in equation (3.37) [143,144].

$$S_{L,ref}^0 = B_m + B_\phi(\phi - \phi_m)^2 \tag{3.37}$$

The terms B_m, B_ϕ and ϕ_m have different values depending on the fuel type. The values of these terms are shown in Table (3.2).

Table 3.2 : Values for B_m , B_ϕ , and ϕ_m in the Metghalchi formula [145].

Fuel	B_m	B_ϕ	ϕ_m
-	(cm/sec)	(cm/sec)	-
Methanol	36.9	-140.5	1.11
Propane	34.2	-138.7	1.08
Izo-Octane	26.3	-84.7	1.13
Gasoline	30.5	-54.9	1.21

The Metghalchi formulation can yield negative values under conditions with very lean or very rich air-fuel mixture excess air ratios. To address this issue, another formulation called the Gülder Formula was developed to determine the reference laminar flame speed. The Gülder formula is represented by equation (3.38) [143].

$$S_{L,ref}^0 = \omega\phi^{\eta}\exp[-\xi(\phi - \sigma)^2] \tag{3.38}$$

The terms ω, η, ξ, and σ are data-fitting coefficients that vary depending on the fuel type. These coefficients are specific to the fuel being used, and their values are determined through data-fitting.

The range for ϕ (equivalence ratio) is defined as $0.65 < \phi < 1.6$. The exponents α and β in the laminar flame speed equation are coefficients that vary with temperature and pressure.

Equations (3.39) and (3.40) provide recommended expressions for α and β based on the equivalence ratio, respectively [146].

$$\alpha = \alpha_1 + \alpha_2 \phi^{\alpha_3} \tag{3.39}$$

$$\beta = \beta_1 + \beta_2 \phi^{\beta_3} \tag{3.40}$$

The suitable values for α_1, α_2, α_3, β_1, β_2, and β_3 obtained using the least squares method, are 2.98, -0.8, 1.0, -0.38, 0.22, and 1.0, respectively [146].

The term F_{dil}, known as diluent's effect, is represented by the suggested equations in (3.41) and (3.42).

$$F_{dil} = 1 - f_{x1} x_{dil}^{f_{x2}} \tag{3.41}$$

$$F_{dil} = 1 - f_{y1} y_{dil}^{f_{y2}} \tag{3.42}$$

The terms x in the equations represent molar units, while the terms y represent mass units. Therefore, x_{dil} represents the diluent molar ratio, and ydil represents the diluent mass ratio. The recommended coefficients based on experimental data are f_{x1}, f_{x2}, f_{y1}, and f_{y2} with values of 2.06, 0.773, 2.3, and 1.0, respectively.

Once the data related to the laminar flame speed is obtained using the equations mentioned earlier, calculations for the turbulent flame speed are performed.

The ratio between the turbulent flame speed and the laminar flame speed is shown in equation (3.43).

$$\frac{S_T^0}{S_L^0} = 1 + I_P \left\{ -\frac{a_4 b_3^2 I_l}{2 b_1 I_F} + \left[\left(\frac{a_4 b_3^2 I_l}{2 b_1 I_F} \right)^2 + a_4 b_3^2 \frac{u' I_l}{S_L^0 I_F} \right]^{1/2} \right\} \tag{3.43}$$

In the equation, I_P represents the flame progress variable, S_L^0 is the laminar flame speed, I_l is the turbulence integral length scale, and I_F is the laminar flame speed thickness [133]. The flame progress variable (I_P) is represented by equation (3.44).

$$I_P = \left[1 - \exp\left(-c_{m2}\frac{t - t_0}{\tau}\right)\right]^{1/2} \tag{3.44}$$

The coefficient c_{m2} in the equation is specifically used in spark ignition engine simulations to find the flame progress variable. It represents the flame development coefficient. The coefficients b_1, b_3, and a_4 in equation (3.43) are obtained from experimental data and are used in the G-Equation combustion model. Their values are 1.5, 1.07, and 0.78, respectively [147]. The majority of the heat released as a result of combustion is generated by the turbulent flame. ANSYS Forte uses the method proposed by Liang to calculate heat release when simulating combustion. The numerical description of the turbulent flame structure is provided in Figure 3.1 [141].

This method assumes that the volumes containing the burned and unburned regions (turbulence-containing vortices) are in small-scale shapes. Here, V_b denotes the volume where combustion occurs, while V_u represents the region where combustion does not occur. The volume where combustion occurs propagates towards the volume where combustion does not occur. It is assumed that the advancing burned volume reaches instantaneous thermodynamic equilibrium under constant pressure and enthalpy. The increase in pressure (deflagration wave theory) is consistent with the flame propagation theory, and it is assumed to remain constant along the flame within the grid.

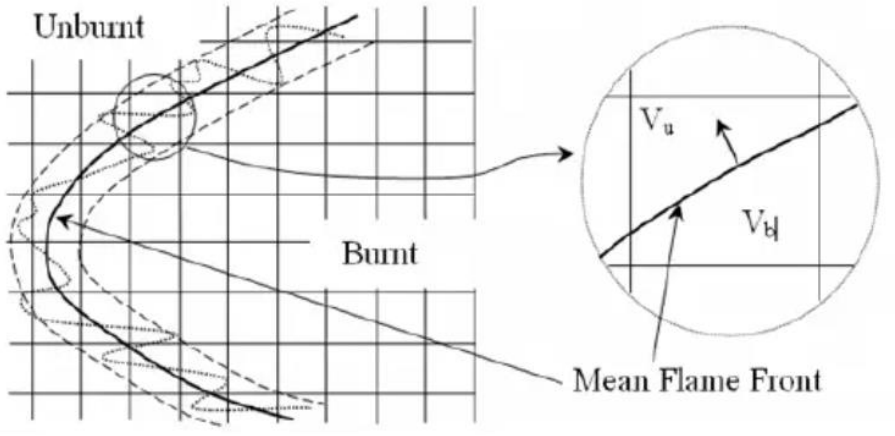

Figure 3.1 : Numerical description of turbulent flame structure [133,141].

The numerical description of the turbulent flame structure begins with determining the equilibrium concentration and adiabatic flame temperature under constant pressure and enthalpy conditions, which, in turn, involves calculating the species transformation rate and the associated primary heat release rate.

For a cell containing a flame, it is assumed that the average flame front crosses the unburned volume V_u within the time step dt. The transformation rate of species k within the time step dt is calculated using equation (3.45), taking into account the part of the mixture within the swept volume V_s that has reached the equilibrium state.

$$\frac{d\rho_k}{dt} = \frac{\rho Y_{k,b} - \rho_k}{dt} \tag{3.45}$$

ρ represents the density of the total mixture, while ρ_k represents the density of the k species. The equation for the swept volume by the burned region is given by equation (3.46) as follows:

$$V_s = A_f S_T dt \tag{3.46}$$

The flame front area (A_f) represents the area of the flame front within the grid, S_T is the turbulent flame speed, and k is the conversion rate of species, which is represented by equation (3.47).

$$\frac{d\rho_k}{dt} = \left(\rho Y_{k,b} - \rho_k\right)\frac{A_f S_T}{V_u} \tag{3.47}$$

In ANSYS Forte, when calculating post-combustion, species conversion and heat release in regions outside the turbulent flame volumes are modeled as processes controlled by chemical kinetics. Particularly, in the calculation cells of the post-flame and final gas regions, chemical processes are assumed to be primarily controlled by reaction pathways defined by chemical kinetic mechanisms. In these regions, the turbulent-kinetic interaction model, including species transformation, can also be included [133].

Some turbulent flames may encounter unburned regions containing oxygen-rich or oxygen-poor mixtures. This interaction can lead to flame quenching, where layering causes the flame to lose its ability to burn, ultimately resulting in flame extinction. These regions where the flame tends to extinguish are known as Flame Quenching

Regions. For laminar flames, the combustibility of the unburned mixture is primarily controlled by the balance between the heat transfer from the preheat region due to chemical heat release and the heat loss from the preheat region to the unburned mixture. However, for turbulent flames, the disturbances caused by turbulence have significant additional effects on the heat transfer balance.

In ANSYS Forte's flame extinction model, local flame extinction is investigated by examining whether the local flame quenching boundary passes from the thin reaction zone regime to the broken reaction zone regime [133].

3.4.2 Spray model

ANSYS Forte is capable of reasonably simulating the preparation of the fuel-air mixture and the physical changes that occur during the fuel injection process before the combustion phase. Therefore, ANSYS Forte incorporates advanced sub-models to simulate multi-component fuel-spray fluid dynamics and interactions with multi-component gases. These sub-models include the Nozzle Flow Model, Breakup Models, Unsteady Gas Jet Model, Collision Model, and Vaporization Models.

3.4.2.1 Nozzle flow model

The Nozzle-Flow model explains the instantaneous flow conditions inside the nozzle. The primary purpose of this model is to provide initial conditions to the spray model. The input parameters for the nozzle flow model include mass flow rate, ambient gas pressure, physical properties of the liquid fuel, geometrical hole diameter, L/D ratio (where L is the length of the injector entrance region), and R/D ratio (where R is the radius of curvature of the injector entrance region). These input parameters are used within the nozzle flow model to determine the instantaneous discharge coefficient (Cd), spray angle, effective injection velocity, and effective flow exit area. The flow exit area is later used to determine the initial size of the injected liquid droplets. Flow through the injector nozzle shown in Figure 3.2 [133].

When the nozzle diameter is not equal to the outlet diameter during the flow, cavitation can occur. In such cases, cavitation can result in flow losses. Taking these flow losses into account, it's necessary to calculate the average flow velocity.

The volumetric average flow velocity (U_{mean}) at the entrance of the nozzle passage for liquid fuel is calculated using equation (3.48) as follows:

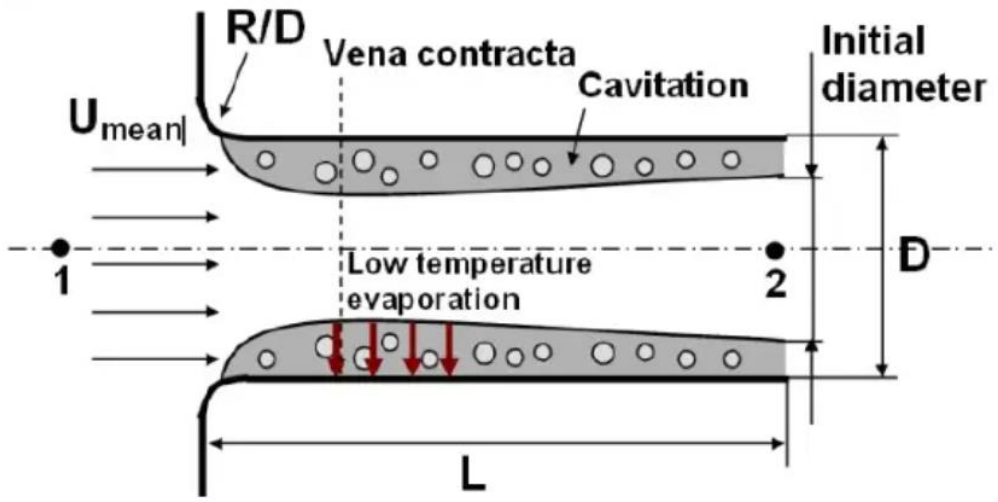

Figure 3.2 : Flow through injector nozzle [133].

$$U_{mean} = \frac{\dot{m}}{\rho_l A} = \frac{4\dot{m}}{\rho_l \pi D^2} \tag{3.48}$$

In the equation, $\dot{m}$ represents the mass flow rate, ρ_l is the density of the liquid fuel, A is the nozzle cross-sectional area, and D is the nozzle diameter. The average mass flow rate at the nozzle exit is always lower than the values estimated by the Bernoulli equation because it decreases due to losses in the flow. These losses occur as a result of expansion and include factors like acceleration, the formation of the inlet velocity profile, throat contraction, and wall friction. The amount of this difference is referred to as the "discharge coefficient (C_d)" and is calculated using equation (3.49).

$$C_d = \frac{U_{mean}}{\sqrt{2\frac{p_1 - p_2}{\rho_1}}} \tag{3.49}$$

p_1 represents the inlet pressure, and p_2 is the outlet pressure. ρ_l is the inlet density of the fluid. If inlet loss coefficients (K_{inlet}) are available in tabular form, the discharge coefficient for wall friction is determined using Blasius or laminar equations and is used as given in equation (3.50).

$$C_d = \frac{1}{\sqrt{K_{inlet} + f.\frac{L}{D} + 1}} \tag{3.50}$$

The friction coefficient f, which can take on a range of values, is proposed to be within the range given by equation (3.51).

$$f = \mathrm{Max}\left(0.316\mathrm{Re}^{0.25}, \frac{64}{\mathrm{Re_D}}\right) \tag{3.51}$$

Re_D is the Reynolds number associated with the nozzle diameter. The initial approximation for the inlet pressure (p_1) in a turbulent environment is determined using equation (3.52).

$$p_1 = p_2 + \frac{\rho_1}{2}\left(\frac{U_{mean}}{C_d}\right)^2 \tag{3.52}$$

In the next step, ANSYS Forte checks for cavitation in the flow under these conditions.

Assuming a uniform velocity profile and using Nurick's expression to calculate the contraction size, the minimum velocity in the smallest flow area is determined based on the principle of continuity.

This continuity principle indicates that the velocity at any section of the flow is related to the flow area and volume. Therefore, with Nurick's expression, the velocity (U_{vena}) at the point where the flow area is reduced is calculated, as shown in equation (3.53).

$$U_{vena} = \frac{U_{mean}}{C_c} \tag{3.53}$$

U_{vena} represents the velocity at the section where the flow area narrows, and C_c is the cavitation coefficient. C_c is given by equation (3.54) as shown below.

$$C_c = \left(2.6 - 11.4\frac{R}{D}\right)^{-0.5} \tag{3.54}$$

In the case of cavitation, the potential flow theory allows the application of Bernoulli's equation from point 1 to point 2 without any losses. In this scenario, equation (3.52) can be used as represented in Equation (3.55) below.

$$p_{vena} = p_1 - \frac{\rho}{2}(U_{vena})^2 \tag{3.55}$$

If p_{vena} is lower than the vapor pressure p_{vapor}, it indicates that the flow is entirely cavitated. In such a case, a new inlet pressure and discharge coefficient are calculated as shown in equation (3.56) and equation (3.57) below.

$$p_1 = p_{vapor} - \frac{\rho}{2}(U_{vena})^2 \tag{3.56}$$

$$C_D = C_c\sqrt{K} = C_c\sqrt{\frac{p_1 - p_{vapor}}{p_1 - p_2}} \tag{3.57}$$

In cases of non-cavitating turbulent flows, the exit velocity of droplets is set to be the same as the average velocity (U_{mean}), and the jet diameter at the nozzle outlet is equal to the nozzle diameter.

However, if cavitation occurs in the nozzle, in that case, the effective injection velocity components are calculated as shown in equation (3.58), and the effective exit area value is calculated as shown in equation (3.59). Additionally, the effective injection exit diameter value is given by equation (3.60).

$$U_{eff} = U_{vena} - \frac{p_2 - p_{vapor}}{p_1 U_{mean}} \tag{3.58}$$

$$A_{eff} = A\frac{U_{mean}}{U_{eff}} \tag{3.59}$$

$$D_{eff} = \sqrt{\frac{4A_{eff}}{\pi}} \tag{3.60}$$

In the nozzle flow model, the spray angle is predicted using an aerodynamic model. This approach is based on Taylor's analysis, which explains high-speed liquid disintegration due to the unstable growth of surface waves resulting in mass shedding. In this approach, the spray angle (θ) is represented by equation (3.61).

$$\tan\left(\frac{\theta}{2}\right) = \frac{4\pi}{A}\sqrt{\frac{\rho_g}{\rho_l}}f(T) \tag{3.61}$$

For the variable A in the equation, equation (3.62) is recommended.

$$A = 3 + 0.28\left(\frac{L}{D}\right) \tag{3.62}$$

The following equation (3.63) and equation (3.64) are used for the function f(T).

$$f(T) = \frac{\sqrt{3}}{6}[1 - \exp(-10T)] \tag{3.63}$$

$$T = \left(\frac{Re}{We}\right)^2 \frac{\rho_l}{\rho_g} \tag{3.64}$$

In ANSYS Forte, users conducting simulations have the option to input experimental constant values for the discharge coefficient and spray angle instead of applying the nozzle flow model. The experimental discharge coefficient is then used to calculate the effective injection velocity and initial droplet size at the nozzle exit [133].

3.4.2.2 Kelvin – Helmholtz / Rayleigh Taylor (KH/RT) break-up models

After the fuel exits the nozzle and encounters the turbulent environment inside the cylinder, the fuel spray undergoes a breakup process under the influence of surface and viscous forces. This breakup process occurs in two stages: primary and secondary breakup.

The breakup of the fuel jet is influenced by the Weber number, representing surface tensions, and the Reynolds number, representing viscous forces. Spray atomization and droplet breakup are modeled using the Kelvin-Helmholtz/Rayleigh-Taylor (KH/RT) hybrid breakup model [148,149].

The KH/RT (Kelvin-Helmholtz/Rayleigh-Taylor) breakup model for sprays combines two types of breakup models: the KH (Kelvin-Helmholtz) and RT (Rayleigh-Taylor) models. The KH breakup model is applied within a certain breakup length (L) from the nozzle exit (Region A). This model separates small droplets from the jet, but the jet still retains a dense liquid core. Beyond the Breakup Length (Region B), the RT model is used in conjunction with the KH model to predict secondary breakup. The breakup steps associated with the model are shown in Figure 3.3 [148–150].

3.4.2.2.1 Kelvin – Helmholtz model

The Kelvin-Helmholtz (KH) model is based on a linear stability analysis of a liquid jet to define the initial breakup region of a liquid jet [151,152]. As a result of linear stability analysis, it is observed that any disturbance applied to the liquid-gas interface can expand as a Fourier series, with the most rapidly growing mode contributing to the breakup and the formation of new droplets.

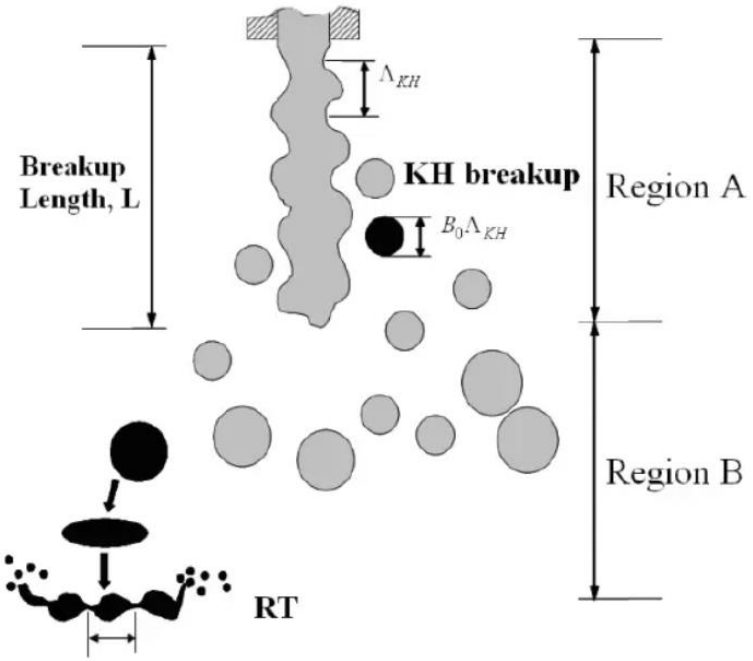

Figure 3.3 : KH/RT break-up model for liquid fuel jet [133].

The growth rate and wavelength of the most rapidly growing mode are numerically calculated and expressed in equations (3.65) and (3.66) as follows [151].

$$\frac{\Lambda_{KH}}{r_p} = 9.02\frac{(1+0.45Z^{0.5})(1+0.4T^{0.7})}{\left(1+0.87We_g^{1.67}\right)^{0.6}} \tag{3.65}$$

$$\Omega_{KH}\left(\frac{\rho_l r_p^3}{\sigma}\right)^{0.5} = \frac{\left(0.34+0.38We_g^{1.5}\right)}{(1+Z)(1+1.4T^{0.6})} \tag{3.66}$$

In the equations, Λ_{KH} represents the wavelength of the fastest growing wave, Ω_{KH} is its growth rate, r_p is the jet radius, σ is surface tension, and We_g is the dimensionless Weber number for gas, as shown in equation (3.67).

$$We_g = \frac{\rho_g U_{rel}^2 r_p}{\sigma} \tag{3.67}$$

U_{rel} represents the magnitude of the relative velocity between the liquid and gas phases. Equation (3.68) is used for relative velocity.

$$U_{rel} = \left|\vec{V}_{gas} + \vec{V}'_{turb} - \vec{u}_d\right| \tag{3.68}$$

The vector $\vec{V}_{gas}$ represents the CFD gas phase constant, and the Weber number for liquid phases is similarly represented using equation (3.69).

$$We_l = \frac{\rho_l U_{rel}^2 r_p}{\sigma} \tag{3.69}$$

Some dimensionless numbers affect the fragmentation of the liquid jet. These include the Ohnesorge number and the Reynolds number, which are respectively represented by equation (3.70) and equation (3.71) below.

$$Z = \frac{\sqrt{We_l}}{Re_l} \tag{3.70}$$

$$Re_l = \frac{\rho_l U_{rel}^2 r_p}{\mu_l} \tag{3.71}$$

μ_l represents the dynamic viscosity of the liquid. Another dimensionless number is the Taylor number, which is represented by equation (3.72).

$$T = Z\sqrt{We_g} \tag{3.72}$$

The relationship between the radius (r_c) of the newly formed droplets during the primary break-up process and the wavelength (Λ_{KH}) is expressed by equation (3.73).

$$r_c = B_{KH}\Lambda_{KH} \tag{3.73}$$

B_{KH} represents the size constant of the Kelvin-Helmholtz (KH) breakup model. ANSYS Forte uses the "blob injection" concept, where it assumes that the liquid jet initially consists of blobs with characteristic sizes equal to the nozzle diameter [153]. Using this concept, primary breakup is modeled as a process where new droplets (with a radius of r_c) are formed from previous droplets (with a radius of r_p). The change in radius due to the mass loss from the previous droplets to the subsequent droplets is defined by the velocity equation. The resulting radius change is followed according to the ratio given in equation (3.74) [153].

$$\frac{r_p - r_c}{\tau_{KH}} \tag{3.74}$$

The droplet radius initially formed (r_p) is either equal to or larger than the droplet radius formed later (r_c). Here, τ_{KH} is the breakup time scale. This relationship is shown in equation (3.75).

$$\tau_{KH} = \frac{3.726 C_{KH} r_p}{\Lambda_{KH} \Omega_{KH}} \quad (3.75)$$

C_{KH} is the time constant of the KH breakup model. In summary, the KH breakup model consists of two steps. The first step gradually reduces the size of the initial droplet (parent droplet) through the velocity equation (equation 3.74), and the second step creates a new particle. During the second breakup step, there are two different options that can be used to determine the droplet sizes and droplet count of the initial and final particles.

In the first option, the droplet count in the initial particle remains the same before and after breakup. The droplet sizes in the initial particle are adjusted based only on the subset received by the final particle. This is the default option used in ANSYS Forte.

In the second option, it is argued that the second breakup step involves the numerical regrouping of droplets and there is no actual breakup event. Therefore, not only the mass conservation between the initial and final particles but also the original Sauter Mean Diameter (SMD) is preserved. Applying this SMD preservation constraint generally results in a slower breakup rate [133].

3.4.2.2.2 Rayleigh - Taylor model

The Rayleigh-Taylor (RT) model is used in conjunction with the KH model to predict the secondary breakup of spray droplets [148,149]. The breakup length is predicted using Levich's theory and is calculated as shown in equation (3.76) [152].

$$L_{brk} = C_b d_{noz} \sqrt{\frac{\rho_l}{\rho_g}} \quad (3.76)$$

In the equation, dnoz represents the nozzle radius, C_b is the RT distance constant, ρ_l is the liquid phase density of the fluid, and ρ_g is the gas phase density of the fluid.

The RT model considers the instability that occurs when two fluids with different densities accelerate in a direction perpendicular to the interfaces during the breakup.

Therefore, it calculates the frequency and wavelength of the fastest-growing wave as suggested by the equations proposed by Bellman as shown below (Equation 3.77 and equation 3.78) [154].

$$\Omega_{RT} = \sqrt{\frac{2}{3\sqrt{3\sigma}} \frac{\left[-a\left(\rho_l - \rho_g\right)\right]^{3/2}}{\rho_l + \rho_g}} \tag{3.77}$$

$$\Lambda_{RT} = 2\pi \sqrt{\frac{3\sigma}{-a\left(\rho_l - \rho_g\right)}} \tag{3.78}$$

The term "a" in the equation represents the deceleration experienced by a droplet moving through the air at high speeds. Similar to the KH model, the RT model also performs calculations based on the breakup of the fastest-growing droplet.

The equations for the radius of the newly formed droplet and the breakup time are proposed as shown in equation (3.79) and equation (3.80) respectively.

$$r_c = B_{RT}\Lambda_{RT} \tag{3.79}$$

$$\tau_{RT} = \frac{C_{RT}}{\Omega_{RT_{RT}}} \tag{3.80}$$

Here, B_{RT} and C_{RT} are two constants. B_{RT} is the RT Breakup Size Constant, and C_{RT} is the RT Breakup Time Constant.

Unlike the KH model, the standard implementation of the RT model does not separate the small-sized final droplets from the initial droplets; instead, it assumes the final droplet as a partial breakup of the initial droplet and assumes that the liquid column of droplets disintegrates at the end, mixing with the surrounding gas.

ANSYS Forte reduces the time step dependency of the RT model by modeling the RT breakup process with a velocity equation, similar to equation (3.74) of the KH model.

$$\frac{dr_p}{dt} = -\frac{r_p - r_c}{\tau_{RT}} \tag{3.81}$$

Here, r_c is estimated using equation (3.79). The initial droplet continuously breaks up at each time step, preventing time step dependency. It is assumed that r_c does not change over time and is analytically solved using equation (3.81).

If equation (3.81) is integrated under the required conditions, the term r_p, as shown in equation (3.82), is analytically obtained.

$$r_p = r_c + (r_{p,0} - r_c)\exp^{\frac{t}{\tau_{RT}}} \quad (3.82)$$

Here, $r_{p,0}$ is the initial radius of the first droplet at the beginning of the breakup. Therefore, the characteristic time τ required for the breakup of the first droplet depends on the initial radius of $r_{p,0}$ [133].

3.4.2.3 Unsteady gas-jet model

The mesh dependency of the KH-RT breakup model arises from the calculation of the liquid-gas relative velocity U_{rel} as described in equation (3.68). In this calculation, U_{rel} is taken as the velocity of the gas inside the CFD cell. ANSYS Forte uses an unsteady gas jet model to eliminate the mesh size dependency of the interaction between the liquid droplet and the surrounding gas [151,155,156].

The gas jet model is based on the theory of an unsteady gas jet, where the relative velocity between the droplet and gas is modeled without the need for differentiation within the CFD grid. Liquid droplets are assumed to behave as a gas jet after breakup, and they are solved within the Unsteady Gas-Jet Model. The visual representation of the model is shown in Figure 3.4.

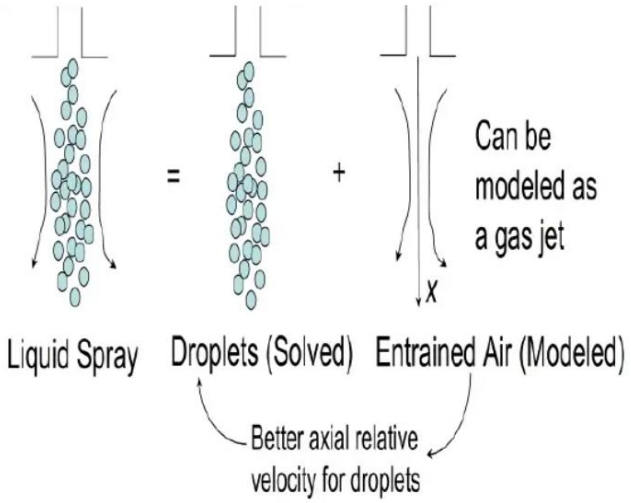

Figure 3.4 : Unsteady gas-jet model [133].

The jet's tip part in the Unsteady Gas-Jet Model evolves as shown in equation (3.83).

$$\frac{dx}{dt} = \frac{3}{K}\frac{U_{inj,eff}(y,t)d_{eq}}{x} \quad \& \quad (x \geq x_0) \quad (3.83)$$

The equation contains the following variables: x, the jet tip penetration; y, the local spray axial location of the particle; K, an entrainment constant; $U_{inj,eff}$, the effective injection velocity; and d_{eq}, the equivalent diameter. The equivalent diameter is related to the nozzle diameter (d_{noz}) and the liquid-gas density ratio. It is shown in equation (3.84).

$$d_{eq} = d_{noz}\sqrt{\frac{\rho_l}{\rho_g}} \tag{3.84}$$

The downstream spray-axial location, denoted as x_0, marks the start of the jet velocity decay, and it is calculated as shown in equation (3.85).

$$x_0 = \frac{3d_{eq}}{K} \tag{3.85}$$

The effective injection velocity ($U_{inj,eff}$) is considered as an indicator of changes in injection velocity. It is obtained by taking the integral of injection velocity from the start of injection (t_0) to the current time (t) (Equation 3.86).

$$U_{inj,eff}(y,t) = U_{inj}(t_0) + \int_{t_0}^{t} R(y,t-\tau)\left(\frac{dU_{inj}(\tau)}{dt}\right)_{\tau} dt \tag{3.86}$$

The response function (R) in the equation is represented by equation (3.87).

$$R(y,t-\tau) = 1 - \exp\left[-\frac{t-\tau}{\tau_v(y,\tau)}\right] \tag{3.87}$$

The response time scale (τ_v) in the equation is related to the local flow time scale (τ_f) and the Stokes Number (St) (Equation 3.88).

$$\tau_v(y,\tau) = St.\,\tau_f(y,\tau) = St\frac{y}{U_{inj}(\tau)} \tag{3.88}$$

All the forces acting on a particle within the flow field cause changes in the particle's velocity. When we track the changes in velocity over time, we can see how the particle responds to the surrounding gas medium. Examining this transformation of the particle within a time scale allows us to determine how long the particle has been present in the flow and in which direction along the local axial location (y) it is situated [143].

The local gas-jet speed along the spray axis direction ($U_{jet,ax}$) is shown by equation (3.89) as follows.

$$U_{jet,ax}(y,t) = \frac{3}{K}\frac{U_{inj,eff}(y,t)d_{eq}}{y} \quad \& \quad (y \geq x_0) \tag{3.89}$$

It is possible to calculate the gas jet velocity in cylindrical coordinates. With the assumption of axisymmetry, the gas jet velocity at any radial position r within the jet cross-section can be calculated as following equation (3.90) [155].

$$U_{jet}(y,r,t) = \frac{3U_{inj,eff}(y,t)d_{eq}}{Ky\left(1+\frac{12r^2}{K^2y^2}\right)} \quad \& \quad (y \geq x_0) \tag{3.90}$$

Using the gas jet velocity in equation (3.90), it is possible to model the drop-gas relative motion given by equation (3.68) with equation (3.91).

$$\frac{d\vec{u}_d}{dt} = \frac{3}{8}C_D\frac{\rho_l}{\rho_g}\frac{1}{D}\left|\vec{V}_{gas}+\vec{V}'_{turb}-\vec{u}_d\right|\left(\vec{V}_{gas}+\vec{V}'_{turb}-\vec{u}_d\right)\vec{g} \tag{3.91}$$

In the equation, $\vec{u}_d$ represents the droplet velocity vector, C_D is the drag coefficient, $\vec{V}'_{turb}$ is the local gas phase turbulent fluctuating velocity vector, and $\vec{g}$ is the gravitational acceleration.

$\vec{V}_{jet}$ from equation (3.91) indicates the corrected mean velocity of the gas jet. The radial and angular components are preserved and therefore do not appear in the equations.

Thus, instead of the term $\vec{V}_{gas}$, the corrected velocity component $\vec{V}_{jet}$ is used. Equation (3.68) takes the following form as equation (3.92).

$$U_{rel} = \left|\vec{V}_{jet}+\vec{V}'_{turb}-\vec{u}_d\right| \tag{3.92}$$

Jet velocities should be calculated using different equations depending on the distance from the injector nozzle. For example, in regions very close to the nozzle, the jet velocity is nearly equal to the injection velocity, while in more distant regions, the jet's velocity is slower. Below are the equations for positional jet velocities relative to the nozzle. When examining Figure 3.5, the variation of the velocity regime with distance for the effective jet velocity can be observed.

$$U_{jet,ax}(y,t) = \begin{cases} \gamma U_{inj,eff}(y,t).\left[1-\left(\frac{x}{x_0}\right)^2\right] & \text{if } y \le x_0 \\ \gamma U_{inj,eff}(y,t).\left[1-\frac{1}{8}\left(\frac{x}{x_0}\right)^2\right] & \text{if } x_0 < y < x_{cvg} \\ \frac{3U_{inj,eff}(y,t)d_{eq}}{Ky} & \text{if } y > x_{cvg} \end{cases} \quad (3.93)$$

The coefficient γ in the equations has a value of 0.6. Applying the parabolic drag gas-jet velocity profile along the spray axis is quite effective in reducing the grid-size dependence of the break-up models. In ANSYS Forte, the gas entrainment constant K in equation (3.83) is a user-defined input. A larger K value increases the gas drag force and, therefore, reduces the spray penetration length. Additionally, the Effective Distance Factor is a dimensionless distance factor used to control the effective range of the gas jet model. The actual effective distance is calculated by multiplying this factor with the breakup length and is measured from the nozzle exit to the spray droplets [133].

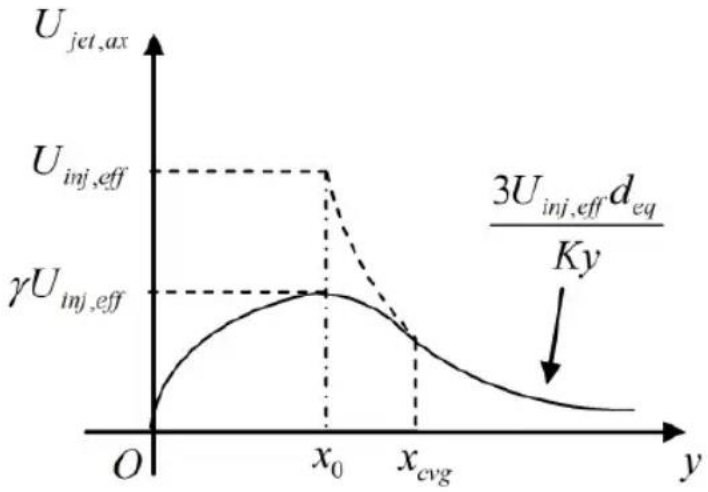

Figure 3.5 : Effective injection velocity in unsteady gas-jet model [133].

3.4.3 Droplet collision and coalescence model

The event of droplet collision and coalescence represents important physical phenomena in dense spray processes. The collision event has been defined by O'Rourke with three fundamental components. These are: first, permanent coalescence; second, the grazing event – in which droplets separate after collision and turn into satellite droplets; and third, shattering events [157]. However, Munnannur and Reitz have added various additional collision outcomes in addition to the collision

results. These additional components include bouncing, stretching, and reflexive separation [158]. The outcome that will occur depends on the forces acting on the colliding droplet pair. At low Weber numbers, surface forces exceed liquid inertia forces, and the droplets tend to coalesce permanently. At higher Weber numbers, liquid inertia forces become more prominent, and grazing collisions can occur. With further increases in the Weber number, dominant liquid inertia forces can lead to the shattering of colliding droplets and the formation of small droplet clusters. ANSYS Forte provides all these outcomes to accurately predict the results of a successful collision [133].

The possible collision outcomes for two colliding droplet fragments are shown in equation (3.94) below.

$$\upsilon = \frac{N_1 N_2}{V_{col}} \rho (r_1 + r_2) \left| \vec{u}_{d,1} - \vec{u}_{d,2} \right| \tag{3.94}$$

The terms N_1 and N_2 in the equation represent the number of droplets in two different parcels, the terms r_1 and r_2 represent the average radius of the droplets in the parcels, and the term V_{col} represents the control volume in which droplet collisions occur [133].

3.4.3.1 Radius of influence (ROI) collision model

In O'Rourke's collision model, spray particles are allowed to collide only if they are in the same computational cell. In a cylindrical grid, the cell size around the spray axis can be very small, which may prevent collisions from occurring. In ANSYS Forte, to eliminate both mesh size dependence and time step dependence in the droplet collision process, the Radius of Influence (ROI) collision model is used [158]. In the ROI method, a particle is allowed to collide only with another particle if it is within the influence radius of the other particle. Droplets that are likely to collide within a specific parcel are searched for within an "influence region" generated near the parcel. All particles within this influence region can be potential collision partners. This approach eliminates the mesh size dependence in the CFD grid [157–159].

The problem of time step dependence was also investigated in a study by Munnannur, taking into account the observation that a particle's travel distance within one time step should be a fraction of the average cell length. Using the Munnanur ROI approach, the mean collision time (MCT) for each cell is suggested as equation (3.95) [133,158].

$$\Delta t_{col} = \frac{C_{col}}{u_{d,max,cell}} \frac{R_{inf}}{N_{ROI}^{1/3}} \tag{3.95}$$

The variable u_d in the equation represents the average droplet velocity, and N_{ROI} denotes the number of parcels within the radius of influence. In ANSYS Forte for ROI model, the influence radius (R_{inf}) is considered as the default value based on Munnannur's recommended value [158].

3.4.3.2 Collision mesh model

ANSYS Forte includes an alternative approach to reduce the solution grid dependency of the collision model, called the "collision mesh model," in addition to the ROI model [160]. The Collision Mesh model creates a separate virtual cylindrical collision solution by segregating the particles present in the computational solution grid. This approach is called the Collision Mesh model and is based on cylindrical coordinates, primarily used in conjunction with coaxial sprays. It ensures that, in cases where the predicted axial symmetry of the spray structure diminishes, cylindrical-coordinate particle groups are always randomly rotated around the spray axis at each time step. This method allows for the possibility of collisions between particles located in the same grid cell. The use of the Collision Mesh grid model requires determining the angular diameter, height, and the number of grids of the collision grid [133].

3.4.4 Multi-compenent droplet vaporization model

In the previous sections, we examined the events related to the breakup, coalescence, and collision of droplets. Now, we will delve into the physical and chemical mechanisms of the evaporation of these broken, combined, and collided droplets. ANSYS Forte uses a discrete multi-component (DMC) fuel evaporation model to represent the evaporation of spray droplets [161]. The DMC evaporation model tracks the individual components (molecules) of a real surrogate fuel during the evaporation process and allows these individual fuel components to interact with reaction kinetics. In the DMC model, an explicit form of the equation (an approximate solution of the quasi-steady energy equation) that determines the heat flux from the droplet-gas interface to the surrounding gas mixture is obtained through an approximate solution [133]. The model is formulated to track each component of the fuel independently, regardless of direction, from evaporation at the droplet surface to re-condensation from

vapor to the droplet surface. Additionally, the DMC evaporation model assumes that a liquid droplet containing a finite number of components evaporates without chemical reactions in a spherical structure. It neglects second-order effects such as radiation, Soret, and Dufour effects [133].

The process of evaporation involves the transition from the liquid phase to the gas phase, so all effects related to the liquid and gas phases must be carefully examined. The distribution of liquid fuel in the surrounding environment is crucial for the evaporation process. Therefore, it is assumed that the ambient gas is not absorbed into the liquid fuel, and the distribution of liquid fuel in the ambient environment is given by equation (3.96) as follows.

$$\frac{d}{dt}\left(y_{i,l}\rho_l\frac{4}{3}\pi R^3\right) = \dot{m}_i 4\pi R^2 \tag{3.96}$$

Here, $y_{i,l}$ is the mass fraction of liquid droplet component i, ρ_l is the mass density of liquid fuel, R is the droplet radius, and $\dot{m}_i$ is the evaporative mass rate per unit area of species i [133].

The change in liquid droplet energy is obtained from the energy conservation equation for a two-phase system consisting of the droplet and the surrounding gas mixture. The equation is shown below as equation (3.97).

$$\frac{d}{dt}\left[\int_0^R c_{v,l}\rho_l 4\pi^2 r^2 T(r)dr\right] = \frac{d}{dt}\left(c_{v,l}\rho_l\frac{4}{3}\pi R^3 T_d\right) = 4\pi R^2\left(q_i - \dot{m}c_{v,l}T_s\right) \tag{3.97}$$

Where, $c_{v,l}$ is the specific heat capacity of the liquid fuel, q_i is the heat transfer rate per unit area from the droplet surface to the inner part of the droplet, and T_d and T_s are, respectively, the average droplet temperature and the droplet surface temperature. The equations related to the gas phase after the liquid phase should be examined carefully. The transport equation for the conservation of species in the gas phase is shown by equation (3.98).

$$\frac{d}{dt}(\rho y_i) + \nabla(\rho y_i \nu) = \nabla(\rho D_i \nabla y_i) + S_{g,i} \tag{3.98}$$

Where, ν is the velocity of the gas mixture, ρ is the density of the gas mixture, y_i and D_i represent the mass fraction and diffusion coefficient of species i, and $S_{g,i}$ is the term

from the vaporization source. Equation (3.98) represents the species i within it. For a diesel engine inside a cylinder, there are typically two species: air and fuel. Therefore, the species conservation equation for the mixture of air and fuel is as shown in equation (3.99) [133].

$$\frac{d}{dt}(\rho y_F) + \nabla(\rho y_F v) = \nabla(\rho \bar{D} \nabla y_F) + S_g \tag{3.99}$$

Here, y_F is the total mass fraction of the fuel species, $\bar{D}$ is the average diffusivity of the fuel species, and S_g is the total evaporation source term. Once the species conservation equation is expressed in equation (3.99), the energy conservation equation for the gas phase with two species (air-fuel) is shown in equation (3.100) [133].

$$\bar{C}_P \frac{\partial}{\partial t}(\rho T) + \bar{C}_P \nabla.(\rho v T) = \nabla.\lambda \nabla T + (\overline{C_{PF} D_F} - C_{PA}\bar{D})\rho \nabla y_F.\nabla T \tag{3.100}$$

Here, T is the temperature, k is the thermal conductivity, $\bar{C}_P$ is the mixture specific heat, C_{PA} is the specific heat of air, and $\overline{C_{PF} D_F}$ represents the average value of the product of the specific heat and the diffusion coefficient of the fuel species. The last term in equation (3.100) represents the energy transport due to the inter-diffusion of species [133].

The equilibrium between the droplet and the surrounding gas phase is based on the assumption that the chemical potential energy is equal for each species in both the liquid and gas phases. Assuming that the mixture (air-fuel) is in the form of an ideal solution, the fuel vapor mass fraction can be determined using Raoult's Law. Raoult's Law suggests an equation relating the mole fractions of species to their partial pressures. Equation (3.101) shows Raoult's Law as follows.

$$p_{i,v} = x_{i,v} P = x_{i,l} P_{sat,i} \tag{3.101}$$

Where, p_i represents the partial pressure of species i in the vapor phase on the droplet's surface, $P_{sat,i}$ is the vapor pressure of species i at temperature T, x is the mole fraction, and v and l indices denote the vapor and liquid phases, respectively. The vapor pressure of a species is determined by the Clausius-Clapeyron equation. The droplet's surface temperature is determined from the heat and mass transfer balance between the droplet

and the surrounding gas. Heat transfer occurs in two different regimes: first, the heat transfer from the inside of the droplet to the surface (q_i), and second, the heat transfer from the external gas to the surface (q_0). The rate of heat transfer balances with the heat required for evaporation at the surface.

$$L(T_s)\dot{m} = q_i + q_0 \tag{3.102}$$

For the equation (3.102), $\dot{m}$ represents the mass vaporization rate, and $L(T_s)$ is the latent heat of the fuel at the surface temperature Ts. Heat transfer occurring inside the droplet is modeled as a convective heat transfer process, taking into account the circulation between the droplet and the surrounding gas. The effective heat transfer coefficient in this heat transfer process is determined from the approximate solution of the energy equation for the vapor phase, considering the effects of inter-species diffusion and Stefan flow. Equation (3.103) combines the temperatures of the droplet and the surrounding gas mixture in a common equation [161].

$$\dot{m}L(T_s) = h_{i,eff}(T_d - T_s) + \frac{\kappa\bar{C}_P\dot{m}}{\exp\left[\frac{2r_0\bar{C}_P\dot{m}}{\lambda Nu} - \frac{(C_A)(y_{Fsur} - y_{F0})}{\lambda}\frac{Sh}{Nu}\right] - 1}(T_{sur} - T_s) \tag{3.103}$$

Equation (3.103) contains $h_{i,eff}$, which represents the droplet convective heat transfer coefficient. It is obtained from thermal conductivity (λ) and the unsteady equivalent thickness of the thermal boundary layer (r_0). Sh and Nu are the Sherwood and Nusselt numbers, respectively. C_p is the average specific heat of the gas mixture including fuel vapor, and the κ term is a correlation factor suggested by Ra and Reitz [162].

C_A represents the inter-diffusional difference in energy flux between fuel and air. The terms y_{F0} and y_{Fsur} in the equation are the fuel mass fractions at the interface and far away from the interface, respectively. T_{sur} is the temperature of the ambient gas. The mass transfer rate at the droplet surface is calculated using the equation for the high mass transfer rate calculated with Spalding's transfer number (Equation 3.104) [163].

$$\dot{m} = g_m \ln(1 + B_M) \tag{3.104}$$

The symbol "g_m" represents the mass transfer coefficient, which is calculated using equation (3.105).

$$g_m = \frac{Sh\rho\overline{D}}{2R} \tag{3.105}$$

The symbol "B_M" represents Spalding's transfer number (STN), and it is shown in equation (3.106).

$$STN = \frac{(y_{Fs} - y_{Fsur})}{(1 - y_{Fs})} \tag{3.106}$$

The boiling model is based on the following three fundamental propositions:

- Unless the droplet undergoes significant surface distortion, surface decay can be neglected.
- Droplets do not suddenly shatter due to internal events (such as micro-explosions).
- As long as the droplet's surface temperature remains in equilibrium, it will remain at the boiling temperature.

Furthermore, it is assumed that the surface temperature (T_S) is equal to the fuel's boiling temperature (T_b). Under these assumptions, equation (3.103) is transformed into the form shown in equation (3.107) [133].

$$\dot{m}L(T_b) = (h_{i,eff,s} - \alpha_{SH})(T_d - T_b) + \frac{\kappa\overline{C}_P\dot{m}}{\exp\left[\frac{2r_0\overline{C}_P\dot{m}}{\lambda Nu} - \frac{(C_A)(y_{Fsur} - 1)}{\lambda}\frac{Sh}{Nu}\right] - 1}(T_{sur} - T_b) \tag{3.107}$$

Where, $h_{i,eff}$ represents the contribution of heat transfer by internal circulation at saturation temperature, and α_{SH} represents the factor that enhances heat transfer through nucleation effects. The evaporation rate calculated based on Spalding's mass transfer number (Equation 3.104) is no longer valid under these conditions [133].

4. NUMERICAL STUDY

A numerical study was conducted to model a compression-ignition diesel engine that had been previously studied in experimental research in the literature [7–9]. In the experiment, a diesel engine was operated in dual-fuel mode, using both diesel and natural gas, and the experimental results were obtained in this manner. The experimental study was conducted at a constant speed of 910 RPM and a fixed indicated mean effective pressure (IMEP) of 4.05 BMEP. The engine's power was adjusted in such a way that 25% was provided by diesel fuel, and the remaining 75% was supplied by natural gas. The experiment examined the effects of different diesel fuel injection timings (10°, 14°, 18°, 22°, 26°, 30°, 34°, 38°, 42°, 46°, and 50° CA BTDC) on the engine's performance under 25% load conditions [7–9]. The conditions used for this experiment were taken into account to establish a numerical model using the CFD program ANSYS Forte. The accuracy of the numerical model was validated by comparing it with the experimental results. Subsequently, various parametric studies were conducted to investigate the effects of alternative fuels on performance and emission values.

4.1 Set of the Numerical Model

ANSYS Forte CFD program was used to establish the numerical model and obtain results. This program, with its compatibility with the chemical kinetics program called Chemkin-Pro, provided practical capabilities for modeling the fuel. In the modeled engine in ANSYS Forte, the injectors are 6-hole and their positions are symmetrical to each other. In such cases, many CFD programs implement a practical application called "sector mesh" to prevent unnecessary processing of both time and data. ANSYS Forte uses this symmetry to allow modeling of the engine by dividing the combustion chamber into slices based on the number of injector nozzle holes, as results will be similar for each injector hole. In this study, since the injector nozzle has 6 holes, the results were obtained for the 60° combustion chamber slice. In this study, the closed-cylinder internal combustion was modeled as a closed process in the ANSYS Forte

CFD program. The analyses started with the intake valve closing (IVC) and ended with the exhaust valve opening (EVO). The grid structure was created within the program itself without the need for any other program.

4.1.1 Model geometry

The modeled engine is a single-cylinder direct-injection heavy-duty diesel engine with six nozzle holes in its injector [7–9].

Table 4.1 : Engine specifications.

Test Engine	Caterpillar 3401
Number of Cylinders	1
Bore x Stroke	137.2 mm x 165.1 mm
Compression Ratio	16.25:1
Stroke Volume	2.44 L
Spray Angle	130º
Spray Cone Angle	15º
Number of Valves	2 intake & 2 exhaust
Diesel Injection	Direct Injection
Natural Gas Injection	Port Injection
Maximum Power	74.6 kW (@2100 rpm)

All geometric parameters used in the experimental conditions have been adapted to the program in the numerical modeling.

Some of these parameters include compression ratio, injection angle, spray cone angle, cylinder volume, and combustion chamber geometry. Engine specifications are shown in Table 4.1.

4.1.2 Initial and boundary conditions

Considering that the study was conducted under partial load conditions and the characteristic features of the heavy-duty engine, as well as the low-speed operation (910 rpm), it is assumed that the swirl ratio is not very high. A swirl ratio of 0.5 is assumed as the initial value [164–166]. The spray angle is obtained as 130°, and the spray cone angle is 15° from the engine specifications.

4.1.3 Adapting experimental conditions to the numerical model

The experiment was conducted on a compression ignition diesel engine operating in dual-fuel mode at partial load (4.05 BMEP - 25%). The engine's energy was supplied by 25% diesel fuel and 75% natural gas. Natural gas was introduced into the cylinder

through a low-pressure gas injector in the intake port, while diesel fuel was injected directly into the combustion chamber.

Table 4.2 : Initial conditions.

Intake Pressure (bar)	1.02
Intake Temperature (K)	360
Turbulent Kinetic Energy (m^2/s^2)	10
Turbulent Length Scale (m)	0.003
Turbulent Model	Rans RNG k-epsilon
Swirl Ratio	0.5
Spray Angle	130^o
Spray Cone Angle	15^o
Nozzle Hole Number	6
Nozzle Hole Diameter (mm)	0.23
IVO (CA BTDC)	358.3^o
IVC (CA BTDC)	169.7^o
EVO (CA ATDC)	145.3^o
EVC (CA ATDC)	348.3^o

The engine power (4.05 BMEP) and speed (910 rpm) were kept constant, and the injection advance of the injected diesel fuel was varied (10°, 14°, 18°, 22°, 26°, 30°, 34°, 38°, 42°, 46°, and 50° CA BTDC) to measure performance and emission values [7–9].

Table 4.3 : Boundary conditions.

Cylinder Head	Wall, 425 K
Piston	Mesh Movement, 450 K
Liner	Wall, 400 K
Segment Cut	Periodic Inlet Outlet

In modeling this experimental study using the ANSYS Forte CFD program, it is crucial to accurately adapt the experimental conditions to the simulation. As mentioned in the previous sections, the geometry of the engine, initial conditions, and boundary conditions were input into the CFD program. The properties of the fuel and the quantities of the fuels used need to be correctly introduced into the program for satisfactory results in the numerical study.

The flexible communication between ANSYS Forte and the Chemkin Pro software provides significant advantages in numerical modeling. When modeling fuel using Chemkin Pro, the program creates a skeletal kinetic mechanism by using three types of files: one containing the reaction mechanisms of species likely to be involved during

combustion, one with the thermodynamic properties of the species, and, if necessary, a transport file that calculates heat transfer and heat flux for interactions between the fuel and the surfaces. This skeletal kinetic mechanism incorporates these three file types to model fuel chemical kinetics. This extensive kinetic mechanism, which contains a high number of species and reactions, can be simplified by removing some species and reactions based on their weak influences, creating a reduced mechanism. This approach allows for obtaining reasonable numerical results more quickly and reduces the computational cost. For the analysis, methane (CH_4) represented natural gas, and n-heptane (n-C_7H_{16}) represented diesel fuel. Consequently, the kinetics of these two fuels were derived from the mechanism files. The mechanism used in the analysis consists of 137 species and 1022 reaction steps [167]. Within the program, the physical properties of n-heptane fuel were replaced with n-tetradecane (n-$C_{14}H_{30}$) to better mimic the physical characteristics of diesel fuel [168]. To model spray characteristics, the effective radius of influence collision model was used, with an impact radius set to 0.2 cm [168].

After modeling the fuel used in the analysis, the fuel quantities used in the test conditions were entered into the program. The fuel quantities for the test conditions are shown in Table 4.4 below. The energy fraction balance between natural gas and diesel fuels in the experiments was ensured by Equation 4.1 [7–9].

$$NG\% = \frac{m_{NG}.LHV_{NG}}{m_{NG}.LHV_{NG} + m_{D}.LHV_{D}} x100 \quad (4.1)$$

Table 4.4 : Test conditions [7–9].

Test Cases	P_{intake}	T_{intake}	Engine Speed	SOI	EOI	Air	Diesel	NG
-	(bar)	(K)	(rpm)	(CA BTDC)	(CA BTDC)	(kg/h)	(kg/h)	(kg/h)
1				10°	3.57°	66.93	0.5238	1.470
2				14°	7.71°	67.21	0.4948	1.389
3				18°	11.81°	67.57	0.4710	1.306
4				22°	15.89°	67.45	0.4503	1.259
5				26°	19.95°	67.08	0.4370	1.237
6	1.05	313	910	30°	23.86°	66.70	0.4552	1.234
7				34°	27.99°	67.24	0.4337	1.215
8				38°	32.01°	67.62	0.4314	1.199
9				42°	36.04°	67.73	0.4167	1.190
10				46°	40.12°	67.65	0.4122	1.179
11				50°	44.15°	67.85	0.4134	1.164

In the equation, m_{NG} and m_D represent the mass of natural gas and diesel fuel per cycle, respectively. LHV_{NG} and LHV_D represent the lower heating values of natural gas and diesel fuels, respectively. LHV_{NG} is assumed to be 50000 kJ/kg, while LHV_D is assumed to be 44640 kJ/kg.

4.1.4 Mesh structure

When setting up the numerical model, the mesh structure plays a crucial role in the accuracy of the results. Having a very fine mesh does not necessarily imply a correct mesh structure. The mesh structure should be created based on regional priorities within the cylinder. In a closed-cycle simulation, a sequence of processes including compression, injection, combustion, and expansion occurs during one cycle. It is known that physical and chemical events have a more significant impact on the cycle at crank angles where injection and combustion processes take place. Therefore, a finer mesh is required for the crank angles where these processes occur, while a reasonable mesh density is sufficient for the compression and expansion processes. CFD program recommendations generally suggest that cell sizes should be a minimum of 0.5 mm and a maximum of 2 mm. The aspect ratio of the mesh structures (the ratio of the longest side to the shortest side of a cell) should preferably be close to 1 or equal to 1 [168,169].

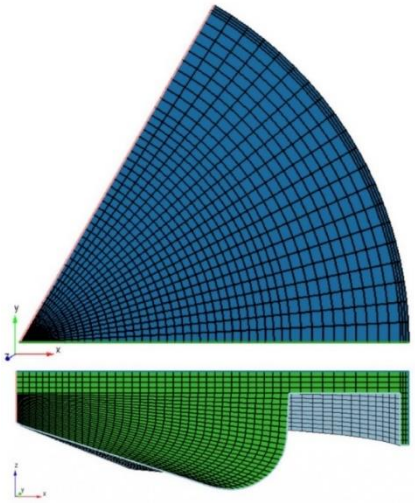

Figure 4.1 : Mesh structure of combustion chamber geometry.

A higher mesh density should be used in the vicinity of the injector and where the injection and combustion processes take place. Structuring the mesh in this way not only prevents unnecessary extension of the analysis but also helps create an economically efficient computational environment for the computer's operating

system. The mesh structure for the modeled engine's combustion chamber is shown in Figure 4.1.

4.2 Grid-Independent Solution

As mentioned earlier, both obtaining reliable numerical results and saving time and computational resources are essential for mesh structure. Another important point is that numerical results should not change as the mesh density increases.

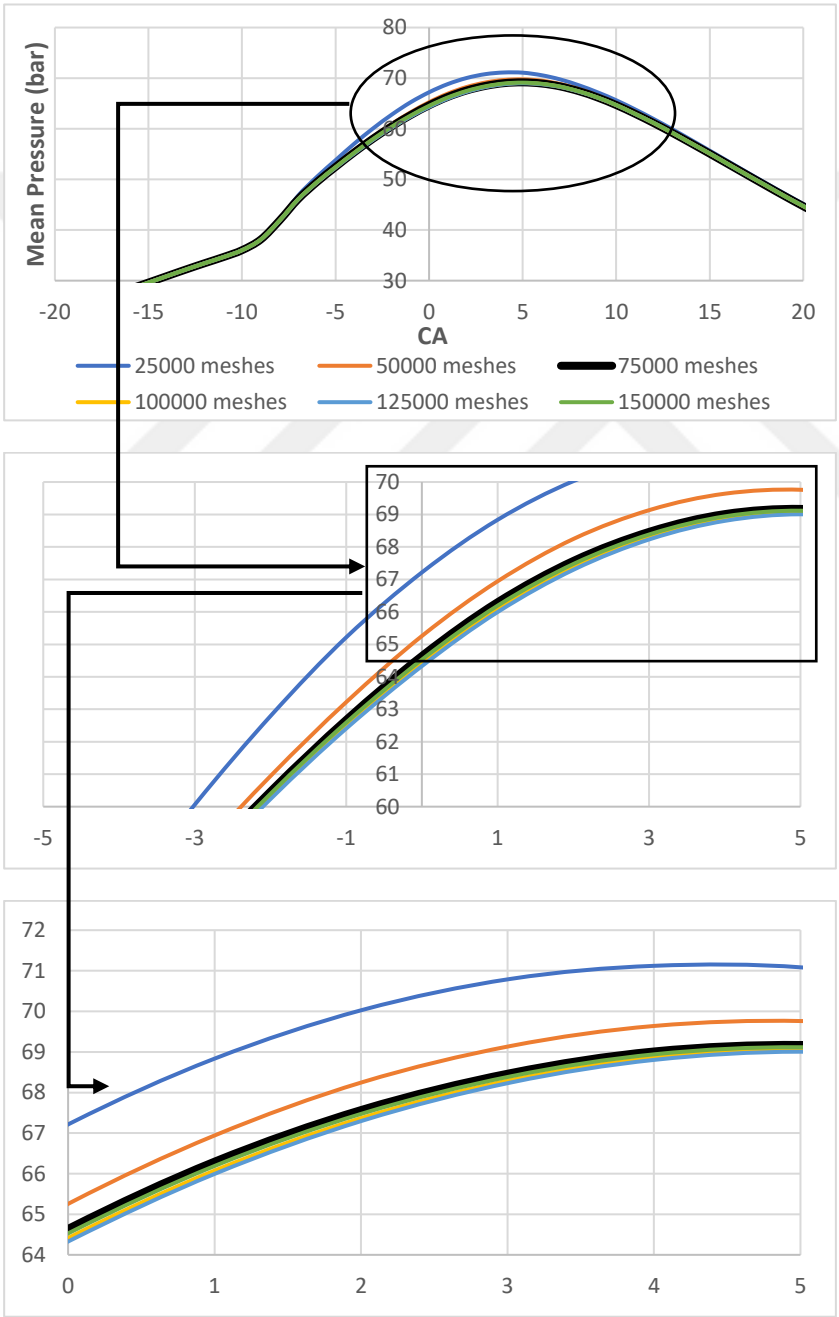

Figure 4.2 : Crank angle - pressure curves for different mesh numbers.

In this study, numerical results were monitored from low mesh densities to high mesh densities. Analyses were repeated for mesh numbers of 25000, 50000, 75000, 100000, 125000, and 150000. For each mesh number examined, pressure and heat release rate (HRR) curves inside the cylinder were obtained and compared with each other.

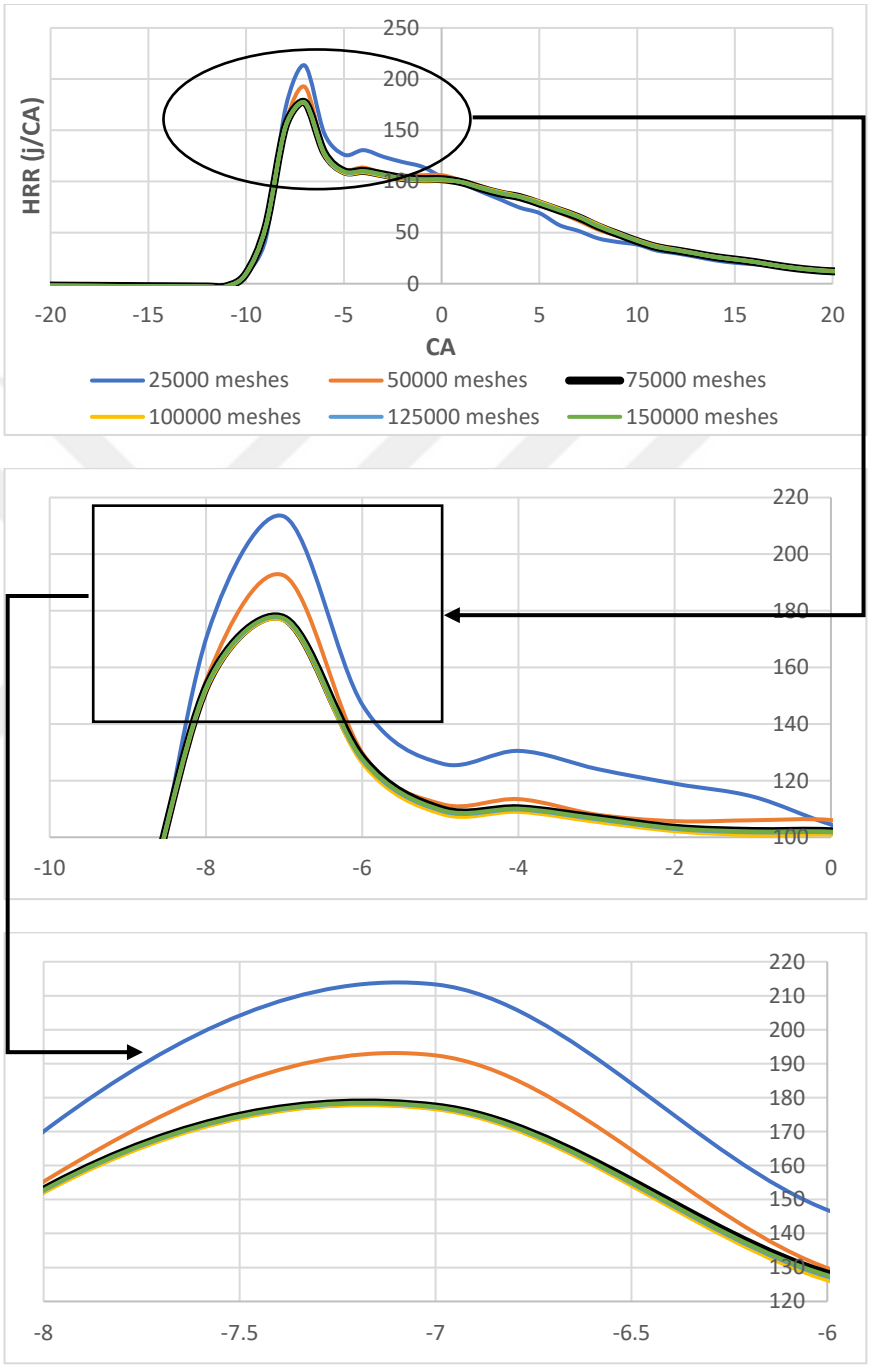

Figure 4.3 : Crank angle - HRR curves for different mesh numbers.

The conditions of pressure curves and heat release rates for different mesh numbers are shown in Figure 4.2 and Figure 4.3, respectively. It can be observed that the results did not change significantly after a mesh number of 75000.

In addition to the conditions of cylinder pressure and heat release rates, the effects of different mesh numbers on certain performance and emission values were also examined. Relative error rates for every 25000 increment in mesh numbers were calculated to ensure a mesh-independent solution. While Table 4.5 shows the relative error rates for increasing mesh numbers, Table 4.6 presents the relative error between the results obtained under test conditions and numerical results.

When examining Table 4.5 and Table 4.6, it can be seen that the results for a mesh number of 75000 fall within a reasonable and acceptable range of relative error rates. Since time is an important factor in obtaining analysis results, there is no need for higher mesh numbers. Moreover, the results do not change significantly with higher mesh numbers.

4.3 Model Validation

After obtaining a mesh-independent solution, the numerical results should be compared to experimental results to demonstrate their reliability. The most crucial indicators in verification studies are the graphs depicting in-cylinder pressure and heat release rate as a function of crank angle. Therefore, pressure curves and heat release rate curves obtained experimentally at different injection timings were compared with the curves obtained from numerical simulations.

It is evident from the indicator diagrams that the experimental results obtained at various injection timings are consistent with the numerical model, indicating that the in-cylinder combustion process occurred in a similar manner.

Considering the numerical results, a relative error rate of at most 2% was observed in terms of pressure values according to the test conditions for different mesh numbers (Table 4.5). However, in order for the HRR curves to be at the values under the test conditions, acceptable relative error rates were possible at higher mesh numbers.

Additionally, NO_x emissions, BMEP (Brake Mean Effective Pressure), ignition delay, and thermal efficiency, which are highly important for the initiation and continuation of the combustion process, were also compared.

The compatibility of experimental and numerical results is shown in Figure 4.4 and Figure 4.5. Table 4.7 shows the relative error rates between experimental and

numerical results for performance parameters (BMEP, Ignition Delay, and Thermal Efficiency).

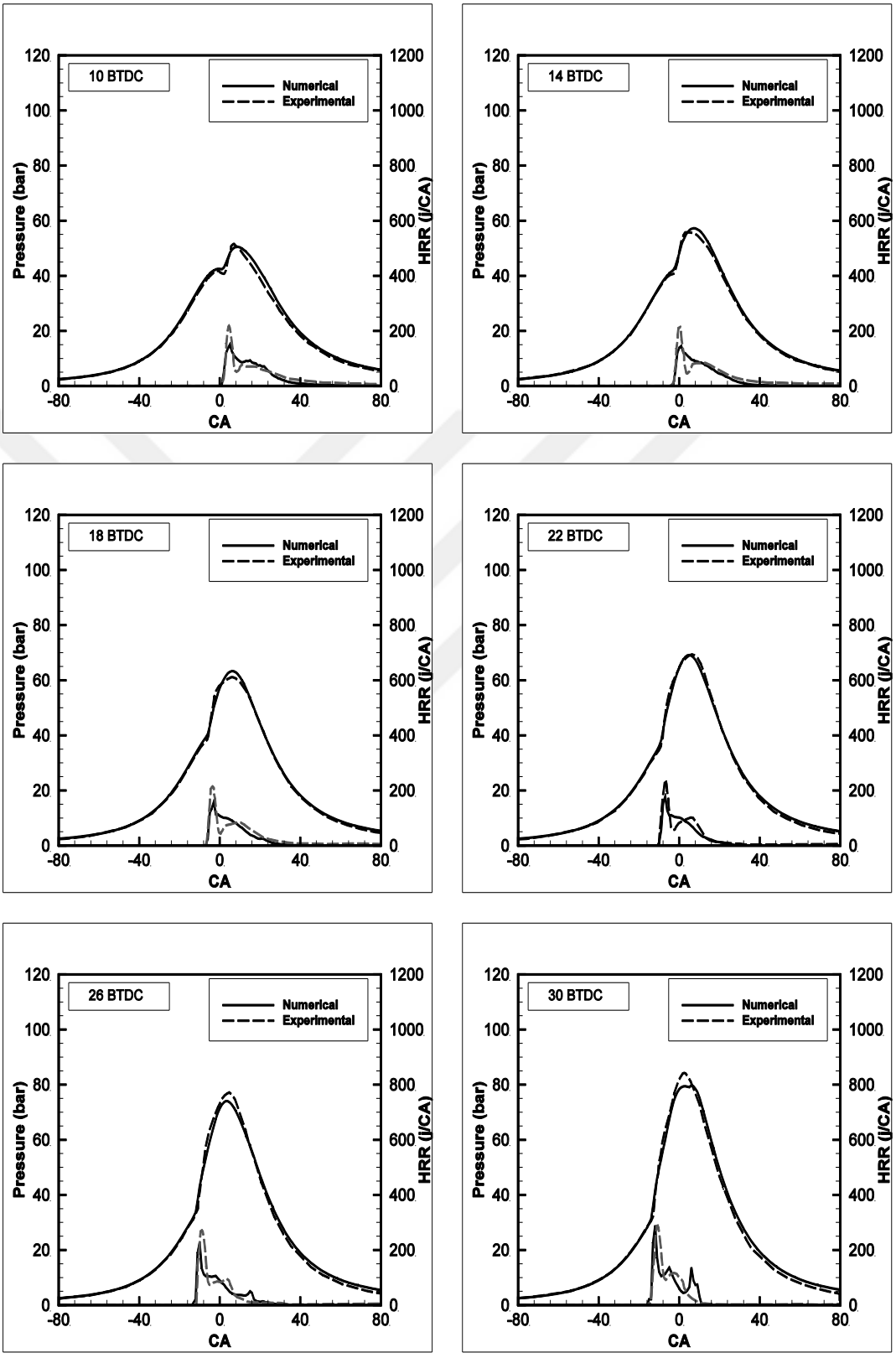

Figure 4.4 : Comparison of pressure and HRR between experimental and numerical results for 10°, 14°, 18°, 22°, 26° and 30° CA BTDC values of SOI.

Table 4.5 : Relative error rates for various engine values across different mesh numbers.

Mesh Numbers	Power	Rel. Err.	Torque	Rel. Err.	BMEP	Rel. Err.	BSFC	Rel. Err.	TE	Rel. Err.	Max. Pressure	Rel. Err.	Max. Mean Temperature	Rel. Err.	NOx	Rel. Err.
-	(kW)	(%)	(N.m)	(%)	(bar)	(%)	(g/kW.h)	(%)	(%)	(%)	(bar)	(%)	(K)	(%)	(ppm)	(%)
25000	9.31	-	97.70	-	4.28	-	182.85	-	34.32	-	71.12	-	1630	-	1396	-
50000	9.21	1.08	96.65	1.08	4.23	1.18	184.94	1.13	33.95	1.09	69.76	1.95	1617	0.80	1365	2.27
75000	9.11	1.09	95.60	1.09	4.18	1.20	187.01	1.11	33.56	1.16	69.17	0.85	1608	0.56	1330	2.63
100000	9.12	0.11	95.70	0.11	4.19	0.24	186.67	0.18	33.62	0.18	68.75	0.61	1607	0.06	1325	0.38
125000	9.04	0.88	94.86	0.88	4.15	0.96	188.42	0.93	33.32	0.90	68.25	0.73	1596	0.69	1318	0.53
150000	9.08	0.44	95.28	0.44	4.16	0.24	187.32	0.59	33.42	0.30	68.87	0.90	1602	0.37	1307	0.84

Table 4.6 : Comparison of results obtained using the number of meshes employed in numerical calculations with measurements obtained in experiments.

	Experimental Result															
	Power	Rel. Err.	ID	Rel. Err.	BMEP	Rel. Err.	CO	Rel. Err.	TE	Rel. Err.	Max. Pressure	Rel. Err.	CO	Rel. Err.	NO_x	Rel. Err.
	(kW)	(%)	(CA)	(%)	(bar)	(%)	(ppm)	(%)	(%)	(%)	(bar)	(%)	(g/kW.h)	(%)	(ppm)	(%)
Test Data	8.82	-	12	-	4.05	-	1074	-	35.45	-	69.43	-	8.46	-	1300	-
75000	9.11	3.29	12	-	4.18	3.21	1163	8.29	33.56	1.89	69.17	0.37	8.67	2.48	1330	2.31

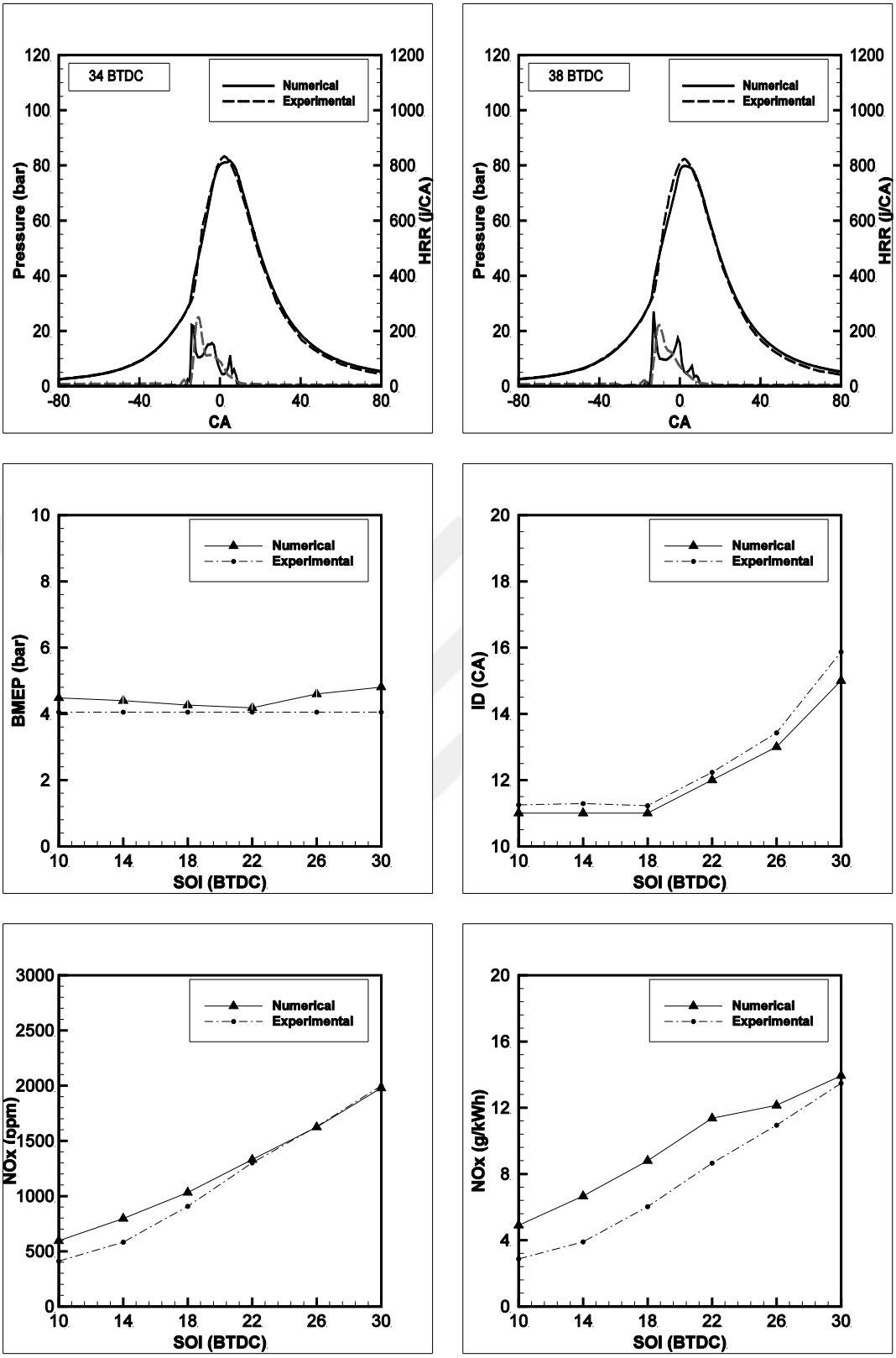

Figure 4.5 : Comparison of pressure and HRR for 34° and 38° CA BTDC values of SOI as well as BMEP, ID and NO_x between test and numerical results.

When the experimental results and the numerical model were compared, the %RE values were obtained as 3.29% for power, 3.21% for BMEP, 8.29% for CO (ppm),

1.89% for TE, 0.37% for pressure and 2.31% for NOx (ppm), respectively (Table 4.6). After acceptable and reasonable results were obtained at all injection timings, and this was followed by the parametric study phase.

Table 4.7 : Relative error between test cases and numerical model.

		SOI (CA BTDC)							
		10º	14º	18º	22º	26º	30º	34º	38º
BMEP (bar)	Test	4.05	4.05	4.05	4.05	4.05	4.05	4.05	4.05
	Numerical	4.47	4.39	4.26	4.18	4.59	4.8	4.53	4.35
	% RE	10.37	8.39	5.18	3.21	13.33	18.51	11.85	7.41
ID (CA)	Test	11.25	11.29	11.22	12.23	13.43	15.87	19.52	23.73
	Numerical	11.02	11.02	11.02	12	13.02	15.01	17.01	20.02
	% RE	2.014	2.39	1.78	1.88	3.05	5.42	12.85	15.63
TE (%)	Test	30.82	33.02	34.62	35.45	35.88	35.02	36.1	36.62
	Numerical	30.83	32.02	32.93	33.56	37.6	39	37.78	36.67
	% RE	0.03	3.03	4.88	5.33	4.79	11.36	4.65	0.13

5. PARAMETRIC STUDY

The effects of a diesel-natural gas dual-fuel operation were investigated in experimental studies [7–9]. The thesis work aims to investigate the effects of hydrogen on a diesel engine. Therefore, to evaluate the results of the effects of alternative fuels on performance and emission values in more detail, hydrogen fuel should also be considered. In the parametric studies in question, numerical studies were conducted in a dual-fuel mode with diesel, natural gas, and hydrogen fuels at different injection timings. The results were evaluated, taking into account two modes in numerical studies. In the first mode of the study, while the injected diesel fuel was kept constant (25% energy fraction), the remaining 75% of the energy was distributed between hydrogen and natural gas fuels. The amount of natural gas fuel was gradually reduced and transferred to hydrogen fuel. This part of the study was named the energy sharing mode and coded as Mode 1.

In the second mode, additional energy transfer to the system was provided. According to this mode, the amount of diesel fuel with 25% energy fraction was kept constant, while 75% energy fraction of natural gas fuel was maintained, and additional hydrogen fuel was sent to the combustion chamber. This part of the study was named the hydrogen energy enrichment mode and coded as Mode 2. Different injection timings were considered for both modes in the study.

As a result of the studies conducted for Mode 1 and Mode 2, the optimum gas-to-fuel ratios and optimum diesel fuel injection timings were determined concerning performance and emission values. The subsequent steps aim to improve the results obtained in the initial stage. The inclusion of hydrogen in the combustion chamber has led to high combustion rates, elevated temperatures, and increased MPRR values. Although performance and some emission types (CO, CO_2, HC and SOOT) have improved significantly, the results in terms of NO_x and MPRR have deteriorated. To ensure that the results are reasonable in all aspects, it is necessary to reduce NO_x and MPRR values. Therefore, various strategies recommended in the literature were applied to meet all the desired conditions in the engine's operation. These strategies

include EGR (Exhaust Gas Recirculation), PI (Pilot Injection), WI (Water Injection) and WVI (Water Vapour Injection), implemented in a combination with PI.

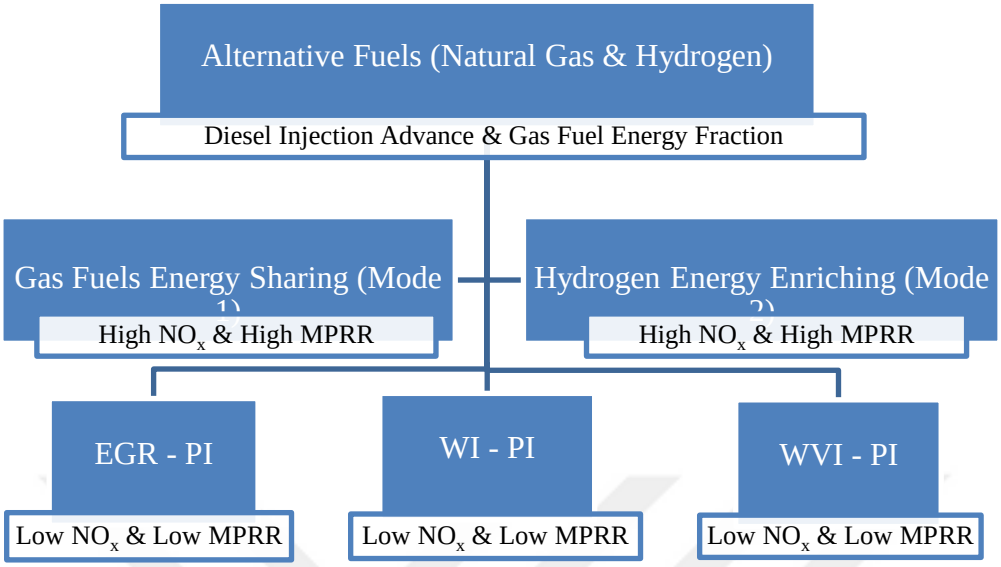

Figure 5.1 : Scheme of parametric studies.

The aim of PI is to reduce MPRR, while other strategies (EGR, WI, and WVI) are aimed at reducing NO_x. The details of these studies will be provided in subsequent sections. All the processes conducted in the thesis work are illustrated in Figure 5.1.

5.1 The Effect of Natural Gas and Hydrogen as Alternative Fuels

The experimental study was conducted under partial load conditions (4.05 BMEP), at a constant engine speed (910 rpm), in the diesel-natural gas dual-fuel mode. In this mode, 25% of the energy was provided from diesel fuel, and the remaining 75% was supplied from natural gas. Furthermore, the effects of various diesel fuel injection timings (10°, 14°, 18°, 22°, 26°, 30°, 34°, 38°, 42°, 46°, and 50° CA BTDC) were also investigated [7–9].

In the scope of the thesis, the effects of hydrogen were investigated by following the guidance of this experimental study. The effects of hydrogen were examined in two different ways. First, with 25% energy fraction in diesel fuel held constant, the 75% natural gas energy fraction was transferred to hydrogen at various ratios. The numerical values of these points with gas fuel energy sharing fractions were calculated at different diesel fuel injection timings (10°, 14°, 18°, 22°, 26°, 30°, 34°, and 38° CA BTDC).

In the second part, 25% diesel energy fraction and 75% natural gas energy fractions were kept constant, and additional hydrogen was introduced into the system. As in the first mode, the effects of different diesel fuel injection timings (10°, 14°, 18°, 22°, 26°, 30°, 34°, and 38° CA BTDC) were investigated in this mode as well.

The effects of the 42°, 46°, and 50° CA BTDC injection timings were not included in the numerical study under the experimental conditions. The results obtained for these injection timings did not provide reasonable results for performance and emission values.

Different numerical studies were conducted for other injection timings using two different modes. These two-stage studies were coded as Mode 1 and Mode 2. The energy distributions of the fuels for Mode 1 and Mode 2 were calculated using equation (5.1) and equation (5.2). The case matrix for the parametric study is shown in Table 5.1. Figure 5.2 is presented for a more concrete understanding of the parametric study.

$$CH_4\% = \frac{m_{CH_4} \text{ x } LHV_{CH_4}}{m_{diesel} \text{ x } LHV_{diesel} + m_{CH_4} \text{ x } LHV_{CH_4} + m_{H_2} \text{ x } LHV_{H_2}} \text{x} 100 \qquad (5.1)$$

$$H_2\% = \frac{m_{H_2} \text{ x } LHV_{H_2}}{m_{diesel} \text{ x } LHV_{diesel} + m_{CH_4} \text{ x } LHV_{CH_4}} \text{x} 100 \qquad (5.2)$$

The codes in the table (Table 5.1) represent the percentage distribution of energy for diesel, natural gas, and hydrogen fuels.

Table 5.1 : Parametric case matrix.

	SOI (CA BTDC)							
Mode 1	10°	14°	18°	22°	26°	30°	34°	38°
D25NG75H00	Case 1	Case 2	Case 3	Case 4	Case 5	Case 6	Case 7	Case 8
D25NG65H10	Case 9	Case 10	Case 11	Case 12	Case 13	Case 14	Case 15	Case 16
D25NG50H25	Case 17	Case 18	Case 19	Case 20	Case 21	Case 22	Case 23	Case 24
D25NG25H50	Case 25	Case 26	Case 27	Case 28	Case 29	Case 30	Case 31	Case 32
D25NG00H75	Case 33	Case 34	Case 35	Case 36	Case 37	Case 38	Case 39	Case 40
	SOI (CA BTDC)							
Mode 2	10°	14°	18°	22°	26°	30°	34°	38°
D25NG75H00	Case 1	Case 2	Case 3	Case 4	Case 5	Case 6	Case 7	Case 8
D25NG75H05	Case 41	Case 42	Case 43	Case 44	Case 45	Case 46	Case 47	Case 48
D25NG75H10	Case 49	Case 50	Case 51	Case 52	Case 53	Case 54	Case 55	Case 56
D25NG75H15	Case 57	Case 58	Case 59	Case 60	Case 61	Case 62	Case 63	Case 64
D25NG75H20	Case 65	Case 66	Case 67	Case 68	Case 69	Case 70	Case 71	Case 72
D25NG75H25	Case 73	Case 74	Case 75	Case 76	Case 77	Case 78	Case 79	Case 80

For example, the working point coded as D25NG65H10 indicates that 25% of the energy is obtained from diesel fuel, 65% from natural gas fuel, and the remaining 10% from hydrogen fuel. This working point is one of the Mode 1 working points because the total energy is kept constant at 100%, and only an energy sharing is made between natural gas and hydrogen.

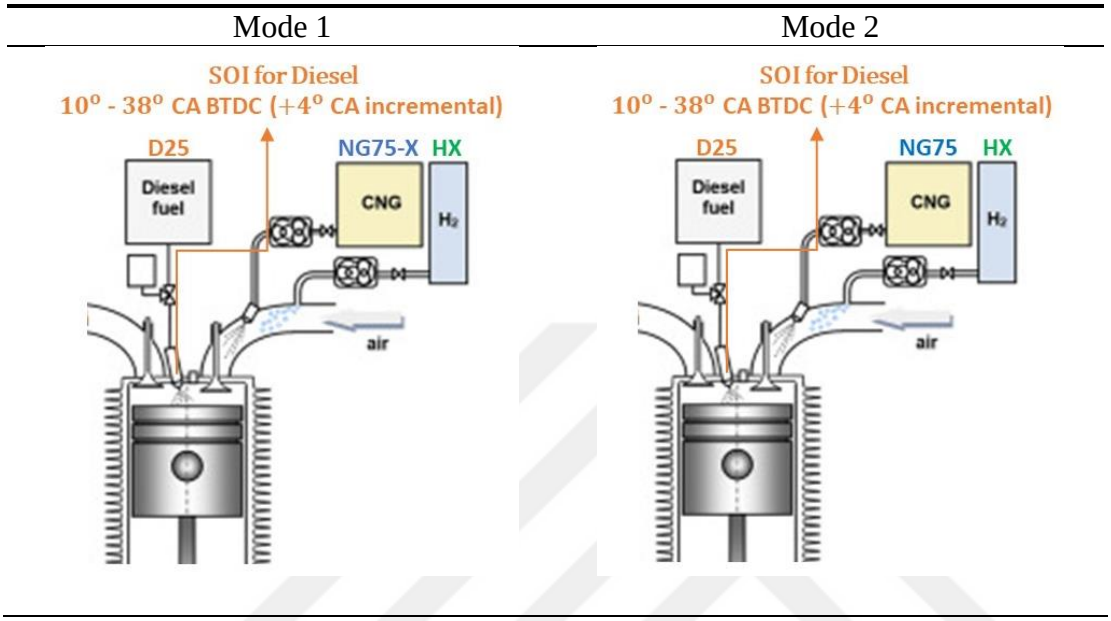

Figure 5.2 : Representative numerical model scheme for Mode 1 and Mode 2 [170].

Let's take another example: D25NG75H20. For this point, under experimental conditions, 25% of diesel energy fraction and 75% of natural gas energy fraction were kept constant, and extra hydrogen fuel was supplied to the system (cylinder) to investigate the effects of hydrogen-enriched natural gas fuel. As seen, the total energy ratio is not 100% but includes an additional energy input, such as 20%. This working point is one of the Mode 2 working points.

5.1.1 Gas fuel energy sharing mode (Mode 1)

The use of hydrogen in compression ignition engines is a common topic in the literature. It contributes greatly to achieving lower emissions as well as higher performance [20,46,171–173].

In this part of our numerical study, the advantages of including hydrogen in the fuel mixture under experimental conditions will be discussed. In this numerical setup, 25% of the energy was maintained as constant from diesel fuel, and the remaining 75% was divided between natural gas and hydrogen gases in varying ratios. Different pilot diesel injection advances were tested, and improvements in performance and emission values

were observed. The increase in hydrogen content in the gas mixture initially improved performance values at low injection advances but started to decline after a certain point, particularly when the hydrogen content exceeded 50% (Figure 5.4). Increasing the hydrogen content at low injection advances had a positive effect on performance values (Figure 5.4). However, when the hydrogen content in the mixture exceeded 50%, the values began to decrease (Figure 5.4 and Figure 5.5).

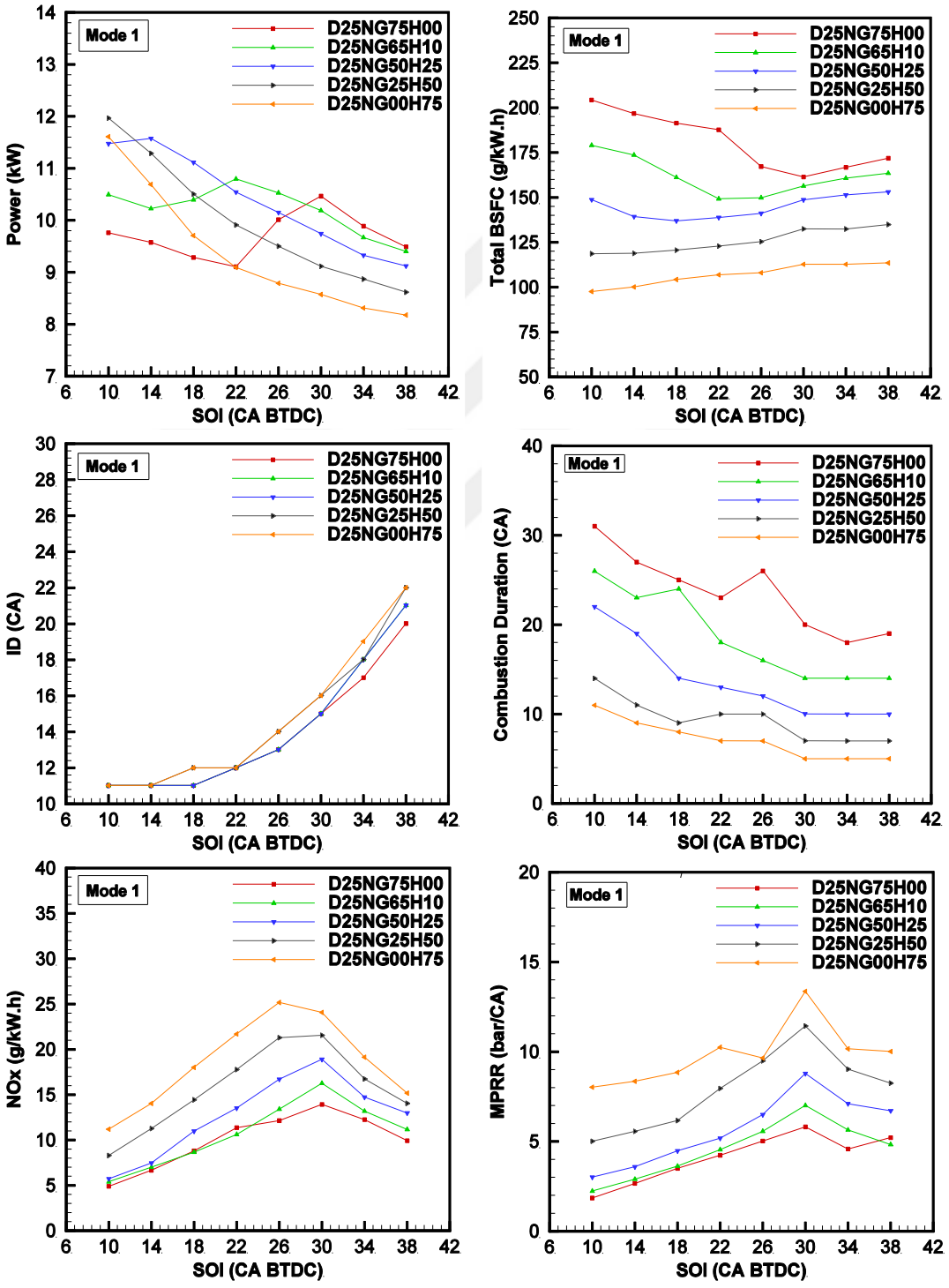

Figure 5.3 : Mode 1 results - The effect of SOI for fixed gas mix.

It is desirable for the crank angle at which the maximum cylinder pressure occurs to be around 7°-15° CA ATDC.

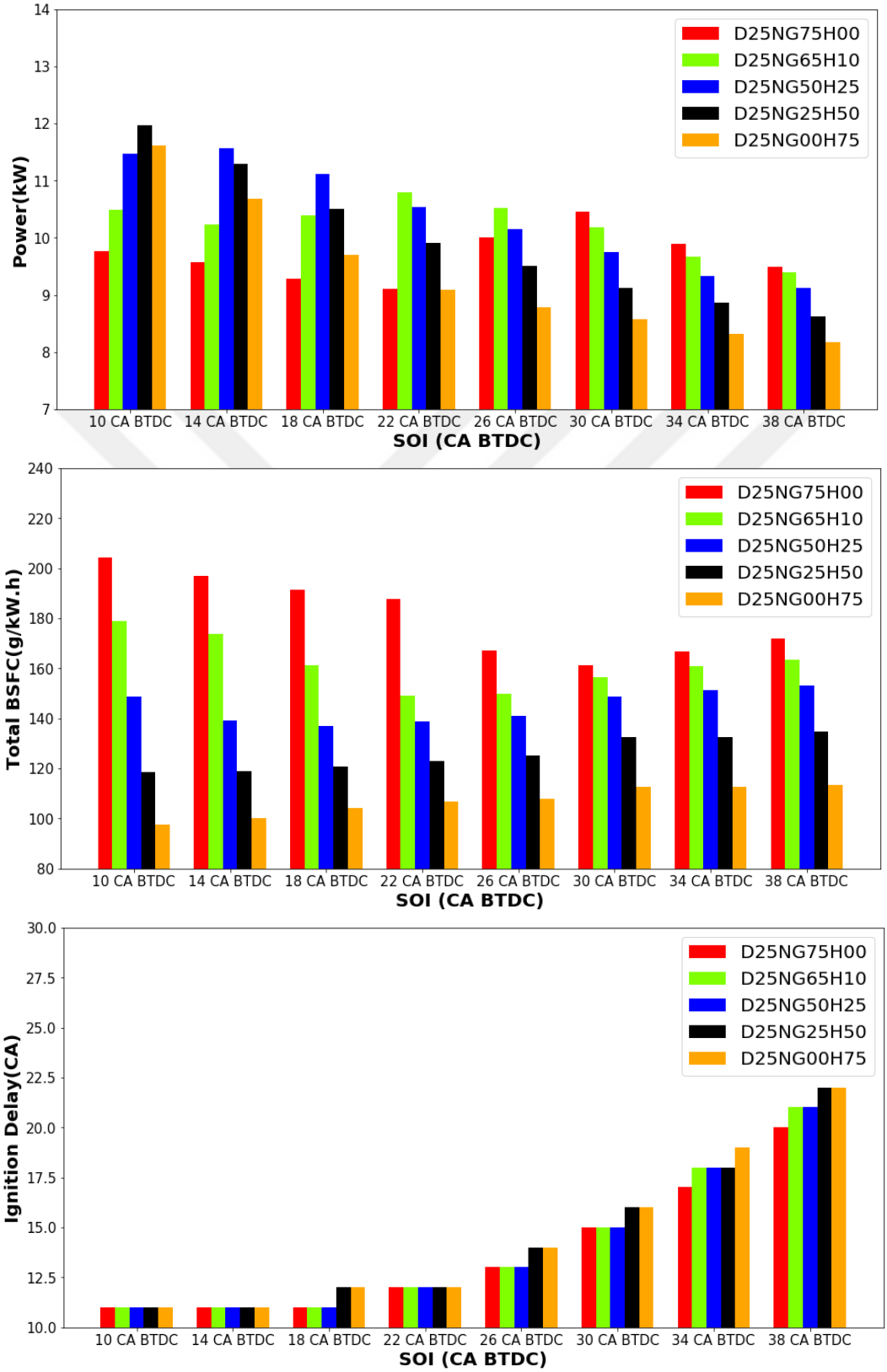

Figure 5.4 : Mode 1 results for Power, BSFC and ID - The effect of gas mix for fixed SOI.

Values before or after this range indicate a loss of power. Hydrogen is a fast-burning fuel compared to natural gas. Increasing the hydrogen content in the gas mixture resulted in a higher burn rate, causing the maximum in-cylinder pressure to move towards the top dead center (Table 5.2). This suggests that excessive increases in injection advance are not suitable for high hydrogen content (Table 5.3). If an increase in hydrogen content is desired, reducing the injection advance is necessary (Table 5.3). At low injection advances, increasing the hydrogen content significantly reduced the specific fuel consumption (Figure 5.4).

Table 5.2 : Results of different gas fuel energy sharing fractions in Mode 1 at 14° CA BTDC value of SOI.

	NG75H00	NG65H10	NG50H25	NG25H50	NG00H75
	Case 2	Case 10	Case 18	Case 26	Case 34
Power (kW)	9.575	10.23	11.58	11.29	10.69
Torque (N.m)	100.477	107.30	121.47	118.45	112.18
BSFC (g/kW.h)	196	171.67	136.27	114.55	95.73
Ignition Delay (CA)	11º	11º	11º	11º	11º
Thermal Efficiency (%)	32.02	34.19	38.71	37.75	35.75
Combustion Duration (CA)	27º	23º	19º	11º	9º
MPRR (bar/CA)	2.66	2.9	3.6	5.57	8.35
Max. Press. (bar)	57.25	60.64	67.45	81.96	85.89
CA for Max. Press. (ATDC)	7º CA	8º CA	8º CA	7º CA	4º CA
Max. Mean Temp. (K)	1504	1593	1779	1963	1997
NO_x (g/kW.h)	6.66	7	7.46	11.27	14
SOOT (g/kW.h)	0.000766	0.00035	0.000172	0.000089	0.00007
CO (g/kW.h)	9.94	6.43	1.42	0.23	0.0036
HC (g/kW.h)	35.21	21.46	4.04	0.98	0.0015

As the injection advance increased, the hydrogen content in the gas fuel caused a decrease in performance values (Figure 5.4). This decreasing trend is observed after the injection advance reaches 22° CA BTDC. This drop in BMEP, power, and torque values indicates that the injection advance has a significant impact on performance values (Figure 5.4). The main reason for this is that the increased injection advance leads to an increase in the amount of fuel inside and a delay in ignition (Figure 5.4). The increased ignition delay suddenly increased cylinder peak pressure and temperature, shortening the combustion duration. The effect of increasing the hydrogen content on ignition delay at low injection advances was almost negligible (Figure 5.4). It played a more effective role at high injection advances. However, the change in injection advance had a more significant effect on ignition delay than the

hydrogen content (Figure 5.3). Taking performance values into account, for Mode 1, it was observed that low injection advances and a gas mixture with a 50% hydrogen content would yield better results.

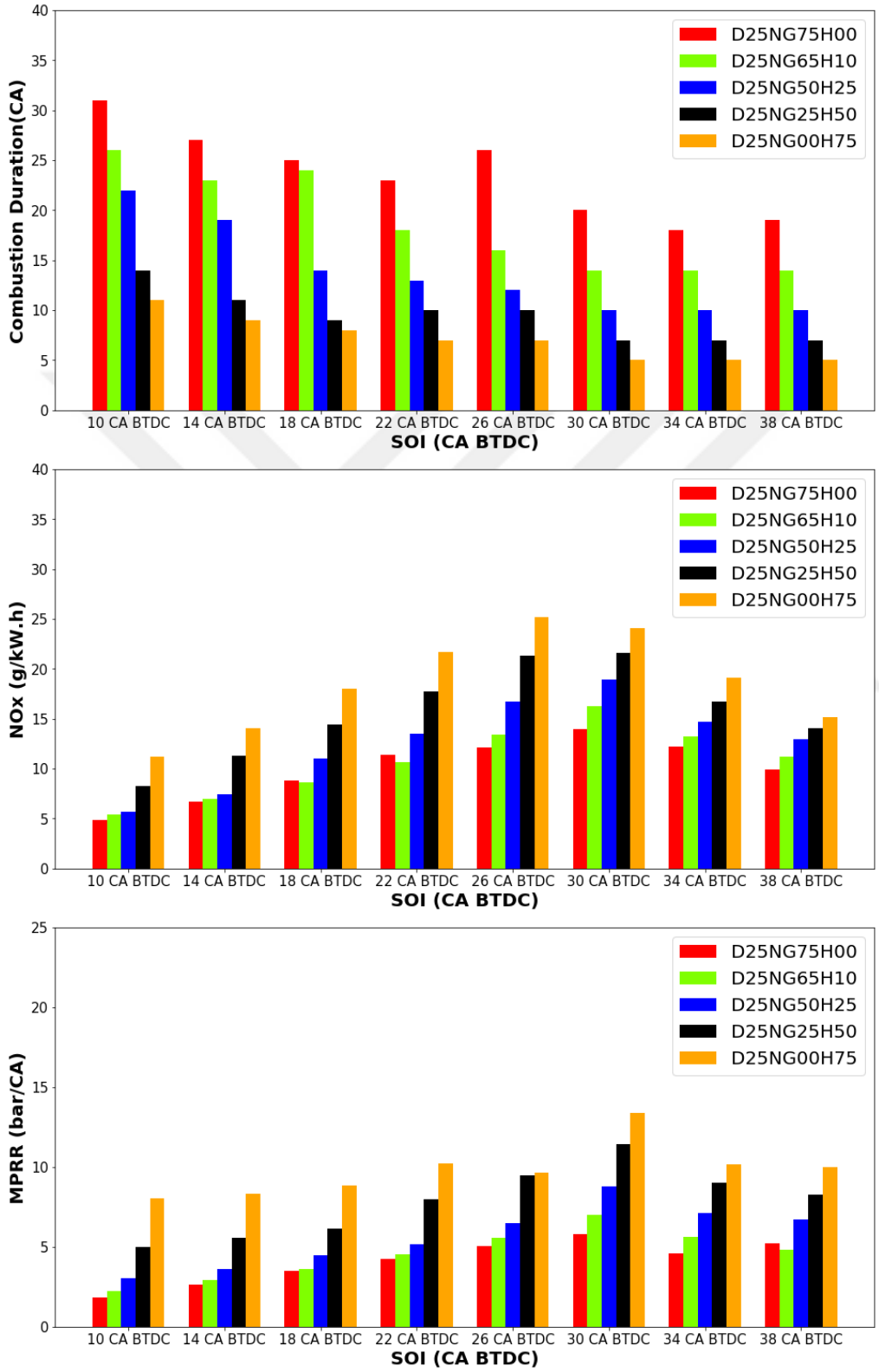

Figure 5.5 : Mode 1 results for CD, NO_x and MPRR – The effect of gas mix for fixed SOI.

In terms of emission values, increasing the injection advance has improved all emissions except NO_x emissions for all gas mixture ratios (Figure 5.3 and Figure 5.4). The increase in hydrogen content has increased cylinder regional temperature values, resulting in an increase in NO_x emissions. When compared to situations where hydrogen is not present in the gas mixture (D25NG75H00), hydrogen has improved all emission values except for NO_x emissions. To reduce NO_x emissions, the natural gas content in the gas mixture needs to be increased (Table 5.2). This way, desired results in terms of performance and emissions can be achieved in low load regions. Natural gas, being slower-burning compared to hydrogen, prevents the increase of cylinder regional temperatures.

As a result, NO_x emissions, which are a function of temperature, are reduced. For this reason, when conditions with hydrogen and conditions without hydrogen (D25NG75H00) are compared, NO_x emissions are higher in the presence of hydrogen.

Table 5.3 : Results of different diesel fuel injection advance values at D25NG50H25 operating points of Mode 1.

SOI of Diesel (CA BTDC)	10º	14º	18º	22º	26º	30º	34º	38º
	Case 17	Case 18	Case 19	Case 20	Case 21	Case 22	Case 23	Case 24
Power (kW)	11.48	11.58	11.11	10.54	10.15	9.74	9.33	9.12
Torque (N.m)	120.42	121.47	116.63	110.64	106.52	102.23	97.88	95.72
BSFC (g/kW.h)	145.52	136.27	133.84	136	138.83	146.85	148.76	150.01
Ignition Delay (CA)	11º	11º	11º	12º	13º	15º	18º	21º
Thermal Efficiency (%)	36.26	38.71	39.41	38.86	38.19	36.36	35.64	35.25
Combustion Duration (CA)	22º	19º	14º	13º	12º	10º	10º	10º
MPRR (bar/CA)	3	3.6	4.48	5.18	6.49	8.78	7.1	6.71
Max. Press. (bar)	58.61	67.45	77.16	85.50	88.40	90.89	89.21	87.57
CA for Max. Press. (ATDC)	11º CA	8º CA	8º CA	4º CA	1º CA	0º CA	0º CA	0º CA
Max. Mean Temp. (K)	1698	1779	1889	1925	1951	1999	1963	1927
NO_x (g/kW.h)	5.73	7.46	10.98	13.52	16.71	18.90	14.73	12.98
SOOT (g/kW.h)	0.00033	0.000172	0.00011	~ 0	~ 0	~ 0	~ 0	~ 0
CO (g/kW.h)	2.38	1.42	0.73	0.69	0.76	0.80	0.76	0.73
HC (g/kW.h)	8.16	4.04	2.99	2.61	2.05	1.58	1.64	1.97

Cylinder peak pressures increase with an increase in hydrogen content in the mixture, which can lead to knocking tendencies and engine noise issues. To avoid these problems, the hydrogen content in the mixture should be kept within a certain range. Excessive hydrogen content in the gas mixture leads to sharper pressure curves, resulting in shorter combustion durations and sudden pressure spikes [26]. The very rapid combustion process can lead to a performance loss when considering that the

area under the pressure curve represents the engine's power. In this case, an energy balance must be achieved with an appropriate mixture of natural gas and hydrogen fuel.

Table 5.4 : Comparison of optimum case for Mode 1 and test case.

	Case 2	Case 18	Variation
Power (kW)	9.575	11.58	+21%
Torque (N.m)	100.477	121.47	+21%
BSFC (g/kW.h)	196	136.27	-30.5%
Ignition Delay (CA)	11º	11º	-
Thermal Efficiency (%)	32.02	38.71	+6.7%
Combustion Duration (CA)	27º	19º	-8º
MPRR (bar/CA)	2.66	3.6	~ +1
Max. Press. (bar)	57.25	67.45	~ +10
CA for Max. Press. (ATDC)	7º CA	8º CA	-
Max. Mean Temp. (K)	1504	1779	+275
NO_x (g/kW.h)	6.66	7.46	+12%
SOOT (g/kW.h)	0.000766	0.000172	-77.5%
CO (g/kW.h)	9.94	1.42	-85.7%
HC (g/kW.h)	35.21	4.04	-88.5%

Hydrogen, with its high thermal energy and rapid combustion characteristics, has reduced the proportion of unburned regions inside the cylinder. The decrease in unburned areas leads to a reduction in emissions of incomplete combustion products such as CO and UHC. Additionally, the absence of carbon atoms in the structure of hydrogen has also resulted in improvements in SOOT emissions (Table 5.2).

The co-operation of hydrogen and natural gas yields more favorable results in combustion. As mentioned earlier, hydrogen has a rapid combustion rate, while natural gas burns more slowly. With suitable fractions of these two gases, optimal results can be achieved in terms of performance and emissions. When Table 5.2 is examined, the condition with 50% natural gas and 25% hydrogen energy fraction has provided ideal performance results. Similarly, the results for other emission types are reasonable, except for NO_x emissions.

Determining the appropriate diesel fuel injection timing for the D25NG50H25 operating point is also crucial. When Table 5.3 is examined, it is seen that 14° CA BTDC has yielded positive results in terms of performance. Higher injection advances have led to the maximum pressure occurring closer to the top dead center (TDC). Considering the Mode 1 analyses, it is observed that the most optimum condition in

terms of both performance and emission values is the mixture of 14° CA BTDC injection timing with 50% natural gas and 25% hydrogen gas (14° CA BTDC D25NG50H25 = Case 18). It has improved engine power by 21% and specific fuel consumption by 30%. There is an approximate 12% increase in NO_x emission values. Excellent results have been achieved for other emission types. There is a reduction of 88% for HC, 77% for SOOT, and 86% for CO emissions, respectively.

Table 5.5 : Results of different diesel fuel injection advance values at D25NG00H75 operating points of Mode 1.

SOI of Diesel (CA BTDC)	10º	14º	18º	22º	26º	30º	34º	38º
	Case 33	Case 34	Case 35	Case 36	Case 37	Case 38	Case 39	Case 40
Power (kW)	11.61	10.69	9.71	9.09	8.79	8.57	8.31	8.18
Torque (N.m)	121.82	112.18	101.85	95.42	92.23	89.96	87.23	85.81
BSFC (g/kW.h)	93.18	95.73	99.82	102.58	104.03	108.93	108.53	109.09
Ignition Delay (CA)	11º	11º	12º	12º	14º	16º	19º	22º
Thermal Efficiency (%)	36.68	35.75	34.42	33.52	33.07	32	31.77	31.60
Combustion Duration (CA)	11º	9º	8º	7º	7º	5º	5º	5º
MPRR (bar/CA)	8	8.35	8.85	10.25	9.65	13.36	10.16	10.01
Max. Press. (bar)	79.83	85.89	87.58	87.69	88.19	89.36	87.71	85.91
CA for Max. Press. (ATDC)	8º CA	4º CA	1º CA	0º CA	0º CA	-1º CA	-1º CA	-1º CA
Max. Mean Temp. (K)	1992	1997	1986	1988	2002	2039	2000	1957
NO_x (g/kW.h)	11.19	14.04	18.01	21.70	25.18	24.08	19.14	15.18
SOOT (g/kW.h)	~ 0	~ 0	~ 0	~ 0	~ 0	~ 0	~ 0	~ 0
CO (g/kW.h)	0.011	0.0036	0.0022	0.0020	0.00086	0.0017	0.0048	0.00022
HC (g/kW.h)	0.0067	0.0015	0.0013	0.0014	0.0003	0.00014	0.0064	0.00017

When comparing the results obtained under test conditions with the results from numerical simulations, it is evident that the performance values and emission levels have improved. By examining Table 5.4, it is clear that, except for NO_x and MPRR, other parameters show more favorable results. The results of the analysis for the Diesel-Hydrogen dual-fuel mode are shown in Table 5.5.

The results indicate that using hydrogen as the sole secondary fuel in a diesel engine is not suitable. Due to hydrogen's rapid combustion characteristics, at all diesel fuel injection timings, high MPRR, high temperatures, and NO_x levels close to top dead center are observed, with maximum pressure even occurring very close to or even before top dead center in some injection timings (In fact, in some injection timings, it even results in negative work, such as at 30° CA BTDC and beyond). To eliminate these issues, the application of natural gas-hydrogen dual-fuel is necessary. The numerical results support this conclusion.

5.1.2 Hydrogen enriching mode (Mode 2)

While keeping the energy distribution at 25% from diesel fuel and 75% from natural gas, additional energy input to the system was provided by hydrogen fuel.

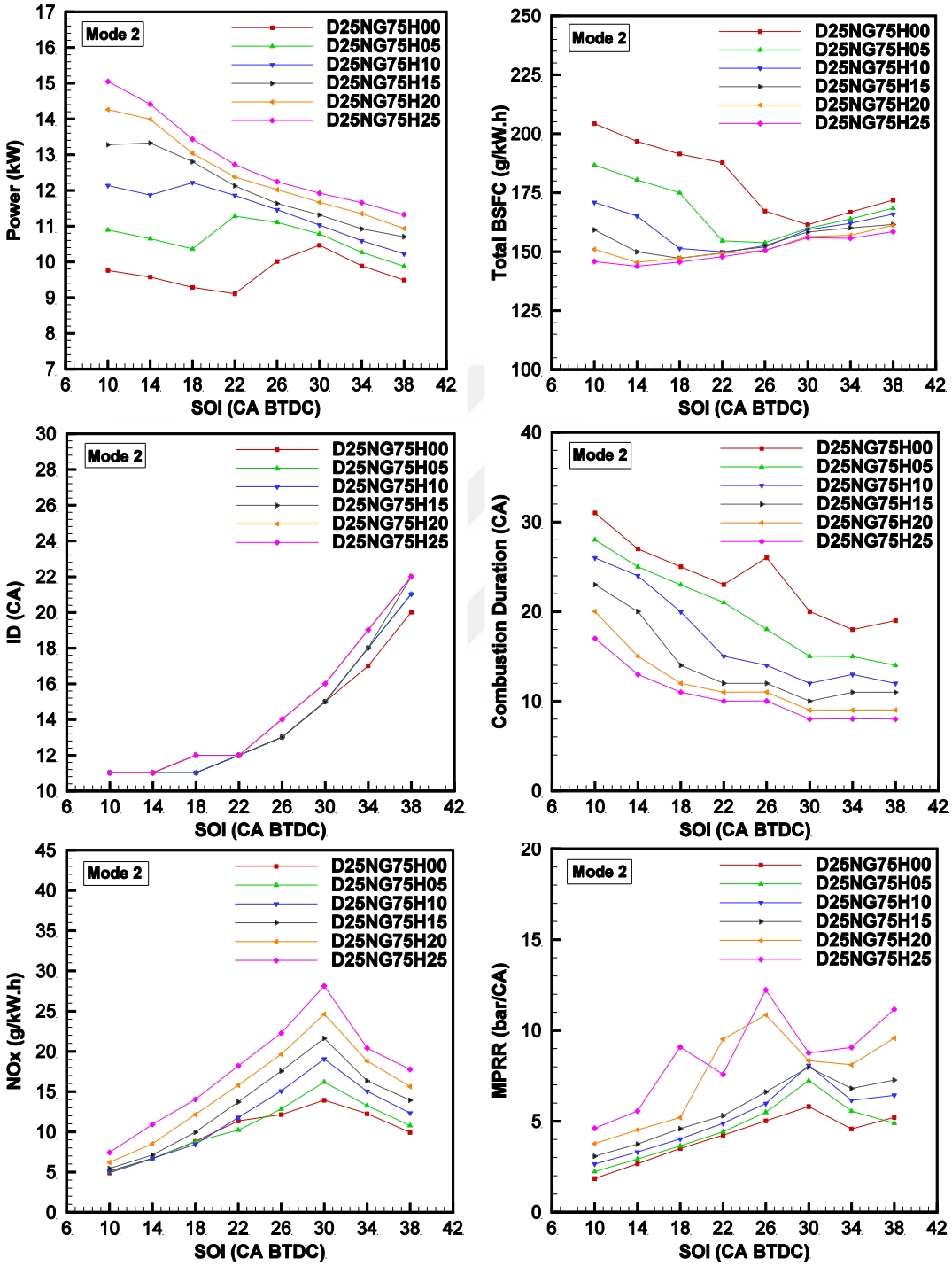

Figure 5.6 : Mode 2 results - The effect of SOI for fixed gas mix.

Various pilot diesel injection timings were used in this mode, resulting in improvements in performance and emission values within this mode. Increased hydrogen proportions for all injection timings have improved performance values.

Especially, increasing the hydrogen content at lower injection timings has significantly enhanced performance values. The effect of hydrogen enrichment on ignition delay is minimal (Figure 5.7). It is observed that the injection timing has a greater effect on ignition delay, just like in Mode 1 (Figure 5.6).

Table 5.6 : Results of different hydrogen enriching fractions in Mode 2 at 10° CA BTDC value of SOI.

	NG75H00	NG75H05	NG75H10	NG75H15	NG75H20	NG75H25
	Case 1	Case 41	Case 49	Case 57	Case 65	Case 73
Power (kW)	9.76	10.89	12.14	13.28	14.27	15.05
Torque (N.m)	102.42	114.29	127.35	139.34	149.69	157.92
BSFC (g/kW.h)	203.85	185.23	168.46	156	147.03	141.09
Ignition Delay (CA)	11º	11º	11º	11º	11º	11º
Thermal Efficiency (%)	30.84	32.77	34.86	36.48	37.56	38.04
Combustion Duration (CA)	31º	28º	26º	23º	20º	17º
MPRR (bar/CA)	1.85	2.23	2.64	3.08	3.77	4.62
Max. Press. (bar)	50.55	52.78	55.76	60.35	65.74	71.94
CA for Max. Press. (ATDC)	9º CA	10º CA	11º CA	12º CA	12º CA	12º CA
Max. Mean Temp. (K)	1477	1574	1688	1809	1933	2057
NO_x (g/kW.h)	4.90	5	5.11	5.44	6.19	7.43
SOOT (g/kW.h)	0.0012	0.00072	0.00034	0.0002	0.00011	0.00015
CO (g/kW.h)	10.25	7.04	3.70	2.02	1.17	0.49
HC (g/kW.h)	36.73	25	15.29	8.76	4.66	2.36

An increase in the hydrogen fraction results in higher thermal efficiency at low diesel fuel injection timings, but this effect diminishes at high injection timings. In fact, beyond 30° CA BTDC injection timing, thermal efficiency starts to decrease (Table 5.7). Similarly, the total specific fuel consumption decreases with an increase in the hydrogen fraction at low diesel fuel injection timings, but the dependency on the injection timing decreases as the injection timing is advanced (Figure 5.6 and Figure 5.7). In terms of emissions, just like in the results of Mode 1, all emissions except NO_x decrease as the injection timing is advanced (Figure 5.9 and Table 5.7). Increasing the hydrogen fraction at fixed diesel fuel injection timings also results in a similar trend (Table 5.6). At low injection timings, increasing the hydrogen fraction in the gas fuel leads to an increase in NO_x emissions; however, this increase is relatively small when compared to high diesel fuel injection timings (Figure 5.8).

If no specific injection strategy or EGR application is employed, it should be noted that increasing the hydrogen fraction along with injection timing can have adverse effects beyond a certain point. Especially at an injection timing of 14° CA BTDC and

a hydrogen enrichment rate exceeding 20%, MPRR and NO_x values rise to critical levels (Figure 5.8).

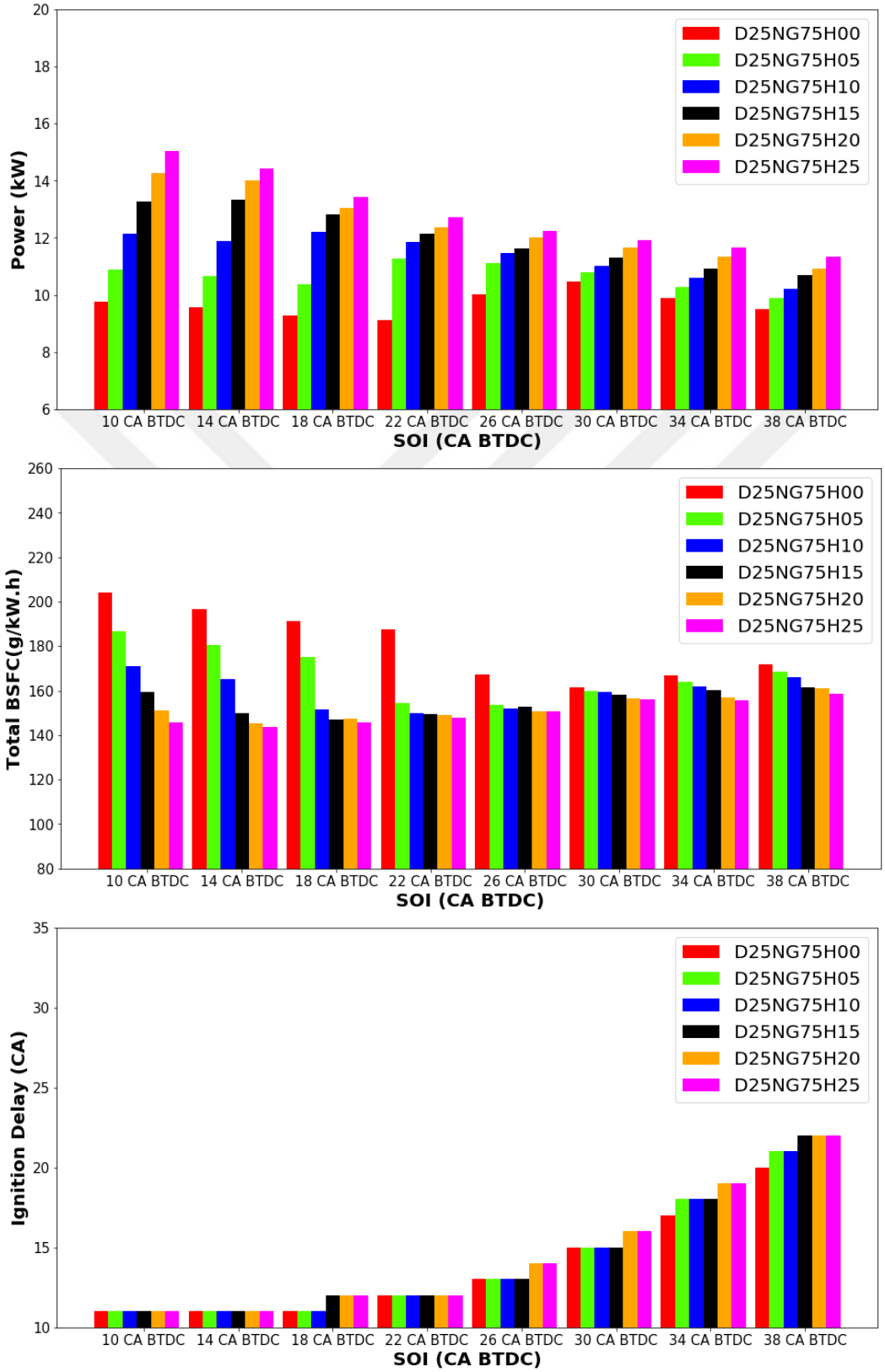

Figure 5.7 : Mode 2 results for power, BSFC and ID - The effect of gas mix for fixed SOI.

Excessive hydrogen content leads to knock events, noise, vibration issues, internal thermal and mechanical deformations, and a significant increase in the harmful NO_x emissions [174,175].

Table 5.7 : Results of different diesel fuel injection advance values at D25NG75H15 operating points of Mode 2.

SOI of Diesel (CA BTDC)	10º	14º	18º	22º	26º	30º	34º	38º
	Case 57	Case 58	Case 59	Case 60	Case 61	Case 62	Case 63	Case 64
Power (kW)	13.28	13.33	12.80	12.13	11.63	11.31	10.92	10.70
Torque (N.m)	139.34	139.84	134.35	127.28	122.08	118.73	114.61	112.31
BSFC (g/kW.h)	156	146.79	143.95	146.56	150.33	156.61	157.55	158.43
Ignition Delay (CA)	11º	11º	12º	12º	13º	15º	18º	22º
Thermal Efficiency (%)	36.48	38.75	39.48	38.88	38.07	36.72	36.29	35.97
Combustion Duration (CA)	23º	20º	14º	12º	12º	10º	11º	11º
MPRR (bar/CA)	3	3.74	4.59	5.31	6.62	7.98	6.81	7.27
Max. Press. (bar)	60.35	69.73	81.46	90.45	94.44	97.37	95.08	93.45
CA for Max. Press. (ATDC)	12º CA	9º CA	9º CA	4º CA	2º CA	0º CA	0º CA	0º CA
Max. Mean Temp. (K)	1809	1885	2000	2043	2073	2126	2079	2041
NO_x (g/kW.h)	5.44	7.13	9.96	13.72	17.55	21.62	16.33	13.94
SOOT (g/kW.h)	~ 0	~ 0	~ 0	~ 0	~ 0	~ 0	~ 0	~ 0
CO (g/kW.h)	2.02	1.26	0.63	0.62	0.68	0.63	0.65	0.71
HC (g/kW.h)	8.76	4.78	3.57	2.62	1.96	1.16	1.37	1.81

Analysis conducted with energy enrichment ratios has shown that a hydrogen fraction of 15% is more suitable for performance, MPRR, and NO_x compared to other analyses (Table 5.6).

Table 5.8 : Comparison of optimum case for Mode 2 and test case.

	Case 1	Case 57	Variation
Power (kW)	9.76	13.28	+36%
Torque (N.m)	102.42	139.34	+36%
BSFC (g/kW.h)	203.85	156	-23.5%
Ignition Delay (CA)	11º	11º	-
Thermal Efficiency (%)	30.84	36.48	+5.64%
Combustion Duration (CA)	31º	23º	-8º
MPRR (bar/CA)	1.85	3	+1.15
Max. Press. (bar)	50.55	60.35	~ +10
CA for Max. Press. (ATDC)	9º CA	12º CA	-
Max. Mean Temp. (K)	1477	1809	+332
NO_x (g/kW.h)	4.9	5.44	+11%
SOOT (g/kW.h)	0.0012	0.000196	-83.6%
CO (g/kW.h)	10.25	2.02	-80.3%
HC (g/kW.h)	36.73	8.76	-76.15%

When considering the results of the D25NG50H25 energy fraction condition under different injection timings, it is observed that a 10° CA BTDC injection timing provides positive results for performance and emissions (Table 5.7).

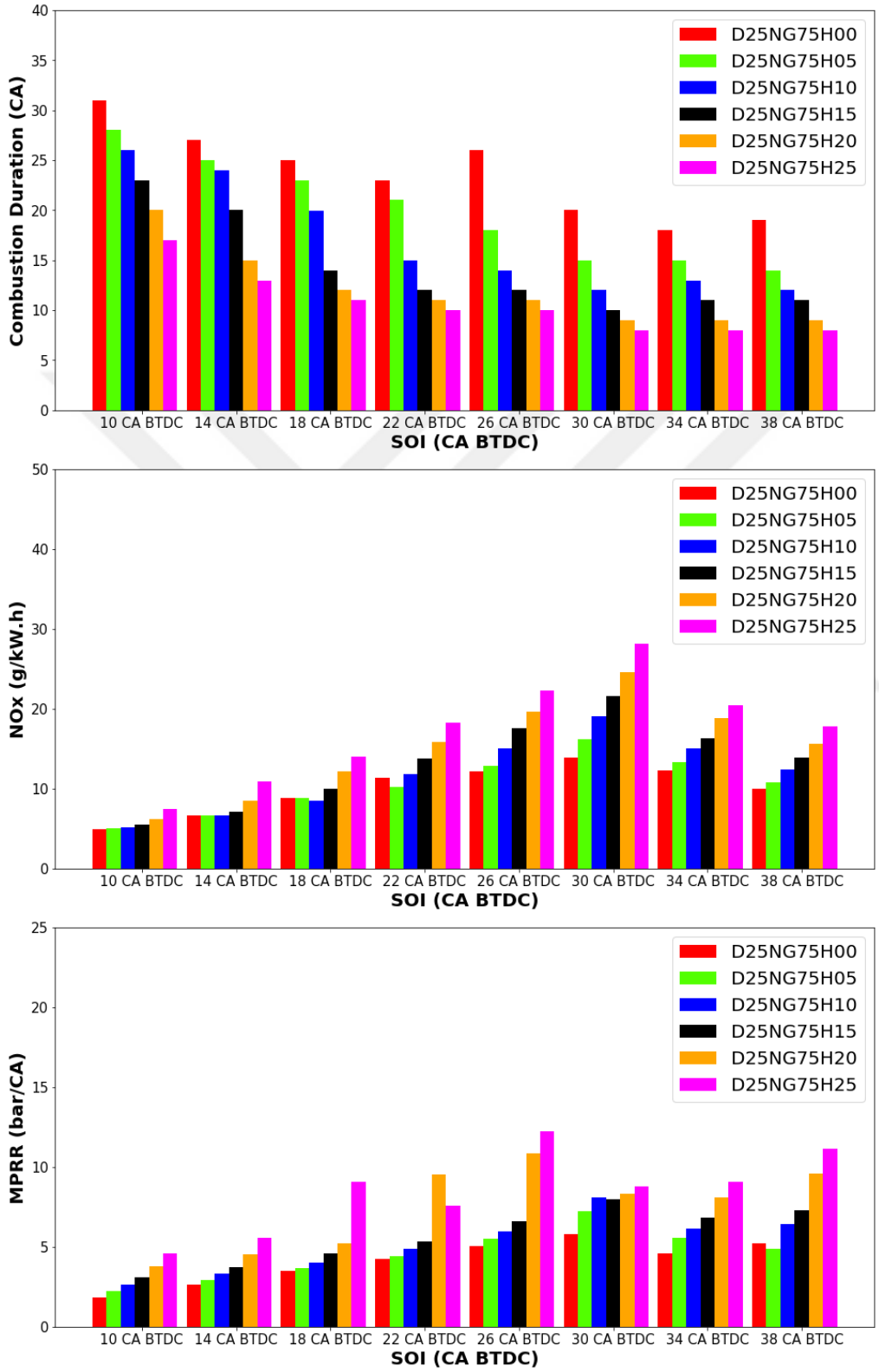

Figure 5.8 : Mode 2 results for CD, NO_x and MPRR – The effect of gas mix for fixed SOI.

MPRR, NO_x, and performance values have produced more reasonable outcomes. When considering the results of Mode 2 analyses, it is observed that the optimal condition for both performance and emission values is a 10° CA BTDC injection timing with a 25% hydrogen enrichment rate (10° CA BTDC D25NG75H15 = Case 57).

Table 5.9 : Results of different diesel fuel injection advance values at D25NG75H25 operating points of Mode 2.

SOI of Diesel (CA BTDC)	10º	14º	18º	22º	26º	30º	34º	38º
	Case 73	Case 74	Case 75	Case 76	Case 77	Case 78	Case 79	Case 80
Power (kW)	15.05	14.42	13.43	12.72	12.24	11.92	11.66	11.32
Torque (N.m)	157.92	151.29	140.95	133.51	128.48	125.10	122.33	118.83
BSFC (g/kW.h)	141.09	139.18	140.85	143.48	146.72	152.67	151.64	153.86
Ignition Delay (CA)	11º	11º	12º	12º	14º	16º	19º	22º
Thermal Efficiency (%)	38.04	38.57	38.11	37.52	36.85	35.59	35.64	35.01
Combustion Duration (CA)	17º	13º	11º	10º	10º	8º	8º	8º
MPRR (bar/CA)	4.62	5.57	9.09	7.59	12.23	8.76	9.07	11.16
Max. Press. (bar)	71.94	86.66	94	97.53	99.13	101.32	99.07	97.4
CA for Max. Press. (ATDC)	12º CA	9º CA	5º CA	2º CA	1º CA	0º CA	0º CA	0º CA
Max. Mean Temp. (K)	2057	2134	2138	2155	2178	2227	2178	2143
NO_x (g/kW.h)	7.43	10.92	14.04	18.20	22.28	28.12	20.41	17.76
SOOT (g/kW.h)	0.00015	~ 0	~ 0	~ 0	~ 0	~ 0	~ 0	~ 0
CO (g/kW.h)	0.49	0.48	0.38	0.36	0.32	0.18	0.24	0.38
HC (g/kW.h)	2.36	1.44	1.52	0.94	0.43	0.2	0.24	0.41

This configuration resulted in a 36% increase in engine power and a 23% improvement in specific fuel consumption. Although there was an approximate 11% increase in NO_x emissions, other emission types showed highly successful results with a 76% reduction in HC, an 83% reduction in SOOT, and an 80% reduction in CO emissions (Table 5.8). The impact of different diesel fuel injection timings with the highest hydrogen enrichment rate is shown in Table 5.9. It can be observed that increasing the hydrogen enrichment rate necessitates reducing the injection timing, especially as MPRR, NO_x, and other performance values reach critical levels.

5.1.3 Comparison of Mode 1 and Mode 2

The increase in performance values resulting from adding hydrogen as an extra energy input to the system (Mode 2) was greater than the performance increase resulting from sharing energy between gas fuels (Mode 1). Under Mode 2 conditions, the proportion of natural gas in the gas mixture is higher when compared to Mode 1 conditions.

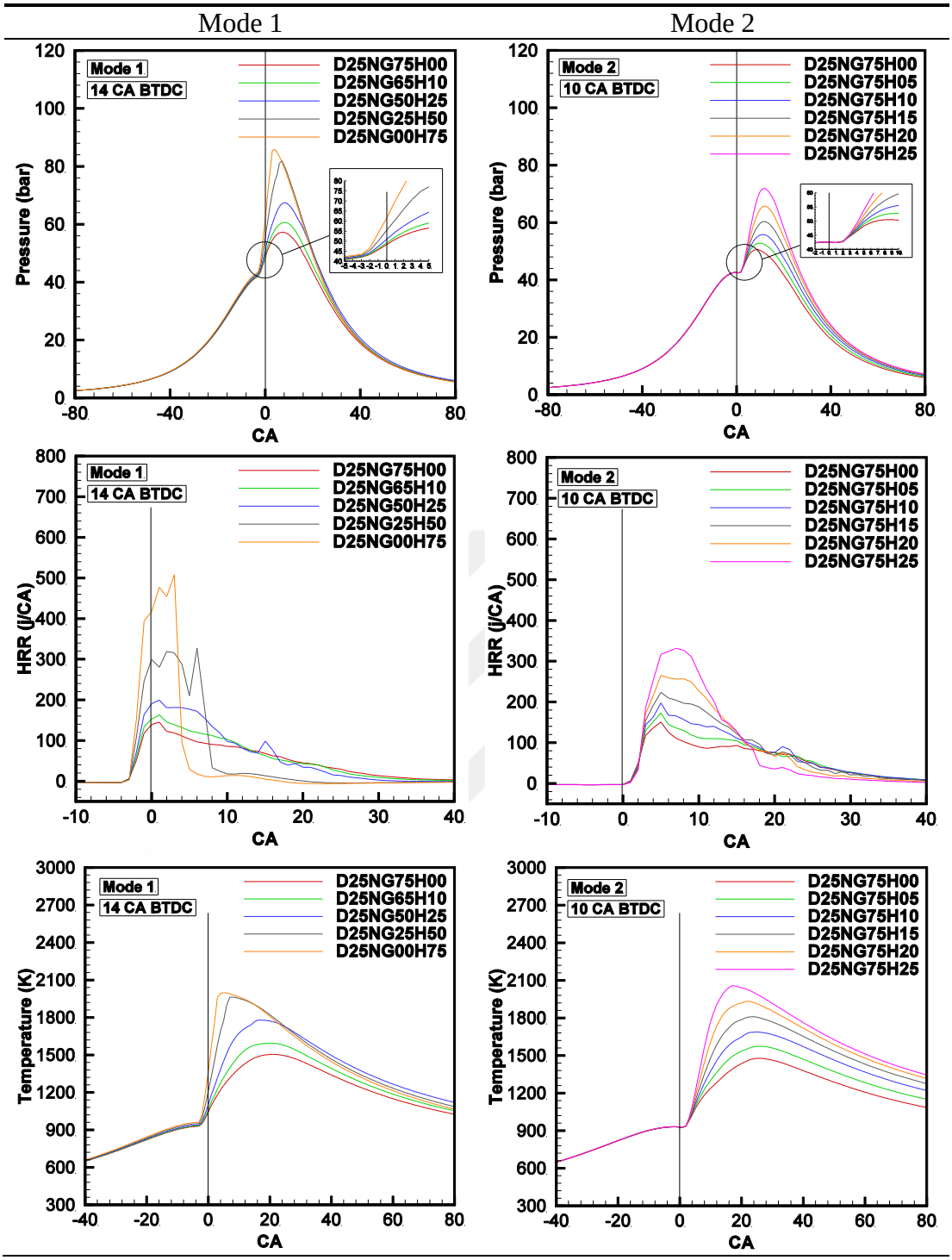

Figure 5.9 : The effect on pressure, HRR and temperature of hydrogen for optimum SOI of Mode 1 (14° CA BTDC) and Mode 2 (10° CA BTDC).

For instance, in Mode 1, a condition with a 14° CA BTDC injection timing and a 10% hydrogen ratio (D25NG65H10 - Case 10) has more hydrogen mass. When Case 50 is normalized to Mode 1 conditions, its hydrogen energy fraction is actually 9%. Similarly, when comparing the natural gas proportions in Case 10 and Case 50 gas mixtures, they are 65% and 68%, respectively.

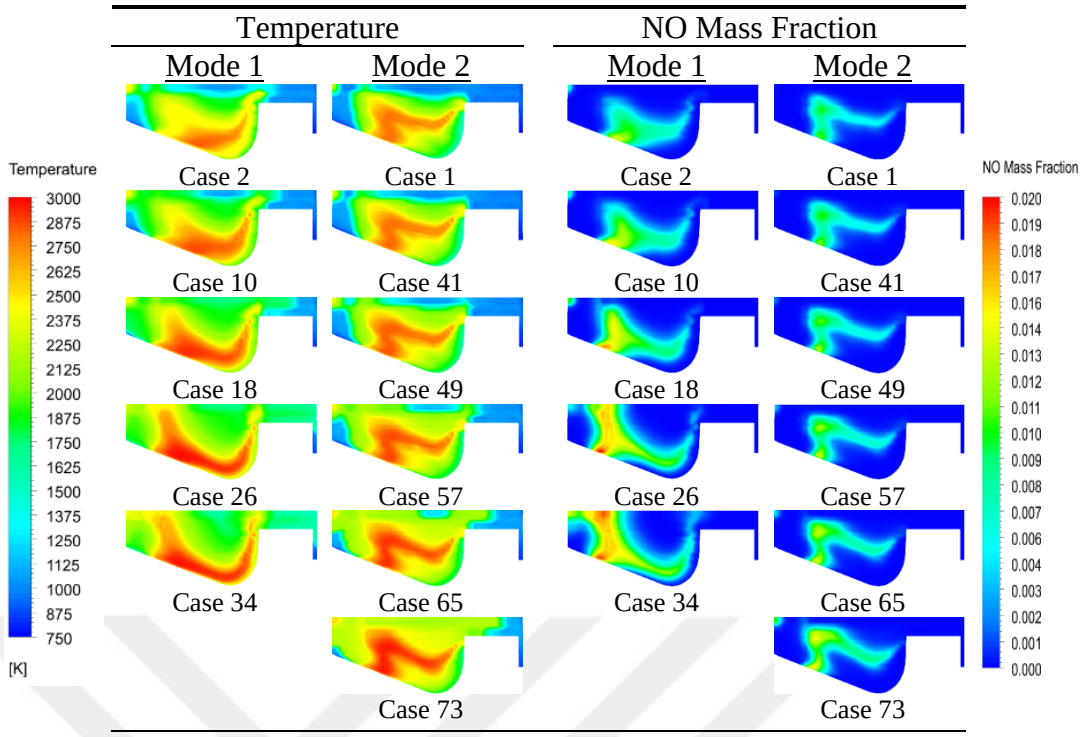

Figure 5.10 : The effect of hydrogen for fixed SOI - Mode 1 (for 14° CA BTDC of SOI) and Mode 2 (for 10° CA BTDC of SOI) temperature and NO_x contours for 10° CA ATDC of piston position.

In terms of diesel fuel content, they are 25% and 23%, respectively. Therefore, in terms of NO_x emissions, the relatively low proportions of hydrogen and diesel make Mode 2 conditions advantageous (Figure 5.10 and Figure 5.12). Additionally, the relatively high natural gas content has extended the combustion duration.

Table 5.10 : Comparison of optimum cases for Mode 1 (D25NG50H25) and Mode 2 (D25NG75H15).

	Case 18	Case 57	Variation
Power (kW)	11.58	13.28	+14.7%
Torque (N.m)	121.47	139.34	+14.7%
BSFC (g/kW.h)	136.27	156	+14.5%
Ignition Delay (CA)	11º	11º	-
Thermal Efficiency (%)	38.71	36.48	-2.23%
Combustion Duration (CA)	19º	23º	+4º
MPRR (bar/CA)	3.6	3	-0.6
Max. Press. (bar)	67.45	60.35	~ -7
CA for Max. Press. (ATDC)	8º CA	12º CA	-
Max. Mean Temp. (K)	1779	1809	+30
NO_x (g/kW.h)	7.46	5.44	-27%
SOOT (g/kW.h)	0.000172	0.000196	~+14%
CO (g/kW.h)	1.42	2.02	~+42%
HC (g/kW.h)	4.04	8.76	+116%

For this reason, Mode 2 has provided more effective results in terms of power and torque values. However, due to the additional fuel input, it has resulted in higher specific fuel consumption values compared to Mode 1 conditions (Table 5.10).

The pressure curve is sharper under Mode 1 conditions compared to the broader curve observed under Mode 2 conditions (Figure 5.9).

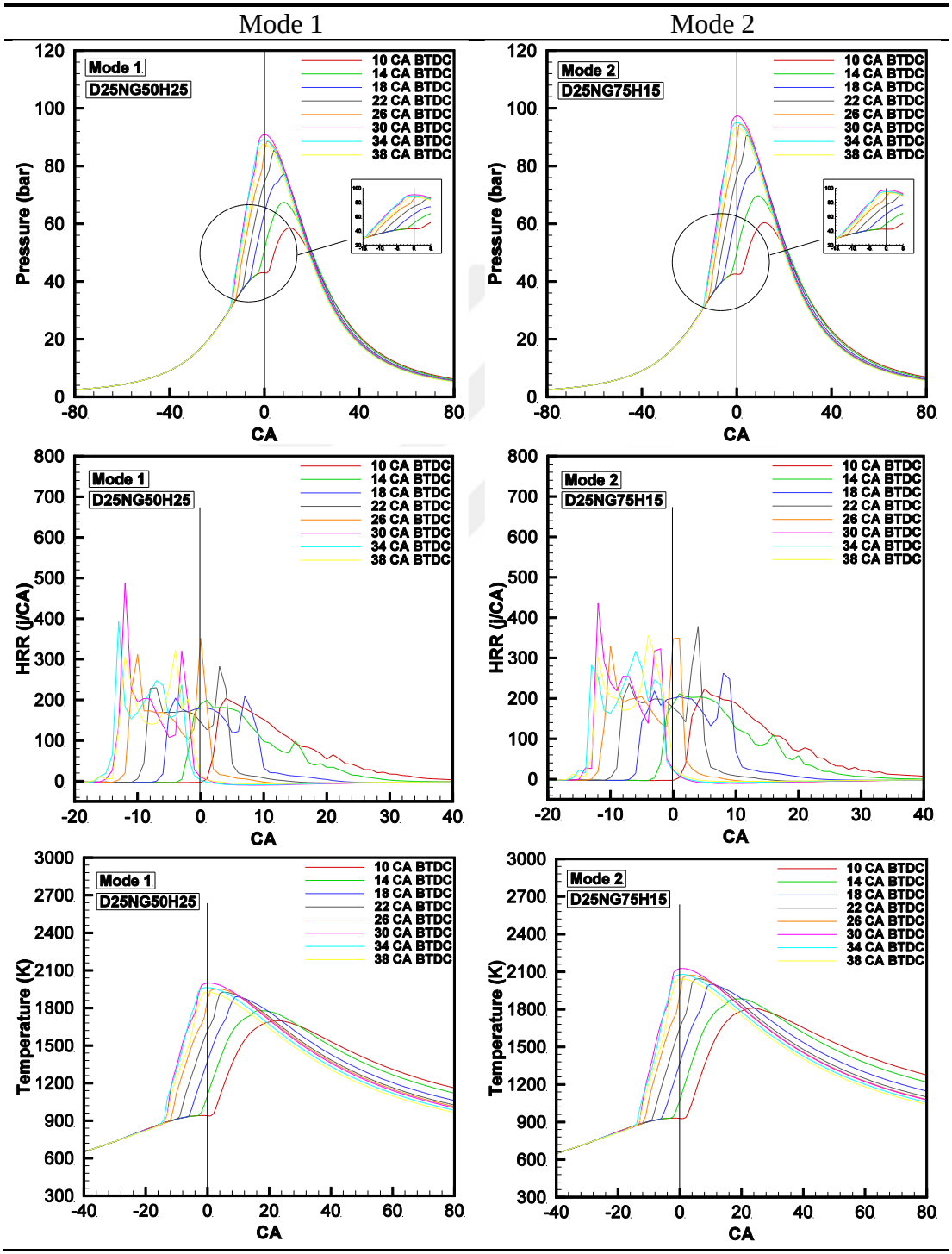

Figure 5.11 : The effect on pressure, HRR and temperature of SOI for optimum hydrogen content of Mode 1 (D25NG50H25) and Mode 2 (D25NG75H15).

This is, once again, a result of the higher hydrogen content under Mode 1 conditions. The ignition delay is shorter under Mode 1 conditions due to the higher hydrogen content in the gas mixture (Table 5.10). This leads to the earlier formation of the maximum pressure value, as seen in Figure 5.9.

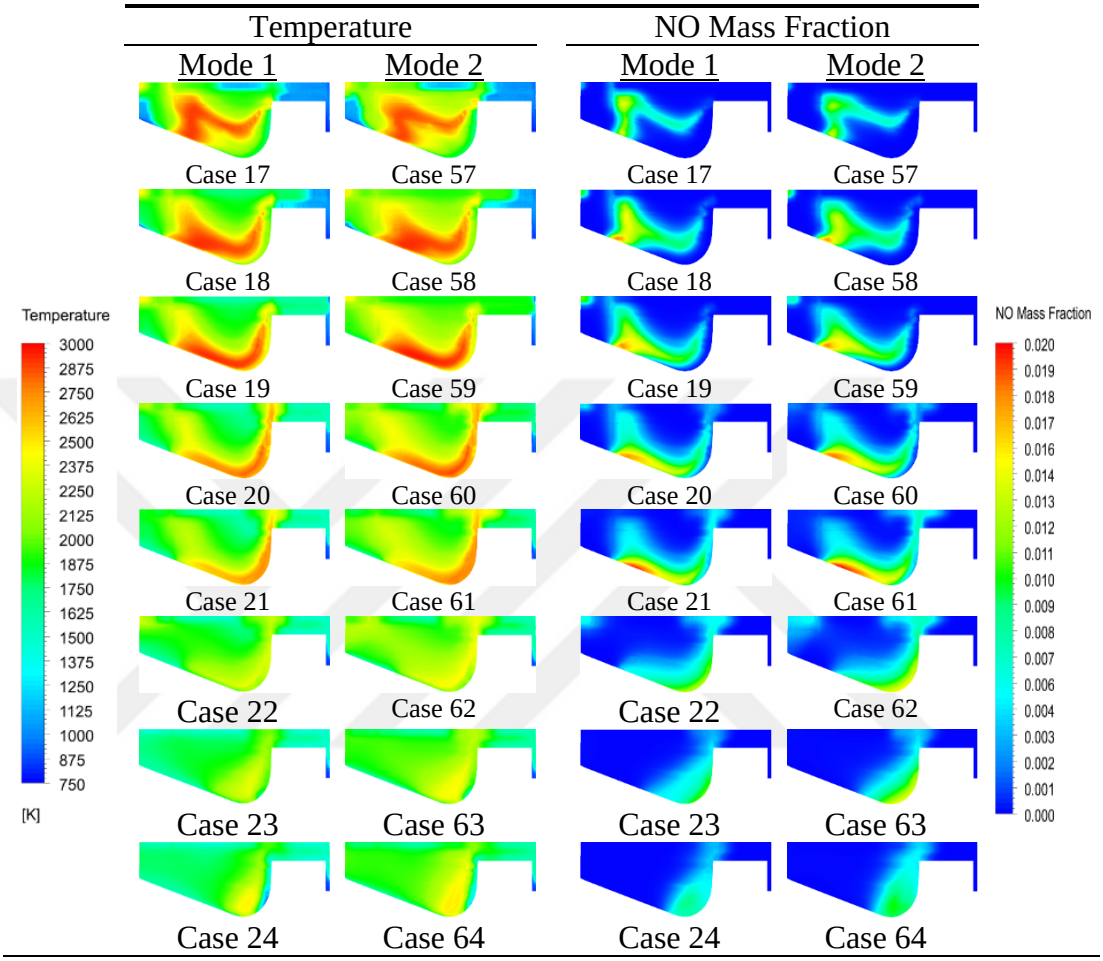

Figure 5.12 : The effect of SOI for fixed hydrogen content - Mode 1 (for D25NG50H25) and Mode 2 (for D25NG75H15) temperature and NO_x contours for 10° CA ATDC of piston position.

While Mode 2 may appear more advantageous in some cases when compared to Mode 1, results from situations without the inclusion of hydrogen (experimental measurements - D25NG75H00) compared to Mode 1 offer promising outcomes. For example, the test results of the condition with 14° CA BTDC injection timing and a 25% hydrogen ratio (Case 18) have resulted in higher performance values when compared to the test case (Case 2). There are also improvements in terms of emissions. In partial loads, incomplete combustion products are a significant issue, particularly in diesel engines. Additionally, in dual-fuel natural gas-diesel engines, despite reductions in incomplete combustion products compared to diesel operation conditions, natural

gas is a hydrocarbon fuel. Hence, PM, CO, and HC emissions are observed. Hydrogen, as a combustion product, only produces water vapor.

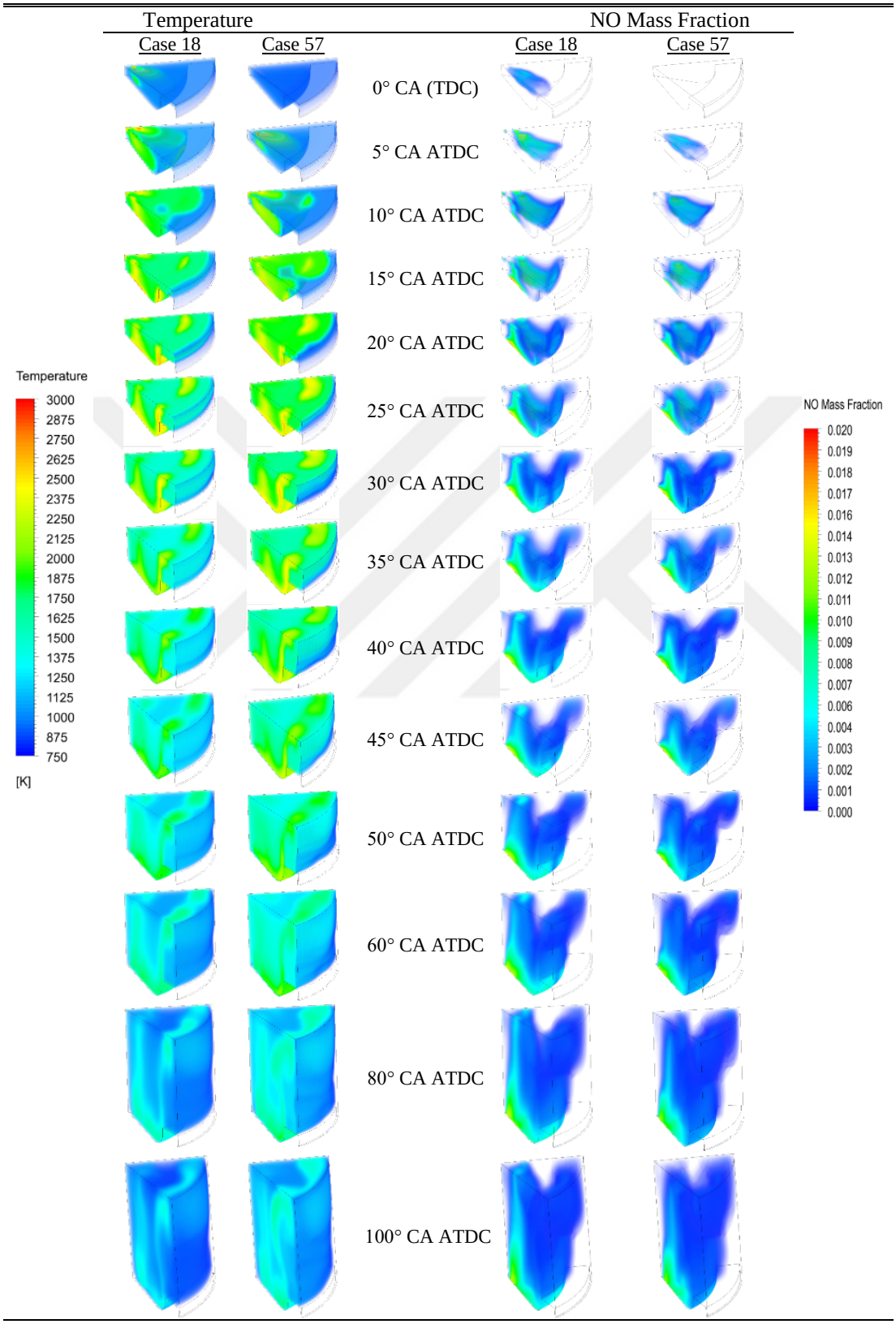

Figure 5.13 : Comparison of optimum cases of Mode 1 and Mode 2 at different combustion chamber positions for temperature and NO_x.

Therefore, by including it in the gas mixture, reductions in incomplete combustion products are achieved (Table 5.4). Similarly, positive results have been obtained when comparing the Mode 2 condition to experimental measurements. For instance, the test results of the condition with a 10° CA BTDC injection timing and an additional 15% hydrogen ratio (approximately 12%) (Case 57) have resulted in higher performance values when compared to the test case (Case 1). There are also improvements in terms of emissions (Table 5.8).

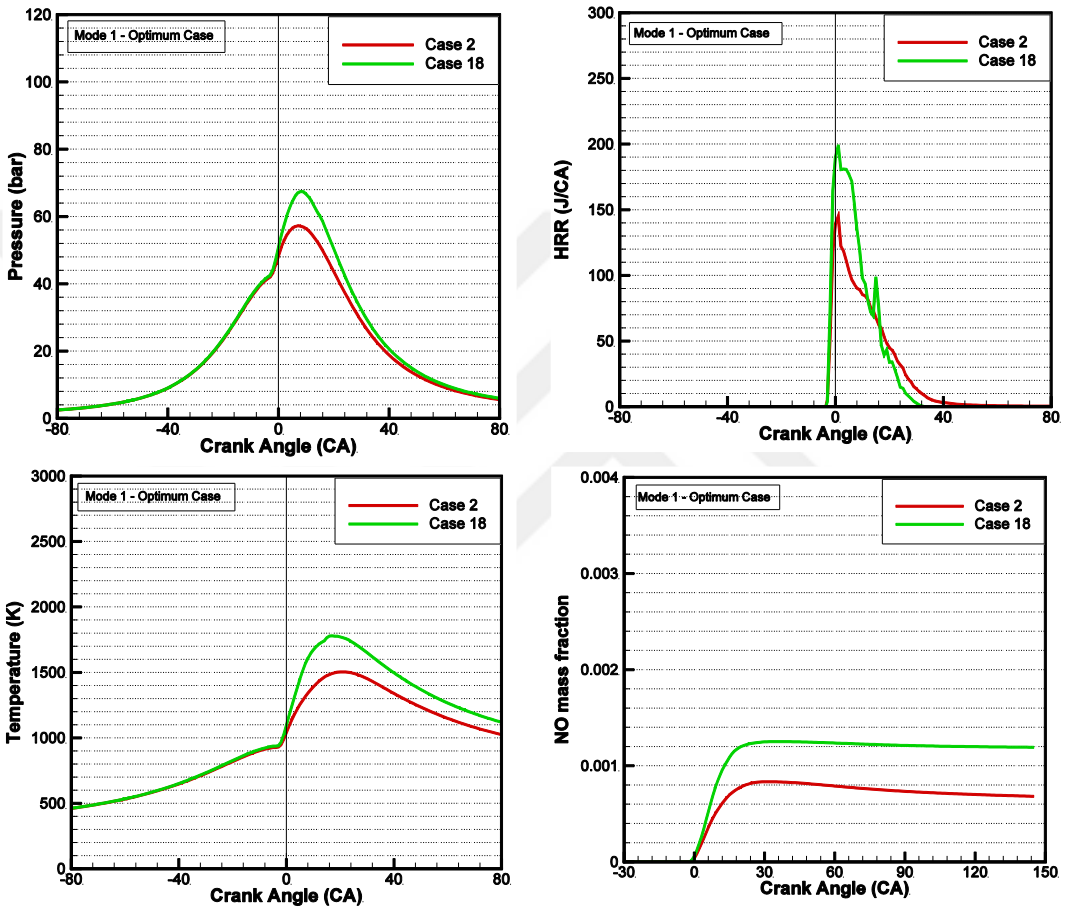

Figure 5.14 : Comparison of test condition (D25NG75H00) and Mode 1 (D25NG50H25).

When comparing the most optimum conditions of Mode 1 and Mode 2, as previously explained, it is evident that higher natural gas content and a slightly lower hydrogen content will yield more favorable results. Due to slow combustion mechanisms, as the natural gas ratio in the mixture increases, temperatures decrease (Figure 5.9). Consequently, NO_x emissions also decrease (Figure 5.10). A reduction in the sharp peak in the Heat Release Rate (HRR) curve, an indicator of sudden ignition, is also observed (Figure 5.9). For other emission types, an increase in the hydrogen content is advantageous in every respect (Table 5.8). It is important to note that the balance

between hydrogen and natural gas fuel needs to be optimized to control both NO_x and other emissions effectively. Within the scope of the study, it is suggested that the hydrogen content limit for Mode 1 should be 50%, while exceeding 25% hydrogen enrichment for Mode 2 is not recommended. These limits can be exceeded with the implementation of certain strategies, as discussed in the subsequent sections of the thesis.

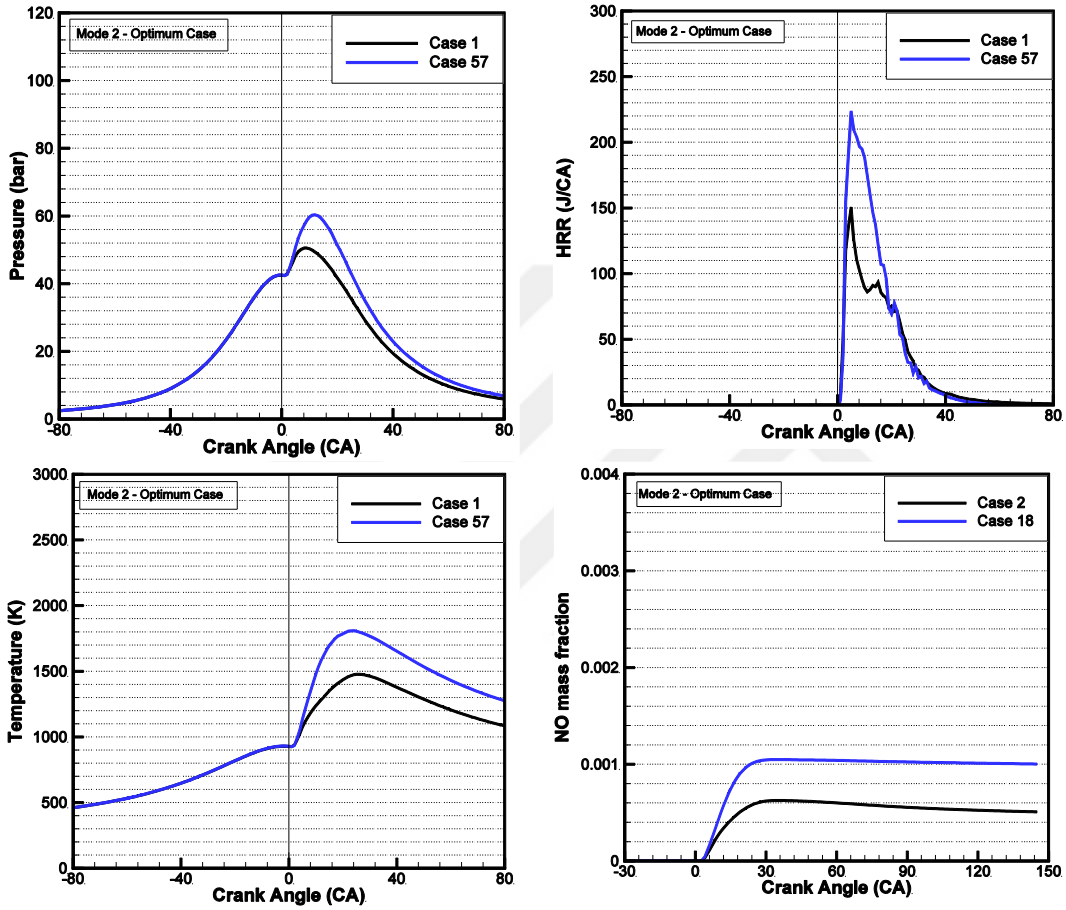

Figure 5.15 : Comparison of test condition (D25NG75H00) and Mode 2 (D25NG75H15).

An increase in the hydrogen energy fraction accelerates the formation of NO_x. When Figure 5.10 is examined for both Mode 1 and Mode 2, the rising trend in temperatures can be clearly observed. As a result of this trend, the formation of NO also increases. An increase in the injection advance causes the maximum pressure to approach the top dead center. This applies to both Mode 1 and Mode 2. The rapid combustion characteristics of hydrogen do not allow for a significant increase in the injection advance (Figure 5.11). Delaying the injection advance reduces the maximum values of pressure, temperature, and heat release rate. Increasing the diesel injection advance leads to an increase in ignition delay, resulting in rapid combustion initiation. When

Figure 5.12 is examined closely, it is evident that with the increase in diesel injection advance, the contour colors of the cylinder's temperature distribution shift from red to yellow (Figure 5.12).

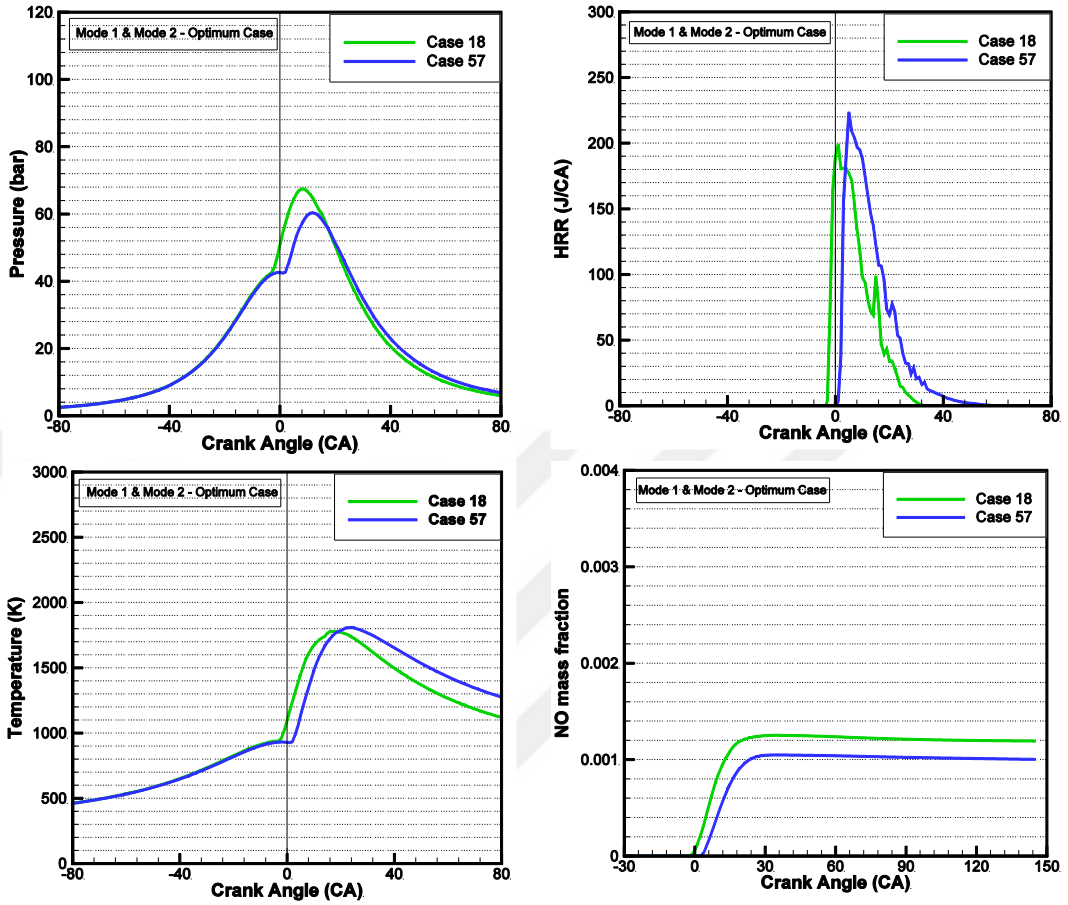

Figure 5.16 : Comparison of Mode 1 (D25NG50H25) and Mode 2 (D25NG75H15).

When comparing the temperature and NO_x levels at varying crank angles for the optimal operating points obtained for Mode 1 and Mode 2, it is observed that Mode 1 exhibits faster combustion and NO_x formation (Figure 5.13). Initially (at 0° CA), the temperature distribution is higher in Mode 1, while at advanced crank angles (at 100° CA), the temperature distribution is higher in Mode 2. This indicates that combustion in Mode 2 takes longer to complete (Table 5.10).

When comparing conditions with and without the inclusion of hydrogen at specific fractions, it is shown that hydrogen increases cylinder pressure, heat release rate, temperature, and NO_x formation for Mode 1 and Mode 2, as illustrated in Figure 5.14 and Figure 5.15, respectively.

When comparing both modes, it can be seen that Mode 1 with a higher hydrogen fraction has curves that are more delayed and have sharper, higher peaks (Figure 5.16).

Figure 5.17 and Table 5.10 show the comparison of the numerical results obtained for Mode 1 and Mode 2 under test conditions.

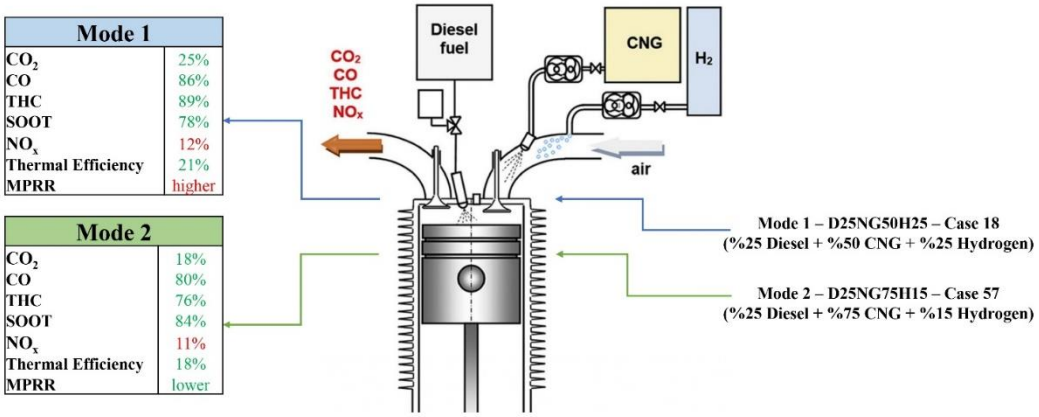

Figure 5.17 : Summary of numerical results obtained for optimum alternative fuel ratios and optimum diesel SOI values [170].

5.1.4 General summary for Mode 1 and Mode 2

Under partial load conditions, the injection timing should not be increased significantly. Having sufficient time for the combustion process and the high combustion rate of hydrogen allows for lower injection timing, reducing losses due to fuel pumping. Injection timing had an impact on performance values after 22° CA BTDC injection timing in Mode 1 conditions. Performance values were found to be similar at 10°, 14°, 18° and 22° CA BTDC injection timing. For Mode 2, after 10° CA BTDC, performance values decrease for all injection timings. Injection timing also has a significant effect on ignition delay. Especially at high injection timings, increasing the hydrogen fraction in the gas mixture has negative effects on engine performance [176–178]. As the hydrogen fraction in the gas mixture is increased, improvements in performance values and all emission types except NO_x emissions have been observed. However, when the hydrogen fraction in the gas mixture exceeds 50%, the situation reverses. To prevent the increase in NO_x emissions, it is recommended to implement different pilot diesel fuel injection strategies or use Exhaust Gas Recirculation (EGR). This way, high-performance values can be maintained, and improvements can be achieved in all emission types, including NO_x emissions [179,180].

The increase in the hydrogen fraction has led to an increase in thermal efficiency and a significant reduction in specific fuel consumption and SOOT (PM) emissions. However, to avoid knocking tendencies, the hydrogen fraction in the gas mixture should be limited. Exceeding a hydrogen fraction of 50% can lead to knocking issues

and deteriorate performance values. An increase in the amount of natural gas in the gas mixture also leads to higher unburned HC, SOOT (PM), and CO emissions. Additionally, adjusting the gas mixture ratio is crucial because it can affect vibrations, mechanical stresses, and thermal load [26,174]. Under 100% diesel fuel conditions, the engine emits higher levels of HC, CO, and SOOT emissions compared to when the engine operates in dual-fuel natural gas-diesel conditions. The addition of hydrogen to the gas mixture can further reduce these emissions. In the study, under Mode 1 conditions, there was an improvement in HC, CO, and SOOT emissions by approximately 88%, 86%, and 77%, respectively, while under Mode 2 conditions, there was an improvement of about 76%, 80%, and 83% in these emissions.

When comparing the two different modes, it is observed that Mode 2 provides more effective results in terms of performance and emission values. In Mode 1 conditions, the higher mass fraction of hydrogen led to higher temperatures. To balance the in-cylinder temperatures, it is essential for the natural gas fuel ratio in the gas mixture not to be too low. Successful results can be achieved when an appropriate mixture of natural gas and hydrogen is ignited with pilot diesel fuel.

In Mode 1 conditions, the optimum situation in terms of performance and emission values was Case 18. It provided a 21% improvement in power and a 29% improvement in Brake Specific Fuel Consumption (BSFC). However, it also resulted in a 12% increase in NO_x emissions. Similarly, in Mode 2 conditions, the optimum situation was Case 57, which led to a 36% improvement in power and a 22% improvement in BSFC. NO_x emissions increased by 11% in this case.

In summary, the suitability of natural gas and hydrogen ratios with injection timing led to optimal results for both modes. However, it was observed that there was an increase in NO_x and MPRR values for both modes under the test conditions. The identification of operating points where all performance (including MPRR) and emission values (including NO_x) are improved requires the implementation of various strategies. By applying EGR, WI, and WVI for NO_x reduction and PI for MPRR reduction, higher performance and lower emissions can be achieved compared to the test conditions. The aim with Mode 1 operating points is to increase performance while reducing all emissions while conserving the same fuel energy. The goal with Mode 2 operating points is to achieve higher efficiency, higher performance, and lower emissions by introducing additional hydrogen into the combustion chamber. However,

the desired results were not achieved for the MPRR performance parameter and the NO_x emissions. Therefore, the scope of the study was expanded to address these issues with the EGR-PI, WI-PI, and WVI-PI strategies.

5.2 EGR – PI Strategies

The results obtained from Mode 1 and Mode 2 have shown that hydrogen and natural gas are valuable alternative fuels for emissions. However, an increase in hydrogen fraction, especially, led to high NO_x emissions and a tendency for knocking. Particularly in the literature, to mitigate these two problems, EGR (Exhaust Gas Recirculation) and pilot injection processes are recommended [57,181–185]. In the numerical simulations at this stage, EGR (Exhaust Gas Recirculation) was used to reduce NO_x emissions, and PI (Pilot Injection) was applied to mitigate knocking tendencies.

In the previous section, the most optimal conditions were determined to be Case 18 (D25NG50H25 - 14° CA BTDC for SOI) for Mode 1 and Case 57 (D25NG75H15 - 10° CA BTDC for SOI) for Mode 2. However, it was observed that NO_x emissions increased compared to the experimental conditions. Additionally, it was noted that the combustion inside the cylinder was more severe, based on the MPRR value. To achieve a smoother combustion, the pilot injection process needed to be investigated. For this study, four different EGR rates and four different pilot injection rates were selected. EGR rates were chosen as 0%, 10%, 15%, and 20%. The purpose here is to start with the situation where EGR is not applied and gradually increase it to light, medium, and high levels in order to jointly optimize NO_x emissions and performance. For the pilot injection process, rates of 0%, 20%, 30%, and 50% were selected to achieve a smoother start of the combustion process. It is known that in diesel engines, there are three different injection strategies: pilot injection, main injection, and post injection. These strategies each have different meanings when applied. Pilot injection is used to achieve a smoother combustion and reduce knocking tendencies. Main injection is used to initiate the main combustion, and post-injection is especially applied to extend the combustion duration and improve SOOT (PM) emissions. In this study, pilot and main injection strategies will be applied, and post-injection will not be used. The reason for not needing post-injection is that with gaseous fuels (Natural Gas and Hydrogen), soot emissions are significantly reduced. In the numerical study, the

pilot injection (PI) timing and injection duration were set to a range of 2.5° CA, with an advance of 40° CA BTDC to 37.5° CA BTDC.

Table 5.11 : Case matrix for EGR and pilot injection processes.

Mode 1		Mode 2	
0% EGR		0% EGR	
PI - 0%	D25NG50H25	PI - 0%	D25NG75H15
PI - 20%	D25NG50H25	PI - 20%	D25NG75H15
PI - 30%	D25NG50H25	PI - 30%	D25NG75H15
PI - 50%	D25NG50H25	PI - 50%	D25NG75H15
0% PI – 100°C EGR		0% PI – 100°C EGR	
EGR - 0%	D25NG50H25	EGR - 0%	D25NG75H15
EGR - 10%	D25NG50H25	EGR - 10%	D25NG75H15
EGR - 15%	D25NG50H25	EGR - 15%	D25NG75H15
EGR - 20%	D25NG50H25	EGR - 20%	D25NG75H15
20% PI – 15% EGR		20% PI – 15% EGR	
100°C - EGR	D25NG50H25	100°C - EGR	D25NG75H15
200°C - EGR	D25NG50H25	200°C - EGR	D25NG75H15
300°C - EGR	D25NG50H25	300°C - EGR	D25NG75H15
20% PI – 100°C EGR		20% PI – 100°C EGR	
EGR – 10%	D25NG50H25	EGR – 10%	D25NG75H15
EGR – 15%	D25NG50H25	EGR – 15%	D25NG75H15
10% EGR – 100°C – 20% PI		10% EGR – 100°C – 20% PI	
D25NG75H00		D25NG75H00	
D25NG65H10		D25NG75H05	
D25NG50H25		D25NG75H10	
D25NG25H50		D25NG75H15	
D25NG00H75		D25NG75H20	
-		D25NG75H25	

Some considerations were taken into account while setting it up this way. The selection of the diesel pilot injection timing in this time interval was based on the temperature distribution inside the cylinder. Diesel fuels evaporate at temperatures between 149°C (420 K) and 371°C (640 K). Therefore, for the effect of the pilot injection process to be observed, the environment should be in the temperature range where the injected fuel evaporates. Because the injected fuel will evaporate, and at the same time, due to the movement of the air inside the cylinder, it will homogenize with the charge in the environment. When ignition is initiated with the main injection, the proportion of evaporated fuel in the environment will increase, resulting in an earlier combustion event. Consequently, the ignition delay will decrease slightly, and the rate of pressure increase per unit crank angle (MPRR) will decrease. In parallel with this development, as temperature distributions decrease, positive results will also be obtained in terms of NO_x emissions. It was observed that the minimum cylinder temperature in the selected

timing range for the pilot injection process was 600 K. Assuming that the injected fuel directly evaporates, considering the evaporation temperature of diesel fuel is between 420 K and 640 K. The analysis was conducted with the pilot injection duration set to 2.5° CA. Additionally, the effects of different EGR temperatures (100°C - Cold EGR, 200°C - Warm EGR, and 300°C - Hot EGR) were examined. All these analyses, as described, are shown in Table 5.11 for both Mode 1 and Mode 2. These analyses were initially initiated at the optimum operating points for Mode 1 and Mode 2. However, they were further expanded to see that higher hydrogen fractions could be achieved with the applied parameters. The table also shows the analysis stages conducted for different gas fuel fractions (Table 5.11).

5.2.1 Optimal condition determination in the EGR – PI co-work

As a result of the previous study, the optimum condition obtained for Mode 1 was D25NG50H25 at 14° CA BTDC for the injection advance. Similarly, in the previous study, the optimum condition for Mode 2 was D25NG75H15 at 10° CA BTDC for the injection advance. Therefore, this study, which is a continuation of the previous one, aims especially to improve the NO_x and MPRR pair. Of course, it also aims to demonstrate the ability to achieve higher hydrogen fractions.

The roadmap of the first study was enriched with EGR and pilot injection processes. The analysis started with gradually increasing the pilot injection rate (0%, 20%, 30%, and 50%) for the optimum conditions of Mode 1 and Mode 2 (Table 5.11). In these analyses, no EGR (0% EGR) was applied. The aim at this stage is to both observe the effects of pilot injection and determine the optimum pilot injection rate.

In the next stage, the effects of different EGR rates (0%, 10%, 15%, and 20%) were investigated without pilot injection (0% PI) (Table 5.11). A temperature of 100°C was used for EGR in this stage. The purpose here is to examine the impact of EGR and determine the optimal EGR rate. With the first two stages, it was understood that 20% PI and 15% EGR rates provided more favorable results in terms of performance and emission values compared to the others. The stage of applying the obtained PI and EGR rates together for Mode 1 and Mode 2 was reached to examine the effects of different EGR temperatures (100°C, 200°C, and 300°C) (Table 5.11). Eventually, the values for PI and EGR rates and EGR temperature were determined as 20%, 15%, and 100°C, respectively. However, since the optimal EGR rate was selected under

conditions without pilot injection (0% PI), the effects of the 10% and 15% EGR rates could not be observed. Therefore, under conditions with pilot injection (20% PI), the effects of the 10% and 15% EGR rates were investigated (Table 5.11).

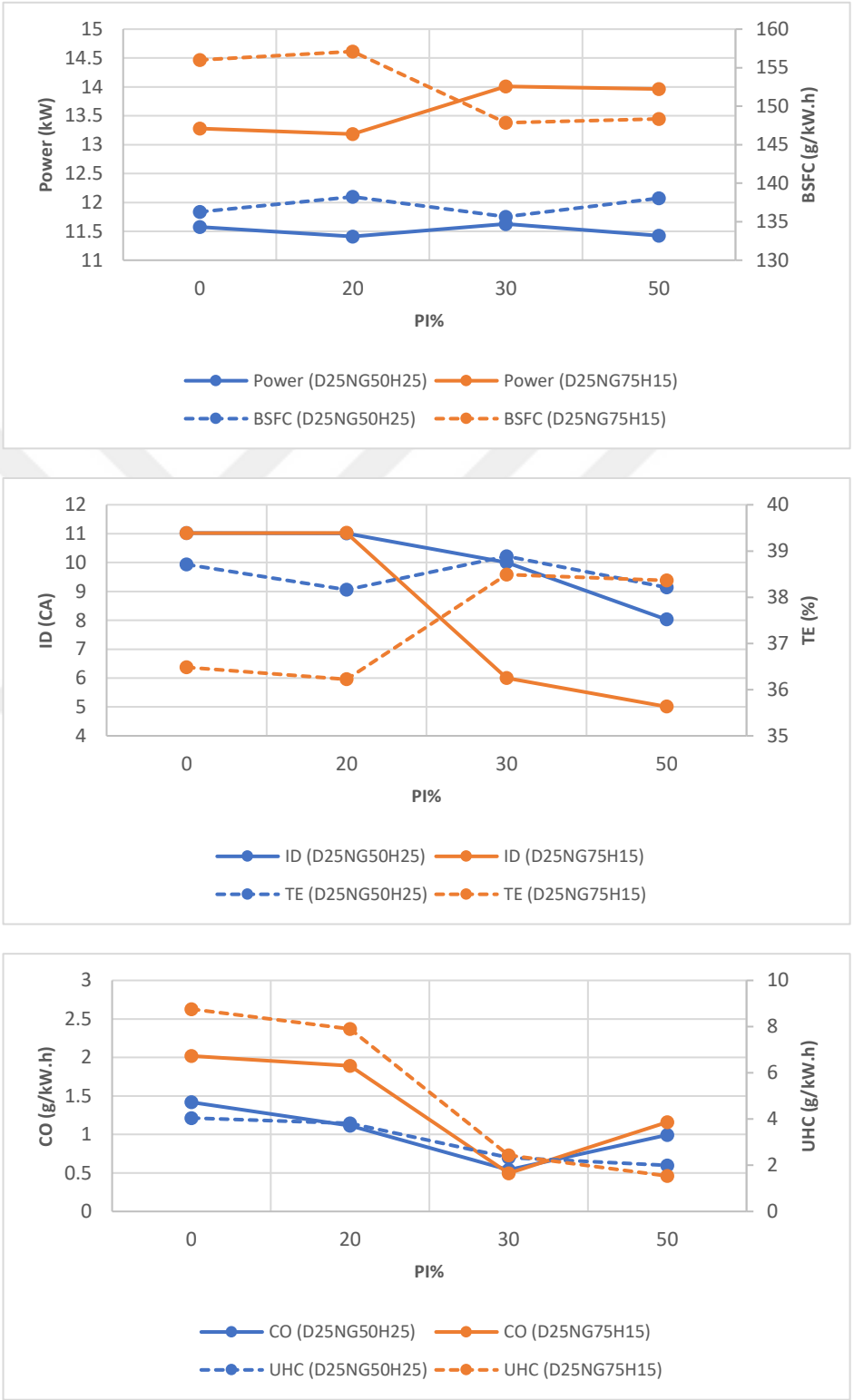

Figure 5.18 : The effect of increasing the pilot injection rate without EGR on power, BSFC, ID, TE, CO, and UHC values.

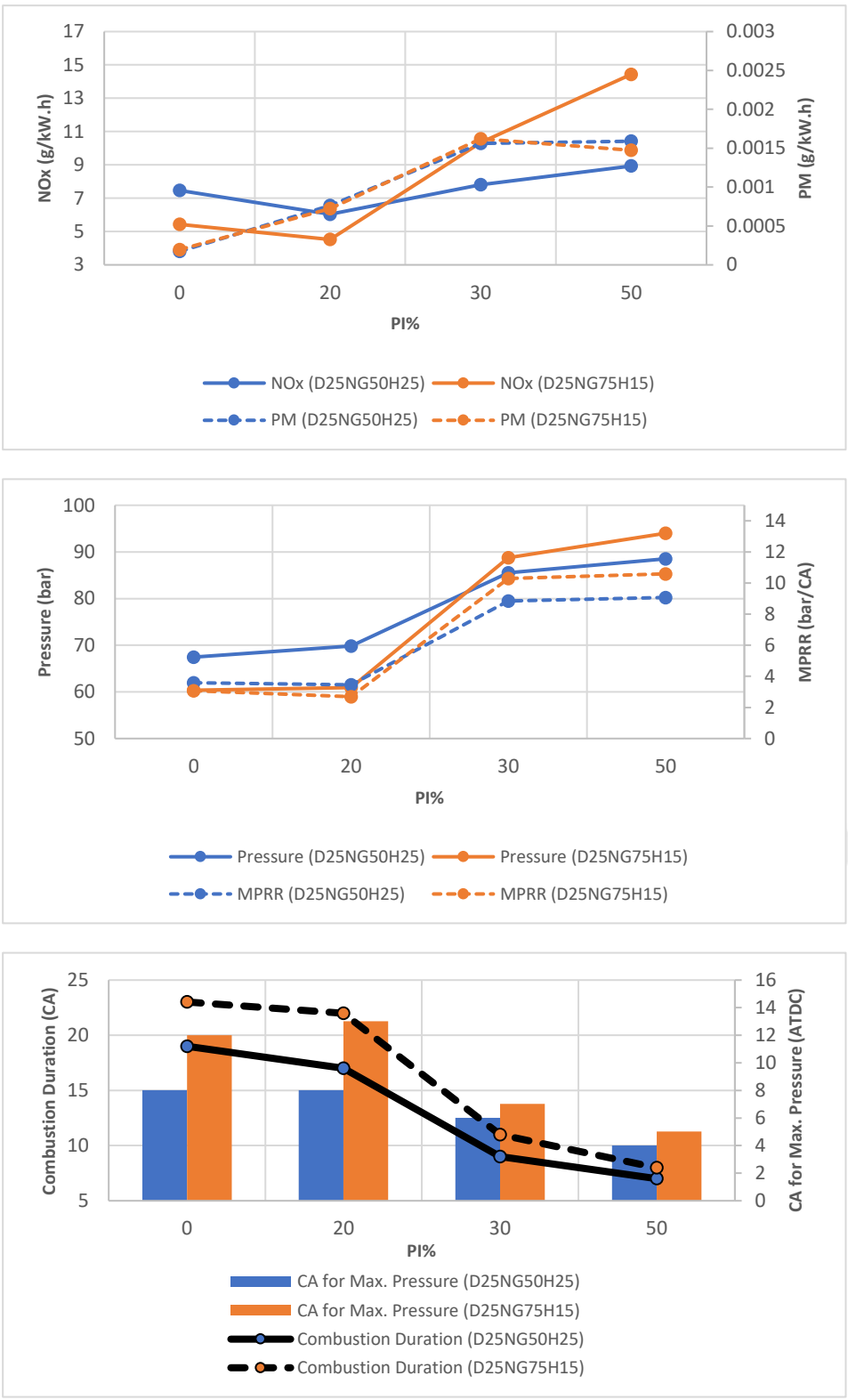

Figure 5.19 : The effect of increasing the pilot injection rate without EGR on NO_x, PM, Pressure, MPRR, CD, and the position of Max. Press. Relative to TDC.

As a result, it was observed that the 10% EGR condition under 20% PI showed more reasonable results in terms of performance and emission values compared to 15%

EGR. In the final stage of the study, the effects of different gas fuel (Natural Gas - Hydrogen) fractions for Mode 1 and different hydrogen enrichment rates for Mode 2 under the optimal conditions (20% PI, 10% EGR, and 100°C EGR Temperature) were examined (Table 5.11).

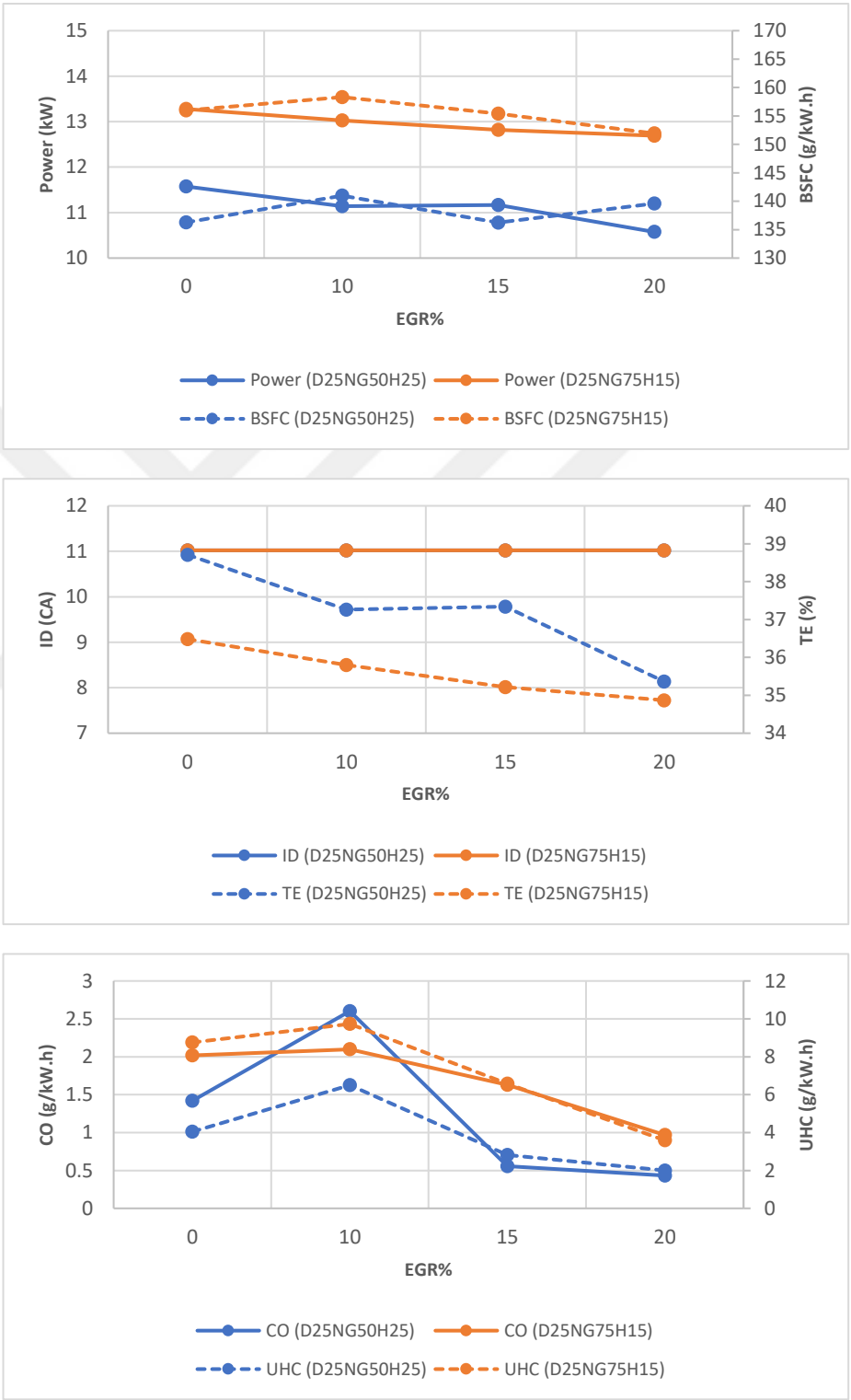

Figure 5.20 : The effect of increasing EGR rate without pilot injection on power, BSFC, ID, TE, CO, and UHC values.

The effect of PI for Mode 1 (D25NG50H25 - 14° CA BTDC for SOI) and Mode 2 (D25NG75H15 - 10° CA BTDC for SOI) is illustrated on the same graphs in Figure 5.18 and Figure 5.19. Mode 1 is represented by the blue color, and Mode 2 is represented by the orange color. When examining the graphs, it can be observed that the power output initially decreases for Mode 1 with an increase in the PI rate up to 20% and then starts to increase. Brake Specific Fuel Consumption (BSFC) first slightly increases and then decreases.

A similar trend is observed for Mode 2 (Figure 5.18). The reason for the increase in performance values after 20% PI is explained by the increased amount of diesel fuel in the combustion chamber before the main injection. The increased accumulation of fuel leads to a reduction in ignition delay (ID), resulting in higher combustion pressure and, consequently, higher temperatures (Figure 5.18 and Figure 5.19).

Table 5.12 : Comparison of numerical results for different EGR rates (10% and 15%) at 20% PI and 100°C EGR temperature for Mode 1 (D25NG50H25).

	20% PI – EGR 100 °C – D25NG50H25		
	10%	15%	Variation
Power (kW)	11.20	10.87	-2.95%
Torque (N.m)	117.48	114.04	-2.93%
BSFC (g/kW.h)	140.33	140	-0.24%
Ignition Delay (CA)	11º	11º	-
Thermal Efficiency (%)	37.44	36.34	-1.1%
Combustion Duration (CA)	20º	12º	-8º
MPRR (bar/CA)	3.36	6.66	+3.3
Max. Press. (bar)	67.31	77.28	+10
CA for Max. Press. (ATDC)	9º CA	8º CA	-1º
Max. Mean Temp. (K)	1738	1950	+212
NO_x (g/kW.h)	4.54	5.93	+30.62%
SOOT (g/kW.h)	0.00121	0.00107	-11.57%
CO (g/kW.h)	1.55	0.49	-68.39%
HC (g/kW.h)	4.45	2.53	-43.15%

Although high pressure results in increased power and combustion efficiency, the results for MPRR and NO_x are not at a reasonable level. When examining the ratios of MPRR and NO_x components in relation to the graphs, it can be seen that the values increase after 20% PI (Figure 5.19). In fact, an increase in performance values has occurred with a tendency toward knocking. This is not the desired outcome. When comparing the results of 20% PI with no pilot injection (0% PI), it is evident that MPRR and NO_x values decrease with 20% PI. Since the main purpose of pilot injection

is to reduce MPRR, it is understood that there is no need to go beyond 20% PI. An increase in PI affects the ID, leading to a reduction in ignition delay. As mentioned earlier, increased PI results in more accumulated fuel before combustion.

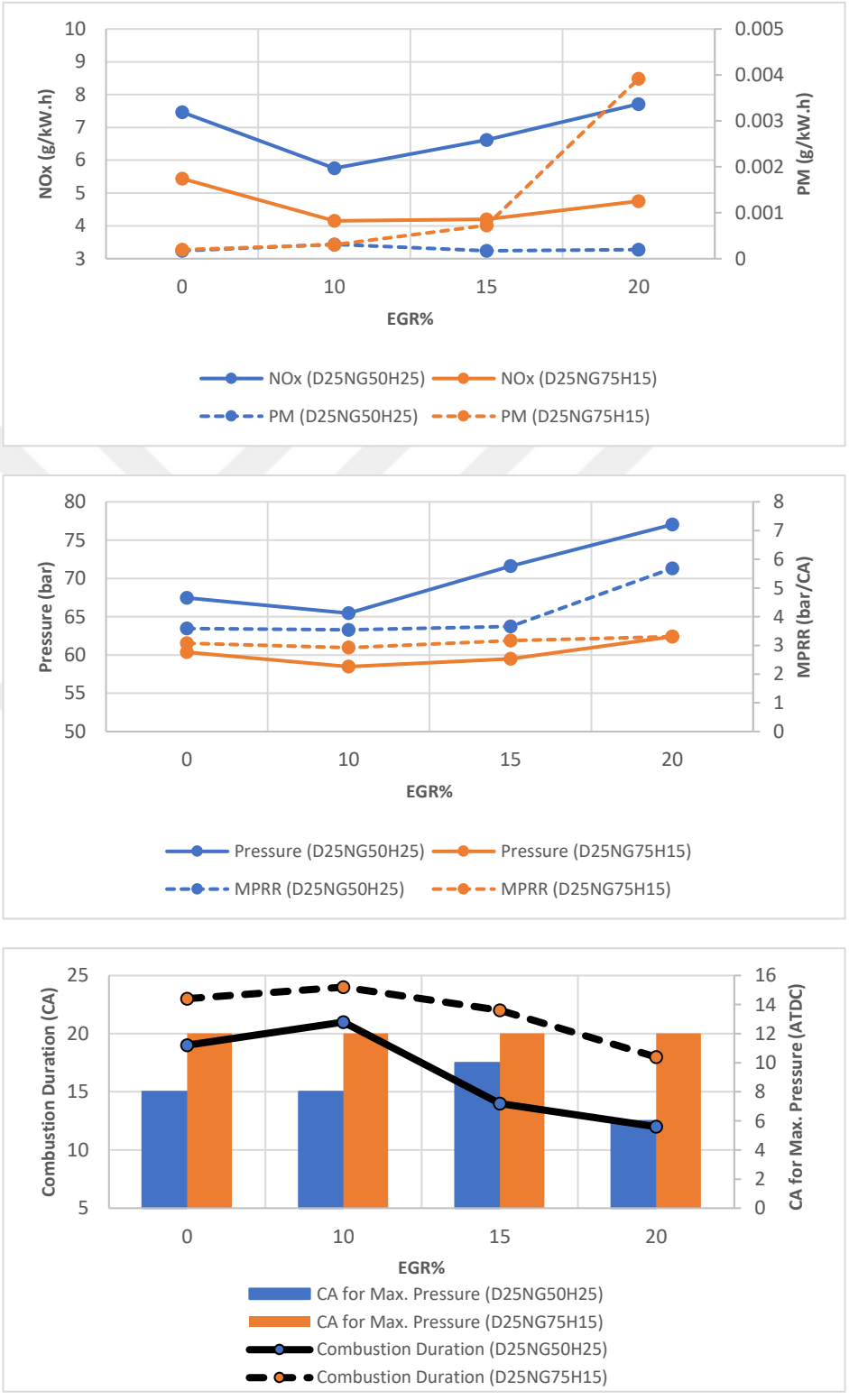

Figure 5.21 : The effect of increasing EGR rate without PI on NO_x, PM, Pressure, MPRR, CD and the position of Max. Press. Relative to TDC.

With increased fuel, the combustion event begins earlier, reducing the ignition delay period (Figure 5.18). Thermal efficiency exhibits a similar trend related to chamber pressure and temperature.

The thermal efficiency showed a change in that direction because of the decrease in pressure and temperature until 20% PI and the subsequent increase trend after 20% PI (Figure 5.18). While CO and UHC emissions decreased until 30% PI, they exhibited an increasing trend after 30% PI. The increase in combustion temperatures indicates an improvement in combustion efficiency. Therefore, CO and UHC emissions decreased until 30% PI due to the increase in combustion efficiency. After 30% PI, there was a sharp decrease in combustion duration, resulting in an increase in unburned product formation (Figure 5.18). PM (SOOT) emissions increased in parallel with the increase in pilot injection (PI) rate. PM emissions are particulate matter composed of carbon particles that form when unburned fuel vapor oxidizes before combustion.

The increase in PI led to an increase in the amount of fuel vapor formed before combustion. Although power and UHC emissions showed positive results up to 30% PI, PM emissions increased in all PI conditions. This is because the increase in pilot injection (PI) led to an increase in the amount of gaseous fuel, resulting in an increase in both burned and unburned gaseous fuel. Especially after 30% PI, as the power gain trend decreased, PM sharply increased (Figure 5.19). The crank angle at which maximum pressure occurs remained almost the same piston position up to 20% PI, but after 20% PI, it moved towards the TDC position (Figure 5.19). This also reduced the generated power. Overall, when the analyses with PI are evaluated, it is understood that more reasonable results were obtained with 20% PI in both Mode 1 and Mode 2 conditions. After obtaining the optimal value for PI, analyses were conducted with different EGR rates. These analyses were carried out without applying PI (0% PI). Performance values, particularly power, gradually decreased as EGR increased. The BSFC value increased slightly up to 10% EGR and then decreased slightly (Figure 5.20). An increase in the EGR rate reduces the oxygen concentration in the cylinder before combustion, which directly affects power and BSFC, as it causes a loss in combustion efficiency. However, this effect was not very significant (Figure 5.20). The relatively minor power and BSFC loss up to 10% EGR, and even the improvement in BSFC, can be attributed to a slight increase in the combustion duration with 10% EGR (Figure 5.21). Ignition delay was not affected by EGR, but thermal efficiency

decreased (Figure 5.20). It's worth noting that EGR is a method used to reduce NO_x emissions. In the numerical study, as EGR increased, NO_x initially decreased and then exhibited an increasing trend.

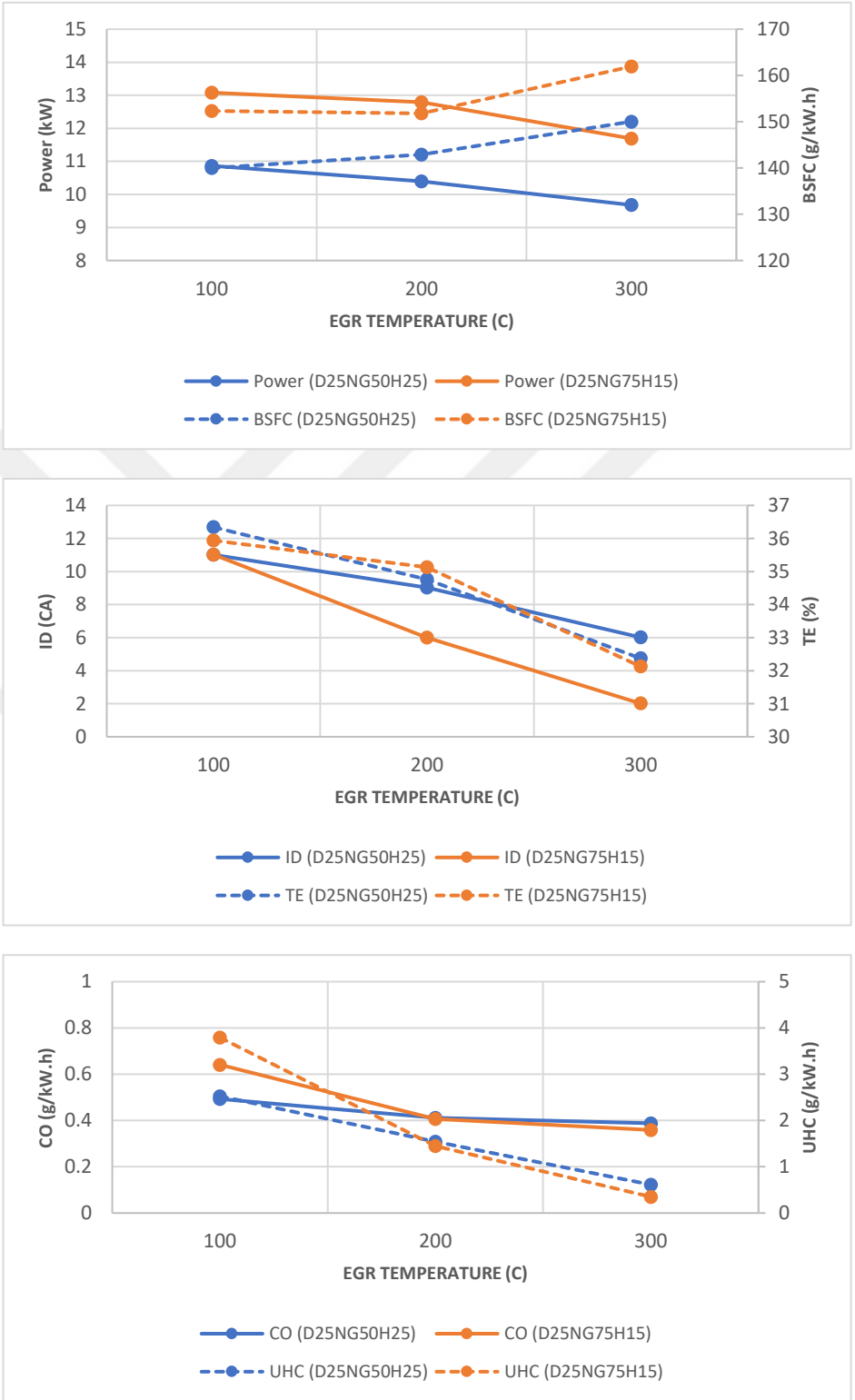

Figure 5.22 : The effect of increasing EGR temperature at 20% PI and 15% EGR rates on power, BSFC, ID, TE, CO, and UHC values.

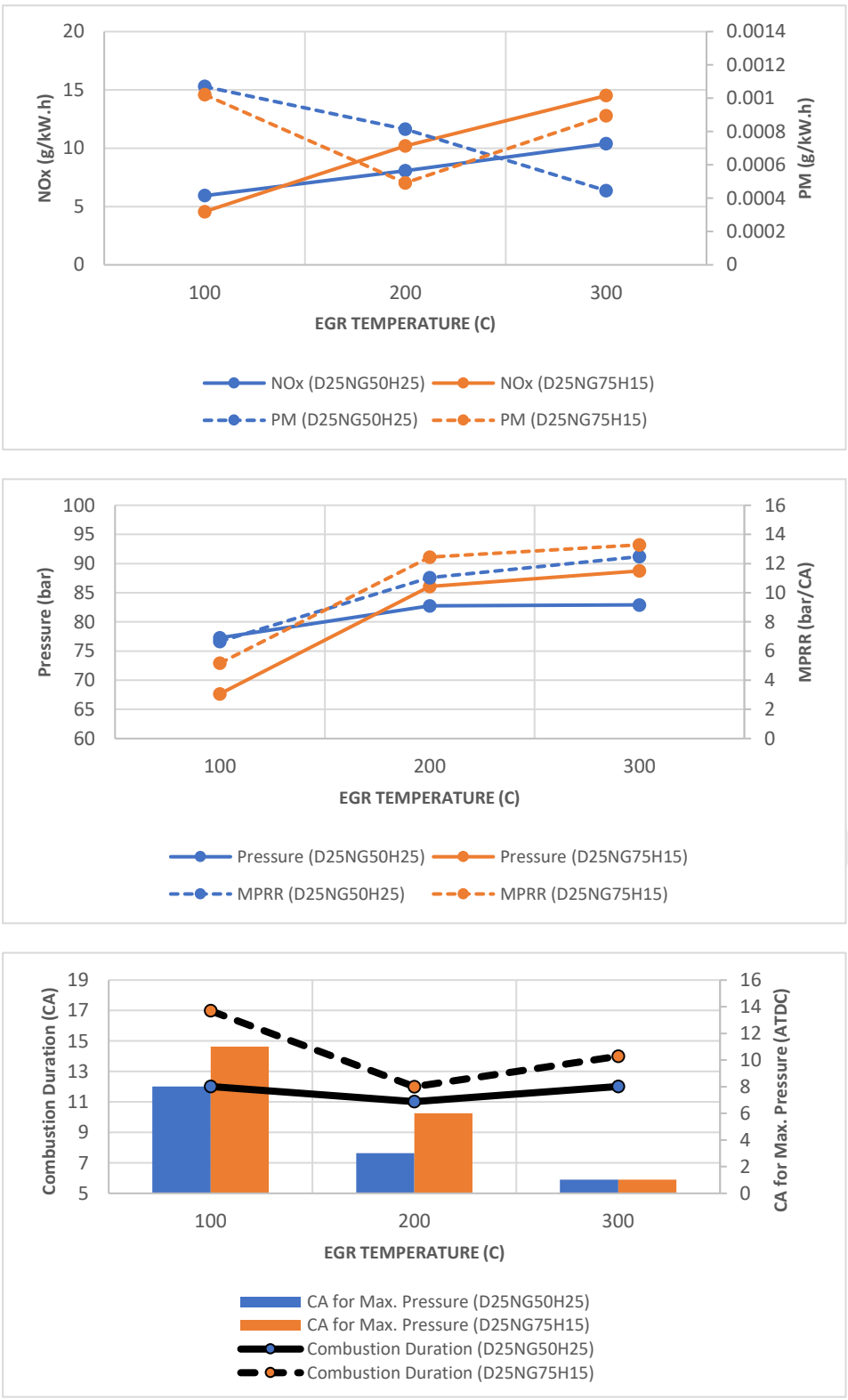

Figure 5.23 : The effect of increasing EGR temperature at 20% PI and 15% EGR rates on NO_x, PM, Pressure, MPRR, CD, and the position of Max. Press. Relative to TDC.

Despite the expected increase in EGR, NO_x emissions exhibited a decreasing trend. However, after reaching 10% EGR, there was an increasing trend in NO_x emissions

(Figure 5.21). The reason for this behavior is the temperature of the applied EGR. Various EGR rates were applied without PI at temperature consistently under 100°C. It is as if the EGR underwent cooling (Cold EGR) before being introduced into the combustion chamber. In the literature, it has been observed that cooled EGR has such effects (increased EGR leading to increased NO_x emissions) [186].

Table 5.13 : Comparison of numerical results for different EGR rates (10% and 15%) at 20% PI and 100°C EGR temperature for Mode 2 (D25NG75H15).

	20% PI – EGR 100 C – D25NG75H15		
	10%	15%	Variation
Power (kW)	12.8	13.08	+2.19%
Torque (N.m)	134.29	137.26	+2.21%
BSFC (g/kW.h)	161.2	152.31	-5.51%
Ignition Delay (CA)	11º	11º	-
Thermal Efficiency (%)	35.16	35.94	+0.78%
Combustion Duration (CA)	25º	17º	-8º
MPRR (bar/CA)	2.31	5.17	+2.86
Max. Press. (bar)	57.92	67.67	+10
CA for Max. Press. (ATDC)	13º CA	11º CA	-2º
Max. Mean Temp. (K)	1779	1970	+191
NO_x (g/kW.h)	3.42	4.56	+33.33%
SOOT (g/kW.h)	0.00122	0.00102	-16.39%
CO (g/kW.h)	2.342	0.64	-72.67%
HC (g/kW.h)	9.557	3.79	-60.34%

The partially non-combustible gas mixture with a 10% EGR rate and a 100°C EGR temperature resulted in reduced oxygen concentration within the cylinder, partially reducing the combustion temperatures. Consequently, both power and NO mass fraction decreased, leading to a decrease in NO_x in g/kW.h. However, beyond 10% EGR, the increase in EGR continued to lower power and the NO mass fraction, but it increased the NO_x in g/kW.h. This can be explained by the fact that higher EGR rates (15% and above) contributed to in-cylinder mixture formation, interacting with the turbulence inside the cylinder, making the air-fuel mixture more homogeneous. Thus, with the influence of hydrogen, combustion occurred more rapidly and efficiently. The quicker combustion can be understood by examining the graph related to the combustion duration (Figure 5.21).

Additionally, monitoring MPRR helps understand this situation (Figure 5.21). UHC emissions followed a similar trend, decreasing after 15% EGR (Figure 5.20). The decrease in power in response to the increase in combustion efficiency was due to the

shorter combustion duration (Figure 5.21). Thermal efficiency is the ratio of the net indicated work to the heat released. The decrease in net work (power) and the increase in in-cylinder temperatures resulted in a decrease in thermal efficiency (Figure 5.20).

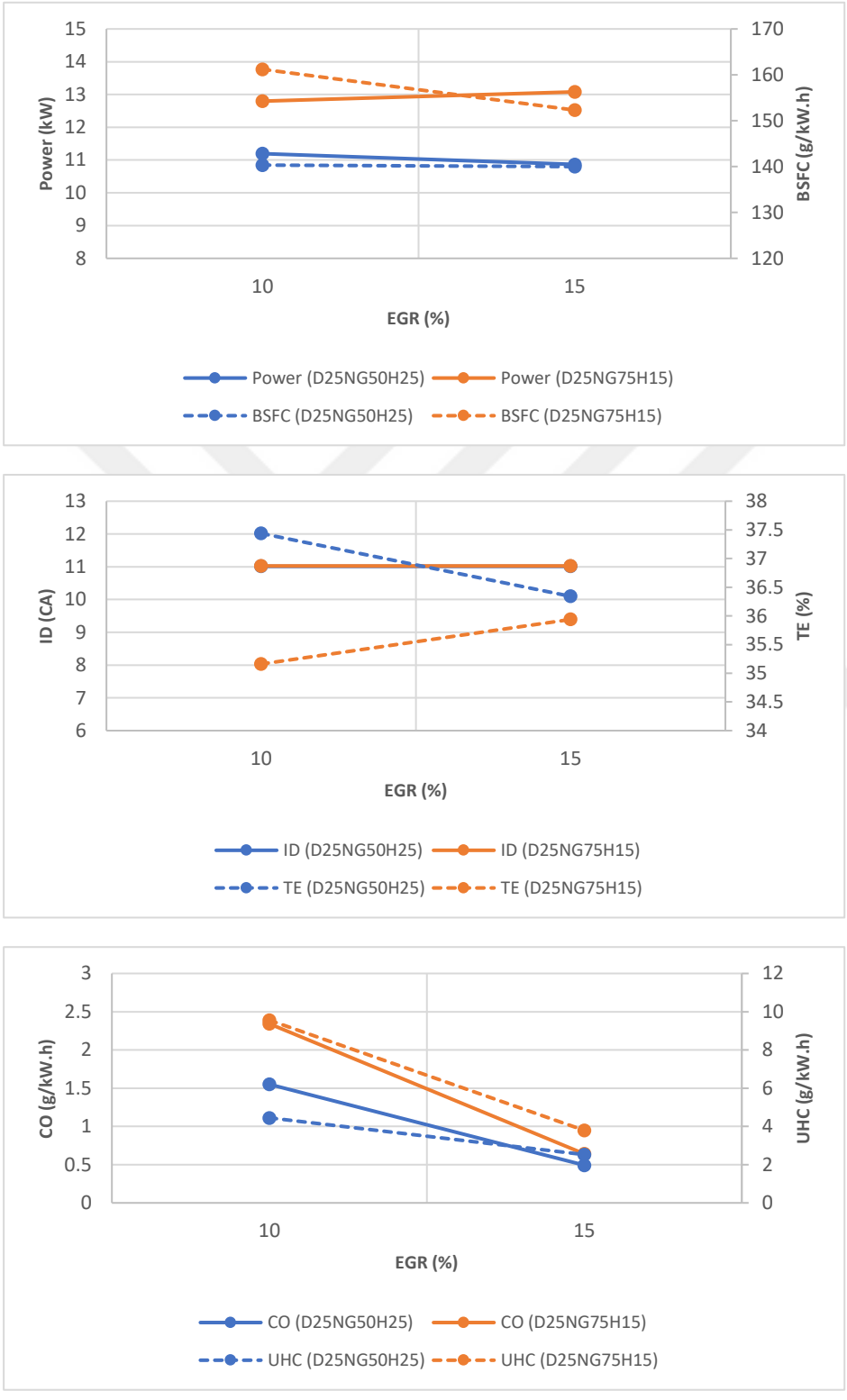

Figure 5.24 : Comparison of 10% and 15% EGR rates at 100°C EGR temperature with 20% PI regarding power, BSFC, ID, TE, CO, and UHC values.

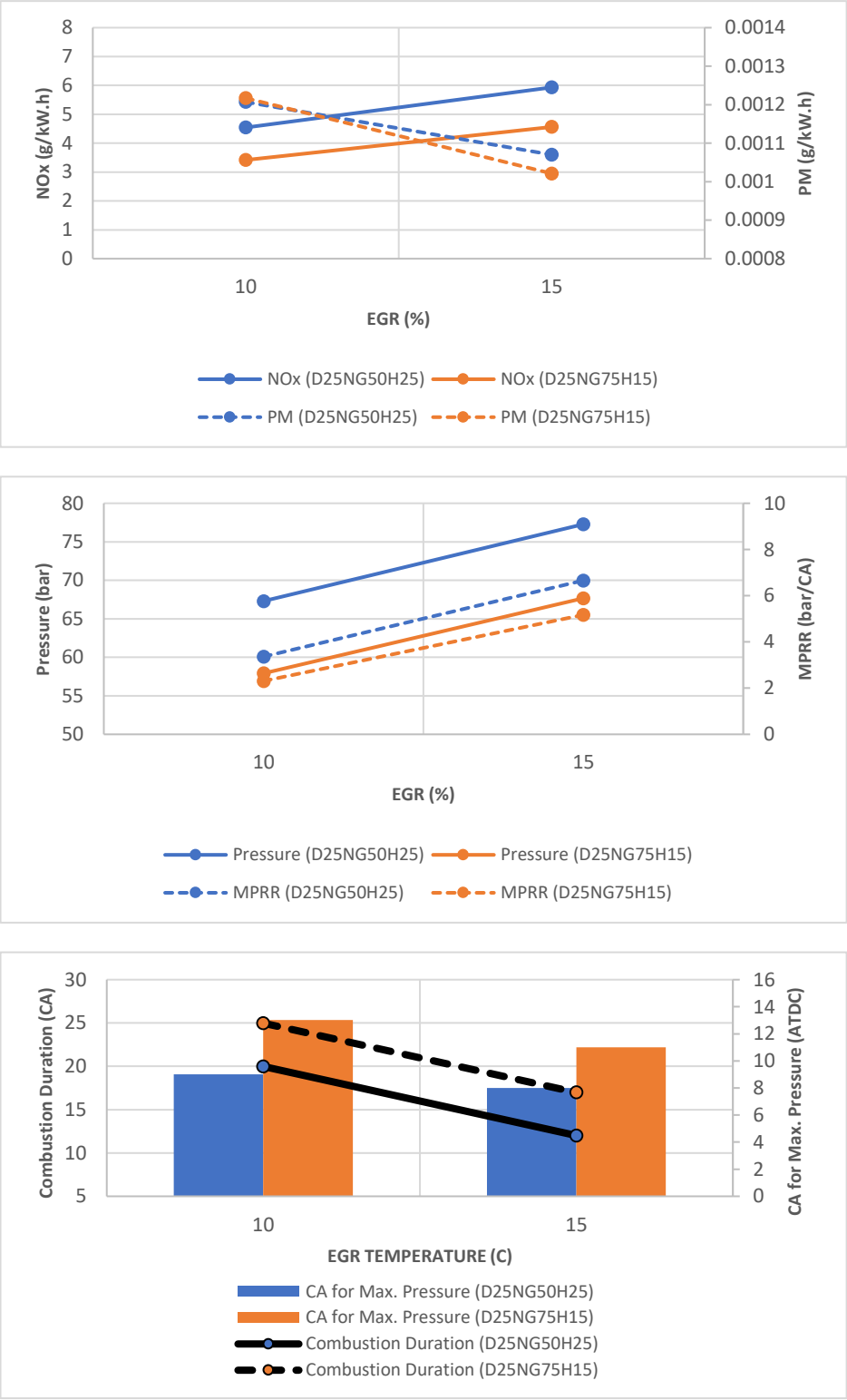

Figure 5.25 : Comparison of 10% and 15% EGR temperature with 20% PI in terms of NO_x, PM, Pressure, MPRR, CD and the position of Max. Press. Relative to TDC.

Ignition delay was unaffected by EGR, but combustion duration was influenced by EGR (Figure 5.20 and Figure 5.21). CO emissions decreased after 15% EGR and beyond. CO is an incomplete combustion product. The increase in combustion rate and

the decrease in combustion duration suggest that combustion efficiency increased, resulting in a decrease in incomplete combustion products (Figure 5.20). The effect of EGR on PM (SOOT) varied for Mode 1 and Mode 2 beyond 10% EGR. After 10% EGR, Mode 1 showed a slight decrease in PM, while Mode 2 exhibited a sharp increase (Figure 5.21). The main reason for this is the difference in hydrogen fractions between Mode 1 and Mode 2. Mode 1, with its higher hydrogen fraction, managed to reduce the proportion of unburned fuel oxidizing before combustion due to higher combustion temperatures. Hydrogen's combustion rate and capability led to a reduction in PM emissions. However, Mode 2, with relatively lower hydrogen fraction, resulted in lower combustion temperatures and, consequently, higher PM emissions (Figure 5.21).

When analyzing all the graphs based on EGR rates, it is evident that 10% and 15% EGR rates are suitable in terms of performance and emission values. However, the decision between 10% and 15% EGR should be based on the specific conditions of the pilot injection, which is the more accurate approach (Figure 5.21).

Table 5.14 : Comparison of numerical results for different PI values (0% and 20%) at 10% EGR rate and 100°C EGR temperature for Mode 1 (D25NG50H25).

	10% EGR 100°C – D25NG50H25		
	0%	20%	Variation
Power (kW)	11.14	11.20	+0.54%
Torque (N.m)	116.93	117.48	+0.47%
BSFC (g/kW.h)	140.98	140.33	-0.46%
Ignition Delay (CA)	11º	11º	-
Thermal Efficiency (%)	37.26	37.44	+0.18%
Combustion Duration (CA)	21º	20º	-1º
MPRR (bar/CA)	3.54	3.36	-0.18
Max. Press. (bar)	65.46	67.31	+1.85
CA for Max. Press. (ATDC)	8º CA	9º CA	+1º
Max. Mean Temp. (K)	1707	1738	+31
NO_x (g/kW.h)	5.76	4.54	-21.18%
SOOT (g/kW.h)	0.00031	0.00121	-
CO (g/kW.h)	2.6	1.55	-40.38%
HC (g/kW.h)	6.5	4.45	-31.54%

Changes in performance and emission values with respect to different EGR temperatures are shown in Figure 5.22 and Figure 5.23. The increase in EGR temperature has led to a decrease in power and an increase in BSFC values (Figure 5.22). The increase in EGR temperature allowed EGR gases to spread over a larger area inside the cylinder, positively contributing to mixture formation.

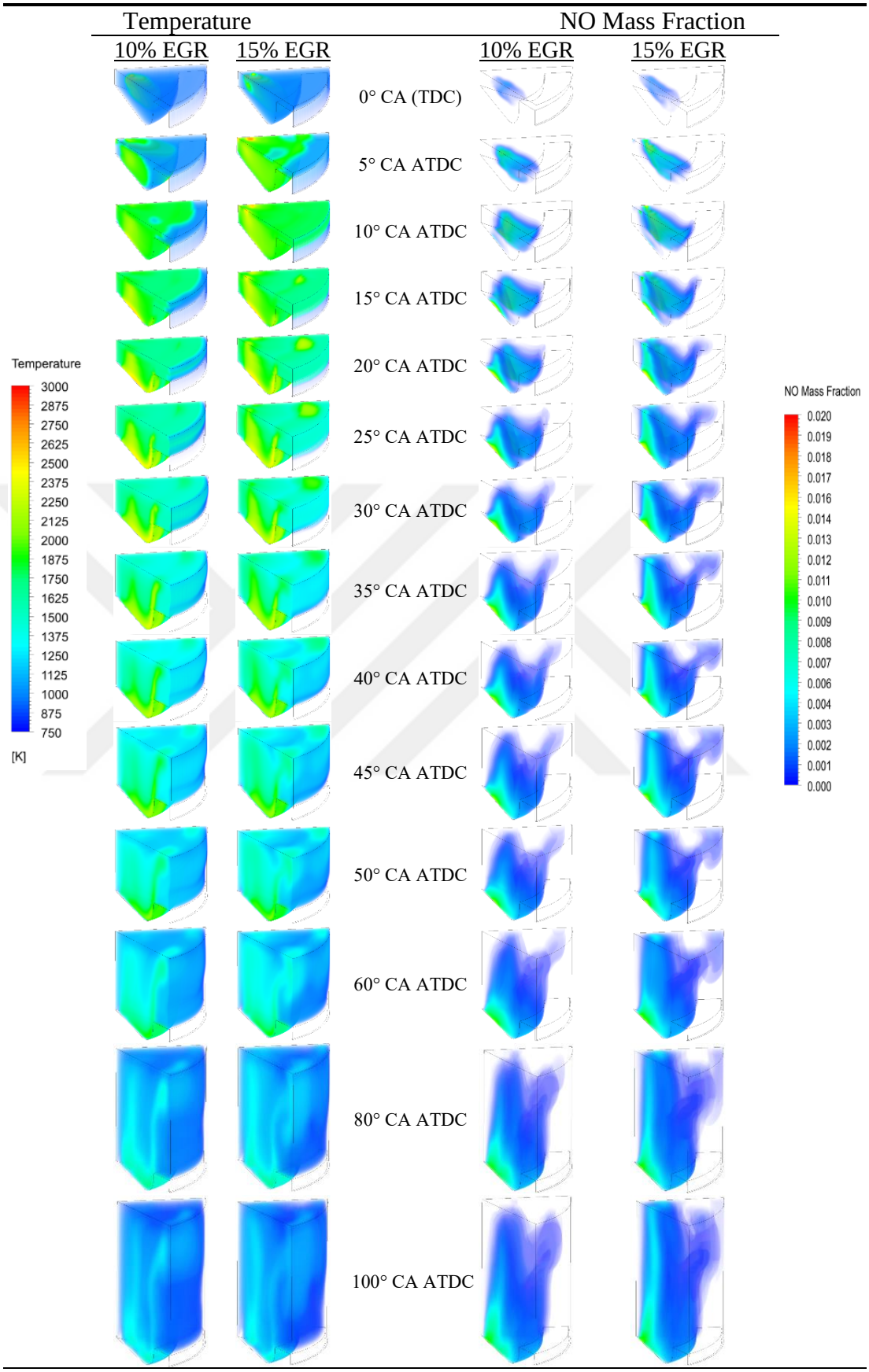

Figure 5.26 : Comparison of temperature and NO mass fraction contours at different piston positions for 10% and 15% EGR ratios for Mode 1 - D25NG50H25 (with 20% PI).

This resulted in increased combustion rates and combustion efficiency but also led to a more intense combustion process. This is clearly observed when examining the pressure and MPRR curves depending on EGR temperature (Figure 5.23). It can also refered to the combustion rate graph in relation to the combustion duration (Figure 5.23). The results in terms of power and BSFC are consistent with the outcomes observed when increasing the EGR ratio, and they are also valid when raising EGR temperatures. As a result, a decrease in CO and UHC emissions would be expected (Figure 5.22). Due to the rapid combustion resulting from this situation, the combustion duration was short, and the generated MPRR value increased. Sudden combustion events bring about high temperatures and NO_x emissions. The NO_x value tends to increase with rising EGR temperatures (Figure 5.23). High EGR temperatures allow fuels (Diesel, Natural Gas, and Hydrogen) to reach their ignition temperatures more quickly, reducing the ignition delay (Figure 5.22).

Thermal efficiency decreased due to the reduction in net work and the increase in heat generation (Figure 5.22). PM emissions were lower due to the increase in combustion efficiency (Figure 5.23). Especially when considering MPRR and NO_x values, it is seen that an EGR temperature of 100°C would be more reasonable.

Table 5.15 : Comparison of numerical results for different PI values (0% and 20%) at 10% EGR rate and 100°C EGR temperature for Mode 2 (D25NG75H15).

	10% EGR 100°C – D25NG75H15		
	0%	20%	Variation
Power (kW)	13.03	12.8	-1.77%
Torque (N.m)	136.73	134.29	-1.78%
BSFC (g/kW.h)	158.32	161.2	+1.82%
Ignition Delay (CA)	11º	11º	-
Thermal Efficiency (%)	35.8	35.16	-0.64%
Combustion Duration (CA)	24º	25º	-1º
MPRR (bar/CA)	2.92	2.31	-0.61
Max. Press. (bar)	58.48	57.92	-
CA for Max. Press. (ATDC)	12º CA	13º CA	+1º
Max. Mean Temp. (K)	1780	1779	-
NO_x (g/kW.h)	4.15	3.42	-17.59%
SOOT (g/kW.h)	0.00031	0.00122	-
CO (g/kW.h)	2.10	2.342	+11.52%
HC (g/kW.h)	9.73	9.557	-1.78%

As recommended earlier, a comparison should be made between the %10 and %15 EGR rates under the conditions where pilot injection is applied. Therefore, a

comparison of the performance and emission values of %10 and %15 EGR rates was made under the conditions of optimal pilot injection rate of %20 PI and optimal EGR temperature of 100 °C. Applying %10 EGR rate along with %20 PI had very positive results for MPRR and NO_x (Figure 5.25).

While similar results were obtained for power, BSFC, TE, and ID, significant differences were observed in terms of combustion and emission values (Figure 5.24 and Figure 5.25). When Table 5.12 for Mode 1 and Table 5.13 for Mode 2 are examined, it will be evident that the %10 EGR rate provides more favorable conditions compared to the %15 EGR rate.

Table 5.16 : Comparison of numerical results with test data (NG75H00*) for different gas fuel fractions (Mode 1) at 20% PI and %10 EGR - 100°C operating point.

	10% EGR 100°C – 20% PI					
	NG75H00*	NG75H00	NG65H10	NG50H25	NG25H50	NG00H75
Power (kW)	9.575	9.66	10.32	11.20	11.04	10.48
Torque (N.m)	100.477	101.34	108.26	117.48	115.88	109.97
BSFC (g/kW.h)	196	193.71	169.5	140.33	116.59	97.25
Ignition Delay (CA)	11º	11º	11º	11º	11º	12º
Thermal Efficiency (%)	32.02	32.30	34.50	37.44	36.93	35.05
Combustion Duration (CA)	27º	25º	22º	20º	11º	9º
MPRR (bar/CA)	2.66	2.42	2.66	3.36	6.11	9.19
Max. Press. (bar)	57.25	57.02	60.85	67.31	80.81	84.81
CA for Max. Press. (ATDC)	7º CA	9º CA	9º CA	9º CA	7º CA	4º CA
Max. Mean Temp. (K)	1504	1524	1620	1738	1954	1994
NO_x (g/kW.h)	6.66	3.80	4.09	4.54	6.87	8.70
SOOT (g/kW.h)	0.00077	0.0022	0.00154	0.00121	0.00082	0.00052
CO (g/kW.h)	9.94	8.68	5.06	1.55	0.23	0.0098
HC (g/kW.h)	35.21	31.91	18.59	4.45	1.03	0.012

Within the scope of the study, the engine operating points that encompass the optimal conditions of a %10 EGR rate, 100°C EGR temperature, and %20 PI have been identified. These operating points are coded as D25NG50H25-10EGR-100°C for Mode 1 and D25NG75H15-10EGR-100°C for Mode 2.

For Mode 1, Figure 5.26 shows the effects of %10 and %15 EGR rates on temperature and NO mass fraction as a function of crank angle, using piston position as the reference. It can be observed that %15 EGR results in higher temperatures and NO mass fractions for Mode 1 (Figure 5.26). A similar situation can be observed for Mode 2 as well (Figure 5.27).

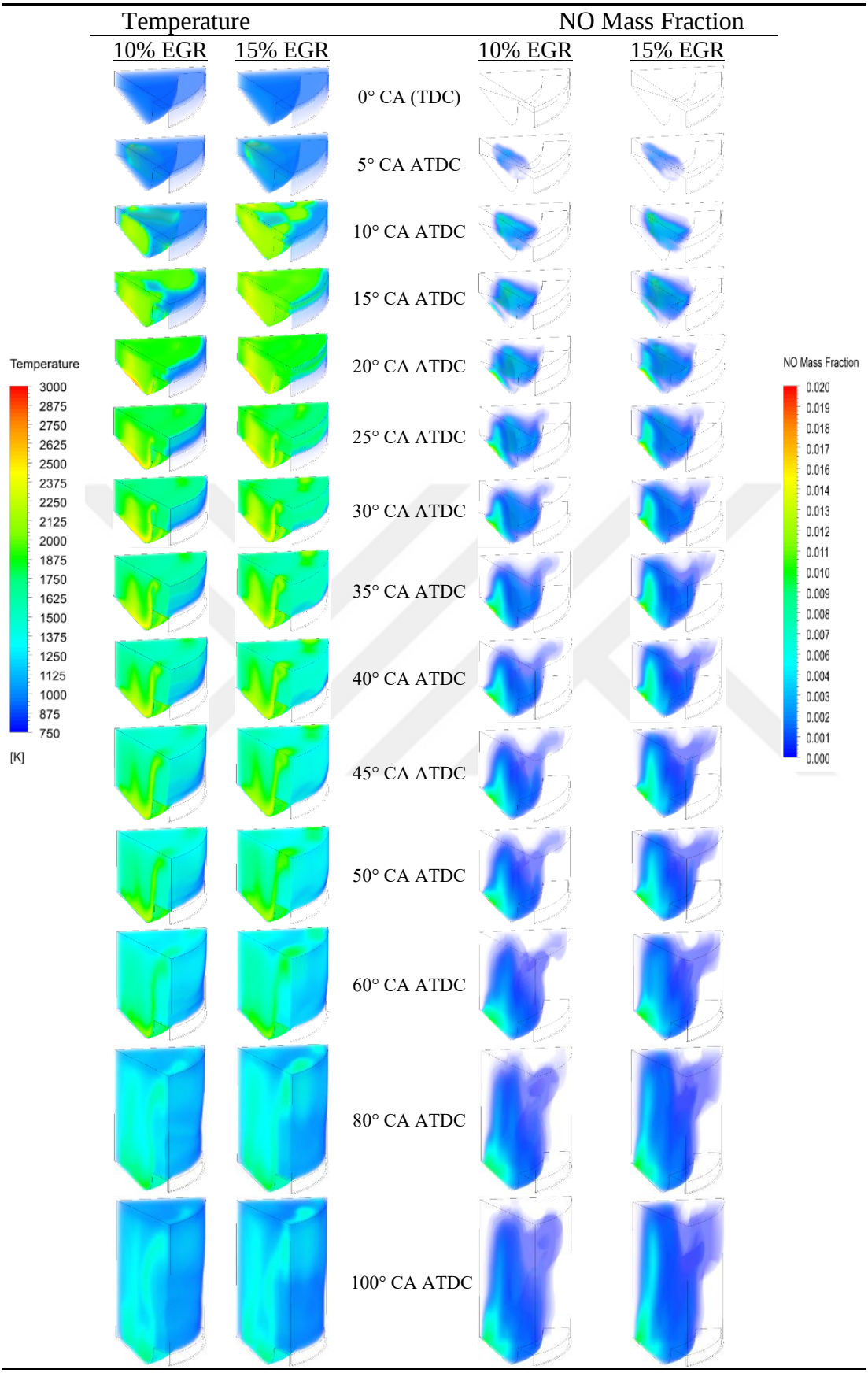

Figure 5.27 : Comparison of temperature and NO mass fraction contours at different piston positions for 10% and 15% EGR ratios for Mode 2 - D25NG75H15 (with 20% PI).

Table 5.14 and Table 5.15, respectively, compare the conditions of %10 EGR and 100°C EGR temperature with and without the application of PI for Mode 1 and Mode 2. The application of PI has improved all parameters for Mode 1 (Table 5.14), including power, torque, BSFC, TE, MPRR, NO_x, CO, and HC. For Mode 2, improvements were observed for NO_x, MPRR, and HC (Table 5.15).

Table 5.17 : Comparison of numerical results with test data for different hydrogen enriching fractions (Mode 2) at 20% PI and %10 EGR - 100°C operating point.

	10% EGR 100°C – 20% PI						
	NG75H00*	NG75H00	NG75H05	NG75H10	NG75H15	NG75H20	NG75H25
Power (kW)	9.76	9.31	10.58	11.78	12.8	13.77	14.53
Torque (N.m)	102.42	97.72	111.02	123.59	134.29	144.49	152.51
BSFC (g/kW.h)	203.85	212.93	189.97	172.92	161.2	151.70	145.48
Ignition Delay (CA)	11º	11º	11º	11º	11º	11º	11º
Thermal Efficiency (%)	30.84	29.42	31.84	33.83	35.16	36.26	36.74
Combustion Duration (CA)	31º	32º	30º	27º	25º	21º	19º
MPRR (bar/CA)	1.85	1.43	1.70	1.90	2.31	2.91	4
Max. Press. (bar)	50.55	48.55	50.55	53.69	57.92	63.58	69.52
CA for Max. Press. (ATDC)	9º CA	10º CA	11º CA	12º CA	13º CA	13º CA	13º CA
Max. Mean Temp. (K)	1477	1429	1542	1668	1779	1885	1993
NO_x (g/kW.h)	4.9	2.77	2.75	3.01	3.42	4.22	5.41
SOOT (g/kW.h)	0.0012	0.0035	0.0027	0.0016	0.00122	0.00108	0.001
CO (g/kW.h)	10.25	12.68	6.73	3.50	2.342	1.58	0.87
HC (g/kW.h)	36.73	40.82	25.86	15.88	9.557	5.11	2.52

Figure 5.28 and Figure 5.29 show the performance and emission effects of different gas fuel fractions with and without EGR-PI strategies for Mode 1. Particularly, improvements in MPRR and NO_x were observed for hydrogen fractions up to 50% and below. However, at high hydrogen fractions (above 50%), the MPRR value remained at critical levels. While the EGR-PI application had little effect on power, BSFC, ID, UHC, and CD (Combustion Duration), it was found to be effective for NO_x, PM, MPRR, and TE. The comparison of results obtained from different gas fuel fraction working points with EGR-PI applied with experimental results for Mode 1 is shown in Table 5.16. The results indicate that the values obtained for the D25NG50H25 working point are preferable compared to the experimental results. For Mode 1, the results show that the working point with 25% hydrogen and 50% natural gas fraction, with 20% PI and 10% EGR under 100°C EGR temperature conditions (D25NG50H25-10EGR-100°C), achieved lower NO_x emissions compared to the experimental results (D25NG75H00) (Table 5.16).

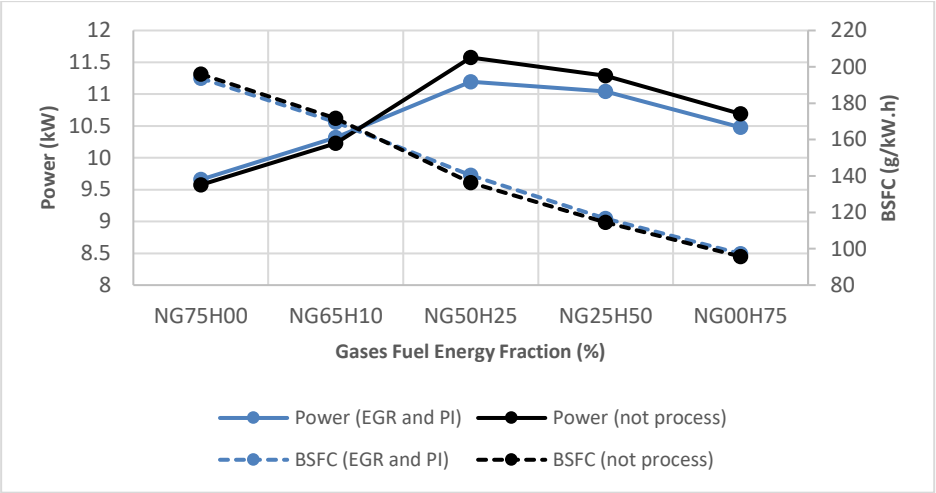

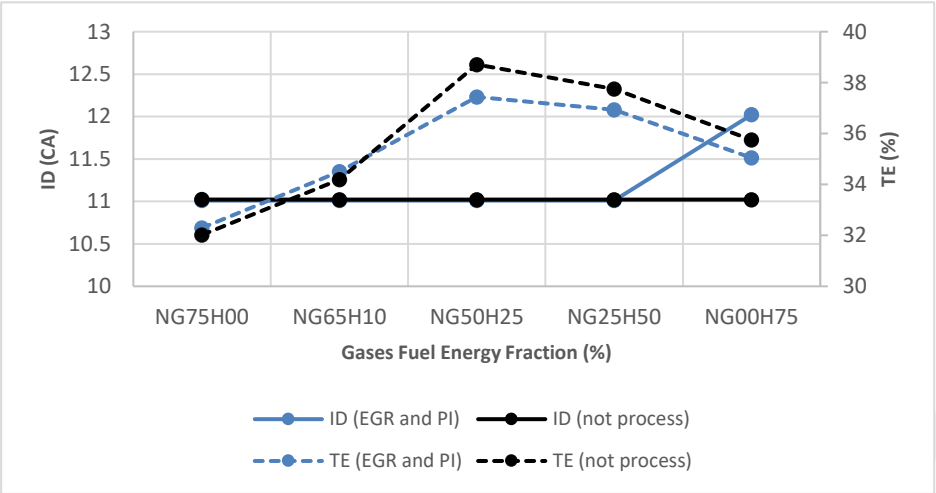

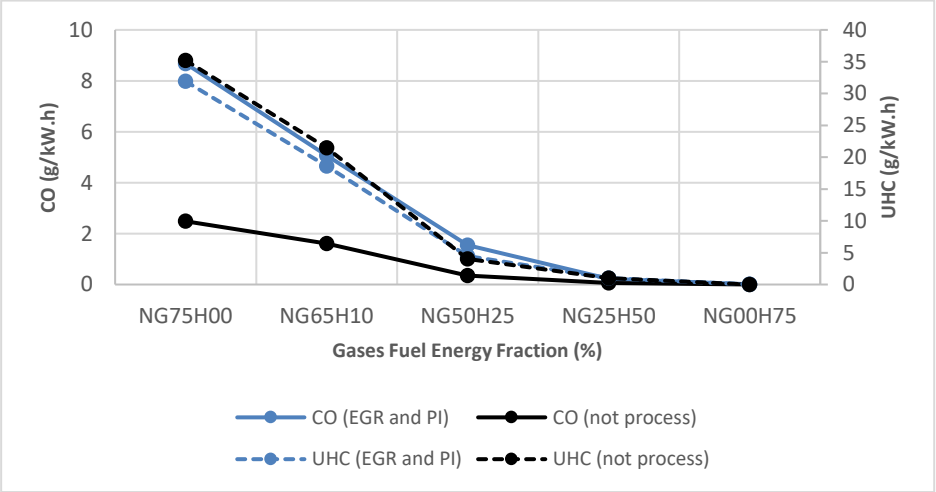

Figure 5.28 : The effect of different fuel composition fractions on power, BSFC, ID, TE, CO, and UHC values for cases with process (20% PI, 10% EGR-100°C) and without process.

The numerical results without the strategy (D25NG50H25) had higher NO_x and MPRR values. However, by applying the EGR-PI collaboration, these were reduced to reasonable levels.

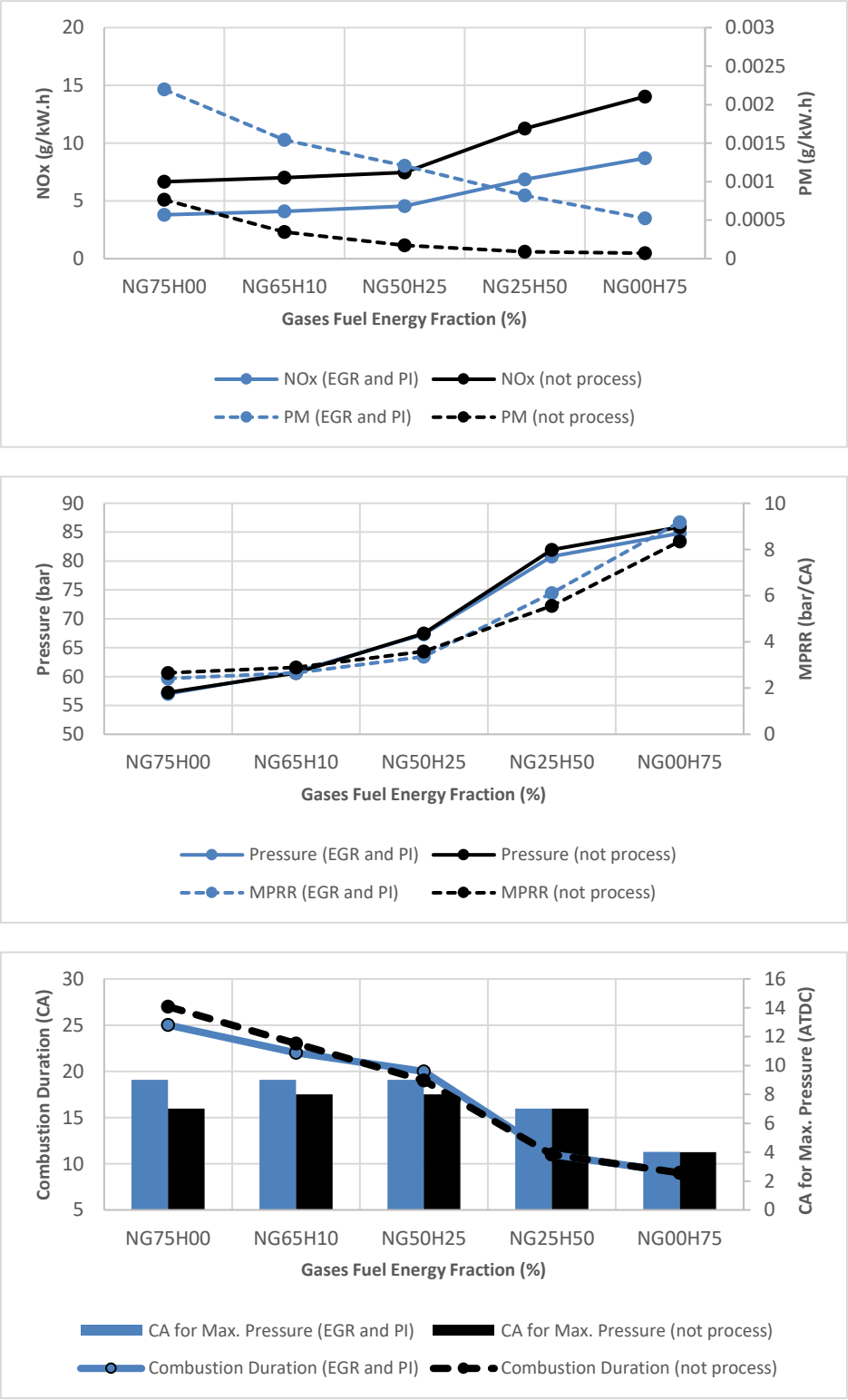

Figure 5.29 : The effect of different fuel composition fractions on NO_x, PM, Pressure, MPRR, CD, and the position of Max. Press. Relative to TDC for cases with process (20% PI, 10% EGR-100°C) and without process.

Figure 5.30 and Figure 5.31 show the performance and emission effects of different hydrogen gas enrichment fractions with and without EGR-PI strategies for Mode 2.

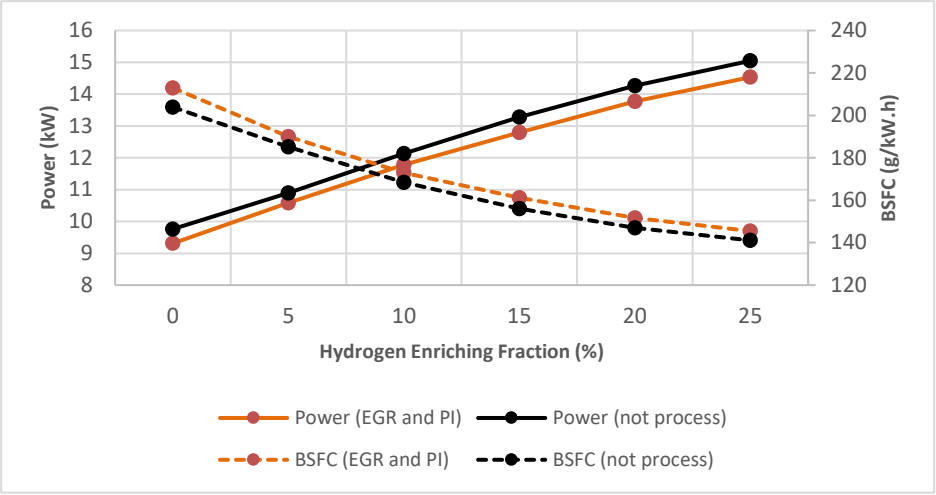

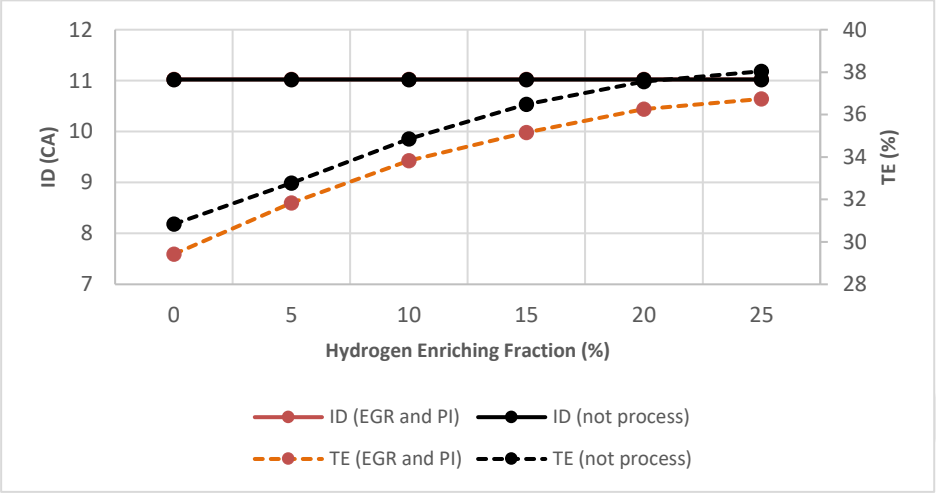

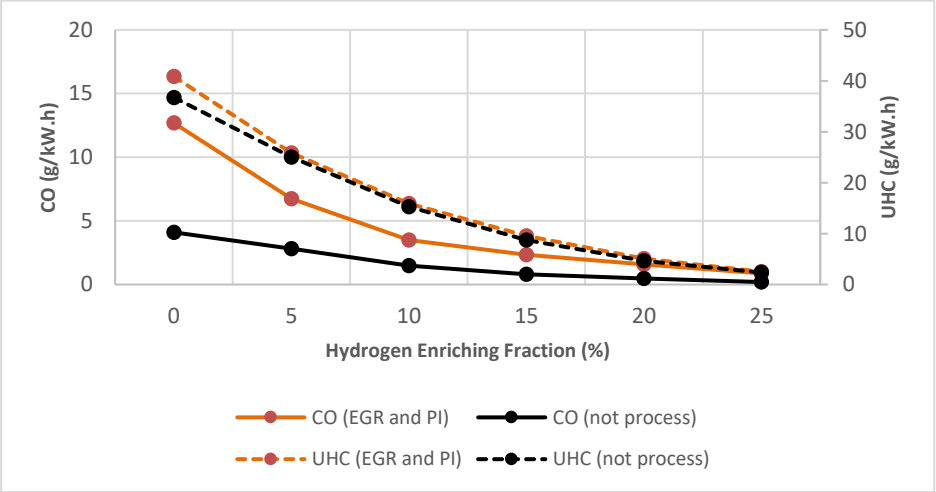

Figure 5.30 : The effect of different hydrogen fuel enrichment fractions on power, BSFC, ID, TE, CO, and UHC values for cases with process (20% PI, 10% EGR-100°C) and without process.

In all hydrogen enrichment fractions, significant improvements, especially in MPRR and NO_x, were observed, and these were within reasonable levels.

Similar to Mode 1, for Mode 2, it was found that the EGR-PI application had a substantial effect on NO_x, PM, MPRR, and TE, while it had little effect on power, BSFC, ID, UHC, and CD.

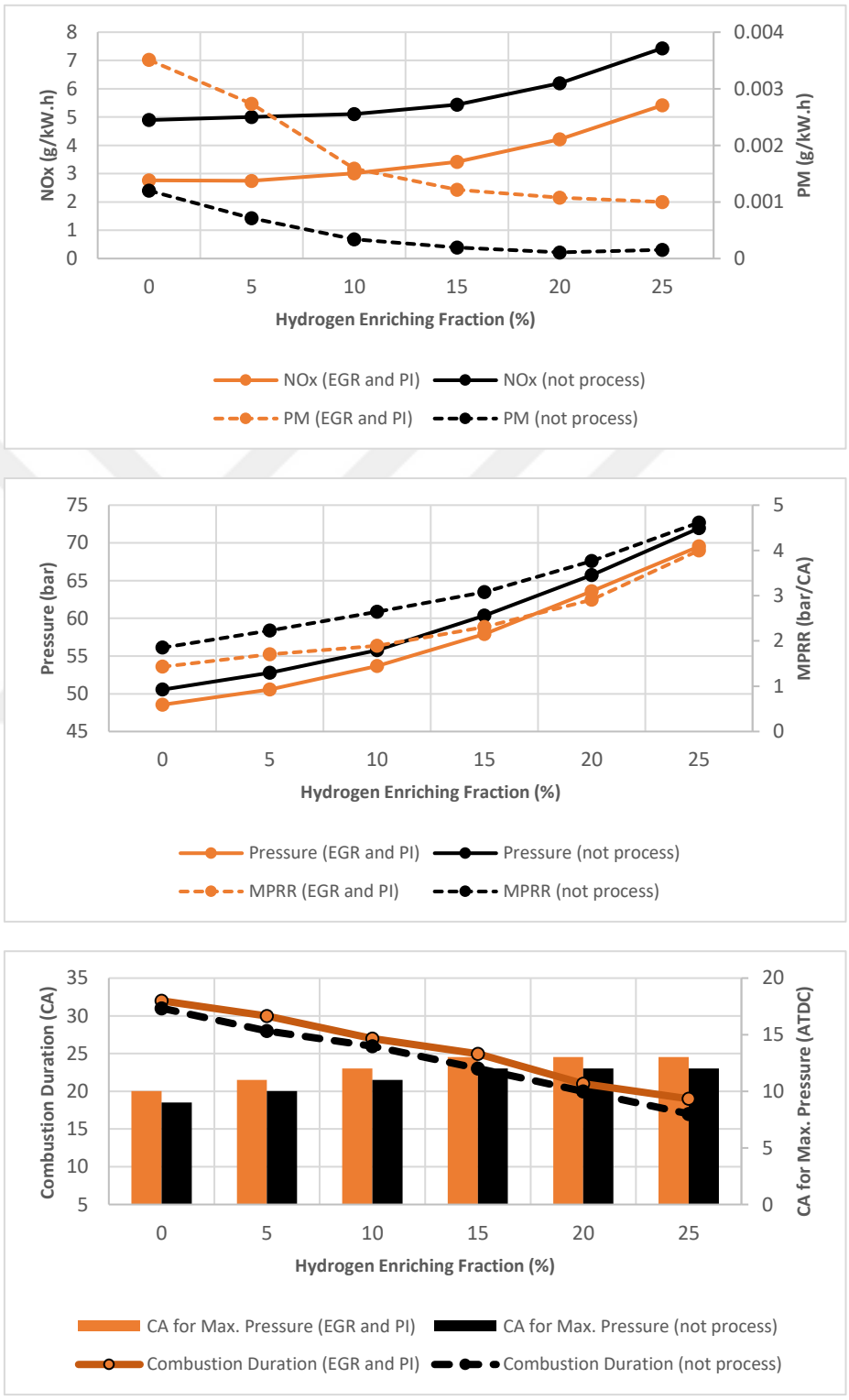

Figure 5.31 : The effect of different hydrogen fuel enrichment fractions on NO_x, PM, Pressure, MPRR, CD, and the position of Max. Press. Relative to TDC for cases with process (20% PI, 10% EGR-100°C) and without process.

The comparison of results obtained from different hydrogen gas enrichment fraction working points with EGR-PI applied with experimental results for Mode 2 is shown in Table 5.17. The results indicate that thanks to the EGR-PI application, high hydrogen enrichment fractions could be achieved. In the subsequent sections, a comparison between the strategies and non-strategies will be presented. This will provide a better understanding of the importance of the EGR-PI combination through those graphics. At this stage, it is evident that the application of EGR-PI for Mode 2 results in highly effective outcomes. The use of hydrogen-enriched natural gas in dual-fuel mode with diesel fuel, in combination with EGR and appropriate PI, leads to preferable results in terms of both emissions and performance (Table 5.17).

The next section aims to demonstrate that with the obtained optimal EGR rate (10%), EGR temperature (100°C), and PI rate (20%), the NO_x and MPRR issues at the working points obtained without the process have been overcome, and higher hydrogen fractions can be achieved.

5.2.2 Comparison of EGR – PI strategy and non – strategy conditions

In the previous section, the results of the EGR-PI application led to the determination of the optimal EGR rate, EGR temperature, and PI rate values. Now, let's compare the performance and emission values of the working points where these values are applied and not applied to see the improvements achieved.

The comparison between the D25NG75H00 gas fuel fraction and the condition with a 14° CA BTDC injection advance (Test Case) and D25NG75H00-10EGR-100°C (14° CA BTDC value of SOI) condition is shown in Figure 5.32 and Table 5.18. While power and BSFC have similar values, CO and UHC emissions are lower in the EGR-PI conditions compared to the test conditions (Figure 5.32). Although there is no significant difference in cylinder pressure, ID, TE, and CD values, differences are observed in terms of MPRR, NO_x, and PM emissions (Figure 5.32).

If 10% EGR and 20% PI are applied at 100°C EGR temperature under test conditions, it results in a 0.89% increase in power, a 0.28% increase in thermal efficiency, a 43% reduction in NO_x emissions, and 13% and 9.37% reductions in CO and UHC emissions, respectively (Table 5.18). MPRR is reduced by 0.24 bar. The comparison between the D25NG50H25 gas fraction working point with EGR-PI strategy and without it and the experimental conditions is provided in Figure 5.33 and Figure 5.34.

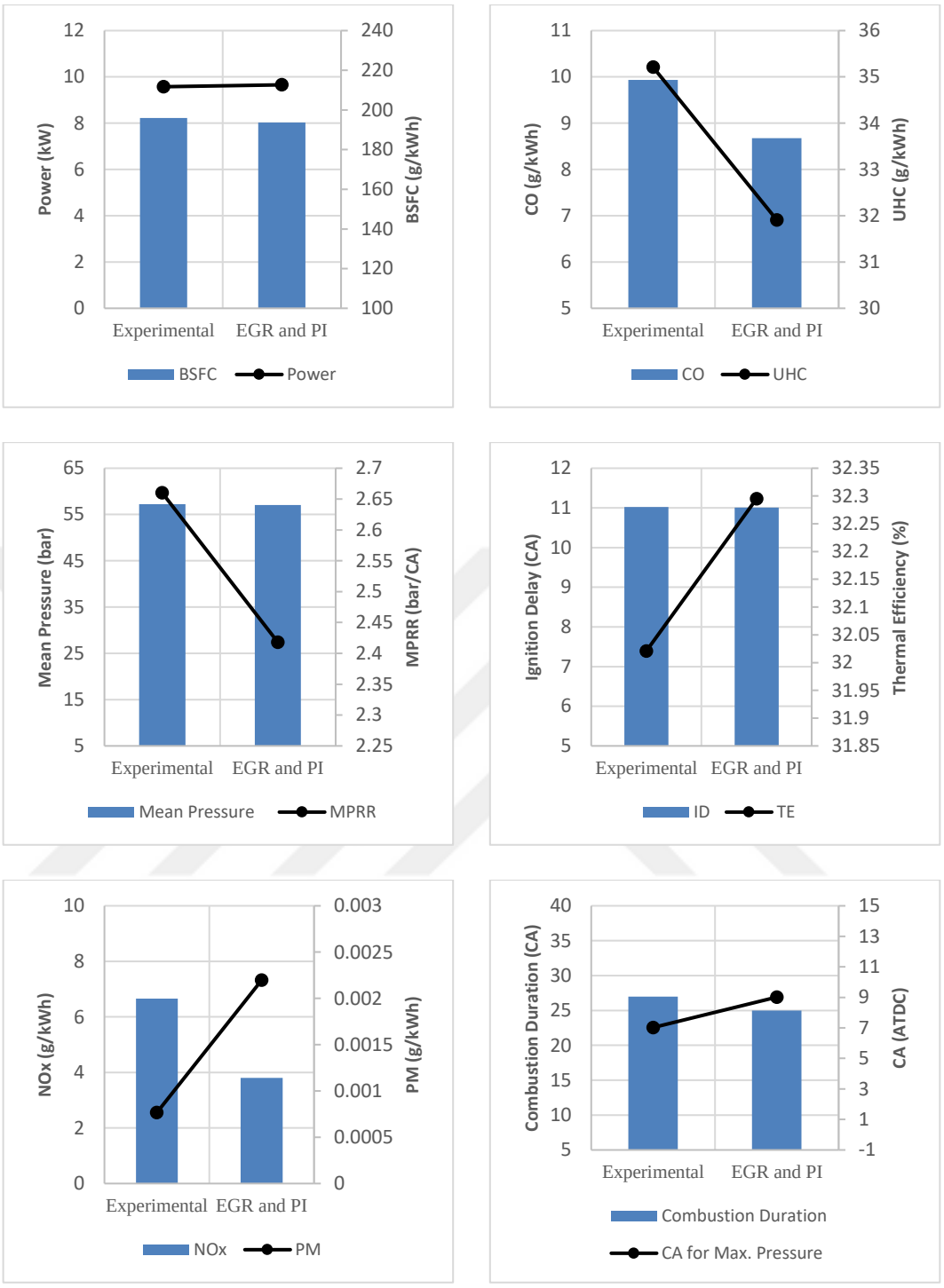

Figure 5.32 : Comparison of power, BSFC, ID, TE, CO, UHC, NO_x, PM, Pressure, MPRR, CD, and the position of Max. Press. Relative to TDC for the case of D25NG75H00 (14° CA BTDC SOI) with process (20% PI, 10% EGR-100°C) and test condition.

According to the experiment, the values of power, BSFC, CO, UHC, and TE in process and processless conditions are at more reasonable levels. Pressure, MPRR, and NO_x did not yield preferable results for the processless (D25NG50H25) working point, as hydrogen presence did not have a significant impact.

Table 5.18 : Comparison of test and processed results for the operating point of D25NG75H00 (14° CA BTDC SOI).

	D25NG75H00	D25NG75H00-20PI-10EGR100°C	Variation
Power (kW)	9.575	9.66	+0.89%
Torque (N.m)	100.477	101.34	+0.86%
BSFC (g/kW.h)	196	193.71	-1.17%
Ignition Delay (CA)	11º	11º	-
Thermal Efficiency (%)	32.02	32.3	+0.28%
Combustion Duration (CA)	27º	25º	-2º
MPRR (bar/CA)	2.66	2.42	-0.24
Max. Press. (bar)	57.25	57	-
CA for Max. Press. (ATDC)	7º CA	9º CA	-
Max. Mean Temp. (K)	1504	1524	+20
NO_x (g/kW.h)	6.66	3.8	-43%
SOOT (g/kW.h)	0.00077	0.0022	-
CO (g/kW.h)	9.94	8.68	~ -13%
HC (g/kW.h)	35.21	31.91	-9.37%

Table 5.19 : Comparison of the optimal result obtained by applying the process for Mode 1 with the test data.

	D25NG75H00	D25NG50H25-20PI-10EGR100°C	Variation
Power (kW)	9.575	11.20	~ +17%
Torque (N.m)	100.477	117.48	~ +17%
BSFC (g/kW.h)	196	140.33	-28.4%
Ignition Delay (CA)	11º	11º	-
Thermal Efficiency (%)	32.02	37.44	+5.42%
Combustion Duration (CA)	27º	20º	-7º
MPRR (bar/CA)	2.66	3.36	+0.7
Max. Press. (bar)	57.25	67.31	~ +10
CA for Max. Press. (ATDC)	7º CA	9º CA	-
Max. Mean Temp. (K)	1504	1738	+234
NO_x (g/kW.h)	6.66	4.54	-32%
SOOT (g/kW.h)	0.00077	0.00121	-
CO (g/kW.h)	9.94	1.55	-84.4%
HC (g/kW.h)	35.21	4.45	-87.4%

The applied processes (10% EGR and 20% PI) have improved the results to even more preferable levels compared to the experimental conditions.

When the experimental conditions (D25NG75H00) are compared to the process condition (D25NG50H25-10EGR-100°C), there is a 17% increase in power, a 28.4% reduction in BSFC, a 5.42% increase in thermal efficiency, a 32% reduction in NO_x emissions, and 84.4% and 87.4% reductions in CO and UHC emissions, respectively (Table 5.19).

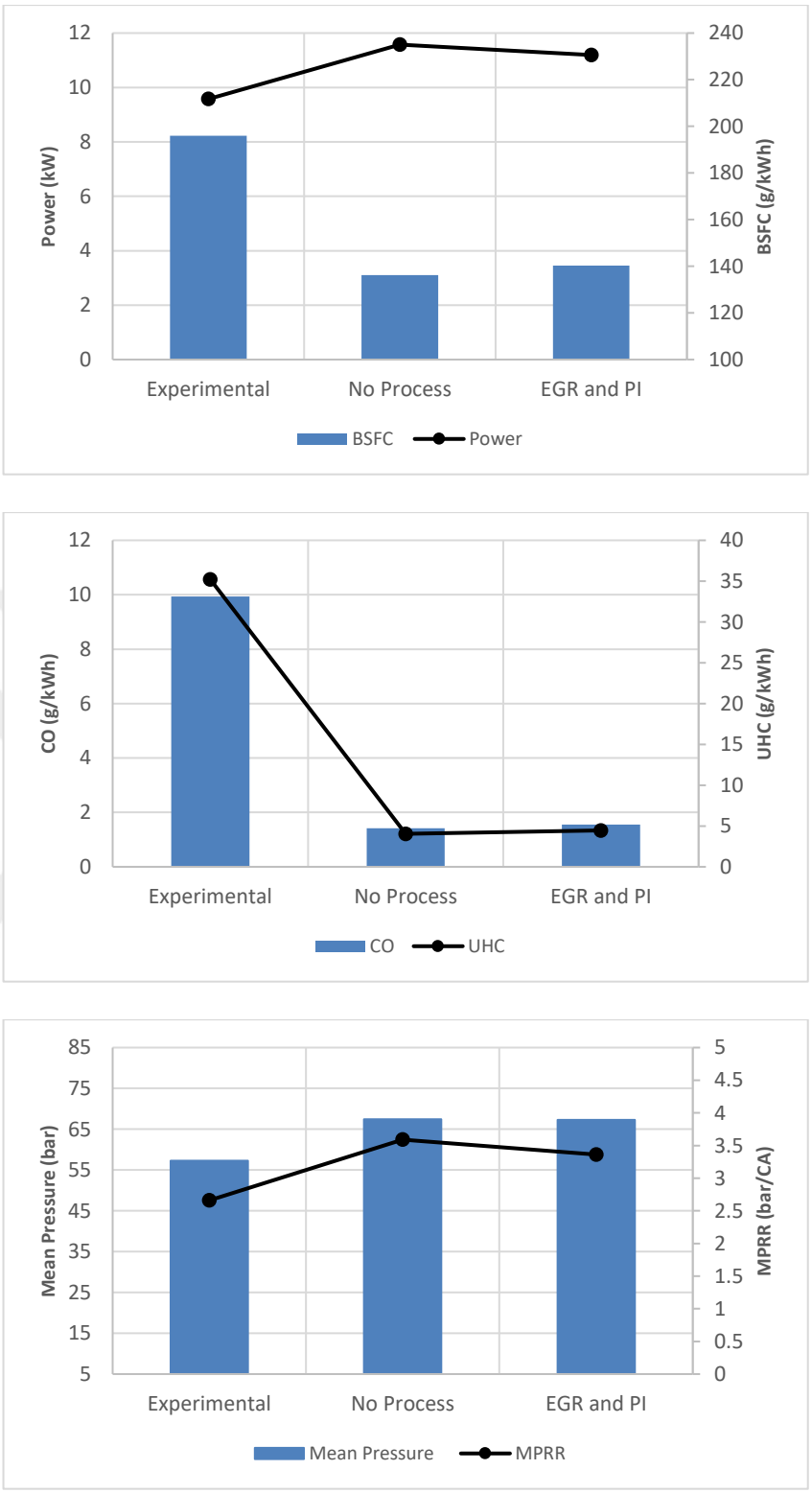

Figure 5.33 : Comparison of power, BSFC, CO, UHC, Pressure, and MPRR between test result and the case of D25NG50H25 with process (20% PI, 10% EGR-100°C) and without process.

When the process condition (D25NG50H25-10EGR-100°C) is compared to the processless condition (D25NG50H25), there is a 3.28% loss in power, but there is a 39% reduction in NO_x emissions and a 0.24 bar improvement in MPRR (Table 5.20).

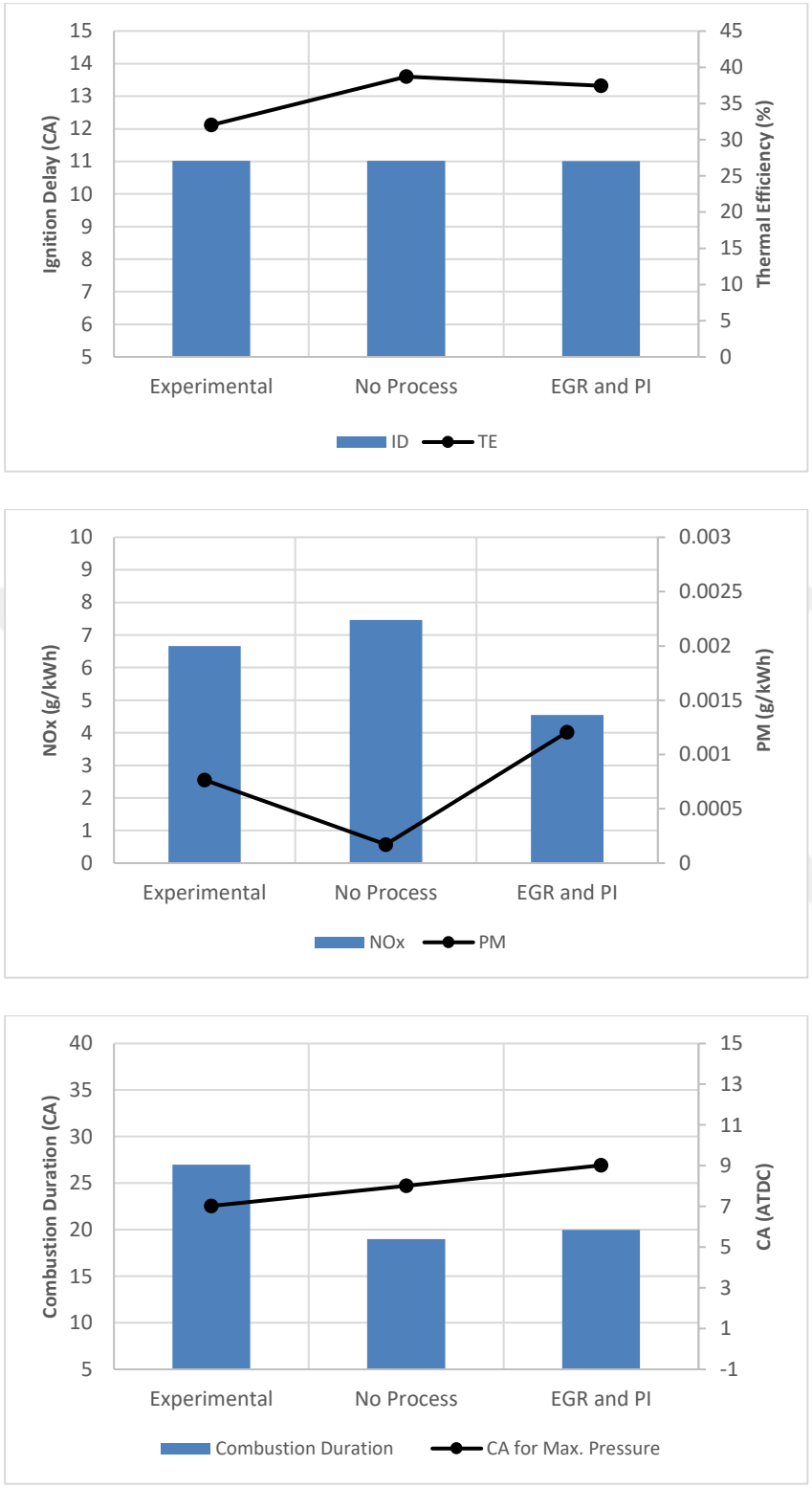

Figure 5.34 : Comparison of ID, TE, NO_x, PM, CD, and the position of Max. Press. Relative to TDC between test result and the case of D25NG50H25 with process (20% PI, 10% EGR-100°C) and without process.

The comparison of the experimental result with the performance and emission values of the process and processless conditions of D25NG00H75, which contains the highest hydrogen fraction for Mode 1, is shown in Figure 5.35 and Figure 5.36. Table 5.21

also displays the numerical results for the process and processless conditions of D25NG00H75.

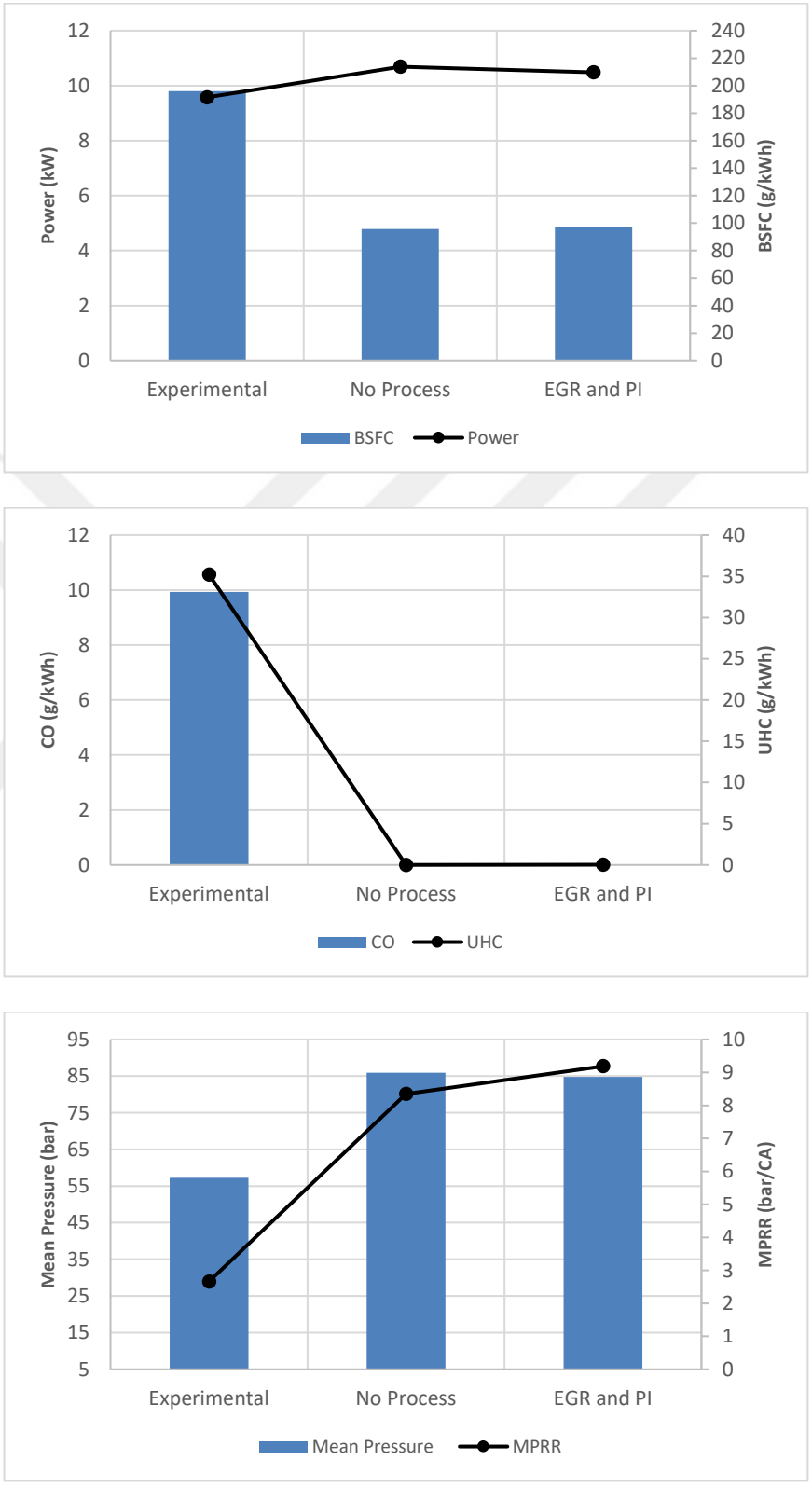

Figure 5.35 : Comparison of power, BSFC, CO, UHC, Pressure, and MPRR between test result and the case of D25NG00H75 with process (20% PI, 10% EGR-100°C) and without process.

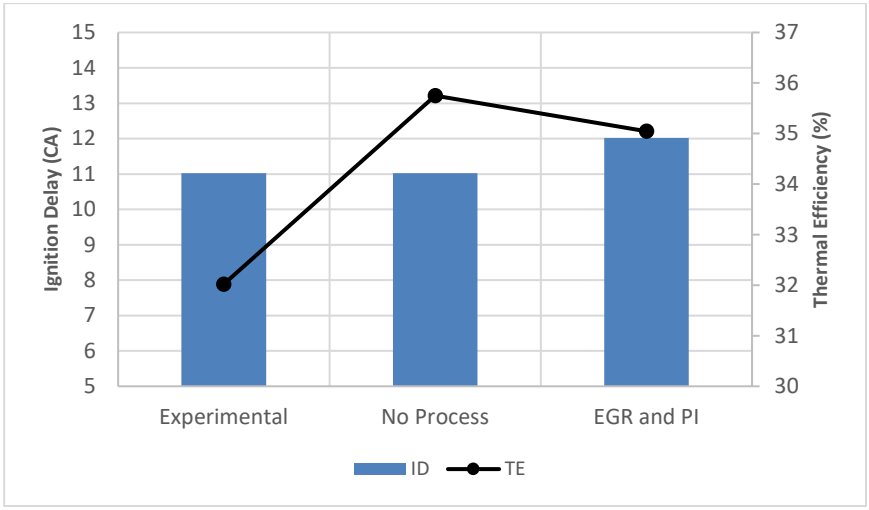

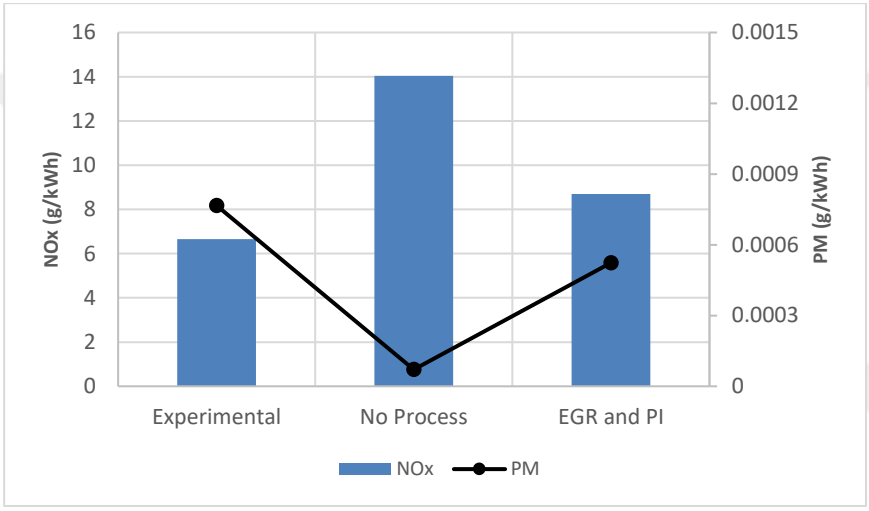

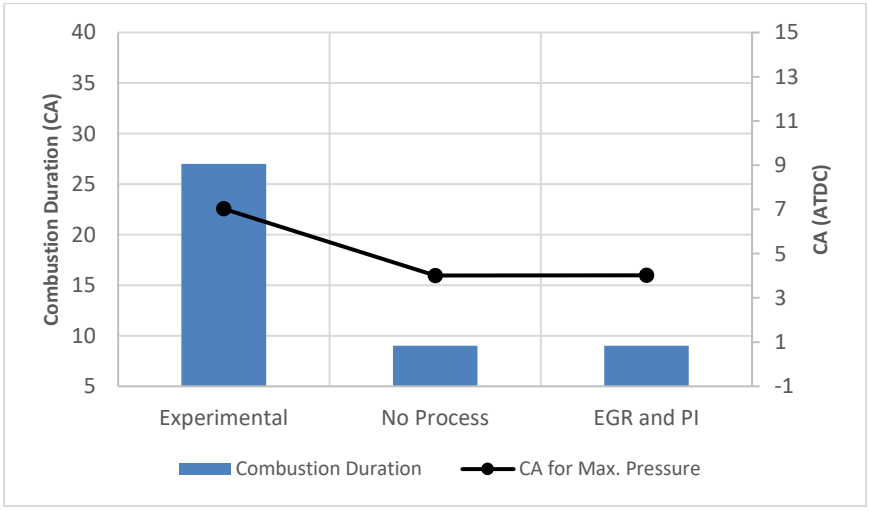

Figure 5.36 : Comparison of ID, TE, NO_x, PM, CD, and the position of Max. Press. Relative to TDC between tets result and the case of D25NG00H75 with process (20% PI, 10% EGR-100°C) and without process.

When the process is applied, a 38% improvement in NO_x emissions is achieved, and the MPRR value is 0.84 bar higher in the process condition.

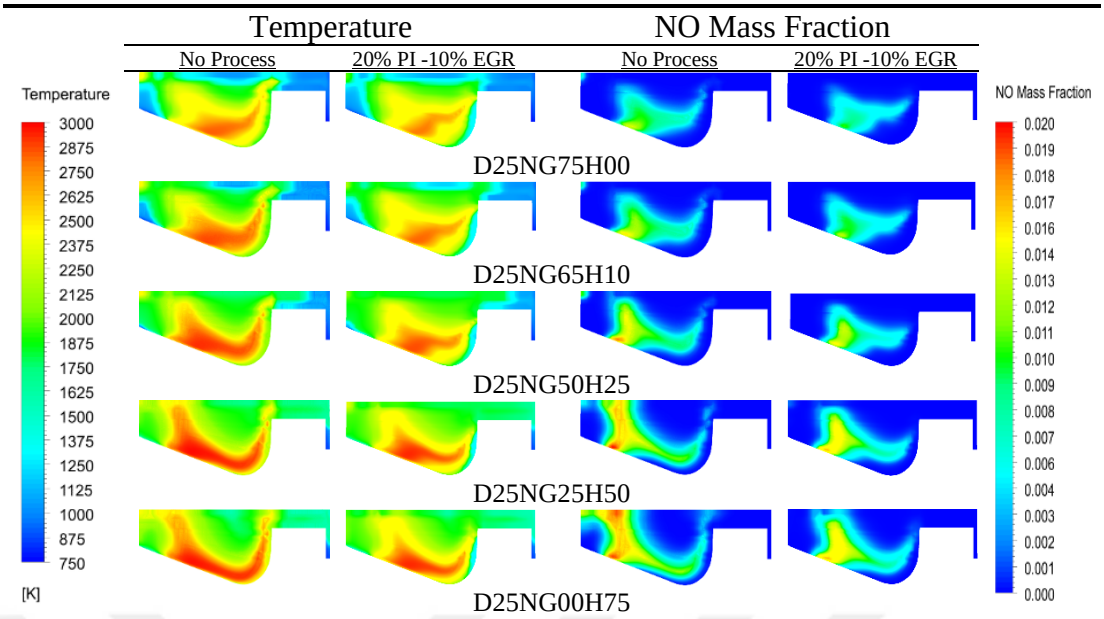

Figure 5.37 : Comparison of temperature and NO mass fraction contours at a piston position of 10° CA ATDC for operating points with applied (20% PI & 10% EGR) and not applied process with different gas fuel fractions for Mode 1.

The reason for this is that the PI application at high hydrogen fractions increases cylinder pressure and temperatures.

Table 5.20 : Comparison of cases with and without process for Mode 1.

	D25NG50H25	D25NG50H25-20PI-10EGR100°C	Variation
Power (kW)	11.58	11.20	-3.28%
Torque (N.m)	121.47	117.48	-3.28%
BSFC (g/kW.h)	136.27	140.33	~ +3%
Ignition Delay (CA)	11º	11º	-
Thermal Efficiency (%)	38.71	37.44	-1.27%
Combustion Duration (CA)	19º	20º	+1º
MPRR (bar/CA)	3.6	3.36	-0.24
Max. Press. (bar)	67.45	67.31	-
CA for Max. Press. (ATDC)	8º CA	9º CA	-
Max. Mean Temp. (K)	1779	1738	-41
NO_x (g/kW.h)	7.46	4.54	-39%
SOOT (g/kW.h)	0.000172	0.00121	-
CO (g/kW.h)	1.42	1.55	+9%
HC (g/kW.h)	4.04	4.45	+10%

The thermodynamic properties of hydrogen (fast combustion and high lower heating value) come into play by promoting the combustion of the premixed diesel fuel sent in advance with pilot injection, increasing the pressure-temperature gradient. Figure 5.37 shows the temperature and NO mass fraction contours for different gas fuel (Natural

Gas - Hydrogen) fractions in Mode 1 under process and processless conditions with the piston positioned at 10° CA ATDC. When examining the figure, it can be observed that in all gas fractions, the temperature and NO mass fraction distributions are darker in the processless condition.

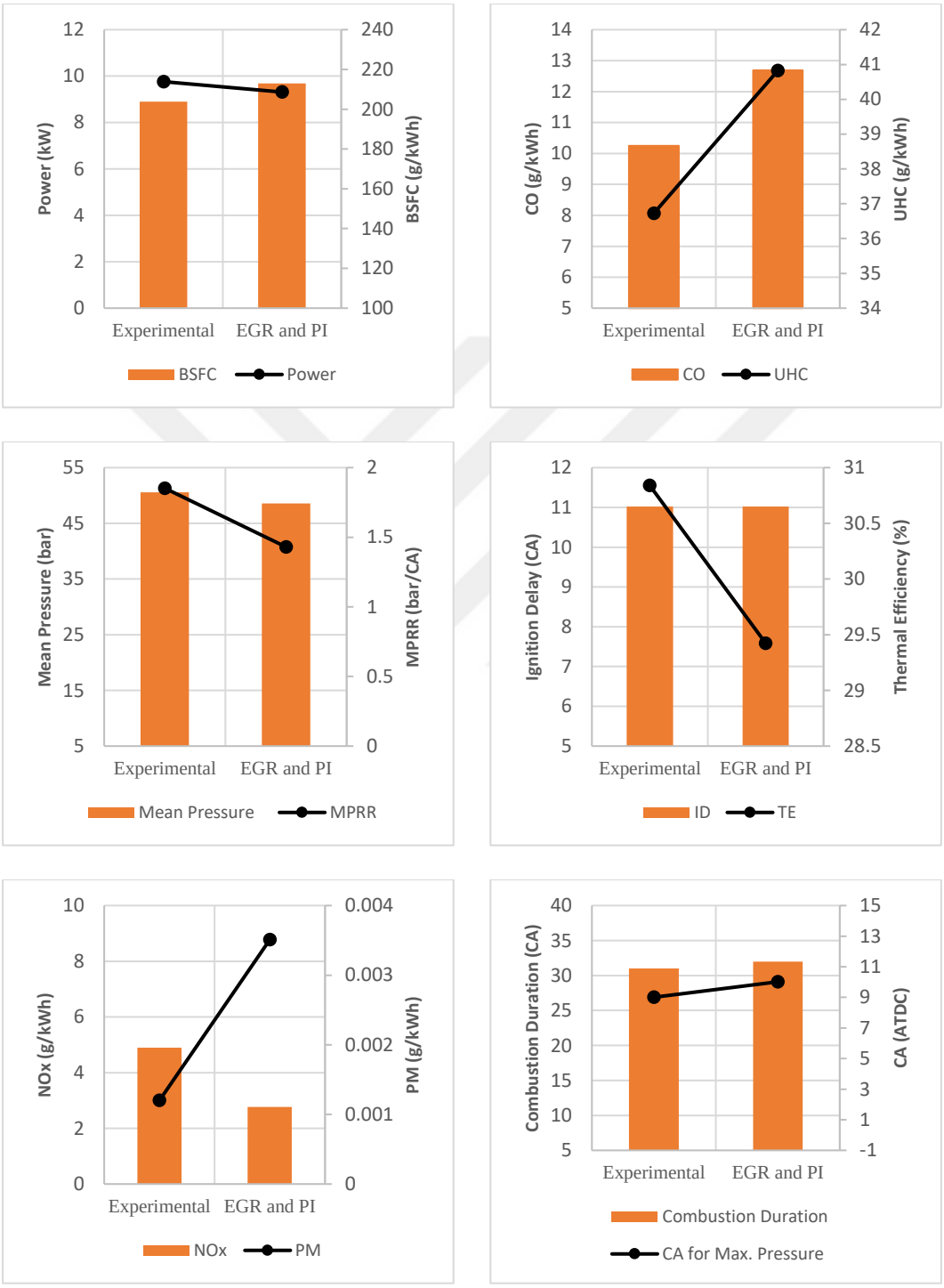

Figure 5.38 : Comparison of power, BSFC, ID, TE, CO, UHC, NO_x, PM, Pressure, MPRR, CD, and the position of Max. Press. Relative to TDC between the case of D25NG75H00 (10° CA BTDC SOI) with process (20% PI, 10% EGR-100°C) and test condition.

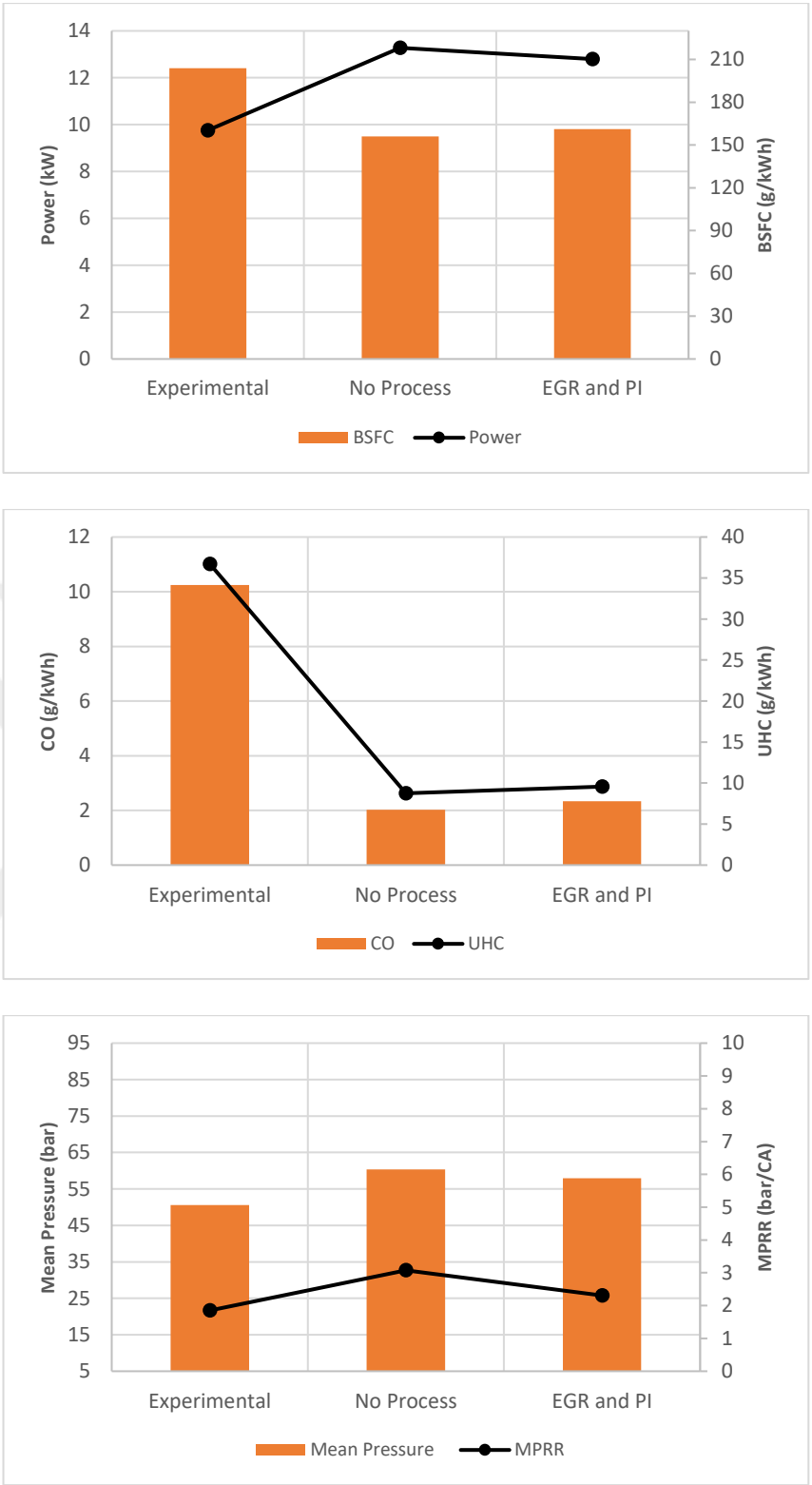

Figure 5.39 : Comparison of power, BSFC, CO, UHC, Pressure, and MPRR between test result and the case of D25NG75H15 with process (20% PI, 10% EGR-100°C) and without process.

D25NG75H00 gas fuel fraction case with a 10° CA BTDC injection advance (Test Case) and D25NG75H00-10EGR-100°C case (10° CA BTDC value of SOI) are compared in terms of performance and emission values in Figure 5.38 and Table 5.22.

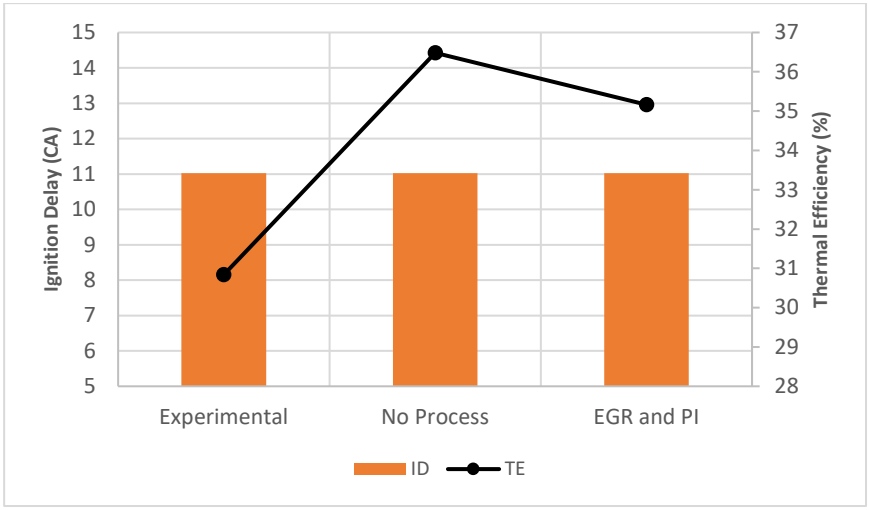

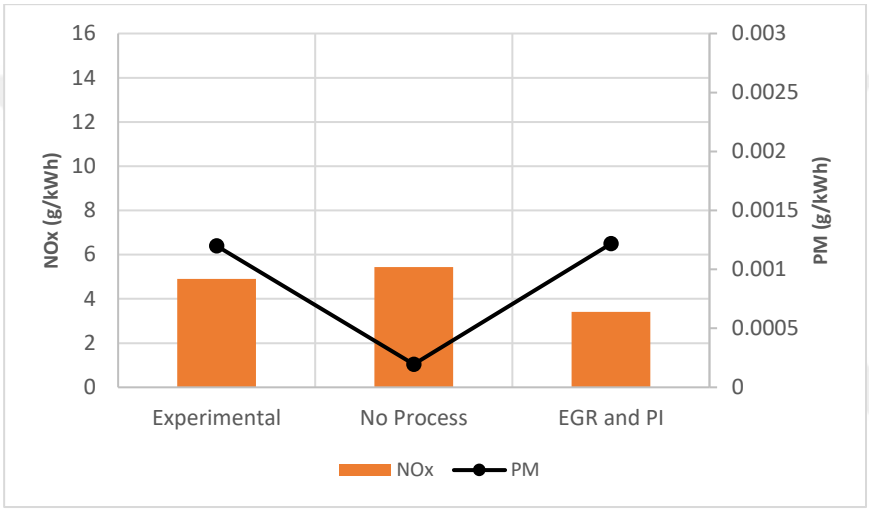

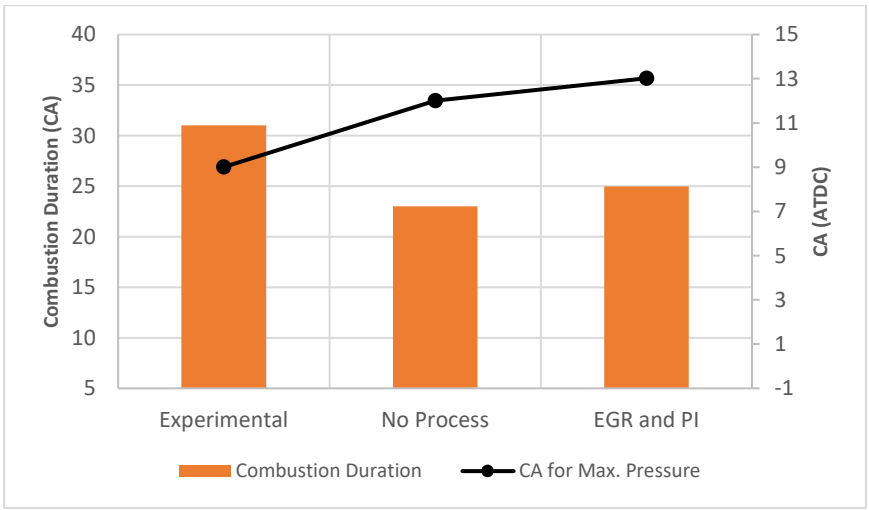

Figure 5.40 : Comparison of ID, TE, NO_x, PM, CD, and the position of Max. Press. Relative to TDC between test result and the case of D25NG75H15 with process (20% PI, 10% EGR-100°C) and without process.

When comparing power and BSFC, it can be seen that the process condition (100°C EGR temperature - 10% EGR - 20% PI) is more preferable, while CO and UHC

emissions are higher in the EGR - PI combination compared to the test conditions (Figure 5.38).

Table 5.21 : Comparison of results with and without the process for D25NG00H75.

	D25NG00H75	D25NG00H75-20PI-10EGR100°C	Variation
Power (kW)	10.69	10.48	-1.96%
Torque (N.m)	112.18	109.97	-1.97%
BSFC (g/kW.h)	95.73	97.25	~ +1.59%
Ignition Delay (CA)	11º	12º	-
Thermal Efficiency (%)	35.75	35.05	-0.7%
Combustion Duration (CA)	9º	9º	-
MPRR (bar/CA)	8.35	9.19	+0.84
Max. Press. (bar)	85.89	84.81	-
CA for Max. Press. (ATDC)	4º CA	4º CA	-
Max. Mean Temp. (K)	1997	1994	-
NO_x (g/kW.h)	14.04	8.7	-38%
SOOT (g/kW.h)	0.000071	0.000524	-
CO (g/kW.h)	0.0036	0.0098	-
HC (g/kW.h)	0.0015	0.0121	-

Although there is no significant difference in in-cylinder pressure, ID, and CD values, differences in MPRR, TE, NO_x, and PM values are observed (Figure 5.38). If 10% EGR and 20% PI are applied at 100°C EGR temperature under the test conditions, there is a 4.6% decrease in power and a 1.42% decrease in thermal efficiency, while there is a 43.5% improvement in NOx emissions.

Table 5.22 : Comparison of test and processed results for the operating point of D25NG75H00 (10° CA BTDC SOI).

	D25NG75H00	D25NG75H00-20PI-10EGR100°C	Variation
Power (kW)	9.76	9.31	-4.6%
Torque (N.m)	102.42	97.72	-4.6%
BSFC (g/kW.h)	203.85	212.93	+4.45%
Ignition Delay (CA)	11º	11º	-
Thermal Efficiency (%)	30.84	29.42	-1.42%
Combustion Duration (CA)	31º	32º	+1º
MPRR (bar/CA)	1.85	1.43	-0.42
Max. Press. (bar)	50.55	48.55	-2
CA for Max. Press. (ATDC)	9º CA	10º CA	-
Max. Mean Temp. (K)	1477	1429	-48
NO_x (g/kW.h)	4.9	2.77	-43.5%
SOOT (g/kW.h)	0.0012	0.0035	-
CO (g/kW.h)	10.25	12.69	+23.8%
HC (g/kW.h)	36.73	40.82	~ +11%

Additionally, CO and UHC emissions increase by 23.8% and 11%, respectively (Table 5.22). A decrease of 0.42 bar is observed in MPRR.

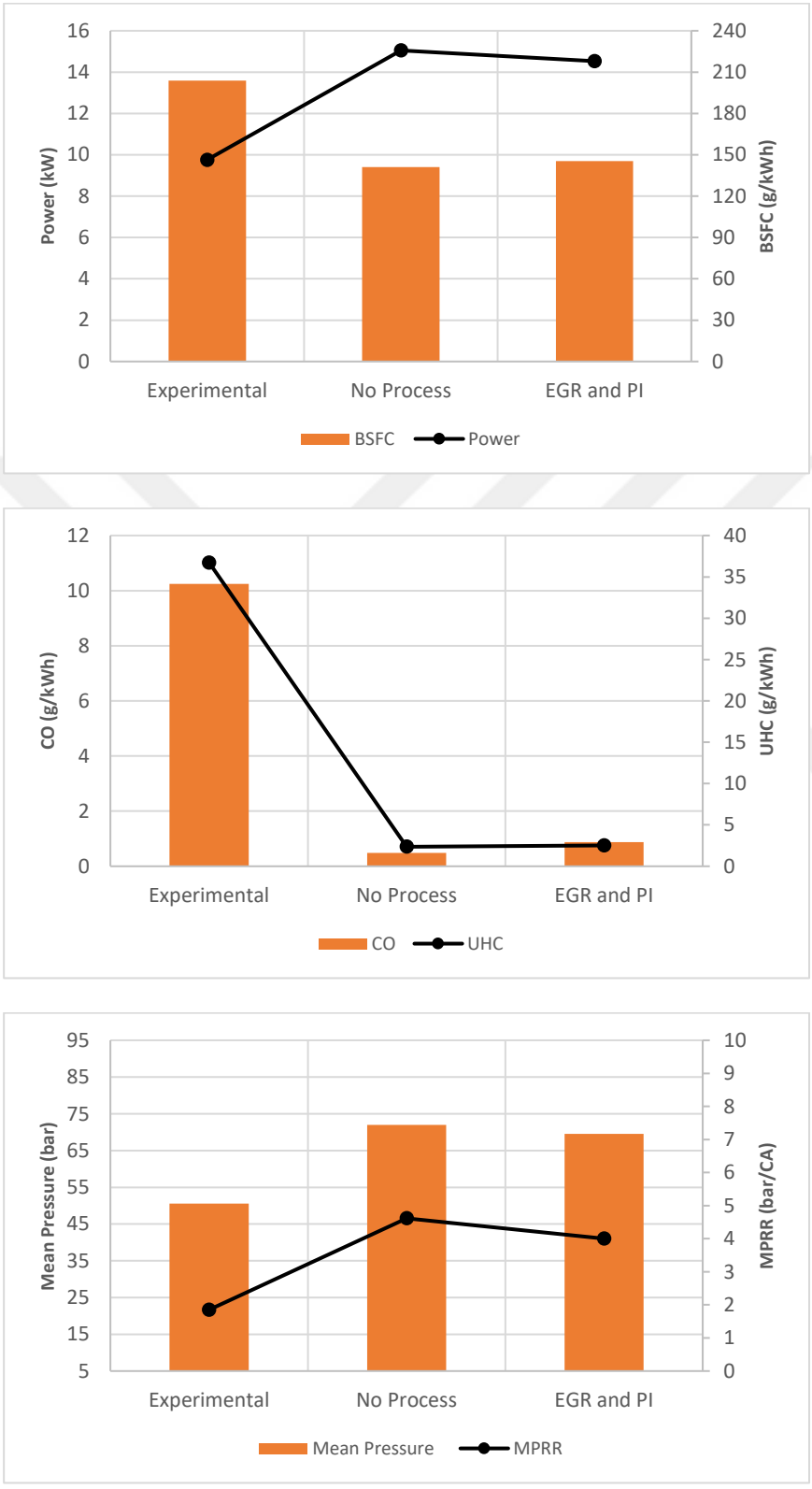

Figure 5.41 : Comparison of power, BSFC, CO, UHC, Pressure, and MPRR between test result and the case of D25NG75H25 with process (20% PI, 10% EGR-100°C) and without process.

Table 5.23 : Comparison of cases with and without process for Mode 2.

	D25NG75H15	D25NG75H15-20PI-10EGR100°C	Variation
Power (kW)	13.28	12.8	-3.61%
Torque (N.m)	139.34	134.29	-3.62%
BSFC (g/kW.h)	155.99	161.2	+3.34%
Ignition Delay (CA)	9º	11º	+2º
Thermal Efficiency (%)	36.48	35.16	-3.62%
Combustion Duration (CA)	23º	25º	+2º
MPRR (bar/CA)	3	2.31	-0.69
Max. Press. (bar)	60.35	57.92	-2.43
CA for Max. Press. (ATDC)	12º CA	13º CA	-
Max. Mean Temp. (K)	1809	1779	-30
NO_x (g/kW.h)	5.44	3.42	-37.13%
SOOT (g/kW.h)	0.0002	0.00122	-
CO (g/kW.h)	2.02	2.342	~ +16%
HC (g/kW.h)	8.76	9.557	+9%

Figure 5.39 and Figure 5.40 compare the performance and emission values of the D25NG75H15 operating point with the process condition D25NG75H15-10EGR-100°C and the test condition (D25NG75H00 - 10° CA BTDC value of SOI). According to the experimental results, the power, BSFC, CO, UHC, and TE values are more reasonable in the process and processless conditions, while the in-cylinder pressure and MPRR values remain higher (Figure 5.39 and Figure 5.40). When comparing the process and processless conditions, the results favor the process condition, with only a small loss in performance values but preferable results in terms of NO_x and MPRR values (Figure 5.39). Ignition delay remains similar under all conditions (experimental, process, and processless) (Figure 5.40).

When comparing the process and processless results for D25NG75H15, there is a 3.61% decrease in power, but a 37.13% improvement in NO_x and a 0.69 bar increase in MPRR (Table 5.23). The comparison of the D25NG75H15-10EGR-100°C condition with the test conditions is provided in Table 5.24. There is a 31.15% increase in power, a 21% decrease in BSFC, a 4.32% improvement in TE, a 30% reduction in NO_x, and a 77.15% and 74% reduction in CO and UHC, respectively. Only a 0.46 bar increase is observed in MPRR.

Figure 5.41 and Figure 5.42 present a comparison of the experimental, process, and processless results for the D25NG75H25 condition, which has the highest hydrogen fraction in Mode 2. While there is no difference in ignition delay, the other parameters show similar distributions to the previous operating points.

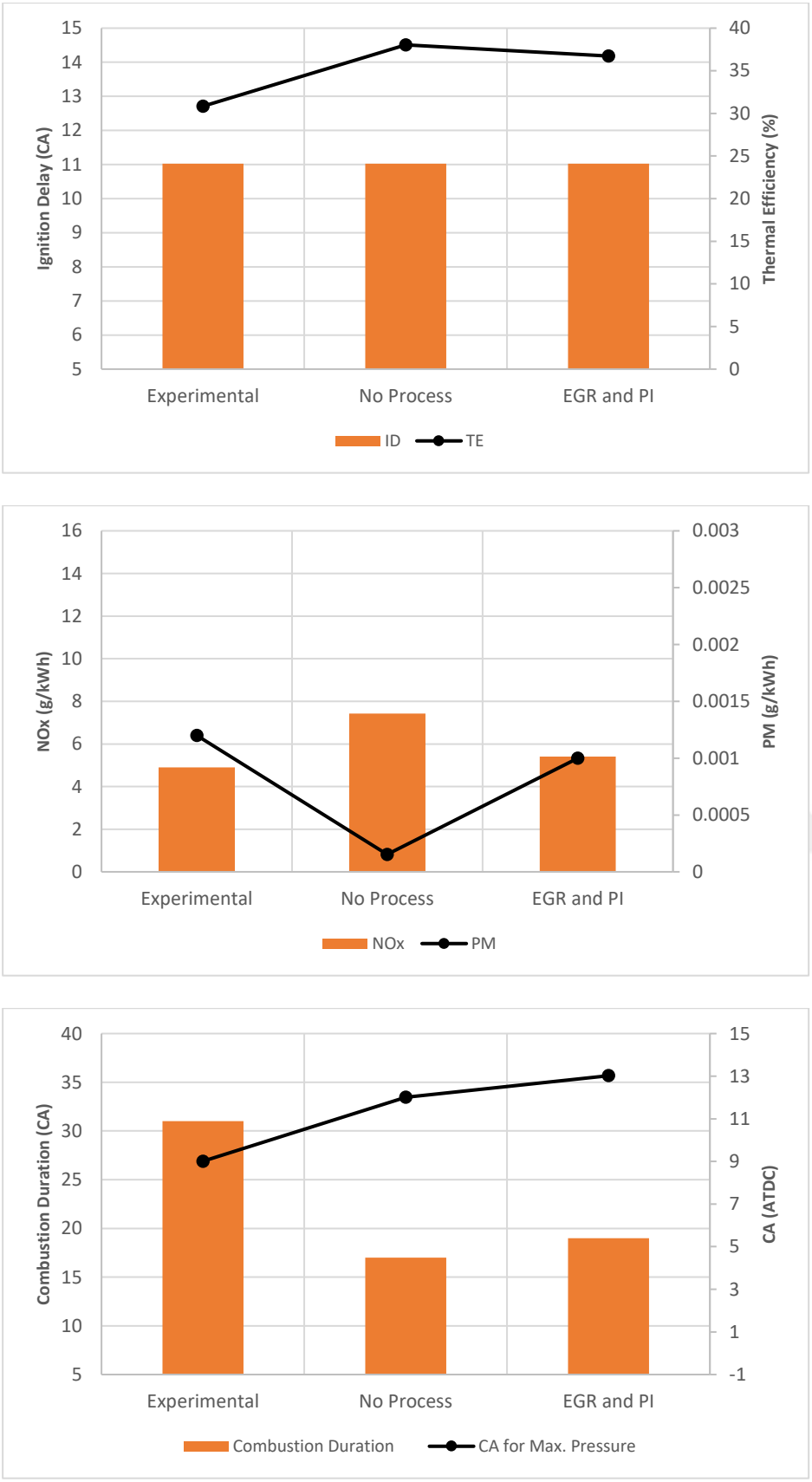

Figure 5.42 : Comparison of ID, TE, NO_x, PM, CD, and the position of Max. Press. Relative to TDC between test result and the case of D25NG75H25 with process (20% PI, 10% EGR-100°C) and without process.

When comparing the process and processless conditions for the D25NG75H15 operating points, the process condition is calculated to be 3.46% lower in power, 3% higher in BSFC, 1.3% lower in TE, 0.62 bar lower in MPRR, and 27% lower in NO_x (Table 5.25).

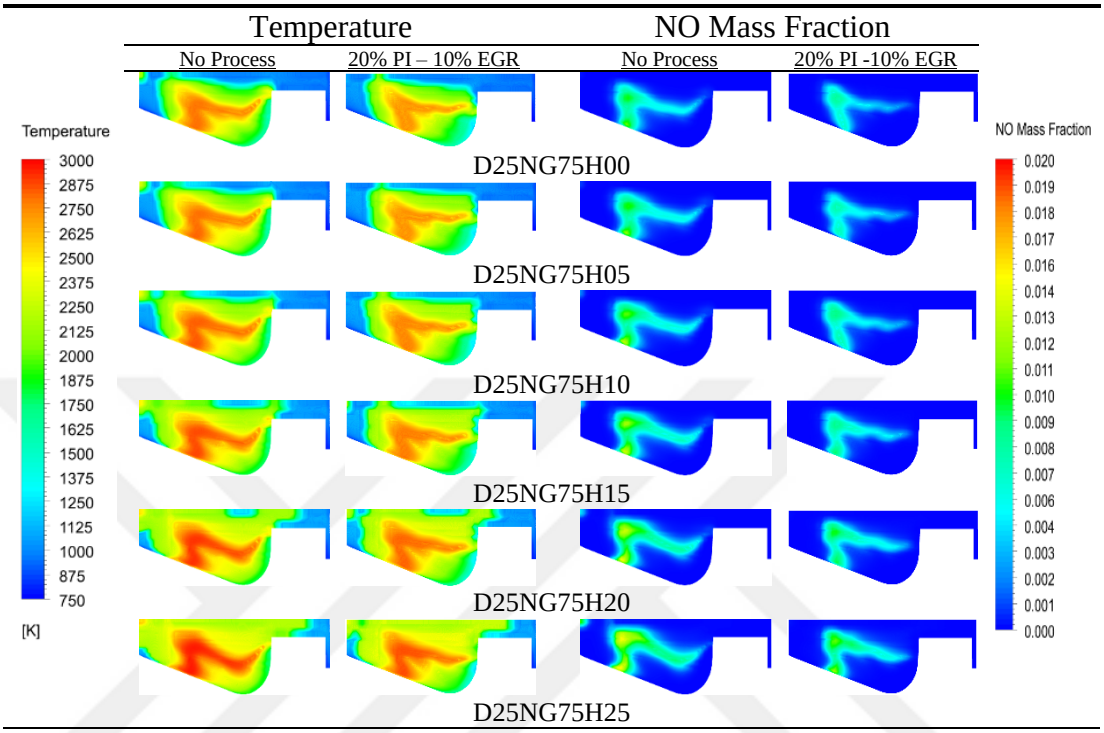

Figure 5.43 : Comparison of temperature and NO mass fraction contours at a piston position of 10° CA ATDC for operating points with applied (20% PI & 10% EGR) and not applied process with different hydrogen enriching fractions for Mode 2.

The temperature and NO mass fraction distributions for the D25NG75H15 operating points in process and processless conditions at the 10° CA BTDC piston position are shown in Figure 5.43. It is evident that the application of EGR and PI, especially for high hydrogen fractions, has a positive impact on the temperature distribution. Mode 1 and Mode 2, a comparison of the optimum conditions obtained with EGR-PI co-work is shown in Table 5.26.

The higher power output of Mode 2 can be explained by the additional hydrogen fraction introduced into the system. However, the most important parameters for comparison here are NO_x and MPRR. The incorporation of hydrogen into the in-cylinder combustion process is crucial for both performance and emission values. Its inclusion in the system should be more of an energy enrichment rather than an energy sharing mode. This is because it's possible to achieve higher performance with lower emissions of all types in Mode 2.

Table 5.24 : Comparison of the optimal result obtained by applying the process for Mode 2 with the test data.

	D25NG75H00	D25NG75H15-20PI-10EGR100°C	Variation
Power (kW)	9.76	12.8	+31.15%
Torque (N.m)	102.42	134.29	+31.12%
BSFC (g/kW.h)	203.85	161.2	~ -21%
Ignition Delay (CA)	11º	11º	-
Thermal Efficiency (%)	30.84	35.16	+4.32%
Combustion Duration (CA)	31º	25º	-6º
MPRR (bar/CA)	1.85	2.31	+0.46
Max. Press. (bar)	50.55	57.92	~ +7
CA for Max. Press. (ATDC)	9º CA	13º CA	-
Max. Mean Temp. (K)	1477	1779	+302
NO_x (g/kW.h)	4.9	3.42	-30%
SOOT (g/kW.h)	0.0012	0.00122	-
CO (g/kW.h)	10.25	2.342	-77.15%
HC (g/kW.h)	36.73	9.557	~ -74%

This results in a 1.05 bar reduction in MPRR and a 24.7% improvement in NO_x (Table 5.26). While CO and UHC emission values may appear higher, when compared to experimental results, D25NG75H15-10EGR-100°C has provided more reasonable results (Table 5.24).

Table 5.25 : Comparison of results with and without the process for D25NG75H25.

	D25NG75H25	D25NG75H25-20PI-10EGR100°C	Variation
Power (kW)	15.05	14.53	-3.46%
Torque (N.m)	157.92	152.51	-3.43%
BSFC (g/kW.h)	141.09	145.48	~ +3%
Ignition Delay (CA)	11º	11º	-
Thermal Efficiency (%)	38.04	36.74	-1.3%
Combustion Duration (CA)	17º	19º	+2º
MPRR (bar/CA)	4.62	4	-0.62
Max. Press. (bar)	71.94	69.52	~ -2.5
CA for Max. Press. (ATDC)	12º CA	13º CA	-
Max. Mean Temp. (K)	2057	1993	-64
NO_x (g/kW.h)	7.43	5.41	-27%
SOOT (g/kW.h)	0.000153	0.001	-
CO (g/kW.h)	0.49	0.874	+78%
HC (g/kW.h)	2.36	2.52	+6.8%

Compared to Mode 1, the presence of more natural gas in the gas mixture in Mode 2 operating conditions resulted in softer combustion conditions. When the results for the D25NG75H25 operation point were examined, the MPRR value remained below 5 bars, providing a more preferable operating opportunity compared to Mode 1.

Table 5.26 : Comparison of the optimal results obtained by applying the process for Mode 1 and Mode 2.

	20% PI – 10% EGR – 100°C		
	D25NG50H25	D25NG75H15	Variation
Power (kW)	11.20	12.8	+14.3%
Torque (N.m)	117.48	134.29	+14.3%
BSFC (g/kW.h)	140.33	161.2	~ 15%
Ignition Delay (CA)	11°	11°	-
Thermal Efficiency (%)	37.44	35.16	-2.28%
Combustion Duration (CA)	20°	25°	+5°
MPRR (bar/CA)	3.36	2.31	-1.05
Max. Press. (bar)	67.31	57.92	~ -10
CA for Max. Press. (ATDC)	9° CA	13° CA	-
Max. Mean Temp. (K)	1738	1779	+41
NO_x (g/kW.h)	4.54	3.42	-24.7%
SOOT (g/kW.h)	0.00121	0.00122	-
CO (g/kW.h)	1.55	2.342	+51%
HC (g/kW.h)	4.45	9.557	-

5.2.3 General summary for EGR – PI strategy

Taking into account all the analyses conducted, it has been determined that EGR plays an extremely important role in reducing NO_x, and PI application contributes to the improvement of MPRR. The appropriate combination of these two strategies is also crucial. With higher PI, combustion rate and intensity increase, which causes MPRR to rise again. On the other hand, higher EGR leads to an increase in combustion efficiency, but rapid and intense combustion results in higher temperatures and, in turn, an increase in NO_x emissions. In both Mode 1 (energy sharing with gaseous fuels) and Mode 2 (hydrogen enrichment mode) operating conditions, the combined use of 10% EGR and 20% PI has yielded more favorable results compared to others. When natural gas is used as an alternative fuel in diesel engines, it is possible to reduce NO_x and MPRR values while improving CO, HC, and CO_2 emissions up to a certain level. However, to nearly neutralize it and make it almost ineffective, hydrogen cooperation is essential. Additionally, incorporating hydrogen leads to improvements in performance as well as a significant enhancement in BSFC values. The use of hydrogen alone in diesel engines is not practically feasible (Table 5.21, Figure 5.35, and Figure 5.36). This is because introducing only hydrogen as the gaseous fuel into the combustion chamber results in increased NO_x and MPRR values due to the rapid combustion and high lower heating value of hydrogen. Even with the use of the EGR-PI combination, it is challenging to achieve desirable results in preventing these issues.

Sending a mixture of natural gas and hydrogen into the combustion chamber, where these two gaseous fuels complement each other, is a more accurate approach. Natural gas possesses slower combustion capabilities, while hydrogen burns rapidly. This combination allows for low NO_x formation with natural gas and high performance, along with low CO, CO_2, and UHC emissions when hydrogen is used. To counter the increased MPRR, PI is applied. This section of the study delves into the detailed balance of the fractions of these two gases and the EGR-PI ratios to achieve reasonable results. In the next section, the effects of water injection (WI) on pilot injection (PI) performance and emission values are examined in detail.

5.3 WI – PI Strategies

Another recommended method in the literature for improving MPRR and NO_x values is water jet injection and pilot injection strategy [50,52,187–190]. In this section of the thesis, the application of water jet injection (WI) to control increased NO_x values when using hydrogen as an alternative fuel and the use of pilot injection (PI) strategy to control MPRR values are discussed. Improved results in terms of performance and emissions were achieved with the combination of these two strategies. Similar to the analysis of the EGR-PI strategies applied in the working points, this section focuses on the effects of the WI-PI combination. Initially, the optimum conditions obtained for Mode 1, Case 18 (D25NG50H25 with 14° CA BTDC for SOI – as explained in Section 5.1), and for Mode 2, Case 57 (D25NG75H15 with 10° CA BTDC for SOI – as explained in Chapter 5.1), were taken as the starting point for the analysis. Within the scope of the study, six different water jet injection ratios were defined, which are 0%, 5%, 10%, 15%, 20%, and 25%. The ratios of injected water jet amounts were calculated as percentages of the mass of the injected diesel fuel.

For example, the case of 20% water jet injection means that 20% of the mass of diesel fuel injected per cycle is taken into account. The reason for not going to higher water jet ratios is that they can have negative effects on performance values. In the previous section (Chapter 5.2), the optimum ratio for pilot injection was determined as 20%, and this value was used in this numerical study.

In this study, the pilot injection (PI) process was carried out with a duration of 2.5° CA, set between 40° CA BTDC and 37.5° CA BTDC. Within the scope of the study, the effects of different water jet temperatures (25°C, 60°C, 75°C, and 90°C) and

different water jet injection advances(20° CA BTDC, 10° CA BTDC, 0° CA BTDC – TDC, and 10° CA ATDC for SOI) were also investigated.

Table 5.27 : Case matrix for WI and PI processes.

Mode 1		Mode 2	
0% PI – 20° CA BTDC SOWI 25°C		0% PI – 20° CA BTDC SOWI 25°C	
WI - 0%	D25NG50H25	WI - 0%	D25NG75H15
WI - 5%	D25NG50H25	WI - 5%	D25NG75H15
WI - 10%	D25NG50H25	WI - 10%	D25NG75H15
WI - 15%	D25NG50H25	WI - 15%	D25NG75H15
WI - 20%	D25NG50H25	WI - 20%	D25NG75H15
WI - 25%	D25NG50H25	WI - 25%	D25NG75H15
0% PI – 25% WI 20° CA BTDC SOWI		0% PI – 25% WI 20° CA BTDC SOWI	
WI - 25°C	D25NG50H25	WI - 25°C	D25NG75H15
WI - 60°C	D25NG50H25	WI - 60°C	D25NG75H15
WI - 75°C	D25NG50H25	WI - 75°C	D25NG75H15
WI - 90°C	D25NG50H25	WI - 90°C	D25NG75H15
20% PI – 25% WI 20° CA BTDC SOWI		20% PI – 25% WI 20° CA BTDC SOWI	
WI - 25°C	D25NG50H25	WI - 25°C	D25NG75H15
WI - 60°C	D25NG50H25	WI - 60°C	D25NG75H15
WI - 75°C	D25NG50H25	WI - 75°C	D25NG75H15
WI - 90°C	D25NG50H25	WI - 90°C	D25NG75H15
20% PI – 25% WI 75°C		20% PI – 25% WI 75°C	
20 CA BTDC SOWI	D25NG50H25	20 CA BTDC SOWI	D25NG75H15
10 CA BTDC SOWI	D25NG50H25	10 CA BTDC SOWI	D25NG75H15
0 CA BTDC SOWI	D25NG50H25	0 CA BTDC SOWI	D25NG75H15
10 CA ATDC SOWI	D25NG50H25	10 CA ATDC SOWI	D25NG75H15
20% PI – 25% WI 20° CA BTDC SOWI 75°C		20% PI – 25% WI 20° CA BTDC SOWI 75°C	
D25NG75H00		D25NG75H00	
D25NG65H10		D25NG75H05	
D25NG50H25		D25NG75H10	
D25NG25H50		D25NG75H15	
D25NG00H75		D25NG75H20	
-		D25NG75H25	
0% PI – 0% WI		0% PI – 0% WI	
D25NG75H00		D25NG75H00	
D25NG65H10		D25NG75H05	
D25NG50H25		D25NG75H10	
D25NG25H50		D25NG75H15	
D25NG00H75		D25NG75H20	
-		D25NG75H25	
20% PI – 0% WI		20% PI – 0% WI	
D25NG75H00		D25NG75H00	
D25NG65H10		D25NG75H05	
D25NG50H25		D25NG75H10	
D25NG25H50		D25NG75H15	
D25NG00H75		D25NG75H20	
-		D25NG75H25	

All the analyses described were performed for both Mode 1 and Mode 2, as shown in Table 5.27. These analyses were initially initiated at the optimum operating points for Mode 1 and Mode 2, but they were expanded to demonstrate that higher hydrogen fraction operating points could be reached with the applied parameters. The table also shows the analysis stages for different gas fuel fractions (Table 5.27).

5.3.1 Optimal condition determination in the WI - PI co-work

In the previous section (Chapter 5.2), detailed explanations were provided about the numerical operating points and results obtained with the EGR – PI strategy. Now, the focus is on another strategy pair, WI – PI. The goal with WI is to improve NO_x values, while with PI, it aims to enhance MPRR values. Additionally, it aims to demonstrate the feasibility of reaching higher hydrogen fractions. The following roadmap was followed to enrich the initial conditions obtained from the first study with the WI and pilot injection processes (PI).

In the first study, the effects of different water jet fractions without pilot injection (0% PI) were investigated at the operation points with D25NG50H25 at 14° CA BTDC injection advance for Mode 1 and D25NG75H15 at 10° CA BTDC injection advance for Mode 2, as obtained from the initial study. The water jet amounts were adjusted based on the percentage of the injected diesel fuel amount, which is 0%, 5%, 10%, 15%, 20%, and 25%. In this case, the temperature of the injected water jet was kept constant at 25°C, and an injection advance of 20° CA BTDC was preferred.

In this phase, the study aimed to investigate both the effects of the water jet fraction and determine the ideal water jet fraction (Table 5.27). The analysis results showed that a 25% WI ratio provided more preferable results. In the subsequent stage, without pilot injection (0% PI) and a constant 25% WI ratio, the effects of different water jet temperatures (25°C, 60°C, 75°C, and 90°C) were examined (Table 5.27).

The goal here was to study the impact of WI temperature and determine the optimum WI temperature. However, the study also aimed to investigate the effects of water jet temperatures (25°C, 60°C, 75°C, and 90°C) when the obtained 25% WI value was used in combination with a 20% pilot injection strategy (PI) (Table 5.27). In this context, a comparison was made between PI and non-PI conditions. The initial stages of the study indicated that 20% PI, 25% WI, and 75°C WI temperature yielded more favorable results in terms of performance and emission values compared to others.

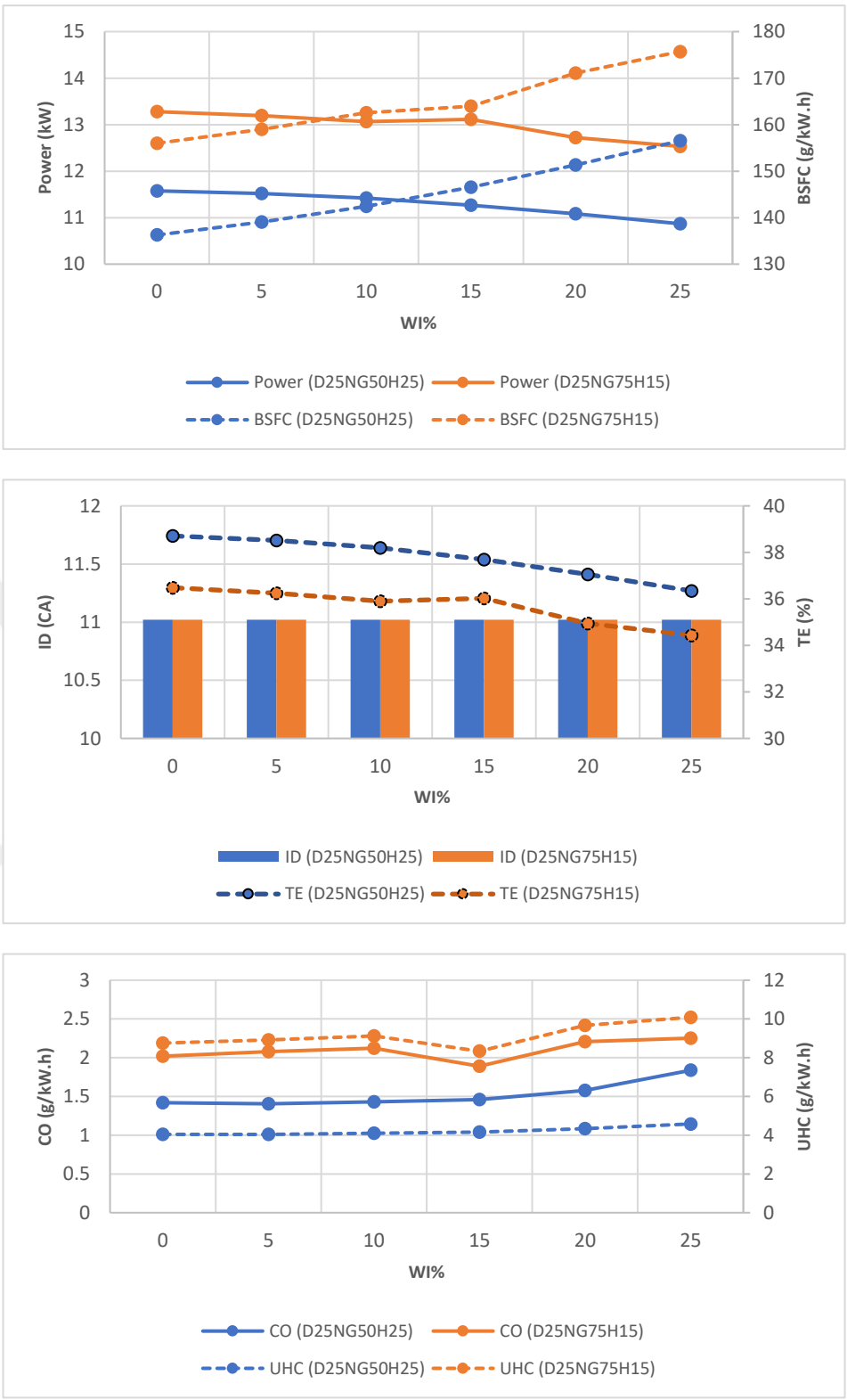

Figure 5.44 : The effect of increasing the WI rate without PI on power, BSFC, ID, TE, CO, and UHC values.

The next phase involved combining the obtained PI and WI ratios and examining the effects of different water jet injection timings (20° CA BTDC, 10° CA BTDC, 0° CA

– TDC, and 10° CA ATDC values for SOWI) for both Mode 1 and Mode 2 (Table 5.27).

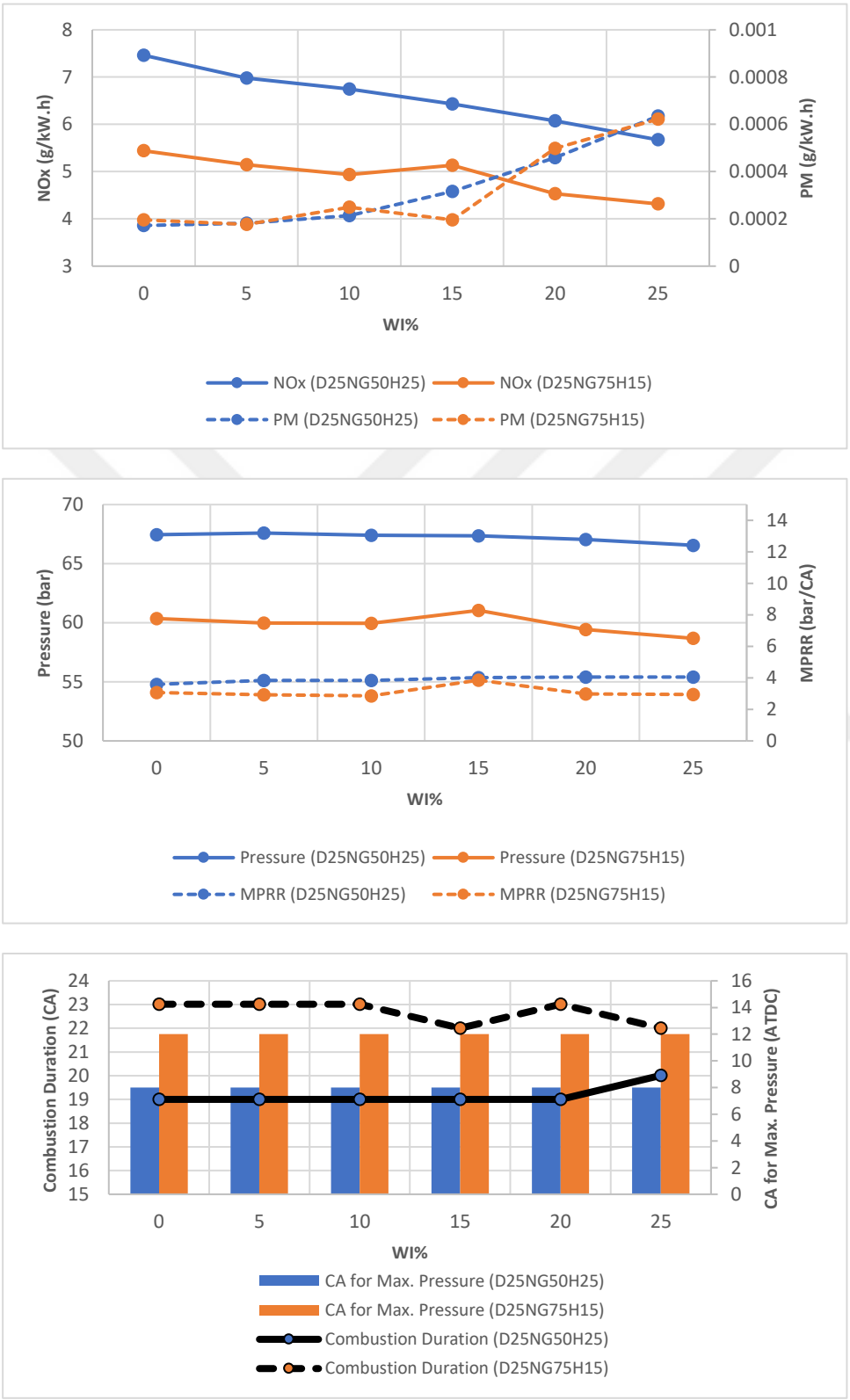

Figure 5.45 : The effect of increasing the WI rate without PI on NO_x, PM, Pressure, MPRR, CD, and the position of Max. Press. Relative to TDC.

Ultimately, values that yielded more reasonable results were determined to be 20% for PI, 25% for WI, and 75°C for WI temperature.

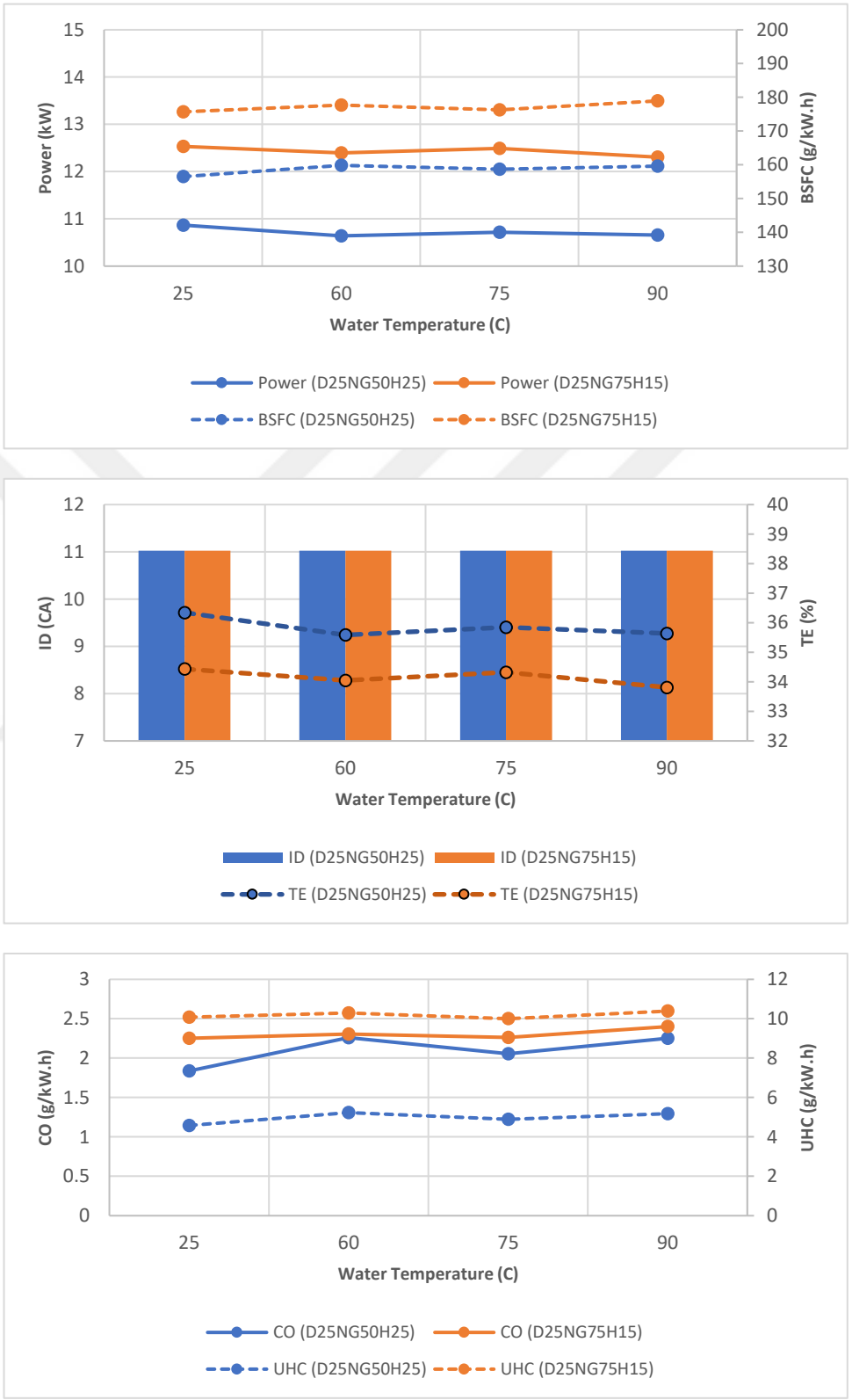

Figure 5.46 : The effect of increasing the WI temperature at fixed the WI rate (25% WI) without PI (0% PI) on power, BSFC, ID, TE, CO, and UHC values.

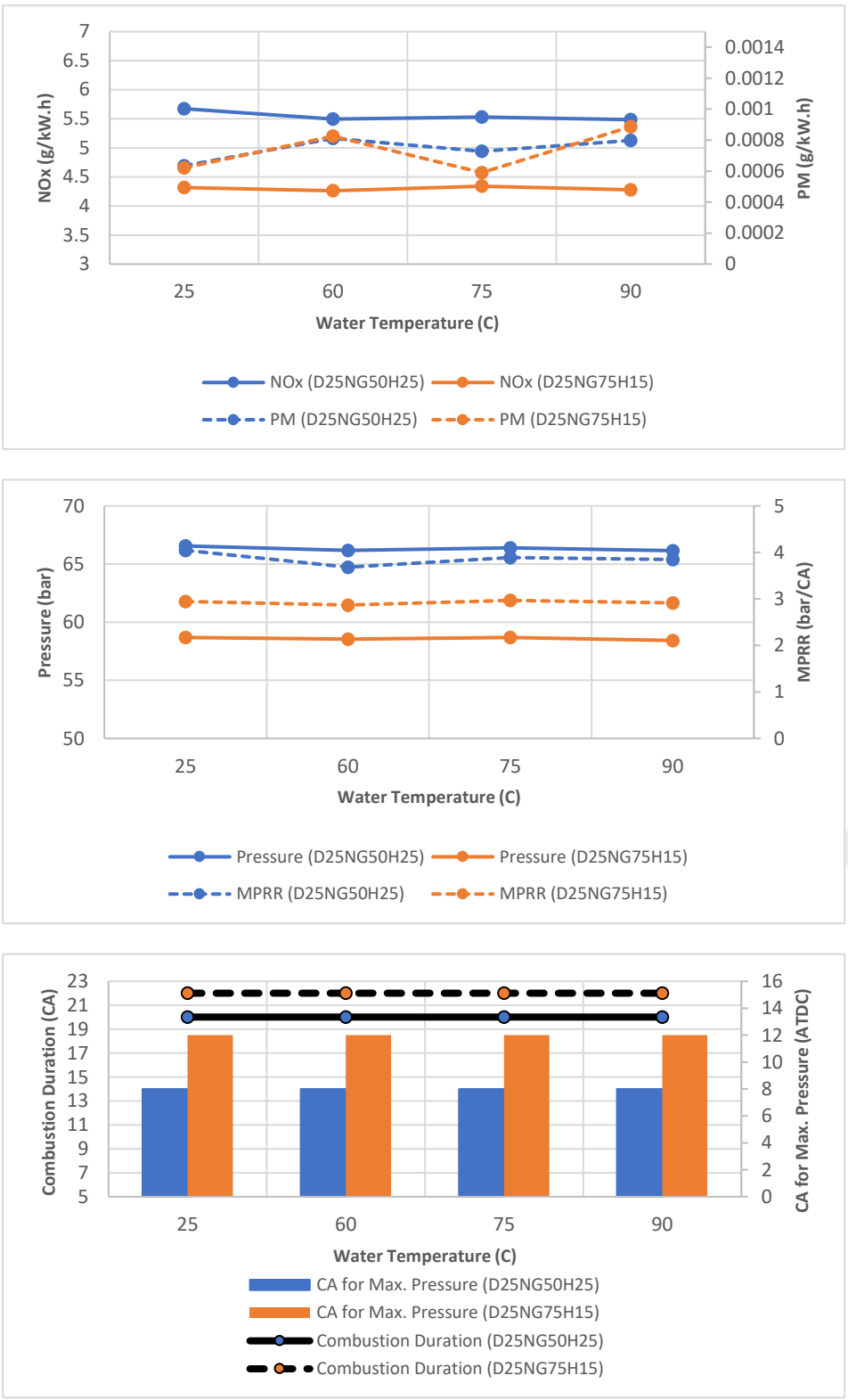

Figure 5.47 : The effect of increasing the WI temperature at fixed the WI rate (25% WI) without PI (0% PI) on NO_x, PM, Pressure, MPRR, CD, and the position of Max. Press. Relative to TDC.

In the final stage of the study, the effects of different gas fuel (Natural Gas - Hydrogen) fractions for Mode 1 and different hydrogen enrichment ratios for Mode 2 were

investigated under the optimum conditions (20% PI, 25% WI, and 75°C WI Temperature) (Table 5.27).

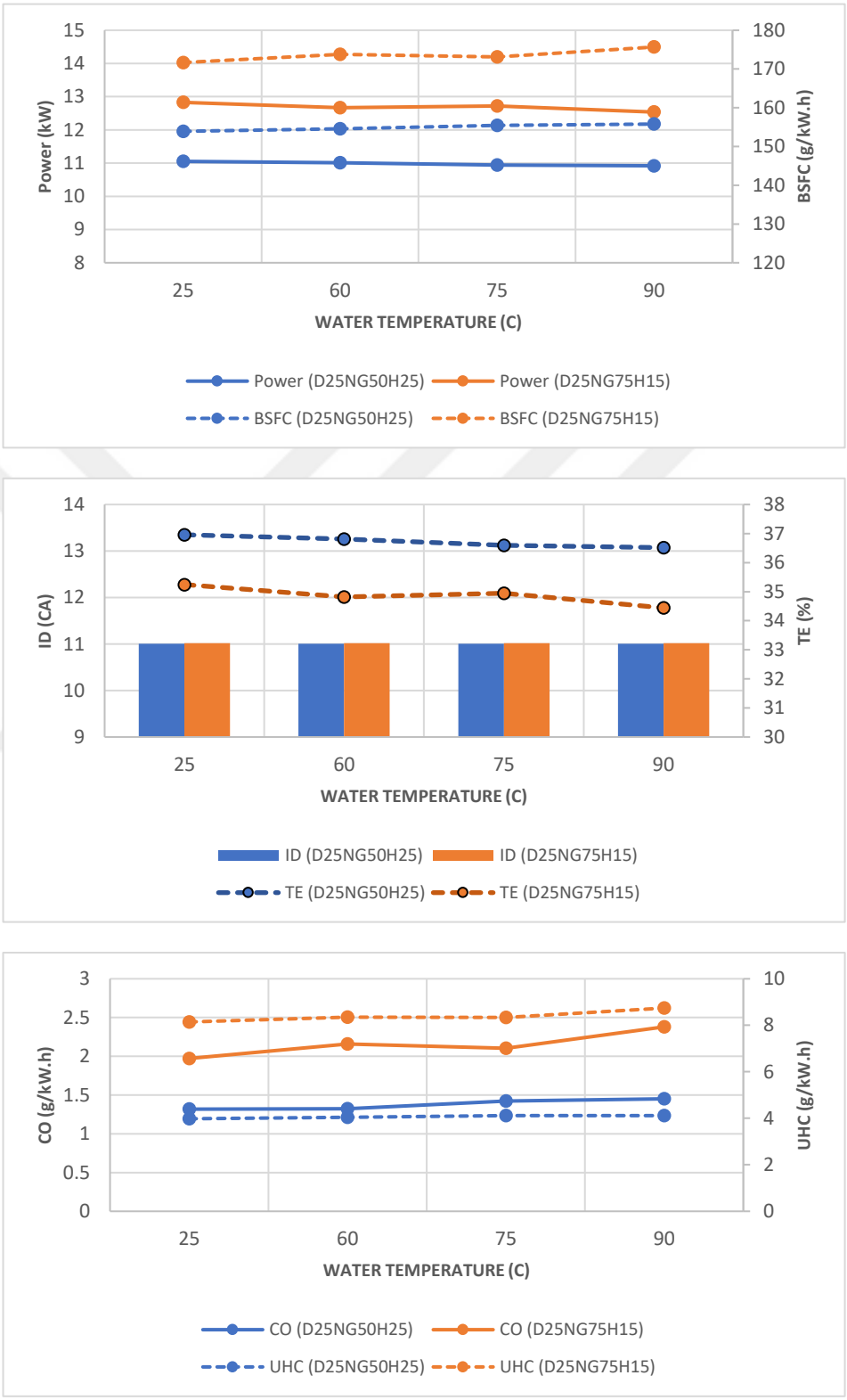

Figure 5.48 : The effect of increasing the WI temperature at fixed the WI rate (25% WI) and PI (20% PI) on power, BSFC, ID, TE, CO, and UHC values.

The impact of increased WI (Water Injection) ratio for Mode 1 (D25NG50H25 - 14° CA BTDC for SOI) and Mode 2 (D25NG75H15 - 10° CA BTDC for SOI) is shown in the same graphs in Figure 5.44 and Figure 5.45.

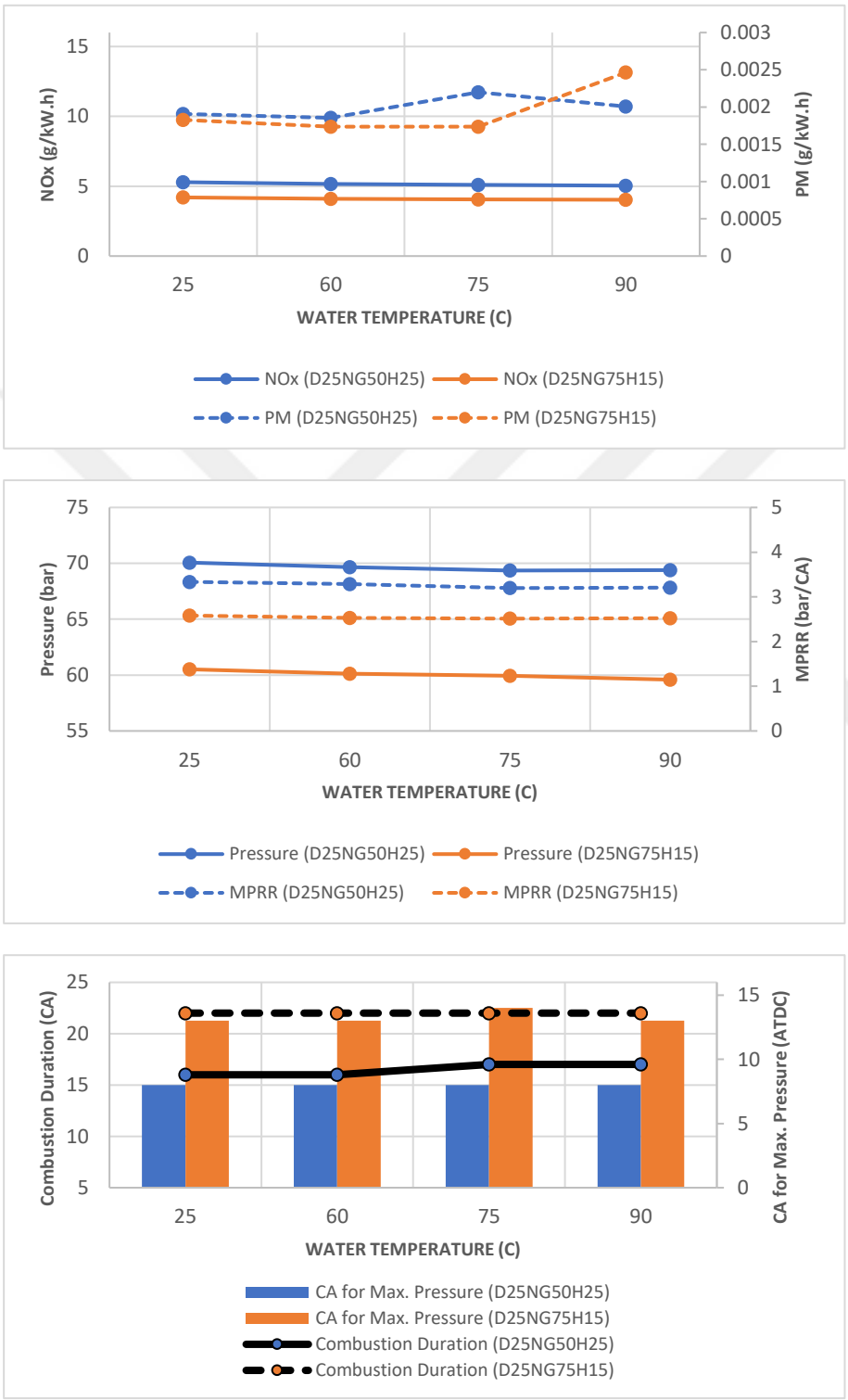

Figure 5.49 : The effect of increasing the WI temperature at fixed the WI rate (25% WI) and PI (20% PI) on NO_x, PM, Pressure, MPRR, CD, and the position of Max. Press. Relative to TDC.

Blue represents Mode 1, while orange represents Mode 2. When examining the graphs, it is observed that the power value showed a slight decrease with increasing WI ratio for Mode 1, while the BSFC continuously increased (Figure 5.44).

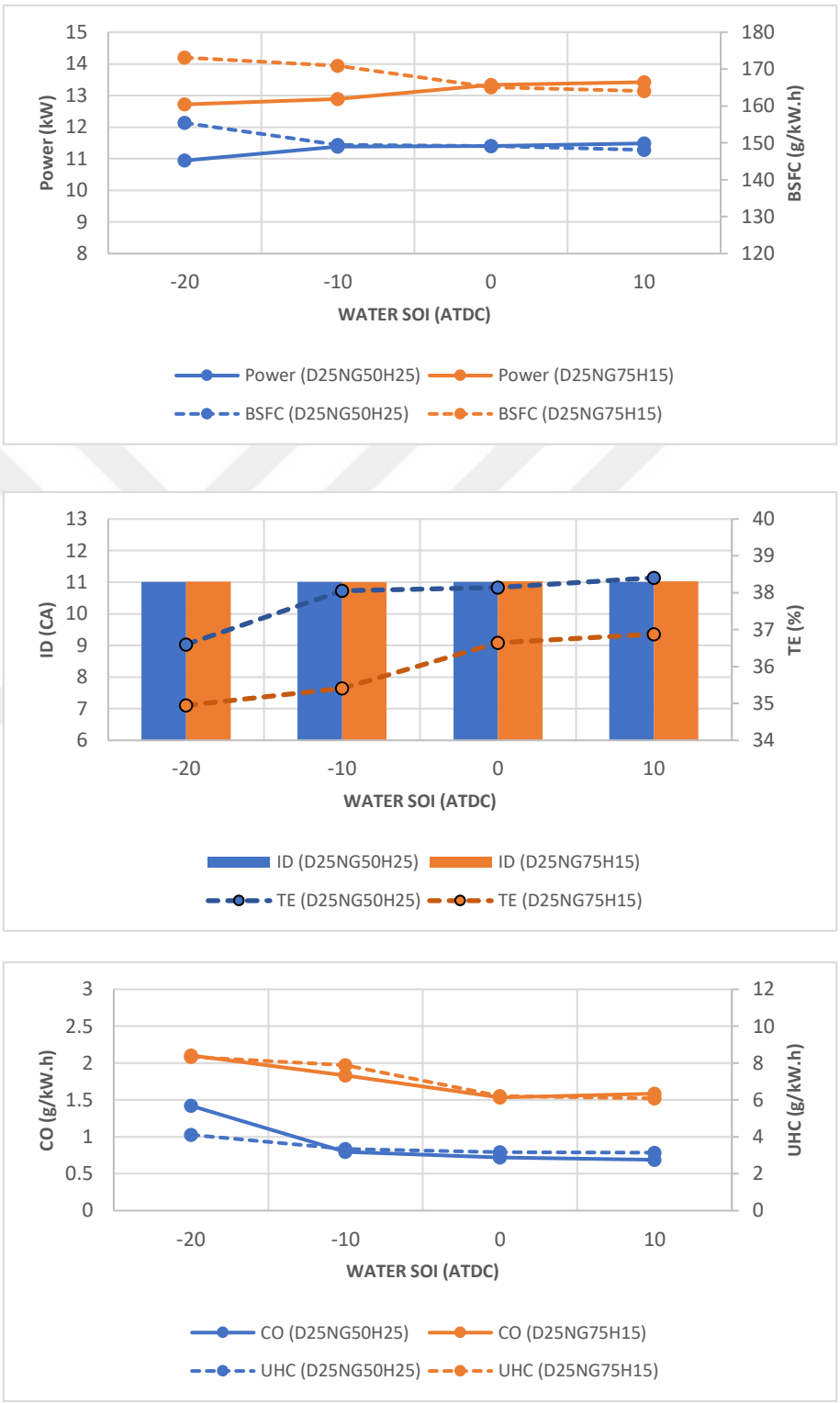

Figure 5.50 : The effect of variation the WI timing at fixed the WI rate (25% WI), the WI temperature (75 °C) and PI (20% PI) on power, BSFC, ID, TE, CO, and UHC values.

Similar changes were observed for Mode 2 (Figure 5.44). The increase in the water jet amount led to a partial decrease in local temperatures, which, in turn, reduced combustion efficiency and worsened performance parameters. For both Mode 1 and Mode 2, ignition delay times were not affected by the WI ratio, but the thermal efficiency (TE) decreased due to the cooling effect of the water jet on the ambient temperature. CO and UHC emissions remained stable and were not significantly affected by the WI ratio (Figure 5.44). The emissions most affected by the WI ratio were NOx and PM (Particulate Matter) emissions (Figure 5.45).

This is because these two types of emissions are directly influenced by local temperatures. Increasing WI resulted in a decrease in local temperatures, which, in turn, reduced NO_x formation. PM emissions result from the oxidation of unburned fuel vapor that doesn't participate in combustion. Therefore, as the combustion temperatures decrease, the probability of this event (oxidation of unburned fuel vapor) increases, leading to higher PM emissions (Figure 5.45). Increasing the WI ratio had minimal effects on in-cylinder pressure and MPRR values (Figure 5.45). It was observed that the 25% WI value, which caused a significant improvement in NO_x at the cost of a slight power loss, was suitable for later analyses. In the next stage, considering the 25% WI value, the effects of different WI temperatures (25°C, 60°C, 75°C, and 90°C) were investigated for cases with and without diesel pilot injection (0% PI and 20% PI). In the case of no diesel pilot injection (0% PI), it was observed that different WI temperatures had no significant effect on power, BSFC, TE, ID, CO, UHC, NO_x, MPRR, in-cylinder pressure, and CD (Combustion Duration) values for both Mode 1 and Mode 2, except for a decrease in PM emissions at 75°C WI temperature (Figure 5.46 and Figure 5.47). A similar situation was observed for 20% PI (Figure 5.48 and Figure 5.49). It can be concluded that WI temperatures had minimal impact on performance and emission values, primarily due to the presence of hydrogen in the gaseous fuel. This is because the high lower heating value of hydrogen and its effect on increasing post-combustion temperatures have a much greater impact than the difference in temperatures between different WI conditions. While there is a significant difference in performance and emission values between the presence and absence of water injection, there is no notable difference in results when water injection is applied at different temperatures. In summary, water injection is an effective method, while water injection temperature has minimal impact on

performance and emission values. Due to its positive contribution to PM emissions, a WI temperature of 75°C was preferred for the next stage (Figure 5.47 and Figure 5.49).

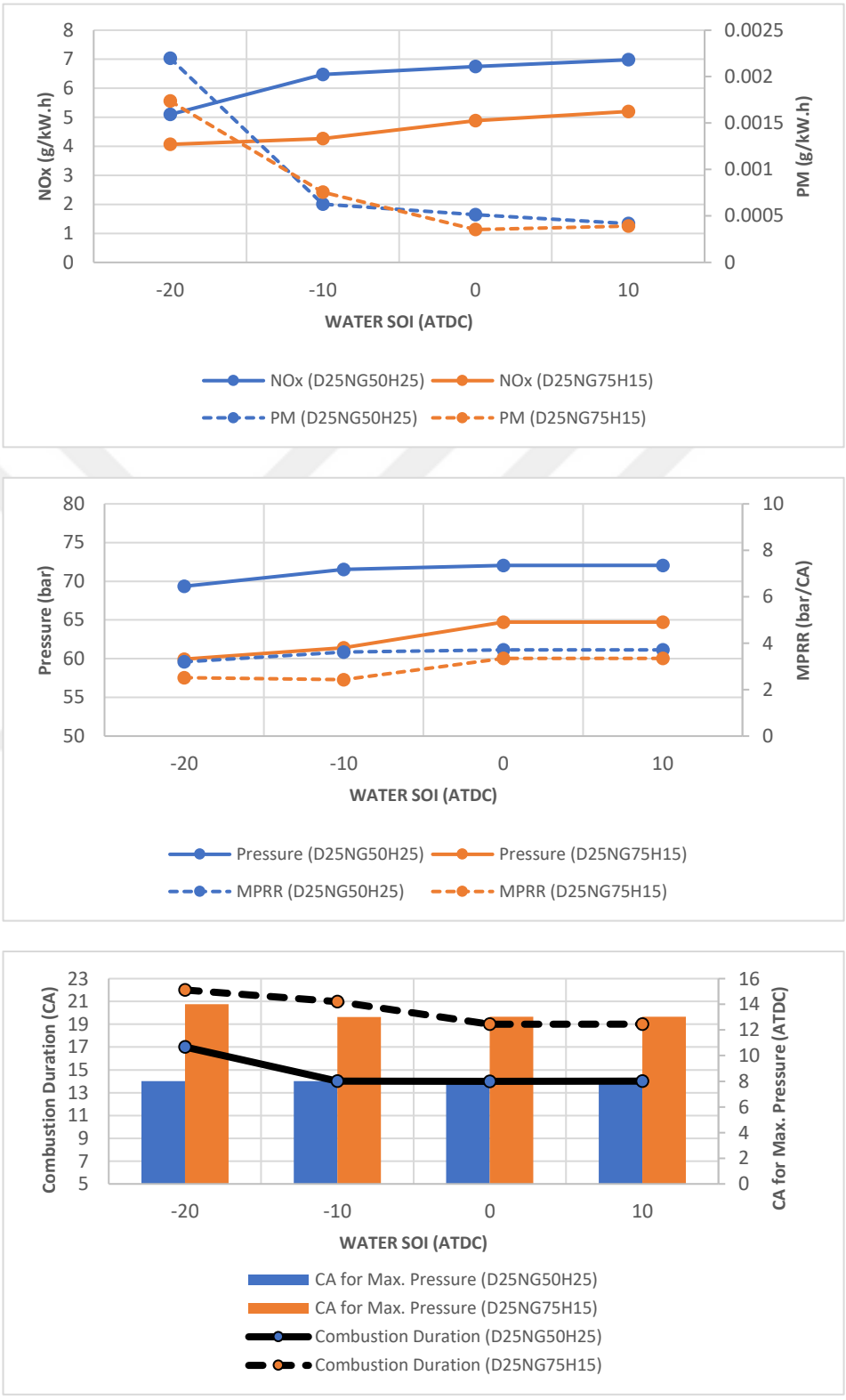

Figure 5.51 : The effect of variation the WI timing at fixed the WI rate (25% WI), the WI temperature (75 °C) and PI (20% PI) on NO_x, PM, Pressure, MPRR, CD, and the position of Max. Press. Relative to TDC.

Up to this point, results were obtained for water injection with an advance value of 20° CA BTDC. The effects of water injection at different advances (20° CA BTDC, 10° CA BTDC, 0° CA BTDC – TDC, and 10° CA ATDC for SOWI) were also analyzed (Figure 5.50 and Figure 5.51). Upon examination of the graphs, it can be seen that reducing the water injection advance for Mode 1 and Mode 2 results in increased power and decreased BSFC (Figure 5.50).

Further delayed water injection had a lesser effect on combustion temperatures compared to early water injection, resulting in less impact on performance values. Therefore, power and BSFC were obtained as more reasonable results for delayed water injection. While ignition delay remained unchanged for both modes with decreasing water injection advance, TE value increased (Figure 5.50).

The increase in TE value can be explained by the fact that delayed water injection has less effect on combustion temperatures. Therefore, higher temperatures indicate high combustion efficiency and low incomplete combustion products. As a result, CO and UHC emissions also decreased (Figure 5.50). However, the situation is the opposite for NO_x. PM emissions also decreased similarly to CO and UHC emissions due to the same reasons (Figure 5.51).

Table 5.28 : Results of different WI temperatures for Mode 1 under constant WI rate (25% WI) and injection advance (20° CA BTDC SOWI), with and without PI.

	25% WI – 20° CA BTDC SOWI – D25NG50H25 (Mode 1)							
	25°C		60°C		75°C		90°C	
	PI		PI		PI		PI	
	0%	20%	0%	20%	0%	20%	0%	20%
Power (kW)	10.87	11.05	10.64	11.01	10.72	10.94	10.67	10.92
Torque (N.m)	114.05	115.97	111.66	115.50	112.49	114.84	111.82	114.58
BSFC (g/kW.h)	156.52	153.91	159.85	154.54	158.67	155.42	159.63	155.78
Ignition Delay (CA)	11º	11º	11º	11º	11º	11º	11º	11º
Thermal Efficiency (%)	36.34	36.96	35.59	36.81	35.85	36.60	35.64	36.52
Combustion Duration (CA)	20º	16º	20º	16º	20º	17º	20º	17º
MPRR (bar/CA)	4.04	3.34	3.68	3.29	3.89	3.20	3.85	3.21
Max. Press. (bar)	66.56	70.07	66.18	69.66	66.40	69.36	66.15	69.40
CA for Max. Press. (ATDC)	8º CA	8º CA	8º CA	8º CA	8º CA	8º CA	8º CA	8º CA
Max. Mean Temp. (K)	1716	1788	1691	1776	1705	1770	1695	1771
NO_x (g/kW.h)	5.67	5.29	5.50	5.15	5.53	5.10	5.49	5.04
SOOT (g/kW.h)	0.00063	0.0019	0.00081	0.0019	0.00073	0.0022	0.00080	0.0020
CO (g/kW.h)	1.84	1.32	2.26	1.33	2.06	1.42	2.25	1.45
HC (g/kW.h)	4.58	3.98	5.23	4.04	4.89	4.11	5.18	4.12

MPRR and in-cylinder pressure values were not significantly affected by water injection advance for Mode 1, but they increased with a reduced water injection advance for Mode 2. The longest combustion duration was observed for the 20° CA

BTDC SOWI value (Figure 5.51). The 20° CA BTDC SOWI value was chosen for NO_x emissions and MPRR as it offered more reasonable results compared to other advances.

Table 5.28 shows the numerical results obtained for different water injection temperatures for Mode 1 (D25NG50H25) with and without diesel fuel pilot injection (0% PI and 20% PI). Water injection conditions were kept at 25% WI and 20° CA BTDC SOWI, and the effects of water injection temperatures were examined for PI and non-PI. When examining the results, it can be seen that the performance, NO_x, and MPRR values at 75 °C water injection temperature are quite successful for 20% PI (Table 5.28). For Mode 2 (D25NG75H15), Table 5.29 shows the numerical results obtained for different water injection temperatures for cases with and without diesel fuel pilot injection (0% PI and 20% PI). The water injection conditions were the same as those for Mode 1. When examining the results for this mode, it can be seen that the performance, NO_x, and MPRR values at 75 °C water injection temperature are successful for 20% PI (Table 5.29).

Table 5.29 : Results of different WI temperatures for Mode 2 under constant WI rate (25% WI) and injection advance (20° CA BTDC SOWI), with and without PI.

	25% WI – 20° CA BTDC SOWI – D25NG75H15 (Mode 2)							
	25°C		60°C		75°C		90°C	
	PI		PI		PI		PI	
	0%	20%	0%	20%	0%	20%	0%	20%
Power (kW)	12.53	12.83	12.39	12.67	12.49	12.72	12.31	12.54
Torque (N.m)	131.52	134.61	130.05	132.98	131.08	133.47	129.14	131.55
BSFC (g/kW.h)	175.70	171.66	177.69	173.78	176.29	173.14	178.94	175.66
Ignition Delay (CA)	11º	11º	11º	11º	11º	11º	11º	11º
Thermal Efficiency (%)	34.44	35.25	34.05	34.82	34.32	34.95	33.81	34.44
Combustion Duration (CA)	22º	22º	22º	22º	22º	22º	22º	22º
MPRR (bar/CA)	2.94	2.58	2.87	2.53	2.97	2.51	2.92	2.53
Max. Press. (bar)	58.68	60.52	58.54	60.12	58.68	59.94	58.42	59.59
CA for Max. Press. (ATDC)	12ºCA	13ºCA	12ºCA	13ºCA	12º CA	14ºCA	12º CA	13ºCA
Max. Mean Temp. (K)	1752	1799	1745	1792	1753	1793	1742	1783
NO_x (g/kW.h)	4.32	4.20	4.26	4.10	4.34	4.07	4.28	4.03
SOOT (g/kW.h)	0.00062	0.0018	0.00083	0.0017	0.00059	0.0017	0.00089	0.0025
CO (g/kW.h)	2.25	1.97	2.31	2.16	2.26	2.10	2.4	2.38
HC (g/kW.h)	10.09	8.14	10.30	8.35	10	8.34	10.39	8.74

When comparing the results for PI and non-PI, it can be observed that the pilot injection process offers lower NO_x and higher MPRR values along with better performance. The highest TE value was also achieved with 20% PI and a 75°C water injection temperature. Reasonable values were observed for CO and UHC emissions as well (Table 5.28 and Table 5.29).

5.3.2 Comparison of WI – PI strategy and non – strategy conditions

For Mode 1 (gas fuel energy sharing mode), numerical results with different gas energy fractions have been compared to experimental results (D25NG75H00 14° CA BTDC for SOI).

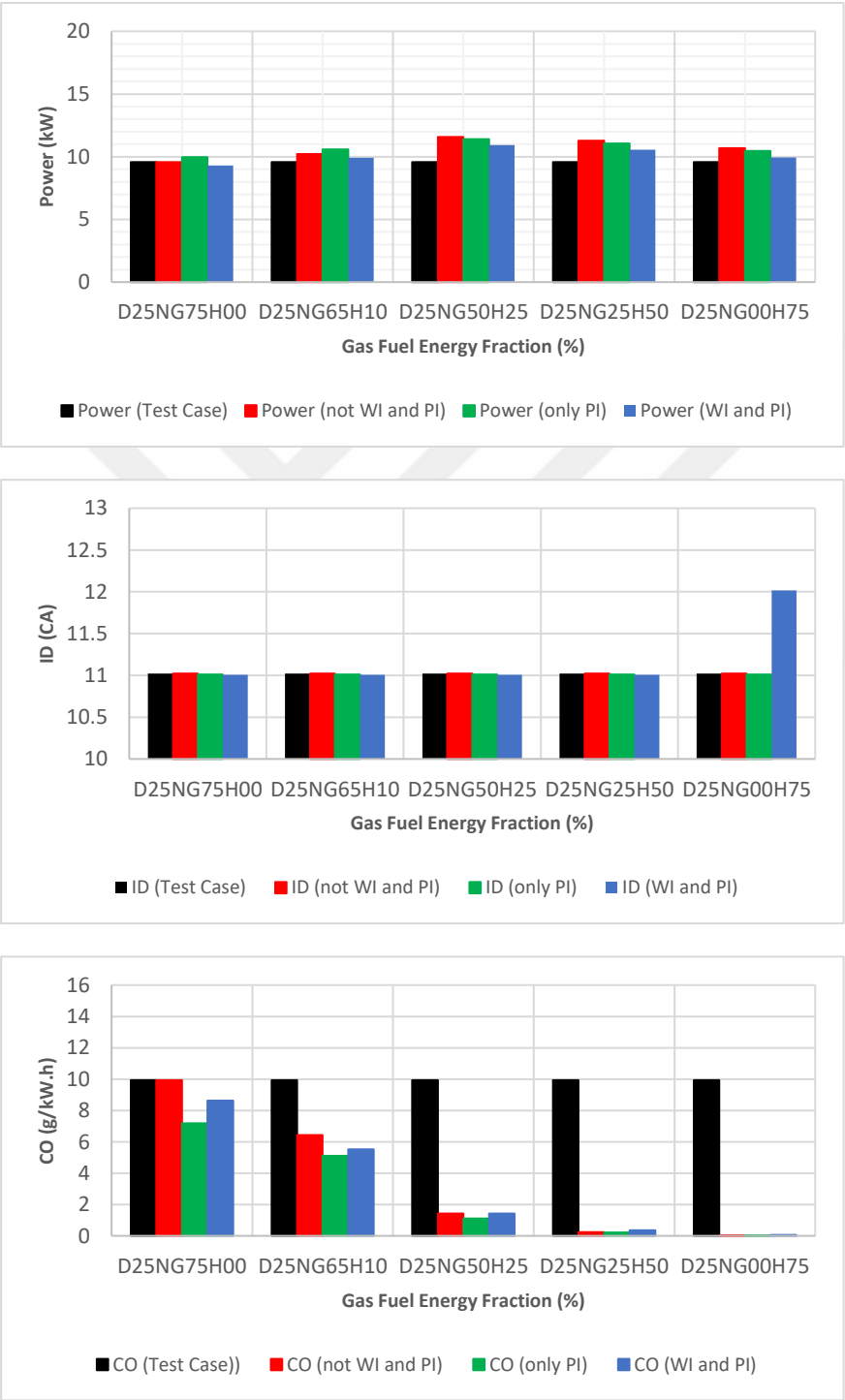

Figure 5.52 : Comparison of test result with the non-process, only PI (20% PI), and both PI and WI conditions (20% PI and 25% WI) in terms of power, ID, and CO emission for Mode 1.

In this case, processes were not applied in any of the gas energy fractions, only pilot injection (20% PI) was applied, and both pilot injection and water injection (20% PI & 25% WI) were applied. The results show that under D25NG75H00 conditions, the highest power value was achieved when only pilot injection was applied (Figure 5.52).

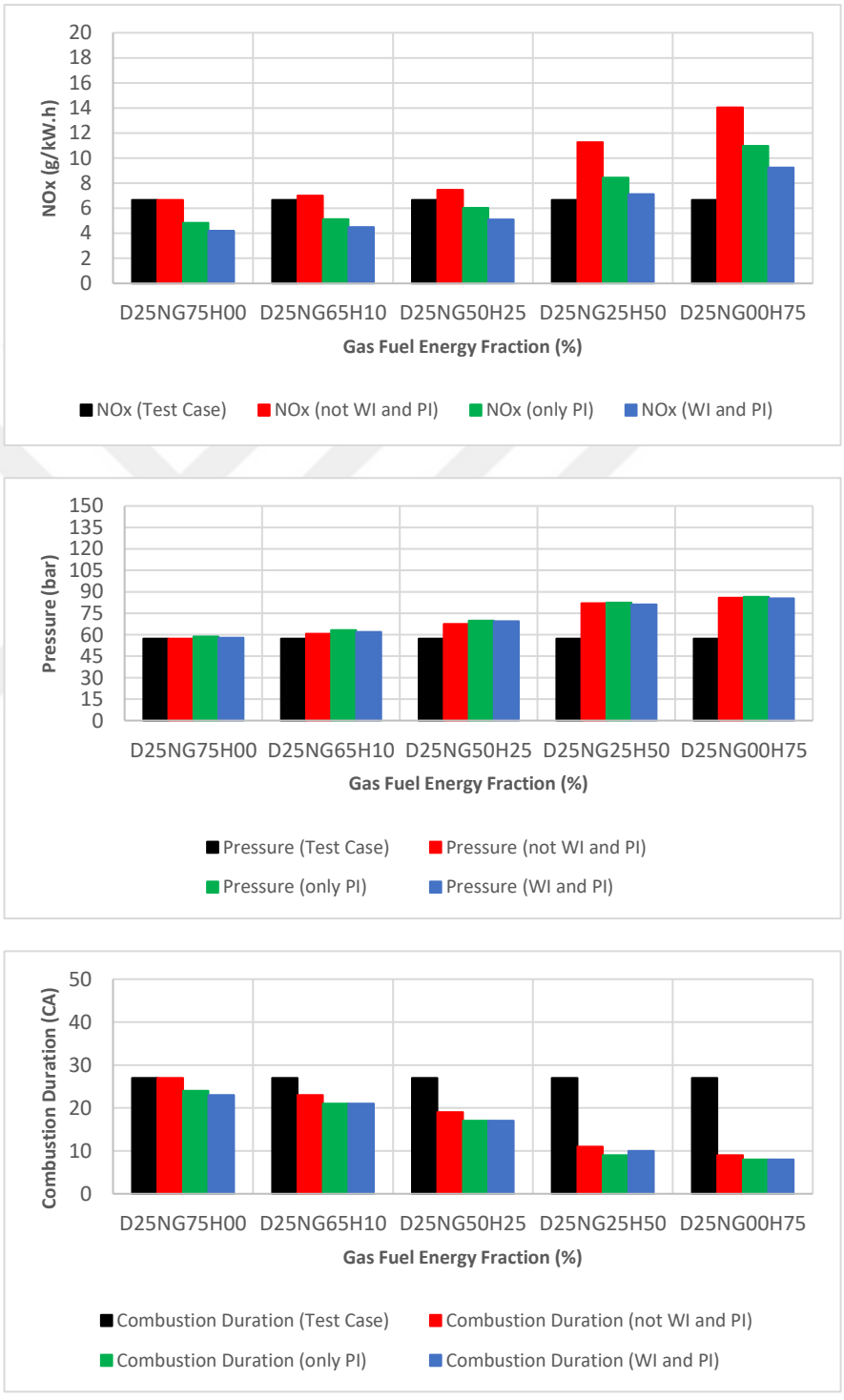

Figure 5.53 : Comparison of test result with the non-process, only PI (20% PI), and both PI and WI conditions (20% PI and 25% WI) in terms of NO_x emissions, Pressure and CD for Mode 1.

In other cases, similar power levels were obtained. D25NG65H10 conditions produced more power and allowed for a greater increase in power when 20% PI was applied. The application of 25% WI with PI caused the power value to decrease back to the levels of the experimental conditions (Figure 5.52).

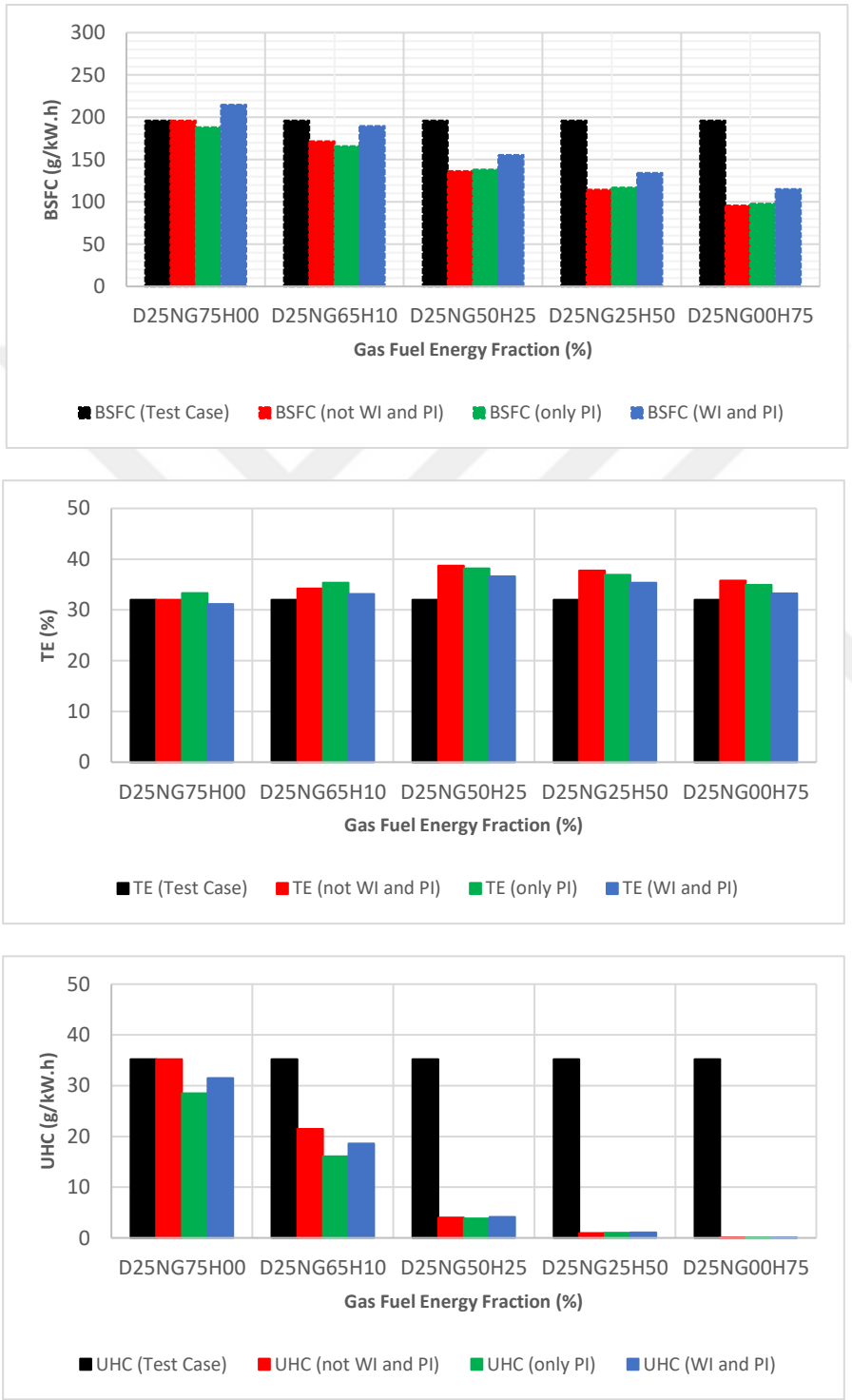

Figure 5.54 : Comparison of test result with the non-process, only PI (20% PI), and both PI and WI conditions (20% PI and 25% WI) in terms of BSFC, TE and UHC emission for Mode 1.

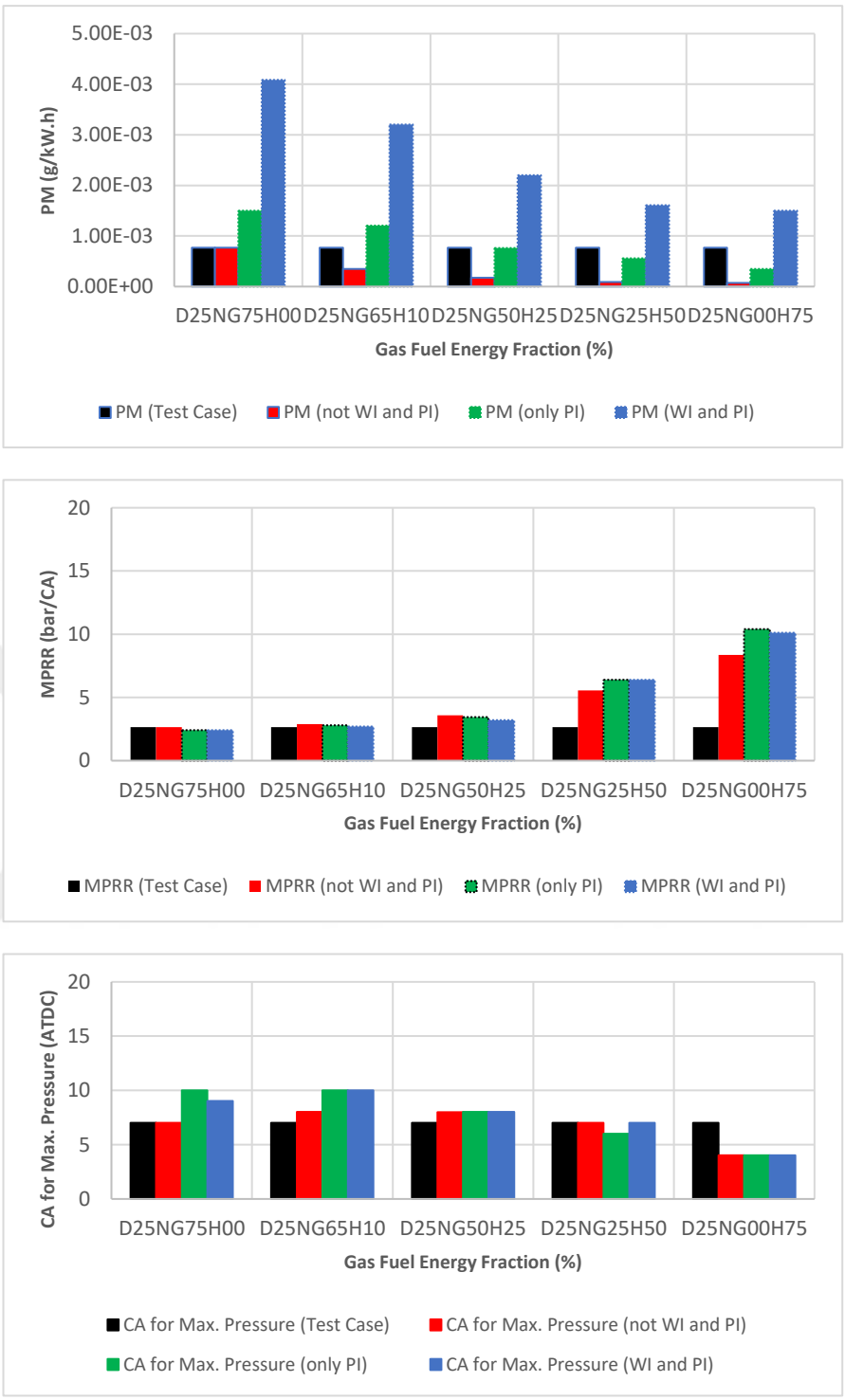

Figure 5.55 : Comparison of test result with the non-process, only PI (20% PI), and both PI and WI conditions (20% PI and 25% WI) in terms of PM emission, MPRR and the position of Max. Press. Relative to TDC for Mode 1.

Increasing the hydrogen fraction in the D25NG50H25 operating point has resulted in a higher power output. However, the application of 20% PI to this operating point has caused a decrease in power. The application of WI, though resulting in a decrease in power, has still provided a higher power value than the test conditions (Figure 5.52).

Increasing the hydrogen fraction counteracts the effect of PI on power output. This is because hydrogen promotes rapid combustion. Pilot injection causes combustion to start slightly earlier and in a more gradual manner. An increase in the hydrogen fraction, in combination with pilot injection, leads to combustion starting early and proceeding rapidly and forcefully. A similar effect can be observed with D25NG00H75 (Figure 5.52). The fluctuations in power values across different gas fuel fractions are also reflected in BSFC due to the same reasons (Figure 5.54).

The ID (Ignition Delay) value has increased as a result of the effect of water injection in the D25NG00H75 condition. In other conditions, it remained stable (Figure 5.52). Although ID appears stable, CD (Combustion Duration) and MPRR (Rate of Maximum Pressure Rise) values have indicated that in high hydrogen fractions, the combustion duration shortened, and MPRR increased (Figure 5.53 and Figure 5.55). In other words, while the start of combustion remains stable, its duration and character have changed. The CD value was highest in the condition without hydrogen (D25NG75H00) and lowest in the D25NG00H75 condition (Figure 5.53). PI and WI applications have shortened the combustion duration slightly. The most important parameter for combustion duration is the hydrogen fraction. MPRR has shown a sharp increase trend when the hydrogen energy fraction is above 50% (Figure 5.55). To improve MPRR, the hydrogen energy fraction in the gas fuel should not exceed 25%. The application of PI does not have a significant impact on reducing MPRR in conditions with high hydrogen energy fractions (Figure 5.55).

When examining the numerical result graphs for NO_x, it's observed that increases occur due to an increase in the hydrogen fraction, especially above 25% hydrogen energy fraction (Figure 5.53). The applied strategies (only PI and PI-WI) have been quite successful in reducing NO_x (Figure 5.53). When the hydrogen fraction is at 50% and above, higher NO_x formation was observed according to the test conditions. Although PI-WI application was performed to achieve a reduction, it couldn't prevent higher NO_x formation compared to the experimental conditions (Figure 5.53). CO and UHC emissions have provided reasonable results in all cases where hydrogen was included (Figure 5.52 and Figure 5.54). Under the same fraction of gas mixture conditions, only PI application has resulted in lower CO and UHC emissions. While there was a slight increase with WI, these emissions remained at lower levels compared to conditions without the process (Figure 5.52 and Figure 5.54).

PM emissions have been influenced by the same magnitudes of local and combustion temperatures. For example, an increase in the hydrogen fraction has resulted in improvement in PM emissions.

The application of PI in the presence of hydrogen has also led to a reduction in PM emissions compared to the experimental conditions (Figure 5.55). When comparing the experimental conditions (D25NG75H00 14° CA BTDC for SOI) with the condition where the WI-PI processes were applied (D25NG50H25-20PI-25WI75°C), improvements of 14.26% for power, 20.7% for BSFC, 4.58% for TE, 23.42% for NO_x, 85.7% for CO, and 88.33% for UHC were observed. Only a slight increase of 0.54 bar was noticed for MPRR (Table 5.30).

Table 5.30 : Comparison between processed by the WI results (20% PI - 25% WI 75°C - 20° CA BTDC SOWI) for D25NG50H25 (Mode 1) and test result.

	D25NG75H00	D25NG50H25-20PI-25WI75°C	Variation
Power (kW)	9.575	10.94	+14.26%
Torque (N.m)	100.477	114.84	+14.29%
BSFC (g/kW.h)	196	155.42	-20.7%
Ignition Delay (CA)	11º	11º	-
Thermal Efficiency (%)	32.02	36.60	+4.58%
Combustion Duration (CA)	27º	17º	-10º
MPRR (bar/CA)	2.66	3.2	+0.54
Max. Press. (bar)	57.25	69.36	~ +12
CA for Max. Press. (ATDC)	7º CA	8º CA	+1º
Max. Mean Temp. (K)	1504	1770	+266
NO_x (g/kW.h)	6.66	5.1	-23.42%
SOOT (g/kW.h)	0.00077	0.0022	-
CO (g/kW.h)	9.94	1.42	-85.7%
HC (g/kW.h)	35.21	4.11	-88.33%

When comparing the conditions without the process (D25NG50H25) to the condition with the WI-PI strategy applied (D25NG50H25-20PI-25WI75°C), the results show a 5.53% decrease in power, a 14% increase in BSFC, a 2.11% decrease in TE, a 0.4 bar improvement in MPRR, and a 31.64% decrease in NO_x (Table 5.31).

In Figure 5.56, the temperature and NO mass fraction distribution contours for the conditions with and without the process in Mode 1 are shown at a piston position of 10° CA ATDC. When examining these contours at this piston position, where the combustion temperatures start to rise, the application of the process has softened the temperature distributions and led to a reduction in NO mass fractions (Figure 5.56).

This is also supported by the improvements in NO_x and MPRR values as shown in Table 5.30 and Table 5.31. Figure 5.57 presents results on temperature and NO_x formation for the D25NG50H25 operating point at different piston positions.

Table 5.31 : Comparison of results with (20% PI - 25% WI 75°C - 20° CA BTDC SOWI) and without the WI process for D25NG50H25 (Mode 1).

	D25NG50H25	D25NG50H25-20PI-25WI75°C	Variation
Power (kW)	11.58	10.94	-5.53%
Torque (N.m)	121.47	114.84	-5.45%
BSFC (g/kW.h)	136.27	155.42	+14%
Ignition Delay (CA)	11º	11º	-
Thermal Efficiency (%)	38.71	36.60	-2.11%
Combustion Duration (CA)	19º	17º	-2º
MPRR (bar/CA)	3.6	3.2	-0.4
Max. Press. (bar)	67.45	69.36	-
CA for Max. Press. (ATDC)	8º CA	8º CA	-
Max. Mean Temp. (K)	1779	1770	-9
NO_x (g/kW.h)	7.46	5.1	-31.64%
SOOT (g/kW.h)	0.000172	0.0022	-
CO (g/kW.h)	1.42	1.42	-
HC (g/kW.h)	4.04	4.11	+1.73%

When observing the temperature distributions starting from Top Dead Center (TDC), it is evident that particularly in conditions with a high hydrogen fraction, temperatures rise to around 3000 K in certain regions of the cylinder.

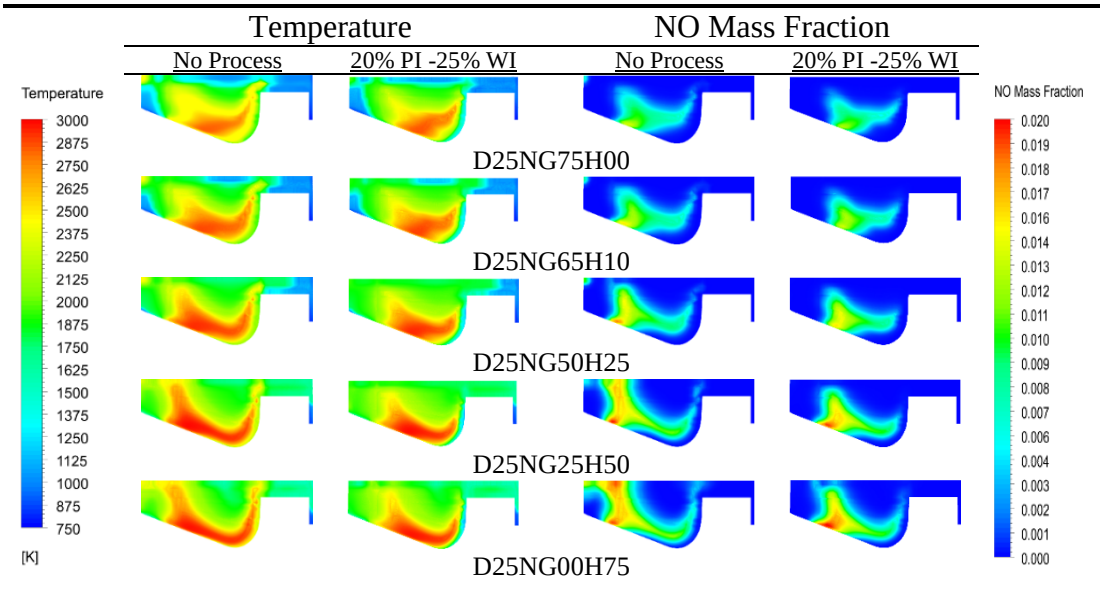

Figure 5.56 : Comparison of temperature and NO mass fraction contours at a piston position of 10° CA ATDC for operating points with applied (20% PI & 25% WI) and not applied process with different gas fuel fractions for Mode 1.

However, with the application of 20% PI and especially 25% WI, these very hot regions are reduced. Correspondingly, when tracking NO_x formation, a decrease in NO mass fraction density is observed (Figure 5.57). For Mode 2 (Hydrogen Enrichment Mode), numerical results with and without the process are compared for all hydrogen energy enrichment fractions, with only pilot injection (20% PI) applied, and with both pilot injection and water injection (20% PI & 25% WI) at a piston position of 10° CA BTDC, as well as with the experimental results (D25NG75H00) in Figure 58 to Figure 61.

Table 5.32 : Comparison between processed by the WI results (20% PI - 25% WI 75°C - 20° CA BTDC SOWI) for D25NG75H15 (Mode 2) and test result.

	D25NG75H00	D25NG75H15-20PI-25WI75°C	Variation
Power (kW)	9.76	12.72	+30.33%
Torque (N.m)	102.42	133.47	+30.32%
BSFC (g/kW.h)	203.85	173.14	~ -15%
Ignition Delay (CA)	11º	11º	-
Thermal Efficiency (%)	30.84	34.95	+4.11%
Combustion Duration (CA)	31º	22º	-9º
MPRR (bar/CA)	1.85	2.51	+0.66
Max. Press. (bar)	50.55	59.94	~ +9
CA for Max. Press. (ATDC)	9º CA	14º CA	+5º
Max. Mean Temp. (K)	1477	1793	+316
NO_x (g/kW.h)	4.9	4.07	~ -17%
SOOT (g/kW.h)	0.0012	0.00174	-45%
CO (g/kW.h)	10.25	2.1	-79.5%
HC (g/kW.h)	36.73	8.34	-77.29%

In the case of the test condition (D25NG75H00), the application of the process did not have a significant impact on power and BSFC values (Figure 5.58 and Figure 5.60). Only when the WI-PI combination was applied did BSFC show a tendency to increase to some extent. It can be said that for the working points with hydrogen present, there is an improvement in power and BSFC compared to the test conditions (D25NG75H00). However, similar values were obtained for the conditions with and without the process (Figure 5.58).

There doesn't appear to be any condition that significantly affects the ignition delay for Mode 2 (Figure 5.58). In Mode 1 conditions, the ignition delay remained stable, similar to the Mode 2 situation. However, stability in this context means that the ignition initiation is constant. To assess the rate, quality, and duration of combustion, it is necessary to look at the CD and MPRR values.

Table 5.33 : Comparison of results with (20% PI - 25% WI 75°C - 20° CA BTDC SOWI) and without the WI process for D25NG75H15 (Mode 2).

	D25NG75H15	D25NG75H15-20PI-25WI75°C	Variation
Power (kW)	13.28	12.72	-4.22%
Torque (N.m)	139.34	133.47	-4.21%
BSFC (g/kW.h)	155.99	173.14	+11%
Ignition Delay (CA)	11°	11°	-
Thermal Efficiency (%)	36.48	34.95	-1.53%
Combustion Duration (CA)	23°	22°	-1°
MPRR (bar/CA)	3.08	2.51	-0.57
Max. Press. (bar)	60.35	59.94	-
CA for Max. Press. (ATDC)	12° CA	14° CA	+2°
Max. Mean Temp. (K)	1809	1793	-16
NO_x (g/kW.h)	5.44	4.07	-25.18%
SOOT (g/kW.h)	0.0002	0.00174	-
CO (g/kW.h)	2.02	2.1	~ +4%
HC (g/kW.h)	8.76	8.34	-4.79%

Combustion duration, especially after 15% hydrogen enrichment fraction, showed a tendency to decrease, and MPRR values showed a tendency to increase. The application of 20% PI helped reduce MPRR to some extent (Figure 5.59 and Figure 5.61). Increased hydrogen enrichment fraction led to an increase in NO_x, especially with the WI strategy. When WI was applied, NO_x was controlled up to 20% hydrogen fraction, and it matched the experimental NO_x values (Figure 5.59). Indeed, the addition of hydrogen resulted in higher performance values while maintaining a smooth combustion characteristic. The increase in hydrogen enrichment fraction led to a decrease in CO and UHC emissions, similar to the trends observed in Mode 1 conditions. Importantly, under the same hydrogen enrichment fraction, the results between process and non-process conditions were very similar, as shown in Figure 5.58 and Figure 5.60. The addition of hydrogen as an extra energy input into the combustion chamber increased thermal efficiency (TE). Notably, under the same hydrogen enrichment fraction, the results in terms of TE were quite similar between process and non-process conditions, as shown in Figure 5.60. Additionally, in terms of particulate matter (PM) emissions, they were lowest in the non-process condition and exhibited a slight increase when PI was applied. The increasing trend continues with the WI application (Figure 5.61). However, it can be reduced with the increase in the hydrogen enrichment fraction. Although PM increases with the PI and WI strategies, the improvements obtained for NO_x and MPRR encourage us not to overlook this increase (Figure 5.59 and Figure 5.61).

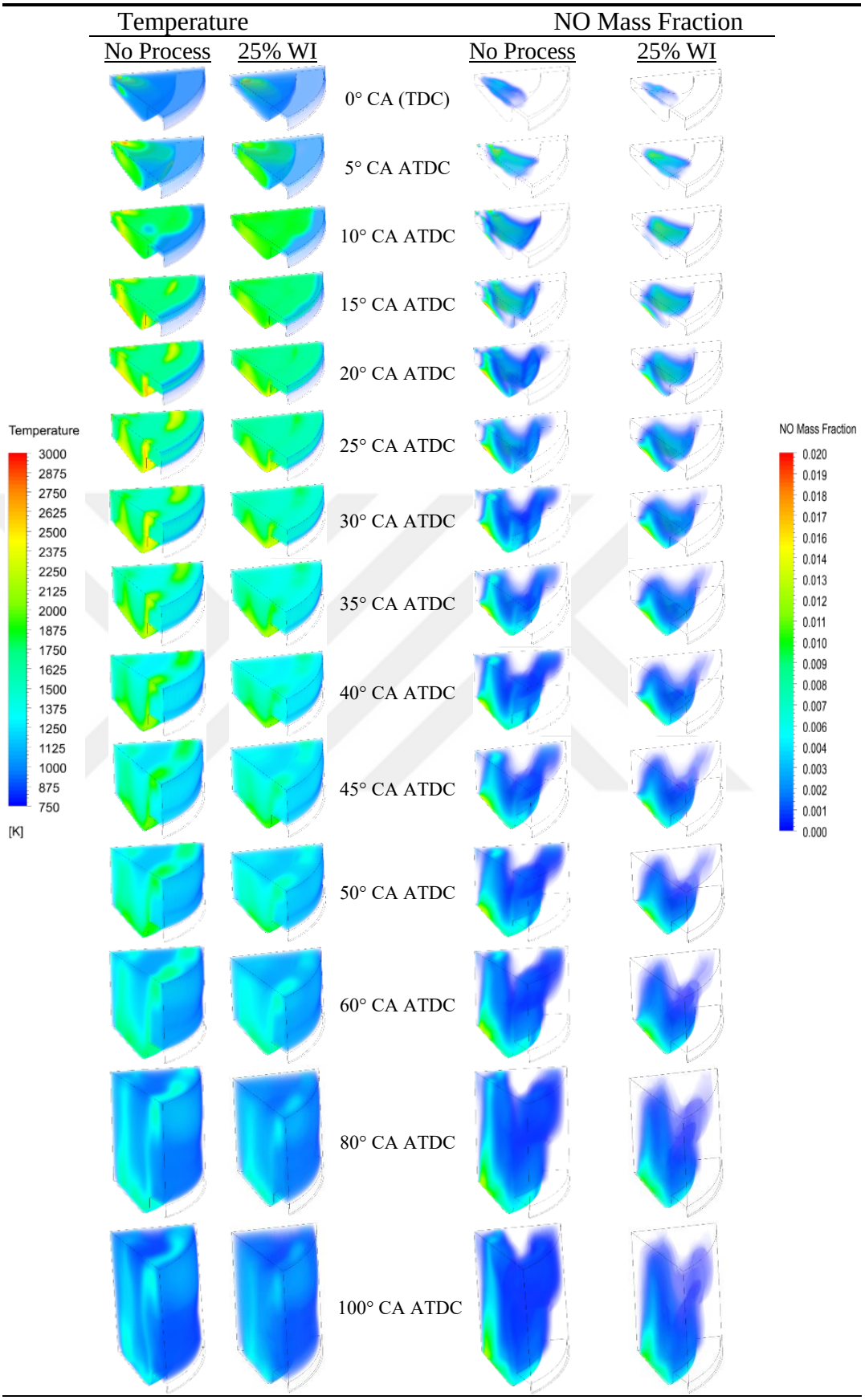

Figure 5.57 : Comparison of temperature and NO mass fraction contours at different piston positions for operating points with applied (20% PI & 25% WI) and not applied process for Mode 1 - D25NG50H25.

Table 5.34 : Comparison of results with and without the WI process for D25NG00H75.

	D25NG00H75	D25NG00H75-20PI-25WI75°C	Variation
Power (kW)	10.69	9.95	-6.92%
Torque (N.m)	112.18	104.44	-6.9%
BSFC (g/kW.h)	95.73	115.25	+20.39%
Ignition Delay (CA)	11º	12º	+1º
Thermal Efficiency (%)	35.75	33.28	-2.47%
Combustion Duration (CA)	9º	8º	-1º
MPRR (bar/CA)	8.35	10.11	+1.76
Max. Press. (bar)	85.89	85.49	-
CA for Max. Press. (ATDC)	4º CA	4º CA	-
Max. Mean Temp. (K)	1997	1989	-8
NO_x (g/kW.h)	14.04	9.23	-34.26%
SOOT (g/kW.h)	~ 0	0.0015	-
CO (g/kW.h)	0.0036	0.067	-
HC (g/kW.h)	0.0015	0.0106	-

When the experimental conditions (D25NG75H00 10° CA BTDC for SOI) are compared with the condition where the WI-PI processes were applied (D25NG75H15-20PI-25WI75°C), it is observed that there are improvements of 30.33% for power, 15% for BSFC, 4.11% for TE, 17% for NO_x, and 79.5% for CO and 77.29% for UHC. Only a 0.66-bar increase is observed for MPRR (Table 5.32). When comparing the condition without the process (D25NG75H15) with the condition where the WI-PI strategy was applied (D25NG75H15-20PI-25WI75°C), it is evident that there is a 4.22% decrease in power, an 11% increase in BSFC, a 1.53% decrease in TE, a 0.57-bar improvement in MPRR, and a 25.18% decrease in NO_x (Table 5.33).

Contour plots of temperature and NO mass fraction distribution for the process and processless operating points in Mode 2 are shown in Figure 5.62. The contours represent a condition with the piston at 10° CA ATDC. At this piston position, as the combustion temperatures start to rise, the application of the process has reduced temperature distributions and decreased NO mass fractions (Figure 5.62). The improvements in NO_x and MPRR values are already presented in Table 5.32 and Table 5.33. Figure 5.63 provides results regarding temperature and NO_x formation for the D25NG75H15 operating point at different piston positions. Starting from Top Dead Center (TDC), when observing temperature distributions, it can be seen that in conditions with a high hydrogen fraction, temperatures rise to around 3000 K in some areas of the cylinder. However, particularly with the application of 20% PI and 25%

WI, it is observed that the proportion of these very hot regions decreases. Simultaneously, while monitoring NO_x formation, a reduction in NO mass fraction is also observed (Figure 5.63).

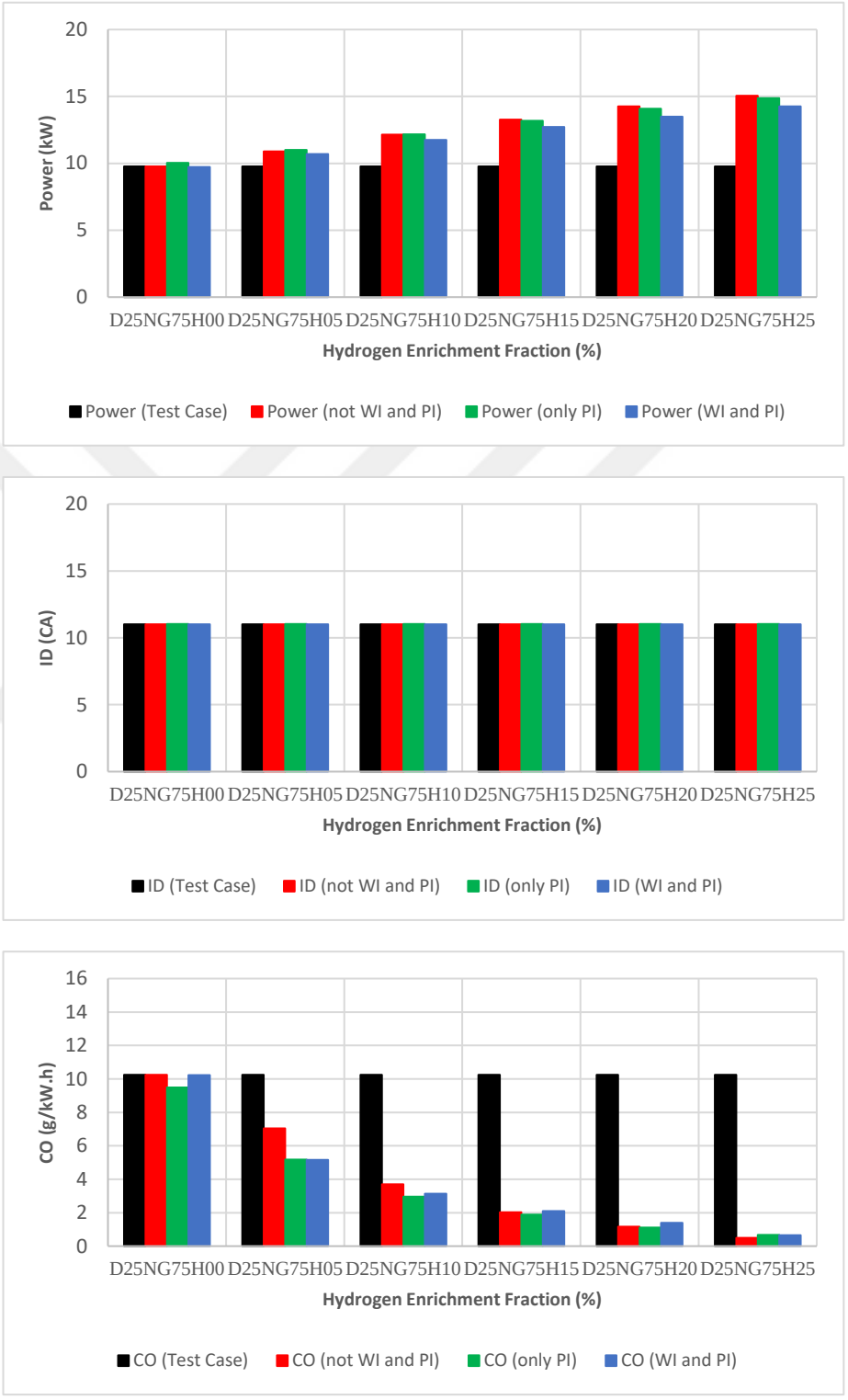

Figure 5.58 : Comparison of test result with the non-process, only PI (20% PI), and both PI and WI conditions (20% PI and 25% WI) in terms of power, ID, and CO emission for Mode 2.

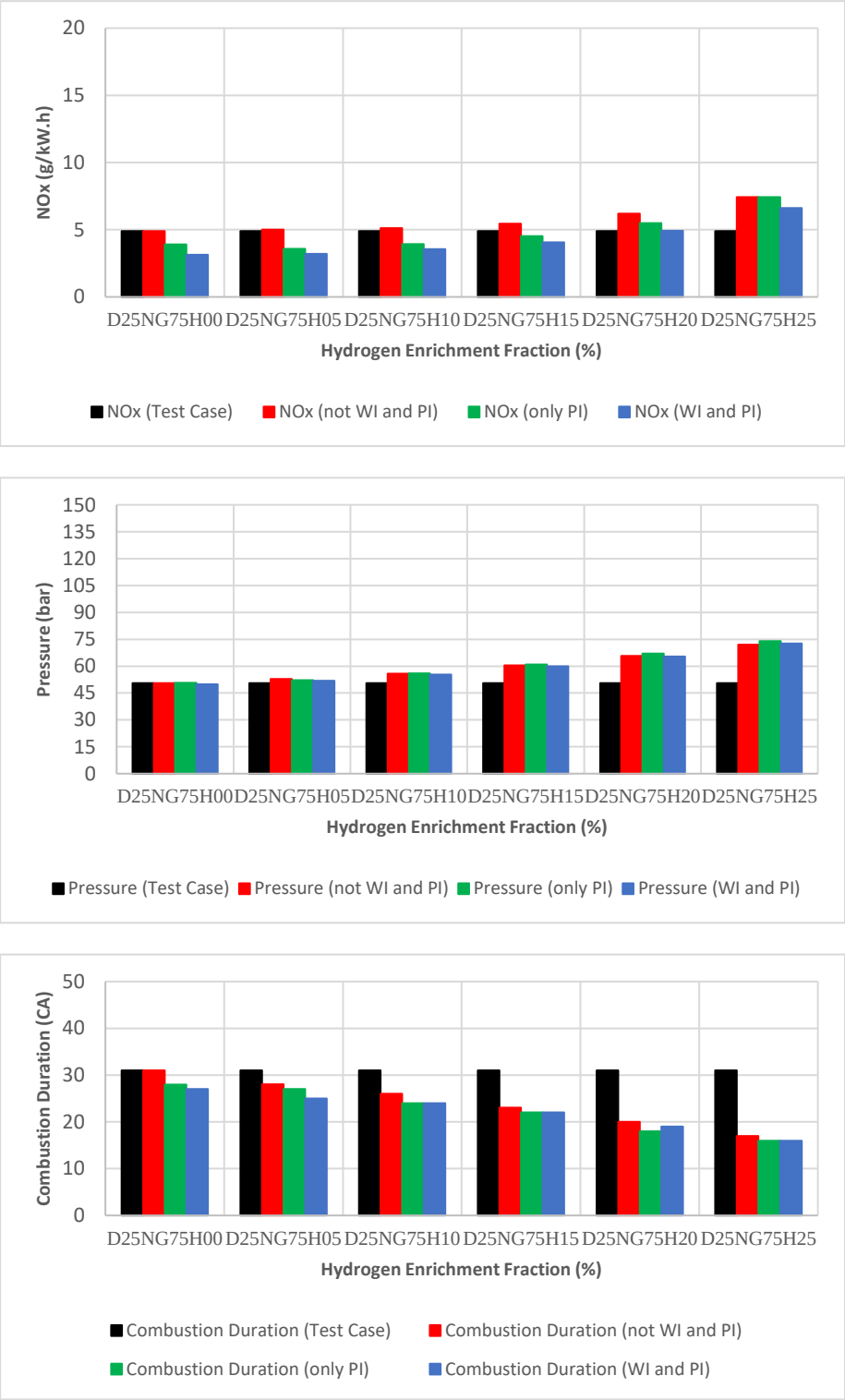

Figure 5.59 : Comparison of test result with the non-process, only PI (20% PI), and both PI and WI conditions (20% PI and 25% WI) in terms of NO_x emissions, Pressure and CD for Mode 2.

Table 5.34 provides the gains and losses when the maximum hydrogen content condition (D25NG00H75) for Mode 1 is subjected to the application of the PI-WI combination. If 20% PI and 25% WI are applied at 75°C, the results show a 6.92%

power loss, a 20.39% increase in BSFC, a 2.47% decrease in TE, a 1.76 bar increase in MPRR, and a 34.26% improvement in NO_x (Table 5.34).

Table 5.35 : Comparison of results with and without the WI process for D25NG75H25.

	D25NG75H25	D25NG75H25-20PI-25WI75°C	Variation
Power (kW)	15.05	14.26	-5.25%
Torque (N.m)	157.92	149.67	-5.22%
BSFC (g/kW.h)	141.09	158.06	~ +12%
Ignition Delay (CA)	11º	11º	-
Thermal Efficiency (%)	38.04	36.05	-2%
Combustion Duration (CA)	17º	16º	-1º
MPRR (bar/CA)	4.62	4.58	-0.04
Max. Press. (bar)	71.94	72.59	-
CA for Max. Press. (ATDC)	12º CA	12º CA	-
Max. Mean Temp. (K)	2057	2030	-27
NO_x (g/kW.h)	7.43	6.62	-11%
SOOT (g/kW.h)	0.00015	0.00115	-
CO (g/kW.h)	0.49	0.65	+32.65%
HC (g/kW.h)	2.36	2.43	+3%

It is evident from these results that the applied processes have been highly effective for NO_x and MPRR. However, an MPRR value of 10.11 bar/CA indicates that the presence of hydrogen in the gas fuel causes a tendency for knock-prone combustion. Table 5.35 provides the gains and losses when the condition with the maximum hydrogen content (D25NG75H25) for Mode 2 is subjected to the application of the PI-WI combination. If 20% PI and 25% WI are applied at 75°C, the results show a 5.25% power loss, a 12% increase in BSFC, a 2% decrease in TE, and an 11% improvement in NO_x (Table 5.35). The MPRR value is the same for both process and non-process conditions, at approximately 4.6 bar/CA, making it a desirable value. While there is a 5.25% decrease in power when comparing process and non-process conditions, there is a significant advantage of a 46% power increase compared to the experimental results.

It is observed that achieving high hydrogen values with PI-WI is possible in Mode 2. Table 5.36 provides the answer to the question of what happens when the PI-WI strategies are applied to the operating point with a main injection advance of 14° CA BTDC (D25NG75H00 14° CA BTDC for SOI). If 20% PI and 25% WI are applied at 75°C, the results show a 2.77% increase in power, a 9.64% increase in BSFC, a 0.88% decrease in TE, a 0.25-bar decrease in MPRR, a 37% improvement in NO_x, and a 13%

reduction in CO and a 10.5% reduction in UHC (Table 5.36). Both performance and emissions are brought to more desirable levels.

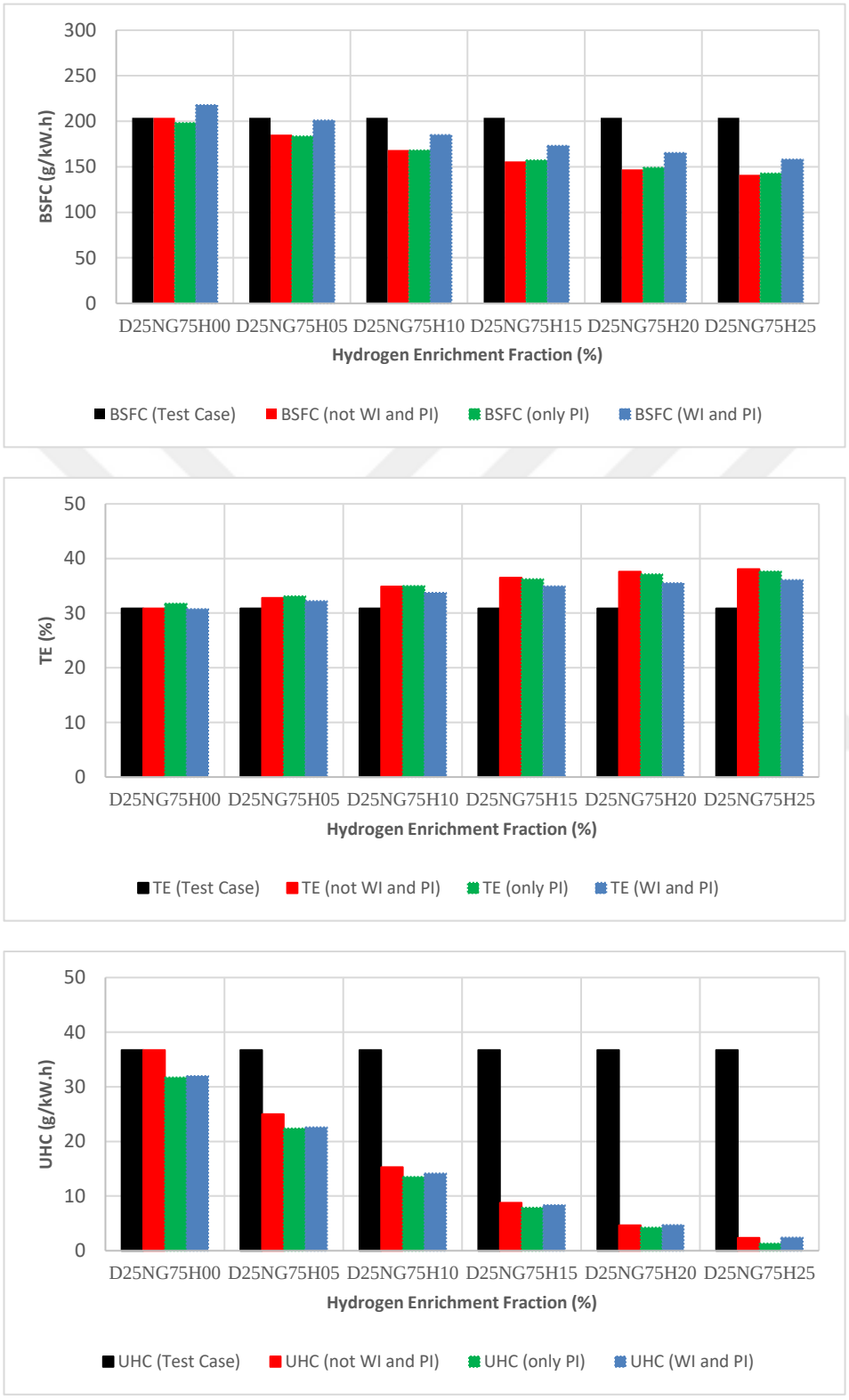

Figure 5.60 : Comparison of test result with the non-process, only PI (20% PI), and both PI and WI conditions (20% PI and 25% WI) in terms of BSFC, TE and UHC emission for Mode 2.

Table 5.36 : Comparison of test and processed by WI results for the operating point of D25NG75H00 (14° CA BTDC SOI).

	D25NG75H00	D25NG75H00-20PI-25WI75°C	Variation
Power (kW)	9.575	9.31	-2.77%
Torque (N.m)	100.477	97.71	-2.75%
BSFC (g/kW.h)	196	214.9	+9.64%
Ignition Delay (CA)	11º	11º	-
Thermal Efficiency (%)	32.02	31.14	-0.88%
Combustion Duration (CA)	27º	23º	-4º
MPRR (bar/CA)	2.66	2.41	-0.25
Max. Press. (bar)	57.25	57.83	-
CA for Max. Press. (ATDC)	7º CA	9º CA	+2º
Max. Mean Temp. (K)	1504	1528	+24
NO_x (g/kW.h)	6.66	4.2	-37%
SOOT (g/kW.h)	0.00077	0.0041	-
CO (g/kW.h)	9.94	8.63	~ -13%
HC (g/kW.h)	35.21	31.5	-10.5%

In a similar situation for test condition with a main injection advance of 10° CA BTDC, the results are as follows: a 0.31% decrease in power, a 6.93% increase in BSFC, a 0.35-bar decrease in MPRR, a 36% improvement in NO_x, and a 13% reduction in HC (Table 5.37). It is easier to control performance and emissions when hydrogen is not included in the gas fuels in the combustion chamber (Test Conditions). The introduction of hydrogen into the combustion chamber triggers a harsh combustion characteristic, leading to an increase in MPRR and NO_x and a decrease in CD.

Table 5.37 : Comparison of test and processed by WI results for the operating point of D25NG75H00 (10° CA BTDC SOI).

	D25NG75H00	D25NG75H00-20PI-25WI75°C	Variation
Power (kW)	9.76	9.73	-0.31%
Torque (N.m)	102.42	102.104	-0.31%
BSFC (g/kW.h)	203.85	217.97	+6.93%
Ignition Delay (CA)	11º	11º	-
Thermal Efficiency (%)	30.84	30.74	-
Combustion Duration (CA)	31º	27º	-4º
MPRR (bar/CA)	1.85	1.5	-0.35
Max. Press. (bar)	50.55	49.89	-
CA for Max. Press. (ATDC)	9º CA	12º CA	+3º
Max. Mean Temp. (K)	1477	1493	+16
NO_x (g/kW.h)	4.9	3.14	-36%
SOOT (g/kW.h)	0.0012	0.0035	-
CO (g/kW.h)	10.25	10.23	-
HC (g/kW.h)	36.73	32	~ -13%

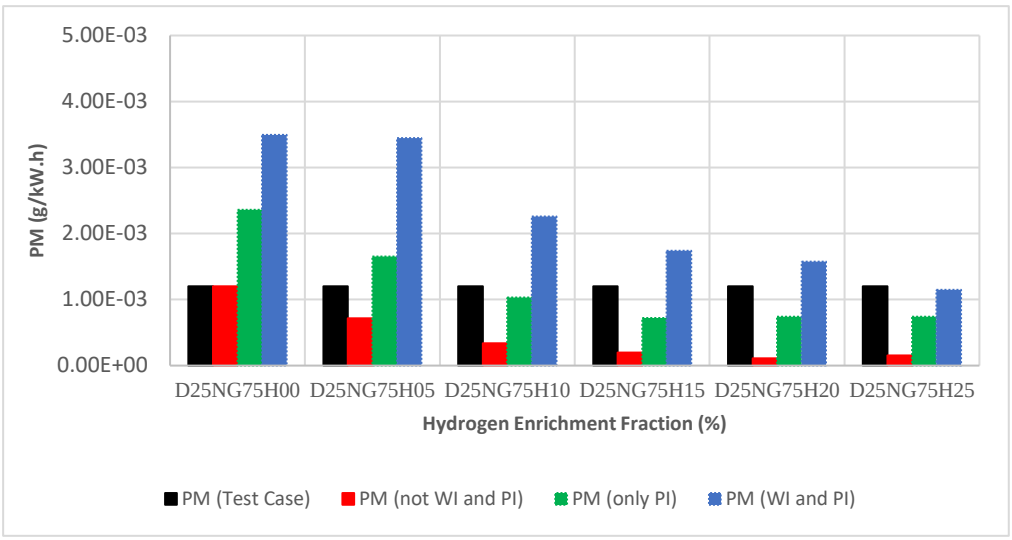

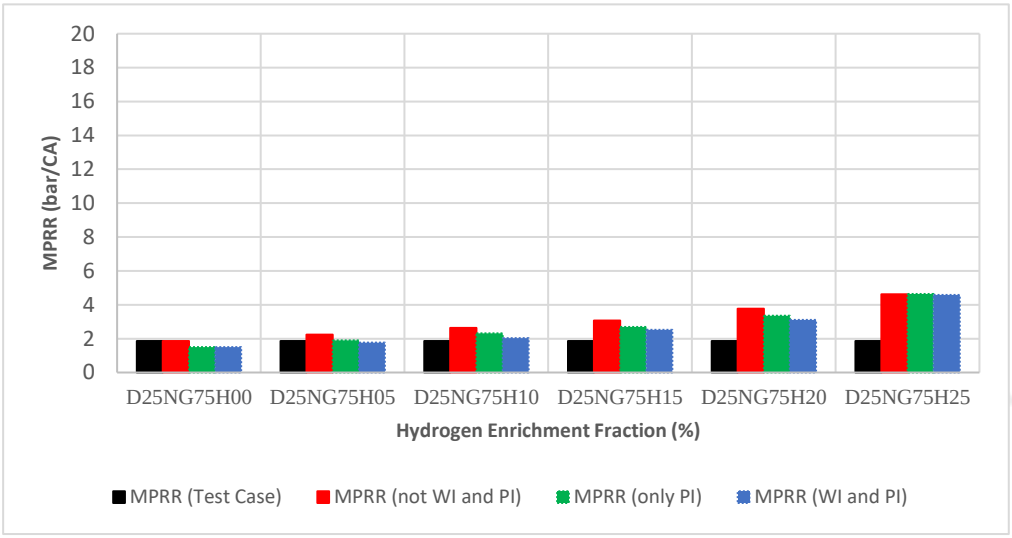

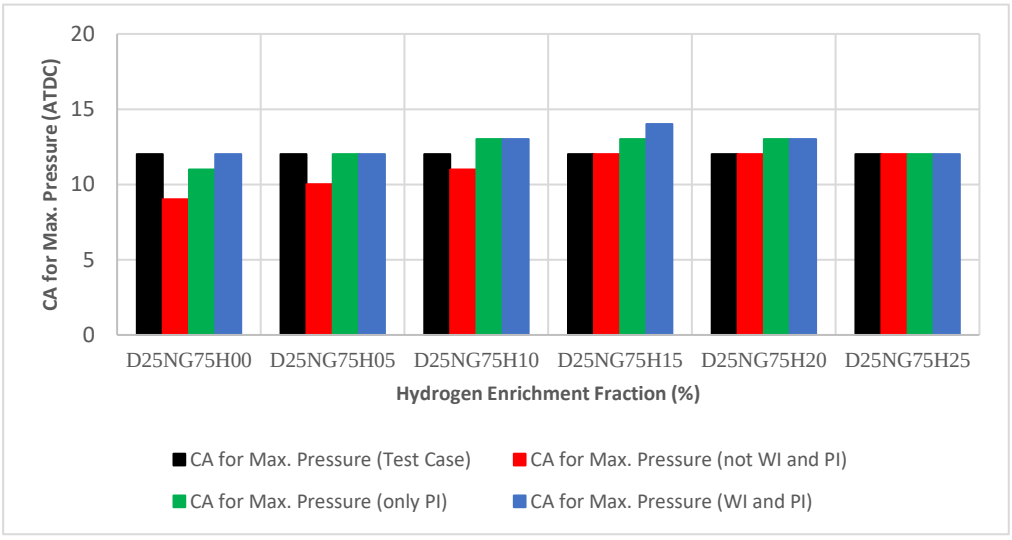

Figure 5.61 : Comparison of test result with the non-process, only PI (20% PI), and both PI and WI conditions (20% PI and 25% WI) in terms of PM emission, MPRR and the position of Max. Press. Relative to TDC for Mode 2.

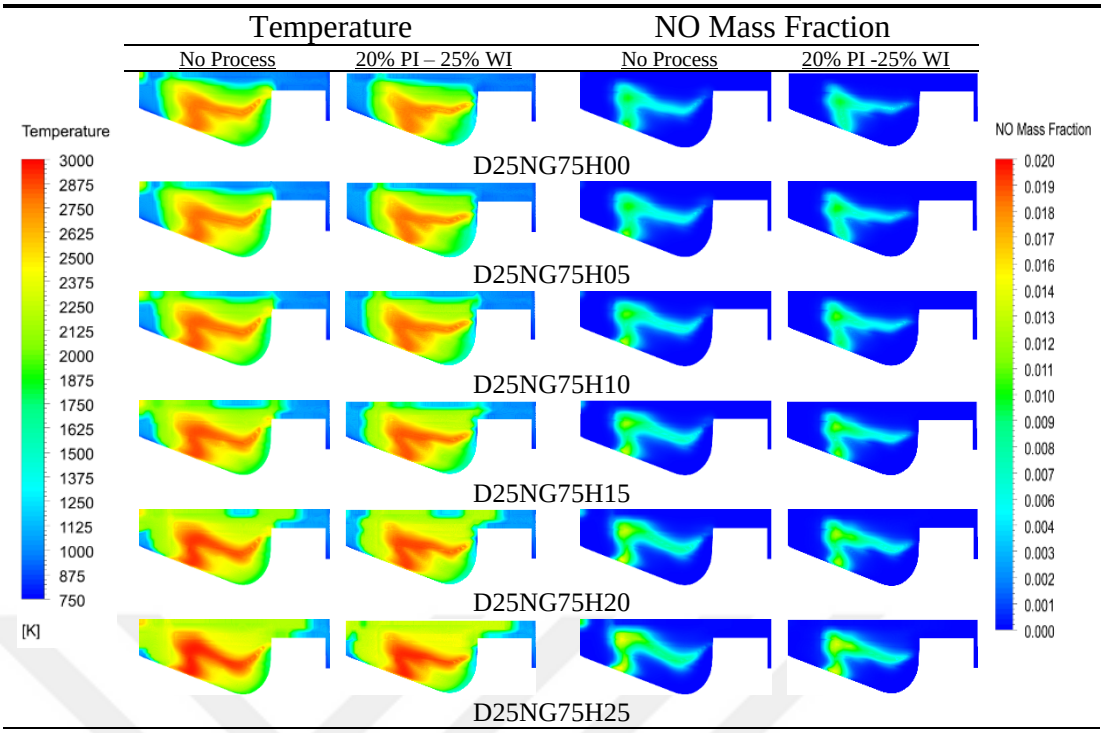

Figure 5.62 : Comparison of temperature and NO mass fraction contours at a piston position of 10° CA ATDC for operating points with applied (20% PI & 25% WI) and not applied process with different hydrogen enriching fractions for Mode 2.

Although the performance values may appear to be improving, the presence of knocking tendencies negates the advantage of increased power. Therefore, an arduous optimization process begins with the aim of establishing a performance-emission balance using the WI-PI strategy for both Mode 1 and Mode 2.

Table 5.38 : Comparison of the optimal results obtained by applying the WI process for Mode 1 and Mode 2.

	20% PI – 25% WI 75°C – 20° CA BTDC SOWI		
	D25NG50H25	D25NG75H15	Variation
Power (kW)	10.94	12.72	+16.27%
Torque (N.m)	114.84	133.47	+16.22%
BSFC (g/kW.h)	155.42	173.14	+11.4%
Ignition Delay (CA)	11°	11°	-
Thermal Efficiency (%)	36.60	34.95	-1.65%
Combustion Duration (CA)	17°	22°	+5°
MPRR (bar/CA)	3.2	2.51	-0.69
Max. Press. (bar)	69.36	59.94	~ -10
CA for Max. Press. (ATDC)	8° CA	14° CA	+6°
Max. Mean Temp. (K)	1770	1793	+23
NO_x (g/kW.h)	5.1	4.07	-20.2%
SOOT (g/kW.h)	0.0022	0.00174	-21%
CO (g/kW.h)	1.42	2.1	-47.89%
HC (g/kW.h)	4.11	8.34	-

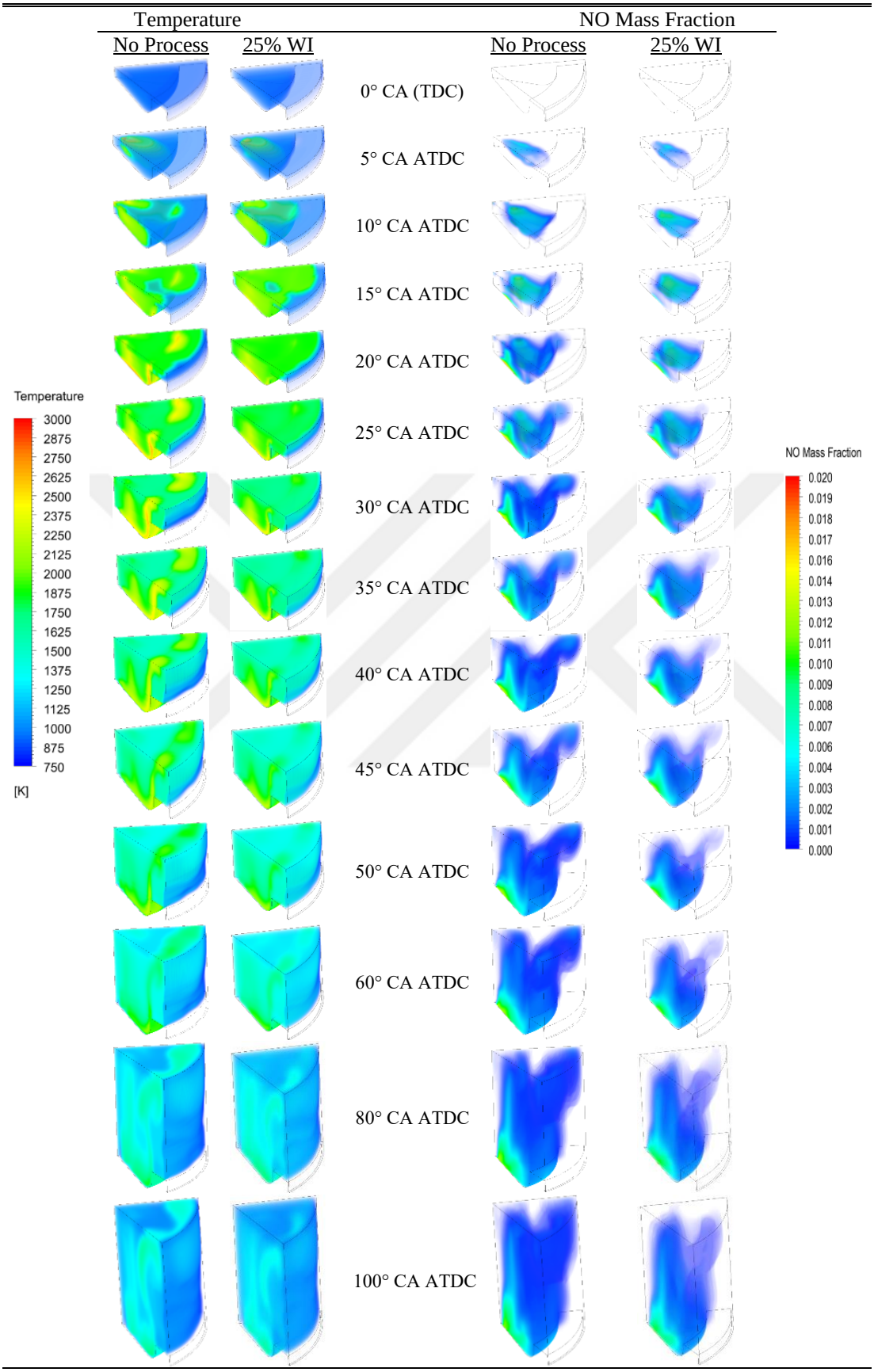

Figure 5.63 : Comparison of temperature and NO mass fraction contours at different piston positions for operating points with applied (20% PI & 25% WI) and not applied process for Mode 2 - D25NG75H15.

Mode 1, containing a relatively higher hydrogen fraction compared to Mode 2, makes MPRR and NO_x control more challenging for Mode 1. When a comparison is made between the most optimal conditions achieved for Mode 1 and Mode 2 with the application of the process, these situations are observed (Table 5.38).

For Mode 2, it is observed that there is 16.27% more power, 11.4% higher BSFC, 1.65% lower TE, 5° CA longer CD, 0.69 bar lower MPRR, 10 bar lower in-cylinder pressure, 20.2% lower NO_x, 21% lower PM, and 47.89% lower CO (Table 5.38). For Mode 1, achieving higher performance and lower emissions while preserving the total fuel energy is easier at lower hydrogen fractions.

Similarly, for Mode 2, to achieve more efficient combustion with extra hydrogen input into the cylinder and attain higher performance and lower emissions, the hydrogen amount should not be increased significantly. In this regard, the assistance of the WI-PI combination is of significant importance in accelerating the achievement of these goals. This has been clearly demonstrated through numerical simulations.

5.3.3 General summary for WI – PI strategy

The analysis began with D25NG50H25 for Mode 1, which is the gaseous fuel energy sharing mode, and D25NG75H15 for Mode 2, which is the hydrogen enrichment mode. From these analyses, the study was expanded by considering the effects of different gaseous fuel fractions on the diesel fuel pilot injection rate (20% PI) with the optimum water jet ratio (25% WI) and water jet temperature (75°C) obtained from these analyses. The aim here is to demonstrate that more hydrogen can be introduced into the system with the application of WI-PI. When the results of the WI-PI study are generally evaluated, it has been shown that it successfully achieves lower NO_x and MPRR values compared to non-process operating points. In the test conditions (D25NG75H00), there is no hydrogen in the gas fuel mixture. The introduction of hydrogen into the combustion chamber as an alternative fuel led to improvements in performance parameters (except MPRR) and emission reductions (except for NO_x). It is crucial to improve the parameters that were not achieved and are of utmost importance to engine combustion. Thus, in this context, just as in the previous section (Chapter 5.2) measures were taken for reducing NO_x using EGR and for reducing MPRR using PI, in this section (Chapter 5.3), measures were taken again for NO_x using WI and for MPRR using PI. By combining these two strategies at different operating

points, the unattainable NO_x and MPRR improvements were achieved in performance and emissions compared to the initial study (Chapter 5.1).

For Mode 1, while maintaining the same lower heating value of the fuel, the WI-PI combination contributed to achieving higher performance and lower overall emissions. When compared to the test results (D25NG75H00 14° CA BTDC for SOI) with the optimum condition for WI-PI application in Mode 1 (D25NG50H25-20PI-25WI75°C), it was observed that there was a 14.26% improvement in power, 20.7% improvement in BSFC, 4.58% improvement in TE, a 23.42% reduction in NO_x, an 85.7% reduction in CO, and an 88.33% reduction in UHC. Compared to the non-process condition (D25NG50H25), the WI-PI combination condition (D25NG50H25-20PI-25WI75°C) resulted in a 0.4 bar decrease in MPRR and a 31.64% reduction in NO_x.

In the case of Mode 2, the significant contribution of the WI-PI combination to achieve the goal of higher efficiency, higher performance values, and lower overall emissions by introducing extra hydrogen into the combustion chamber is evident. When compared to the test results (D25NG75H00 10° CA BTDC for SOI) with the optimum condition for WI-PI application in Mode 2 (D25NG75H15-20PI-25WI75°C), a 30.33% improvement in power, 15% improvement in BSFC, 4.11% improvement in TE, a 17% reduction in NO_x, a 79.5% reduction in CO, and a 77.29% reduction in UHC were achieved. Compared to the non-process condition (D25NG75H15), the WI-PI combination condition (D25NG75H15-20PI-25WI75°C) resulted in a 0.57 bar decrease in MPRR and a 25.18% reduction in NO_x. After examining the effect of water injection in this section, the effects of introducing water in vapor phase into the combustion chamber will be analyzed. The advantages and disadvantages of injection in both liquid and vapor phases will be discussed in detail in the following section (Chapter 5.4).

5.4 WVI – PI Strategies

In the previous section, the effects of the combination of water jet injection and pilot diesel fuel injection on performance and emission values were examined. In this section, numerical studies were conducted by introducing water into the combustion chamber in vapor phase. As mentioned earlier, the literature recommends EGR and water injection, particularly for NO_x reduction.

Table 5.39 : Case matrix for WVI and PI processes.

Mode 1		Mode 2	
0% PI – 20° CA BTDC SOWVI 100°C		0% PI – 20° CA BTDC SOWVI 100°C	
WV - 0%	D25NG50H25	WV - 0%	D25NG75H15
WV - 5%	D25NG50H25	WV - 5%	D25NG75H15
WV - 10%	D25NG50H25	WV - 10%	D25NG75H15
WV - 15%	D25NG50H25	WV - 15%	D25NG75H15
WV - 20%	D25NG50H25	WV - 20%	D25NG75H15
WV - 25%	D25NG50H25	WV - 25%	D25NG75H15
0% PI – 15% WVI 20° CA BTDC SOWVI		0% PI – 15% WVI 20° CA BTDC SOWVI	
WV - 100°C	D25NG50H25	WV - 100°C	D25NG75H15
WV - 125°C	D25NG50H25	WV - 125°C	D25NG75H15
WV - 150°C	D25NG50H25	WV - 150°C	D25NG75H15
WV - 200°C	D25NG50H25	WV - 200°C	D25NG75H15
20% PI – 15% WVI 20° CA BTDC SOWVI		20% PI – 15% WVI 20° CA BTDC SOWVI	
WV - 100°C	D25NG50H25	WV - 100°C	D25NG75H15
WV - 125°C	D25NG50H25	WV - 125°C	D25NG75H15
WV - 150°C	D25NG50H25	WV - 150°C	D25NG75H15
WV - 200°C	D25NG50H25	WV - 200°C	D25NG75H15
20% PI – 15% WVI 100°C		20% PI – 15% WVI 100°C	
20 CA BTDC SOWI	D25NG50H25	20 CA BTDC SOWI	D25NG75H15
10 CA BTDC SOWI	D25NG50H25	10 CA BTDC SOWI	D25NG75H15
0 CA BTDC SOWI	D25NG50H25	0 CA BTDC SOWI	D25NG75H15
10 CA ATDC SOWI	D25NG50H25	10 CA ATDC SOWI	D25NG75H15
20% PI-15% WVI 20° CA BTDC SOWVI 100°C		20% PI-15% WVI 20° CA BTDC SOWVI 100°C	
D25NG75H00		D25NG75H00	
D25NG65H10		D25NG75H05	
D25NG50H25		D25NG75H10	
D25NG25H50		D25NG75H15	
D25NG00H75		D25NG75H20	
-		D25NG75H25	
0% PI – 0% WVI		0% PI – 0% WVI	
D25NG75H00		D25NG75H00	
D25NG65H10		D25NG75H05	
D25NG50H25		D25NG75H10	
D25NG25H50		D25NG75H15	
D25NG00H75		D25NG75H20	
-		D25NG75H25	
20% PI – 0% WVI		20% PI – 0% WVI	
D25NG75H00		D25NG75H00	
D25NG65H10		D25NG75H05	
D25NG50H25		D25NG75H10	
D25NG25H50		D25NG75H15	
D25NG00H75		D25NG75H20	
-		D25NG75H25	

Studies involving the injection of water vapor have shown that NO_x emissions can be reduced, and reasonable performance results can be achieved. Research involving water vapor injection and the simultaneous examination of various engine parameters

(EGR, Compression Ratio, Injection Strategies, etc.) is intensively conducted to investigate NO_x and MPRR values [187,191–196].

In this section of the thesis, water vapor injection (WVI) into the combustion chamber, especially in combination with pilot diesel fuel injection (PI) strategy, has been applied to control increased NO_x emissions and MPRR values in the combustion of a high lower heating value fuel such as hydrogen, known for its fast combustion characteristics. The combination of these two strategies, referred to as WVI - PI, has led to improvements in performance and emission characteristics. The optimum pilot injection rate obtained in the previous section (Chapter 5.2), which is 20%, was also used in this study. Within the scope of the study, two different operating modes, Mode 1 and Mode 2, which were previously described in detail in Chapter 5.1, were considered. For Mode 1, the optimal condition was Case 18 (D25NG50H25 - SOI at 14° CA BTDC), and for Mode 2, the optimal condition was Case 57 (D25NG75H15 - SOI at 10° CA BTDC). Analyses of WVI were conducted at these operating points, similar to the analysis of EGR and water jet injections (WI).

For water vapor injection (WVI), the ratios used for water jet injection (WI) in the previous section (0%, 5%, 10%, 15%, 20%, and 25%) have been determined. The amount of injected water vapor has been calculated as a percentage of the mass of the injected diesel fuel. The optimal 20% ratio obtained for pilot injection in previous sections was used. Furthermore, the timing and injection duration of the pilot injection process are valid in this study, with a 2.5° CA duration in the range of 40° CA BTDC to 37.5° CA BTDC.

In this study, different water vapor temperatures (100°C, 125°C, 150°C, and 200°C) and different water vapor injection timings (20° CA BTDC, 10° CA BTDC, 0° CA BTDC - TDC, and 10° CA ATDC for SOI) were examined. All of these analyses are shown in Table 5.39 for both Mode 1 and Mode 2. Additionally, the analysis stages for different gas fuel fractions (gas fuel energy sharing - hydrogen enrichment) are also included in the table.

5.4.1 Optimal condition determination in the WVI – PI co-work

The conditions for water jet injection (WI) analysis have been explored within the scope of the analysis for water vapor injection (WVI). The comparison of the results of vapor and water jet conditions is presented in the next section (Chapter 5.5).

Initially, the analysis for different water vapor ratios aimed to find a reasonable water vapor ratio.

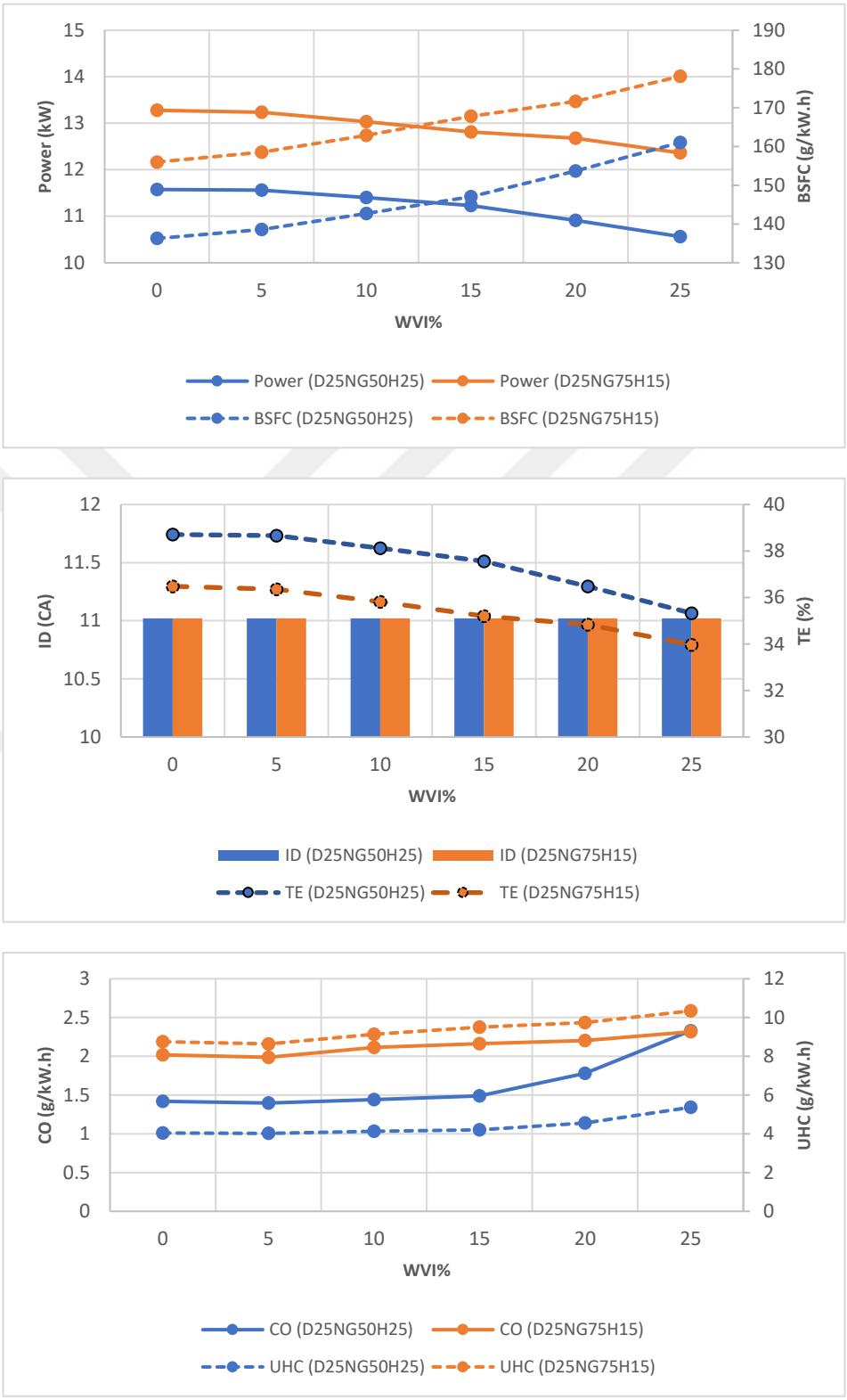

Figure 5.64 : The effect of increasing the WVI rate without PI on power, BSFC, ID, TE, CO, and UHC values.

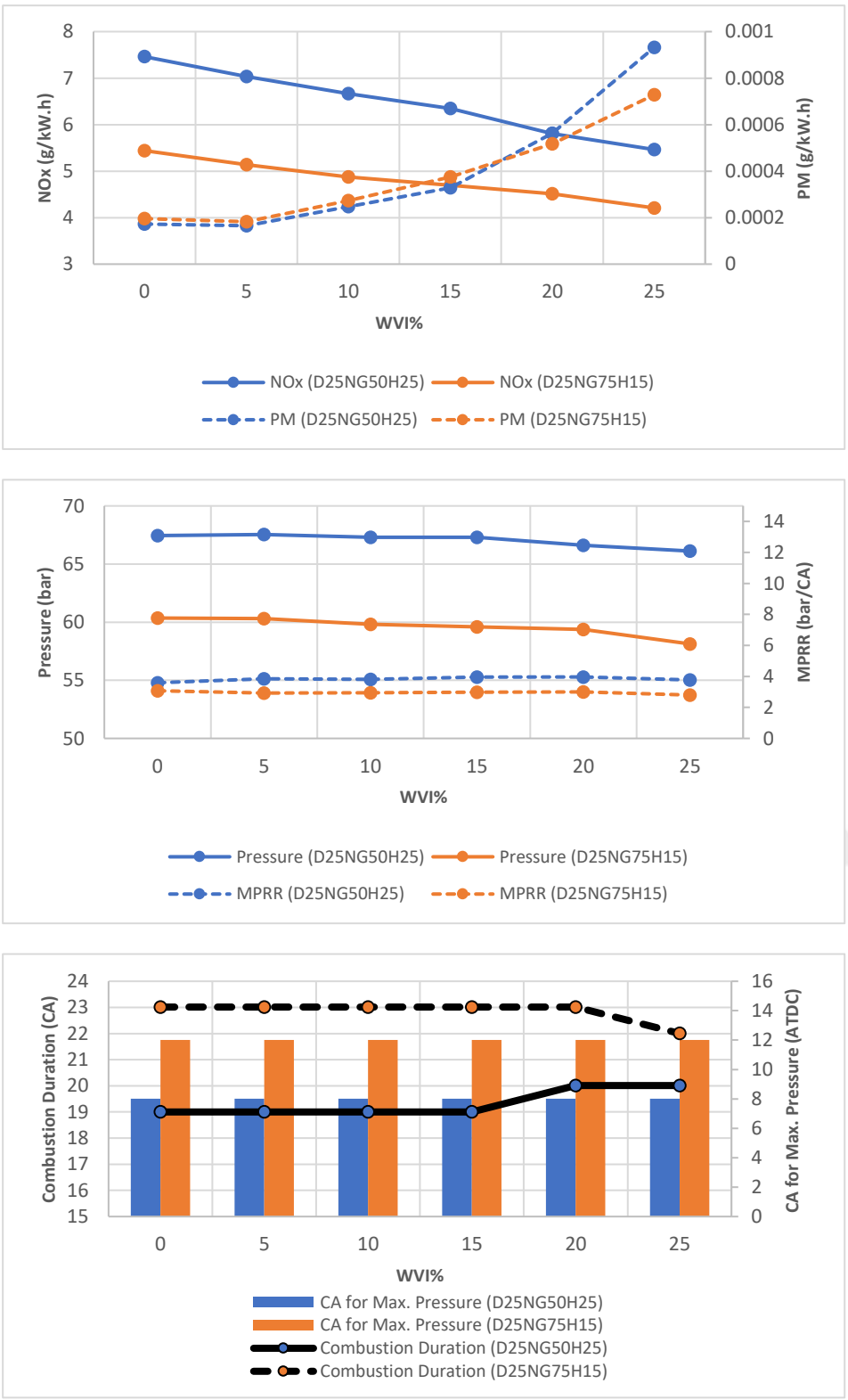

Figure 5.65 : The effect of increasing the WVI rate without PI on NO_x, PM, Pressure, MPRR, CD, and the position of Max. Press. Relative to TDC.

For these analyses, a water vapor temperature of 100°C was used. Six different water vapor ratios (0%, 5%, 10%, 15%, 20%, and 25%) were examined for Mode 1 and Mode 2 cases based on the optimal gas fraction points obtained from previous studies

(Mode 1 - D25NG50H25, 14° CA BTDC for SOI & Mode 2 - D25NG75H15, 10° CA BTDC for SOI) (Table 5.39). In the analyses conducted without pilot injection (0% PI), the start of water vapor injection (SOWVI) was set to 20° CA BTDC.

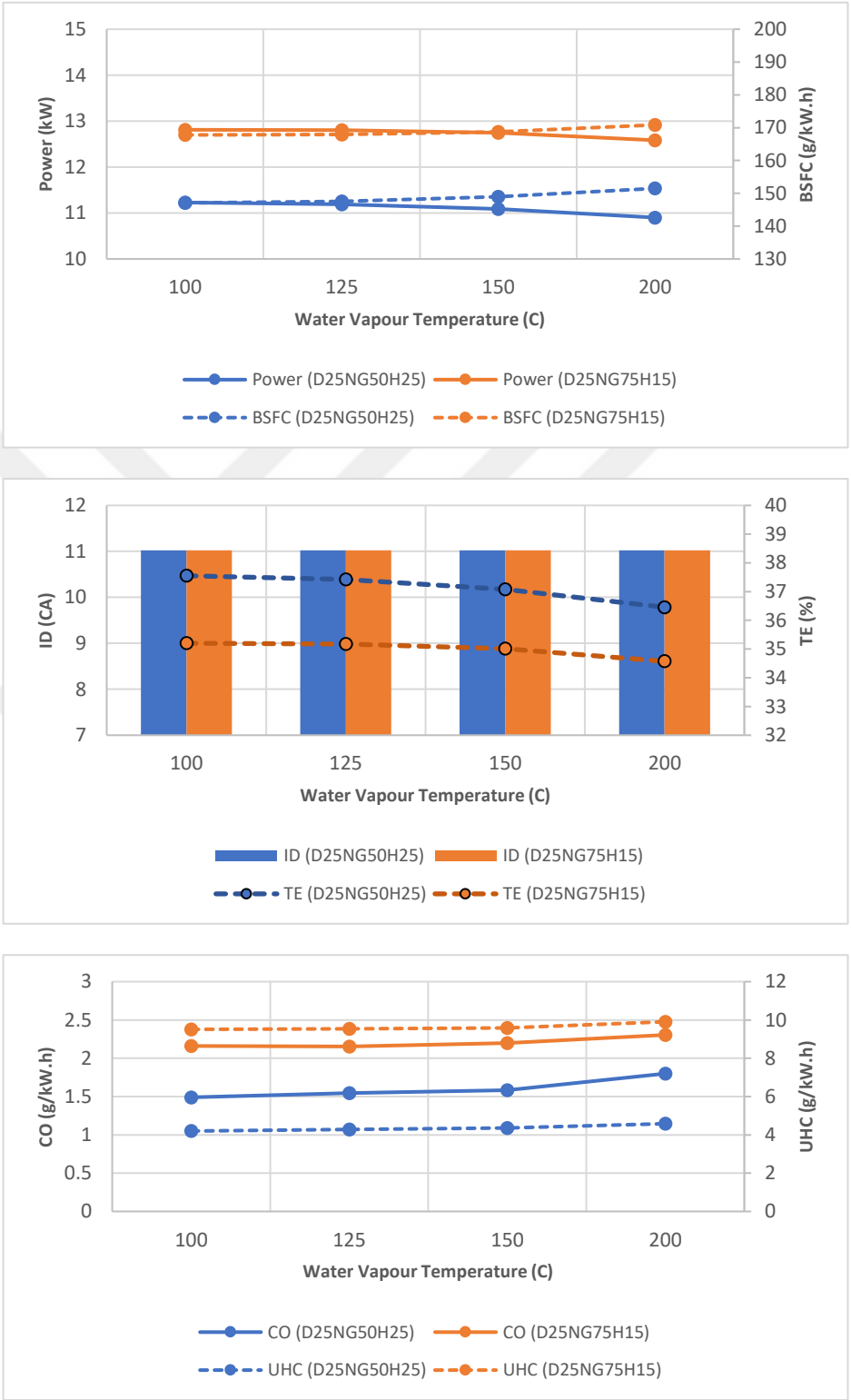

Figure 5.66 : The effect of increasing the WVI temperature at fixed the WVI rate (15% WI) without PI (0% PI) on power, BSFC, ID, TE, CO, and UHC values.

The goal here was to both examine the effects of water vapor injection and determine the water vapor ratio that provides reasonable results. Numerical results have shown that a 15% WVI ratio is preferable.

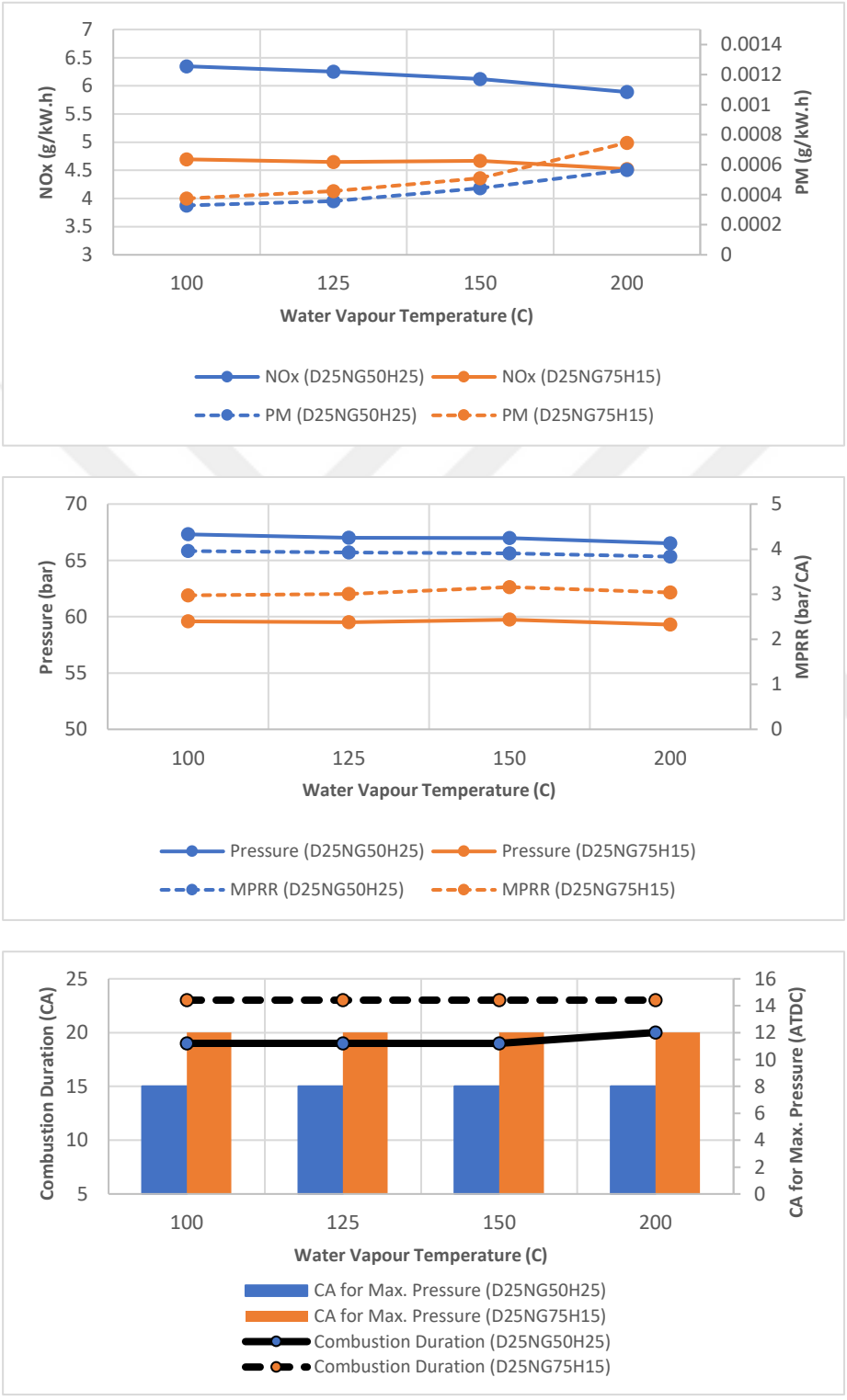

Figure 5.67 : The effect of increasing the WVI temperature at fixed the WVI rate (15% WI) without PI (0% PI) on NO_x, PM, Pressure, MPRR, CD, and the position of Max. Press. Relative to TDC.

Table 5.40 : Results of different WVI temperatures for Mode 1 under constant WVI rate (15% WVI) and injection advance (20° CA BTDC SOWVI), with and without PI.

	15% WVI – 20° CA BTDC SOWVI – D25NG50H25 (Mode 1)							
	100°C		125°C		150°C		200°C	
	PI		PI		PI		PI	
	0%	20%	0%	20%	0%	20%	0%	20%
Power (kW)	11.23	11.24	11.19	11.20	11.09	11.15	10.90	11.06
Torque (N.m)	117.83	117.94	117.44	117.57	116.34	116.97	114.39	116.09
BSFC (g/kW.h)	147.07	146.94	147.58	147.40	148.97	148.16	151.50	149.28
Ignition Delay (CA)	11º	11º	11º	11º	11º	11º	11º	11º
Thermal Efficiency (%)	37.55	37.59	37.43	37.47	37.07	37.28	36.46	37
Combustion Duration (CA)	19º	16º	19º	16º	19º	15º	20º	15º
MPRR (bar/CA)	3.96	3.37	3.93	3.37	3.91	3.48	3.83	3.41
Max. Press. (bar)	67.31	70.46	67.01	70.49	66.97	70.31	66.51	70.43
CA for Max. Press. (ATDC)	8º CA	8º CA	8º CA	8º CA	8º CA	8º CA	8º CA	8º CA
Max. Mean Temp. (K)	1754	1811	1747	1808	1741	1800	1719	1800
NO_x (g/kW.h)	6.35	5.69	6.25	5.69	6.12	5.67	5.89	5.67
SOOT (g/kW.h)	0.00033	0.00131	0.00036	0.0016	0.00044	0.0018	0.00057	0.0020
CO (g/kW.h)	1.49	1.19	1.55	1.20	1.58	1.27	1.8	1.34
HC (g/kW.h)	4.2	3.83	4.29	3.86	4.36	3.90	4.58	3.94

Subsequently, the effects of different water vapor temperatures (100°C, 125°C, 150°C, and 200°C) were investigated using a 15% WVI ratio (Table 5.39). In the examination of vapor temperature, two different branches were analyzed: without pilot diesel fuel injection (0% PI) and with pilot diesel fuel injection (20% PI). The results indicated that a 100°C vapor temperature had a more positive impact on performance and emission values. Up to this stage, an SOWVI value of 20° CA BTDC was used. Different SOWVI values (20° CA BTDC, 10° CA BTDC, 0° CA BTDC - TDC, and 10° CA ATDC) were examined to determine the appropriate timing for water vapor injection (Table 5.39).

The findings indicated that 20° CA BTDC is the appropriate timing to continue with. Finally, all the obtained optimal values were applied to different gas fuel fraction points (Table 5.39). With increasing WVI, the power decreased, and the BSFC increased for both Mode 1 (D25NG50H25, 14° CA BTDC for SOI) and Mode 2 (D25NG75H15, 10° CA BTDC for SOI) (Figure 5.64). The applied WVI reduced the oxygen concentration within the combustion chamber, leading to a decrease in combustion efficiency. Lower combustion efficiency resulted in reduced ambient temperatures, leading to a decrease in TE (Figure 5.64). The ID was not significantly affected by the WVI ratio (Figure 5.64). ID is mainly influenced by the pilot diesel fuel advance and the hydrogen fraction within the combustion chamber. CO and UHC emissions increased sharply after the 15% WVI ratio.

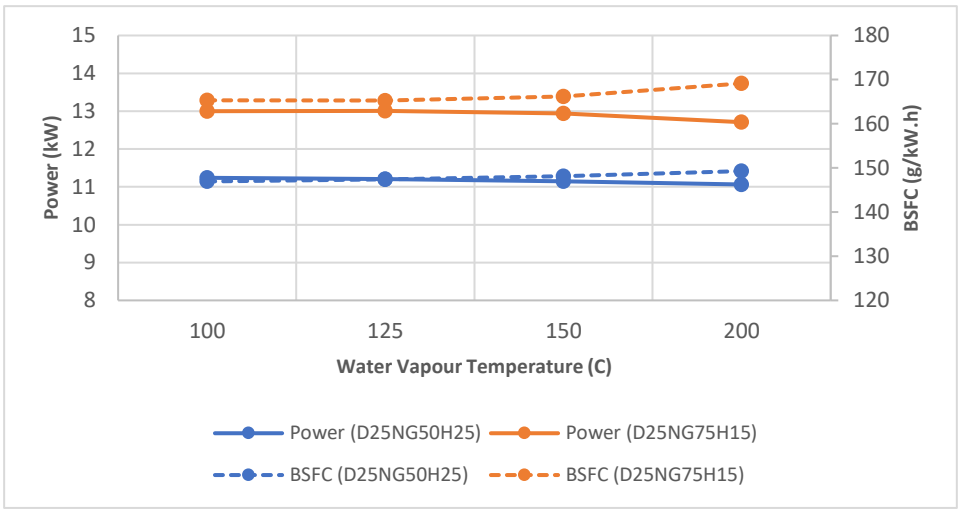

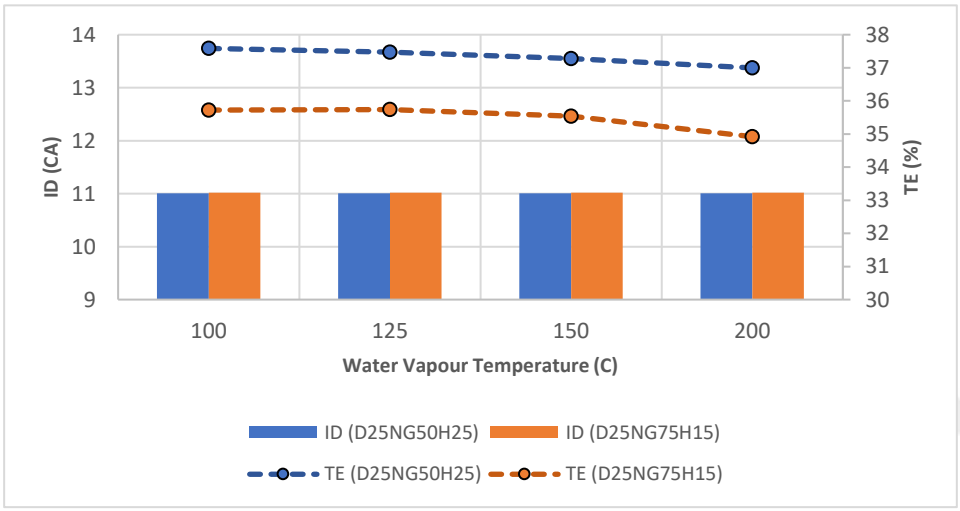

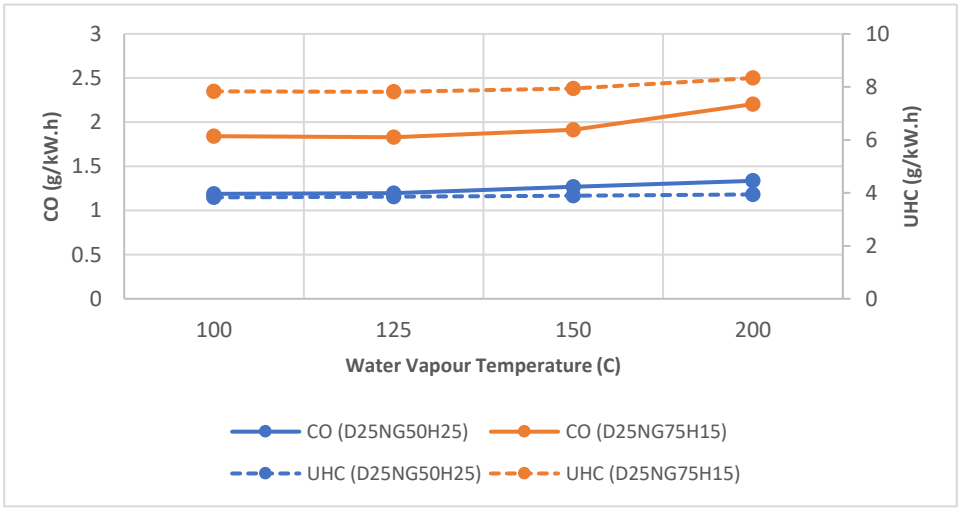

Figure 5.68 : The effect of increasing the WVI temperature at fixed the WVI rate (15% WI) and PI (20% PI) on power, BSFC, ID, TE, CO, and UHC values.

The increase in WVI reduced power and, due to the decrease in oxygen concentration, led to increased incomplete combustion products, namely CO and UHC (Figure 5.64).

As regional temperatures decreased in parallel, it resulted in an improvement in NO_x emissions. The decrease in PM after 15% WVI has shifted to an increasing trend. Especially after 15% WVI, PM increased significantly (Figure 5.65).

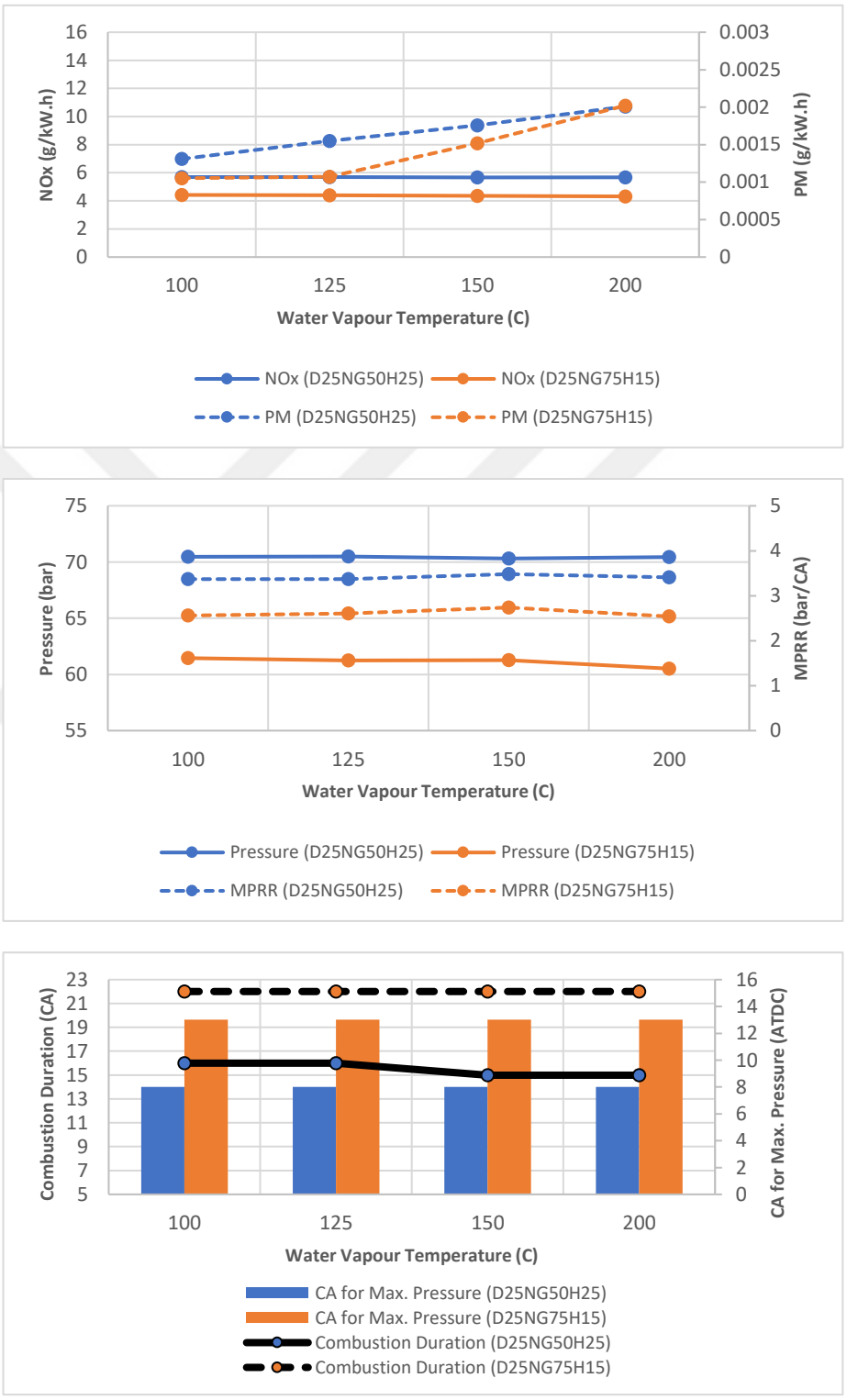

Figure 5.69 : The effect of increasing the WVI temperature at fixed the WVI rate (15% WI) and PI (20% PI) on NO_x, PM, Pressure, MPRR, CD, and the position of Max. Press. Relative to TDC.

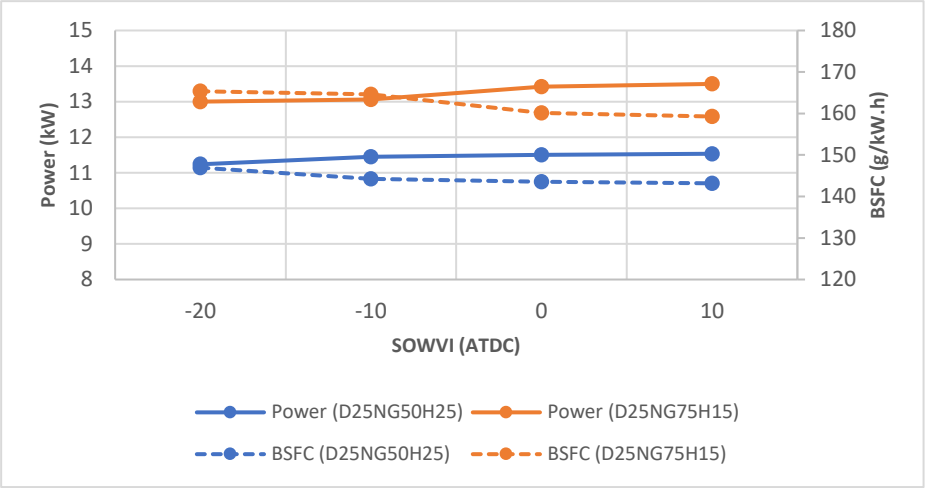

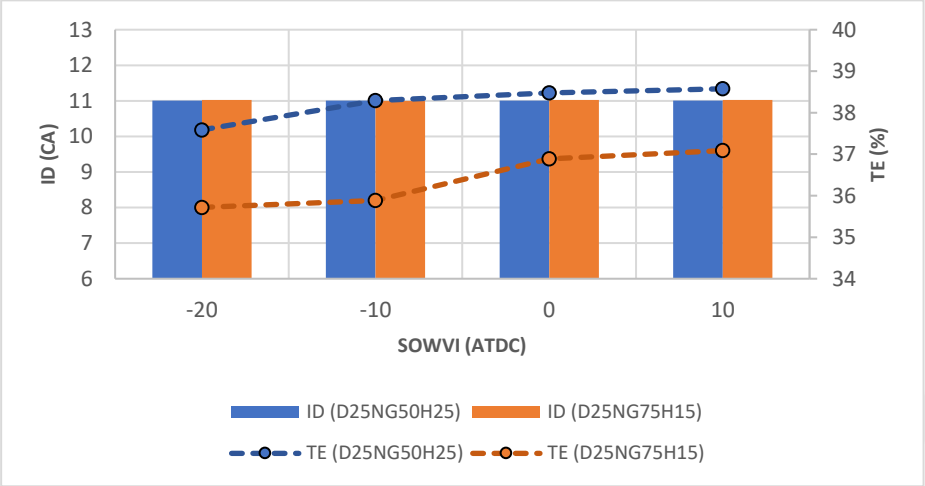

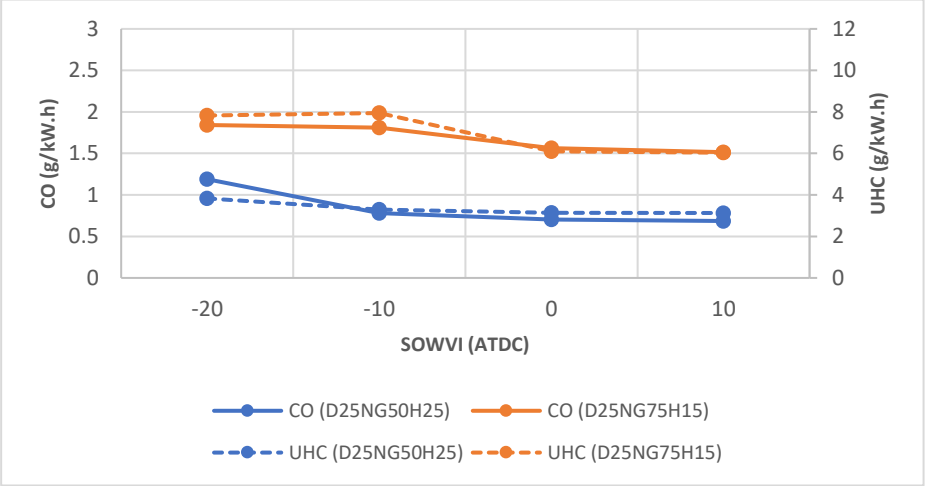

Figure 5.70 : The effect of variation the WVI timing at fixed the WVI rate (15% WI), the WVI temperature (100°C) and PI (20% PI) on power, BSFC, ID, TE, CO, and UHC values.

The MPRR value was not significantly affected by WVI (Figure 5.65). For Mode 1, the combustion duration increased after 15% WVI, while for Mode 2, it decreased after 20% WVI (Figure 5.65). The analysis of the suitable water vapor injection rate showed

that 15% WVI provided more effective results. In the water jet injection analysis (Chapter 5.3), the suitable rate was 25% WI. In this section, the suitable water vapor injection rate was found to be 15% WVI. Because the vapor phase occupies a larger volume compared to the liquid phase, this rate is 10% lower. The tendency to reduce oxygen concentration (with a negative effect on volumetric efficiency) is much higher in the vapor phase. In the next stage, using the 15% WVI value, the effects of different water vapor temperatures (100°C, 125°C, 150°C, and 200°C) were investigated for pilot injection without (0% PI) and with pilot injection (20% PI) conditions.

As the water vapor temperature increased, the water vapor exhibited a more diffusive character. This has triggered negative effects on volumetric efficiency. Therefore, especially after 150°C, the potential for a decrease in performance values became more pronounced (Figure 5.66 and Figure 5.68).

While thermal efficiency (TE) decreased with increasing water vapor temperatures, the in-cylinder pressure (ID) was not significantly affected. The decrease in performance values can be attributed to worsened combustion. The deterioration in combustion quality also led to an increase in CO and UHC emissions (Figure 5.66 and Figure 5.68). This adverse effect on the combustion process has been beneficial for NO_x due to the decrease in combustion temperatures. PM, on the other hand, increased sharply, especially after the 150°C water vapor temperature.

Pressure fluctuations, combustion durations, and MPRR values were not significantly affected by water vapor temperatures (Figure 5.67 and Figure 5.69). These observations represent the effects of WVI temperatures for both pilot injection-off (0% PI) and pilot injection-on (20% PI) cases. Due to the limited impact of WVI temperatures on performance and emission values, the 100°C WVI temperature, which provided the highest performance, was preferred, and the analysis was continued with different SOWVI (Start of Water Vapour Injection) values. These analyses were conducted at the working points where the pilot diesel fuel injection process (20% PI) was considered.

Delaying the start of water vapor injection (reducing WVI advance) had positive effects on power, TE, CO, UHC, and PM (Figure 5.70 and Figure 5.71). However, the situation was different for NO_x, MPRR, and CD values (Figure 5.70 and Figure 5.71). Since the goal is to achieve more power with lower emissions than the experimental

conditions, priority was given to NOx and MPRR. This is because the process of adding hydrogen to the combustion already improved power, BSFC, TE, CO, UHC, and PM values.

Table 5.41 : Results of different WVI temperatures for Mode 2 under constant WVI rate (15% WVI) and injection advance (20° CA BTDC SOWI), with and without PI.

	15% WVI – 20° CA BTDC SOWVI – D25NG75H15 (Mode 2)							
	100°C		125°C		150°C		200°C	
	PI		PI		PI		PI	
	0%	20%	0%	20%	0%	20%	0%	20%
Power (kW)	12.81	13	12.80	13	12.74	12.94	12.58	12.71
Torque (N.m)	134.45	136.42	134.35	136.50	133.73	135.75	132.04	133.37
BSFC (g/kW.h)	167.79	165.35	167.91	165.27	168.69	166.19	170.85	169.14
Ignition Delay (CA)	11º	11º	11º	11º	11º	11º	11º	11º
Thermal Efficiency (%)	35.20	35.72	35.18	35.74	35.02	35.54	34.57	34.92
Combustion Duration (CA)	23º	22º	23º	22º	23º	22º	23º	22º
MPRR (bar/CA)	2.97	2.56	3	2.60	3.16	2.74	3.03	2.54
Max. Press. (bar)	59.59	61.45	59.51	61.25	59.73	61.27	59.29	60.52
CA for Max. Press. (ATDC)	12º CA	13º CA	12º CA	13º CA	12º CA	13º CA	12º CA	13º CA
Max. Mean Temp. (K)	1772	1811	1771	1809	1770	1807	1758	1795
NO_x (g/kW.h)	4.70	4.42	4.65	4.39	4.67	4.36	4.52	4.32
SOOT (g/kW.h)	0.00037	0.0011	0.00042	0.0011	0.00051	0.0015	0.00075	0.0020
CO (g/kW.h)	2.16	1.84	2.15	1.83	2.20	1.92	2.31	2.21
HC (g/kW.h)	9.51	7.83	9.54	7.81	9.58	7.94	9.91	8.33

However, NO_x, MPRR, and CD values deteriorated. To improve the deteriorating results, the optimal SOWVI value was selected as 20° CA BTDC. The positive effect of the pilot diesel fuel injection process (20% PI) was reflected in the results for each WVI temperature. In Table 5.40, it is seen that it is possible to maintain performance values and reduce emission values for Mode 1. In Table 5.40, a comparison is made between the conditions of pilot diesel fuel injection without pilot injection (0% PI) and with pilot injection (20% PI) for D25NG50H25 with a 15% WVI rate (Comparison of 0% PI and 20% PI for D25NG50H25-15WVI).

Power, BSFC, TE, MPRR, NO_x, CO, and UHC values were more reasonable in the PI condition. It can be understood from this that the combination of WVI and PI applications yielded more favorable results (Table 5.40). The power value was slightly lower in the non-PI condition (0% PI) compared to the pilot injection condition (20% PI). The reason for this is that even though PI does not change the ignition delay value of the diesel fuel sent to the combustion chamber beforehand, it affects the combustion process. The combustion occurred faster, and the peak pressure increased. However, the increase in the combustion rate was more gradual rather than sharp. This can be observed through the decrease in the MPRR value (Table 5.40 and Table 5.41).

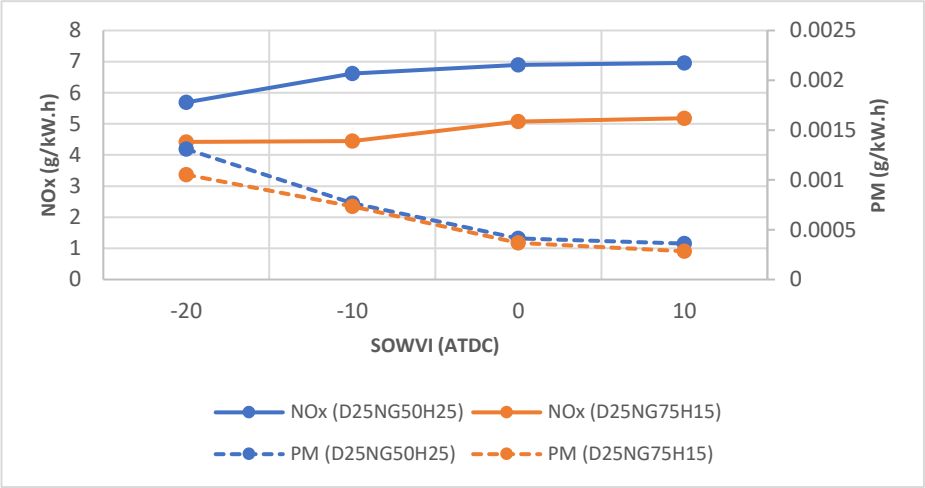

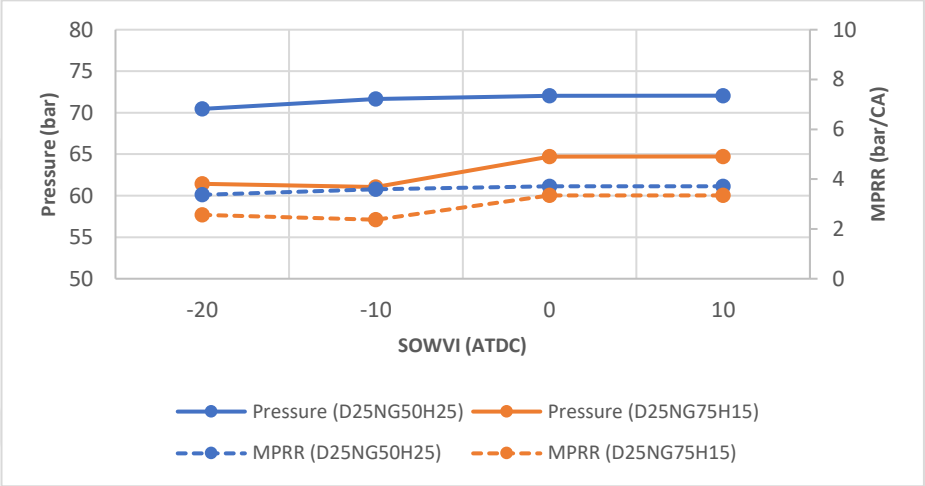

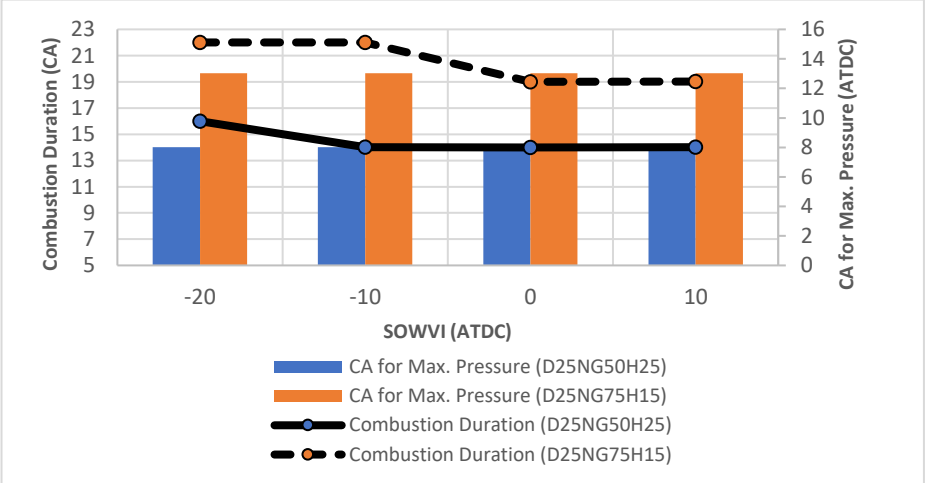

Figure 5.71 : The effect of variation the WVI at fixed the WVI rate (15% WI), the WVI temperature (100°C) and PI (20% PI) on NO_x, PM, Pressure, MPRR, CD, and the position of Max. Press. Relative to TDC.

If we consider power as the area under the pressure-volume diagram, power can increase in two ways. First, when the curve is broader with a fixed peak point, the area under the curve increases. This can be achieved with an extended combustion duration.

In the second scenario, power increases due to the curve's peak point rising and the curve becoming narrower. In this case, MPRR must be controlled to avoid knocking tendencies in combustion. For Mode 1 and Mode 2, power increased with the pilot injection process due to the second scenario, while MPRR decreased. With pilot injection, combustion duration decreased, and the peak pressure value slightly increased. This resulted in a gradual rapid combustion process rather than a sudden increase in combustion. As a result, both performance and emissions, including NO_x, improved (Table 5.40 and Table 5.41). Achieving high hydrogen fractions is possible through the collaborative use of WVI and PI strategies in appropriate proportions. An increase in WVI temperature increases the specific volume of the injected water vapor into the combustion chamber, leading to a decrease in volumetric efficiency and a subsequent reduction in combustion efficiency.

Increasing the hydrogen fraction can be accompanied by an increase in WVI temperature. However, it should be noted that this recommendation is valid for hydrogen fractions where knocking tendencies do not occur. If the WVI temperature is increased in hydrogen fractions with high MPRR values, it may have a diminishing effect, but this might not lead to a sufficient improvement. The same situation applies when examining Mode 2 (Comparison of 0% PI and 20% PI for D25NG75H15-15WVI). Similarly, performance and emissions improved with the pilot diesel fuel injection (Table 5.41). For higher hydrogen enrichment, WVI temperature can be increased while monitoring MPRR.

5.4.2 Comparison of WVI – PI strategy and non – strategy conditions

In this chapter, WVI analyses (15% WVI and 20% PI) were compared to other conducted analysis results (Test Case, non-Process, only PI – 20% PI). For Mode 1 (gas fuel sharing mode), the power output was slightly higher when only pilot injection was applied in cases where hydrogen was not included or included at low fractions (D25NG75H00 and D25NG65H10). Higher hydrogen fractions, at 25% and above, resulted in higher power levels for non-process analyses (Figure 5.72). It can be concluded that the effect of hydrogen on power increase is more significant than the influence of the applied processes. Although there are differences in power values, they are very close to each other. The highest power output was obtained for D25NG50H25 in the non-process case. The lowest power was observed for

D25NG75H00 (test case) (Figure 5.72). BSFC was most affected by the hydrogen fraction (Figure 5.74). The lowest value was obtained for the highest hydrogen fraction (D25NG00H75).

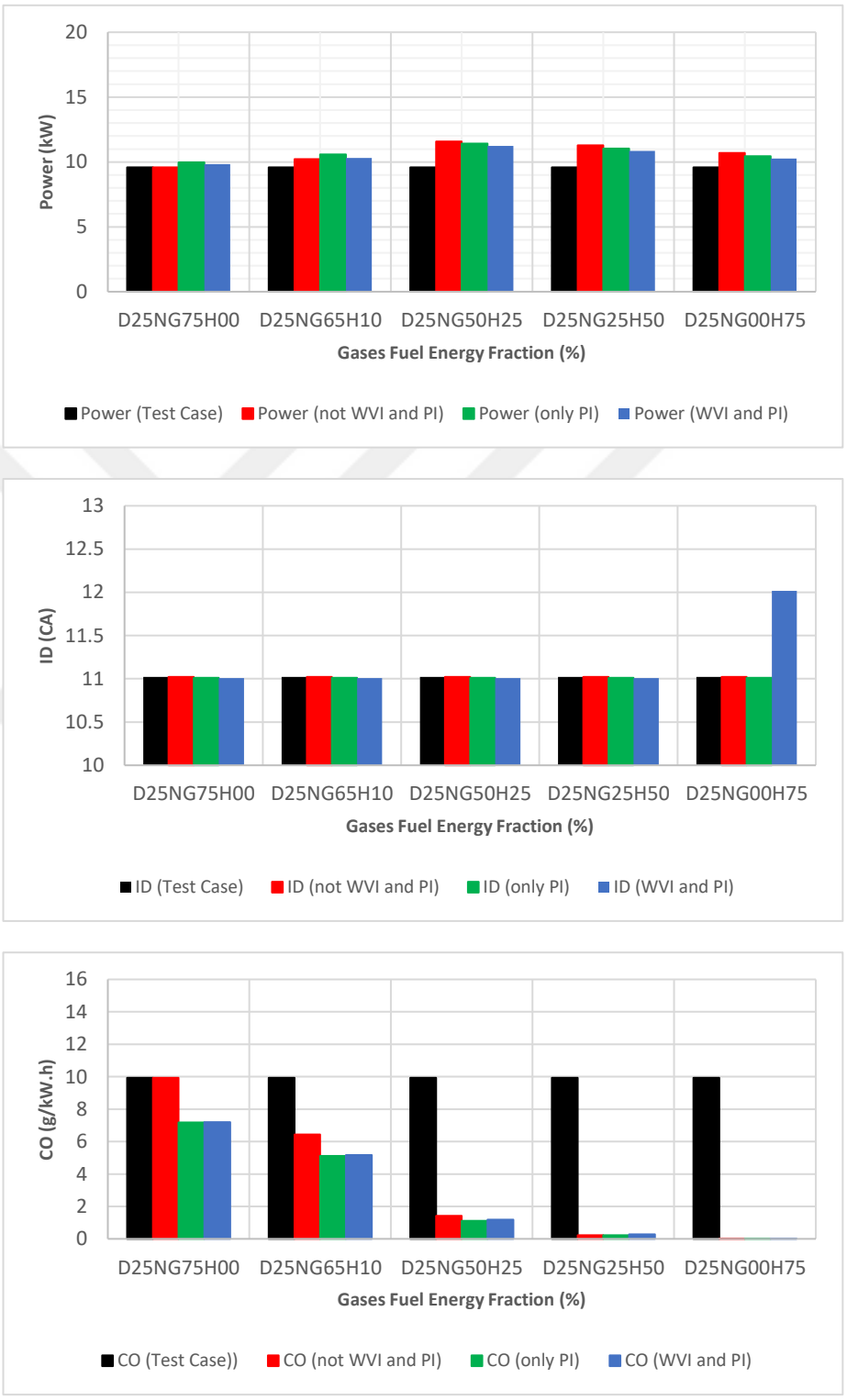

Figure 5.72 : Comparison of test result with the non-process, only PI (20% PI), and both PI and WVI conditions (20% PI and 15% WVI) in terms of power, ID, and CO emission for Mode 1.

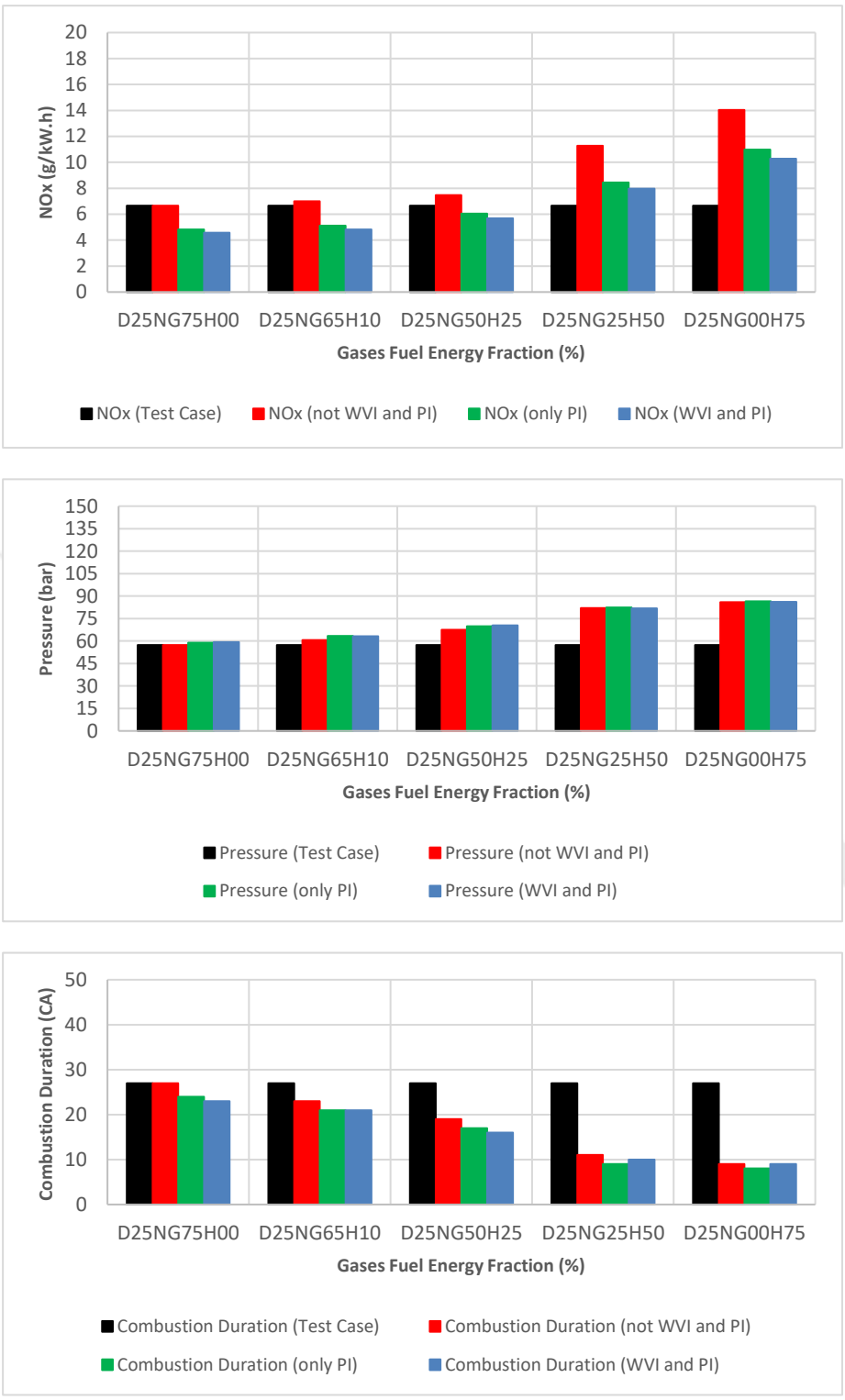

Figure 5.73 : Comparison of test result with the non-process, only PI (20% PI), and both PI and WVI conditions (20% PI and 15% WVI) in terms of NO_x emissions, Pressure and CD for Mode 1.

The highest BSFC was observed for D25NG75H00-20PI-15WVI with water vapor injection (Figure 5.74). ID (Ignition Delay) was not significantly influenced by hydrogen fraction and applied processes, except for an increase when water vapor

injection was used in the case with the highest hydrogen fraction (Figure 5.72). The Thermal Efficiency (TE) showed a decreasing trend beyond hydrogen fractions of up to 25% in the gas-fuel mixture.

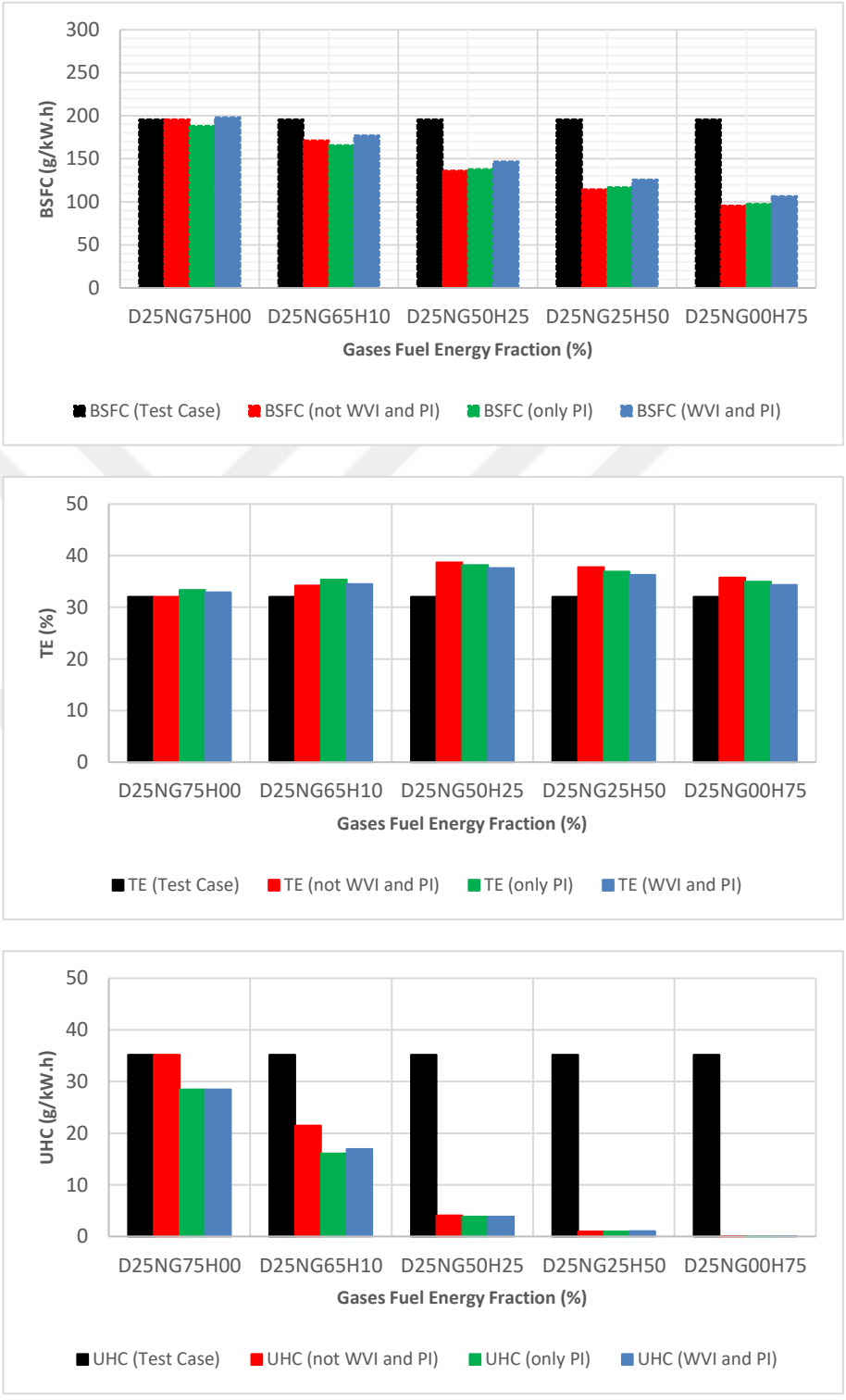

Figure 5.74 : Comparison of test result with the non-process, only PI (20% PI), and both PI and WVI condition (20% PI and 15% WVI) in terms of BSFC, TE and UHC emission for Mode 1.

The highest TE was observed at the D25NG50H25 operating point under non-process conditions. The lowest value was recorded for the test conditions without hydrogen (D25NG75H00) (Figure 5.74). Although there was an increase in NO_x levels parallel to the increase in hydrogen fraction due to the effect of raising temperatures, reasonable results were achieved as a result of the applied processes. Significant improvements were particularly observed for high hydrogen fractions (D25NG25H50 and D25NG00H75) compared to non-process conditions (Figure 5.73).

Table 5.42 : Comparison between processed by the WVI results (20% PI - 15% WVI 100°C - 20° CA BTDC SOWVI) for D25NG50H25 (Mode 1) and test result.

	D25NG75H00	D25NG50H25-20PI-15WVI100°C	Variation
Power (kW)	9.575	11.24	+17.39%
Torque (N.m)	100.477	117.94	+17.38%
BSFC (g/kW.h)	196	146.94	-25%
Ignition Delay (CA)	11º	11º	-
Thermal Efficiency (%)	32.02	37.59	+5.57%
Combustion Duration (CA)	27º	16º	-11º
MPRR (bar/CA)	2.66	3.37	+0.71
Max. Press. (bar)	57.25	70.46	+13.21
CA for Max. Press. (ATDC)	7º CA	8º CA	+1º
Max. Mean Temp. (K)	1504	1811	+307
NO_x (g/kW.h)	6.66	5.69	-14.56%
SOOT (g/kW.h)	0.00077	0.00131	-
CO (g/kW.h)	9.94	1.19	-88%
HC (g/kW.h)	35.21	3.83	-89.12%

Contrary to the decrease in NO_x, PM has increased. Only the application of PI reduced PM to below test conditions, but its inclusion with water vapor injection led to an increase in PM (Figure 5.75). As for CO and UHC emissions, an increase in the hydrogen fraction has had a very positive effect, and this effect was further enhanced by the applied processes. In other words, very low values were achieved for CO and HC emissions compared to test conditions (Figure 5.72 and Figure 5.74). MPRR can be controlled with pilot diesel fuel injection for hydrogen fractions up to 25%, but it cannot prevent MPRR from increasing for hydrogen fractions of 25% and above (Figure 5.75). It can be observed from this that PI is not suitable for high hydrogen fractions. The crank angle at which the maximum pressure occurs has shifted towards TDC due to the acceleration of combustion with an increase in hydrogen. The pilot diesel fuel injection process delayed the occurrence of the maximum pressure crank angle (beyond TDC) for conditions with low to medium hydrogen fractions

(D25NG75H00, D25NG65H10, and D25NG50H25), but this effect was not observed later (Figure 5.75).

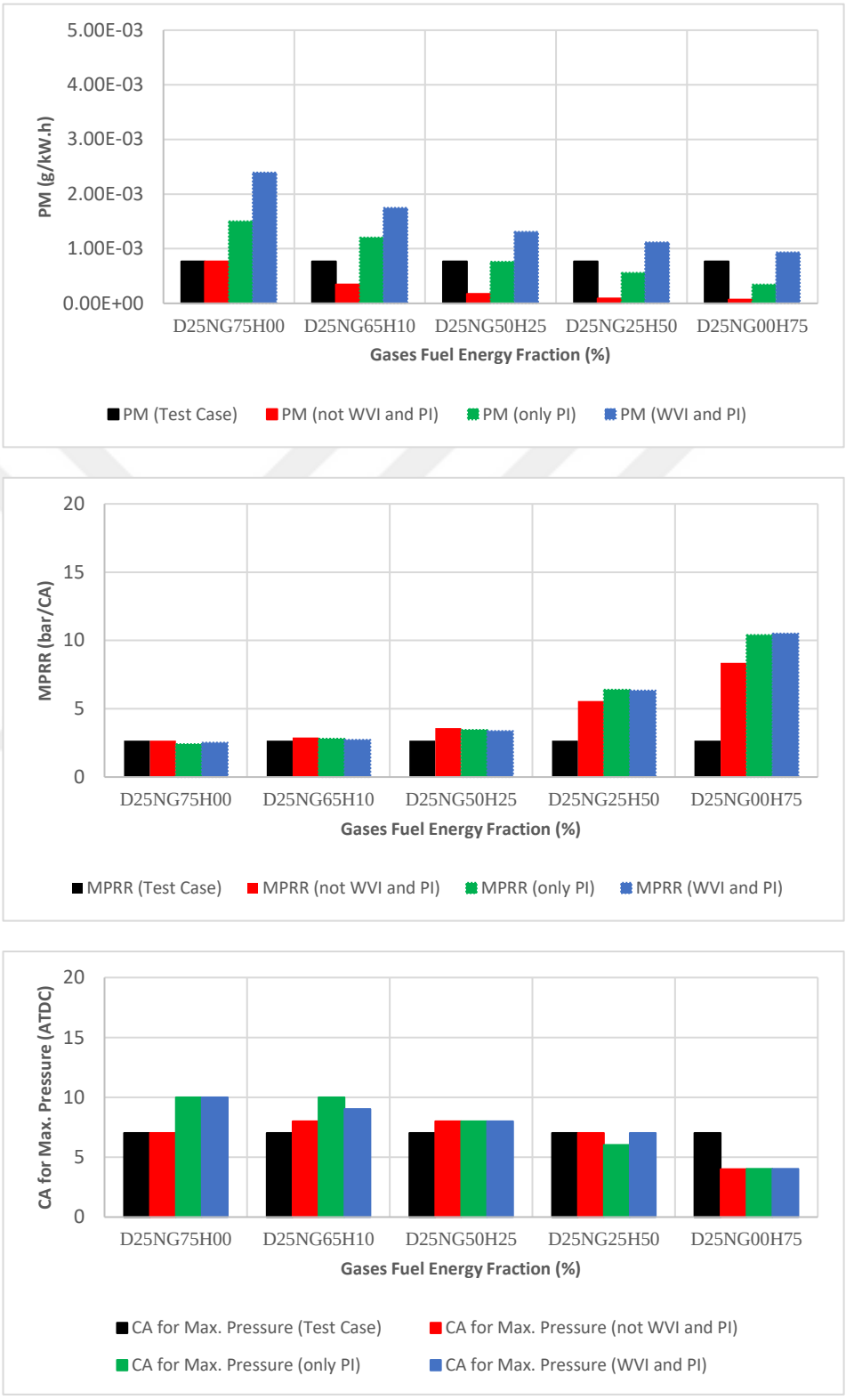

Figure 5.75 : Comparison of test result with the non-process, only PI (20% PI), and both PI and WVI conditions (20% PI and 15% WVI) in terms of PM emission, MPRR and the position of Max. Press. Relative to TDC for Mode 1.

Considering the D25NG50H25 conditions, both the application of only PI and WVI-PI have yielded more reasonable results compared to other conditions. Using only PI has already resulted in reductions in NO_x and MPRR. However, with the combination of WVI-PI, further improvements in lower NO_x and MPRR can be achieved. Beyond a hydrogen fraction of 50%, the effects of only PI and WVI-PI were not as significant. For D25NG25H50, performance improved under moderately intense combustion conditions (with MPRR ranging from 5 to 10 bar/CA) while keeping NO_x levels close to test conditions. Compared to the non-process condition, both only-PI and WVI-PI applications offer preferable results for D25NG25H50 (Figure 5.72 – Figure 5.75).

Table 5.43 : Comparison of results with (20% PI - 15% WVI 100°C - 20° CA BTDC SOWVI) and without the WVI process for D25NG50H25 (Mode 1).

	D25NG50H25	D25NG50H25-20PI-15WVI100°C	Variation
Power (kW)	11.58	11.24	-2.94%
Torque (N.m)	121.47	117.94	-2.91%
BSFC (g/kW.h)	136.27	146.94	+7.83%
Ignition Delay (CA)	11º	11º	-
Thermal Efficiency (%)	38.71	37.59	-1.12%
Combustion Duration (CA)	19º	16º	-3º
MPRR (bar/CA)	3.6	3.37	-0.23
Max. Press. (bar)	67.45	70.46	+3
CA for Max. Press. (ATDC)	8º CA	8º CA	-
Max. Mean Temp. (K)	1779	1811	+32
NO_x (g/kW.h)	7.46	5.69	-23.73%
SOOT (g/kW.h)	0.000172	0.00131	-
CO (g/kW.h)	1.42	1.19	-16.2%
HC (g/kW.h)	4.04	3.83	-5.2%

Table 5.42 provides a comparison between the test conditions (D25NG75H00 14° CA BTDC for SOI) and the application of WVI-PI (15% WVI and 20% PI). Compared to the test conditions, power improved by 17.39%, BSFC improved by 25%, TE improved by 5.57%, NO_x improved by 14.56%, and there were 88% and 89.12% improvements in CO and UHC, respectively. However, MPRR only increased by 0.71 bar (Table 5.42). When comparing WVI-PI (D25NG50H25-20PI-15WVI) to non-process (D25NG50H25), power deteriorated by 2.94%, BSFC worsened by 7.83%, and TE reduced by 1.12%. Nonetheless, there were improvements of 0.23 bar in MPRR, 23.73% in NO_x, 16.2% in CO, and 5.2% in UHC (Table 5.43).

Figure 5.76 illustrates the comparative conditions of different gas fuel fractions for Mode 1 (gas fuel energy sharing mode) at a piston position of 10° CA ATDC for

temperature and NO mass fraction under non-process and WVI-PI scenarios. The influence of PI and WVI is clearly visible on the graph, especially in high hydrogen fractions.

When examining the developments in temperature and NO mass fraction with respect to crank angle, it is observed that the maximum temperature values occur at 25° CA ATDC, while NO_x formation shows a continuous trend (Figure 5.77). This is because temperatures above 1800 K lead to reactions between the nitrogen in the air and the oxygen in the combustion chamber, resulting in the formation of NO and its derivatives.

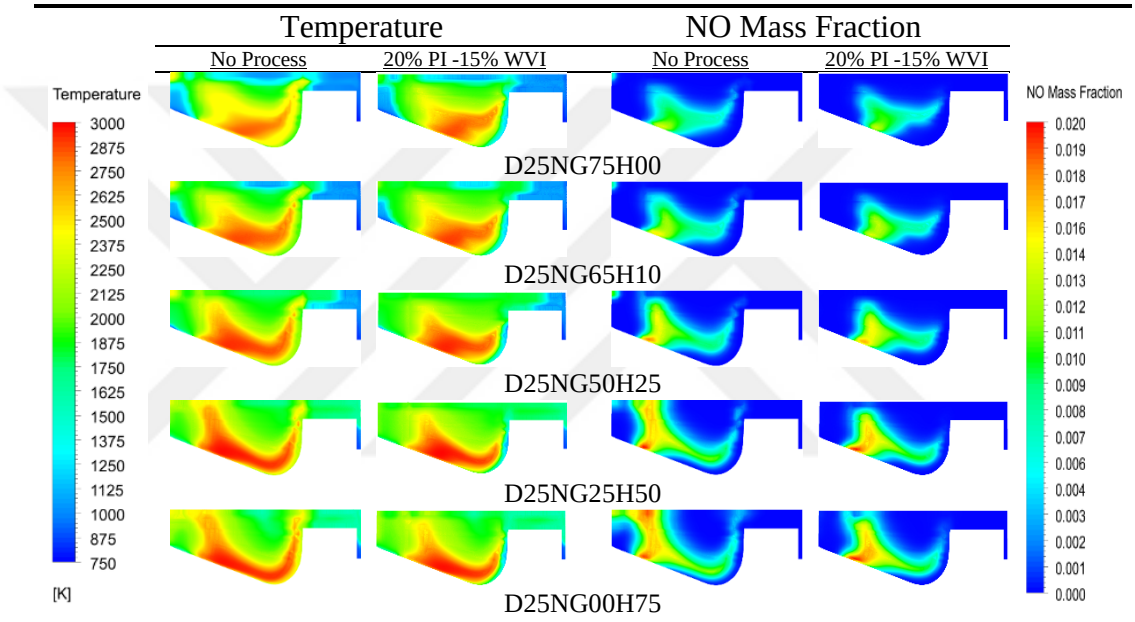

Figure 5.76 : Comparison of temperature and NO mass fraction contours at a piston position of 10° CA ATDC for operating points with applied (20% PI & 15% WVI) and not applied process with different gas fuel fractions for Mode 1.

The formation of NO_x derivatives involves equilibrium reactions where they break down into nitrogen and oxygen, given sufficient time. However, in engine combustion conditions, there is not enough time for these equilibrium reactions to occur.

As a result, the levels of NO_x remain high and are expelled into the exhaust gases. As a result, the rate of increase in NO_x, especially in-cylinder combustion after the maximum temperature, slows down, and there is no transition to reverse reaction mechanisms. This is because combustion is completed very quickly, and there is not enough time for the equilibrium reactions of NO_x to occur, so it remains at a maximum level. When Figure 5.77 is examined, a change in color distribution in temperature

contours is observed after the piston position of 30° CA ATDC, whereas the color content is similar for NO mass fraction distributions.

Table 5.44 : Comparison between processed by the WVI results (20% PI - 15% WI 100°C - 20° CA BTDC SOWVI) for D25NG75H15 (Mode 2) and test result.

	D25NG75H00	D25NG75H15-20PI-15WVI100°C	Variation
Power (kW)	9.76	13	+33.2%
Torque (N.m)	102.42	136.42	+33.2%
BSFC (g/kW.h)	203.85	165.35	~ -18.89%
Ignition Delay (CA)	11º	11º	-
Thermal Efficiency (%)	30.84	35.72	+4.88%
Combustion Duration (CA)	31º	22º	-9º
MPRR (bar/CA)	1.85	2.56	+0.71
Max. Press. (bar)	50.55	61.45	~ +11
CA for Max. Press. (ATDC)	9º CA	13º CA	+4º
Max. Mean Temp. (K)	1477	1811	+334
NO_x (g/kW.h)	4.9	4.42	-9.8%
SOOT (g/kW.h)	0.0012	0.0011	-8.33%
CO (g/kW.h)	10.25	1.84	-82%
HC (g/kW.h)	36.73	7.83	-78.68%

When comparing the results of non-process, only PI, and WVI-PI applied to Mode 2 (hydrogen-enrichment mode) with the test conditions, it is observed that the highest power value was obtained in the non-process condition of the D25NG75H25 operating point (Figure 5.78).

This result was achieved with a high hydrogen content. Within the same hydrogen fraction conditions, when PI was applied at low hydrogen enrichment levels (5% and 10%), it was observed that there was a slight increase in power compared to the non-process condition. However, as the hydrogen fraction increased, PI was not very effective in increasing power. For D25NG75H05, an increase in power was achieved with WVI (Figure 5.78). This indicates that performance improvements can be achieved in steam injection applications. The applied 15% WVI has cooperated with turbulence at this operating point, positively contributing to mixture formation, which has had a positive effect on TE, CO, UHC, and NO_x values (Figure 5.78 - Figure 5.80). The effect of hydrogen enrichment fraction and applied processes on ID was not significant (Figure 5.78). For CO and UHC emissions, it was observed that there were reductions due to an increase in hydrogen energy fraction, as well as with the application of PI and WVI (Figure 5.78 and Figure 5.80). In all hydrogen enrichment operating points, CO and UHC values remained lower than the test conditions.

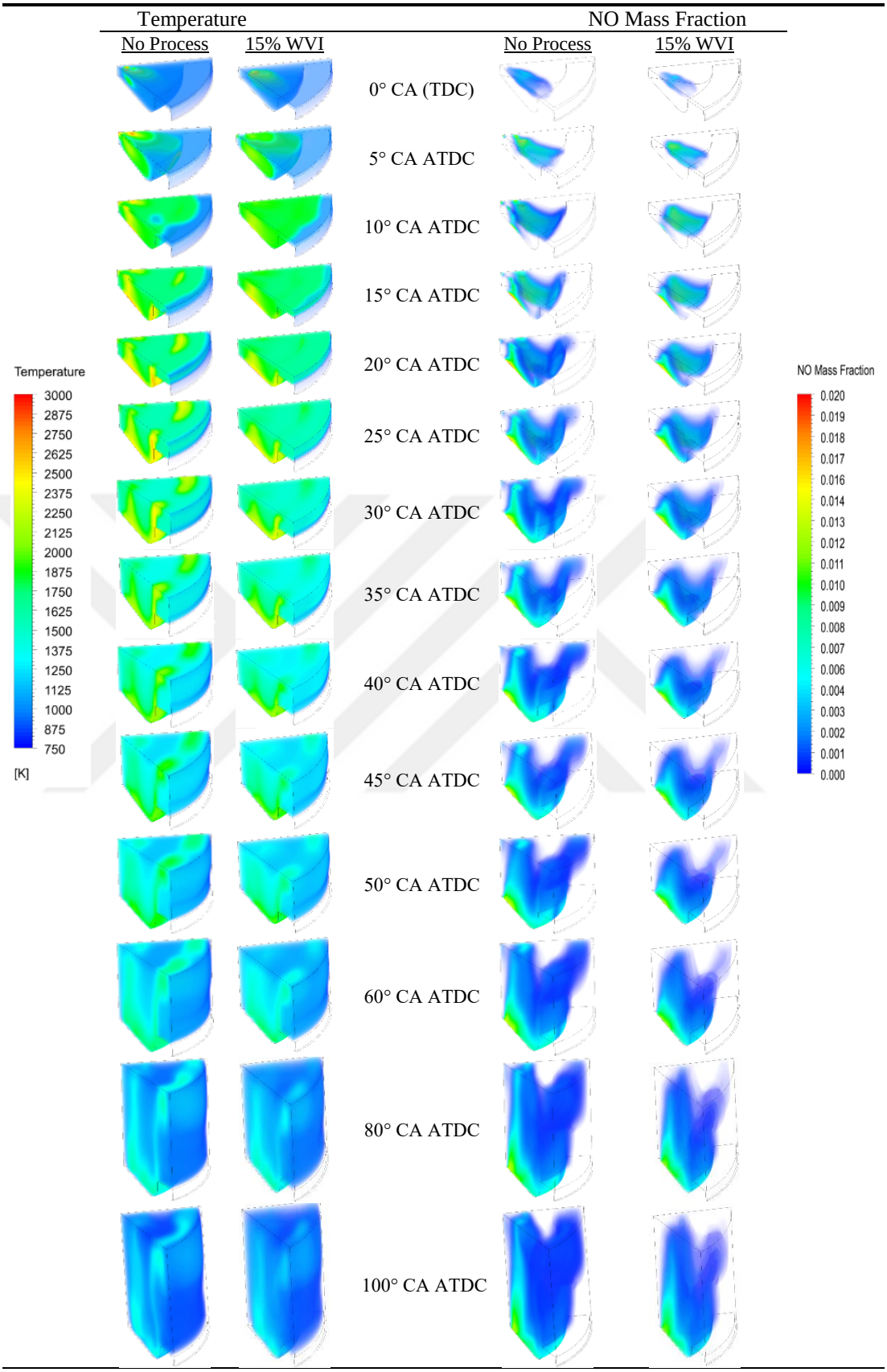

Figure 5.77 : Comparison of temperature and NO mass fraction contours at different piston positions for operating points with applied (20% PI & 15% WVI) and not applied process with different hydrogen enriching fractions for Mode 1 - D25NG50H25.

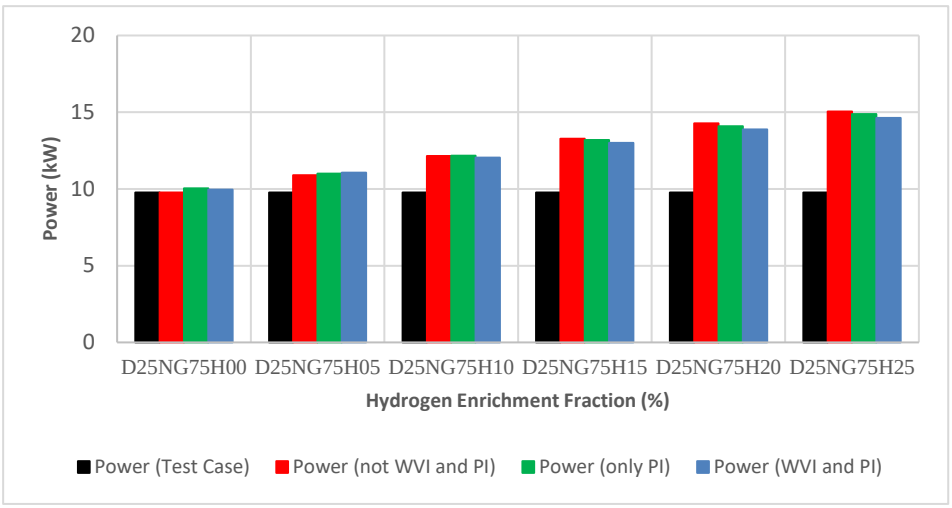

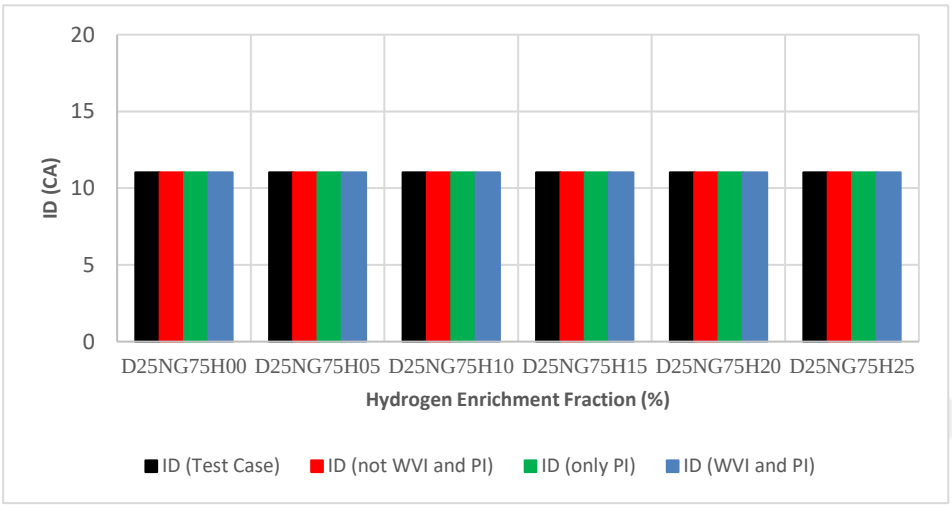

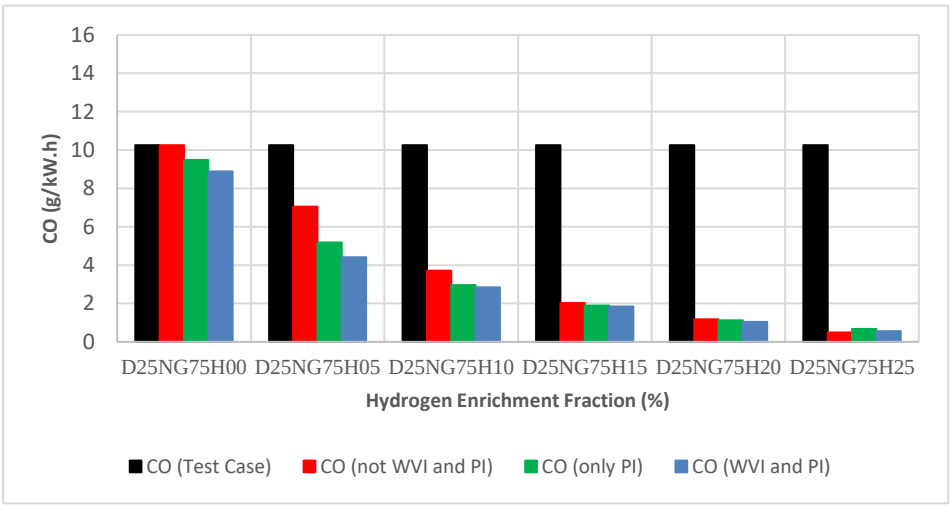

Figure 5.78 : Comparison of test result with the non-process, only PI (20% PI), and both PI and WVI conditions (20% PI and 15% WVI) in terms of power, ID, and CO emission for Mode 2.

Although the application of PI led to a decrease in NO_x for all hydrogen fractions, PI was not very effective for D25NG75H25 (Figure 5.79). At high hydrogen fractions,

temperatures rise rapidly due to abrupt combustion, and the combustion duration decreases.

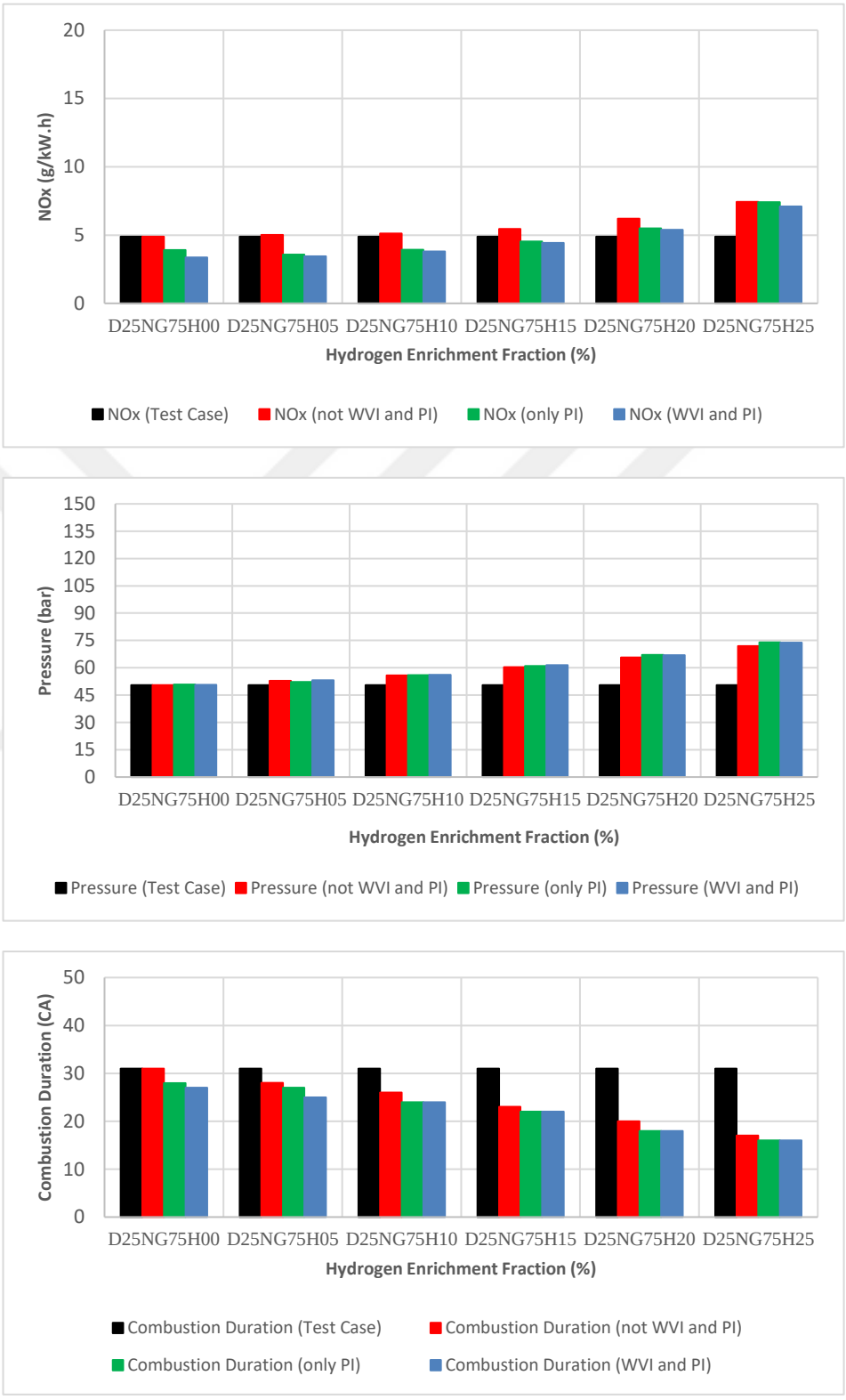

Figure 5.79 : Comparison of test result with the non-process, only PI (20% PI), and both PI and WVI conditions (20% PI and 15% WVI) in terms of NO_x emissions, Pressure and CD for Mode 2.

Table 5.45 : Comparison of results with (20% PI - 15% WVI 100°C - 20° CA BTDC SOWVI) and without the WVI process for D25NG75H15 (Mode 2).

	D25NG75H15	D25NG75H15-20PI-15WVI100°C	Variation
Power (kW)	13.28	13	-2.11%
Torque (N.m)	139.34	136.42	-2.1%
BSFC (g/kW.h)	155.99	165.35	+6%
Ignition Delay (CA)	11º	11º	-
Thermal Efficiency (%)	36.48	35.72	-0.76%
Combustion Duration (CA)	23º	22º	-1º
MPRR (bar/CA)	3.08	2.56	-0.52
Max. Press. (bar)	60.35	61.45	~ +1
CA for Max. Press. (ATDC)	12º CA	13º CA	+1º
Max. Mean Temp. (K)	1809	1811	-
NO_x (g/kW.h)	5.44	4.42	-18.75%
SOOT (g/kW.h)	0.0002	0.0011	-
CO (g/kW.h)	2.02	1.84	-8.91%
HC (g/kW.h)	8.76	7.83	-10.62%

For this reason, the application of PI at the 25% hydrogen enrichment level did not have a positive effect on MPRR and NO_x. However, with WVI application, a decrease in NO_x was observed (Figure 5.79). The lowest value for NO_x was achieved with the D25NG75H00-20PI-15WVI condition, while the highest value was observed in the D25NG75H25 non-process condition. PM, on the other hand, was observed to be highest with D25NG75H00-20PI-15WVI and lowest in the condition where the highest NO_x values were observed.

Table 5.46 : Comparison of results with and without the WVI process for D25NG00H75.

	D25NG00H75	D25NG00H75-20PI-15WVI100°C	Variation
Power (kW)	10.69	10.27	-3.93%
Torque (N.m)	112.18	107.77	-3.93%
BSFC (g/kW.h)	95.73	106.88	+11.65%
Ignition Delay (CA)	11º	12º	+1º
Thermal Efficiency (%)	35.75	34.35	-1.4%
Combustion Duration (CA)	9º	9º	-
MPRR (bar/CA)	8.35	10.51	+2.16
Max. Press. (bar)	85.89	86	-
CA for Max. Press. (ATDC)	4º CA	4º CA	-
Max. Mean Temp. (K)	1997	2000	-
NO_x (g/kW.h)	14.04	10.28	-26.78%
SOOT (g/kW.h)	~ 0	0.00093	-
CO (g/kW.h)	0.0036	0.018	-
HC (g/kW.h)	0.0015	0.012	-

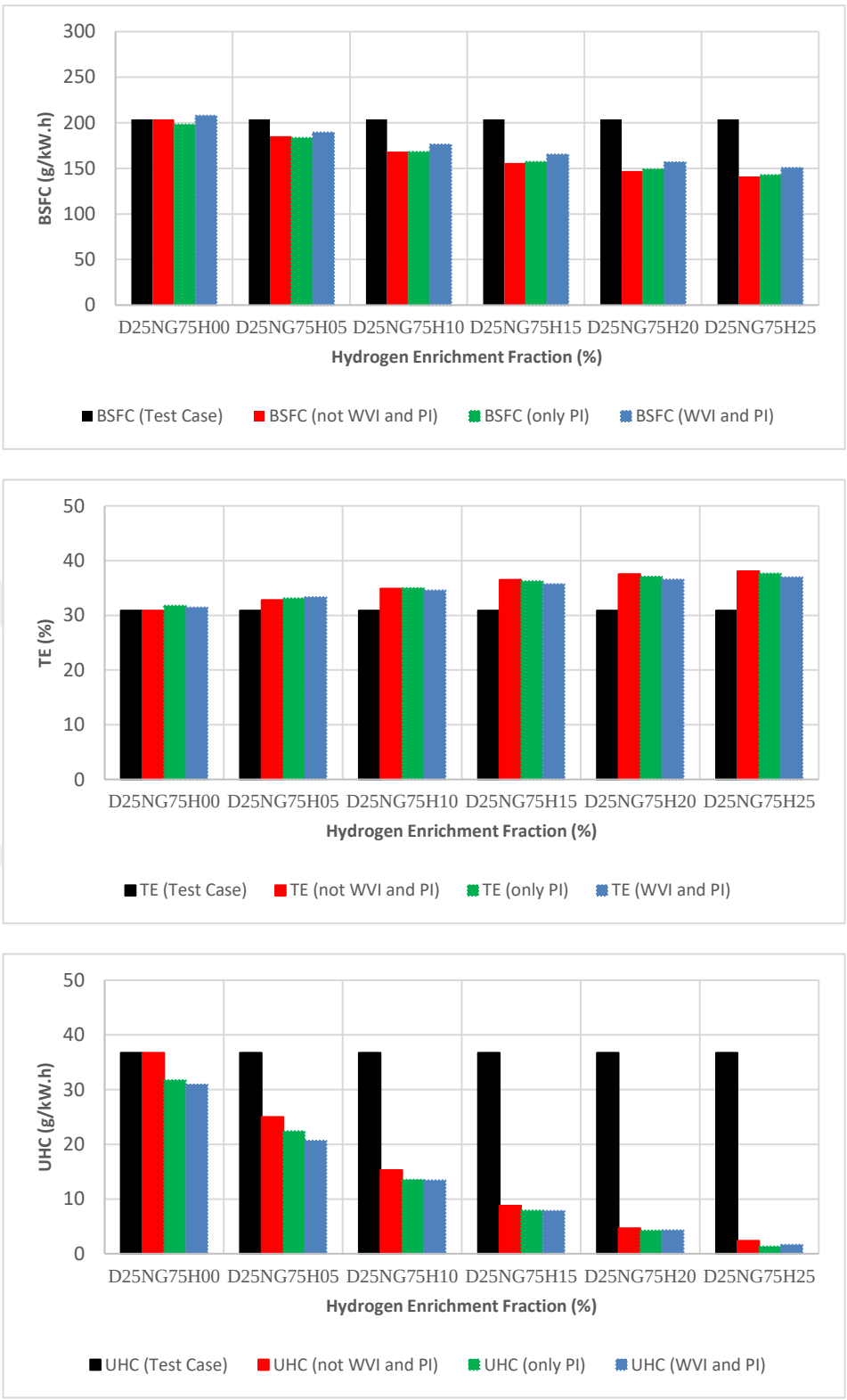

Figure 5.80 : Comparison of test result with the non-process, only PI (20% PI), and both PI and WVI conditions (20% PI and 15% WVI) in terms of BSFC, TE and UHC emission for Mode

While PM increased with WVI, its values remained close to those of the test conditions, not overshadowing the improvements in other parameters.

In fact, it was even lower than the value in the experiment with D25NG75H15 (Figure 5.81). When all the results are considered, the collaboration of WVI and PI applied at the D25NG75H15 operating point is seen to lead to favorable results. Beyond the 15% hydrogen fraction, NO_x and MPRR values remain higher than those under test conditions (Figure 5.79 and Figure 5.81). As the hydrogen enrichment fraction increased, the function of PI decreased. The combination of WVI and PI led to the delayed occurrence of peak pressure and a shorter combustion duration at all hydrogen enrichment ratios. This resulted in an increase in peak pressure.

Table 5.47 : Comparison of results with and without the WVI process for D25NG75H25.

	D25NG75H25	D25NG75H25-20PI-15WVI100°C	Variation
Power (kW)	15.05	14.63	-2.79%
Torque (N.m)	157.92	153.50	-2.80%
BSFC (g/kW.h)	141.09	150.52	+6.68%
Ignition Delay (CA)	11º	11º	-
Thermal Efficiency (%)	38.04	36.98	-1.06%
Combustion Duration (CA)	17º	16º	-1º
MPRR (bar/CA)	4.62	4.71	+0.09
Max. Press. (bar)	71.94	73.74	+1.8
CA for Max. Press. (ATDC)	12º CA	12º CA	-
Max. Mean Temp. (K)	2057	2060	-
NO_x (g/kW.h)	7.43	7.10	-4.44%
SOOT (g/kW.h)	0.00015	0.00074	-
CO (g/kW.h)	0.49	0.56	+14.29%
HC (g/kW.h)	2.36	1.61	-31.78%

The shape of the pressure-volume diagram becomes sharper, and the area underneath it has increased. Ideal results were obtained for hydrogen fractions that are within the knock limits (25% and below) while an increase in power beyond the knock limits is not meaningful. An increase in power as a result of harsh combustion (MPRR > 10 bar/CA) is an undesirable condition. Table 5.44 shows the differences between D25NG75H00 (test case) and D25NG75H15-20PI-15WVI.

Compared to the test conditions, there was an improvement of 33.2% in power, 18.89% in BSFC, 4.88% in TE, 9.8% in NO_x, 82% in CO, and 78.68% in UHC, while MPRR increased by only 0.71 bars. When comparing non-process and WVI – PI for D25NG75H15, there was a deterioration in power by 2.11%, BSFC by 6%, and TE by 0.76%. However, improvements were observed in NO_x by 18.75%, CO by 8.91%, UHC by 10.62%, and MPRR by 0.52 bars when compared to the test conditions (Table

5.45). After achieving a 33.2% increase in power under the test conditions, the 2.11% loss due to WVI application may not be strongly felt.

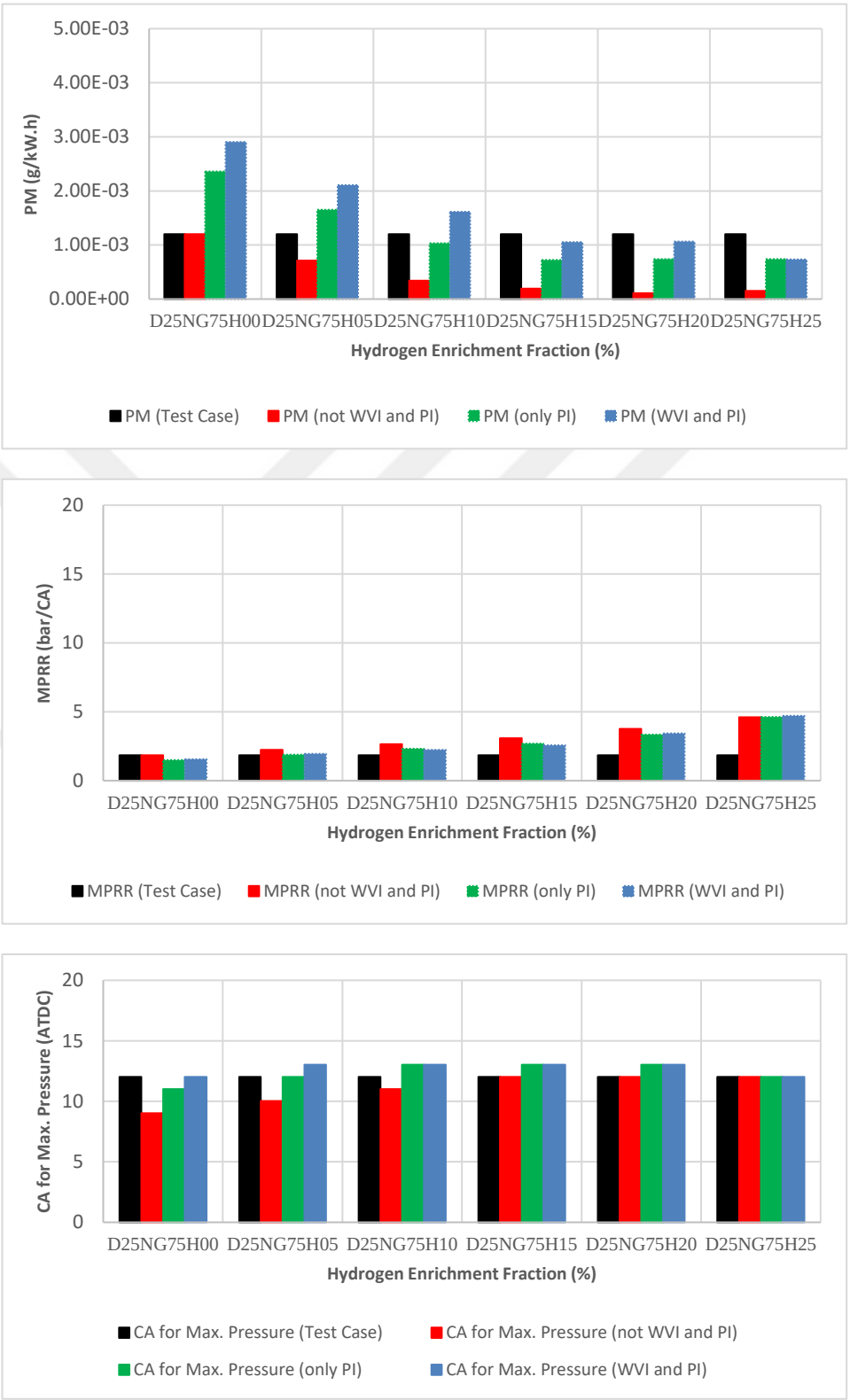

Figure 5.81 : Comparison of test result with the non-process, only PI (20% PI), and both PI and WVI conditions (20% PI and 15% WVI) in terms of PM emission, MPRR and the position of Max. Press. Relative to TDC for Mode 2.

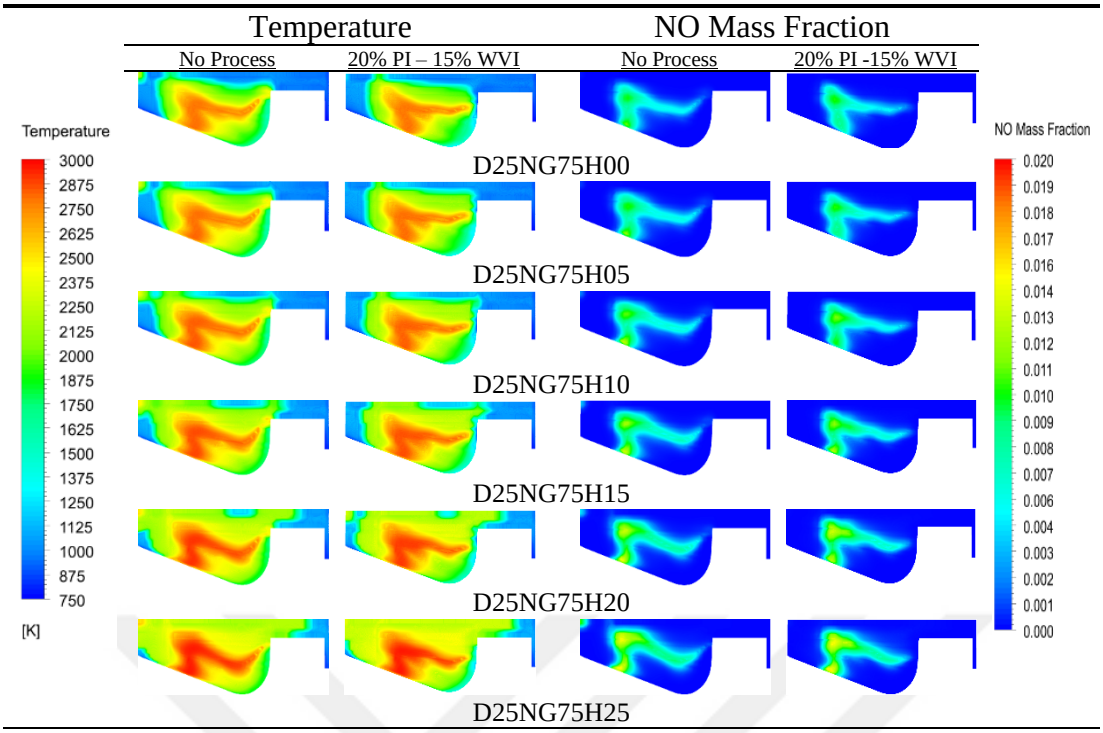

Figure 5.82 : Comparison of temperature and NO mass fraction contours at a piston position of 10° CA ATDC for operating points with applied (20% PI & 15% WVI) and not applied process with different hydrogen enriching fractions for Mode 2.

Still, considering that MPRR remains within acceptable limits, this suggests a successful outcome. For Mode 2, temperature and NO mass fraction contours at a piston position of 10° CA ATDC are displayed for different hydrogen enrichment fractions (Figure 5.82).

Table 5.48 : Comparison of test and processed by WVI results for the operating point of D25NG75H00 (14° CA BTDC SOI).

	D25NG75H00	D25NG75H00-20PI-15WVI100°C	Variation
Power (kW)	9.575	9.83	+2.66%
Torque (N.m)	100.477	103.15	+2.66%
BSFC (g/kW.h)	196	198.52	+1.29%
Ignition Delay (CA)	11º	11º	-
Thermal Efficiency (%)	32.02	32.87	+0.85%
Combustion Duration (CA)	27º	23º	-4º
MPRR (bar/CA)	2.66	2.51	-0.15
Max. Press. (bar)	57.25	59.18	~ +2
CA for Max. Press. (ATDC)	7º CA	10º CA	+3º
Max. Mean Temp. (K)	1504	1561	+57
NO_x (g/kW.h)	6.66	4.58	-31.23%
SOOT (g/kW.h)	0.00077	0.0024	-
CO (g/kW.h)	9.94	7.21	-27.46%
HC (g/kW.h)	35.21	28.46	-19.17%

It's evident that the applied WVI - PI leads to a reduction in high-temperature and NO formation rates. When examining the temperature and NO_x development concerning crank angle, just as in Mode 1, after the crank angle where maximum temperature values occur (after 30° CA ATDC), the NO formation remains stable, and its rate decreases for Mode 2 as well (Figure 5.83).

Table 5.49 : Comparison of test and processed by WVI results for the operating point of D25NG75H00 (10° CA BTDC SOI).

	D25NG75H00	D25NG75H00-20PI-15WVI100°C	Variation
Power (kW)	9.76	9.95	+1.95%
Torque (N.m)	102.42	104.41	+1.94%
BSFC (g/kW.h)	203.85	207.89	+1.98%
Ignition Delay (CA)	11º	11º	-
Thermal Efficiency (%)	30.84	31.44	+0.6%
Combustion Duration (CA)	31º	27º	-4º
MPRR (bar/CA)	1.85	1.57	-0.28
Max. Press. (bar)	50.55	50.69	-
CA for Max. Press. (ATDC)	9º CA	12º CA	+3º
Max. Mean Temp. (K)	1477	1505	+28
NO_x (g/kW.h)	4.9	3.37	-31.22%
SOOT (g/kW.h)	0.0012	0.0029	-
CO (g/kW.h)	10.25	8.88	-13.37%
HC (g/kW.h)	36.73	30.96	-15.71%

The answer to the question of how much the condition with the highest hydrogen fraction for Mode 1 can be improved by applying WVI - PI strategies is quite clear from Table 5.46. When examining the table, it can be seen that the MPRR value is above the critical limit. As previously explained, in conditions with high hydrogen energy fractions, PI has an adverse effect, leading to an increase in the MPRR value. In the non-process condition, the MPRR, which was 8.35 bar/CA, was calculated as 10.51 bar/CA under 15% WVI and 20% PI strategies. This value is above the preferred limit under engine operating conditions. For Mode 2, when comparing the condition with the highest hydrogen enrichment fraction with non-process and WVI - PI, it can be observed that the MPRR value is at reasonable levels, and there are improvements that can be considered effective in terms of NO_x (Table 5.47). A 2.79% power loss, a 6.68% increase in BSFC, and a 1.06% decrease in TE resulted in a 4.44% improvement in NO_x. Here, the presence of WVI influence was more noticeable than the PI effect. To understand the response of the experimental conditions to WVI - PI application, it can refer to Table 5.48 and Table 5.49.

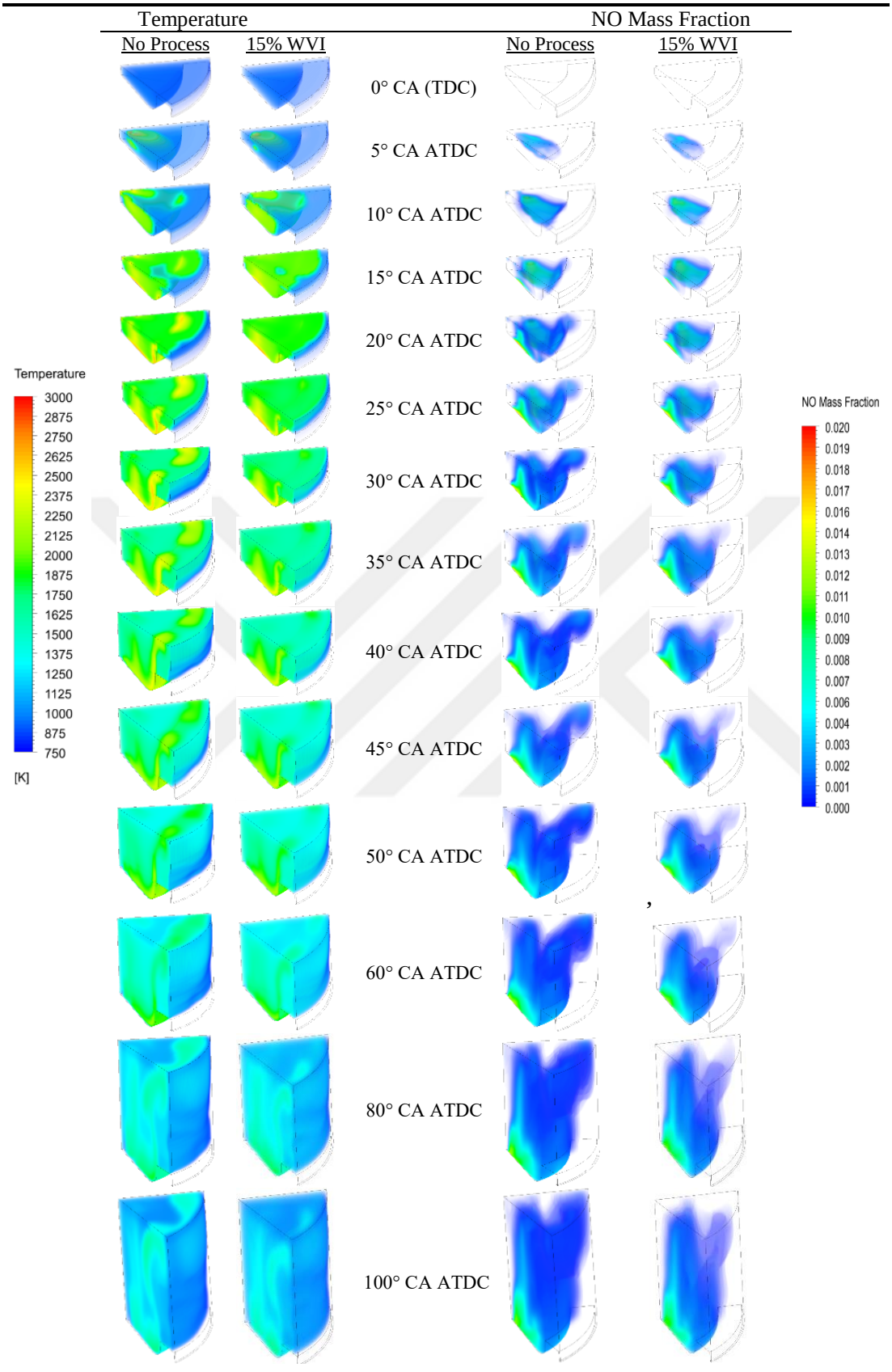

Figure 5.83 : Comparison of temperature and NO mass fraction contours at different piston positions for operating points with applied (20% PI & 15% WVI) and not applied process with different hydrogen enriching fractions for Mode 2 - D25NG75H15.

When 15% WVI and 20% PI are applied to the D25NG75H00 14° CA BTDC (test case) operating point, a 2.66% improvement in power, 0.85% in TE, 0.15 bar in MPRR, 31.23% in NO_x, 27.46% in CO, and 19.17% in UHC can be observed (Table 5.48). When the D25NG75H00 10° CA BTDC (test case) operating point is examined, there is a 1.95% improvement in power, 0.6% in TE, 0.28 bar in MPRR, 31.22% in NO_x, 13.37% in CO, and 15.71% in UHC (Table 5.49).

Table 5.50 : Comparison of the optimal results obtained by applying the WVI process for Mode 1 and Mode 2.

	20% PI – 15% WVI 100°C – 20° CA BTDC SOWVI		
	D25NG50H25	D25NG75H15	Variation
Power (kW)	11.24	13	+15.66%
Torque (N.m)	117.94	136.42	+15.67%
BSFC (g/kW.h)	146.94	165.35	+12.53%
Ignition Delay (CA)	11º	11º	-
Thermal Efficiency (%)	37.59	35.72	-1.87%
Combustion Duration (CA)	16º	22º	+6º
MPRR (bar/CA)	3.37	2.56	-0.81
Max. Press. (bar)	70.46	61.45	-9
CA for Max. Press. (ATDC)	8º CA	13º CA	+5º
Max. Mean Temp. (K)	1811	1811	-
NO_x (g/kW.h)	5.69	4.42	-22.32%
SOOT (g/kW.h)	0.00131	0.0011	-16%
CO (g/kW.h)	1.19	1.84	-54.62%
HC (g/kW.h)	3.83	7.83	-

When comparing the numerical results obtained by applying the 15% WVI and 20% PI strategies to the optimal gas fraction working points of Mode 1 and Mode 2, Mode 2 conditions are more advantageous compared to Mode 1. Specifically, Mode 2 has a 15.66% higher power, 1.87% higher thermal efficiency (TE), 0.81 bar higher maximum pressure rise rate (MPRR), 22.32% lower NO_x emissions, 16% lower SOOT emissions, and 54.62% lower CO emissions compared to Mode 1 (Table 5.50). The D25NG75H15 condition, with 15% more energy input compared to the D25NG50H25 condition, has achieved 22.32% lower NO_x emissions, lower CO emissions, and reduced PM formation, while being closer to the goal of low emissions at high power.

5.4.3 General summary for WVI – PI strategy

The analysis of WVI and PI showed that they could improve the harsh combustion characteristics and high NO_x levels under non-process conditions. However,

increasing the vapor injection rate and vapor temperature reduced performance values. The increase in vapor concentration and temperature caused a decrease in oxygen concentration in the combustion chamber, worsening combustion, and reducing NO_x emissions. The fundamental difference between WI and WVI is the volume they occupy. The vapor phase occupies more volume, so it has a greater impact on volumetric efficiency. This is why the optimal ratio is 25% for water jet injection analysis, while it's 15% for vapour injection. Furthermore, in water jet injection, the liquid phase needs to draw heat from the combustion chamber to convert into the vapor phase. This leads to a decrease in post-combustion temperatures due to both the heat extraction and the vapor phase reducing oxygen concentration and worsening combustion, causing a decrease in temperature. Consequently, in terms of NO_x emissions, the liquid phase was more effective. For Mode 1 and Mode 2, the application of 15% WVI and 20% PI resulted in power increases of 17.39% and 33.2%, respectively, compared to test conditions. At the same time, NO_x emissions decreased by 14.56% and 9.8%, respectively. The increase in power with WVI at the D25NG75H05 operating point was due to the introduction of 15% WVI into the combustion chamber, which, together with its turbulence effect, led to the fragmentation of the liquid diesel fuel jet into smaller droplets. Smaller droplets mean a larger surface area-to-volume ratio, resulting in improved combustion efficiency and, consequently, an increase in power.

In terms of combustion efficiency, the decrease in UHC and the increase in TE can be observed (Figure 5.80). In both Mode 1 and Mode 2, there was no significant impact of PI at high hydrogen fractions. Beyond a certain point, particularly after 50% hydrogen fraction for Mode 1 and 25% hydrogen enrichment for Mode 2, the results became less significant. Especially beyond these ratios, high MPRR and NO_x production occurred. Delaying the injection timing of steam led to positive results in terms of performance, but it also resulted in high NO_x values. The effect of pilot diesel fuel injection was pronounced in low to medium hydrogen fractions (up to 50% for Mode 1 and 20% for Mode 2) and contributed to lower MPRR values. In operating points with high hydrogen fractions, PI application should not be preferred due to the associated drawbacks. Because the purpose of pilot diesel fuel is to ensure early fuel vaporization in the combustion chamber, preventing an increase in ignition delay and promoting a smooth and gradual ignition. However, in high hydrogen fractions, the

high lower heating value of hydrogen and its high ignition rate, combined with the effect of pilot diesel fuel, lead to a sharp and sudden ignition. Consequently, this triggers high-pressure and temperature increases. As a result, MPRR and NO_x values increase.

Finally, the optimum conditions for Mode 1 and Mode 2 are recommended as D25NG50H25-20PI-15WVI100°C and D25NG75H15-20PI-15WVI100°C, respectively.

5.5 Comparison of All Strategies

In this chapter, a comparison of the operating points obtained in the previous sections (Chapter 5.1, Chapter 5.2, Chapter 5.3, and Chapter 5.4) will be carried out. For Mode 1, the results of the D25NG50H25 operating point under EGR - PI, WI - PI, and WVI - PI conditions are compared with the test results, as shown in Table 5.51. Here, the working points considered are D25NG50H25-20PI-10EGR100°C for EGR - PI, D25NG50H25-20PI-25WI75°C for WI - PI, and D25NG50H25-20PI-15WVI100°C for WVI - PI.

The working point considered as the test case is D25NG75H00 (14° CA BTDC for SOI), as shown in the table. Naturally, the highest power value is achieved in the no-process (D25NG50H25) condition (Table 5.51 and Figure 5.84). In this working point, there is no EGR, PI, or water jet/vapor injection applied. The presence of hydrogen has led to an increase in power. It is worth noting that, in terms of NO_x, the highest value has also been obtained in this condition (Figure 5.85). In terms of NO_x, a value higher than the test conditions has been obtained. The NO_x value has been improved the most by the EGR - PI strategy (Figure 5.85). In fact, EGR - PI (10% EGR for 100 °C - 20% PI) and WVI - PI (15% WVI for 100 °C - 20% PI) strategies show similarities in terms of application. EGR was applied as a mixture of CO_2-H_2O-N_2-O_2, while WVI was applied only as water vapor. The reason for lower NO_x formation with EGR is that EGR is present in the intake process along with being in the combustion chamber, whereas the WVI strategy provides injection into the combustion chamber at 20° CA BTDC. Therefore, the effect of the EGR process on temperatures has started earlier. With EGR, the influence on oxygen concentration in the mixture formation started earlier, leading to lower temperatures (Table 5.51) [197].

Table 5.51 : Comparison of test result with optimally obtained results from processes for Mode 1 – D25NG50H25 (EGR, WI and WVI).

	Test Case	No Process	EGR	WI	WVI
Power (kW)	9.575	11.58	11.20	10.94	11.24
Torque (N.m)	100.477	121.47	117.48	114.84	117.94
BSFC (g/kW.h)	196	136.27	140.33	155.42	146.94
Ignition Delay (CA)	11º	11º	11º	11º	11º
Thermal Efficiency (%)	32.02	38.71	37.44	36.60	37.59
Combustion Duration (CA)	27º	19º	20º	17º	16º
MPRR (bar/CA)	2.66	3.6	3.36	3.2	3.37
Max. Press. (bar)	57.25	67.45	67.31	69.36	70.46
CA for Max. Press. (ATDC)	7º CA	8º CA	9º CA	8º CA	8º CA
Max. Mean Temp. (K)	1504	1779	1738	1770	1811
NO_x (g/kW.h)	6.66	7.46	4.54	5.1	5.69
SOOT (g/kW.h)	0.00077	0.000172	0.00121	0.0022	0.00131
CO (g/kW.h)	9.94	1.42	1.55	1.42	1.19
HC (g/kW.h)	35.21	4.04	4.45	4.11	3.83

EGR has had a similar impact on the mixture gas fractions in the pre-combustion phase (especially up to 20° CA BTDC) and the post-combustion phase. Therefore, the combustion duration was longer for EGR.

WVI injection was highly effective for both just before and after combustion (the phase after 20° CA BTDC), but it had no effect on the phase well before combustion. When we divide combustion into homogeneous combustion and diffusion combustion, the fuels pre-mixed in the combustion chamber (Hydrogen - Natural Gas and pilot diesel fuel) represent homogeneous combustion, while the fuels added later (diesel fuel by main injection) represent diffusion combustion. Since WVI initially affected diffusion combustion and later had an impact on homogeneous combustion, the combustion duration was shorter (Figure 5.85) [188].

Looking at the CO and SOOT emissions as well as the BSFC values, it can be said that WVI has a greater impact on diffusion combustion compared to homogeneous combustion (Table 5.51). Higher SOOT formation despite higher power suggests that the diffusion flame is weaker. The power increase has compensated for this in homogeneous combustion. WVI, with lower CO emissions, indicates that the homogeneous combustion flame is stronger than the diffusion flame. Despite the higher power, the slightly higher BSFC value shows that the phase representing a higher mass of fuel was somewhat affected. Additionally, a somewhat more intense combustion occurred compared to the EGR process. In rapid and intense combustion,

temperatures are high, leading to higher TE, NO_x, and MPRR values. When WI (D25NG50H25-20PI-25WI75°C) and WVI (D25NG50H25-20PI-15WVI100°C) are compared, WI involves the injection of the liquid phase into the combustion chamber, which necessitates heat withdrawal from the environment for the transition from the liquid phase to the vapor phase. This resulted in lower power, NO_x, TE, lower BSFC, and higher values for CO, UHC, and SOOT (Figure 5.84 and Figure 5.85).

Table 5.52 : Comparison of test result with optimally obtained results from processes for Mode 2 – D25NG75H15 (EGR, WI and WVI).

	Test Case	No Process	EGR	WI	WVI
Power (kW)	9.76	13.28	12.8	12.72	13
Torque (N.m)	102.42	139.34	134.29	133.47	136.42
BSFC (g/kW.h)	203.85	155.99	161.2	173.14	165.35
Ignition Delay (CA)	11º	11º	11º	11º	11º
Thermal Efficiency (%)	30.84	36.48	35.16	34.95	35.72
Combustion Duration (CA)	31º	23º	25º	22º	22º
MPRR (bar/CA)	1.85	3.08	2.31	2.51	2.56
Max. Press. (bar)	50.55	60.35	57.92	59.94	61.45
CA for Max. Press. (ATDC)	9º CA	12º CA	13º CA	14º CA	13º CA
Max. Mean Temp. (K)	1477	1809	1779	1793	1811
NO_x (g/kW.h)	4.9	5.44	3.42	4.07	4.42
SOOT (g/kW.h)	0.0012	0.0002	0.00122	0.00174	0.0011
CO (g/kW.h)	10.25	2.02	2.342	2.1	1.84
HC (g/kW.h)	36.73	8.76	9.557	8.34	7.83

The ID value showed similarities at all operating points (Figure 5.84). ID varies more depending on the main injection and pilot diesel injection timings and the sharp changes in the hydrogen fraction. While the no-process condition may seem reasonable in terms of performance values, it has not provided a preferable outcome, especially for NO_x emissions. Therefore, when considering emissions, the EGR - PI application has yielded significant results. The degrees to which the applied processes (EGR - PI, WI - PI, and WVI - PI) affect the homogeneous and diffusion phases of combustion can be seen in Figure 5.86.

Considering that the injection advance for D25NG50H25 is 14° CA BTDC, diffusion combustion has ended with TDC, and homogeneous combustion continues. When examining the contours, it can be observed that the contours for the EGR - PI condition are of a lighter color. This indicates that for WI and WVI, the homogeneous phase continues at higher temperatures [198]. The more effective role of the EGR - PI process in terms of diffusion flames was explained in Table 5.51, Figure 5.84, and

Figure 5.85. It can be seen that a significant portion of NOx formation occurs in homogeneous combustion (Figure 5.87). The effects of reducing temperatures can be examined using the applied processes in Figure 5.88. The figure shows the contour lines for points at 2500 K temperature at different piston positions.

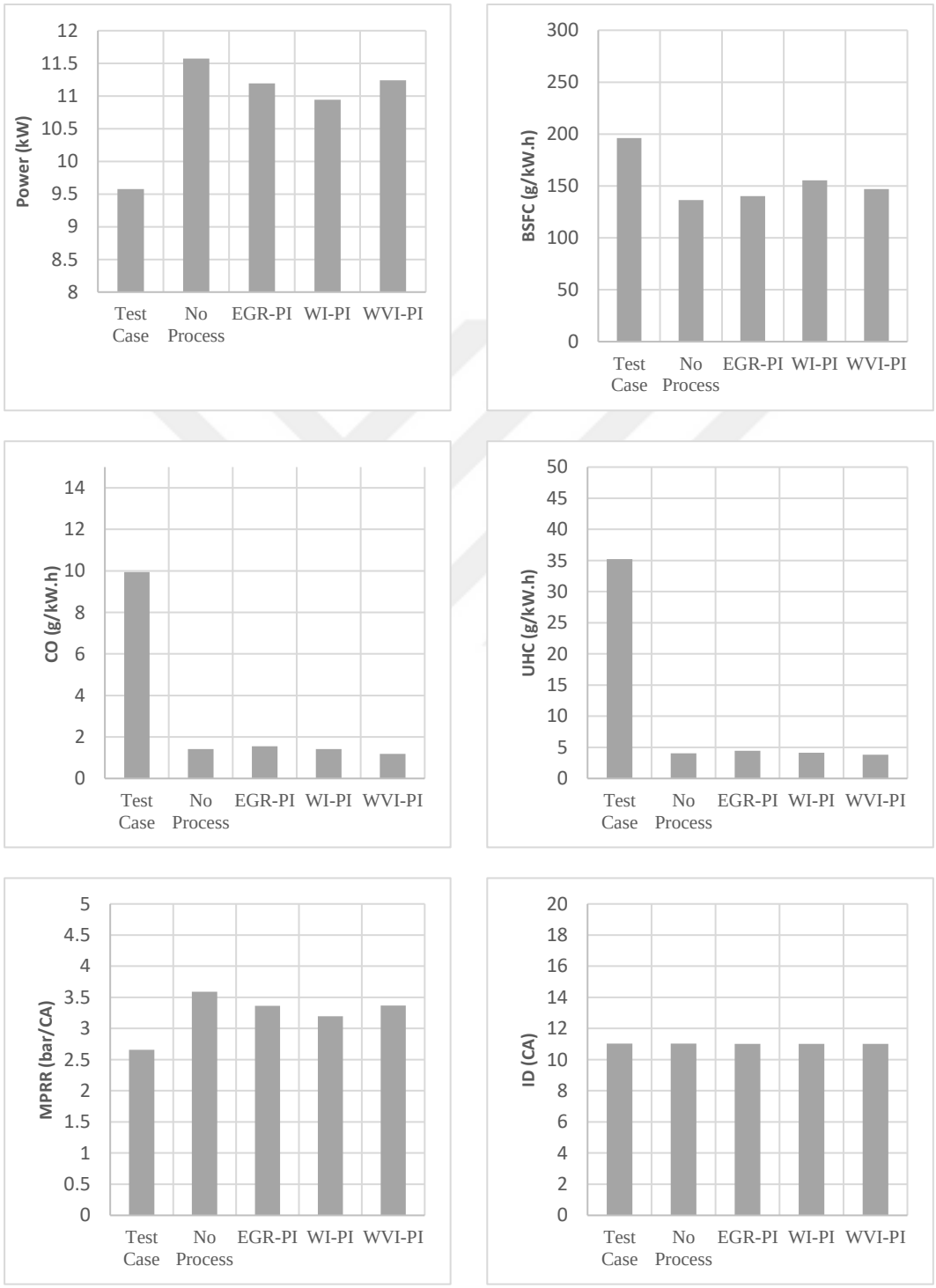

Figure 5.84 : Comparison of test data and results without the process with all obtained optimal states from applied processes in terms of power, BSFC, CO, UHC, MPRR and ID (for Mode 1).

It is evident that the high temperatures in the no-process condition are significantly reduced with EGR, WI, and WVI (Figure 5.88) [199]. Additionally, it can be observed that homogeneous combustion is more effectively realized with the WVI strategy compared to the EGR strategy (Figure 5.88).

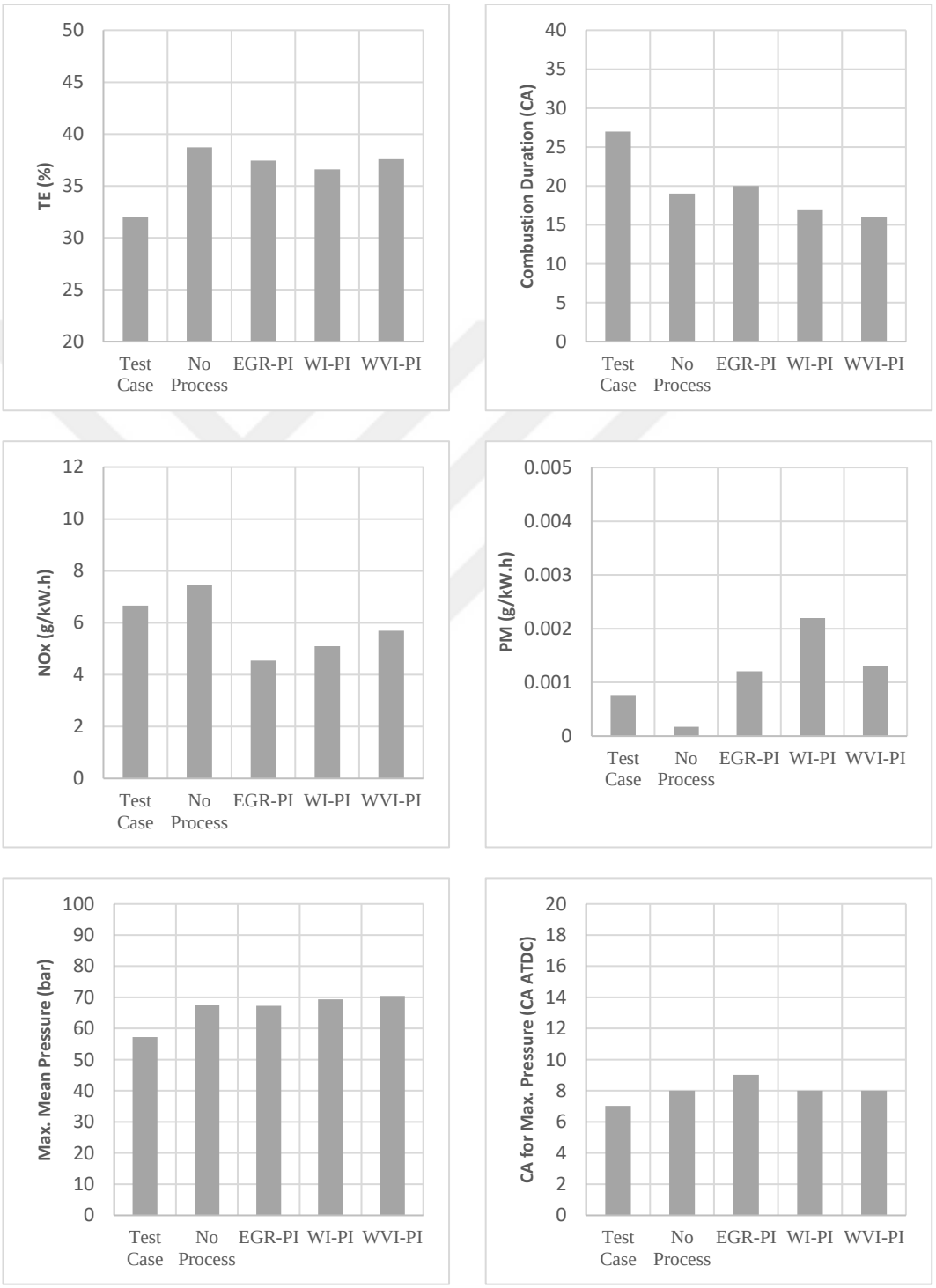

Figure 5.85 : Comparison of test data and results without the process with all obtained optimal states from applied processes in terms of TE, CD, NO_x, PM, Max. Press. and the position of Max. Press. Relative to TDC (for Mode 1).

The density of points with a temperature of 2500 K near the TDC position of the piston is higher for WVI than for EGR. It has been mentioned before that the WVI process deteriorates diffusion combustion and has a higher homogeneous combustion efficiency. Although the diffusion combustion phase of EGR is superior to the WVI process, it is not significantly behind in terms of homogeneous combustion.

EGR is effective in distributing homogeneously throughout the combustion chamber, while WVI is more effective in the region where it is injected and its vicinity. This is why diffusion combustion is less efficient for WVI. The progression of combustion has been similar for EGR and WVI, with only minor differences in the initial stages. The diffusion flame for WVI and the initial stages of homogeneous combustion for EGR have developed somewhat differently, but they have shown similarities in the later stages of combustion (Figure 5.86 and Figure 5.88).

The results of the no-process (D25NG75H15), EGR - PI (D25NG75H15-20PI-25WI75°C), and WVI - PI (D25NG75H15-20PI-15WVI100°C) operating points obtained for Mode 2 have been compared with the experimental results of D25NG75H00 (10° CA BTDC for SOI) (Table 5.52 and Figure 5.89 - Figure 5.93). It is evident that the performance values will increase with the additional energy input of hydrogen into the combustion chamber. However, the goal here is to achieve higher performance with lower overall emissions, which is why it was investigated for Mode 2. The no-process (D25NG75H15) resulted in increased NO_x and MPRR values, and to improve these values, EGR, WI, and WVI processes were applied.

The lowest values for NO_x and MPRR were achieved with the application of the EGR - PI (20% PI and 10% EGR for 100 °C) process in D25NG75H15-20PI-10EGR100°C. Even though the fuel fractions were the same at the operating point where EGR, WI, and WVI processes were applied (D25NG75H15), their effects on combustion were different. WI and WVI were more effective in the diffusion flame, while EGR played a more significant role in the homogeneous combustion phase. EGR, when distributed throughout the cylinder, can have a slightly disruptive effect on the combustion of hydrogen-natural gas-pilot diesel fuels. WI and WVI strategies, on the other hand, show disruptive effects, especially in the region where they are injected. The similarity between the region where the main diesel fuel injection occurs and the region where water jet/vapour injection occurs, and the initiation of combustion from this region, is the reason why WI and WVI strategies affect the diffusion flame.

The homogeneous combustion phase occurs more rapidly, while the diffusion flame takes place more slowly. In fact, this situation is due to the slower combustion of diesel fuel compared to hydrogen. When we look at it, even though the combustion rate of natural gas and hydrogen is slowed down, the combustion rate of hydrogen-enriched natural gas is higher compared to diesel.

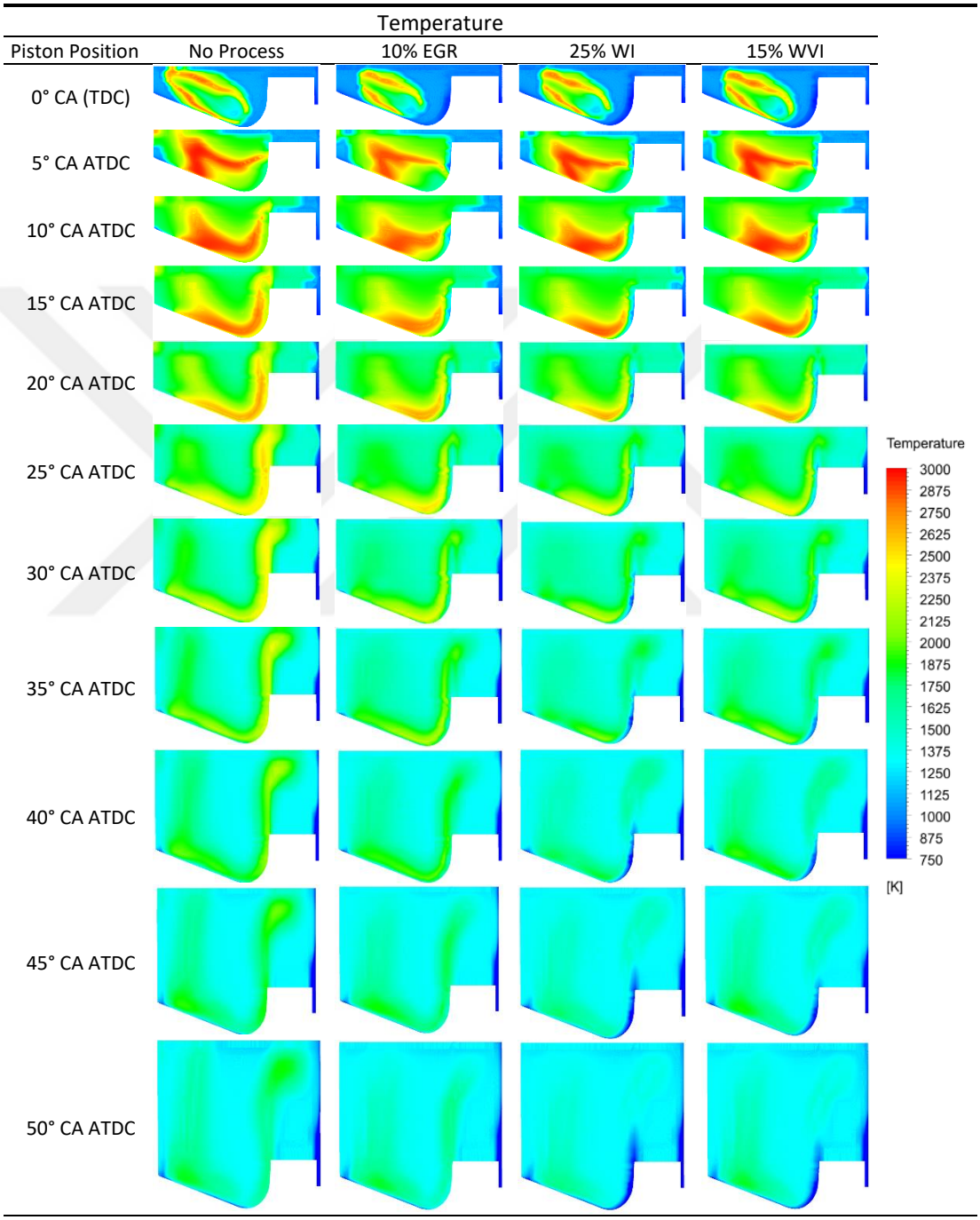

Figure 5.86 : Temperature contours at different piston positions for the optimal operating points obtained by applying no process and various types of processes (20% PI - 10% EGR, 20% PI - 25% WI and 20% PI - 15% WVI) to D25NG50H25 (Mode 1).

In the homogeneous combustion phase, the heat release rate (HRR) is accelerating, which results in relatively higher temperatures and pressures. Therefore, for WI and WVI, NO_x, MPRR, and in-cylinder pressure values are higher, while the combustion duration (CD) is shorter (Figure 5.89 and Figure 5.90). Compared to EGR, combustion is more abrupt and intense for WI and WVI.

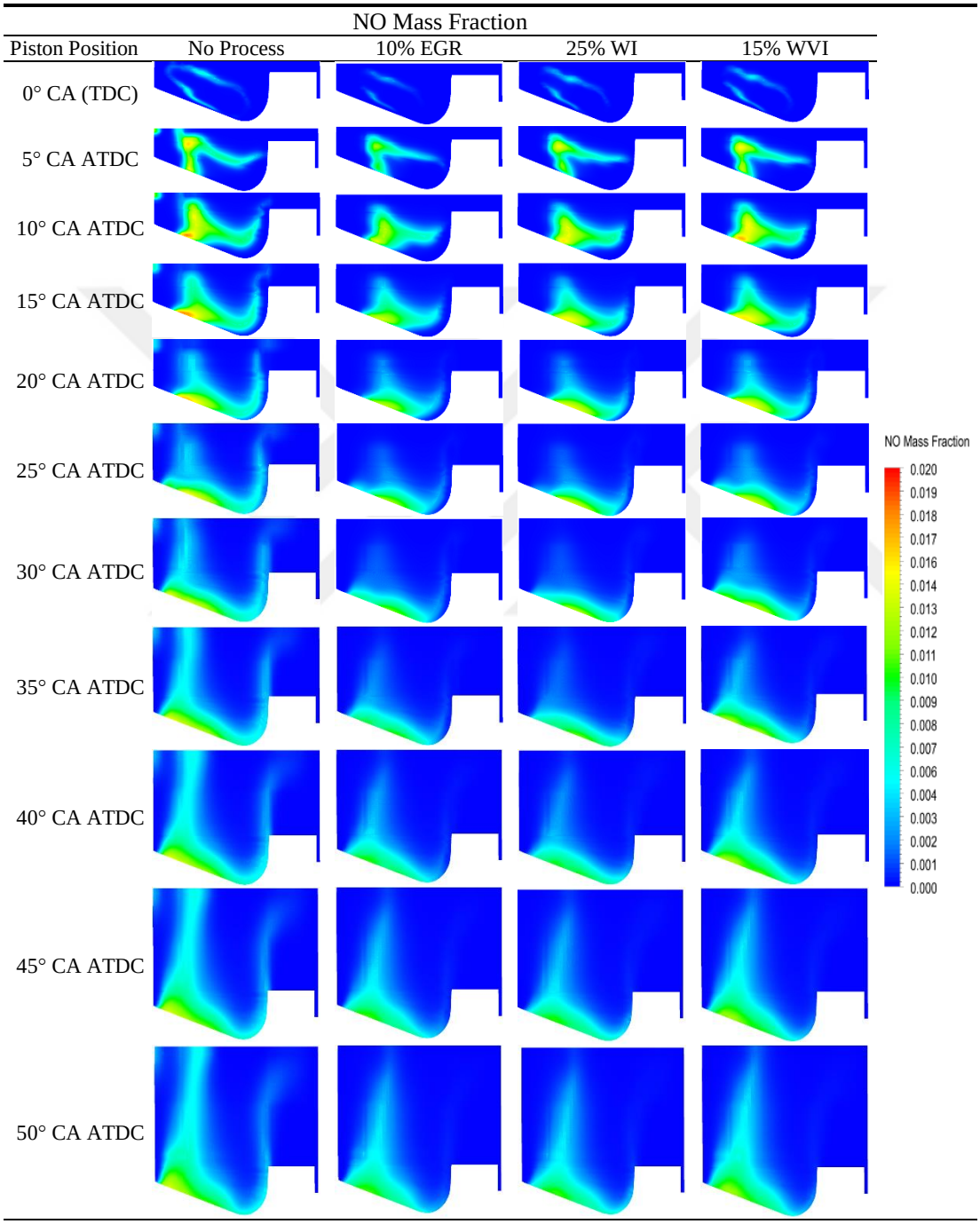

Figure 5.87 : NO mass fraction contours at different piston positions for the optimal operating points obtained by applying no process and various types of processes (20% PI - 10% EGR, 20% PI - 25% WI and 20% PI - 15% WVI) to D25NG50H25 (Mode 1).

Table 5.53 : Comparison of results with (EGR, WI and WVI) or without processes for Mode 1 – D25NG75H00 (SOI 14° CA BTDC).

	No Process	EGR	WI	WVI
Power (kW)	9.575	9.66	9.31	9.83
Torque (N.m)	100.477	101.34	97.71	103.15
BSFC (g/kW.h)	196	193.71	214.9	198.52
Ignition Delay (CA)	11º	11º	11º	11º
Thermal Efficiency (%)	32.02	32.3	31.14	32.87
Combustion Duration (CA)	27º	25º	23º	23º
MPRR (bar/CA)	2.66	2.42	2.41	2.51
Max. Press. (bar)	57.25	57	57.83	59.18
CA for Max. Press. (ATDC)	7º CA	9º CA	9º CA	10º CA
Max. Mean Temp. (K)	1504	1524	1528	1561
NO_x (g/kW.h)	6.66	3.8	4.2	4.58
SOOT (g/kW.h)	0.00077	0.0022	0.0041	0.0024
CO (g/kW.h)	9.94	8.68	8.63	7.21
HC (g/kW.h)	35.21	31.91	31.5	28.46

Although the combustion durations are equal for WI and WVI, the combustion for WVI occurred at higher pressures, resulting in higher temperatures. This has led to higher NO_x and MPRR values (Figure 5.89 and Figure 5.90). WVI has produced lower CO and HC emissions. Combustion of the premixed fuel with 75% natural gas and 20% PI content in the homogeneous combustion phase is more dominant for WVI compared to WI. For this reason, the power value is higher, and CO and UHC emissions are lower (Figure 5.89). Considering that the power is the area under the pressure-volume curve, WVI, which has a larger area, results in a higher power value.

The highest TE value was observed for no-process and WVI (Figure 5.90). For no-process, the reason is the absence of any additional processes. However, for WVI, the higher TE compared to EGR and WI is indirectly due to regional temperature values. EGR simultaneously reduces the oxygen concentration inside the combustion chamber, which partially reduces combustion efficiency and subsequently results in a decrease in TE due to the lower temperatures.

Similarly, with WI, the liquid jet that is sprayed needs heat from the combustion chamber to evaporate, which in turn lowers the temperatures and leads to a decrease in TE.

When looking at WVI, it can be observed that apart from the region where vapor is injected, the homogenization of the premixed fuel with air is more effective, leading to a higher quality of homogeneous combustion, and consequently, a higher TE value.

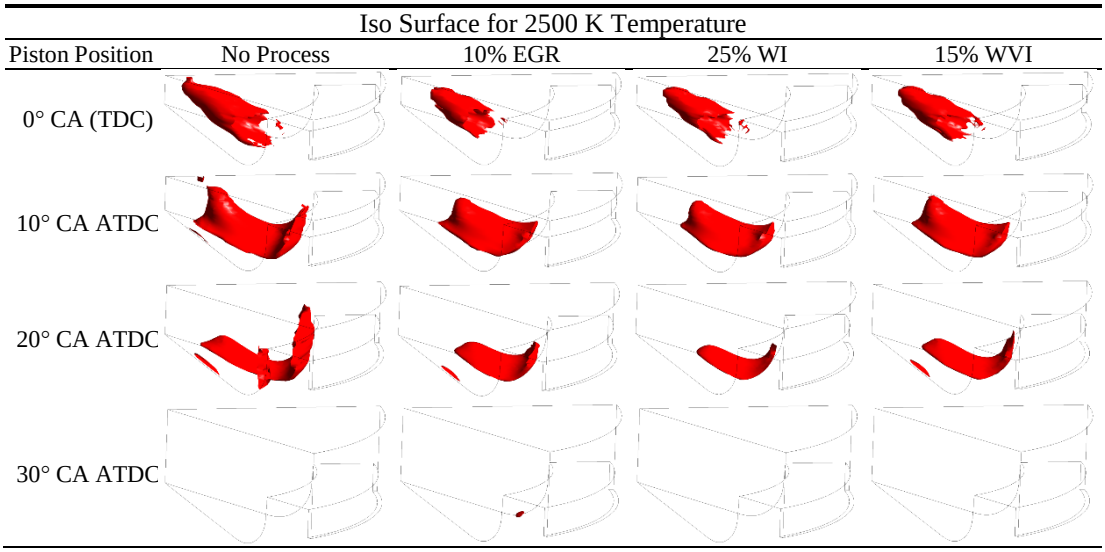

Figure 5.88 : Comparison of Iso Surfaces for temperature of 2500 K at different piston positions for the optimal operating points obtained by applying no process and various types of processes (20% PI - 10% EGR, 20% PI - 25% WI and 20% PI - 15% WVI) to D25NG50H25 (Mode 1).

As a result, the TE value remains higher for WVI compared to EGR and WI. PM emissions were observed to be highest in the case of water injection (WI) (Figure 5.90). WI is the strategy that affects both diffusion and homogeneous combustion the most. This is because the water injected in liquid phase into the diffusion combustion region disrupts the combustion of the core region of diesel fuel injected with the main spray and simultaneously lowers the temperatures in the homogeneous combustion regions, affecting the quality of homogeneous combustion.

SOOT (PM) emissions refer to fuel that has burned before oxidizing, and they increase the amount of fuel oxidizing in the core and its surroundings. NO_x emissions are highest in the case of WVI among the applied EGR, WI, and WVI processes. The WVI strategy, with higher temperatures in homogeneous combustion regions compared to EGR and WI, has produced higher values of NO_x emissions, in line with this situation. When examining the contours showing the temperature and NO mass fraction distributions for a piston position at 10° CA ATDC, it can be observed that the EGR process generates lower temperature values (Figure 5.91 and Figure 5.92).

Although the processes (EGR, WI, and WVI) have different effects on the combustion phases (diffusion and homogeneous combustion phases), the temperature distributions generally show similarities (Table 5.52 and Figure 5.93). This indicates that the processes' effects start differently after the beginning of the diffusion combustion process, but the progression of combustion is similar. When examining the effects of

process applications (EGR - PI, WI - PI, and WVI - PI) under experimental conditions with a 14° CA BTDC injection advance (D25NG75H00 14° CA BTDC for SOI), it is observed that the most suitable strategy implementation is WVI (Table 5.53 and Figure 5.94 - Figure 5.98).

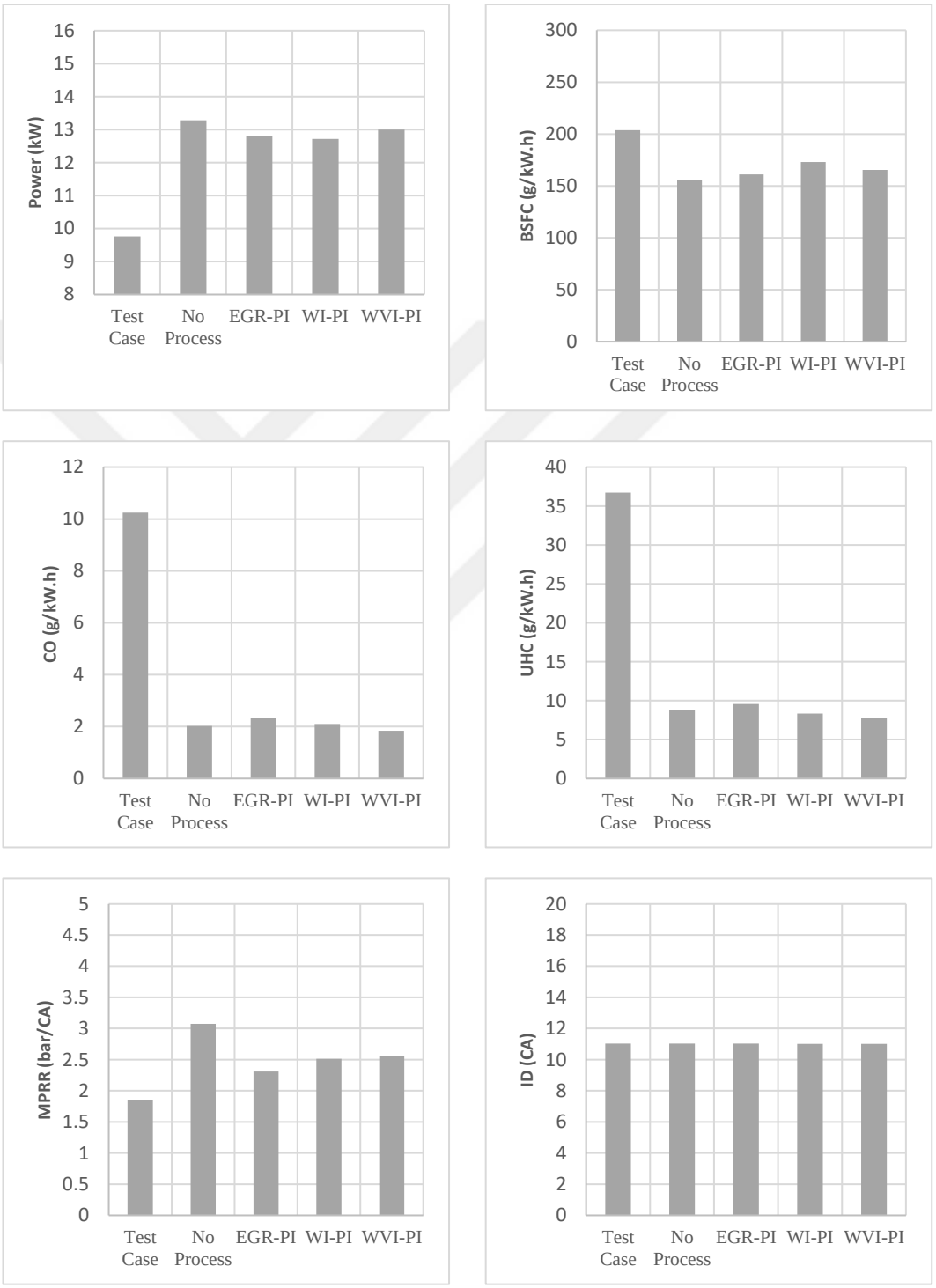

Figure 5.89 : Comparison of test data and results without the process with all obtained optimal states from applied processes in terms of power, BSFC, CO, UHC, MPRR and ID (for Mode 2).

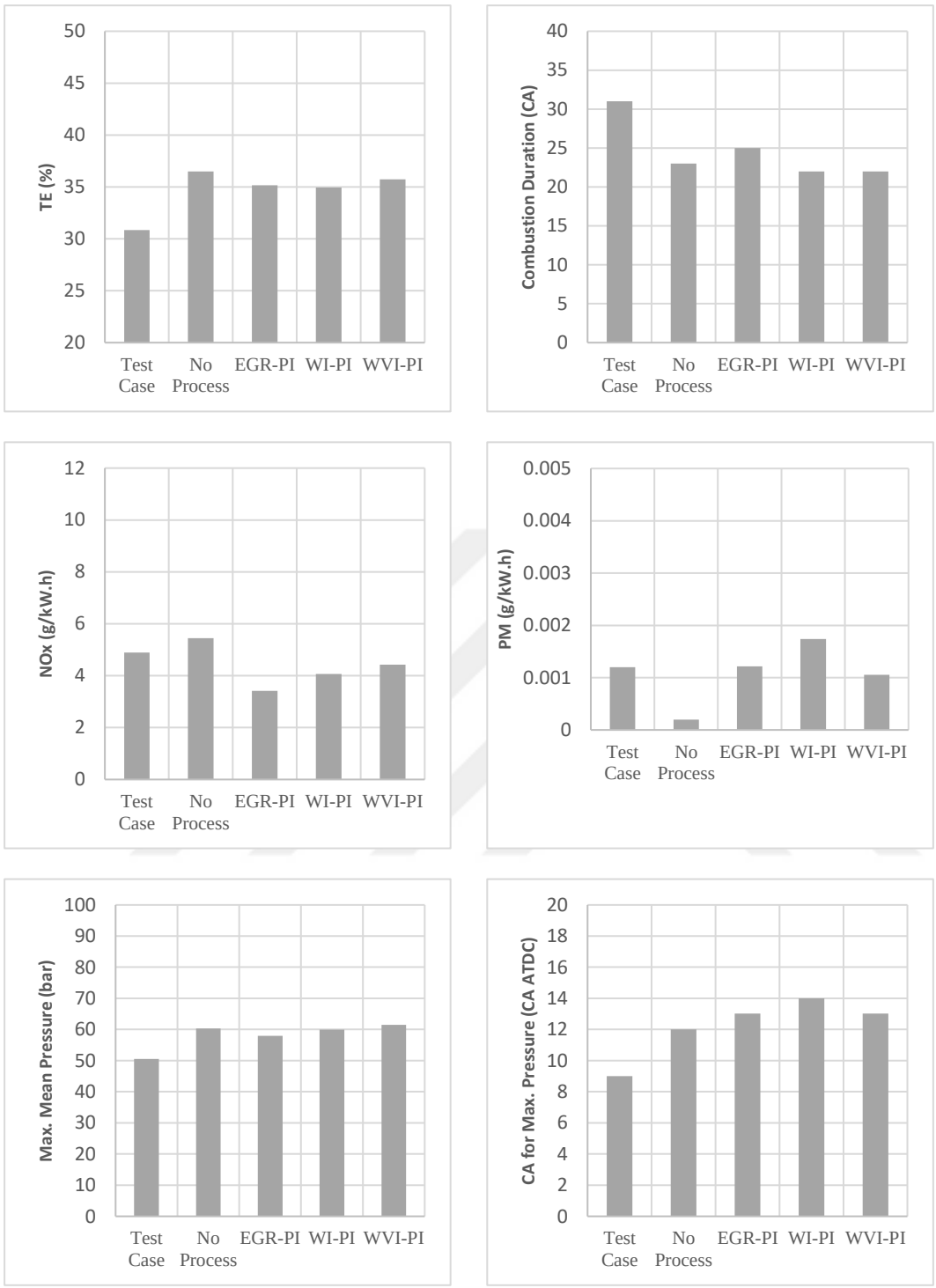

Figure 5.90 : Comparison of test data and results without the process with all obtained optimal states from applied processes in terms of TE, CD, NO_x, PM, Max. Press. and the position of Max. Press. Relative to TDC (for Mode 2).

Since there is no hydrogen in the gas mixture at the D25NG75H00 operating point, the homogeneous combustion phase was smoother (lower MPRR) and the combustion rate was lower (Figure 5.94 and Figure 5.95). In fact, the power value was even higher with the WVI under the test conditions (Figure 5.94). The increase in power according to

the test conditions was provided by the application of pilot diesel fuel (20% PI). The reason why the WVI strategy offers higher performance values compared to the EGR and WI strategies is due to the reasons explained in the previous sections.

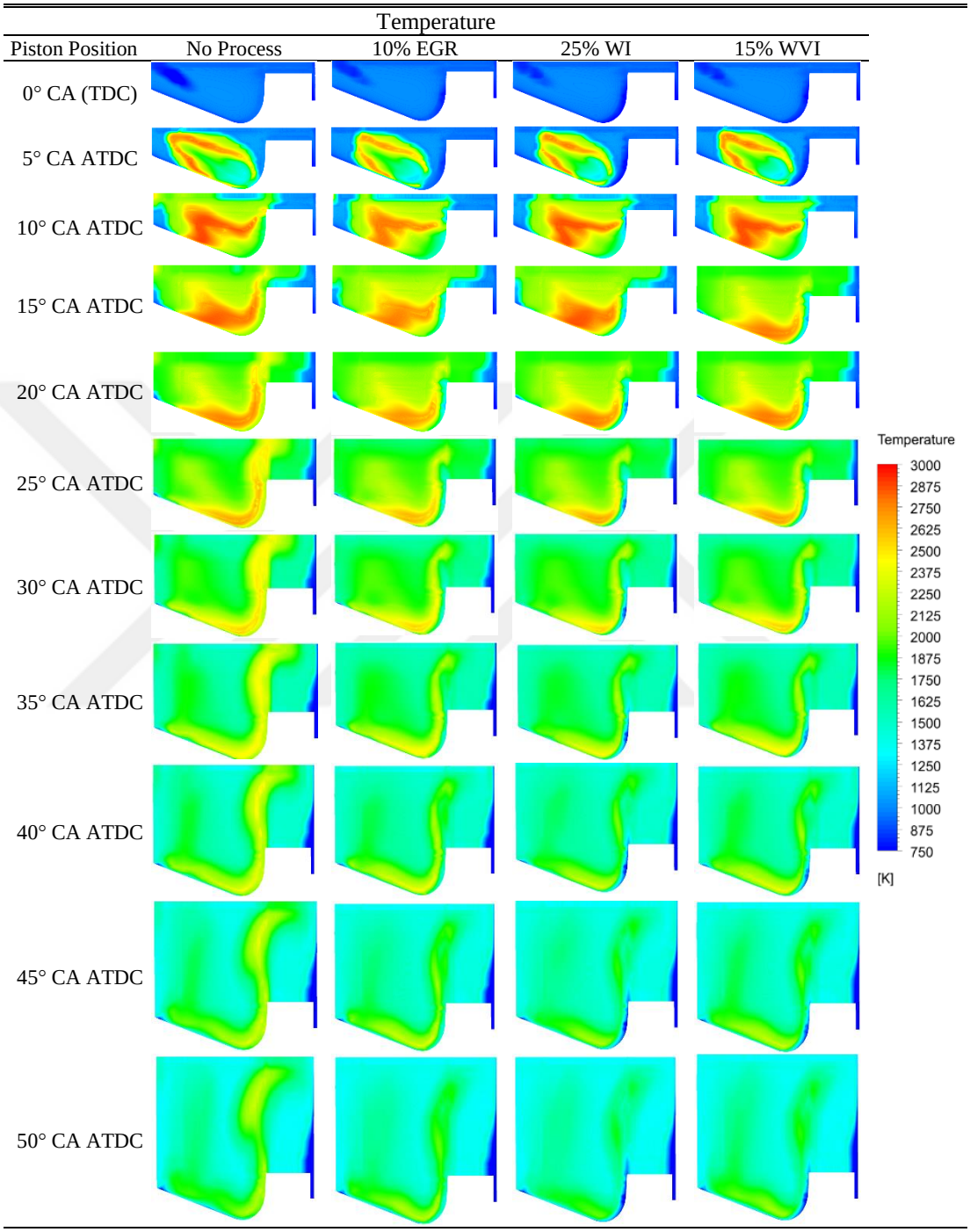

Figure 5.91 : Temperature contours at different piston positions for the optimal operating points obtained by applying no process and various types of processes (20% PI - 10% EGR, 20% PI - 25% WI and 20% PI - 15% WVI) to D25NG75H15 (Mode 2).

Under test conditions, the mixture in the homogeneous combustion phase contains a combination of natural gas and pilot diesel fuel. Since natural gas is a fuel with a low

combustion rate, the combustion duration is longer compared to the other operating points where hydrogen is included. The highest power and TE values were observed at the D25NG75H00-20PI-15WVI100°C operating point (Figure 5.94 and Figure 5.95). Power and TE increase were observed in all processes except WI - PI according to the test conditions.

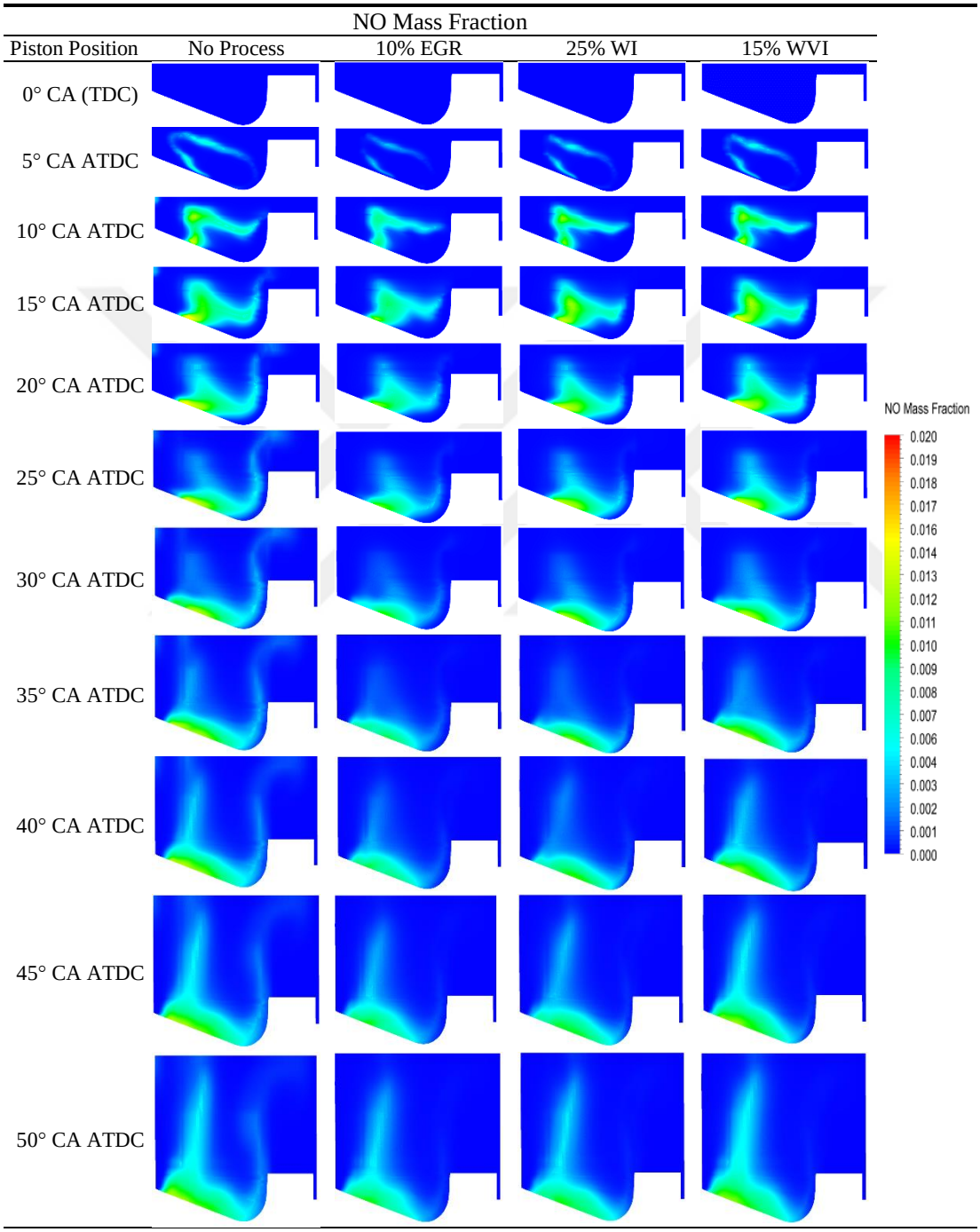

Figure 5.92 : NO mass fraction contours at different piston positions for the optimal operating points obtained by applying no process and various types of processes (20% PI - 10% EGR, 20% PI - 25% WI and 20% PI - 15% WVI) to D25NG75H15 (Mode 2).

The reason for not observing it in WI is that water needs to extract heat from the environment to transition from the liquid phase to the vapor phase. After the heat is absorbed, the combustion efficiency decreases, resulting in a reduction in TE and power.

The EGR process affects the mixture formation in all areas of the combustion chamber, which is why TE and power values have lagged behind the WVI process. The 20% PI strategy applied to all processes has improved the efficiency of the homogeneous combustion phase, contributing to the reduction of CO and UHC emissions (Figure 5.94). The WI process, which has the most influence on the diffusion combustion phase (D25NG75H00-20PI-25WI75°C), has led to the highest PM emissions (Figure 5.95). The MPRR values have remained reasonable and similar levels due to the hydrogen-free premixture (Figure 5.94).

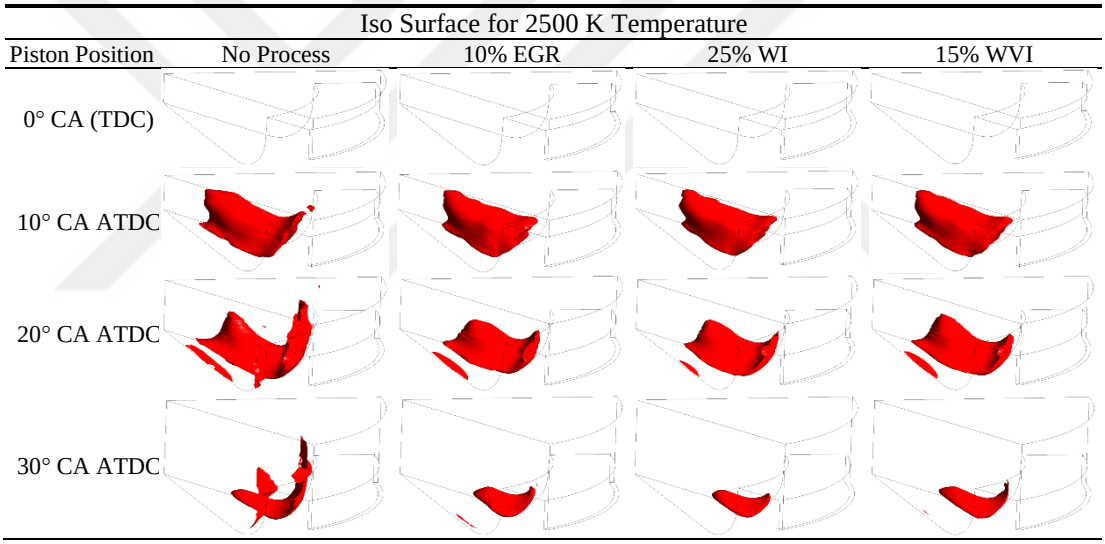

Figure 5.93 : Comparison of Iso Surfaces for temperature of 2500 K at different piston positions for the optimal operating points obtained by applying no process and various types of processes (20% PI - 10% EGR, 20% PI - 25% WI and 20% PI - 15% WVI) to D25NG75H15 (Mode 2).

The influence of EGR, WI, and WVI processes on the homogeneous combustion phase is clearly visible in Figure 5.96. In particular, it can be seen that EGR and WI have temperature contours distributed in lighter colors. When the NO mass fraction distributions are examined, it is observed that EGR – PI application produces less NO_x, while more formation is observed for WVI (Figure 5.97).

When isocontours at 2500 K temperature are followed for EGR, WI, and WVI at different piston positions, it is observed that the points with the highest temperature of 2500 K are formed after the test conditions with WVI. While temperatures are

extinguished more quickly for WI (water jet injection), similar point density can be mentioned for EGR and WVI (Figure 5.98) [200].

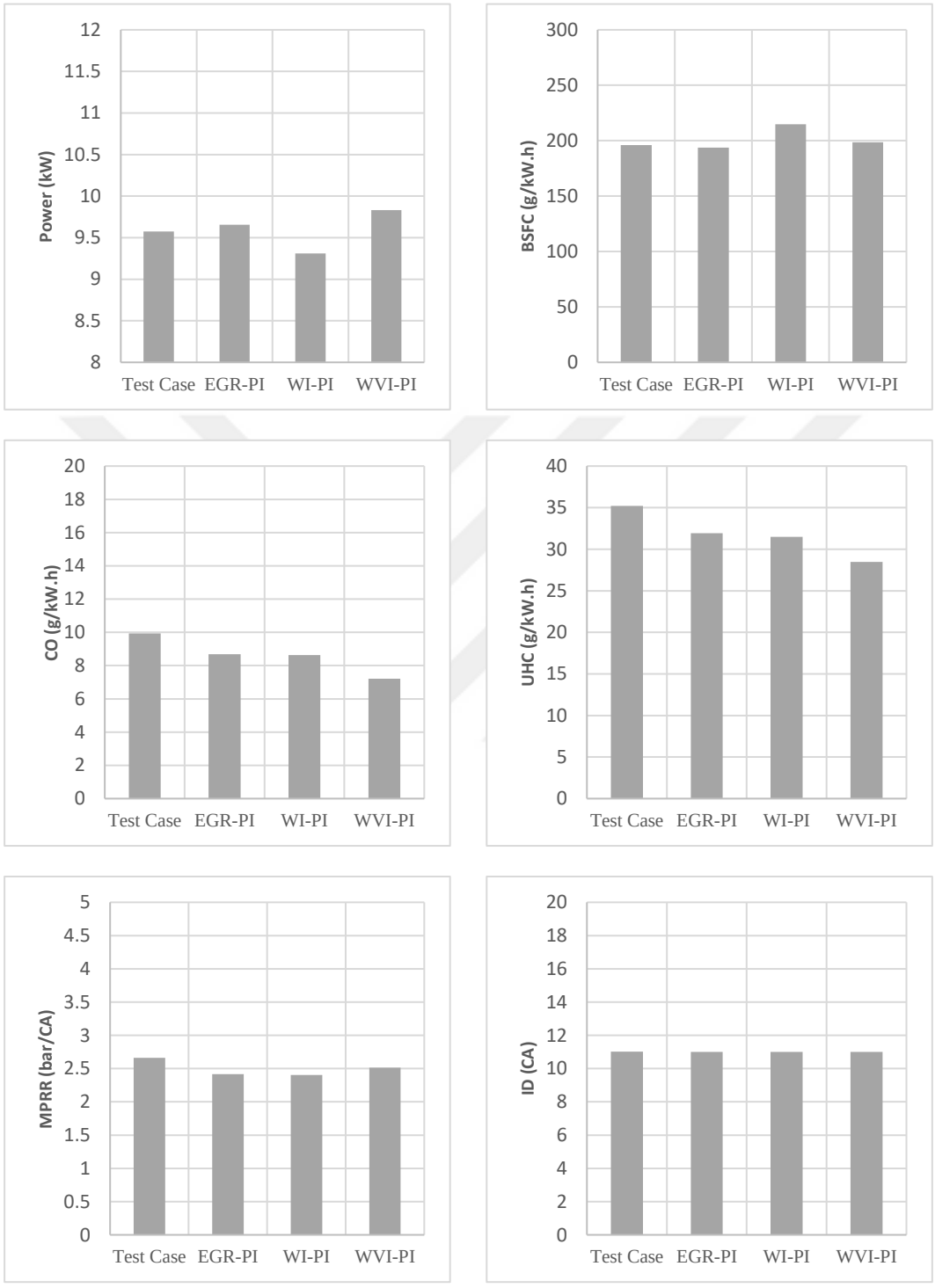

Figure 5.94 : Comparison of test and process-applied (EGR, WI, and WVI) results for D25NG75H00 (14° CA BTDC SOI) in terms of power, BSFC, CO, UHC, MPRR, and ID.

The effects of the applied processes (EGR, WI, and WVI) on the test conditions for a working point with a 10° CA BTDC injection advance (D25NG75H00 10° CA BTDC

for SOI) resulted in improvements in performance and emission values (Table 5.54 and Figure 5.99 – Figure 5.103). The highest values for power and TE are achieved with WVI, while the lowest values for CO and UHC are observed (Figure 5.99 – Figure 5.100). The BSFC value increases with EGR and WI processes, but it remains close to the test conditions with WVI (Figure 5.99). The MPRR value has been lowered by the applied strategies. The ID has decreased in the EGR – PI case, while in other processes, it is similar to the test conditions (Table 5.54 and Figure 5.99).

Table 5.54 : Comparison of results with (EGR, WI and WVI) or without processes for Mode 2 – D25NG75H00 (SOI 10° CA BTDC).

	No Process	EGR	WI	WVI
Power (kW)	9.76	9.31	9.73	9.95
Torque (N.m)	102.42	97.72	102.104	104.41
BSFC (g/kW.h)	203.85	212.93	217.97	207.89
Ignition Delay (CA)	11º	9º	11º	11º
Thermal Efficiency (%)	30.84	29.42	30.74	31.44
Combustion Duration (CA)	31º	32º	27º	27º
MPRR (bar/CA)	1.85	1.43	1.5	1.57
Max. Press. (bar)	50.55	48.55	49.89	50.69
CA for Max. Press. (ATDC)	9º CA	10º CA	12º CA	12º CA
Max. Mean Temp. (K)	1477	1429	1493	1505
NO_x (g/kW.h)	4.9	2.77	3.14	3.37
SOOT (g/kW.h)	0.0012	0.0035	0.0035	0.0029
CO (g/kW.h)	10.25	12.69	10.23	8.88
HC (g/kW.h)	36.73	40.82	32	30.96

The combustion duration (CD) has increased with EGR – PI, but it has decreased below the test conditions with WI – PI and WVI – PI. NO_x is lower in all processes compared to the test results, with the lowest NO_x being achieved with EGR – PI. PM emissions, inversely related to NO_x, reached the highest value with EGR – PI and the lowest value with WVI – PI (Figure 5.100). The point of maximum pressure occurred later in the crank angle with all applied processes, moving to the right of TDC. It can be observed that for the test conditions with a 14° CA BTDC injection advance, combustion began during the compression stroke, while for the test conditions with a 10° CA BTDC injection advance, combustion started at the end of the compression stroke and TDC position. In the case of EGR – PI application, the combustion duration is slightly longer and softer, with maximum pressure being lower (Figure 5.100) [179,201]. The presence of fuel that starts to ignite earlier than other processes and test conditions has caused a decrease in power.

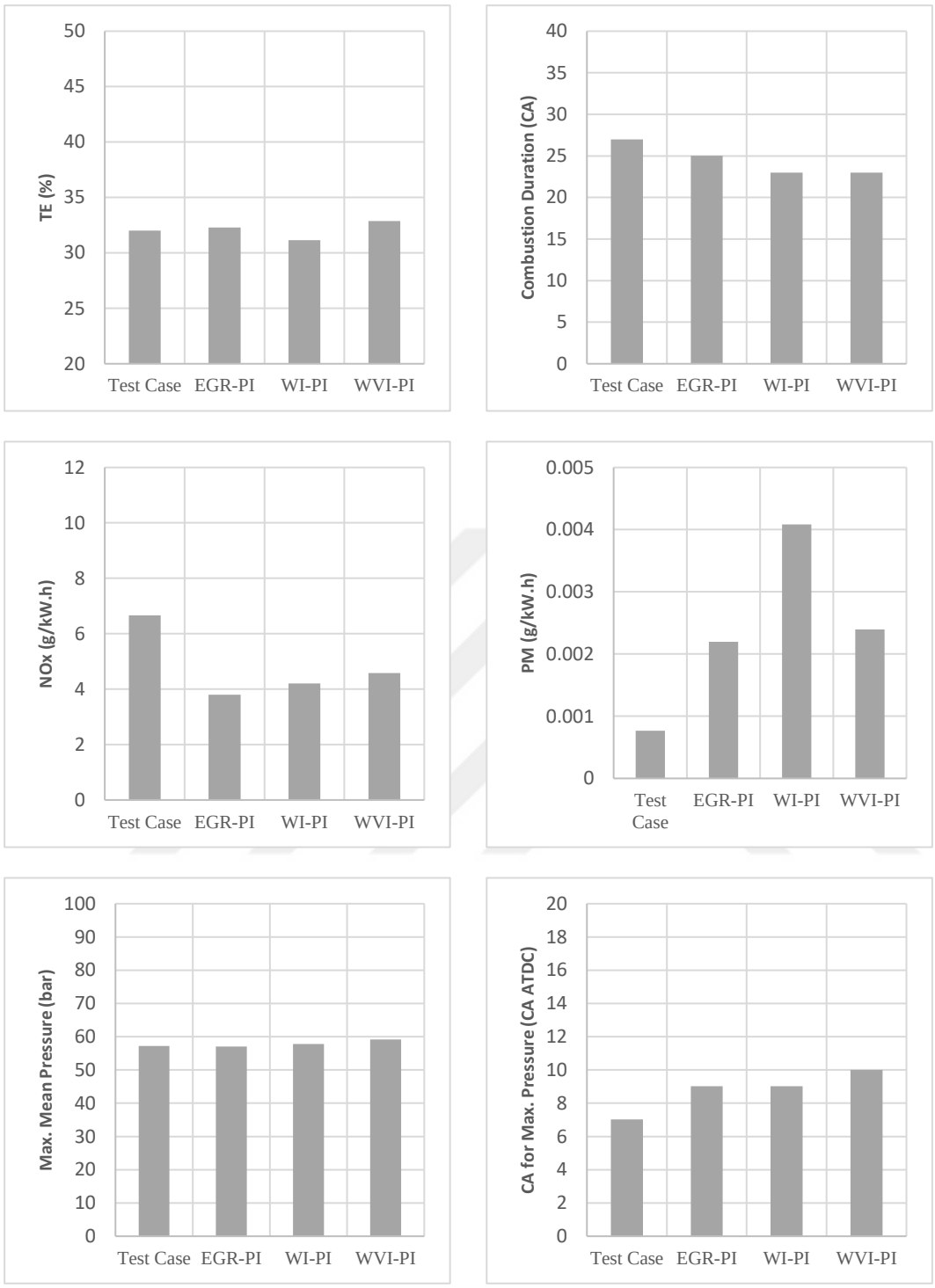

Figure 5.95 : Comparison of test and process-applied (EGR, WI, and WVI) results for D25NG75H00 (14° CA BTDC SOI) in terms of TE, CD, NO_x, PM, Max. Press. and the position of Max. Press. Relative to TDC.

The higher strength of the homogeneous combustion phase with the WVI strategy, along with the interaction of vapor with turbulence, allows for better atomization of the injected fuel particles, increasing combustion efficiency. Therefore, power and TE values have increased, while BSFC, UHC, and CO values have decreased (Figure 5.99

and Figure 5.100). Although to a lesser extent, the increase in combustion pressure and temperatures has also increased NO_x emission levels. Since EGR and WI have a more significant effect on the diffusion combustion phase, the highest PM values have been observed in these processes. Figures 5.101 and 5.102 show that the EGR process has the most significant effect on temperature and NO_x distribution.

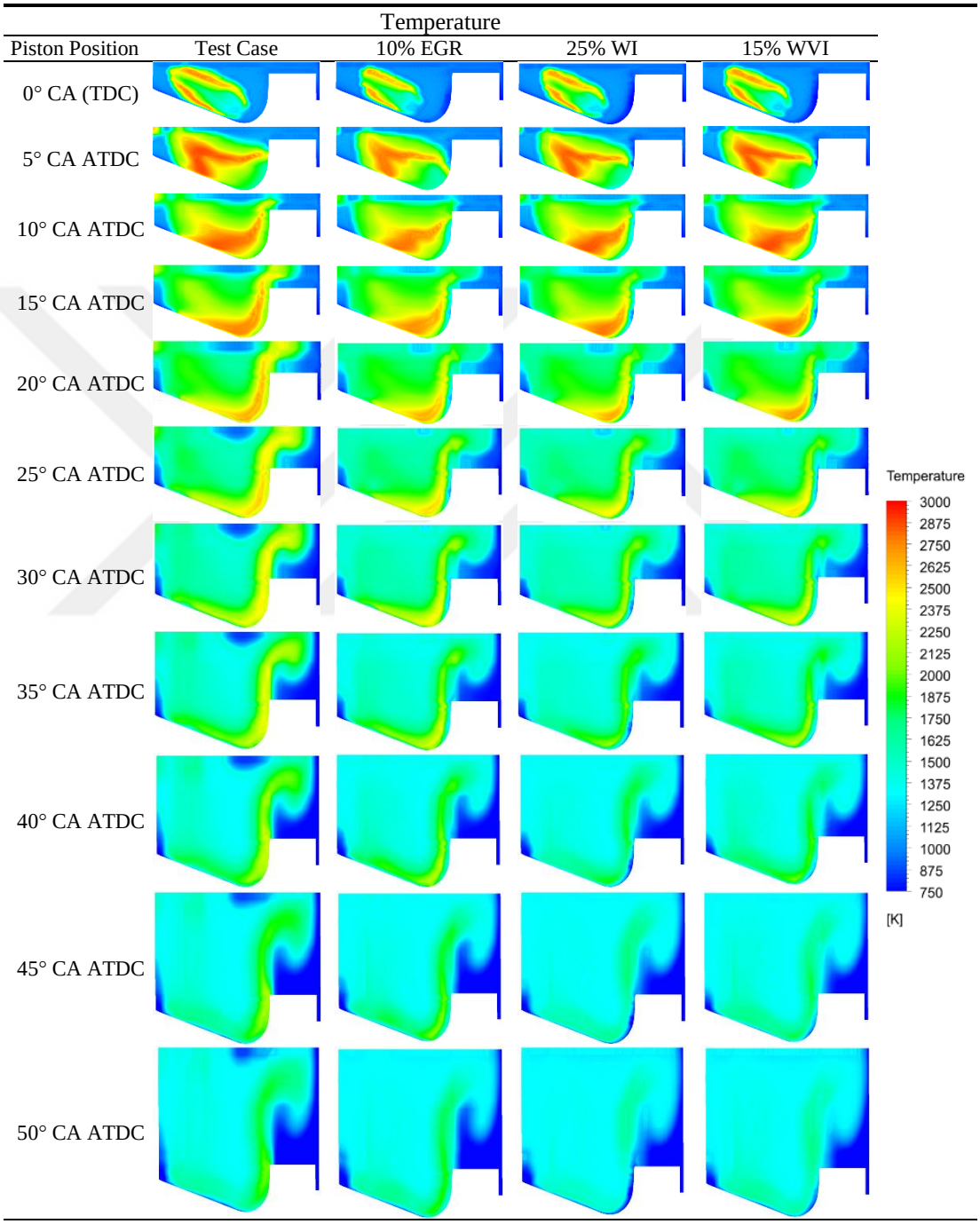

Figure 5.96 : Comparison of temperature contours at different piston positions between test case with the optimal operating points obtained by applying various types of processes (20% PI - 10% EGR, 20% PI - 25% WI and 20% PI - 15% WVI) to D25NG75H00 (SOI of 14° CA BTDC).

It was previously mentioned that combustion consists of diffusion and homogeneous combustion phases. Based on this, it can be observed that the EGR process has a more significant effect on homogeneous combustion, while the WVI and WI processes are more effective on diffusion combustion (Figure 5.101 and Figure 5.102).

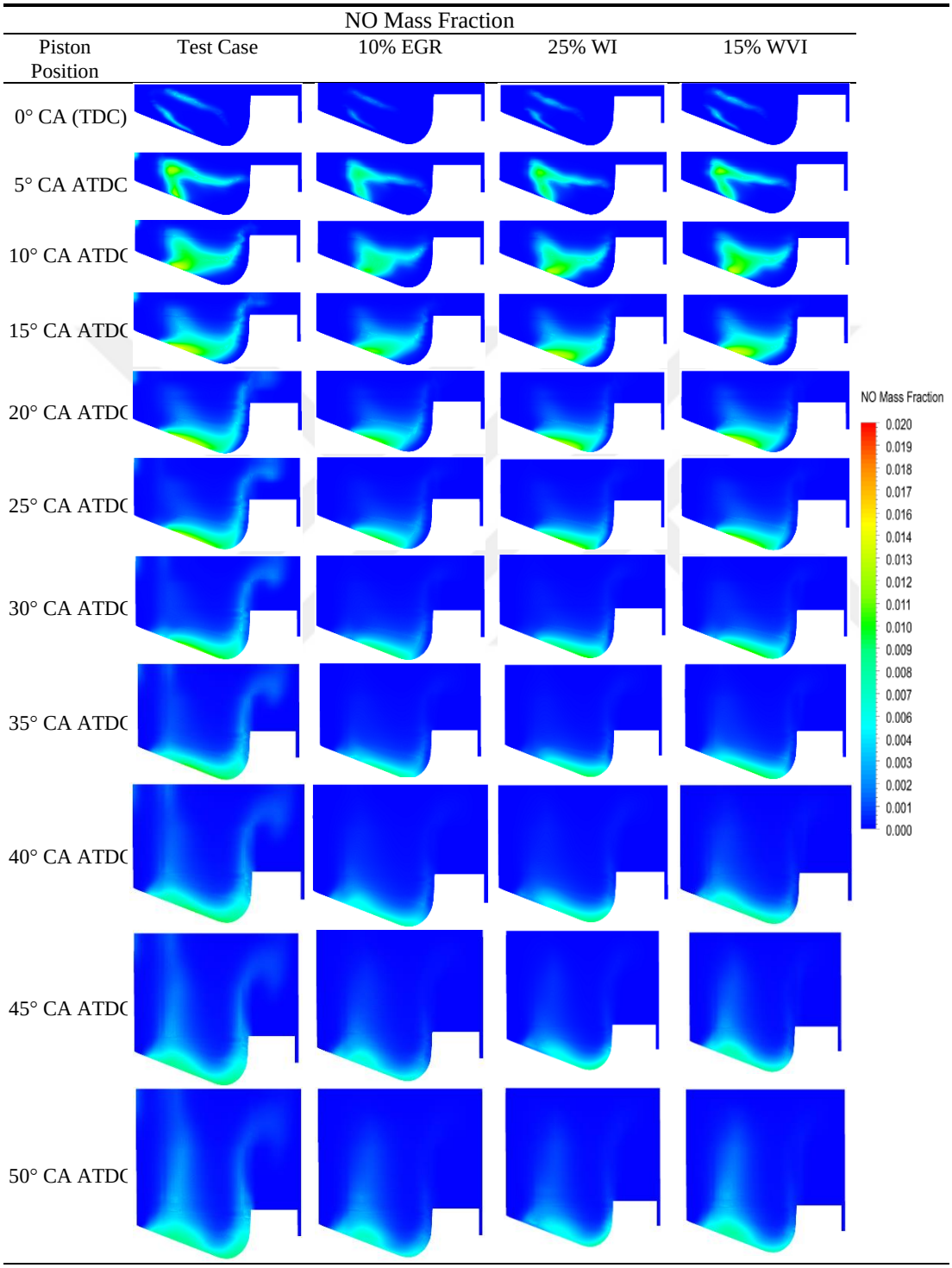

Figure 5.97 : Comparison of NO mass fraction contours at different piston positions between test case with the optimal operating points obtained by applying various types of processes (20% PI - 10% EGR, 20% PI - 25% WI and 20% PI - 15% WVI) to D25NG75H00 (SOI of 14° CA BTDC).

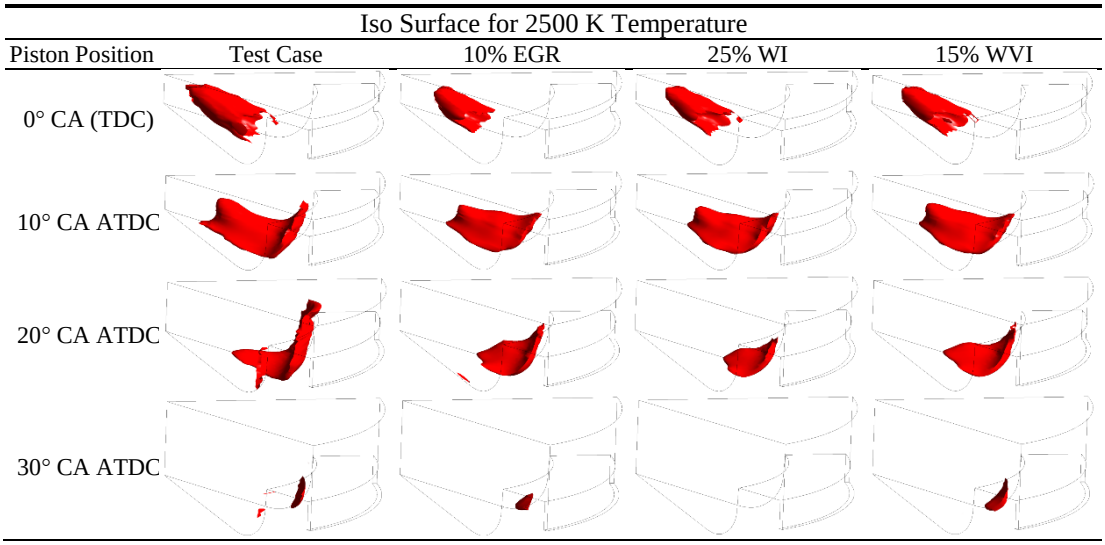

Figure 5.98 : Comparison of Iso Surfaces for temperature of 2500 K at different piston positions between test case with the optimal operating points obtained by applying various types of processes (20% PI - 10% EGR, 20% PI - 25% WI and 20% PI - 15% WVI) to D25NG75H00 (SOI of 14° CA BTDC).

EGR distributed throughout the combustion chamber much earlier and directly affected the air-natural gas-pilot diesel fuel premixture. In contrast, the WI and WVI processes were introduced into the combustion chamber later, making them more effective on the diffusion flame, which, in turn, leads to an increase in PM emissions.

As mentioned earlier, when comparing WI to WVI, the WI process had a more significant impact on both the diffusion flame and the homogeneous combustion phase. The transition of the liquid phase to the vapor phase, which requires heat to be drawn from the environment, reduced combustion efficiency.

When examining points with combustion temperatures of 2500 K at different piston positions, it is evident that similar results are obtained for all processes (Figure 5.103). However, the similarity of temperatures at 2500 K does not necessarily imply the same for other temperatures. From the results, it can be seen that EGR application leads to lower temperature distributions.

NO_x formation is observed at all temperatures of 1800 K and above. Therefore, when looking at the range between 1800-2500 K, the process with the highest uniform temperature distribution in this temperature range will be observed with WVI. Following that, the ranking will be WI and EGR. In the case of D25NG00H75, which has the highest hydrogen fraction for Mode 1, it was observed that the Pilot Injection (PI) had a negative impact when the processes (EGR - PI, WI - PI, and WVI - PI) were examined.

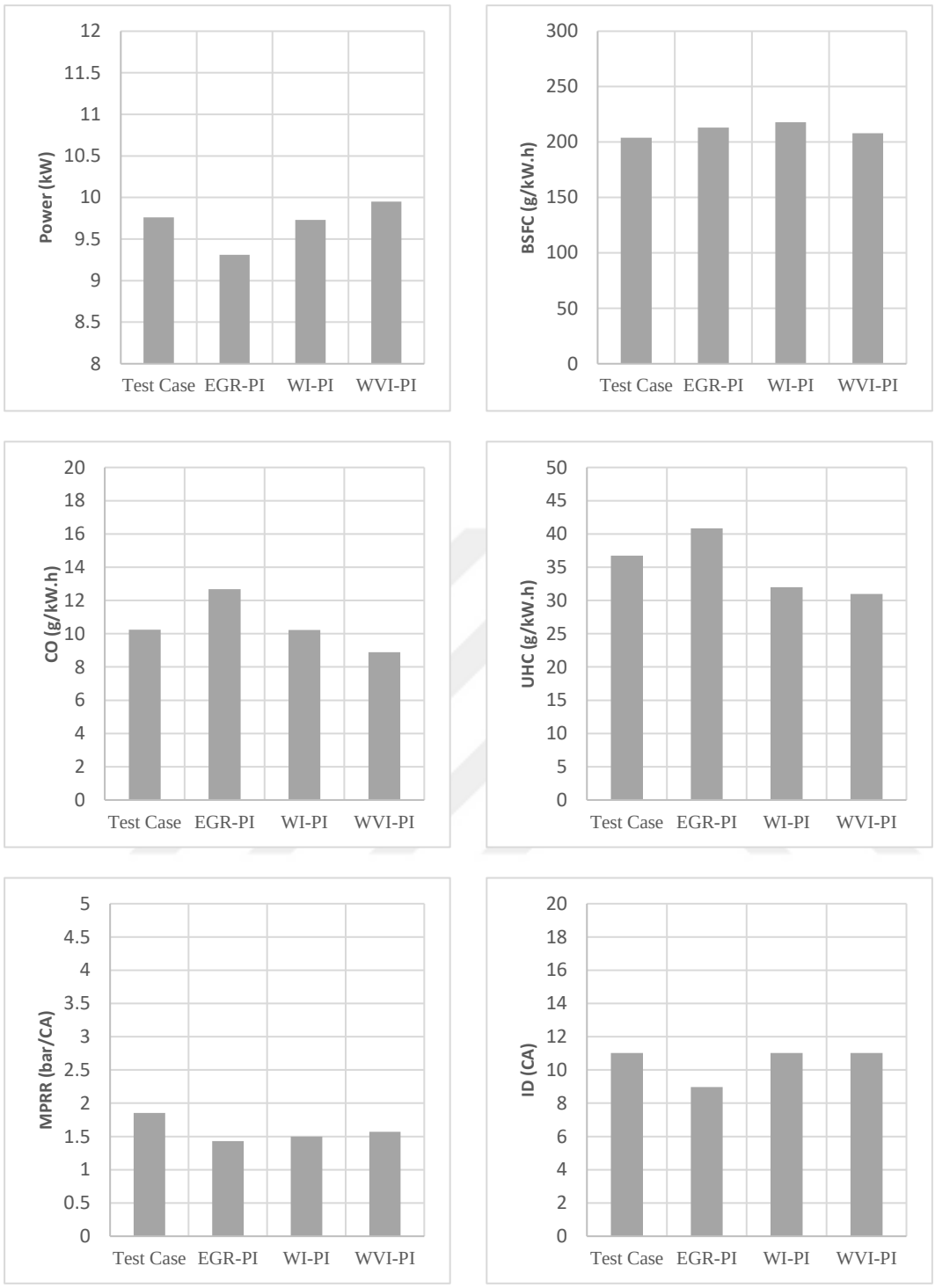

Figure 5.99 : Comparison of test and process-applied (EGR, WI, and WVI) results for D25NG75H00 (10° CA BTDC SOI) in terms of power, BSFC, CO, UHC, MPRR, and ID.

The reason for the negative effect of applying PI (20%) at high hydrogen fraction working points is that it increases the premixing ratio accumulating in the combustion chamber until the ignition starts, causing combustion to start abruptly and intensively. The rapid combustion and high lower heating value of hydrogen in the premix further

exacerbate these abrupt and intense combustion conditions. Consequently, the MPRR value is higher with PI than without it (Table 5.55 and Figure 5.104). However, the applied EGR, WI, and WVI, while causing decreases, could not lead to a reducing effect, especially for NO_x.

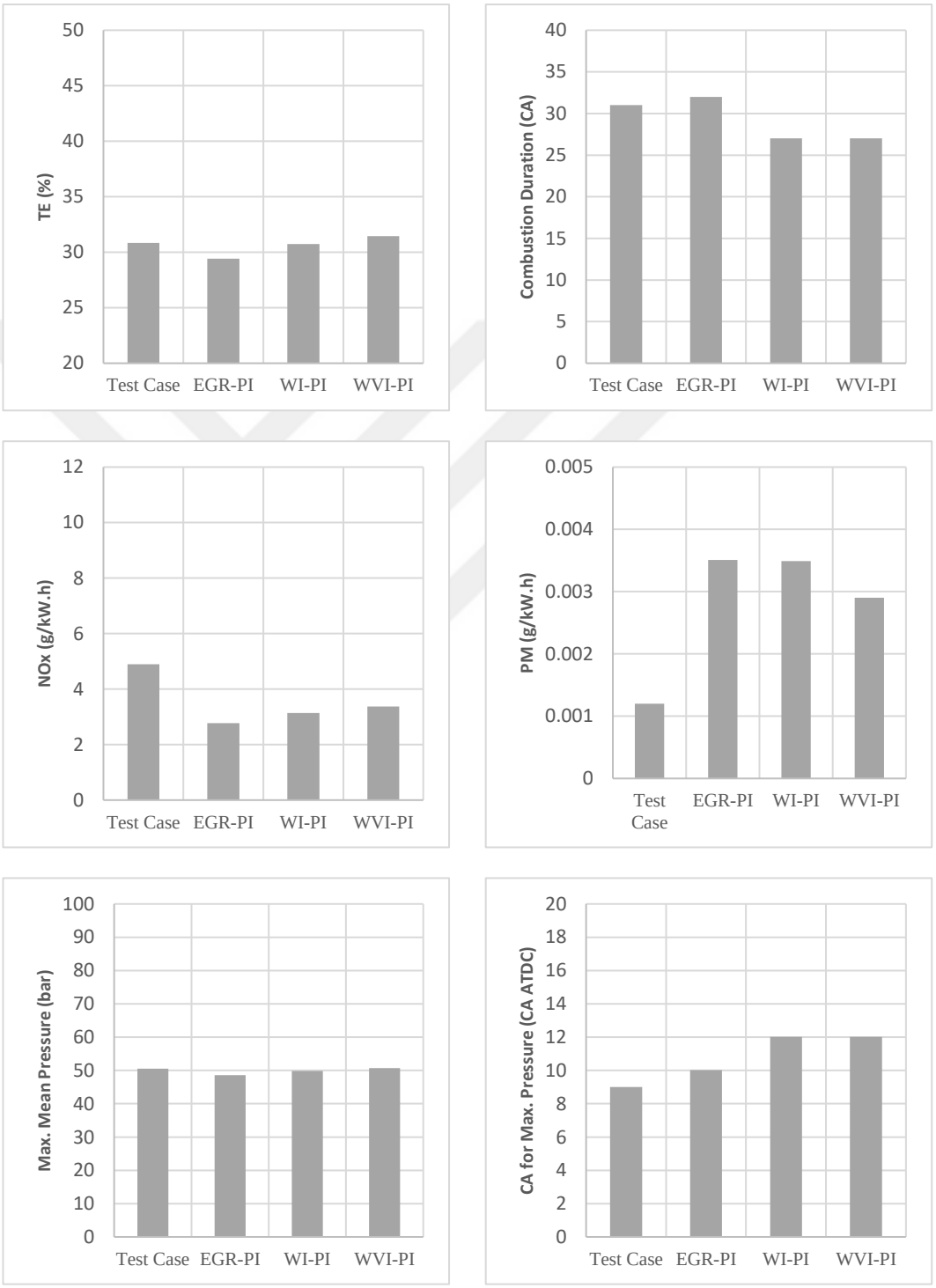

Figure 5.100 : Comparison of test and process-applied (EGR, WI, and WVI) results for D25NG75H00 (10° CA BTDC SOI) in terms of TE, CD, NO_x, PM, Max. Press. and the position of Max. Press. Relative to TDC.

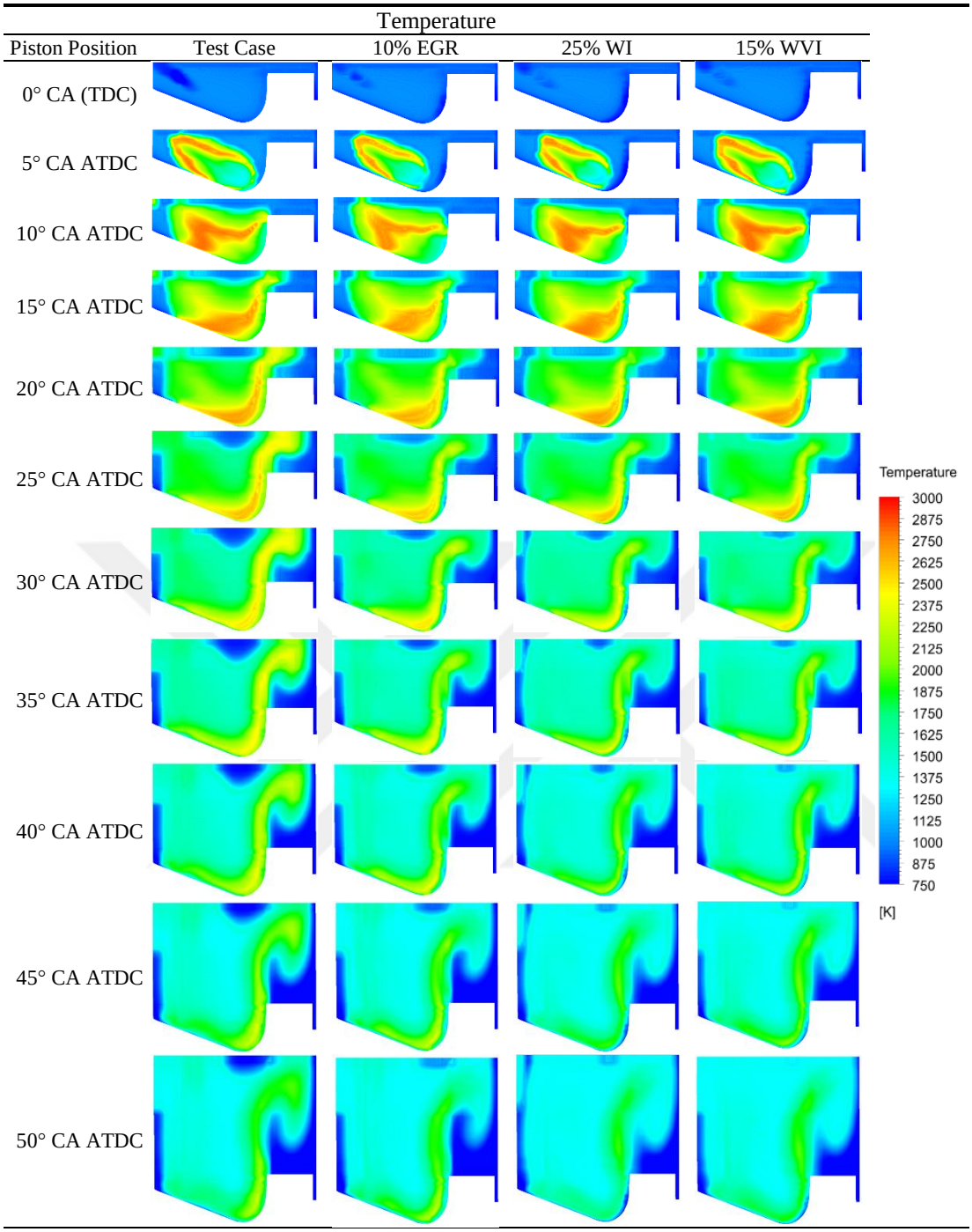

Figure 5.101 : Comparison of temperature contours at different piston positions between test case with the optimal operating points obtained by applying various types of processes (20% PI - 10% EGR, 20% PI - 25% WI and 20% PI - 15% WVI) to D25NG75H00 (SOI of 10° CA BTDC).

While temperatures and pressures have increased, the TE value has decreased. As is known, in cases of abrupt and intense combustion, combustion durations are short, and the crank angle at which maximum pressure occurs is close to TDC. In such combustion events, the area under the pressure-volume curve will decrease, leading to a deterioration in performance values.

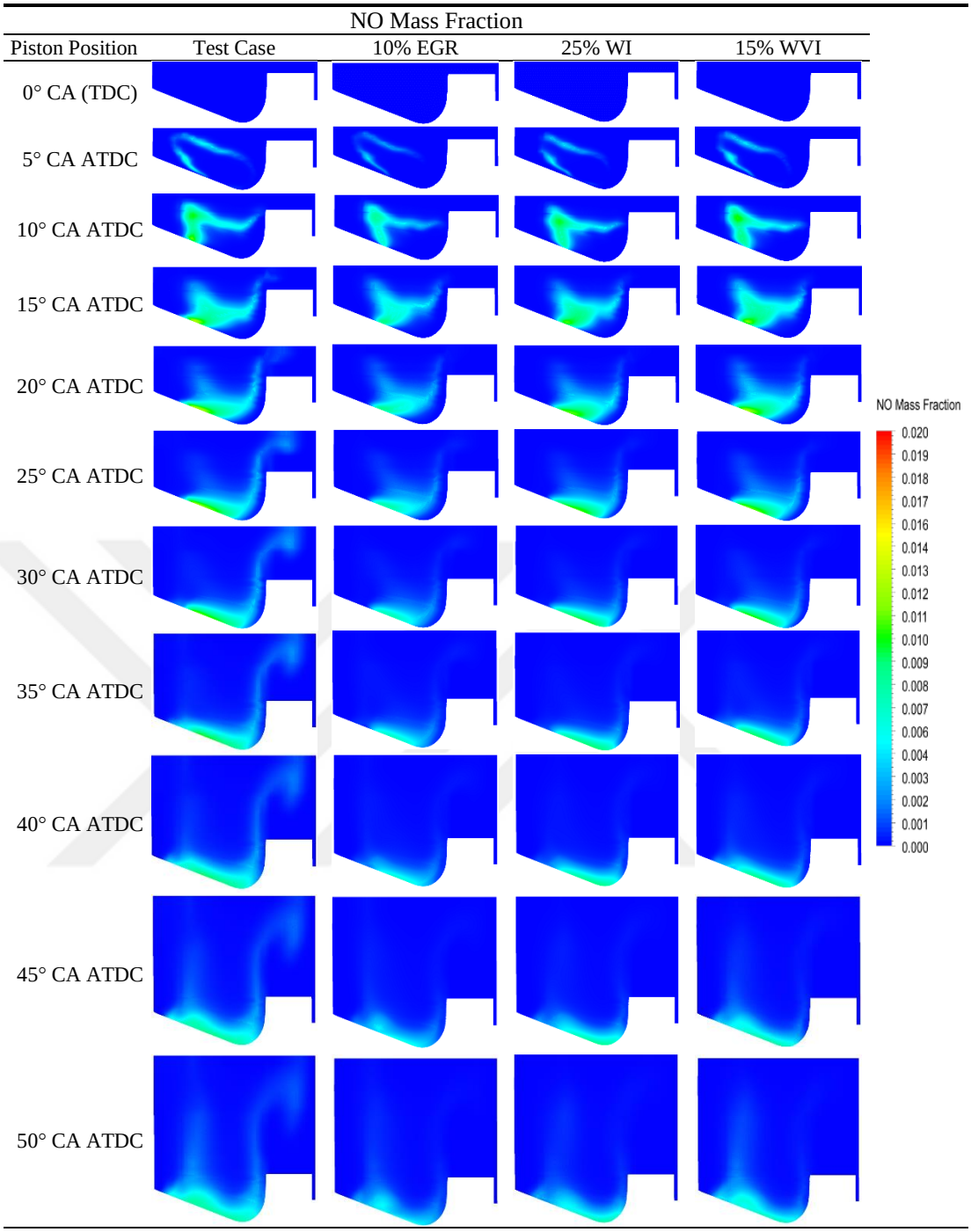

Figure 5.102 : Comparison of NO mass fraction contours at different piston positions between test case with the optimal operating points obtained by applying various types of processes (20% PI - 10% EGR, 20% PI - 25% WI and 20% PI - 15% WVI) to D25NG75H00 (SOI of 10° CA BTDC).

Although CO and UHC emissions have increased compared to the no-process condition due to the applied processes (EGR, WI, and WVI), these increases are at very small levels, so they have minimal impact on the environment (Figure 5.104). The lowest value for NO_x was observed with EGR - PI, while the highest value for MPRR was achieved with WVI (Figure 5.105). It is once again understood that the use

of hydrogen at high fractions does not yield reasonable results in a diesel engine, and the hydrogen-natural gas collaboration is more recommended for achieving better results. It should be noted that using only hydrogen in the gas mixture leads to a tendency for knocking in the combustion process due to high pressure and temperature, and achieving reasonable results with the applied strategies (EGR, WI, WVI, and PI) is not very possible, so it is not recommended. It should be known that operation points with hydrogen-natural gas fractions are a more accurate choice.

Table 5.55 : Comparison of results with (EGR, WI and WVI) or without processes for Mode 1 – D25NG00H75.

	No Process	EGR	WI	WVI
Power (kW)	10.69	10.48	9.95	10.27
Torque (N.m)	112.18	109.97	104.44	107.77
BSFC (g/kW.h)	95.73	97.25	115.25	106.88
Ignition Delay (CA)	11º	12º	12º	12º
Thermal Efficiency (%)	35.75	35.05	33.28	34.35
Combustion Duration (CA)	9º	9º	8º	9º
MPRR (bar/CA)	8.35	9.19	10.11	10.51
Max. Press. (bar)	85.89	84.81	85.49	86
CA for Max. Press. (ATDC)	4º CA	4º CA	4º CA	4º CA
Max. Mean Temp. (K)	1997	1994	1989	2000
NO_x (g/kW.h)	14.04	8.7	9.23	10.28
SOOT (g/kW.h)	0.000071	0.000524	0.0015	0.00093
CO (g/kW.h)	0.0036	0.0098	0.067	0.018
HC (g/kW.h)	0.0015	0.0121	0.0106	0.012

The dominant effect of the homogeneous combustion phase is reflected in temperature and NO mass fraction contours for D25NG00H75 because the gas mixture consists entirely of hydrogen (Figure 5.106 and Figure 5.107). The formation of a darker color distribution indicates the dominance transitioning from the diffusion flame to the homogeneous combustion phase.

The hydrogen-rich homogeneous combustion phase implies higher temperatures and a faster rate of combustion (Table 5.55). This situation indicates the occurrence of knock-prone rapid and intense combustion. In the presence of a high fraction of hydrogen, the applied EGR, WI, and WVI applications have only resulted in positive outcomes in terms of NO_x (Figure 5.107) [202]. We can also see that combustion is completed rapidly and in a shorter time period based on the graph depicting points with a temperature of 2500 K (Figure 5.108). When looking at the rate of decrease in point density between two different crank angles (10° CA ATDC and 20° CA ATDC)

at 2500 K, the situation regarding the combustion rate becomes evident. This is particularly clear with the WI process. The combustion duration is 1° CA shorter for WI. When the combustion duration is less than 10° CA, a difference of 1° CA is highly significant.

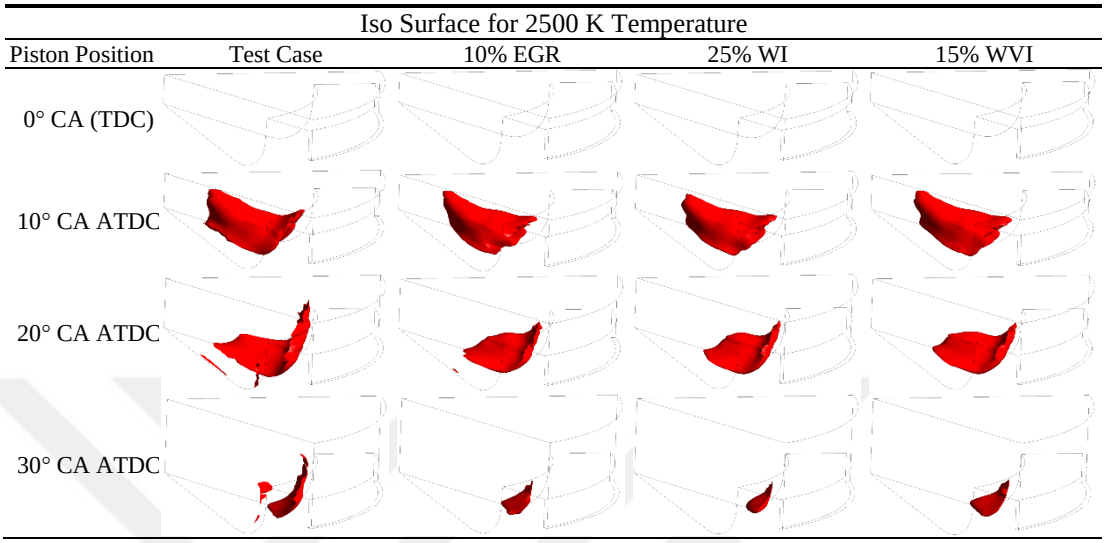

Figure 5.103 : Comparison of Iso Surfaces for temperature of 2500 K at different piston positions between test case with the optimal operating points obtained by applying various types of processes (20% PI - 10% EGR, 20% PI - 25% WI and 20% PI - 15% WVI) to D25NG75H00 (SOI of 10° CA BTDC).

In the case of D25NG75H25 with the highest hydrogen fraction for Mode 2, the application of EGR, WI, and WVI strategies resulted in the highest power and thermal efficiency (TE) values when WVI was applied (D25NG75H25-20PI-15WVI100°C) (Table 5.56 and Figure 5.109). The MPRR values for WVI and WI applications were higher than those in the EGR case, primarily due to their influence on the diffusion flame rather than the homogeneous combustion zones (Figure 5.109).

PM emissions were minimized with WVI because the partial disruption of the diffusion flame by WVI could lead to increased fuel particles oxidizing due to the high temperature of the homogeneous combustion phase, which, in turn, significantly reduced PM emissions.

In the case of WI, the water particles transitioning from the liquid phase to the vapor phase extracted excess heat from the environment, which weakened both the diffusion flame and the homogeneous combustion phase. The weakening of the diffusion flame, in turn, resulted in higher PM emissions as fuel particles oxidized due to increased combustion (SOOT) remained at elevated levels in the homogeneous combustion phase (Figure 5.110).

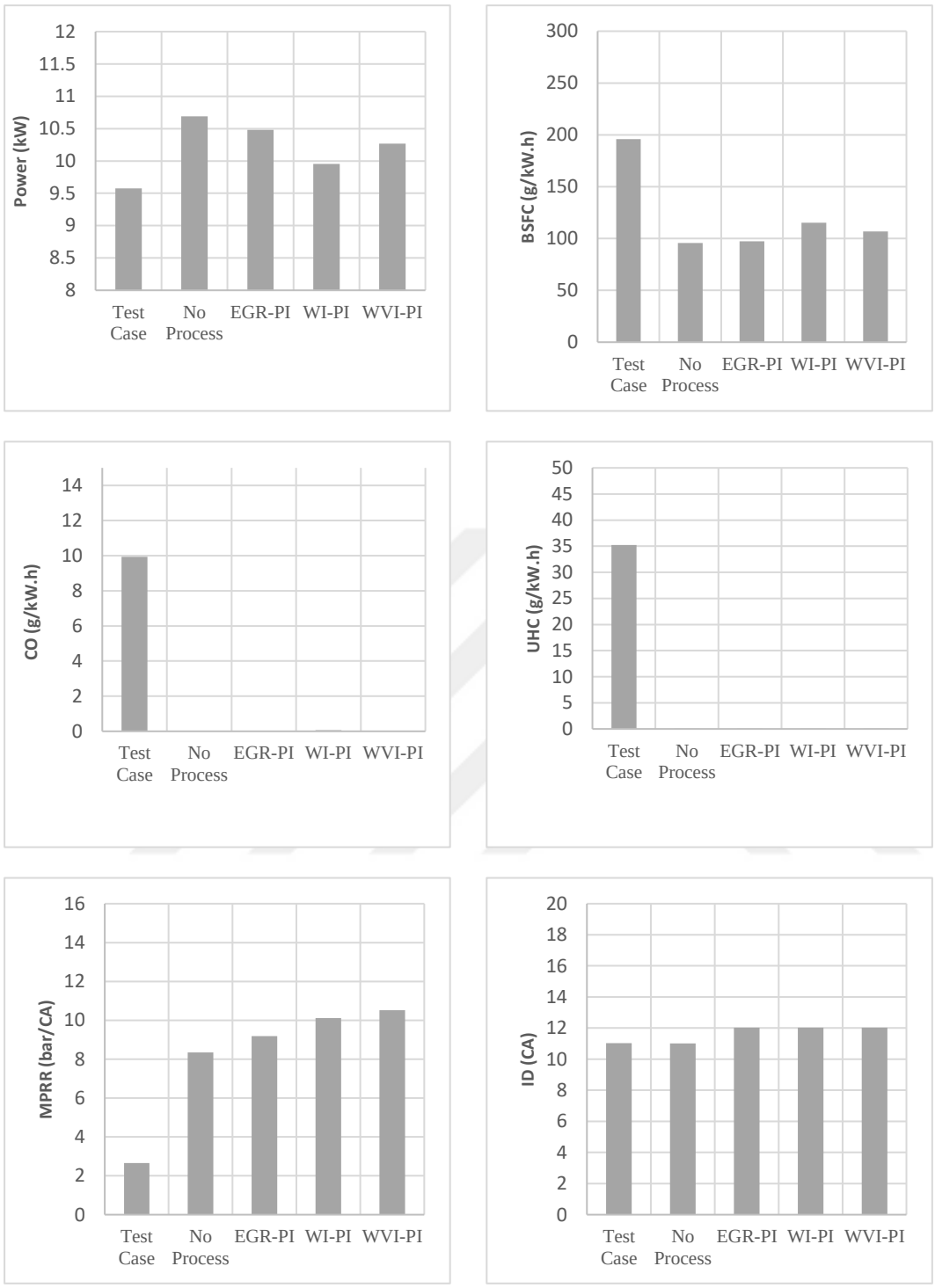

Figure 5.104 : Comparison of results in terms of power, BSFC, CO, UHC, MPRR, and ID with and without processes (EGR, WI, and WVI) at the highest hydrogen-enriched operating point (D25NG00H75) applied for Mode 1, with test result.

The EGR process was less effective on the homogeneous combustion phase compared to the WI process. The impact on combustion occurs in two ways: first, by affecting oxygen concentration through distribution, which reduces combustion efficiency, and second, by drawing heat from the environment to lower temperatures, which also

reduces combustion efficiency. EGR reduces combustion efficiency through the first effect, while WI acts through both the first and the second effect.

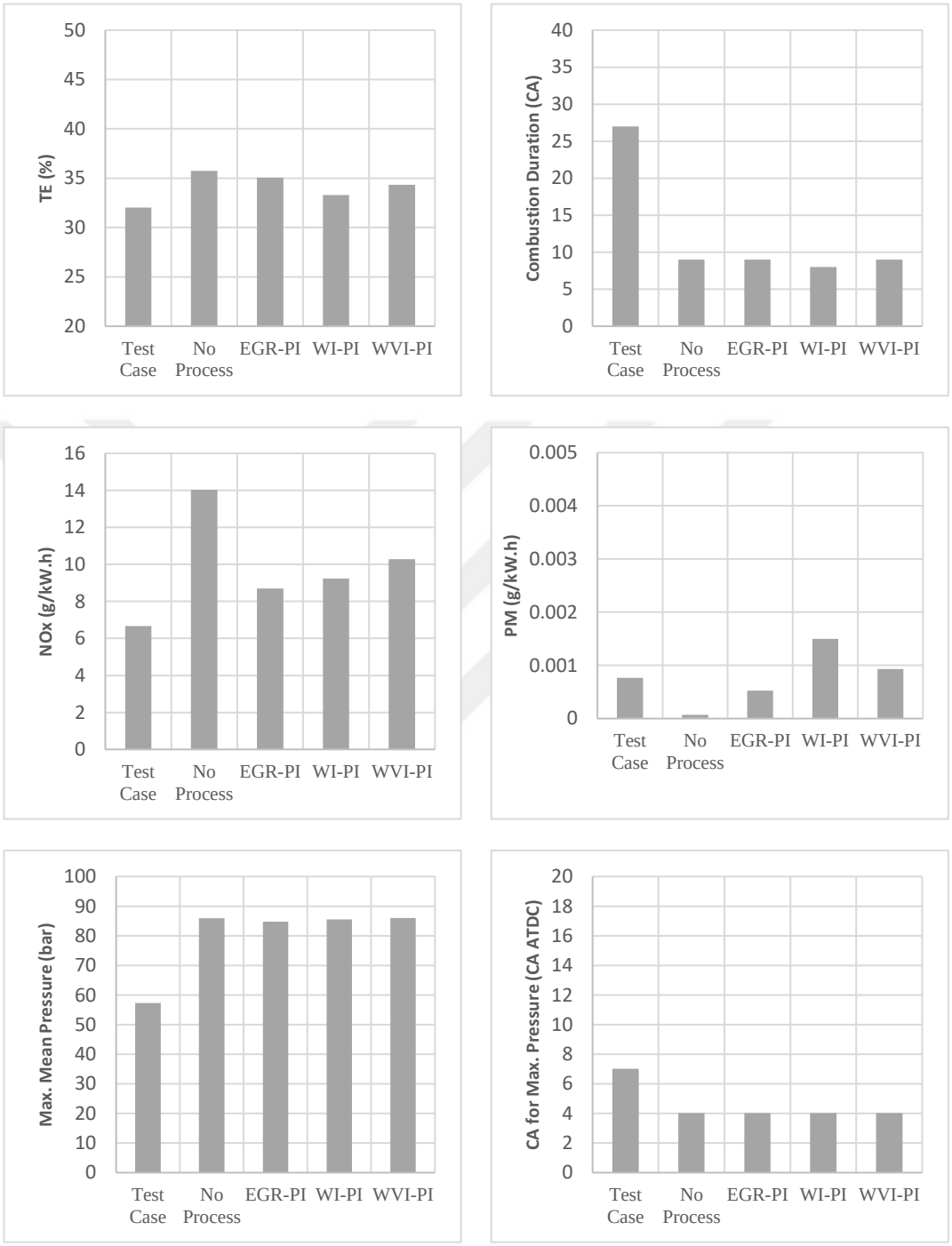

Figure 5.105 : Comparison of results in terms of TE, CD, NO_x, PM, Max. Press. and the position of Max. Press. Relative to TDC with and without processes (EGR, WI, and WVI) at the highest hydrogen-enriched operating point (D25NG00H75) applied for Mode 1, with test result.

However, the delayed introduction of the water jet into the combustion chamber made the second effect more dominant. If the water jet were introduced into the combustion

chamber much earlier, like EGR, the first effect would be overwhelmingly dominant. For WVI, again, the second effect is dominant. As previously analyzed in Chapters 5.3 and 5.4, the temperature of water jet/vapour injections has been found to be less influential on performance and emission values than their fractions.

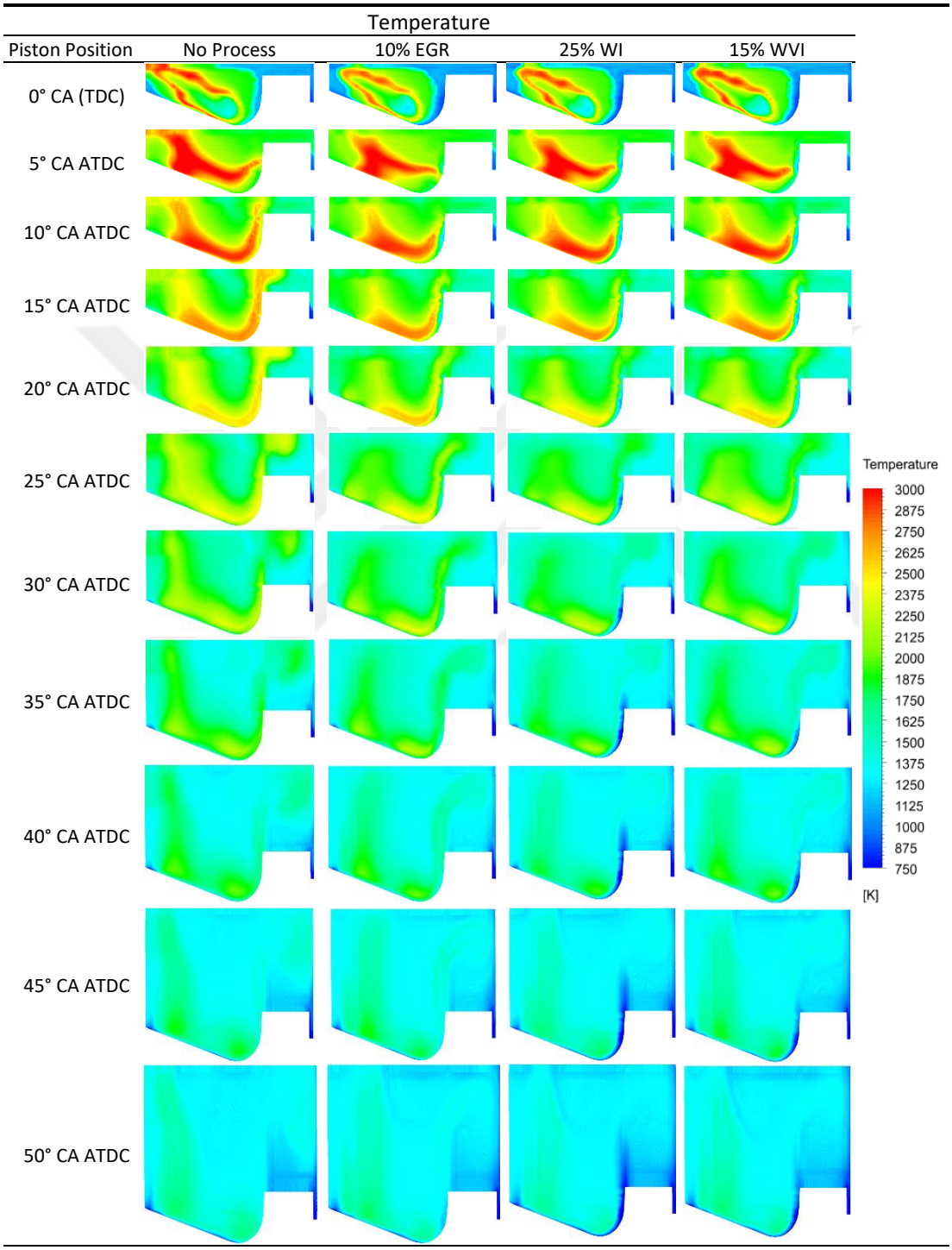

Figure 5.106 : Comparison of temperature contours at different piston positions between no process point with the optimal operating points obtained by applying various types of processes (20% PI - 10% EGR, 20% PI - 25% WI and 20% PI - 15% WVI) to D25NG00H75.

CO and UHC emissions, in order from low to high based on the strength of the homogeneous combustion phase, were WVI, WI, and EGR (Figure 5.109). WVI has less impact on the diffusion flame compared to WI and has a similar effect on the homogeneous combustion phase.

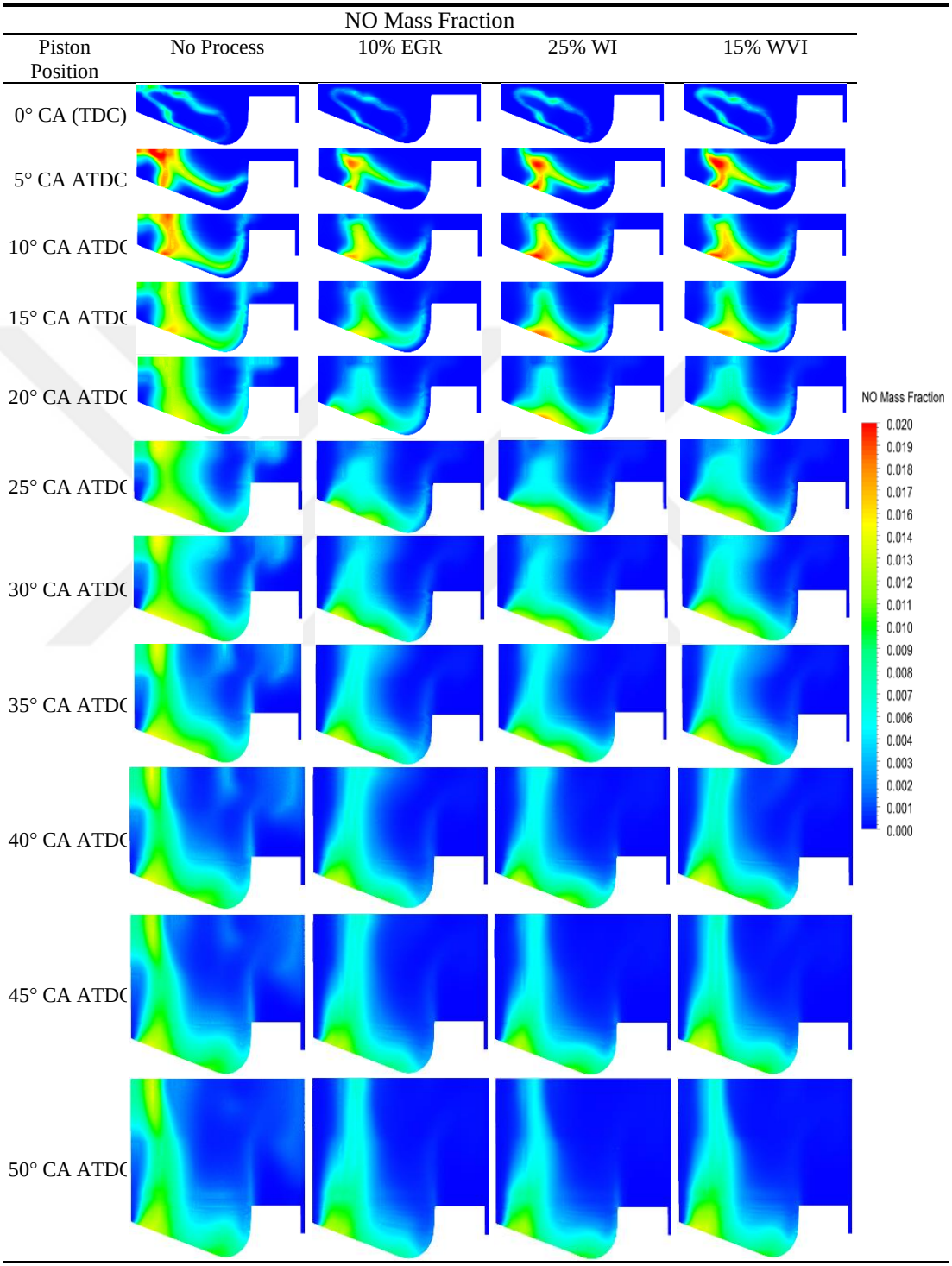

Figure 5.107 : Comparison of NO mass fraction contours at different piston positions between no process point with the optimal operating points obtained by applying various types of processes (20% PI - 10% EGR, 20% PI - 25% WI and 20% PI - 15% WVI) to D25NG00H75.

Table 5.56 : Comparison of results with (EGR, WI and WVI) or without processes for Mode 2 – D25NG75H25.

	No Process	EGR	WI	WVI
Power (kW)	15.05	14.53	14.26	14.63
Torque (N.m)	157.92	152.51	149.67	153.50
BSFC (g/kW.h)	141.09	145.48	158.06	150.52
Ignition Delay (CA)	11º	11º	11º	11º
Thermal Efficiency (%)	38.04	36.74	36.05	36.98
Combustion Duration (CA)	17º	19º	16º	16º
MPRR (bar/CA)	4.62	4	4.58	4.71
Max. Press. (bar)	71.94	69.52	72.59	73.74
CA for Max. Press. (ATDC)	12º CA	13º CA	12º CA	12º CA
Max. Mean Temp. (K)	2057	1993	2030	2060
NO_x (g/kW.h)	7.43	5.41	6.62	7.10
SOOT (g/kW.h)	0.000153	0.001	0.00115	0.00074
CO (g/kW.h)	0.49	0.874	0.65	0.56
HC (g/kW.h)	2.36	2.52	2.43	1.61

EGR, on the other hand, has had a more significant impact on the homogeneous combustion phase. Processes with a strong homogeneous combustion phase produce less CO and UHC.

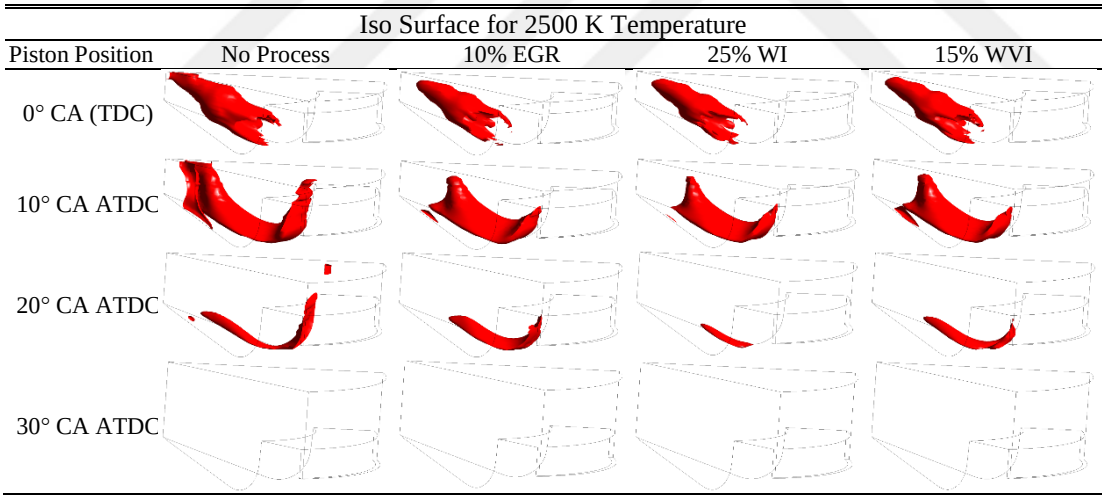

Figure 5.108 : Comparison of Iso Surfaces for temperature of 2500 K at different piston positions for the optimal operating points obtained by applying no process and various types of processes (20% PI - 10% EGR, 20% PI - 25% WI and 20% PI - 15% WVI) to D25NG00H75.

While WI may disrupt both the diffusion flame and the homogeneous combustion phase by drawing heat from the environment, it affects the partial region of the combustion chamber's premixing. Significant premixed regions that are not affected by heat withdrawal have helped maintain the strength of homogeneous combustion. Therefore, in terms of the strength of homogeneous combustion, WI is more effective

than the EGR process. The longer and smoother combustion in the EGR is due to the diffusion flame being stronger than the other processes (Figure 5.109 and Figure 5.110). At the same time, the low strength of homogeneous combustion has contributed to this situation.

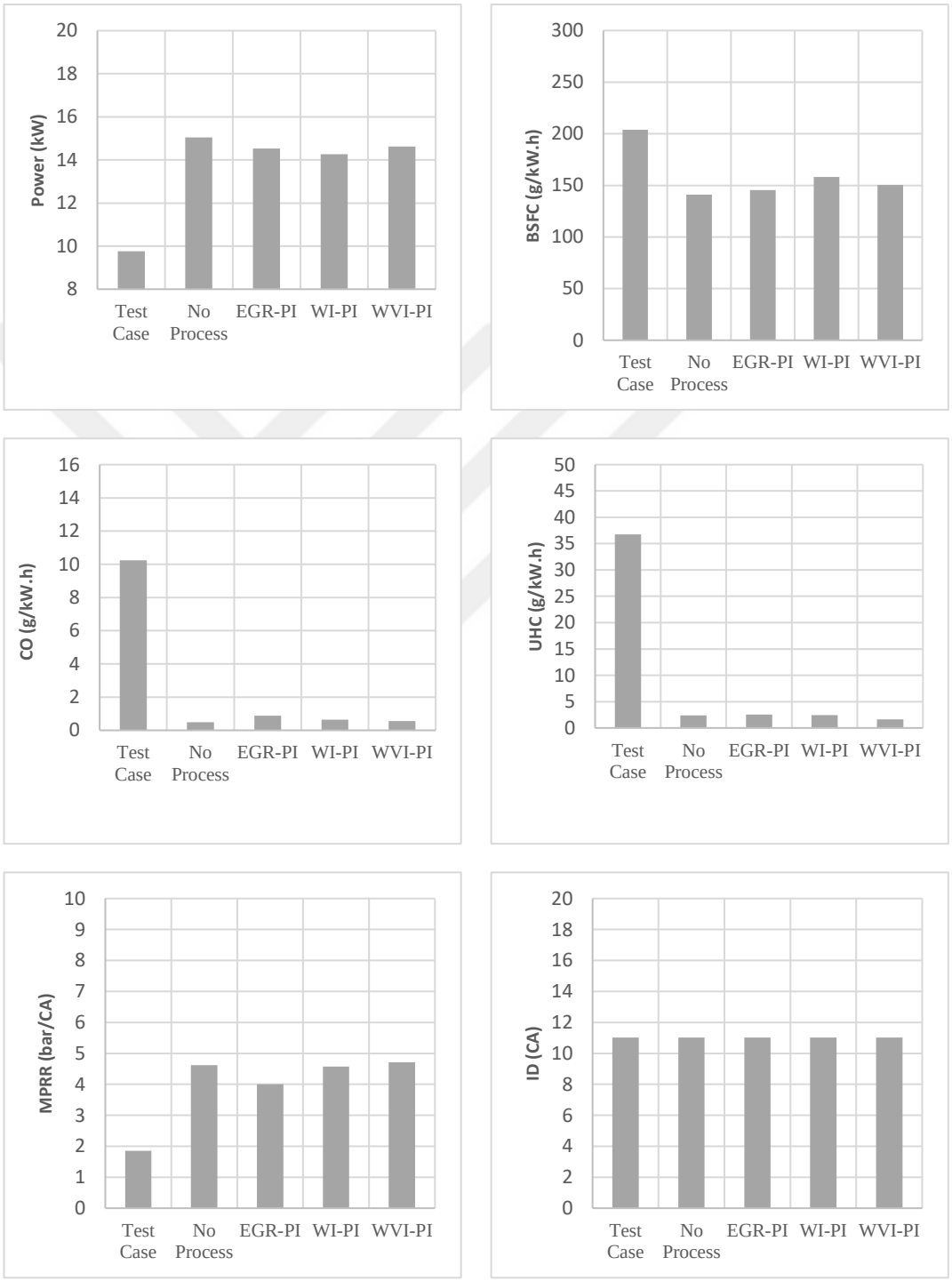

Figure 5.109 : Comparison of results in terms of power, BSFC, CO, UHC, MPRR, and ID with and without processes (EGR, WI, and WVI) at the highest hydrogen-enriched operating point (D25NG75H25) applied for Mode 2, with test result.

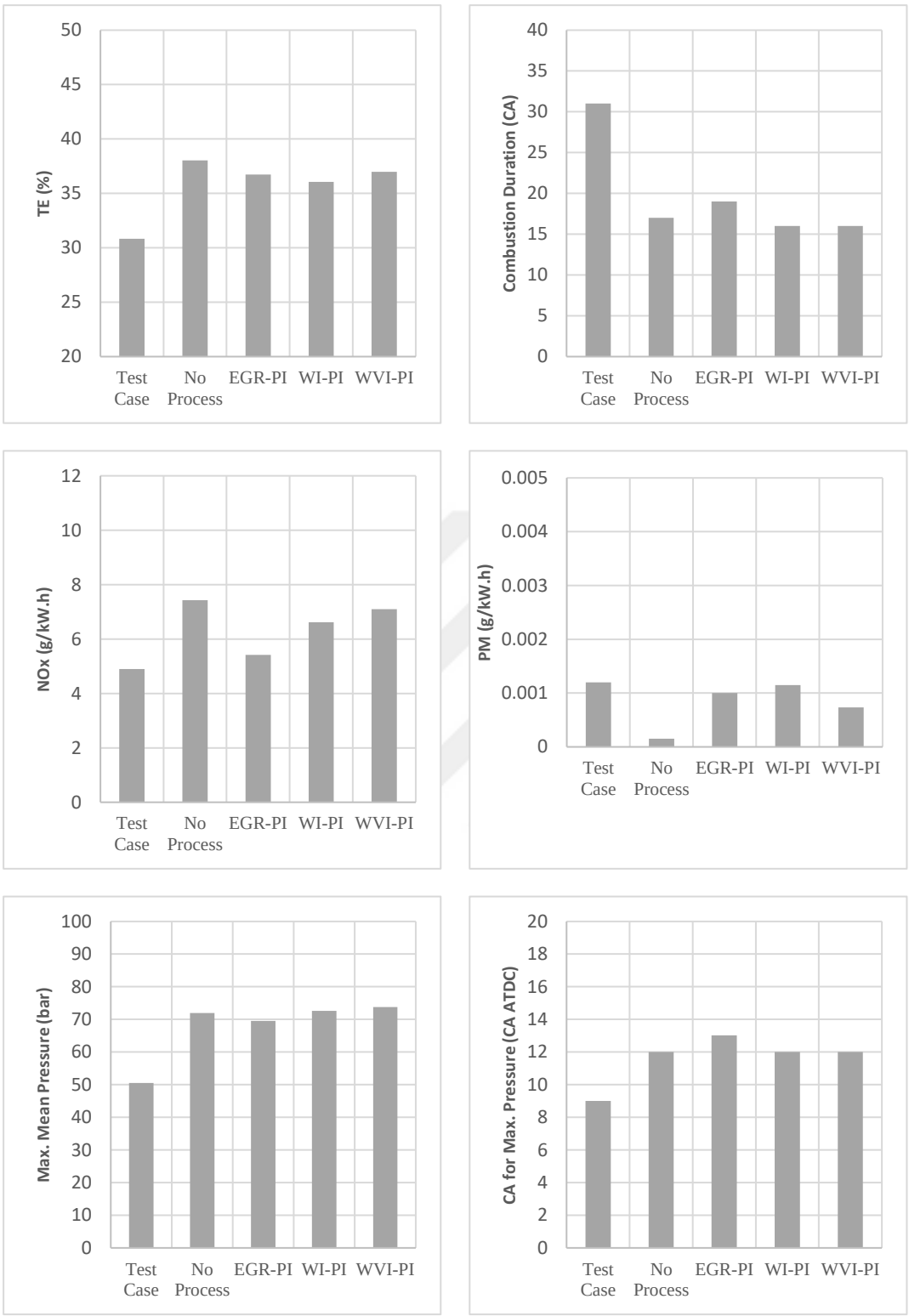

Figure 5.110 : Comparison of results in terms of TE, CD, NO_x, PM, Max. Press. and the position of Max. Press. Relative to TDC with and without processes (EGR, WI, and WVI) at the highest hydrogen-enriched operating point (D25NG75H25) applied for Mode 2, with test result.

The variation in the strength of premixed combustion (homogeneous combustion phase) with respect to the applied processes (EGR, WI, and WVI) at different piston

positions can be observed through the temperature distribution shown in the graph (Figure 5.111).

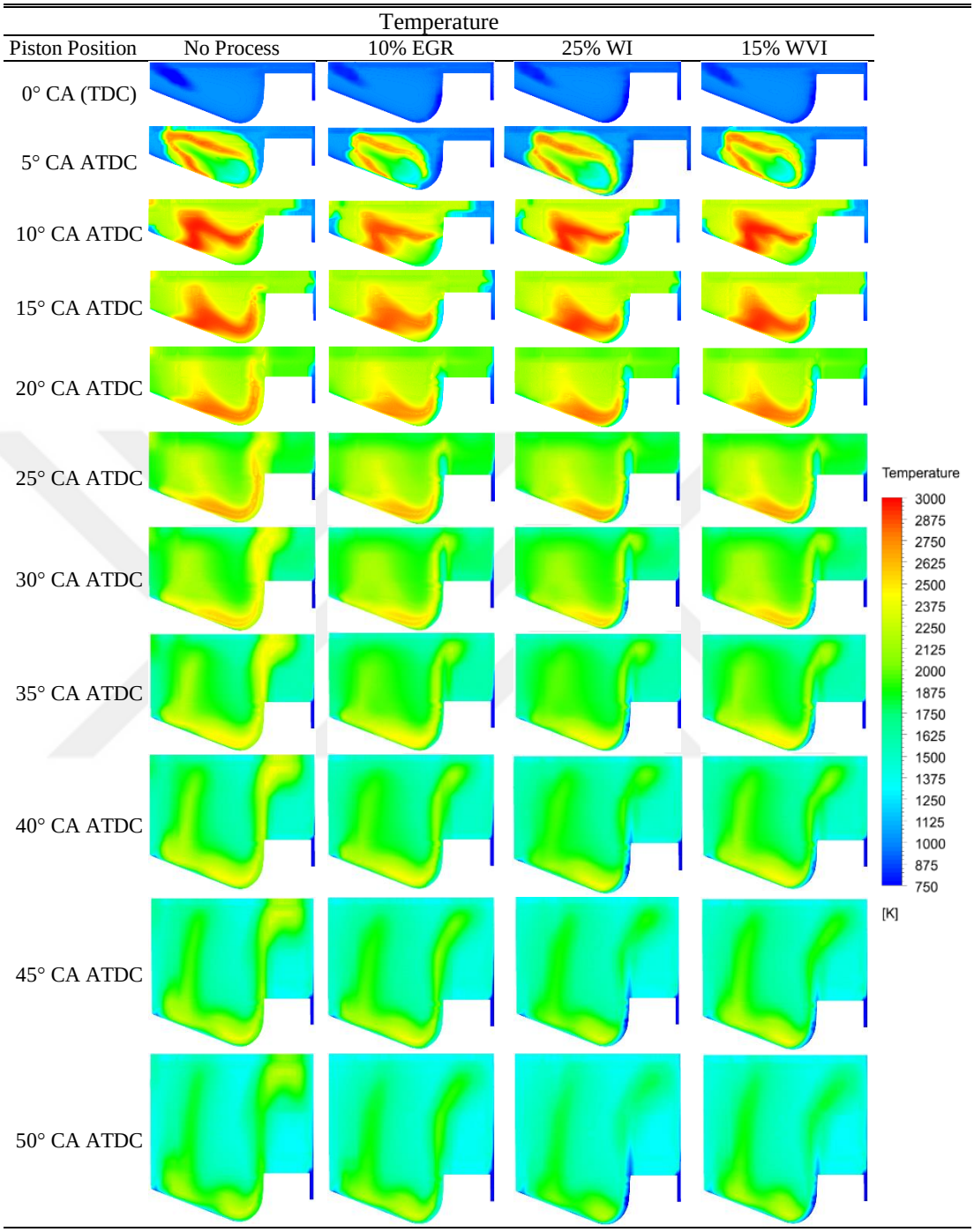

Figure 5.111 : Comparison of temperature contours at different piston positions between no process point with the optimal operating points obtained by applying various types of processes (20% PI - 10% EGR, 20% PI - 25% WI and 20% PI - 15% WVI) to D25NG75H25.

The condition with the highest temperature distribution is WVI, while the lowest is EGR. Detailed explanations of the reasons were given earlier. Corresponding to the temperature distribution, when we look at the NO mass fraction distributions, we can

see that the darkest distribution is WVI, and the least dark distribution is EGR (Figure 5.112).

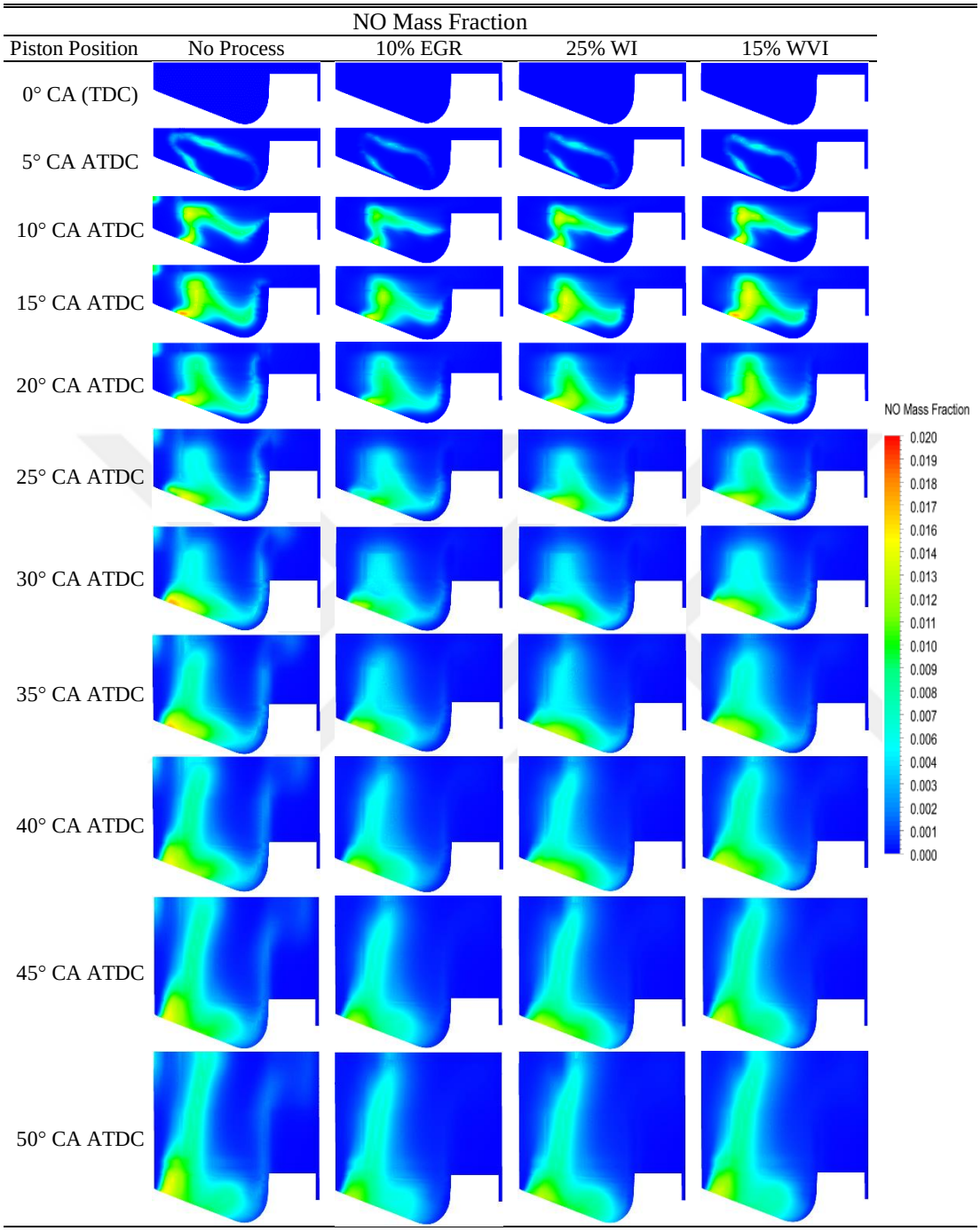

Figure 5.112 : Comparison of NO mass fraction contours at different piston positions between no process point with the optimal operating points obtained by applying various types of processes (20% PI - 10% EGR, 20% PI - 25% WI and 20% PI - 15% WVI) to D25NG75H25.

Figure 5.113 also shows that the most intense condition for points with a temperature of 2500 K is WVI, while in the WI process, due to the shorter combustion duration of the burning regions compared to EGR, it appears as if the burning regions have gone

out more quickly, resulting in seemingly lower temperature generation compared to EGR (Figure 5.113). However, a graph showing the temperature distribution more frequently with crank angles shows that EGR produces lower temperatures and lower NO_x emissions compared to the WI process (Table 5.56, Figure 5.111, and Figure 5.112).

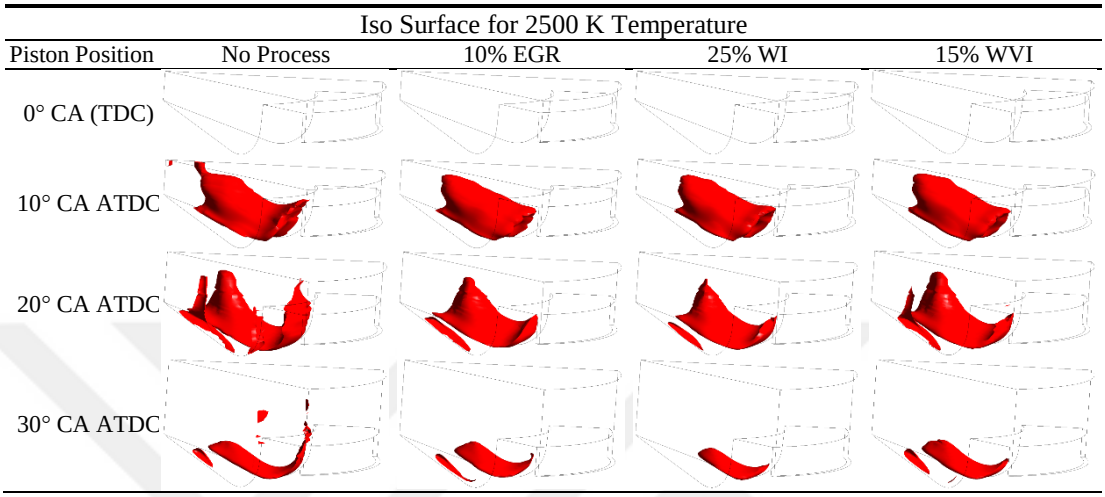

Figure 5.113 : Comparison of Iso Surfaces for temperature of 2500 K at different piston positions for the optimal operating points obtained by applying no process and various types of processes (20% PI - 10% EGR, 20% PI - 25% WI and 20% PI - 15% WVI) to D25NG75H25.

6. CONCLUDING REMARKS AND RECOMMENDATIONS

The numerical results obtained in the scope of the thesis demonstrate that hydrogen and natural gas are highly valuable alternative fuels for emissions. Considering various energy fractions of hydrogen-natural gas operating points and the effects of different diesel fuel injection timings, it is observed that the inclusion of hydrogen in the combustion chamber leads to higher performance and lower emission values. However, an increase in the hydrogen fraction, especially, brought along the issues of high NO_x emissions and a tendency for knock (higher MPRR).

To mitigate these two problems, EGR-PI, WI-PI, and WVI-PI processes were applied to the operating points where hydrogen was included. If these processes are selected at appropriate ratios and timings, an increase in the fraction of hydrogen in the combustion chamber may occur. Because a high hydrogen content implies high NO_x emissions and MPRR (knock tendency), it has been observed that with pilot injection (PI) and, especially, water vapor injection (WVI), higher hydrogen fractions in the combustion chamber can be achieved. Thus, we can transition to zero-carbon hydrogen by meeting the energy needs of the engine from diesel and natural gas fuels. This would lead to more environmentally friendly results [50,179,189,190,203–205].

In the first phase of the study, the effects of natural gas-hydrogen fuels in the form of energy sharing and the impacts of additional hydrogen incorporation with hydrogen-enriched natural gas (hythane) fuel were investigated.

In this way, two working points were defined in two Modes (Mode 1 and Mode 2). The second phase of the study focused on emission improvement studies related to EGR-pilot injection strategies and the effects of water jet and vapor injection into the combustion chamber at partial loads, which were a continuation of the first phase efforts.

A review of the literature reveals a scarcity of studies examining these parameters (EGR, WI, and WVI) in dual-fuel diesel-natural gas-hydrogen engines. The present thesis study aims to address this gap in the literature, providing insights for future researchers working on hydrogen and natural gas, the fuels of the future.

6.1 General Remarks

In compression-ignition engines (CI), diesel fuel is preferred both in terms of performance and for economic reasons. Heavy-duty engines, especially those used in applications such as marine engines, require high torque, necessitating engines with a long stroke. In this context, CI engines fulfill this requirement. CI engines are characterized by high compression ratios due to these features. According to the working principle of compression-ignition engines, a fuel with a high auto-ignition function is required. Unfortunately, there is currently no fuel that can compete with diesel, especially in achieving high engine speeds and meeting the conditions requiring maneuverability, due to its automatic ignition feature. However, issues such as the current reserve problem and the emission of exhaust gases into the air above standards have increased interest in alternatives to diesel. Although these problems are valid for diesel fuel, the automatic ignition function and fuel efficiency features are crucial in the significance of diesel fuel.

The most important emphasis intended with this study is to avoid running the engine with 100% diesel (pure diesel) and instead enable diesel to participate in combustion in very small energy fractions. Here, the most significant contribution of diesel fuel is to initiate combustion by providing ignition, and then ensuring the continuation of combustion with other alternative fuels. Therefore, it is aimed to take advantage of the characteristics of diesel while simultaneously reducing its effectiveness to keep the environment cleaner. This concept will contribute to extending the current reserve life. In the current thesis, the contribution of diesel to the in-cylinder combustion process was kept constant at 25% energy fraction, while the majority was allocated to alternative gas fuels. Natural gas and hydrogen possess notable thermodynamic properties. Natural gas, besides being low in carbon content, has a high lower heating value. Hydrogen is carbon-free and has combustion characteristics at wide air/fuel ratio values, along with a high lower heating value. While these fuels can be easily used alone in SI (Spark Ignition) engines, it is not feasible to use them independently in CI (Compression Ignition) engines. Certainly, ignition by a different fuel is required. This fuel, as previously mentioned, must not only have a high automatic ignition capability but should also initiate combustion under various engine loads and speed conditions. Currently, diesel fuel takes the forefront with these characteristics. Alternative gas fuels also have their own set of disadvantages. While natural gas has a

low C/H ratio, its carbon content contributes to the release of CO, CO_2, and UHC emissions into the environment. However, in terms of NO_x, natural gas is advantageous due to its low combustion temperatures. Hydrogen, on the other hand, has disadvantages such as rapid combustion and high combustion temperatures. By sending a mixture of both fuels into the combustion chamber, the contrast in disadvantages can be turned into an advantage.

As known, diffusion combustion occurs in situations where the air and fuel mixture develops instantaneously (heterogeneous). In other words, diffusion combustion is a combustion type where the formation of the mixture ends just before combustion or where fuel supply can continue during combustion. Another type of combustion is homogeneous combustion. In this type of combustion, the mixture is prepared well in advance, and the mixture is provided homogeneously. The combustion of this mixture develops rapidly and abruptly. In conventional SI (Spark Ignition) engines, this type of combustion is observed. In fact, the fundamental difference between the two types of combustion is the time of mixture formation. The diffusion combustion is created by directly injecting diesel fuel into the combustion chamber, while in the case of alternative gas fuels, the mixture of these fuels is provided in the intake port before entering the combustion chamber, creating a homogeneous charge, and later, this charge forms the homogeneous combustion phase. The diffusion combustion phase leads to SOOT (PM) emissions, while the homogeneous combustion phase triggers the formation of high NO_x due to the high temperatures involved.

Within the scope of the thesis, reducing the energy fraction of diesel was aimed at decreasing the efficiency of diffusion combustion, while the efficiency of homogeneous combustion was increased by creating homogeneous mixtures of alternative gaseous fuels. The presence of hydrogen in the gas mixture further accelerates the high temperatures associated with homogeneous combustion, thereby hastening the increase in NO_x. Therefore, it is crucial to implement measures that reduce combustion temperatures, especially in homogeneous combustion phases involving hydrogen.

Measures recommended in the literature, such as EGR, water injection (WI), or water vapor injection (WVI), contribute to NO_x improvements, while pilot injection processes (PI) can prevent high-pressure increases. Hydrogen, with its high combustion speed and elevated combustion temperatures, leads to pressure increases

and a reduction in combustion duration. To facilitate a smoother and gradual onset of combustion, it is of particular importance to introduce a portion of the diesel fuel into the combustion chamber through pre-injection.

Another consideration when incorporating hydrogen into combustion is the need to address high temperatures. Exhaust Gas Recirculation (EGR) involves introducing intake air into the combustion chamber before combustion, thereby reducing the oxygen concentration within the cylinder. This has a mitigating effect on post-combustion temperatures. Particularly in the case of the phase of homogeneous combustion, this reduction in oxygen concentration results in decreased efficiency, accompanied by a parallel decrease in temperatures.

When examining Water Injection (WI), it has been observed that it is effective in reducing in-cylinder temperatures. The WI process has been decisive for both diffusion combustion and the phase of homogeneous combustion, impacting NO_x and PM emissions. Since the injection region of water (WI) corresponds to the injection region of diesel fuel, WI has proven to be the most effective process for the diffusion combustion phase.

The efficiency of homogeneous combustion has been affected because water, in transitioning from the liquid to the gas phase, draws heat from the combustion chamber. It significantly influenced the number of fuel particles oxidizing before combustion in the region where diffusion combustion occurs, exerting greater dominance over SOOT (PM) emissions compared to other applications.

Water Vapor Injection (WVI) has affected the oxygen concentration within the combustion chamber, similar to EGR application. However, this effect has occurred not throughout the entire combustion chamber, as in EGR, but specifically in the diffusion combustion region. The process with the least impact on the homogeneous combustion phase, WVI, has been observed to increase the combustion duration.

In the premixed combustion of natural gas and hydrogen, if the hydrogen fraction is increased excessively, preventing the NO_x and MPRR values above the critical level after combustion will not be possible with any process. Firstly, the critical hydrogen fraction suitable for each operating condition (engine load and engine speed) should be determined, and then a preventive application (EGR-PI, WI-PI, and WVI-PI) should be selected for the high NO_x and MPRR values that occur subsequently.

6.2 Conclusions

In the current thesis work, a diesel engine that had been experimentally studied in dual-fuel mode (diesel-natural gas) in previous literature was utilized to create the numerical model. The experimental study investigated the effects of different diesel fuel injection timings (10°, 14°, 18°, 22°, 26°, 30°, 34°, 38°, 42°, 46°, and 50° CA BTDC) at 25% load (partial load) where 25% of the energy was obtained from diesel fuel and 75% from natural gas, under constant engine speed (910 RPM) and constant mean effective pressure (4.05 BMEP) [7–9].

A numerical model was developed using a Computational Fluid Dynamics (CFD) program, ANSYS Forte, considering the conditions of the experiment. The accuracy of the established numerical model was validated by comparing it with experimental results. Subsequently, parametric studies were conducted using the validated model to investigate the effects of alternative fuels, specifically natural gas and hydrogen at different ratios.

In the parametric studies, results were obtained considering two modes. In the first mode of the system, the total fuel energy and the injected diesel fuel were kept constant (25% energy fraction), with the remaining 75% of energy being distributed between hydrogen and natural gas fuels. The amount of natural gas fuel was gradually reduced, and the energy was transferred to hydrogen fuel step by step (D25NG75H00, D25NG65H10, D25NG50H25, D25NG25H50, and D25NG00H75). For this part of the study, the energy sharing mode was termed as "Mode 1 working points" in the nomenclature. In the second mode, additional energy transfer to the system was provided, keeping the diesel fuel quantity constant with a 25% energy fraction and the natural gas fuel quantity constant with a 75% energy fraction. Extra hydrogen fuel was injected into the combustion chamber (D25NG75H00, D25NGH05, D25NG75H10, D25NG75H15, D25NG75H20, and D25NG75H25). The naming convention for this mode was termed as "hydrogen enrichment mode" and abbreviated as "Mode 2 working points." Working points were defined for both modes, considering different diesel fuel injection advances (10°, 14°, 18°, 22°, 26°, 30°, 34°, and 38° CA BTDC). These analyses constituted the initial stage of the numerical study.

The second stage aimed to improve the NO_x and MPRR values obtained in the first stage of the numerical results. For MPRR, pilot injection (PI) was considered, while

for NO_x reduction, EGR, water jet injection (WI), and water vapor injection (WVI) processes were applied. To simultaneously reduce NO_x and MPRR, dual processes were implemented (EGR-PI, WI-PI, and WVI-PI). The pilot injection (PI) ratio, expressed as a fraction of the total diesel fuel amount, was examined at values of 0%, 20%, 30%, and 50%. For EGR, the ratios were 0%, 10%, 15%, and 20%, while for WI and WVI, they were set at 0%, 5%, 10%, 15%, 20%, and 25%. The effects of different temperatures were also investigated for EGR, WI, and WVI. These temperatures were considered as follows: 100 °C, 200 °C, and 300 °C for EGR; 25 °C, 60 °C, 75 °C, and 90 °C for WI; and 100 °C, 125 °C, 150 °C, and 200 °C for WVI. Lastly, the effects of different injection timings were also examined for WI and WVI. The injection timings considered for water jet/vapour were 20° CA BTDC, 10° CA BTDC, 0° CA BTDC (TDC), and 10° CA ATDC.

The obtained numerical results for the first stage of the current thesis, which involves determining the fractions of alternative gas fuels (natural gas-hydrogen) and diesel fuel injection timings, can be summarized as follows (Chapter 5.1).

- Advanced injection timing significantly negatively impacts performance and emission values during partial load combustion events where hydrogen is involved. It has been observed that the optimum diesel fuel advance for Mode 1 and Mode 2 operating points is 14° CA BTDC and 10° CA BTDC, respectively.
- The value of the diesel fuel injection advance has a significant impact on ignition delay. It has been observed that a higher injection advance leads to a higher ignition delay. Specifically, advancing the injection before 22° CA BTDC has significantly increased ignition delay.
- For Mode 1, there is a sharp decrease in performance values for diesel fuel injection advances earlier than 22° CA BTDC, while similar results are observed for subsequent diesel fuel advances (10°, 14°, 18°, and 22° CA BTDC) in terms of performance. For Mode 2, a decreasing trend in performance is observed for all diesel fuel injection advances before 10° CA BTDC.
- The increase in the hydrogen fraction in the gas mixture particularly has a negative impact on performance values, especially at high injection advances (before 22° CA BTDC), and has led to an increase in regional temperatures inside the cylinder.
- In order to achieve balanced control of in-cylinder combustion temperatures, natural gas needs to be present in the gas mixture to a certain extent (at least 50%).

Although the presence of natural gas tends to increase CO, UHC, and SOOT (PM) emissions, it has been observed that these emissions can be reduced by enriching natural gas with hydrogen.

- With hydrogen energy fraction below 50%, performance and all emissions except NO_x have been improved. However, results have reversed when hydrogen exceeds 50%. For Mode 1 operating points, the optimum natural gas and hydrogen ratio is 50% and 25% respectively (D25NG50H25), while for Mode 2, these values are 75% and 15% respectively (D25NG75H15).
- The increase in hydrogen in the gas mixture leads to an increase in MPRR values, so it is crucial to accurately determine the critical value suitable for the engine operating conditions (engine load and speed). For 25% load and 910 rpm, the numerical results indicate that the critical hydrogen level is determined as 50%. Beyond this ratio, hydrogen fractions have led to MPRR values reaching 10 bar/CA, resulting in knocking tendencies.
- Hydrogen has had a positive effect on thermal efficiency. For Mode 1 (Case 18 - D25NG50H25) and Mode 2 (Case 57 - D25NG75H15), there has been an improvement of 21% and 18%, respectively, in terms of thermal efficiency at the optimum operating points. For Mode 1, there was a 21% improvement in power and a 29% improvement in BSFC, while for Mode 2, there was a 36% improvement in power and a 22% improvement in BSFC.
- The presence of hydrogen has had a negative impact on NO_x emissions. It has caused an increase of 12% for Mode 1 and 11% for Mode 2. However, there have been significant improvements in UHC, CO, and SOOT (PM) emissions. For Mode 1, there were improvements of 88% for UHC, 86% for CO, and 77% for SOOT (PM). For Mode 2, the improvements were 76% for UHC, 80% for CO, and 83% for SOOT (PM).

The second stage aimed to improve the conditions regarding MPRR and NO_x. The EGR-PI pair was initially implemented in this stage. Through these processes, when compared to the experimental conditions, it was observed that overall performance and emissions, including NO_x and MPRR, were improved. The numerical results obtained from the EGR-PI strategies are summarized below (Chapter 5.2).

- The increase in the PI value (after 20% PI) resulted in a decrease in ignition delay. The increase in PI caused an increase in the accumulated fuel in the cylinder before

the main injection, leading to an increase in temperatures and pressures, and consequently an increase in power and combustion efficiency. However, this increase in performance occurred due to the formation of hard combustion conditions, resulting in deteriorated NO_x and MPRR values.

- When analyses with no PI applied (0% PI) were compared with analyses with 20% PI, it was observed that NO_x and MPRR values improved. Considering that the primary goal of the second stage was to improve these two values and the results deteriorated after 20% PI, it is understood that the critical limit for PI is 20%.
- The increase in the EGR ratio led to a decrease in performance values since it affected the cylinder's oxygen concentration. Because EGR was introduced into the cylinder before combustion through the intake process, it showed a homogeneous distribution. It directly influenced both diffusion flame and homogeneous combustion phases. Therefore, it proved to be highly effective for both SOOT (PM) and NO_x. Considering both performance and emission values, optimum values were observed for a 10% EGR ratio.
- The increase in EGR temperature led to a decrease in thermal efficiency (TE) and a shortening of the combustion duration. The rapid onset of harsh combustion conditions increased both NO_x and MPRR while decreasing the power value. Reasonable results were obtained with the examined EGR temperatures of 100 °C (Cold EGR), 200 °C, and 300 °C, with the most favorable outcomes achieved at 100 °C.
- When comparing the test conditions (D25NG75H00 14° CA BTDC for SOI) with the operating point created by combining the optimal gas fraction condition obtained in the first stage for Mode 1 with the optimal PI (20%), EGR (10%) ratios, and temperature (100 °C) values (D25NG50H25-20PI-10EGR100°C), improvements of 17%, 28.4%, 5.42%, 32%, 84.4%, and 87.4% were observed in power, BSFC, TE, NO_x, CO, and UHC values, respectively. When comparing the operating point obtained by applying the optimum EGR-PI ratios (D25NG75H15-20PI-10EGR100°C) for Mode 2 with the test conditions (D25NG75H00 10° CA BTDC for SOI), improvements were observed in power, BSFC, TE, NO_x, CO, and UHC values by 31.15%, 21%, 4.32%, 30%, 77.15%, and 74%, respectively.
- When the optimum EGR-PI processes (10% EGR & 20% PI) were applied under test conditions (D25NG75H00 14° CA BTDC for SOI), improvements were

observed in power, BSFC, TE, MPRR, NO_x, CO, and UHC by 0.89%, 1.17%, 0.28%, 0.24 bar, 43%, 13%, and 9.37%, respectively. For the other test condition (D25NG75H00 10° CA BTDC for SOI), the EGR-PI combination has led to deteriorations in power, BSFC, TE, CO, and UHC by 4.6%, 4.45%, 1.42%, 23.8%, and 11%, respectively. However, improvements of 43.5% for NO_x and 0.42 bar for MPRR have been observed. It can be understood from this that, in cases where hydrogen is not present in the gas mixture, increasing the main diesel fuel injection advance yields more reasonable results in terms of performance.

- For D25NG50H25 (Mode 1), applying EGR-PI resulted in decreases of 39% for NO_x and 0.24 bar for MPRR. For D25NG75H15 (Mode 2), these values were obtained as 37.13% for NO_x and 0.69 bar for MPRR, respectively.
- In Mode 1, the condition with the highest hydrogen fraction (D25NG00H75) was observed to have very high MPRR values (10 bar/CA). While EGR-PI resulted in a 38% decrease in NO_x, the application of PI led to an increase of 0.84 bar in MPRR. The application of PI should be avoided in cases where the hydrogen fraction in the gas mixture is very high, as it leads to negative outcomes, particularly a reverse effect on MPRR. In the case of the highest hydrogen enrichment fraction for Mode 2 (D25NG75H25), the applied EGR-PI strategies (D25NG75H25-20PI-10EGR100°C) have resulted in a reduction of 27% in NO_x and 0.62 bar in MPRR. When comparing the test conditions (D25NG75H00 10° CA BTDC for SOI) with the EGR-PI processed condition (D25NG75H25-20PI-10EGR100°C), improvements have been observed in power, BSFC, TE, CO, and UHC by 48.87%, 28.63%, 5.9%, 91.47%, and 93.14%, respectively. However, NO_x increased by 10.41%, and MPRR increased by 2.15 bars.

Another strategy applied is the direct injection of a water jet (WI) into the combustion chamber. This process was implemented in the form of WI-PI along with 20% PI. The goal here is to improve MPRR with PI and NO_x with WI. The information obtained from these processes is summarized below (Chapter 5.3).

- An increase in the WI rate has led to a slight decrease in performance values, especially in terms of NO_x, resulting in reasonable outcomes. Although the power value tends to decrease with increasing WI, it has been higher when compared to the test results (D25NG75H00 14° CA BTDC for SOI). Therefore, due to its

success in improving NO_x emissions, the optimum value for WI has been determined as 25%.

- The increase in the WI rate has had a minimal impact on ignition delay (ID) and MPRR. Due to its effect on reducing regional temperatures, WI has mostly influenced NO_x and TE. CO and UHC emission values, like ID, have shown a stable trend. PM (SOOT) emissions have increased due to the WI strategy lowering temperatures in the diffusion flame region.
- The increase in WI temperature (25 °C, 60 °C, 75 °C, and 90 °C) has not shown a dominant feature in terms of performance and emission values for both Mode 1 (D25NG50H25) and Mode 2 (D25NG75H15). The PM emissions reached their minimum value at a WI temperature of 75 °C. The weak influence of the increase in WI temperature on performance and emission values is attributed to the presence of hydrogen in the fuel mixture. This situation is explained by the fact that the difference between WI temperature values is much lower than the temperature values generated during the combustion of hydrogen. The WI temperature value of 75 °C, which contributes positively to PM emissions, has been preferred for use in subsequent analyses.
- It has been observed that reducing the WI advance value (20° CA BTDC, 10° CA BTDC, 0° CA BTDC – TDC, and 10° CA ATDC for SOWI) improves performance for both Mode 1 and Mode 2. The delayed WI results in higher combustion temperatures, leading to positive effects on performance parameters such as power, BSFC, and thermal efficiency (TE). In terms of emissions, PM, CO, and UHC decrease, while NO_x shows a notable increase tendency. Although MPRR and in-cylinder pressure values were not affected by WI advance in Mode 1 operation points, they increased in Mode 2 operation points as the WI advance was reduced. The sharp increase in NO_x values with the decrease in WI advance led to the preference of 20° CA BTDC as the optimum WI advance.
- The obtained optimum values (25% WI - 75 °C for WI temperature - 20° CA BTDC for SOWI) were considered, and non-PI (0% PI) and 20% PI conditions were compared. It was observed that performance increased and MPRR and NO_x values decreased with 20% PI.
- For Mode 1, when the processes were applied to the operating point (D25NG50H25-20PI-25WI75°C-20°CABTDCSOWI), the test results were

compared with those of (D25NG75H00 14° CA BTDC for SOI). It was observed that there were improvements in power, BSFC, TE, NO_x, CO, and UHC by 14.26%, 20.7%, 4.58%, 23.42%, 85.7%, and 88.33%, respectively. there was only a 0.54 bar increase in MPRR. Similarly, for Mode 2 (D25NG75H15-20PI-25WI75°C-20°CABTDCSOWI), when compared to the test conditions (D25NG75H00 10° CA BTDC for SOI), there were improvements in power, BSFC, TE, NO_x, CO, and UHC by 30.33%, 15%, 4.11%, 17%, 79.5%, and 77.29%, respectively. However, MPRR showed only a 0.66 bar increase.

- The application of WI-PI (25% WI & 20% PI) strategies to the experimental operating points resulted in a slight decrease in performance but a significant improvement in emission values. When WI-PI was applied for the test condition with an injection advance of 14° CA BTDC (D25NG75H00), power, BSFC, and TE experienced losses of 2.77%, 9.64%, and 0.88%, respectively. However, improvements were observed in NO_x, CO, UHC, and MPRR, with values of 37%, 13%, 10.5%, and 0.25 bar, respectively. For the other test condition with an injection advance of 10° CA BTDC for SOI (D25NG75H00), there was a loss of 0.31% in power and 6.93% in BSFC. However, improvements were observed in NO_x, UHC, and MPRR, with values of 36%, 13%, and 0.35 bar, respectively.
- For D25NG50H25 (Mode 1), the application of WI-PI resulted in a decrease of 31.64% in NO_x and 0.4 bar in MPRR. For D25NG75H15 (Mode 2), the corresponding values were 25.18% decrease in NO_x and a 0.57 bar decrease in MPRR.
- It was previously mentioned that the condition with the highest hydrogen fraction within Mode 1 operating points (D25NG00H75) had very high MPRR values (10 bar/CA). In this operating point, WI-PI provides a reduction of 34.26% for NO_x, but due to the applied PI, MPRR has increased by 1.76 bar. In the mode with the highest hydrogen enrichment fraction for Mode 2 (D25NG75H25), the applied WI-PI (D25NG75H25-20PI-25WI75°C-20°CABTDCSOWI) strategies have reduced NO_x and MPRR by 11% and 0.04 bar, respectively. When comparing the test conditions (D25NG75H00 10° CA BTDC for SOI) with the WI-PI processed state, improvements of 46.11%, 22.46%, 5.21%, 93.66%, and 93.38% are observed in power, BSFC, TE, CO, and UHC, respectively. However, there is an increase of 35.1% in NO_x and 2.73 bar in MPRR.

Within the scope of the thesis, the final process applied is the injection of water vapor into the combustion chamber (WVI). This process was implemented in conjunction with 20% PI, resulting in various WVI-PI operating points. The numerical results obtained from WVI-PI are summarized below (Chapter 5.4).

- An increase in water vapor injection (WVI) rate has had a negative impact on power, BSFC, and TE values for both Mode 1 (D25NG50H25) and Mode 2 (D25NG75H15). However, it has yielded positive results in terms of NO_x. Just like in the WI process, there is a significant increase compared to the test conditions (D25NG75H00) in the WVI process. Therefore, the performance loss resulting from the application of the WVI-PI pair is not very significant compared to the process without it. The substantial decrease in NO_x has mitigated the significance of this performance loss.
- It has been observed that CO, UHC, and SOOT (PM) emissions sharply increase after the WVI ratio reaches 15%. To prevent performance loss and the increase in emissions, the optimum value for WVI has been considered to be 15%. While the optimum ratio was 25% in WI analyses, it is 15% in WVI analyses. The main reason for this is that water in the gas phase occupies more volume inside the cylinder, effectively reducing the oxygen concentration.
- The increase in WVI temperature (100 °C, 125 °C, 150 °C, and 200 °C) has a significant impact on volumetric efficiency, especially after 150 °C, leading to a noticeable deterioration in performance. While power and thermal efficiency decrease, ID (Ignition Delay), MPRR, and CD (Combustion Duration) values are not significantly affected. In line with the decrease in combustion performance, CO, UHC, and PM emissions have increased. The optimum temperature for WVI is considered to be 100 °C in terms of both performance and emission values.
- Reducing WVI advance results in positive outcomes for power, TE, CO, UHC, and PM, while it leads to negative effects on NO_x, MPRR, and CD. However, despite the results being this way compared to the non-process condition (0% WVI & 0% PI for Mode 1 - D25NG50H25 and Mode 2 - D25NG75H15), the use of a 20° CA BTDC value for WVI is understood to be necessary due to its enabling higher performance and lower emissions concerning test conditions (D25NG75H00 10° and 14° CA BTDC for SOI).

- Taking into account the obtained optimum values (15% WVI - 100 °C WVI temperature - 20° CA BTDC SOWVI), a comparison was made between non-PI (0% PI) and 20% PI conditions. It was observed that there is an improvement in performance and a decrease in MPRR and NO_x values with 20% PI.
- Compared to the test conditions of the operational point where the processes were applied in Mode 1 (D25NG50H25-20PI-15WVI100°C-20°CABTDCSOWVI) with the test conditions of D25NG75H00 14° CA BTDC for SOI, improvements were observed in power, BSFC, TE, NO_x, CO, and UHC by 17.39%, 25%, 5.57%, 14.56%, 88%, and 89.12%, respectively. There was only a 0.71 bar increase in MPRR. Similarly, for Mode 2 (D25NG75H15-20PI-15WVI100°C-20°CABTDCSOWVI), compared to the test conditions (D25NG75H00 10° CA BTDC for SOI), there were improvements in power, BSFC, TE, NO_x, CO, and UHC by 33.2%, 18.89%, 4.88%, 9.8%, 82%, and 78.68%, respectively, while there was only a 0.71 bar increase in MPRR.
- Applying WVI-PI (15% WVI & 20% PI) strategies to the experimental operating points resulted in a certain improvement in power, TE, and MPRR, while a slight deterioration was observed in BSFC values. However, it was observed that all emission values, including NO_x, were improved to reasonable levels. When WVI-PI was applied to the test condition with a injection advance of 14° CA BTDC (D25NG75H00), improvements of 2.66% for power, 0.85% for TE, and 0.15 bar for MPRR were observed, with only a 1.29% increase in BSFC. Improvements of 31.23%, 27.46%, and 19.17% were achieved for NO_x, CO, and UHC, respectively. For the other test condition (D25NG75H00 10° CA BTDC for SOI), there were improvements of 1.95% for power, 0.6% for TE, and 0.28 bar for MPRR, with only a 1.98% increase in BSFC.
- For D25NG50H25 (Mode 1), applying WVI-PI resulted in a decrease of 23.73% for NO_x and 0.23 bar for MPRR. For D25NG75H15 (Mode 2), these values were determined as a decrease of 18.75% for NO_x and 0.52 bar for MPRR.
- In Mode 1 operation points, when PI is applied in the condition where hydrogen fraction is the highest, combustion becomes more intense and closer to knocking limits (10 bar/CA for MPRR). In this operating point, while WVI-PI achieves a decrease of 26.78% for NO_x, the applied PI causes an increase of 2.16 bars for MPRR. In Mode 2, in the condition with the highest hydrogen enrichment fraction

(D25NG75H25), applied WVI-PI (D25NG75H25-20PI-15WVI100°C-20°CABTDCSOWVI) strategies resulted in a 4.44% improvement for NO_x, while there was a 0.09 bar increase in MPRR. When comparing the test conditions (D25NG75H00 10° CA BTDC for SOI) with the WVI-PI processed condition, there was an improvement in power, BSFC, TE, CO, and UHC by 49.9%, 26.16%, 6.14%, 94.54%, and 95.62%, respectively, while NO_x and MPRR showed an increase of 44.9% and 2.86 bar, respectively.

The first phase of the current study involved introducing hydrogen into a compression-ignition diesel engine, resulting in improved performance parameters (except MPRR) and all emissions except NO_x. In the second phase, EGR-PI, WI-PI, and WVI-PI dual processes were applied for NO_x and MPRR. In a broader scope, optimal operating points were identified under partial load conditions, achieving higher performance and lower overall emissions.

6.3 Recommendations

The thesis study presents a detailed analysis of the effects of different fractions of diesel-natural gas-hydrogen fuels on the engine performance and emission values of a compression-ignition engine at partial load (25%) and a constant engine speed (910 rpm). Furthermore, the study thoroughly investigates the effects of Exhaust Gas Recirculation (EGR), Pilot Injection (PI), Water Injection (WI), and Water Vapor Injection (WVI) processes. Based on the numerical results obtained in the study, the following recommendations are provided to contribute to a more comprehensive understanding of the use of alternative fuels in compression-ignition engines (CI).

- Since the studies have been limited to a constant engine speed and partial load, it would be highly beneficial for the literature to explore the effects of different engine loads (medium and full loads) and speeds.
- Furthermore, within the scope of the study, direct injection of water and water vapor into the combustion chamber has been implemented. Readers may explore the effects of injecting the water jet/steam into the intake port as well.
- In the thesis study, ignition was carried out by diesel fuel with a 25% energy fraction. As it is known, diesel fuel has a high C/H ratio, and it may be interesting to investigate how engine performance and exhaust gas emissions would be

affected when ignition is achieved with another liquid or gas fuel with a lower C/H ratio (such as low-C alcohols).

- Another suggestion is to investigate whether the 25% energy fraction of diesel fuel can be reduced further. Diversifying the study by gradually reducing the energy load of diesel and transferring it to gaseous fuels (hydrogen and natural gas) can be explored.
- The most crucial suggestion is to explore ways to reduce the energy share of diesel fuel in the current study, especially diverting this energy to hydrogen fuel. This is because the inadequacy of diesel fuel in meeting emission standards and the current reserve problem worldwide has made diesel fuel a significant actor in recent times. The more the share of diesel fuel can be reduced in studies, the less emission will be produced.

While a fuel that completely eliminates diesel may not currently exist, the knowledge accumulated through the current thesis and the suggested studies above can pave the way for the near future. With this information, it is likely that compression ignition engines can operate within a wide combustion range without the need for diesel fuel.

REFERENCES

[1] **Url-1** <*http://www.aecc.eu*>, date retrieved 29.09.2023.

[2] **Url-2** <*http://safety4sea.com* >, date retrieved 29.09.2023.

[3] **Url-3** <*http://www.greencarcongress.com*>, date retrieved 29.09.2023.

[4] **Url-4** <*http://www.myseatime.com*>, date retrieved 30.09.2023.

[5] **Url-5** <*http://www.enginebuildermag.com*>, date retrieved 30.09.2023.

[6] **Url-6** <*https://www.egcsa.com*>, date retrieved 30.09.2023.

[7] **H. Guo, B. Liko, and J. Littlejohns,** "Combustion and greenhouse gas emissions of a natural gas-Diesel dual fuel engine at low and high load conditions," in *Internal Combustion Engine Division Fall Technical Conference*, American Society of Mechanical Engineers, 2019, p. V001T02A004.

[8] **H. Guo, B. Liko, L. Luque, and J. Littlejohns,** "Combustion performance and unburned hydrocarbon emissions of a natural gas–diesel dual fuel engine at a low load condition," *J. Eng. Gas Turbines Power*, vol. 140, no. 11, p. 112801, 2018.

[9] **H. Guo, W. S. Neill, and B. Liko,** "An Experimental Investigation on the Combustion and Emissions Performance of a Natural Gas–Diesel Dual Fuel Engine at Low and Medium Loads," presented at the *ASME 2015 Internal Combustion Engine Division Fall Technical Conference*, American Society of Mechanical Engineers Digital Collection, Jan. 2016. doi: 10.1115/ICEF2015-1041.

[10] **X. Liu, G. Seberry, S. Kook, Q. N. Chan, and E. R. Hawkes,** "Direct injection of hydrogen main fuel and diesel pilot fuel in a retrofitted single-cylinder compression ignition engine," *Int. J. Hydrog. Energy*, vol. 47, no. 84, pp. 35864–35876, 2022.

[11] **K. Bayramoğlu and S. Yılmaz,** "Emission and performance estimation in hydrogen injection strategies on diesel engines," *Int. J. Hydrog. Energy*, vol. 46, no. 57, pp. 29732–29744, 2021.

[12] **A. Jamrozik, K. Grab-Rogaliński, and W. Tutak,** "Hydrogen effects on combustion stability, performance and emission of diesel engine," *Int. J. Hydrog. Energy*, vol. 45, no. 38, pp. 19936–19947, 2020.

[13] **I. T. Yilmaz and M. Gumus,** "Effects of hydrogen addition to the intake air on performance and emissions of common rail diesel engine," *Energy*, vol. 142, pp. 1104–1113, 2018.

[14] **N. Castro, M. Toledo, and G. Amador,** "An experimental investigation of the performance and emissions of a hydrogen-diesel dual fuel compression ignition internal combustion engine," *Appl. Therm. Eng.*, vol. 156, pp. 660–667, 2019.

[15] **L. Wang, D. Liu, Z. Yang, H. Li, L. Wei, and Q. Li,** "Effect of H2 addition on combustion and exhaust emissions in a heavy-duty diesel engine with EGR," *Int. J. Hydrog. Energy*, vol. 43, no. 50, pp. 22658–22668, 2018.

[16] **O. H. Ghazal,** "Performance and combustion characteristic of CI engine fueled with hydrogen enriched diesel," *Int. J. Hydrog. Energy*, vol. 38, no. 35, pp. 15469–15476, 2013.

[17] **X. Liu, A. Srna, H. L. Yip, S. Kook, Q. N. Chan, and E. R. Hawkes,** "Performance and emissions of hydrogen-diesel dual direct injection (H2DDI) in a single-cylinder compression-ignition engine," *Int. J. Hydrog. Energy*, vol. 46, no. 1, pp. 1302–1314, 2021.

[18] **R. Juknelevičius, A. Rimkus, S. Pukalskas, and J. Matijošius,** "Research of performance and emission indicators of the compression-ignition engine powered by hydrogen-Diesel mixtures," *Int. J. Hydrog. Energy*, vol. 44, no. 20, pp. 10129–10138, 2019.

[19] **R. A. Bakar *et al.*,** "Experimental analysis on the performance, combustion/emission characteristics of a DI diesel engine using hydrogen in dual fuel mode," *Int. J. Hydrog. Energy*, 2022.

[20] **T. Tsujimura and Y. Suzuki,** "The utilization of hydrogen in hydrogen/diesel dual fuel engine," *Int. J. Hydrog. Energy*, vol. 42, no. 19, pp. 14019–14029, 2017.

[21] **N. Khatri and K. K. Khatri,** "Hydrogen enrichment on diesel engine with biogas in dual fuel mode," *Int. J. Hydrog. Energy*, vol. 45, no. 11, pp. 7128–7140, 2020.

[22] **S. Kanth, S. Debbarma, and B. Das,** "Effect of hydrogen enrichment in the intake air of diesel engine fuelled with honge biodiesel blend and diesel," *Int. J. Hydrog. Energy*, vol. 45, no. 56, pp. 32521–32533, 2020.

[23] **S. Das, S. Kanth, B. Das, and S. Debbarma,** "Experimental evaluation of hydrogen enrichment in a dual-fueled CRDI diesel engine," *Int. J. Hydrog. Energy*, vol. 47, no. 20, pp. 11039–11051, 2022.

[24] **H. M. Rahimi, S. A. Jazayeri, and M. Ebrahimi,** "Hydrogen energy share enhancement in a heavy duty diesel engine under RCCI combustion fueled with natural gas and diesel oil," *Int. J. Hydrog. Energy*, vol. 45, no. 35, pp. 17975–17991, 2020.

[25] **R. Juknelevicius, S. Szwaja, M. Pyrc, and M. Gruca,** "Influence of hydrogen co-combustion with diesel fuel on performance, smoke and combustion phases in the compression ignition engine," *Int. J. Hydrog. Energy*, vol. 44, no. 34, pp. 19026–19034, 2019.

[26] **S. Nag, P. Sharma, A. Gupta, and A. Dhar,** "Experimental study of engine performance and emissions for hydrogen diesel dual fuel engine with exhaust gas recirculation," *Int. J. Hydrog. Energy*, vol. 44, no. 23, pp. 12163–12175, 2019.

[27] **P. Dimitriou, M. Kumar, T. Tsujimura, and Y. Suzuki,** "Combustion and emission characteristics of a hydrogen-diesel dual-fuel engine," *Int. J. Hydrog. Energy*, vol. 43, no. 29, pp. 13605–13617, 2018.

[28] **J. You, Z. Liu, Z. Wang, D. Wang, and Y. Xu,** "Experimental analysis of inert gases in EGR on engine power and combustion characteristics in a stoichiometric dual fuel heavy-duty natural gas engine ignited with diesel," *Appl. Therm. Eng.*, vol. 180, p. 115860, 2020.

[29] **C. D. Rakopoulos, D. C. Rakopoulos, G. C. Mavropoulos, and G. M. Kosmadakis,** "Investigating the EGR rate and temperature impact on diesel engine combustion and emissions under various injection timings and loads by comprehensive two-zone modeling," *Energy*, vol. 157, pp. 990–1014, 2018.

[30] **V. S. Yaliwal, N. R. Banapurmath, M. E. M. Soudagar, A. Afzal, and P. Ahmadi,** "Effect of manifold and port injection of hydrogen and exhaust gas recirculation (EGR) in dairy scum biodiesel-low energy content gas-fueled CI engine operated on dual fuel mode," *Int. J. Hydrog. Energy*, vol. 47, no. 10, pp. 6873–6897, 2022.

[31] **H.-W. Wu and Z.-Y. Wu,** "Investigation on combustion characteristics and emissions of diesel/hydrogen mixtures by using energy-share method in a diesel engine," *Appl. Therm. Eng.*, vol. 42, pp. 154–162, 2012.

[32] **Y. Suzuki and T. Tsujimura,** "The combustion improvements of hydrogen/diesel dual fuel engine," *SAE Technical Paper*, 2015.

[33] **B. Shin, Y. Cho, D. Han, S. Song, and K. M. Chun,** "Hydrogen effects on NOx emissions and brake thermal efficiency in a diesel engine under low-temperature and heavy-EGR conditions," *Int. J. Hydrog. Energy*, vol. 36, no. 10, pp. 6281–6291, 2011.

[34] **M. Kumar, S. Bhowmik, and A. Paul,** "Effect of pilot fuel injection pressure and injection timing on combustion, performance and emission of hydrogen-biodiesel dual fuel engine," *Int. J. Hydrog. Energy*, vol. 47, no. 68, pp. 29554–29567, 2022.

[35] **G. Tripathi, P. Sharma, A. Dhar, and A. Sadiki,** "Computational investigation of diesel injection strategies in hydrogen-diesel dual fuel engine," *Sustain. Energy Technol. Assess.*, vol. 36, p. 100543, 2019.

[36] **V. Chintala, D. Benaerjee, P. K. Ghodke, and E. Porpatham,** "Hydrogen rich exhaust gas recirculation (H2EGR) for performance improvement and emissions reduction of a compression ignition engine," *Int. J. Hydrog. Energy*, vol. 44, no. 33, pp. 18545–18558, 2019.

[37] **M. Talibi, P. Hellier, and N. Ladommatos,** "The effect of varying EGR and intake air boost on hydrogen-diesel co-combustion in CI engines," *Int. J. Hydrog. Energy*, vol. 42, no. 9, pp. 6369–6383, 2017.

[38] **H.-W. Wu, T.-T. Hsu, J.-Y. He, and C.-M. Fan,** "Optimal performance and emissions of diesel/hydrogen-rich gas engine varying intake air temperature and EGR ratio," *Appl. Therm. Eng.*, vol. 124, pp. 381–392, 2017.

[39] **D. T. Hountalas, G. C. Mavropoulos, and K. B. Binder,** "Effect of exhaust gas recirculation (EGR) temperature for various EGR rates on heavy duty DI diesel engine performance and emissions," *Energy*, vol. 33, no. 2, pp. 272–283, 2008.

[40] **S. Verma, L. M. Das, S. C. Kaushik, and S. S. Bhatti,** "The effects of compression ratio and EGR on the performance and emission characteristics of diesel-biogas dual fuel engine," *Appl. Therm. Eng.*, vol. 150, pp. 1090–1103, 2019.

[41] **M. Karimi, X. Wang, J. Hamilton, and M. Negnevitsky,** "Numerical investigation on hydrogen-diesel dual-fuel engine improvements by oxygen enrichment," *Int. J. Hydrog. Energy*, vol. 47, no. 60, pp. 25418–25432, 2022.

[42] **X. Shan, Y. Qian, L. Zhu, and X. Lu,** "Effects of EGR rate and hydrogen/carbon monoxide ratio on combustion and emission characteristics of biogas/diesel dual fuel combustion engine," *Fuel*, vol. 181, pp. 1050–1057, 2016.

[43] **A. Jain, A. P. Singh, and A. K. Agarwal,** "Effect of split fuel injection and EGR on NOx and PM emission reduction in a low temperature combustion (LTC) mode diesel engine," *Energy*, vol. 122, pp. 249–264, 2017.

[44] **S. Sathishkumar and M. M. Ibrahim,** "Investigation on the effect of injection schedule and EGR in hydrogen energy share using common rail direct injection dual fuel engine," *Int. J. Hydrog. Energy*, vol. 46, no. 20, pp. 11494–11510, 2021.

[45] **X. Zhou, W. Qian, M. Pan, R. Huang, L. Xu, and J. Yin,** "Potential of n-butanol/diesel blends for CI engines under post injection strategy and different EGR rates conditions," *Energy Convers. Manag.*, vol. 204, p. 112329, 2020.

[46] **A. I. Jabbr and U. O. Koylu,** "Influence of operating parameters on performance and emissions for a compression-ignition engine fueled by hydrogen/diesel mixtures," *Int. J. Hydrog. Energy*, vol. 44, no. 26, pp. 13964–13973, 2019.

[47] **P. Sharma and A. Dhar,** "Compression ratio influence on combustion and emissions characteristic of hydrogen diesel dual fuel CI engine: Numerical Study," *Fuel*, vol. 222, pp. 852–858, 2018.

[48] **B. Wang, C. Yang, H. Wang, D. Hu, B. Duan, and Y. Wang,** "Study on injection strategy of ammonia/hydrogen dual fuel engine under different compression ratios," *Fuel*, vol. 334, p. 126666, 2023.

[49] **K. Shojae, M. Mahdavian, and E. Baghshani,** "Investigation of piston bowl geometry, injection timing, and EGR mass fraction to improve the performance of ISM 370 diesel engine," *Fuel*, vol. 324, p. 124422, 2022.

[50] **X. Sun, J. Ning, X. Liang, G. Jing, Y. Chen, and G. Chen,** "Effect of direct water injection on combustion and emissions characteristics of marine diesel engines," *Fuel*, vol. 309, p. 122213, 2022.

[51] **R. Adnan, H. H. Masjuki, and T. M. I. Mahlia,** "Performance and emission analysis of hydrogen fueled compression ignition engine with variable water injection timing," *Energy*, vol. 43, no. 1, pp. 416–426, 2012.

[52] **H. Taghavifar, S. Anvari, and A. Parvishi,** "Benchmarking of water injection in a hydrogen-fueled diesel engine to reduce emissions," *Int. J. Hydrog. Energy*, vol. 42, no. 16, pp. 11962–11975, 2017.

[53] **H. Taghavifar,** "Experimental and numerical engine cycle setup for a dual fuel hydrogen, methane, and hythane with diesel to assess the effect of water injection and nozzle geometry," *Environ. Prog. Sustain. Energy*, vol. 42, no. 1, p. e13936, Jan. 2023, doi: 10.1002/ep.13936.

[54] **B. Tesfa, R. Mishra, F. Gu, and A. D. Ball,** "Water injection effects on the performance and emission characteristics of a CI engine operating with biodiesel," *Renew. Energy*, vol. 37, no. 1, pp. 333–344, 2012.

[55] **M. A. Benbellil, M. S. Lounici, K. Loubar, and M. Tazerout,** "Investigation of natural gas enrichment with high hydrogen participation in dual fuel diesel engine," *Energy*, vol. 243, p. 122746, 2022.

[56] **J. Zareei, A. Rohani, and J. R. N. Alvarez,** "The effect of EGR and hydrogen addition to natural gas on performance and exhaust emissions in a diesel engine by AVL fire multi-domain simulation, GPR model, and multi-objective genetic algorithm," *Int. J. Hydrog. Energy*, vol. 47, no. 50, pp. 21565–21581, 2022.

[57] **W. Zhang, T. Feng, Z. Li, Z. Chen, and J. Zhao,** "EGR thermal and chemical effects on combustion and emission of diesel/natural gas dual-fuel engine," *Fuel*, vol. 302, p. 121161, 2021.

[58] **S. Ouchikh, M. S. Lounici, K. Loubar, L. Tarabet, and M. Tazerout,** "Effect of diesel injection strategy on performance and emissions of CH4/diesel dual-fuel engine," *Fuel*, vol. 308, p. 121911, 2022.

[59] **S. K. Pathak, A. Nayyar, and V. Goel,** "Optimization of EGR effects on performance and emission parameters of a dual fuel (Diesel+ CNG) CI engine: an experimental investigation," *Fuel*, vol. 291, p. 120183, 2021.

[60] **S. Vadlamudi, S. K. Gugulothu, J. K. Panda, B. Deepanraj, and P. V. Kumar,** "Paradigm analysis of performance and exhaust emissions in CRDI engine powered with hydrogen and Hydrogen/CNG fuels: A green fuel approach under different injection strategies," *Int. J. Hydrog. Energy*, 2022.

[61] **G. Tripathi, P. Sharma, and A. Dhar,** "Computational study of diesel injection strategies for methane-diesel dual fuel engine," *Clean. Eng. Technol.*, vol. 6, p. 100393, 2022.

[62] **Y. Chen *et al.*,** "Study of injection pressure couple with EGR on combustion performance and emissions of natural gas-diesel dual-fuel engine," *Fuel*, vol. 261, p. 116409, 2020.

[63] **F. Liu, Y. Kang, H. Wu, C.-F. Lee, and Y. Li,** "Effect of hydrogen volume ratio on the combustion characteristics of CNG-diesel dual-fuel engine," *SAE Technical Paper*, 2017.

[64] **S. Ouchikh, M. S. Lounici, L. Tarabet, K. Loubar, and M. Tazerout,** "Effect of natural gas enrichment with hydrogen on combustion characteristics of a dual fuel diesel engine," *Int. J. Hydrog. Energy*, vol. 44, no. 26, pp. 13974–13987, 2019.

[65] **Url-7** <*http://www.britannica.com*>, date retrieved 03.10.2023.

[66] **Url-8** <*http://www.x-engineer.org*>, date retrieved 03.10.2023.

[67] **J. B. Heywood,** *Internal combustion engine fundamentals*. McGraw-Hill Education, 2018.

[68] **R. S. Benson and N. D. Whitehouse,** *Internal combustion engines: in 2 volumes ; a detailed introduction to the thermodynamics of spark and compression ignition engines, their design and development*, Reprinted. in Pergamon international library of science, technology, engineering and social studies. Oxford u.a: Pergamon Press, 1983.

[69] **B. Challen and R. Baranescu,** "Diesel engine reference book", 1999.

[70] **K. Kannan and M. Udayakumar,** "Modeling of nitric oxide formation in single cylinder direct injection diesel engine using diesel-water emulsion," *Am. J. Appl. Sci.*, vol. 6, no. 7, p. 1313, 2009.

[71] **H. O. Hardenberg and F. W. Hase,** "An empirical formula for computing the pressure rise delay of a fuel from its cetane number and from the relevant parameters of direct-injection diesel engines," *SAE Trans.*, pp. 1823–1834, 1979.

[72] **D. N. Assanis, Z. S. Filipi, S. B. Fiveland, and M. Syrimis,** "A predictive ignition delay correlation under steady-state and transient operation of a direct injection diesel engine," *J Eng Gas Turbines Power*, vol. 125, no. 2, pp. 450–457, 2003.

[73] **H. Yasar, H. S. Soyhan, H. Walmsley, B. Head, and C. Sorusbay,** "Double-Wiebe function: An approach for single-zone HCCI engine modeling," *Appl. Therm. Eng.*, vol. 28, no. 11–12, pp. 1284–1290, 2008.

[74] **A. G. Charalambides,** "Homogenous charge compression ignition (HCCI) engines," *Adv. Intern. Combust. Engines Fuel Technol.*, pp. 119–148, 2013.

[75] **J. E. Dec,** "Advanced compression-ignition engines—understanding the in-cylinder processes," *Proc. Combust. Inst.*, vol. 32, no. 2, pp. 2727–2742, 2009.

[76] **J. G. Antunes, R. Mikalsen, and A. P. Roskilly,** "An investigation of hydrogen-fuelled HCCI engine performance and operation," *Int. J. Hydrog. Energy*, vol. 33, no. 20, pp. 5823–5828, 2008.

[77] **G. Li, C. Zhang, and J. Zhou,** "Study on the knock tendency and cyclical variations of a HCCI engine fueled with n-butanol/n-heptane blends," *Energy Convers. Manag.*, vol. 133, pp. 548–557, 2017.

[78] **D. Yap, S. M. Peucheret, A. Megaritis, M. L. Wyszynski, and H. Xu,** "Natural gas HCCI engine operation with exhaust gas fuel reforming," *Int. J. Hydrog. Energy*, vol. 31, no. 5, pp. 587–595, 2006.

[79] **M. M. Andreae, W. K. Cheng, T. Kenney, and J. Yang,** "On HCCI engine knock," *SAE Trans.*, pp. 355–363, 2007.

[80] **J. E. Dec and Y. Yang,** "Boosted HCCI for high power without engine knock and with ultra-low NOx emissions-using conventional gasoline," *SAE Int. J. Engines*, vol. 3, no. 1, pp. 750–767, 2010.

[81] **S. Gan, H. K. Ng, and K. M. Pang,** "Homogeneous charge compression ignition (HCCI) combustion: implementation and effects on pollutants in direct injection diesel engines,"*Appl. Energy*, vol.88, no.3, pp.559–567, 2011.

[82] **A. W. Gray III and T. W. Ryan III,** "Homogeneous charge compression ignition (HCCI) of diesel fuel," *SAE Trans.*, pp. 1927–1935, 1997.

[83] **N. P. Komninos and G. M. Kosmadakis,** "Heat transfer in HCCI multi-zone modeling: Validation of a new wall heat flux correlation under motoring conditions," *Appl. Energy*, vol. 88, no. 5, pp. 1635–1648, 2011.

[84] **X.-C. Lü, W. Chen, and Z. Huang,** "A fundamental study on the control of the HCCI combustion and emissions by fuel design concept combined with controllable EGR. Part 2. Effect of operating conditions and EGR on HCCI combustion," *Fuel*, vol. 84, no. 9, pp. 1084–1092, 2005.

[85] **M. Nakano, Y. Mandokoro, S. Kubo, and S. Yamazaki,** "Effects of exhaust gas recirculation in homogeneous charge compression ignition engines," *Int. J. Engine Res.*, vol. 1, no. 3, pp. 269–279, Jun. 2000, doi: 10.1243/1468087001545173.

[86] **D. Mei, S. Yue, X. Zhao, K. Hielscher, and R. Baar,** "Effects of center of heat release on combustion and emissions in a PCCI diesel engine fuelled by DMC-diesel blend," *Appl. Therm. Eng.*, vol. 114, pp. 969–976, 2017.

[87] **T. Fuyuto, M. Taki, R. Ueda, Y. Hattori, H. Kuzuyama, and T. Umehara,** "Noise and emissions reduction by second injection in diesel PCCI combustion with split injection," *SAE Int. J. Engines*, vol. 7, no. 4, pp. 1900–1910, 2014.

[88] **H. Ikeda, N. Iida, H. Kuzuyama, T. Umehara, and T. Fuyuto,** "An investigation of controlling two-peak heat release rate for combustion noise reduction in split-injection PCCI engine using numerical calculation," *SAE Technical Paper*, 2014.

[89] **Z. Peng, B. Liu, W. Wang, and L. Lu,** "CFD investigation into diesel PCCI combustion with optimized fuel injection," *Energies*, vol. 4, no. 3, pp. 517–531, 2011.

[90] **S. d'Ambrosio and A. Ferrari,** "Effects of exhaust gas recirculation in diesel engines featuring late PCCI type combustion strategies," *Energy Convers. Manag.*, vol. 105, pp. 1269–1280, 2015.

[91] **W. L. Hardy and R. D. Reitz,** "A study of the effects of high EGR, high equivalence ratio, and mixing time on emissions levels in a heavy-duty diesel engine for PCCI combustion," *SAE Technical Paper*, 2006.

[92] **B. V. S. Chauhan, I. Sayyed, A. Vedrantam, A. Garg, S. Bharti, and M. Shukla,**"State of the Art in Low-Temperature Combustion Technologies: HCCI, PCCI, and RCCI," in *Advanced Combustion for Sustainable Transport*, A. K. Agarwal, A. G. Martínez, A. Kalwar, and H. Valera, Eds., in Energy, Environment, and Sustainability., Singapore: Springer Singapore, 2022, pp. 95–139. doi: 10.1007/978-981-16-8418-04.

[93] **E. Shim, H. Park, and C. Bae,** "Comparisons of advanced combustion technologies (HCCI, PCCI, and dual-fuel PCCI) on engine performance and emission characteristics in a heavy-duty diesel engine," *Fuel*, vol. 262, p. 116436, 2020.

[94] **G. D. Neely, S. Sasaki, Y. Huang, J. A. Leet, and D. W. Stewart,** "New diesel emission control strategy to meet US Tier 2 emissions regulations," *SAE Trans.*, pp. 512–524, 2005.

[95] **X. Liang, Z. Zheng, H. Zhang, Y. Wang, and H. Yu,** "A review of early injection strategy in premixed combustion engines," *Appl. Sci.*, vol. 9, no. 18, p. 3737, 2019.

[96] **J. Benajes, S. Molina, A. García, and J. Monsalve-Serrano,** "Effects of low reactivity fuel characteristics and blending ratio on low load RCCI (reactivity controlled compression ignition) performance and emissions in a heavy-duty diesel engine," *Energy*, vol. 90, pp. 1261–1271, 2015.

[97] **J. Li, W. Yang, and D. Zhou,** "Review on the management of RCCI engines," *Renew. Sustain. Energy Rev.*, vol. 69, pp. 65–79, 2017.

[98] **A. P. Singh, V. Kumar, and A. K. Agarwal,** "Evaluation of comparative engine combustion, performance and emission characteristics of low temperature combustion (PCCI and RCCI) modes," *Appl. Energy*, vol. 278, p. 115644, 2020.

[99] **M. Sonachalam and V. Manieniyan,** "Performance and Emission Analysis of RCCI Engine Fuelled with Acetylene Gas," in *Advances in IC Engines and Combustion Technology*, A. K. Gupta, H. C. Mongia, P. Chandna, and G. Sachdeva, Eds., in Lecture Notes in Mechanical Engineering. , Singapore: Springer Singapore, 2021, pp. 113–123. doi: 10.1007/978-981-15-5996-9_9.

[100] **J. Dierickx, Q. Dejaegere, J. Peeters, L. Sileghem, and S. Verhelst,** "Performance and emissions of a high-speed marine dual-fuel engine operating with methanol-water blends as a fuel," *Fuel*, vol. 333, p. 126349, 2023.

[101] **Q. Wang, L. Wei, W. Pan, and C. Yao,** "Investigation of operating range in a methanol fumigated diesel engine," *Fuel*, vol. 140, pp. 164–170, 2015.

[102] **A. J. Reiter and S.-C. Kong,** "Demonstration of Compression-Ignition Engine Combustion Using Ammonia in Reducing Greenhouse Gas Emissions," *Energy Fuels*, vol. 22, no. 5, pp. 2963–2971, Sep. 2008, doi: 10.1021/ef800140f.

[103] **J. R. Cooper, R. J. Crookes, J. W. Rose, and A. Mozafari,** "Ammonia as a Fuel for the IC Engine," 1991.

[104] **P. Berwal, S. Kumar, and B. Khandelwal,** "A comprehensive review on synthesis, chemical kinetics, and practical application of ammonia as future fuel for combustion," *J. Energy Inst.*, vol. 99, pp. 273–298, 2021.

[105] **J. Li *et al.*,** "A review on combustion characteristics of ammonia as a carbon-free fuel," *Front. Energy Res.*, vol. 9, p. 760356, 2021.

[106] **H. Chen, J. He, and X. Zhong,** "Engine combustion and emission fuelled with natural gas: a review," *J. Energy Inst.*, vol. 92, no. 4, pp. 1123–1136, 2019.

[107] **T. Li, M. Eremia, and M. Shahidehpour,** "Interdependency of natural gas network and power system security," *IEEE Trans. Power Syst.*, vol. 23, no. 4, pp. 1817–1824, 2008.

[108] **C. Hall and M. Kassa,** "Advances in combustion control for natural gas–diesel dual fuel compression ignition engines in automotive applications: A review," *Renew. Sustain. Energy Rev.*, vol. 148, p. 111291, 2021.

[109] **G. A. Karim,** "A review of combustion processes in the dual fuel engine—the gas diesel engine," *Prog. Energy Combust. Sci.*, vol. 6, no. 3, pp. 277–285, 1980.

[110] **A. Wagemakers and C. A. J. Leermakers,** "Review on the effects of dual-fuel operation, using diesel and gaseous fuels, on emissions and performance," *SAE Int. J. Engines*, vol. 2012010869, no. 2012-01–0869, pp. 1–18, 2012.

[111] **M. Ciniviz and H. Köse,** "Hydrogen use in internal combustion engine: a review," *Int. J. Automot. Eng. Technol.*, vol. 1, no. 1, pp. 1–15, 2012.

[112] **B. Shadidi, G. Najafi, and T. Yusaf,** "A review of hydrogen as a fuel in internal combustion engines," *Energies*, vol. 14, no. 19, p. 6209, 2021.

[113] **T. Gatts, S. Liu, C. Liew, B. Ralston, C. Bell, and H. Li,** "An experimental investigation of incomplete combustion of gaseous fuels of a heavy-duty diesel engine supplemented with hydrogen and natural gas," *Int. J. Hydrog. Energy*, vol. 37, no. 9, pp. 7848–7859, 2012.

[114] **I. T. Yilmaz,** "Effect of using dual fuel (biogas-diesel) on the performance and emissions of a low heat rejection diesel engine," *PhD Marmara Univ. Inst. Pure Appl. Sci. Istanb.*, 2015.

[115] **I. T. Yilmaz and M. Gumus,** "Investigation of the effect of biogas on combustion and emissions of TBC diesel engine," *Fuel*, vol. 188, pp. 69–78, 2017.

[116] **K. Von Mitzlaff,** *Engines for biogas*. Deutsche Zentrum fur Entwicklungstechnologien, 1988.

[117] **H. N. Gupta,** *Fundamentals of internal combustion engines*. PHI Learning Pvt. Ltd., 2012.

[118] **H. Bockhorn,** *Soot formation in combustion: mechanisms and models*, vol. 59. Springer Science & Business Media, 2013.

[119] **R. D. Meininger *et al.*,** "Knock criteria for aviation diesel engines," *Int. J. Engine Res.*, vol. 18, no. 7, pp. 752–762, Sep. 2017, doi: 10.1177/1468087416669882.

[120] **L. Shi, K. Deng, Y. Cui, S. Qu, and W. Hu,** "Study on knocking combustion in a diesel HCCI engine with fuel injection in negative valve overlap," *Fuel*, vol. 106, pp. 478–483, 2013.

[121] **A. Taghizadeh-Alisaraei and A. Rezaei-Asl,** "The effect of added ethanol to diesel fuel on performance, vibration, combustion and knocking of a CI engine," *Fuel*, vol. 185, pp. 718–733, 2016.

[122] **K. Wannatong, N. Akarapanyavit, S. Siengsanorh, and S. Chanchaona,** "Combustion and knock characteristics of natural gas diesel dual fuel engine," SAE Technical Paper, 2007.

[123] **H. Wu *et al.*,** "Effect of injection timing on knock combustion and pollutant emission of heavy-duty diesel engines at low temperatures," *Chemosphere*, vol. 305, p. 135519, 2022.

[124] **H. Chen, X. Guo, H. Huang, and B. Wang,** "The effect of a pine oil/diesel blend on the particulate emission characteristics of a diesel engine under a pre-injection strategy with EGR," *Sustain. Energy Fuels*, vol. 7, no. 15, pp. 3644–3653, 2023.

[125] **W. Gu and W. Su,** "Study on the Effects of Exhaust Gas Recirculation and Fuel Injection Strategy on Transient Process Performance of Diesel Engines," *Sustainability*, vol. 15, no. 16, p. 12403, 2023.

[126] **Z. Han, A. Uludogan, G. J. Hampson, and R. D. Reitz,** "Mechanism of soot and NOx emission reduction using multiple-injection in a diesel engine," *SAE Trans.*, pp. 837–852, 1996.

[127] **D. Tan *et al.*,** "Utilization of renewable and sustainable diesel/methanol/n-butanol (DMB) blends for reducing the engine emissions in a diesel engine with different pre-injection strategies," *Energy*, vol. 269, p. 126785, 2023.

[128] **D. Wang, C. Zhang, and Y. Wang,** "A Numerical Study of Multiple Fuel Injection Strategies for NO_x Reduction from DI Diesel Engines," *Int. J. Green Energy*, vol. 4, no. 4, pp. 453–470, Jul. 2007, doi: 10.1080/15435070701465912.

[129] **Url-9** <*http://www.dieselnet.com*>, date retrieved 15.10.2023.

[130] **E. Öztürk and Ö. Can,** "Effects of EGR, injection retardation and ethanol addition on combustion, performance and emissions of a DI diesel engine fueled with canola biodiesel/diesel fuel blend," *Energy*, vol. 244, p. 123129, 2022.

[131] **A. Parlak, V. Ayhan, İ. Cesur, and B. Boru,** "Endirekt enjeksiyonlu bir dizel motoruna buhar enjeksiyonunun etkilerinin araştırılması," in *6th International Advanced Technologies Symposium*, 2011, pp. 16–18.

[132] **Y. Murthy, G. Y. K. Sastry, and M. R. S. Satyanaryana,** "Experimental investigation of performance and emissions on low speed diesel engine with dual injection of solar generated steam and pongamia methyl ester," *Indian J. Sci. Technol.*, vol. 4, no. 1, pp. 29–33, 2011.

[133] **"ANSYS Forte Reaction Design."** in Forte Theory Manual. 2018.

[134] **V. Yakhot and S. A. Orszag,** "Renormalization group analysis of turbulence. I. Basic theory," *J. Sci. Comput.*, vol. 1, no. 1, pp. 3–51, 1986.

[135] **H. Hiroyasu and T. Kadota,** "Models for combustion and formation of nitric oxide and soot in direct injection diesel engines," *SAE Trans.*, pp. 513–526, 1976.

[136] **J. Nagle and R. F. Strickland-Constable,** "Oxidation of carbon between 1000–2000 C," in *Proceedings of the fifth conference on carbon*, Elsevier, 1962, pp. 154–164.

[137] **D. Kong, R. K. Eckhoff, and F. Alfert,** "Auto-ignition of CH4air, C3H8air, CH4/C3H8/air and CH4/CO2/air using a 11 ignition bomb," *J. Hazard. Mater.*, vol. 40, no. 1, pp. 69–84, 1995.

[138] **S.-C. Kong and R. D. Reitz,** "Use of detailed chemical kinetics to study HCCI engine combustion with consideration of turbulent mixing effects," *J Eng Gas Turbines Power*, vol. 124, no. 3, pp. 702–707, 2002.

[139] **N. Peters, H. Wenzel, and F. A. Williams,** "Modification of the turbulent burning velocity by gas expansion," *Proc. Combust. Inst.*, vol. 28, no. 1, pp. 235–243, 2000.

[140] **L. Liang and R. D. Reitz,** "Spark ignition engine combustion modeling using a level set method with detailed chemistry," *SAE Technical Paper*, 2006.

[141] **L. Liang, R. D. Reitz, C. O. Iyer, and J. Yi,** "Modeling knock in spark-ignition engines using a G-equation combustion model incorporating detailed chemical kinetics," *SAE technical paper*, 2007.

[142] **Z. Tan and R. D. Reitz,** "An ignition and combustion model based on the level-set method for spark ignition engine multidimensional modeling," *Combust. Flame*, vol. 145, no. 1–2, pp. 1–15, 2006.

[143] **C. T. Crowe, J. D. Schwarzkopf, M. Sommerfeld, and Y. Tsuji,** *Multiphase flows with droplets and particles*. CRC press, 2011.

[144] **M. Metghalchi and J. C. Keck,** "Burning velocities of methanol, ethanol and iso-octane-air mixtures," in *19th Symposium (International) on Combustion/The combustion Institute*, 1983, p. 275.

[145] **Z. Han and R. D. Reitz,** "A temperature wall function formulation for variable-density turbulent flows with application to engine convective heat transfer modeling," *Int. J. Heat Mass Transf.*, vol. 40, no. 3, pp. 613–625, 1997.

[146] **Z. Han and R. D. Reitz,** "Turbulence Modeling of Internal Combustion Engines Using RNG κ-ε Models," *Combust. Sci. Technol.*, vol. 106, no. 4–6, pp. 267–295, Jan. 1995, doi: 10.1080/00102209508907782.

[147] **A. Kazakov and M. Frenklach,** "Dynamic modeling of soot particle coagulation and aggregation: Implementation with the method of moments and application to high-pressure laminar premixed flames," *Combust. Flame*, vol. 114, no. 3–4, pp. 484–501, 1998.

[148] **J. C. Beale and R. D. Reitz,** "Modeling spray atomization with the Kelvin-Helmholtz/Rayleigh-Taylor hybrid model," *At. Sprays*, vol. 9, no. 6, 1999.

[149] **T. F. Su, M. A. Patterson, R. D. Reitz, and P. V. Farrell,** "Experimental and numerical studies of high pressure multiple injection sprays," *SAE Trans.*, pp. 1281–1292, 1996.

[150] **Y. Wang, H.-W. Ge, and R. D. Reitz,** "Validation of mesh-and timestep-independent spray models for multi-dimensional engine CFD simulation," *SAE Int. J. Fuels Lubr.*, vol. 3, no. 1, pp. 277–302, 2010.

[151] **R. Reitz,** "Modeling atomization processes in high-pressure vaporizing sprays," *At. Spray Technol.*, vol. 3, no. 4, pp. 309–337, 1987.

[152] **V. G. Levich,** *Physicochemical hydrodynamics:(by) veniamin G. Levich. Transl. by scripta technica, inc*. Prentice-Hall, 1962.

[153] **R. D. Reitz and R. Diwakar,** "Effect of drop breakup on fuel sprays," *SAE Trans.*, pp. 218–227, 1986.

[154] **R. Bellman and R. H. Pennington,** "Effects of surface tension and viscosity on Taylor instability," *Q. Appl. Math.*, vol. 12, no. 2, pp. 151–162, 1954.

[155] **N. Abani *et al.*,** "An improved spray model for reducing numerical parameter dependencies in diesel engine CFD simulations," SAE technical paper, 2008.

[156] **X. Yang, Y. Takamoto, A. Okajima, T. Obokata, and W. Long,** "Comparison of computed and measured high-pressure conical diesel sprays," *SAE Trans.*, pp. 1092–1101, 2000.

[157] **P. J. O'Rourke and A. A. Amsden,** "The TAB method for numerical calculation of spray droplet breakup," *SAE technical paper*, 1987.

[158] **A. Munnannur,** *Droplet collision modeling in multi-dimensional engine spray computation*. University of Wisconsin–Madison, 2007.

[159] **D. P. Schmidt and C. J. Rutland,** "A new droplet collision algorithm," *J. Comput. Phys.*, vol. 164, no. 1, pp. 62–80, 2000.

[160] **Y. Sun and R. D. Reitz,** "Modeling low-pressure injections in diesel HCCI engines," in *Proceedings of ILASS Americas, 20th annual conference on liquid atomization and spray systems*, 2007.

[161] **Y. Ra and R. D. Reitz,** "A vaporization model for discrete multi-component fuel sprays," *Int. J. Multiph. Flow*, vol. 35, no. 2, pp. 101–117, 2009.

[162] **Y. Ra and R. D. Reitz,** "The application of a multicomponent droplet vaporization model to gasoline direct injection engines," *Int. J. Engine Res.*, vol. 4, no. 3, pp. 193–218, 2003.

[163] **W. A. Sirignano,** "Fuel droplet vaporization and spray combustion theory," *Prog. Energy Combust. Sci.*, vol. 9, no. 4, pp. 291–322, 1983.

[164] **A. Yousefi, H. Guo, and M. Birouk,** "An experimental and numerical study on diesel injection split of a natural gas/diesel dual-fuel engine at a low engine load," *Fuel*, vol. 212, pp. 332–346, 2018.

[165] **A. Yousefi, H. Guo, and M. Birouk,** "Effect of swirl ratio on NG/diesel dual-fuel combustion at low to high engine load conditions," *Appl. Energy*, vol. 229, pp. 375–388, 2018.

[166] **A. Yousefi, H. Guo, and M. Birouk,** "Effect of diesel injection timing on the combustion of natural gas/diesel dual-fuel engine at low-high load and low-high speed conditions," *Fuel*, vol. 235, pp. 838–846, 2019.

[167] **"ANSYS Forte Theory Guide."** in Chemical Reaction Mechanism. 2019.

[168] **"ANSYS Forte Best Practices."** in Sector Mesh Generation. 2019.

[169] **A. CFD, "Solver users guide [z],"** *AVL FIRE*, 2013.

[170] **F. Ekin, O. A. Ozsoysal, and H. Arslan,** "The effect of using hydrogen at partial load in a diesel-natural gas dual fuel engine," *Int. J. Hydrog. Energy*, vol. 47, no. 42, pp. 18532–18550, May 2022, doi: 10.1016/j.ijhydene.2022.03.287.

[171] **Y. Karagöz, T. Sandalcı, L. Yüksek, A. S. Dalkılıç, and S. Wongwises,** "Effect of hydrogen–diesel dual-fuel usage on performance, emissions and diesel combustion in diesel engines," *Adv. Mech. Eng.*, vol. 8, no. 8, p. 1687814016664458, 2016.

[172] **N. Saravanan, G. Nagarajan, G. Sanjay, C. Dhanasekaran, and K. M. Kalaiselvan,** "Combustion analysis on a DI diesel engine with hydrogen in dual fuel mode," *Fuel*, vol. 87, no. 17–18, pp. 3591–3599, 2008.

[173] **S. Szwaja and K. Grab-Rogalinski,** "Hydrogen combustion in a compression ignition diesel engine," *Int. J. Hydrog. Energy*, vol. 34, no. 10, pp. 4413–4421, 2009.

[174] **R. Kavtaradze, T. Natriashvili, and S. Gladyshev,** "Hydrogen-diesel engine: Problems and prospects of improving the working process," SAE Technical Paper, 2019.

[175] **U. Rajak, P. Nashine, T. N. Verma, I. Veza, and Ü. Ağbulut,** "Numerical and experimental investigation of hydrogen enrichment in a dual-fueled CI engine: A detailed combustion, performance, and emission discussion," *Int. J. Hydrog. Energy*, vol. 47, no. 76, pp. 32741–32752, 2022.

[176] **N. Saravanan and G. Nagarajan,** "Experimental investigation in optimizing the hydrogen fuel on a hydrogen diesel dual-fuel engine," *Energy Fuels*, vol. 23, no. 5, pp. 2646–2657, 2009.

[177] **N. Saravanan and G. Nagarajan,** "Performance and emission study in manifold hydrogen injection with diesel as an ignition source for different start of injection," *Renew. Energy*, vol. 34, no. 1, pp. 328–334, 2009.

[178] **W. Fang, B. Huang, D. B. Kittelson, and W. F. Northrop,** "Dual-fuel diesel engine combustion with hydrogen, gasoline, and ethanol as fumigants: effect of diesel injection timing," *J. Eng. Gas Turbines Power*, vol. 136, no. 8, p. 081502, 2014.

[179] **H. Huang, Q. Wang, C. Shi, Q. Liu, and C. Zhou,** "Comparative study of effects of pilot injection and fuel properties on low temperature combustion in diesel engine under a medium EGR rate," *Appl. Energy*, vol. 179, pp. 1194–1208, 2016.

[180] **Q. Fang, J. Fang, J. Zhuang, and Z. Huang,** "Influences of pilot injection and exhaust gas recirculation (EGR) on combustion and emissions in a HCCI-DI combustion engine," *Appl. Therm. Eng.*, vol. 48, pp. 97–104, 2012.

[181] **M. M. Abdelaal and A. H. Hegab,** "Combustion and emission characteristics of a natural gas-fueled diesel engine with EGR," *Energy Convers. Manag.*, vol. 64, pp. 301–312, 2012.

[182] **S. Saravanan,** "Effect of exhaust gas recirculation (EGR) on performance and emissions of a constant speed DI diesel engine fueled with pentanol/diesel blends," *Fuel*, vol. 160, pp. 217–226, 2015.

[183] **K. Ryu,** "Effects of pilot injection pressure on the combustion and emissions characteristics in a diesel engine using biodiesel–CNG dual fuel," *Energy Convers. Manag.*, vol. 76, pp. 506–516, 2013.

[184] **R. S. Kishna, K. Nanthagopal, B. Ashok, R. Srinath, M. P. Kumar, and P. Bhowmick,** "Investigation on pilot injection with low temperature combustion of Calophyllum inophyllum biodiesel fuel in common rail direct injection diesel engine," *Fuel*, vol. 258, p. 116144, 2019.

[185] **H. Wei *et al.*,** "Experimental investigations of the effects of pilot injection on combustion and gaseous emission characteristics of diesel/methanol dual fuel engine," *Fuel*, vol. 188, pp. 427–441, 2017.

[186] **L. Niranjan, S. Thomas, and V. Sajith,** "Experimental investigation on the effects of cold and hot EGR using diesel and bio-diesel as Fuel," in *international Conference on Energy and Environment*, 2006, pp. 28–30.

[187] **W. Mingrui, N. T. Sa, R. F. Turkson, L. Jinping, and G. Guanlun,** "Water injection for higher engine performance and lower emissions," *J. Energy Inst.*, vol. 90, no. 2, pp. 285–299, 2017.

[188] **S. Zhu *et al.*,** "A review of water injection applied on the internal combustion engine," *Energy Convers. Manag.*, vol. 184, pp. 139–158, 2019.

[189] **V. Ayhan and Y. M. Ece,** "New application to reduce NOx emissions of diesel engines: Electronically controlled direct water injection at compression stroke," *Appl. Energy*, vol. 260, p. 114328, 2020.

[190] **Z. Chen, Y. Cai, G. Xu, H. Duan, and M. Jia,** "Exploring the potential of water injection (WI) in a high-load diesel engine under different fuel injection strategies," *Energy*, vol. 243, p. 123074, 2022.

[191] **A. Krishnasamy,** "Effects of compression ratio and water vapor induction on the achievable load limits of a light duty diesel engine operated in HCCI mode," *SAE Technical Paper*, 2019.

[192] **R. Chaurasiya and A. Krishnasamy,** "A single fuel port and direct injected low temperature combustion strategy to reduce regulated pollutants from a light-duty diesel engine," *Fuel*, vol. 335, p. 127114, 2023.

[193] **S. Gowrishankar, P. Rastogi, P. Bhasker, and A. Krishnasamy,** "Comparison of Diesel-Water Emulsion and Water Vapor Induction Methods for Simultaneous Reduction in NO x and Smoke Emissions of a Diesel Engine," *SAE Technical Paper*, 2020.

[194] **X. Tauzia, A. Maiboom, and S. R. Shah,** "Experimental study of inlet manifold water injection on combustion and emissions of an automotive direct injection diesel engine," *Energy*, vol. 35, no. 9, pp. 3628–3639, 2010.

[195] **M. Kettner *et al.*,** "Investigating the influence of water injection on the emissions of a diesel engine," *J. Mech. Eng. Sci.*, vol. 10, no. 1, pp. 1863–1881, 2016.

[196] **A. Maiboom, X. Tauzia, and J.-F. Hétet,** "Experimental study of various effects of exhaust gas recirculation (EGR) on combustion and emissions of an automotive direct injection diesel engine," *Energy*, vol. 33, no. 1, pp. 22–34, 2008.

[197] **X. Wei *et al.*,** "Effects of coupling port water injection and EGR on the spray water evolution, combustion and emission of a premixed stoichiometric natural gas engine: A numerical study," *Fuel*, vol. 324, p. 124315, 2022.

[198] **E. P. Kopyev, I. S. Anufriev, E. Y. Shadrin, E. L. Loboda, M. V. Agafontsev, and M. A. Mukhina,** "Studying the diesel flame structure in superheated water vapor jets by using IR thermography," *Infrared Phys. Technol.*, vol. 102, p. 103028, 2019.

[199] **S. Wang, Y. Zhai, Z. Wang, R. Hou, T. Zhang, and C. Ji,** "Comparison of air and EGR with different water fractions dilutions on the combustion of hydrogen-air mixtures," *Fuel*, vol. 324, p. 124686, 2022.

[200] **G. G. Naik and H. M. Dharmadhikari,** "Methods for reducing NOx and PM emissions in compression ignition engine: A review," *Mater. Today Proc.*, vol. 72, pp. 1406–1412, 2023.

[201] **M. Choi, K. Mohiuddin, N. Kim, and S. Park,** "Investigation of the effects of EGR rate, injection strategy and nozzle specification on engine performances and emissions of a single cylinder heavy duty diesel engine using the two color method," *Appl. Therm. Eng.*, vol. 193, p. 117036, 2021.

[202] **X. Jiang, H. Wei, L. Zhou, and R. Chen,** "Numerical study on the effects of multiple-injection coupled with EGR on combustion and NOx emissions in a marine diesel engine," *Energy Procedia*, vol. 158, pp. 4429–4434, 2019.

[203] **F. Jaliliantabar *et al.*,** "A comprehensive study on the effect of pilot injection, EGR rate, IMEP and biodiesel characteristics on a CRDI diesel engine," *Energy*, vol. 194, p. 116860, 2020.

[204] **G. Kökkülünk, A. Parlak, V. Ayhan, I. Cesur, G. Gonca, and B. Boru,** "Theoretical and experimental investigation of steam injected diesel engine with EGR," *Energy*, vol. 74, pp. 331–339, 2014.

[205] **O. H. Ghazal,** "Combustion analysis of hydrogen-diesel dual fuel engine with water injection technique," *Case Stud. Therm. Eng.*, vol. 13, p. 100380, 2019.

CURRICULUM VITAE

Name Surname **:** Ferhat EKİN

EDUCATION **:**

- **B.Sc.** **:** 2013, Yıldız Technical University, Naval Architecture and Maritime Faculty, Naval Architecture and Marine Engineering
- **Second B.Sc.** **:** 2021, İstanbul - Cerrahpaşa University, Engineering Faculty, Mechanical Engineering
- **M.Sc.** **:** 2017, İstanbul Technical University, Naval Architecture and Marine Science Faculty, Naval Architecture and Marine Engineering

PROFESSIONAL EXPERIENCE AND REWARDS:

- 2014-2023 İstanbul Technical University, Research Assistant
- 2023- Van Yüzüncü Yıl University, Research Assistant

PUBLICATIONS, PRESENTATIONS AND PATENTS ON THE THESIS:

- **Ekin, F.,** Ozsoysal, O. A., & Arslan, H. (2022). The effect of using hydrogen at partial load in a diesel-natural gas dual fuel engine. *International Journal of Hydrogen Energy*, *47*(42), 18532-18550.

OTHER PUBLICATIONS, PRESENTATIONS AND PATENTS:

- **Ekin, F.,** Kafalı, M., Ozsoysal, O. A. 2018: A Numerical Study of the Effects of Spray Angle and Swirl Ratio on Combustion and Emission of Diesel Engines. International Congress on Engineering and Life Science (ICELIS), April 26-29, 2018 Kastamonu, Turkey.
- **Ekin, F.,** Ozsoysal, O. A. 2019: A Numerical Study for Different Humidity Ratios of Intake Air in A CNG Engine about the Effects on the Performance and Emission Values. International Congress on Engineering and Life Science (ICELIS), April 11-14, 2019 Kastamonu, Turkey.
- **Ekin, F.** 2019: A Numerical Study About the Effects of Spray Angle and Injector Nozzle Diameter on the Performance and Emission Values in A Diesel Engine. International Congress on Engineering and Life Science (ICELIS), April 11-14, 2019 Kastamonu, Turkey.

- **Ekin, F.** 2019: A Numerical Study about the Effects of Amount of Intake Air Humidity and Different Injection Strategies on Performance and Emission Values in a Turbo-Charged Diesel Engine. Congress on Thermal Science and Technology (CTST), September 11-14, 2019 Kocaeli, Turkey.
- Öncüoğlu Ö., **Ekin, F.** 2020: Dizel Motorda Enjektör Püskürtme Açısı ve Silindir İçi Döngü Oranının Performans ve Emisyonlara Etkisinin Sayısal Olarak İncelenmesi. International Conference on Materials Science, Mechanical and Automotive Engineerings and Technology (IMSMATEC), June 24-26, 2020 Nevşehir, Turkey.